

# PHASE 2 INITIAL BOREHOLE DRILLING AND TESTING AT IG\_BH04/05/06 IGNACE AREA

*WP06 Data Report Hydraulic Testing for IG\_BH05*

**APM-REP-01332-0395**

**November 2023**

**WSP Canada Inc.**

**nwmo**

NUCLEAR WASTE  
MANAGEMENT  
ORGANIZATION

SOCIÉTÉ DE GESTION  
DES DÉCHETS  
NUCLÉAIRES

**Nuclear Waste Management Organization**  
22 St. Clair Avenue East, 4<sup>th</sup> Floor  
Toronto, Ontario  
M4T 2S3  
Canada

Tel: 416-934-9814  
Web: [www.nwmo.ca](http://www.nwmo.ca)



## REPORT

# Phase 2 Initial Borehole Drilling and Testing at IG\_BH04/05/06, Ignace Area

*WP06 Data Report - Hydraulic Testing for IG\_BH05*

Submitted to:

**Nuclear Waste Management Organization**

4th Floor  
22. St. Clair Avenue East  
Toronto, Ontario M4T 2S3

Submitted by:

**WSP Canada Inc.**

6925 Century Avenue, Suite #600, Mississauga, Ontario, L5N 7K2, Canada

+1 905 567 4444

20253946 (5060)

NWMO Report: APM-REP-01332-0395

November 3, 2023

## Distribution List

e-copy: NWMO

e-copy: WSP Canada Inc.

## WP06 DATA REPORT

### HYDRAULIC TESTING FOR IG\_BH05

#### CLIENT INFORMATION

Project Name: Phase 2 Initial Borehole Drilling and Testing at IG\_BH04/05/06, Ignace Area  
Project Number: 20253946  
Client PO Number: 2001102  
Document Name: 20253946 (5060) ig\_bh05\_wp06\_report\_r1a

Client: Nuclear Waste Management Organization (NWMO)  
Address: 22 St. Clair Avenue East, 4th Floor  
City: Toronto  
Province: Ontario  
Postal Code: M4T 2S3  
Client Contact: Ryan Abrams      Warwick Watt      Natacha Lugo Bizarro  
Email: rabrams@nwmo.ca      wwatt@nwmo.ca      nlugo@nwmo.ca

**ISSUE/REVISION INDEX**

Issue Code	Revision					Revision Details
	No.	By	Rev'd.	App.	Date	
RR	R0a	STH	ML	JC	March 20, 2023	Draft released for review and comment
RI	R1a	STH	ML	JC	November 3, 2023	Final Released for Information

Issue Codes: RR = Released for Review and Comments, RI = Released for Information

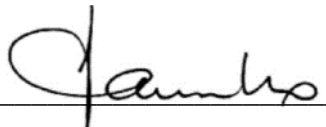
**SIGNATURES**

Prepared by: 

Steve Hales, P.Geo.  
Hydrogeologist

Reviewed by: 

Michael Lemon, P.Eng.  
Lead Geological Engineer

Approved by: 

Joe Carvalho, Ph.D., P.Eng.  
Principal Geotechnical Engineer

# Table of Contents

<b>1.0 INTRODUCTION .....</b>	<b>1</b>
<b>2.0 BACKGROUND INFORMATION.....</b>	<b>1</b>
2.1 Geological Setting .....	1
2.2 Purpose .....	6
2.3 Roles and Responsibilities .....	6
<b>3.0 TESTING EQUIPMENT .....</b>	<b>6</b>
3.1 Packer Inflation.....	9
3.2 Data Acquisition .....	10
3.3 Tool Assembly.....	12
3.4 Tool Operation Checks .....	16
3.4.1 Leak Test #1 – Start of Testing Prior to Test HT001 .....	16
3.4.2 Leak Test #2 – End of Testing .....	17
<b>4.0 TEST INTERVAL SELECTION.....</b>	<b>18</b>
<b>5.0 TESTING METHODOLOGY .....</b>	<b>19</b>
<b>6.0 TEST ANALYSIS .....</b>	<b>23</b>
6.1 Input Parameters.....	24
6.1.1 Test Pressure.....	24
6.1.2 Wellbore Storage .....	24
6.2 Output Parameters.....	26
6.2.1 Transmissivity and Hydraulic Conductivity .....	27
6.2.2 Storativity .....	27
6.2.3 Formation Pressure .....	28
6.2.4 Skin Zone .....	28
6.2.5 Flow Dimension.....	28
<b>7.0 SUMMARY OF RESULTS .....</b>	<b>29</b>
<b>8.0 REFERENCES .....</b>	<b>33</b>

## TABLES

Table 1: List of Downhole Equipment.....	7
Table 2: List of Surface Equipment .....	8
Table 3: Summary of Test Results .....	30

## FIGURES

Figure 1: Location of IG_BH05 in relation to the Ignace Area.....	4
Figure 2: Geological Setting and Location of Boreholes IG_BH04, IG_BH05, and IG_BH06 in the Northern Portion of the Revell Batholith.....	5
Figure 3: DataCan Surface Readout Box, Model 105421 .....	11
Figure 4: DataCan Gauge Carrier and Transducers with Outer Protective Casing Removed.....	12
Figure 5: Tool Schematic.....	13
Figure 6: Work area tent with flatpack and pressure vessel (packer inflation manifold with pressure gauge on right side of cage) (see Figure 8) .....	14
Figure 7: Work area tent with flatpack and red DHSIV activation pump below flatpack at center .....	15
Figure 8: Pressure vessel (front) and packer inflation manifold with pressure gauge and nitrogen bottle on side of flatpack cage.....	15
Figure 9: Leak Test #1 Pressure Plot .....	17
Figure 10: Leak Test #2 Pressure Plot .....	18
Figure 11: IG_BH05 WP06 Test Plan Flow Chart .....	20
Figure 12: Typical Pulse Test Procedure, IG_BH05_HT003.....	21
Figure 13: Semi-log Plot of IG_BH05_HT029 analyses showing the pressure recovery of the PSR phase (dark blue) and extrapolated static pressure fit line (red).....	22
Figure 14: Transmissivity.....	32
Figure 15: Hydraulic Conductivity.....	32

## APPENDICES

### APPENDIX A

Equipment Photographs

### APPENDIX B

Calibration Certificates

### APPENDIX C

Test Results



## 1.0 INTRODUCTION

The Phase 2 Initial Borehole Drilling and Testing at IG\_BH04/05/06 project in the Wabigoon Lake Ojibway Nation (WLON) – Ignace area of Ontario, is part of the Phase 2 Geoscientific Preliminary Field Investigations of the Nuclear Waste Management Organization's (NWMO) Adaptive Phased Management (APM) Site Selection Phase.

This project involves testing of deep borehole IG\_BH04 and the drilling and testing of deep boreholes IG\_BH05 and IG\_BH06 in the Revell site within the identified Potential Repository Area (PRA). The work comprised of a total of eleven work packages and was carried out by a team led by Golder Associates Ltd. (now WSP Canada Inc.) on behalf of the NWMO. The IG\_BH05 program is described in a Borehole Characterization Plan (BCP) for IG\_BH05.

This report describes the methodology, activities and results for Work Package 6 (WP06): Hydraulic Testing for IG\_BH05. Borehole IG\_BH05 is an inclined hole and all depths referred to in this report are in meters below ground surface along the length of the borehole (mbgs along hole), rather than true vertical depth.

## 2.0 BACKGROUND INFORMATION

### 2.1 Geological Setting

The approximately 2.7-billion year old Revell batholith is located in the western part of the Wabigoon Subprovince of the Archean Superior Province. The batholith is roughly elliptical in shape trending northwest, is approximately 40 km in length, 15 km in width, and covers an area of approximately 455 km<sup>2</sup>. Based on geophysical modelling, the batholith is approximately 2 km to 3 km thick through the center of the northern portion (SGL, 2015). The batholith is surrounded by supracrustal rocks of the Raleigh Lake (to the north and east) and Bending Lake (to the southwest) greenstone belts (Figure 2).

IG\_BH05 is located within an investigation area of approximately 19 km<sup>2</sup> in size, situated in the northern portion of the Revell batholith. Bedrock exposure in the area is generally very good due to minimal overburden, few water bodies, and relatively recent logging activities. Ground elevations generally range from 400 to 450 m above sea level. The ground surface broadly slopes towards the northwest as indicated by the flow direction of the main rivers in the area. Local water courses tend to flow to the southwest towards Mennin Lake (Figure 1).

Four main rock units are identified in the supracrustal rock group: mafic metavolcanic rocks, intermediate to felsic metavolcanic rocks, metasedimentary rocks, and mafic intrusive rocks (Figure 2). Sedimentation within the supracrustal rock assemblage was largely synvolcanic, although sediment deposition in the Bending Lake area may have continued past the volcanic period (Stone, 2009; Stone, 2010a; Stone, 2010b). All supracrustal rocks are affected, to varying degrees, by penetrative brittle-ductile to ductile deformation under greenschist- to amphibolite-facies metamorphic conditions (Blackburn and Hinz, 1996; Stone et al., 1998). In some locations, primary features, such as pillow basalt or bedding in sedimentary rocks are preserved, in other locations, primary relationships are completely masked by penetrative deformation. Uranium-lead (U-Pb) geochronological analysis of the supracrustal rocks produced ages that range between 2734.6 +/-1.1 Ma and 2725 +/-5 Ma (Stone et al. 2010).

Three main suites of plutonic rock are recognized in the Revell batholith, including, from oldest to youngest: a Biotite Tonalite to Granodiorite suite, a Hornblende Tonalite to Granodiorite suite, and a Biotite Granite to Granodiorite suite (Figure 2). Plutonic rocks of the Biotite Tonalite to Granodiorite suite occur along the

southwestern and northeastern margins of the Revell batholith. The principal type of rock within this suite is a white to grey, medium-grained, variably massive to foliated or weakly gneissic, biotite tonalite to granodiorite. One sample of foliated and medium-grained biotite tonalite produced a U-Pb age of  $2734.2 \pm 0.8$  Ma (Stone et al. 2010). The Hornblende Tonalite to Granodiorite suite occurs in two irregularly-shaped zones surrounding the central core of the Revell batholith. Rocks of the Hornblende Tonalite to Granodiorite suite range compositionally from tonalite through granodiorite to granite and also include significant proportions of quartz diorite and quartz monzodiorite. One sample of coarse-grained grey mesocratic hornblende tonalite produced a U-Pb age of  $2732.3 \pm 0.8$  Ma (Stone et al. 2010). Rocks of the Biotite Granite to Granodiorite suite underlie most of the northern, central and southern portions of the Revell batholith. Rocks of this suite are typically coarse-grained, massive to weakly foliated, and white to pink in colour. The Biotite Granite to Granodiorite suite ranges compositionally from granite through granodiorite to tonalite. A distinct potassium (K)-Feldspar Megacrystic Granite phase of the Biotite Granite to Granodiorite suite occurs as an oval-shaped body in the central portion of the Revell batholith (Figure 2). One sample of coarse-grained, pink, massive K-feldspar megacrystic biotite granite produced a U-Pb age of  $2694.0 \pm 0.9$  Ma (Stone et al. 2010).

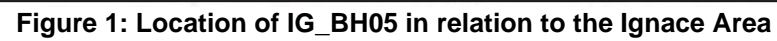
The bedrock surrounding IG\_BH05 is composed mainly of massive to weakly foliated felsic intrusive rocks that vary in composition between granodiorite and tonalite, and together form a relatively homogeneous intrusive complex. Bedrock identified as tonalite transitions gradationally into granodiorite and no distinct contact relationships between these two rock types are typically observed (SRK and Golder, 2015; Golder and PGW, 2017). Massive to weakly foliated granite is identified at the ground surface to the northwest of the feldspar-megacrystic granite. The granite is observed to intrude into the granodiorite-tonalite bedrock, indicating it is distinct from, and younger than, the intrusive complex (Golder and PGW 2017).

West-northwest trending mafic dykes interpreted from aeromagnetic data extend across the northern portion of the Revell batholith and into the surrounding greenstone belts. One mafic dyke occurrence, located to the northwest of IG\_BH01, is approximately 15-20 m wide (Figure 2). All of these mafic dykes have a similar character and are interpreted to be part of the Wabigoon dyke swarm. One sample from the same Wabigoon swarm produced a U-Pb age of  $1887 \pm 13$  Ma (Stone et al., 2010), indicating that these mafic dykes are Proterozoic in age. It is assumed based on surface measurements that these mafic dykes are sub-vertical (Golder and PGW 2017).

Long, narrow valleys are located along the western and southern limits of the investigation area (Figure 1). These local valleys host creeks and small lakes that drain to the southwest and may represent the surface expression of structural features that extend into the bedrock. A broad valley is located along the eastern limits of the investigation area and hosts a more continuous, un-named water body that flows to the south. The linear and segmented nature of this waterbody's shorelines may also represent the surface expression of structural features that extend into the bedrock.

Regional observations from mapping have indicated that structural features are widely spaced (typical 30 to 500 cm spacing range) and dominantly comprised of sub-vertical joints with two dominant orientations, northeast and northwest trending (Golder and PGW 2017). Interpreted bedrock lineaments generally follow these same dominant orientations in the northern portion of the Revell batholith (Figure 2; DesRoches et al., 2018). Minor sub-horizontal joints have been observed with minimal alteration, suggesting they are younger and perhaps related to glacial unloading. One mapped regional-scale fault, the Washeibemaga Lake fault, trends east and is located to the west of the Revell batholith (Figure 2). Ductile lineaments, also shown on Figure 2, follow the trend of foliation

mapped in the surrounding greenstone belts. Additional details of the lithological units and structures found at surface within the investigation area are reported in Golder and PGW (2017).





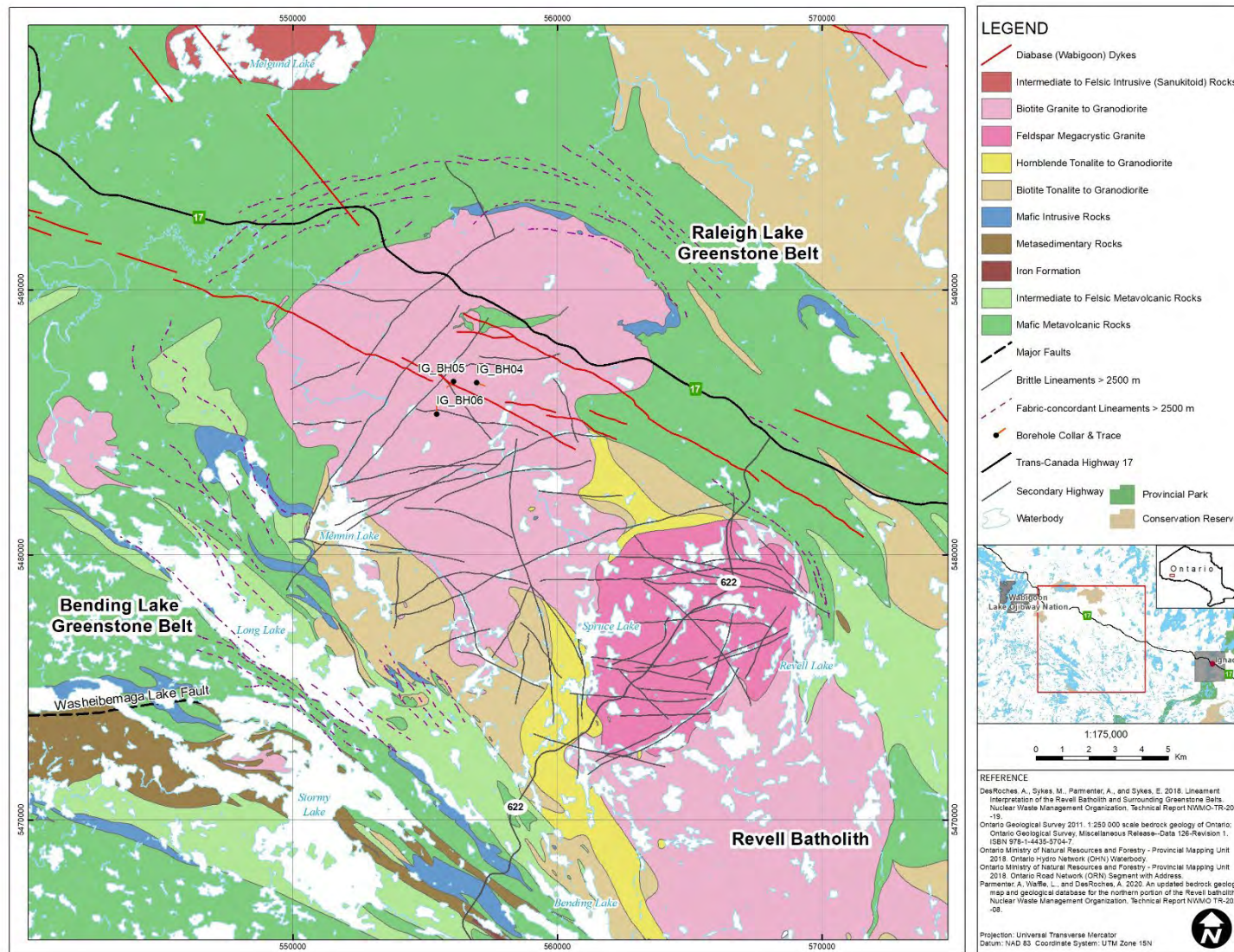


Figure 2: Geological Setting and Location of Boreholes IG\_BH04, IG\_BH05, and IG\_BH06 in the Northern Portion of the Revell Batholith

## 2.2 Purpose

The purpose of WP06 is to estimate the hydraulic properties of the crystalline rock units at selected depths in borehole IG\_BH05. The borehole was drilled in 96 mm (HQ) diameter at an inclination of 70° from horizontal and an azimuth of 220° to a total depth of 1000.63 m along hole. Additional borehole details are presented in the report WP02 Data Report – Borehole Drilling and Coring for IG\_BH05 (Golder, 2022). Testing occurred after the completion of drilling and logging. Selection of test intervals considered potential water conductive zones based on review of the earlier stages of work that included the following:

- WP02 – Borehole Drilling and Coring;
- WP03 – Geological and Geotechnical Core Logging, Photography, and Sampling;
- WP05 – Geophysical Logging and Interpretation; and
- WP07 – Opportunistic Groundwater Sampling.

The scientific objective is the collection of high quality and reliable test data that will support the estimation of high-confidence hydraulic properties including:

- Hydraulic conductivity (transmissivity / thickness);
- Inferred hydraulic pressure in the rock;
- Test zone compressibility, including the rock within the isolated interval, water within the test zone and the test tool;
- Borehole skin factor; and
- Specific storage (storativity / thickness).

The procedures for the collection, analyses and reporting of the test data were developed by WSP and reviewed by the NWMO. These procedures for data collection are summarized in the following sections.

For the purpose of test analysis, the static formation pressure was estimated by extrapolation of the test interval pressure response.

## 2.3 Roles and Responsibilities

Testing was carried out by a team of testing specialists from WSP. Drill rig operation support was provided by Rodren Drilling Ltd., based in Winnipeg, Manitoba. Testing was carried out on a 24-hour, 7 days per week basis. Day shifts ran from 7 am to 7 pm, and night shifts from 7 pm to 7 am. A driller and helper were on site for each day and night shift, and a drilling foreman was typically present during the day shifts, or as required. Work was performed under direction and review from WSP's WP06 lead. WSP's WP06 lead communicated with the NWMO's WP06 lead regarding the development of the test plan and decisions during field testing based on preliminary test results.

## 3.0 TESTING EQUIPMENT

The equipment used for hydrogeological testing of borehole IG\_BH05 consisted of a straddle packer tool with a 20 m long test interval, integrated downhole shut-in valve (DHSIV) for isolating the test interval from the test

tubing to reduce wellbore storage, and real-time multi-zone pressure and temperature monitoring. Real-time pressure from test tubing, and above, between and below the packers was monitored at surface using DataCan pressure transducers mounted in a gauge carrier directly above the DHSIV. A separate pressure transducer with internal memory, manufactured by Pioneer Petrotech Services (PPS), was positioned within the interval to collect data for test analyses directly from the test interval. A list of equipment used downhole is provided in Table 1, and a list of equipment used at surface is provided in Table 2. Photos of the testing equipment are provided in Appendix A. Pressure transducers were calibrated following manufacturers' instructions, and calibration certificates are provided in Appendix B.

**Table 1: List of Downhole Equipment**

Item Name	Manufacturer and Model	Item Description
Packers (2x)	Baski MD-2.7, Medium Duty, Sliding-Head Type	Inflatable packers for isolating test zone Uninflated OD = 69 mm Largest recommended hole size = 127 mm Mandrel pipe size = 25 mm Uninflated element length = 1016 mm Max differential pressure rating in 102 mm hole = 5.5 MPa
Test Tubing above tool	Boart Longyear	BQ threaded pipe with O-ring sealed joints OD = 55.7 mm ID = 46.1 mm Length = 3 m
Test Tubing within interval	Boart Longyear	ARQTK threaded perforated pipe between packers OD = 44.7 mm ID = 37.5 mm Length = 1.5 m
Multi-zone pressure transducers (4x)	DataCan Multi-Gauge Piezo Bottom Pressure Gauge, Model 108931	Absolute pressure monitoring in test interval between packers, bottom zone below lower packer, annulus above upper packer and test tubing above DHSIV. Max operating pressure rating = 41.37 MPa Accuracy: Pressure = 0.022% FS Temperature = 0.25°C Resolution: Pressure = 0.0003% FS Temperature = 0.005°C
Multi-zone pressure transducer protective casing	DataCan	Protective metal gauge carrier for Multi-Gauge real-time pressure transducers, installed in-line above the DHSIV
Interval pressure transducer	PPS25 pressure transducer	Absolute pressure monitoring in test interval for data analyses Max operating pressure rating = 41.37 MPa Accuracy: Pressure = 0.03% FS Temperature = 0.5°C Resolution: Pressure = 0.0003% FS Temperature = 0.01°C

Item Name	Manufacturer and Model	Item Description
Swabbing Tool	BQ size, rubber flexible cups on articulated shaft with an attachment for wireline	Used for the removal of water from test tubing for slug/pulse tests Cup diameter = 44.7 mm (unexpanded)
Downhole Shut-in Valve (DHSIV)	IPI Downhole Shut-in Valve (DSHIV)	Hydraulically actuated single line for isolation of the test interval from the test tubing OD = 70mm Zero-volume displacement 100% sealing ball valve Pressure rating up to 68.9 MPa
In-line adapter (ILA) (4x)	Baski	Steel adapter to feed pressure lines from outside of the packer string through the packer OD = 69 mm
Centralizers (6x)	Baski	Positioned above the DataCan gauge carrier, above and below each packer and within the test interval OD = 82.6 mm Length = 300 mm
Flatpack and Spool	Baski	Santoprene encased integrated pressure and electric cable line system 0.0343 m x 0.00104 m x 1400 m 1x 6.35 mm OD x 0.71 mm wall tubing encapsulated single conductor cable 3x 6.35 mm OD x 0.89 mm wall Duplex 2205 stainless steel Motorized metal spool 2 m diameter, 1 m wide 1800 kg weight
Pressure transducer for wellbore storage estimation	Solinst 3001 LT Barologger, M1.5	Lowered inside test tubing during the opening of the DHSIV to measure the volume displacement to estimate the test zone compressibility and wellbore storage Max operating pressure rating= 14.71 kPa Accuracy: Pressure = 0.05 kPa Temperature = 0.05°C Resolution: Pressure = 0.002% FS Temperature = 0.003°C

**Table 2: List of Surface Equipment**

Item Name	Manufacturer and Model	Item Description
Inflation Pressure Vessel	Misc.	20-liter capacity, 8.0 MPa pressure rating. Filled with water and pressurized using nitrogen to inflate packers.
Packer Inflation Control Manifold and Hoses	Misc.	A manifold to control nitrogen flow for packer inflation,



Item Name	Manufacturer and Model	Item Description
		8.0 MPa pressure rating
Nitrogen Pressure Regulator	Misc.	High pressure regulator for controlling pressure outflow from nitrogen cylinder used for packer inflation.
Nitrogen Cylinders	Praxair Canada Inc., Dryden, Ontario	Compressed nitrogen gas cylinder for pressurizing the packer inflation pressure vessel.
DHSIV Activation Pump	CVS Controls Ltd.	Manual high-pressure pump for DHSIV operation. Maximum Injection Pressure = 20.68 MPa
Barometric Pressure Transducer	Solinst 3001 LT Barologger, M1.5	Barometric pressure monitoring for correcting absolute pressure downhole gauges Max operating pressure rating= 14.71 kPa Accuracy: Pressure = 0.05 kPa Temperature = 0.05°C Resolution: Pressure = 0.002% FS Temperature = 0.003°C
Master Pressure Gauge, Packer Pressure Monitoring	Omega DPG4000-2K	Digital pressure gauge for field calibration check of pressure transducers and monitoring of packer inflation pressure Max pressure = 13.79 MPa Accuracy = $\pm 0.05\%$
Data Acquisition System	DataCan Surface Readout Box, Model 105421	Data logger with real-time communication, collection and storing of downhole and surface sensor data with 20M sample capacity, USB set-up/ download

### 3.1 Packer Inflation

Water was used for packer inflation instead of gas to reduce the required packer inflation pressure, and the compressibility of the packers and the inflation lines which contribute to the test interval compressibility. A surface pressure vessel filled with water was pressurized using compressed nitrogen to achieve the desired packer inflation pressure.

Packer inflation pressure is calculated following the manufacturer's recommendations and recorded in the Field Data tab of the Data Quality Confirmation workbook. The inflation pressure at surface was set at 2.1 MPa, which is the summation of several criteria:

- Hydrostatic Pressure* – Pressure exerted on the external surface of the packers. When inflating packers with water, the external pressure on the packer is balanced by the equivalent internal hydrostatic pressure in the inflation line resulting in an assumed net pressure of zero.
- Packer stretch (or packer seating pressure)* – Pressure required to expand and seat the packer to the borehole wall. This pressure is dependent on the borehole diameter and provided in the manufacturer's user manual (equals 0.7 MPa for HQ borehole).

- c) *Test Differential Pressure (or packer sealing pressure)* – Packer pressure required to prevent leakage across the packer when maximum differential pressure is exerted at the test interval during the test execution. A maximum test pressure of 1.0 MPa was applied for the inflation pressure calculation as the maximum test differential pressure was 0.76 MPa; however, the target minimum differential pressure as defined in the Test Plan was 100 kPa.
- d) *Factor of Safety* – Extra applied pressure to ensure the required packer inflation pressure is maintained through the entire test. The factor of safety accounts for any slow leakage in the system, temperature variations at surface, and fluid density variation between the water within the inflation system and the borehole fluid. A factor of safety of 0.35 MPa was applied for all tests.

The required packer inflation pressure is first set at the nitrogen cylinder using the pressure regulator. This pressure is then transferred to the packer inflation manifold, where a more precise adjustment of the required inflation pressure can be achieved using an Omega analog pressure gauge. The pressure from the packer inflation manifold is then diverted to the pressure vessel where it pressurizes the water within, forcing it into the packer inflation line in the flatpack to inflate the packers. The two packers were inflated using two separate inflation lines allowing for individual inflating and deflating of the packers.

## 3.2 Data Acquisition

In order to collect accurate pressure and temperature data, the following instruments were used:

- **Real-time Multi-zone Downhole Pressure Measurements** - Downhole pressure is monitored in four isolated zones using transducers manufactured by DataCan, Model Number 108931. Pressure readings are communicated in real-time to the surface via dedicated cable in the flatpack. Data are recorded with a DataCan surface readout box (Figure 3) connected to a field laptop via USB. The real-time pressure readings are used to monitor the test progress, verify packer seal of the test zone and allow for estimation of preliminary transmissivity values during testing. The DataCan transducers are housed within a protective carrier mounted above the DHSIV as shown in Figure 4. The zones monitored during testing include:
  - Test interval between the packers;
  - Open borehole below the lower packer to confirm adequate seal at the bottom of the test interval;
  - Annular space above the upper packer between the test tubing and borehole wall to confirm adequate seal at the top of the test interval; and
  - Test tubing above the DHSIV to measure the magnitude of the induced slug or pulse.
- **Test Interval Pressure Data (for analyses)** - Pressure and temperature data were recorded directly in the test interval with a single pressure transducer manufactured by Pioneer Petrotech Services Inc. (PPS), Model PPS25. The PPS transducer is self-contained with integrated internal memory and battery. The transducer was positioned inside a perforated pipe below the upper packer and the recorded pressures from this transducer were used for the final test analyses since it provided a complete borehole pressure history from the start of testing.
- **Packer Pressure** - Packer pressures were monitored at surface with the Omega DPG4000-2K pressure gauge connected to the packer inflation vessel. Packer pressures were monitored during the testing to ensure no leakage in the packer inflation system occurred. Packer pressures at the start and end of each test were

recorded in the Field Data tab of the Data Quality Confirmation (DQC) workbook included in the electronic deliverable under separate cover.

- **Barometric Pressure** – Barometric pressure was recorded at the drill rig during testing using a Solinst 3001 LT Barologger, M1.5. Barometric pressure and air temperature were recorded every minute for barometric pressure correction of the downhole absolute pressure transducers. Barometric pressure was used to compensate the downhole transducer pressures by subtracting the barometric pressure from the downhole transducer absolute pressure reading to provide gauge pressure at depth. The range of barometric pressure recorded over the duration of each test was included in the Field Data tab of the DQC workbook.

All electronic instruments were calibrated following the manufacturer's instructions prior to arrival on site. Calibration checks are recorded in the Tool Assembly tab of the DQC workbook. Calibration certificates are provided in Appendix B.



**Figure 3: DataCan Surface Readout Box, Model 105421**



**Figure 4: DataCan Gauge Carrier and Transducers with Outer Protective Casing Removed**

### **3.3 Tool Assembly**

The tool configuration as shown in Figure 5 was used for all tests.

Due to its length, the testing tool was mobilized in modules and assembled on site from bottom-up as it was lowered into the borehole. The tool assembly sequence was as follows:

- The bottom packer was threaded to the perforated transducer carrier.
- The pre-programmed, battery powered, interval pressure transducer (PPS25) with internal memory was threaded inside the transducer carrier. The recording frequency was set to 5 second intervals allowing for several months of data recording and storage.
- The perforated transducer carrier was threaded to ARQTK interval test tubing which was threaded to the bottom of the top packer with the DHSIV positioned above the upper packer.
- The DataCan multi-zone pressure transducer protective casing is positioned above the DHSIV.

Prior to lowering the tool down the borehole, the packers and the inflation lines were filled with water to remove the air from the system.

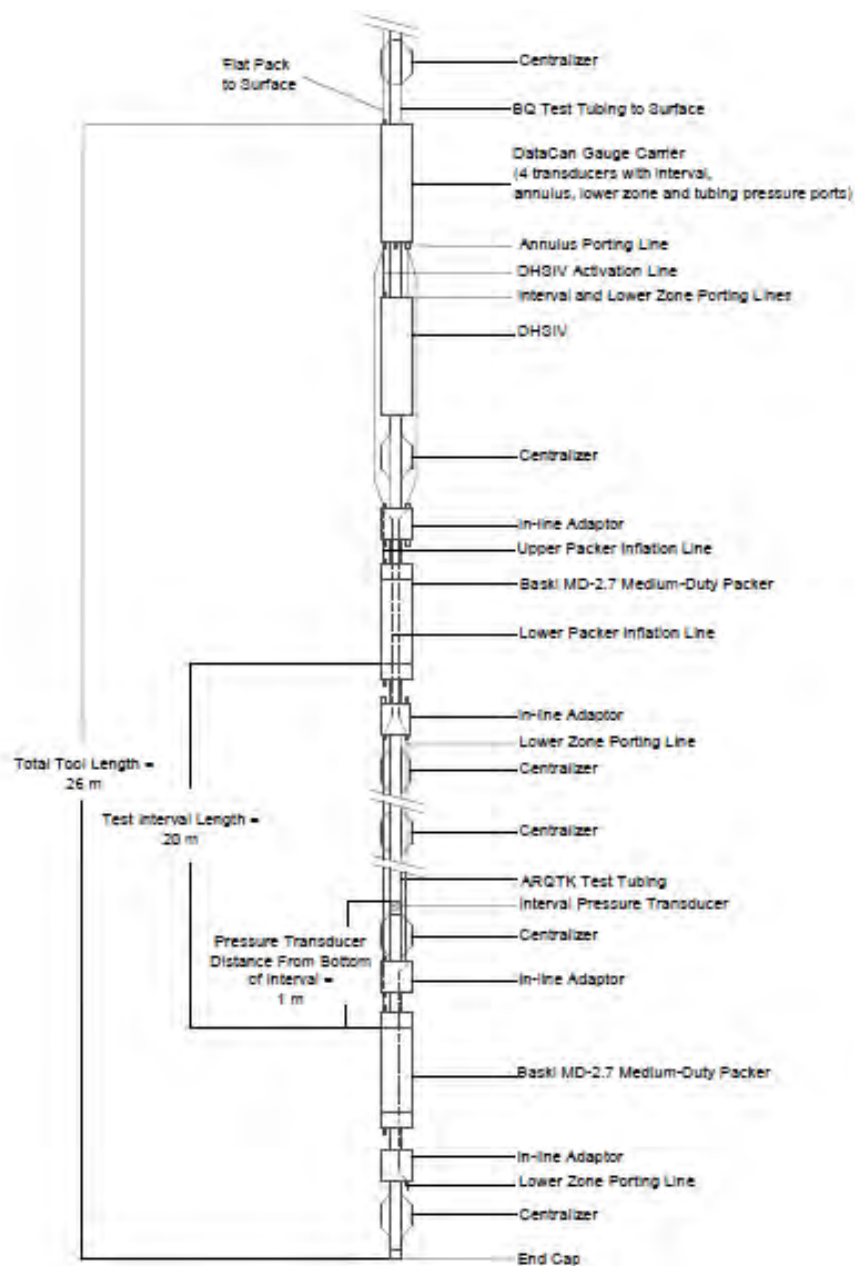


**Figure 5: Tool Schematic**

The end of the flatpack was positioned directly above the multi-zone pressure transducer carrier and the three stainless steel lines in the flatpack were connected to the upper packer, the lower packer, and the DHSIV lines. The electrical cable was connected to the common lead (cable head) from the pressure transducers.

BQ drill rods were used to lower the tool to the selected test depths and the flatpack was secured to the outside of the test tubing with duct tape. The joints of the drill rods were sealed with a rubber O-ring and tightened using pipe wrenches. Rod joint leakage less than the measured magnitude of the interval transmissivity observed during testing had no impact on the pulse test results because the fluid in the tubing is isolated from the test interval by the closed DHSIV.

The pressure required to inflate the packers was supplied from a compressed nitrogen gas cylinder at the surface. A high-pressure regulator was directly attached to the cylinder and connected to packer inflation control manifold. The control manifold was used to inflate packers by pressurizing the water-filled inflation pressure vessel. A manual activation pump was used to operate the DHSIV (Figures 6, 7 and 8).



**Figure 6: Work area tent with flatpack and pressure vessel (packer inflation manifold with pressure gauge on right side of cage) (see Figure 8)**





**Figure 7: Work area tent with flatpack and red DHSIV activation pump below flatpack at center**



**Figure 8: Pressure vessel (front) and packer inflation manifold with pressure gauge and nitrogen bottle on side of flatpack cage**

### 3.4 Tool Operation Checks

Quality assurance (QA) testing of the tool operation was performed on the packer inflation lines and DHSIV activation line inside the surface casing to check for leaks in the system. Data from the quality assurance testing is documented in the DQC workbook.

Two QA tests (Leak Tests) were performed inside the surface casing. Leak tests were performed at the start of testing prior to test HT001 and at the end of the testing program. The leak tests measure the leakage of the testing system at the maximum anticipated test differential pressures and allow for the estimation of an equivalent transmissivity of the cased interval to confirm the testing tool met the project's requirement of accurately measuring test interval hydraulic conductivity to  $10^{-13}$  m/sec.

The leak tests performed are summarized in the following subsections. Details on each test are provided in the DQC workbook.

#### 3.4.1 Leak Test #1 – Start of Testing Prior to Test HT001

Leak Test #1 was performed on September 2, 2021 at the start of testing prior to test HT001. The pressure data collected during the test are presented in Figure 9. The testing tool with a test interval length of 20.02 m was lowered into the surface casing below the water level. The packers were inflated to 2.51 MPa surface pressure (20% above the anticipated inflation pressure during testing) and monitored for leakage. No leakage was observed from the testing system. With the packers inflated, the DHSIV was closed to simulate the PSR phase and the water level in the test tubing was lowered by 0.195 MPa, the maximum available water column above the test tool, in preparation for a slug withdrawal (SW) phase. No hydraulic connection was observed between the annulus, tubing, and test interval. The DHSIV was then opened introducing the pressure change to the test interval, and the interval pressure was monitored for 30 minutes. Following the SW phase, the DHSIV was closed for 210 minutes for a shut-in recovery phase (SWS) with no observable hydraulic connection above and below the test interval.

With the DHSIV open, transmissivity of  $1\text{E-}10$  m<sup>2</sup>/sec and an equivalent hydraulic conductivity of  $5\text{E-}12$  m/sec for the 20.02 m test interval length was derived for the testing tool from the slug withdrawal phase (SW) data. These values are estimated due to the magnitude of the SW recovery being at the lower limit of the transducer range of measurement; also, these values can be considered the lower limit of the testing tool for slug tests. The analyses of the data from shut-in recovery phase (SWS) resulted in a transmissivity of  $7\text{E-}14$  m<sup>2</sup>/sec or an equivalent hydraulic conductivity of  $4\text{E-}15$  m/sec for the 20.02 m test interval length. Leak Test #1 confirmed the tool performance met the project's requirement of accurately measuring test interval hydraulic conductivity down  $10^{-13}$  m/sec.



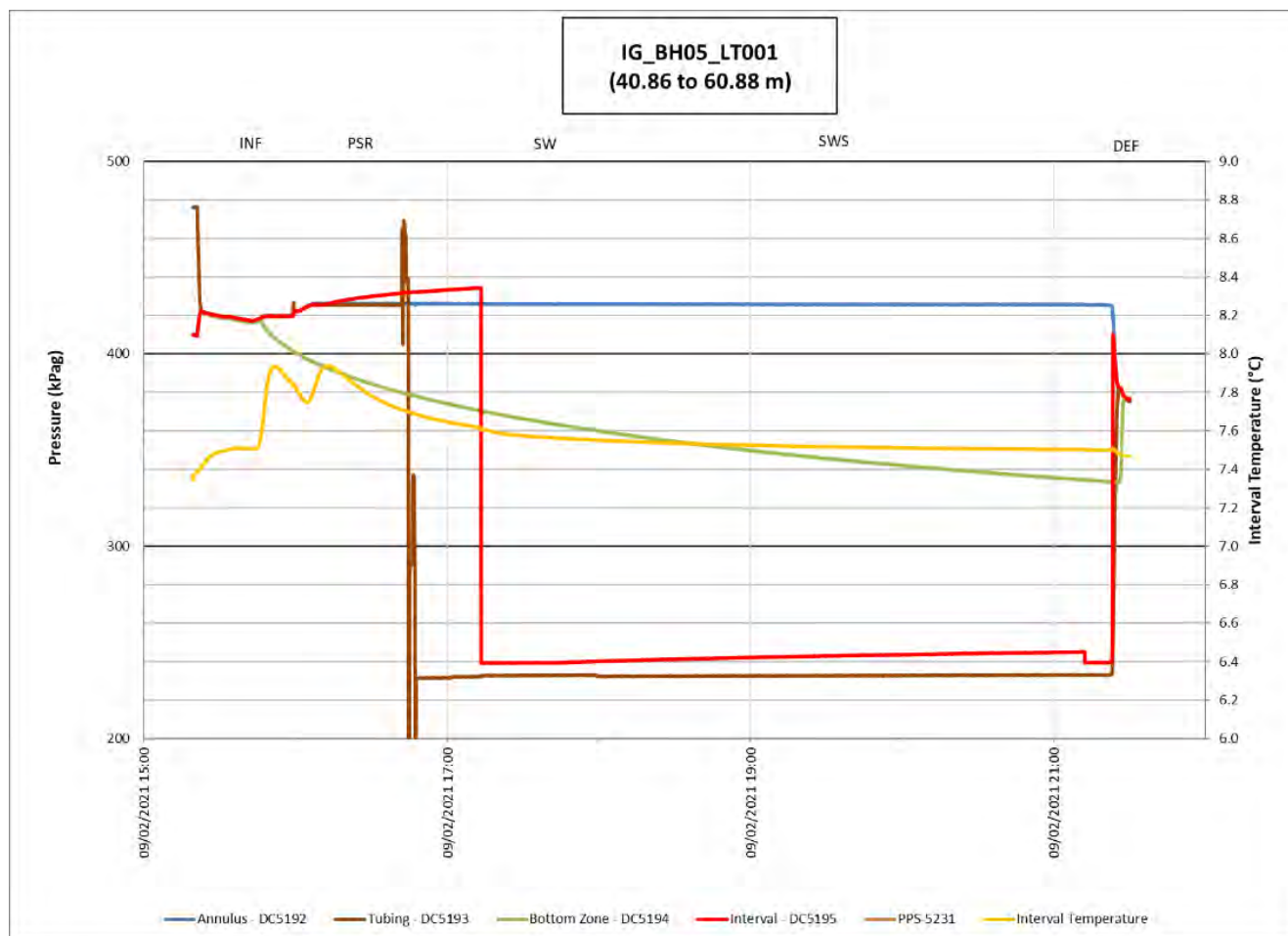


**Figure 9: Leak Test #1 Pressure Plot**

### 3.4.2 Leak Test #2 – End of Testing

Leak Test #2 was performed on October 3, 2021, after the completion of test HT030. The pressure data collected during the test are presented in Figure 10. The testing tool with a test interval length of 20.02 m was pulled into the surface casing below the water level. The packers were inflated to 2.57 MPa surface pressure (20% above the anticipated inflation pressure during testing) and monitored for leakage. No leakage was observed from the testing system. With the packers inflated, the DHSIV was closed to simulate the PSR phase and the water level in the test tubing was raised by 0.309 MPa in preparation for a slug injection (SI) phase. No hydraulic connection was observed between the annulus, tubing, and test interval. The DHSIV was then opened introducing the pressure change to the test interval, and the interval pressure was monitored for 30 minutes. Following the SI phase, the DHSIV was closed for 30 minutes for a shut-in recovery phase (SIS) with no observable hydraulic connection above and below the test interval.

With the DHSIV open, transmissivity of  $9\text{E-}11 \text{ m}^2/\text{sec}$  and an equivalent hydraulic conductivity of  $4\text{E-}12 \text{ m}/\text{sec}$  for the 20.02 m test interval length was derived for the testing tool from the slug injection phase (SI) data. The analyses of the data from shut-in recovery phase (SIS) resulted in a transmissivity of  $2\text{E-}13 \text{ m}^2/\text{sec}$  or an equivalent hydraulic conductivity of  $1\text{E-}14 \text{ m}/\text{sec}$  for the 20.02 m test interval length. Leak Test #2 confirmed the

tool performance met the project's requirement of accurately measuring test interval hydraulic conductivity down to  $10^{-13}$  m/sec.

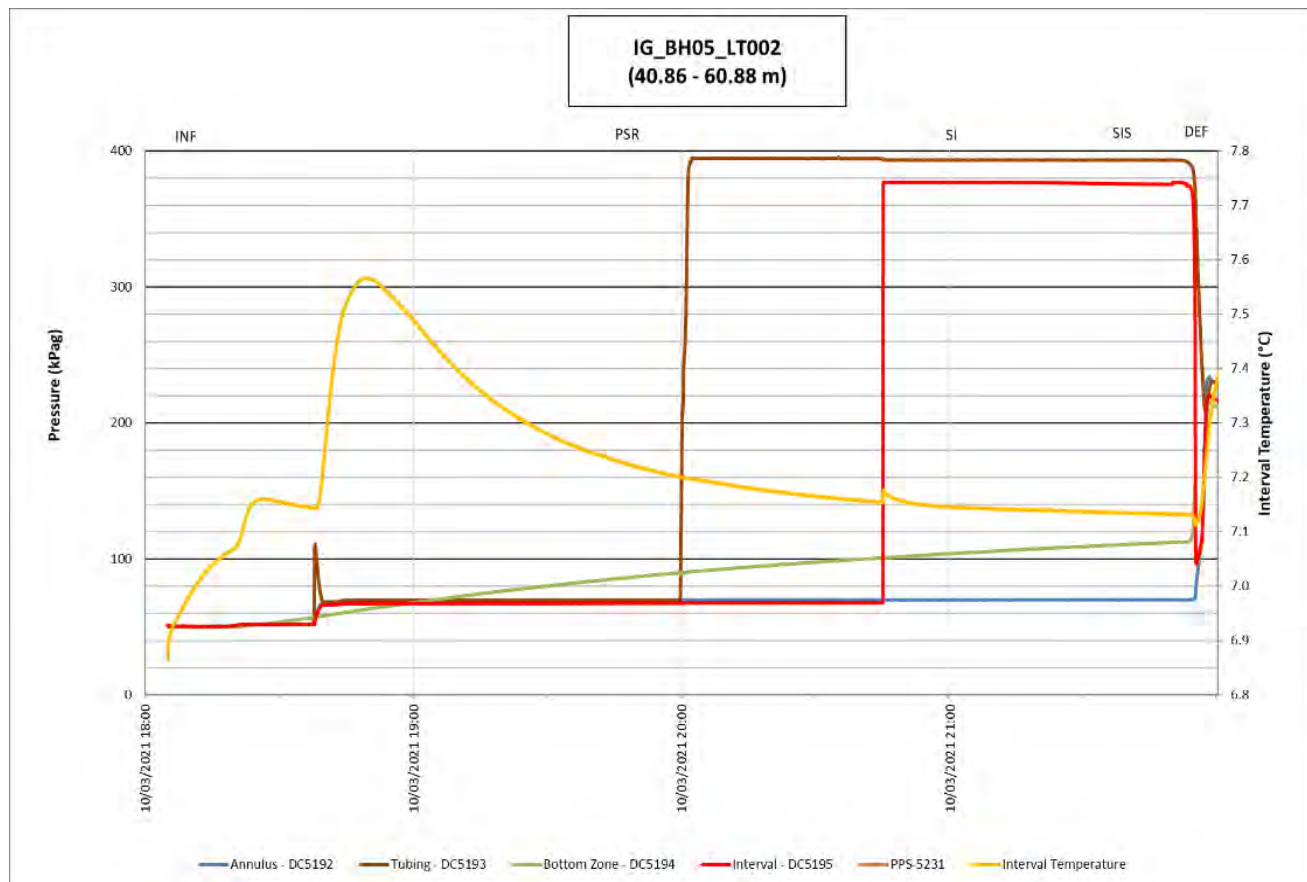


Figure 10: Leak Test #2 Pressure Plot

## 4.0 TEST INTERVAL SELECTION

The selection of test intervals was determined in a collaborative workshop with the NWMO and WSP technical leads based on the findings from drilling, core logging, and geophysical logging. The objectives for test interval selection consisted of:

- Confirm low rock mass hydraulic conductivity in potential repository depths (below 500 m below ground surface (mbgs)) and directly above potential repository depths (above 500 mbgs);
- Determine hydraulic conductivity of identified higher fracture frequency intervals within and in proximity to the repository horizon; and
- Develop an initial understanding of the general trend in hydraulic properties with depth.

The final selection of the test intervals considered the following criteria:

- **Acceptable packer element placement.** Packer element placement is based on the borehole condition. Geophysical caliper logs (WP05) were reviewed to confirm the borehole had a consistent diameter (no washouts) to ensure the differential pressure rating of the packers would apply. Acoustic televiewer imagery (WP05) and core photos (WP03) were reviewed to ensure the packers were seated in sections of the borehole free of fractures to ensure no packer bypass.
- **Location of hydrogeologic features.** The presence of broken fractures, and zones of increased porosity or weathering can influence the hydraulic response of the bulk rock mass. These features were identified and incorporated into the test interval selection decision to ensure that low hydraulic conductivity intervals as well as intervals containing potentially conductive features are tested to assess the range of hydraulic conductivities within the borehole. Flow logging was performed under static (non-pumping) and dynamic (pumping) conditions to identify the potentially water conductive fractures. The selection of potentially water conductive fractures was carried out during Drilling and Coring (WP02), Geological and Geotechnical Core Logging, Photography and Sampling (WP03), and Fluid Temperature and Resistivity Log and Flowing Fluid Electrical Conductivity Log (WP05).

Observations from these data are summarized in the Cover Page of the DQC workbook.

A total of thirty (30) intervals were identified based on the testing objectives and the test interval selection criteria. The intervals were tested in sequence as the tool was being lowered downhole. The testing was carried out from September 2, 2021 through October 3, 2021.

## 5.0 TESTING METHODOLOGY

The planned hydraulic testing methodology is illustrated in Figure 11. However, due to the overall low to very low hydraulic conductivity of the selected test intervals in borehole IG\_BH05, only two test types were performed:

- 1) Pulse withdrawal tests in all intervals;
- 2) Slug tests in seven intervals HT001, HT002, HT006, HT015, HT023, HT024, and HT026 (in addition to pulse test).

The individual test sequences are described in detail in the following sections.

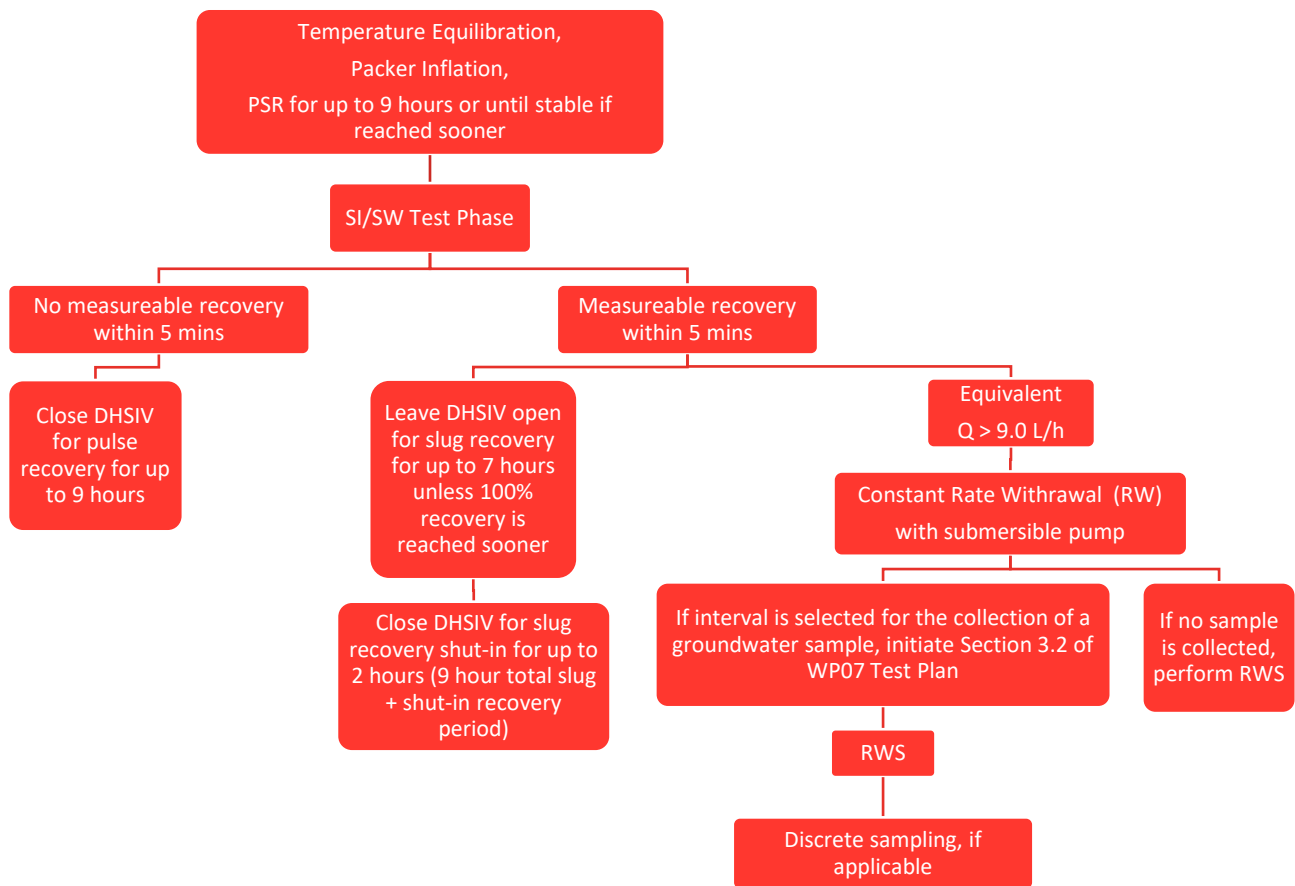


**Figure 11: IG\_BH05 WP06 Test Plan Flow Chart**

A graphical representation of a typical pulse test as demonstrated in Test HT003 is shown in Figure 12. The test included a PSR phase, pulse withdrawal phase, and recovery phase. The hydraulic isolation of the test interval is demonstrated by the different pressure responses from the borehole annulus (blue), tubing (brown), bottom zone (green), and test interval (red and orange). The figure also shows a relative stabilization in the interval temperature that occurs prior to the initiation of the pulse.

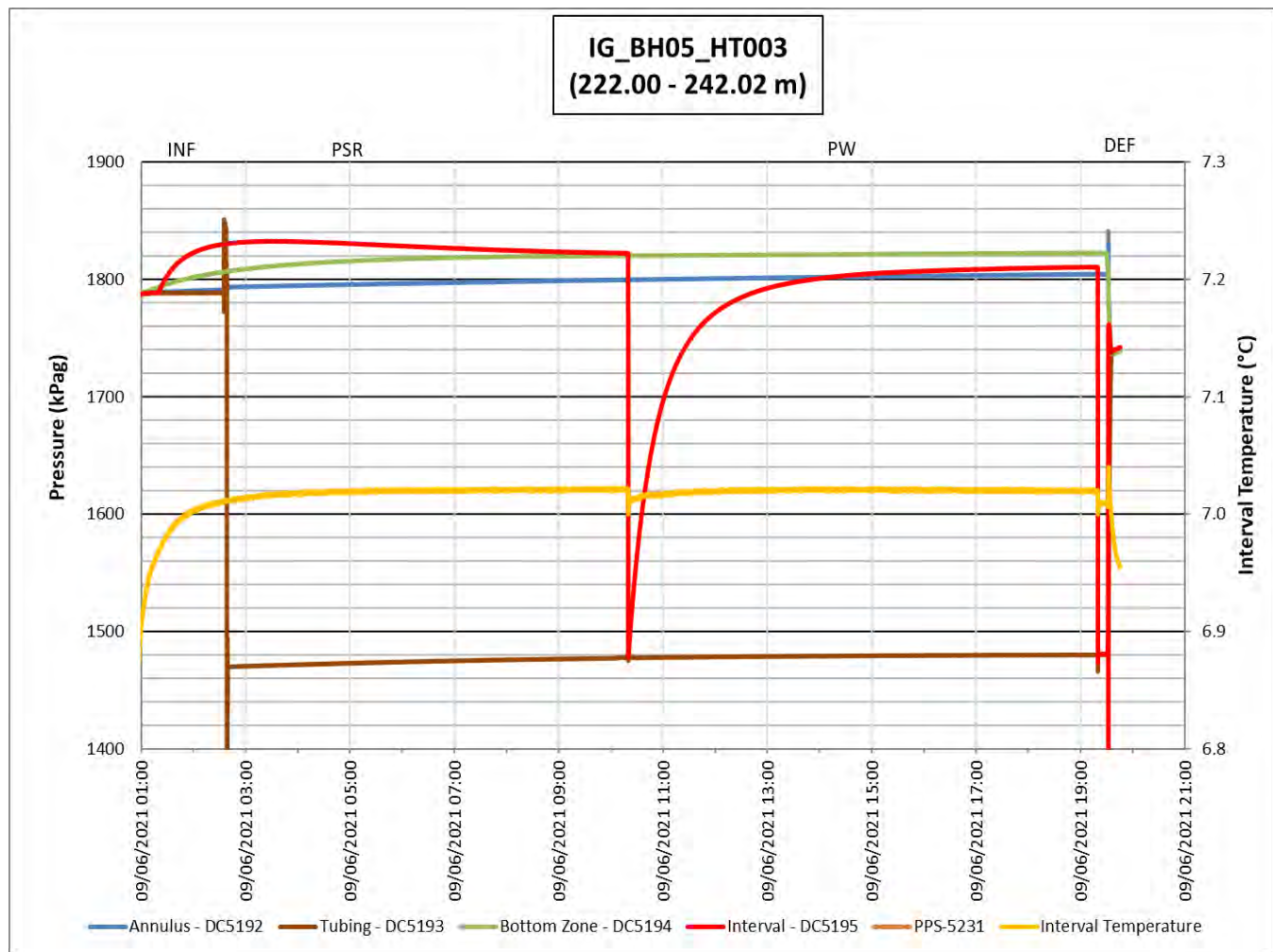


**Figure 12: Typical Pulse Test Procedure, IG\_BH05\_HT003**

### **Packer Inflation**

The required packer inflation pressure was first set at the nitrogen cylinder using a pressure regulator. This pressure was then directed through the packer inflation manifold to the pressure vessel that pressurized the water within the flatpack inflation lines and the packers. The packer inflation pressure was monitored at the pressure vessel with a digital pressure gauge. The nitrogen pressure was applied to the pressure vessel until the water level in the vessel remained stable, indicating the packers have inflated to their full size against the borehole wall. The typical duration of the packer inflation was approximately 25 minutes.

After the packers were inflated, the packer seals were confirmed by monitoring the real-time pressure responses in the bottom zone below the lower packer and the borehole annulus above the upper packer (see zone pressure responses during the INF phase of HT003 in Figure 12). If the expected pressure responses were not discernable (i.e., enough to raise the water column at least one meter), several litres of drilling supply water were poured between the surface casing and the test tubing while monitoring the interval transducer for any change in pressure. The interval temperature was monitored until it stabilized before initiating the pressure static recovery phase. The packer pressure (start and end of test) was recorded in the Field Data tab in the DQC workbook.

**Pressure Static Recovery (PSR) Phase**

The PSR phase is intended to assess the initial pressure within the test interval prior to testing. After the packers were inflated at the selected depth interval, the PSR phase was initiated by closing the DHSIV. The DHSIV pressure was adjusted and controlled manually using a 4-litre water-filled high-pressure pump diverted to the DHSIV via the flatpack.

Closing and opening the DHSIV was completed within a relatively short period of time (a few seconds). The PSR phase was initiated by closing the DHSIV, effectively separating the hydrostatic pressure within the test section from the rest of the test tubing while the pressure in the test interval starts equilibrating. The PSR phase was monitored in real-time by the interval transducer and continued until the rate of pressure change stabilized relative to the transducer resolution or could be extrapolated with confidence by examining the semi-log Horner plot in WSP’s analysis software HydroBench. The semi-log Horner plot for test HT029 is shown as Figure 13 below as an example.

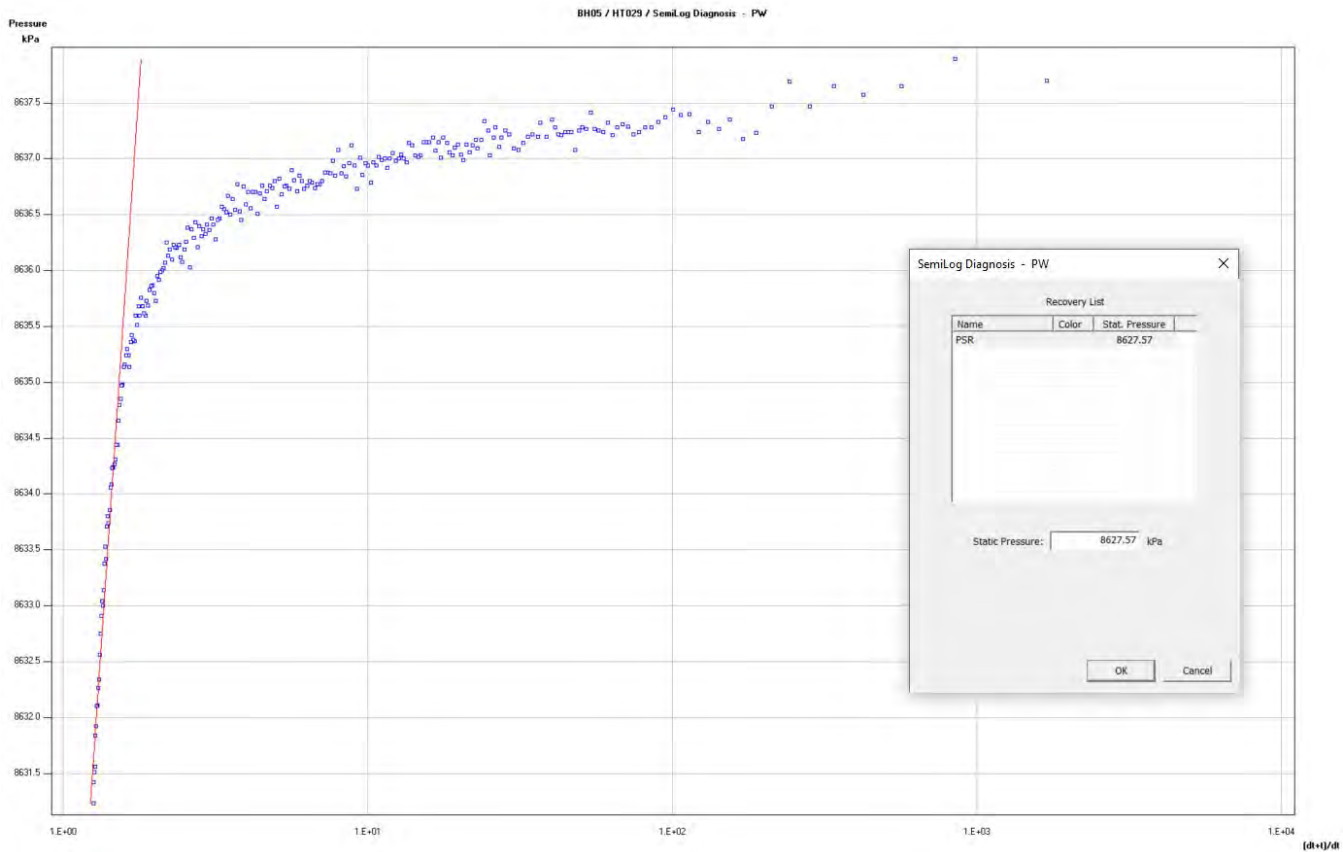


**Figure 13: Semi-log Plot of IG\_BH05\_HT029 analyses showing the pressure recovery of the PSR phase (dark blue) and extrapolated static pressure fit line (red)**

The PSR phase details including start time, end time, and stabilized pressure were recorded in the Field Data tab of the DQC workbook. In addition to assessing the initial test interval pressure prior to testing, the PSR Phase served to dissipate a portion of the borehole pressure and temperature history effects to minimize their influence on the derivation of hydraulic parameters for the test interval.



### ***Creating Test Differential Pressure***

The water level within the test tubing was typically within 20 m of the ground surface, which allowed for the differential pressure for each test to be created by withdrawing water from the test tubing. The pressure differential was created using a swabbing tool lowered on the rig wireline inside the test tubing (BQ drill pipe) to various depths ranging from 16 to 77 m with the DHSIV closed. The swabbing tool was raised to surface, removing the column of water and inducing a differential pressure in the test interval. Pressure differentials achieved for the tests ranged from approximately 0.155 MPa to 0.759 MPa. After removing water from the test tubing, the DHSIV was opened, introducing the pressure change to the test interval for several seconds. The DHSIV was then closed to begin the pulse recovery phase (PW).

### ***Test Pressure Recovery for Very Low Conductivity Test Intervals***

For 23 out of 30 test intervals with very low transmissivity (i.e.,  $< 1\text{E-}10 \text{ m}^2/\text{s}$ ) the interval pressure did not recover from the PW within the pre-determined recovery duration of 9 hours. The interval pressure recovery was monitored in real-time with the DataCan interval pressure transducer and assessed in the field using WSP's analysis software HydroBench. This field assessment of real-time data was used to ensure a high level of confidence was achieved for the derived formation parameters prior to terminating each interval test.

### ***Test Pressure Recovery for Low Conductivity Test Intervals***

Seven test intervals (HT001, HT002, HT006, HT015, HT023, HT024, and HT026) had sufficient transmissivity for the interval pressure to nearly recover within 9 hours. For these seven intervals, a slug withdrawal (SW) was performed at the end of the PW phase by opening the DHSIV. The interval pressure during the SW phase was monitored with the DHSIV open. The length of the slug recovery phase depended on the remaining pre-determined recovery time.

The interval pressure recovery was monitored in real-time with the interval pressure transducer and assessed in the field using WSP's analysis software HydroBench. This field assessment of real-time data was used to determine the duration of the interval pressure recovery phases (SW) to ensure a high level of confidence has been achieved for the derived formation parameters prior to terminating each interval test.

The observed pressure recovery curves indicated that none of the tested intervals demonstrated sufficiently high transmissivity values to warrant constant-rate withdrawal testing.

### ***Packer Deflation***

At the termination of each test, the packers were deflated by releasing the nitrogen pressure from the pressure vessel. The pressures in the bottom, interval, and annulus zones were monitored in real-time for pressure equilibration to confirm the packers had unseated from the borehole wall. The tool was moved to the next test interval when the level of water in the pressure vessel had returned to the pre-inflation level, which indicated the packers were fully deflated.

## **6.0 TEST ANALYSIS**

In fractured crystalline rock settings, it is expected that the rock mass would have low bulk hydraulic conductivity, and main contribution to hydraulic conductivity and total porosity comes from localized conductive fractures. Under these conditions, the volume of rock actually influenced during a borehole hydraulic test can be quite limited. For relatively short duration test that were completed for this program, it is expected that near borehole

conditions dominate the test response with only limited transition to the undisturbed formation response further away from the borehole. The approach was to apply wellbore storage with a composite flow model (i.e., inner skin zone with outer formation zone) try matching the test interval pressure responses.

The final analyses of the hydraulic tests were carried out using nSIGHTS (n-dimensional Stochastic Inverse Graphical Hydraulic Test Simulator) version 2.50 freely available online (Geofirma and INTERA, 2011). nSIGHTS is a well-test code developed for Sandia National Laboratories by Geofirma. Non-linear parameter-estimation methods are used in nSIGHTS to find the optimal values of the model fitting parameters (formation hydraulic conductivity (K), formation specific storage ( $S_s$ ), inferred formation pressure, flow dimension, skin K, and skin thickness) that provide the best statistical match to the observed test data.

A comparison of the best fit and median value for each model fitting parameter was performed to identify which was the best statistical match to the field data. In general, the difference between the best fit and median values was less than an order of magnitude for each parameter, however, there were several instances (up to 25% of the tests) where the difference was slightly greater than an order of magnitude. There was no significant trend, some parameters were higher in some tests while lower in others. There was no indication that the median value produced a more representative value than the best fit. For this reason, the best fit results will be reported.

Input parameters used for each test analysis are listed in Appendix C. The parameters are defined in the following subsections.

## **6.1 Input Parameters**

### **6.1.1 Test Pressure**

Final analyses were completed at the end of the WP06 testing program using the interval pressure data from the PPS transducer positioned inside the test interval. The recorded pressures from this transducer were used for the final test analyses since it is positioned directly inside the test interval and the data do not require depth correction. The pressure measured with the PPS transducer was corrected for barometric pressure by subtracting the barometric pressure measured at the surface (drill rig) using a Solinst Barologger.

### **6.1.2 Wellbore Storage**

Wellbore storage is the response of the test zone to the change in pressure as a result of the compressibility of the fluid in the system (test interval + test tubing), the packer tool, and the rock formation within the interval. For test interval sections of low hydraulic conductivity, the phase of the pressure response dominated by wellbore storage can mask the pressure response of the rock. Wellbore storage is identified with an early unit slope of the pressure change derivative plotted on the log-log plot. nSIGHTS produces this graph for assessing the wellbore storage phase during testing.

Wellbore storage is a sensitive parameter in the estimation of hydraulic parameters in low transmissivity rock. There are two types; open tubing wellbore storage where the fluid level is changing in the tubing with the DHSIV open, and shut-in wellbore storage where pressure is recovering within the test interval with the DHSIV closed. For slug tests, the open tubing wellbore storage coefficient is determined by the test tubing radius where the fluid column change is measured.

#### **Open Tubing Wellbore Storage**

For slug tests, wellbore storage C ( $\text{m}^3/\text{Pa}$ ) is calculated by the equation below



$$C(DHSIV\ open) = \frac{\pi * r_u^2}{\rho * g}$$

where:

- $r_u$  is the equivalent test tubing radius =  $\text{SQRT}((\text{tubing radius})^2/\sin(\text{borehole inclination})) = 0.02378\text{ m}$ 
  - where tubing radius = 0.02305 m and borehole inclination = 70 degrees
- $\rho$  is the density of water at 10°C = 999.7 kg/m<sup>3</sup>
- $g$  is the earth gravity acceleration = 9.81 m/s<sup>2</sup>

Applying these values,  $C$  (SI open) = 1.8E-07 m<sup>3</sup>/Pa, was applied for all slug test analyses.

### Shut-in Wellbore Storage

For test phases where the DHSIV is closed,  $C$  (m<sup>3</sup>/Pa) is determined by the change in volume required to produce the corresponding change in pressure for the pulse test, which is determined by the compressibility of the system (drill fluid column + interval rock matrix + packer tool). This compressibility is estimated during the pulse phase of the test by measuring the change in water level within the test tubing using a datalogger (Solinst Barologger). The datalogger was lowered into the test tubing from the surface after lowering the water level in the tubing in preparation for the pulse to measure the change in volume induced from the pulse activation (opening and closing the DHSIV) then removed from the test tubing for the recovery phase.

Wellbore Storage was calculated using the following equation:

$$C(DHSIV\ closed) = \frac{(dP_{tubing}) * \pi * r_u^2}{\rho * g} * \frac{1}{(dP_{interval})}$$

where:

- $\rho$  is the density of the fluid (kg/m<sup>3</sup>)
- $g$  is the earth gravity acceleration (m/s<sup>2</sup>)
- $r_u$  is the equivalent test tubing radius =  $\text{SQRT}((\text{tubing radius})^2/\sin(\text{borehole inclination})) = 0.02378\text{ m}$ 
  - where tubing radius = 0.02305 m and borehole inclination = 70 degrees
- $dP_{tubing}$  is the change in pressure measured in the test tubing as a result of the pulse (Pa)
- $dP_{interval}$  is the change in pressure measured in the test interval as a result of the pulse (Pa)

The wellbore storage measurements ranged from 7E-11 m<sup>3</sup>/Pa (HT029) to 3E-08 m<sup>3</sup>/Pa (HT001).

Dividing the wellbore storage by the test interval volume, a total test zone compressibility ranged from of 5E-10 1/Pa (HT029) to 2E-07 1/Pa (HT001) with most tests ranging from 5E-10 1/Pa to 4E-9 1/Pa. Casing tests carried out for the Swiss National Cooperative for the Disposal of Radioactive Waste (NAGRA) report water and test tool compressibility values that typically approach 2E-09 1/Pa to 6E-10 1/Pa (Kennedy and Davidson 1989). Total test zone compressibility typically averages 2E-09 1/Pa (Ostrowski et al. 1992).

## 6.2 Output Parameters

The input parameters applied to the test analysis have different degrees of uncertainty that impact the uncertainty of the transmissivity estimates (output parameters) from the test analyses. The analysis approach follows a systematic, hierarchical workflow to minimize uncertainty:

- Tests were performed to minimize factors that increase uncertainty such as borehole history and temperature effects.
- Establish a conceptual model using pressure data input and defining test sequences.
- Diagnostic analyses by generating pressure-derivative plots to determine base case of fitting parameters (hydraulic conductivity, skin, storativity, inferred formation pressure, and flow model). The flow model and parameter estimates from the diagnostic analysis were used as input in the forward simulation in nSIGHTS.
- Inverse parameter estimation was performed by using the flow model and parameter estimates using non-linear regression techniques. The result gave best-fit parameters to match the well test behavior and statistical information on model errors. The first (forward simulation) and the second (optimization) of these two analysis steps were completed. The parameters (also known as model constraints) including flow dimension, formation hydraulic conductivity, formation specific storage, skin hydraulic conductivity, skin thickness, and static formation pressure were used as fitting parameters for the optimization. Flow dimension and static formation pressure were varied in a linear scale while the other constraints will be varied in a logarithmic scale.
- Residual analyses applied the model errors to determine their distribution to statistically verify the inferred flow model;
- Perturbation analysis to evaluate the uniqueness of the base case parameters (i.e., check for parametric correlations). This process was repeated a number of times to determine if the non-linear regression algorithm was converging to a unique global minimum or if local minima were obscuring the results. Typically, 200 perturbations with perturbation span of 0.40 was performed. The subsequent perturbation analysis used the last optimization value for its initial estimate of parameters. The final number of perturbations is dependant on the best-fit parameter values for each test.

A summary of the test results is provided in Appendix C. Appendix C presents a brief summary of each test interval, plot of pressures and temperature from all monitored zones, test tubing pressure during the DHSIV activation for WBS calculation, table with nSIGHTS fitted parameter output ranges, and the following analyses plots produced by nSIGHTS:

- Pressure plot showing best fit simulation and best fit results. Test data is shown as red points, best fit simulation is shown as a green line;
- Deconvolved pressure change (red points) and pressure derivative plot (blue points) showing the best fit simulation (magenta line);
- XY scatter plot of each fitted parameter vs the fit value (to check the uniqueness of the best fit value); and
- XY scatter plot showing the relation between selected pairs of fitted parameters, using symbols colored according to the corresponding fit value. (to check the degree of correlation between fitted parameters).

Data Quality Confirmation forms are provided within the Data Deliverable package.

The analysis includes the following main steps:

- Define fitting parameters using results of the preliminary HydroBench analyses;
- Define minimum and maximum values for each fitting parameter (approximately two orders of magnitude below and above the initially assumed values for conductivity and specific storage,  $\pm 200$  kPa around the initial value of the static formation pressure, 0.001 m and 1 m for the radial thickness of the skin-zone, 1 and 3 for flow dimension);
- Define the test phases to be included in fitting (typically Pulse and / or Slug);
- Define fit types for each selected test phase (typically normalized pressure vs. time, deconvolved pressure and derivative vs. time, and cartesian plot of pressure vs. time.)
- Define a composite fit using a proper combination of individual fits;
- Define the number of perturbations (200 in each case) and the perturbation span (0.4, i.e., 40% of the domain defined by min and max values, centered around the initial guess value);
- Perform perturbation run; and
- Analyze the results by creating appropriate tables (e.g., best fit parameter values, statistics of fitted parameter values) and plots (pressure plot showing best fit simulation, cumulative distribution function plot of each fitting parameter, XY scatter plot of selected pairs of fitted parameters, XY scatter plot of each fitted parameter vs the fit value).

### 6.2.1 Transmissivity and Hydraulic Conductivity

The nSIGHTS analysis produces the test interval transmissivity. Hydraulic conductivity is derived from transmissivity by applying the measured transmissivity over the length of the test interval contributing to that transmissivity. It was assumed for all tests that the test interval is homogeneous (i.e., the entire test interval contributes equally to the measured transmissivity). Thus, hydraulic conductivity was calculated by dividing the measured transmissivity by the interval length.

### 6.2.2 Storativity

Storativity is a fitting parameter in nSIGHTS, which is directly correlated with skin effect and cannot be uniquely determined from a single hole test. While storativity directly impacts skin, it has less of an impact on the determination of transmissivity.

Storativity is calculated using the following equation:

$$S = \rho * g * \emptyset * c_t * h$$

Where

- $\rho$  is the density of water
- $g$  is the acceleration of gravity
- $\emptyset$  is the formation effective porosity
- $c_t$  is the formation compressibility in 1/Pa
- $h$  is the length of the test interval in m

The formation compressibility and effective porosity were varied to produce the best fit storativity parameter.

### 6.2.3 Formation Pressure

It should be noted that the accuracy of the derived initial formation pressure is strongly dependent on the borehole pressure history. Generally, the longer and more complicated is the borehole pressure history period, the greater are the uncertainties in the analysis. Lower transmissivities are more strongly influenced by uncertainties in the borehole pressure history. To reduce the influence of borehole pressure history on the derivation of transmissivity, a PSR phase was included at the start of each test to dissipate a portion of the borehole pressure history prior to initiation of the active phases, and each test was completed with a relatively long duration shut-in recovery phase when borehole pressure history effects will be minimal compared to the early portion of the test.

Formation pressure is a fitting parameter in nSIGHTS.

### 6.2.4 Skin Zone

Skin is a dimensionless term that is used to quantify the hydraulic properties of the rock around a borehole which may be enhanced by an increased fracturing caused by drilling or reduced by drilling debris and/or mud invasion. The skin magnitude correlates to the ratio of the change in permeability as a factor to the thickness of the skin relative to the borehole diameter. Diagnostic tools are used to identify the hydraulic properties (transmissivity and radial thickness) of the “skin zone” based on the shape and the slopes of the semi-log derivative of the specific drawdown on the log-log plot produced in nSIGHTS. A negative skin value corresponds to an increase in transmissivity within the skin zone. A positive skin value corresponds to a decrease in transmissivity within the skin zone. The effects of the skin are then separated from the portion of the data that is primarily influenced by the undisturbed rock properties. nSIGHTS applies skin thickness and magnitude as fitting parameters to the simulation match which influences the shape of the pressure derivative.

### 6.2.5 Flow Dimension

nSIGHTS can apply multi-dimensional flow models. If there is a slope in the derivative data that is characteristic for a flow geometry other than two-dimensional radial flow such as one dimensional linear (positive half slope) or three-dimensional spherical flow (negative half slope), alternative non-radial flow geometry produces a better match to the test response. The slope of derivative data is equal to  $1-n/2$  where  $n$  is the flow dimension; therefore, for linear flow which has a flow dimension of one (1) as flow area does not increase with distance from well results in a positive half slope in the derivative data. Inputting a flow dimension of 1 into the equation above yields a derivative slope of  $1/2$  on the log-log plot.

In low permeability setting, a composite flow response is often observed that is consistent with a near well zone of higher transmissivity with a flow dimension of 2 and outer zone of lower transmissivity more representative of the undisturbed formation. Allowing flow geometry to be a fitted parameter in manual or automated matching provides an improved match because there are more parameters applied to the fit, but results in a flow model that may not be consistent with the measured data and conceptual geologic understanding. Therefore, the additional fitted parameters would only be used to compensate for inaccuracies in representing the borehole history effects and results in more uncertainty (although improving the match).

## 7.0 SUMMARY OF RESULTS

Hydraulic testing was completed in 30 intervals in borehole IG\_BH05. Transmissivity values were estimated to be in the range of  $3\text{E-}13$  to  $3\text{E-}07$   $\text{m}^2/\text{s}$  with hydraulic conductivities in the range of  $2\text{E-}14$  to  $2\text{E-}08$   $\text{m/s}$ .

All tests showed a very minor hydraulic connection between the borehole annulus and the test tubing (likely caused by minor leakage at threaded tubing joints), but this connection did not impact the analyses of the pulse test as the test tubing is not hydraulically connected to the test interval when the DHSIV is closed during the test. The leakage from the test tubing also did not impact the slug test recoveries of tests HT001, HT002, HT006, HT015, HT023, HT024, and HT026 as the magnitude of the leakage was less than the fluid loss to the formation during each of the slug test recoveries.

The primary uncertainties in estimation of transmissivity are the uncertainty in the input parameters, inherent uncertainties due to borehole pressure history effects and, to a lesser degree, temperature transients. Uncertainty in hydraulic conductivity also stems from the assumption of formation length across which flow occurs.

There were several steps taken to minimize the uncertainty as summarized below:

- Test tool included a downhole shut-in valve to minimize wellbore storage and pressure gauges with a relatively high degree of accuracy.
- Leak tests within casing and the tool function checks were performed during the testing program to estimate the lower transmissivity limit of the tool and confirm that the packer seals were adequate.
- Measurement of the change in the interval volume during the pulse induction to estimate test zone compressibility.
- Test design and performance included the following:
  - PSR phase to dissipate part of the borehole pressure history and temperature history effects; and
  - Test phases optimal to the magnitude of transmissivity with slug phases for higher transmissivity and pulse phases for lower transmissivity.

Based on WSP's experience with hydraulic testing and sensitivity analyses for nuclear repository programs (e.g., Enachescu et al., 1997), for test intervals with transmissivity in the magnitude of  $1\text{E-}11$   $\text{m}^2/\text{s}$  to  $1\text{E-}09$   $\text{m}^2/\text{s}$ , the inherent uncertainty in hydraulic parameters is considered to range between plus/minus a factor of 5 to plus or minus a factor of 10 as borehole pressure history and temperature history effects become more material in this transmissivity range and difficult to accurately replicate in the analysis.

Test results are presented in Appendix C and shown on Figure 14 and Figure 15.

**Table 3: Summary of Test Results**

TEST ID	Top of Interval along Borehole (mbgs)	Bottom of Interval along Borehole (mbgs)	Interval Length (m)	Inferred Formation Pressure (kPa)	WBS (m <sup>3</sup> /Pa)		Transmissivity (m <sup>2</sup> /sec)	Bulk Hydraulic Conductivity <sup>1</sup> (m/sec)
					DHSIV Open - Tubing Related	DHSIV Closed		
HT001	87.00	107.02	20.02	809	2E-07	3E-08	2E-08	8E-10
HT002	157.37	177.39	20.02	1449	2E-07	2E-08	3E-07	2E-08
HT003	222.00	242.02	20.02	2017	2E-07	9E-11	5E-12	3E-13
HT004	260.00	280.02	20.02	2356	2E-07	7E-11	3E-11	1E-12
HT005	280.70	300.72	20.02	2558	2E-07	2E-10	9E-11	5E-12
HT006	309.00	329.02	20.02	2808	2E-07	9E-11	2E-10	1E-11
HT007	347.05	367.07	20.02	3170	2E-07	8E-11	2E-11	8E-13
HT008	383.00	403.02	20.02	3488	2E-07	7E-11	1E-11	6E-13
HT009	404.00	424.02	20.02	3668	2E-07	8E-11	1E-11	6E-13
HT010	429.02	449.04	20.02	3932	2E-07	8E-11	3E-13	2E-14
HT011	462.00	482.02	20.02	4209	2E-07	8E-11	1E-12	5E-14
HT012	518.00	538.02	20.02	4758	2E-07	8E-11	5E-12	3E-13
HT013	564.02	584.04	20.02	5204	2E-07	8E-11	7E-12	4E-13
HT014	594.20	614.22	20.02	5502	2E-07	7E-11	4E-12	2E-13
HT015	614.20	634.22	20.02	5627	2E-07	8E-11	1E-09	6E-11
HT016	634.20	654.22	20.02	5847	2E-07	8E-11	7E-12	4E-13
HT017	653.90	673.92	20.02	6024	2E-07	9E-11	1E-11	5E-13
HT018	673.90	693.92	20.02	6200	2E-07	7E-11	8E-12	4E-13

TEST ID	Top of Interval along Borehole (mbgs)	Bottom of Interval along Borehole (mbgs)	Interval Length (m)	Inferred Formation Pressure (kPa)	WBS (m <sup>3</sup> /Pa)		Transmissivity (m <sup>2</sup> /sec)	Bulk Hydraulic Conductivity <sup>1</sup> (m/sec)
					DHSIV Open - Tubing Related	DHSIV Closed		
HT019	693.90	713.92	20.02	6493	2E-07	8E-11	1E-12	5E-14
HT020	713.80	733.82	20.02	6567	2E-07	7E-11	2E-12	1E-13
HT021	733.80	753.82	20.02	6756	2E-07	9E-11	3E-12	2E-13
HT022	753.52	773.54	20.02	6962	2E-07	8E-11	3E-12	1E-13
HT023	772.99	793.01	20.02	7087	2E-07	9E-11	3E-07	1E-08
HT024	792.31	812.33	20.02	7273	2E-07	8E-11	2E-10	1E-11
HT025	814.13	834.15	20.02	7478	2E-07	7E-11	8E-12	4E-13
HT026	848.70	868.72	20.02	7835	2E-07	2E-09	2E-09	1E-10
HT027	907.00	927.02	20.02	8558	2E-07	8E-11	2E-12	1E-13
HT028	924.00	944.02	20.02	8476	2E-07	7E-11	1E-12	5E-14
HT029	945.00	965.02	20.02	8747	2E-07	7E-11	8E-13	4E-14
HT030	967.00	987.02	20.02	8911	2E-07	5E-10	4E-11	2E-12

Notes:

- 1) Bulk hydraulic conductivity is calculated by transmissivity / interval length.

Transmissivity and hydraulic conductivity results are plotted relative to depth on Figure 14 and Figure 15.

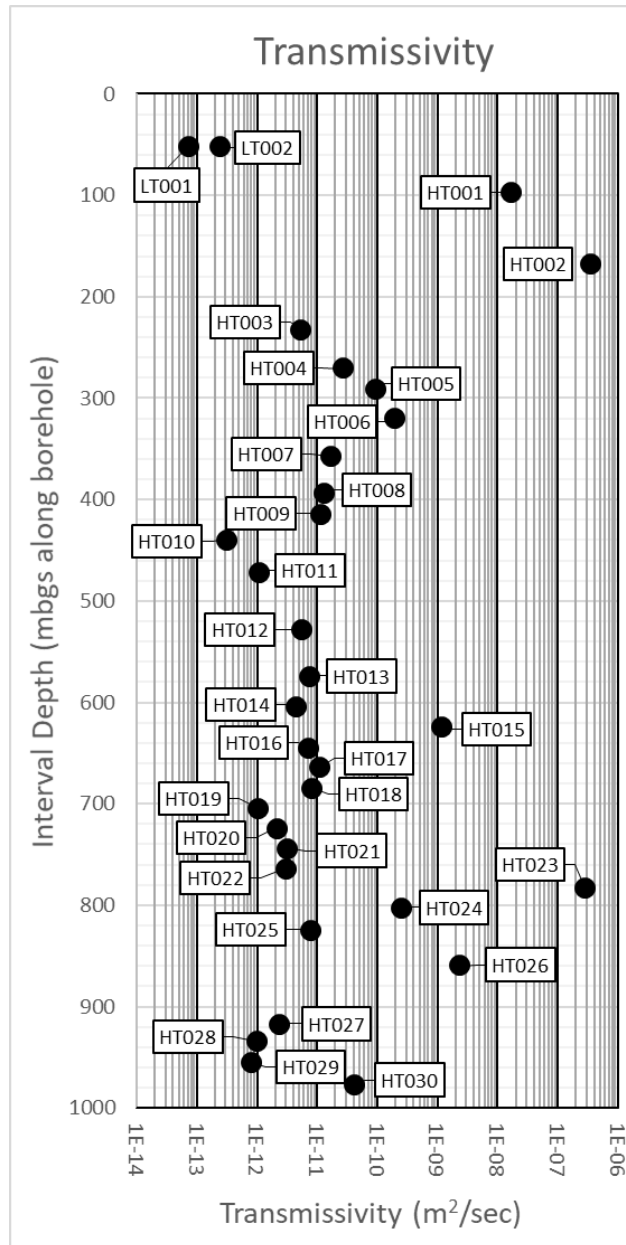


Figure 14: Transmissivity

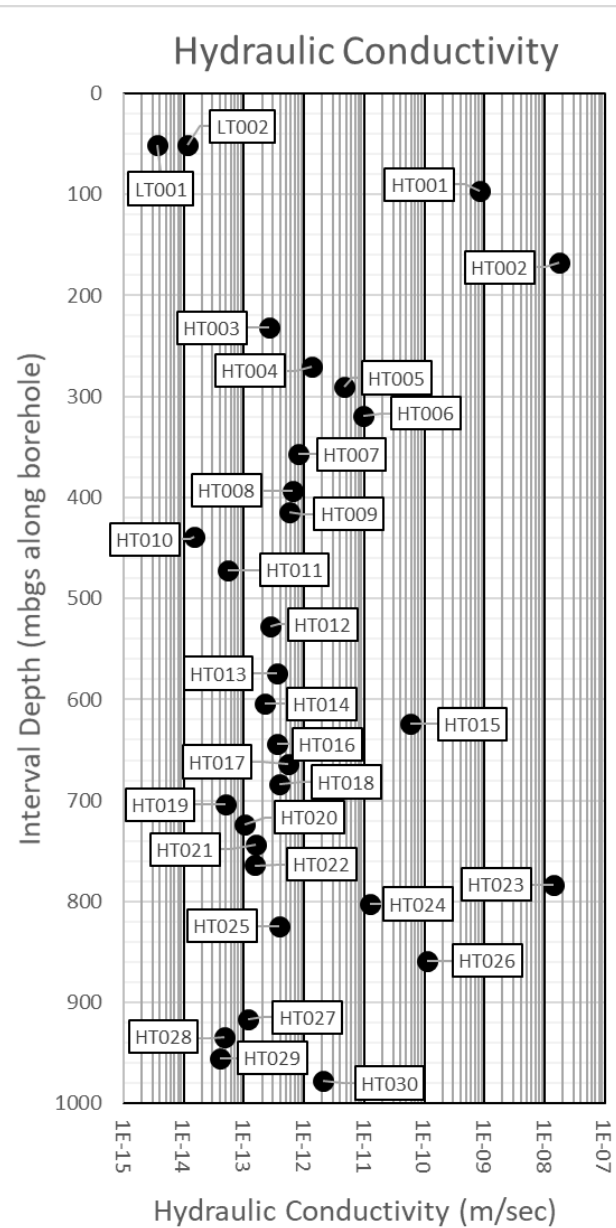


Figure 15: Hydraulic Conductivity



## 8.0 REFERENCES

- Blackburn, C.E. and Hinz, P., 1996. Gold and base metal potential of the northwest part of the Raleigh Lake greenstone belt, northwestern Ontario-Kenora Resident Geologist's District; in Summary of Field Work and Other Activities 1996, Ontario Geological Survey, Miscellaneous Paper 166, p.113-115.
- DesRoches, A., Sykes, M., Parmenter, A. and Sykes, E., 2018. Lineament Interpretation of the Revell Batholith and Surrounding Greenstone Belts (Nuclear Waste Management Organization. No. NWMO-TR-2018-19).
- Enachescu, C., J-M Lavanchy, L. Ostrowski, R. Senger and J. Wozniwicz, 1997. Hydrological Investigations at Wellenberg: Hydraulic Packer Testing in Boreholes SB4a/v and SB4a/s. Methods and Field Results. NAGRA Technical Report 95-02.
- Geofirma Engineering Ltd. and INTERA Inc., 2011. nSIGHTS Version 2.50 User Manual.
- Golder and PGW (Paterson Grant and Watson Ltd.), 2017. Phase 2 Geoscientific Preliminary Assessment, Geological Mapping, Township of Ignace and Area, Ontario: APM-REP-01332-0225.
- Golder, 2022. Phase 2 Initial Borehole Drilling and Testing at IG\_BH04/05/06, Ignace Area, WP02 Data Report – Borehole Drilling and Coring for IG\_BH05. NWMO Report Number: APM-REP-01332-0243.
- Kennedy, K.G. and Davidson, L.M., 1989. Oberbauenstock (OBS) 1987: Results of the hydrogeological testing program OBS-1. – Nagra Technical Report, NTB 88-03, Nagra, Baden.
- OGS (Ontario Geological Survey), 2011. 1:250 000 scale bedrock geology of Ontario, Ontario Geological Survey, Miscellaneous Release Data 126 - Revision 1.
- Ostrowski, L.P., Enachescu, C., Haborth, B. and Kloska, M.B, 1992. Hydrological Investigations at Wellenberg: Hydraulic Packer Testing in Boreholes SB3, SB4 and SB6, Methods and Field Results. Nagra Technical Report, NTB 92-05; Nagra, Wettingen.
- Parmenter, A., Waffle, L. and DesRoches, A., 2020. An updated bedrock geology map and geological database for the northern portion of the Revell batholith (No. NWMO-TR-2020-08). Nuclear Waste Management Organization.
- SGL (Sander Geophysics Limited), 2015. Phase 2 Geoscientific Preliminary Assessment, Acquisition, Processing and Interpretation of High-Resolution Airborne Geophysical Data, Township of Ignace, Ontario. Prepared for Nuclear Waste Management Organization (NWMO). NWMO Report Number: APM-REP-06145-0002.
- SRK (SRK Consulting, Inc). and Golder, 2015. Phase 2 Geoscientific Preliminary Assessment, Observation of General Geological Features, Township of Ignace, Ontario. Prepared for Nuclear Waste Management Organization. NWMO Report Number: APM-REP-06145-0004.
- Stone, D., 2009. Geology of the Bending Lake Area, Northwestern Ontario; *in* Summary of Field Work and Other Activities 2009. Ontario Geological Survey. Open File Report 6240.
- Stone, D., 2010a. Geology of the Stormy Lake Area, Northwestern Ontario; *in* Summary of Field Work and Other Activities 2010. Ontario Geological Survey, Open File Report 6260.
- Stone, D., 2010b. Precambrian geology of the central Wabigoon Subprovince area, northwestern Ontario. Ontario Geological Survey, Open File Report 5422.

Stone, D., Halle, J. and Chaloux, E., 1998. Geology of the Ignace and Pekagoning Lake Areas, Central Wabigoon Subprovince; *in* Summary of Field Work and Other Activities 1998, Ontario Geological Survey, Misc. Paper 169.

Stone, D., Davis, D.W., Hamilton, M.A. and Falcon, A., 2010. Interpretation of 2009 Geochronology in the Central Wabigoon Subprovince and Bending Lake Areas, Northwestern Ontario, *in* Summary of Field Work and Other Activities 2010, Ontario Geological Survey, Open File Report 6260.

**APPENDIX A**

# Equipment Photographs



Photo 1 – Packer testing tool with lower packer shown on left. Datalogger, DHSIV and upper packer shown on right.



Photo 2 – Datalogger, DHSIV and upper packer shown assembled at drill rig.



Photo 3 – Stitched photograph showing entire tool. Top of tool is shown in upper right, bottom of tool shown on lower left.

**APPENDIX B**

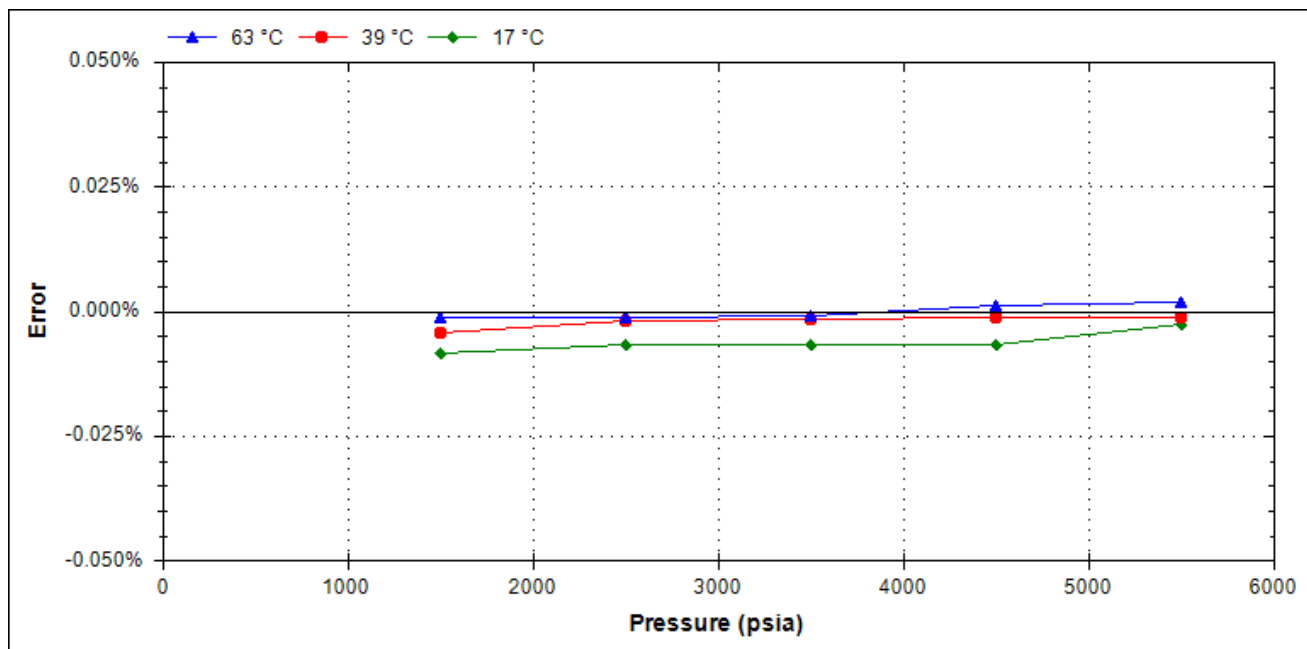
# Calibration Certificates

<b>Calibration Date:</b>	29-Mar-21	<b>Calibration System:</b>	CALIBRATION04
<b>Max Pressure Error:</b>	0.009% F.S.	<b>Batch Number:</b>	20210325.160414
<b>Max Temperature Error:</b>	0.132 °C		
<b>Part Number:</b>	108931		
<b>Serial Number:</b>	DC5192		

## 0.75 OD\_Multi-Gauge\_Piezo\_Bottom\_1/4 Wire\_SS

Max Pressure		Max Temperature	
psi	kPa	°F	°C
6,000	41,369	185	85

**Accuracy:** As shown in the graph below, this DataCan Pressure gauge conforms to within +/- 0.030% F.S. of the pressure standard used in calibration, which is accurate to within +/- 0.01% of reading.

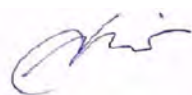


### Working Standards

Sun Electronic Systems Environmental Chamber, Model: EC127, Serial: EC0180  
DHI Instruments Pressure Controller, Model: PPCH-200M (30,000psi Reference), Serial: 3171

### Traceability Statement

All working standards are traceable to nationally or internationally recognized standards.



Approved By:  
DataCan Services Corp.

Calibrated By:  
Angelo Pulido

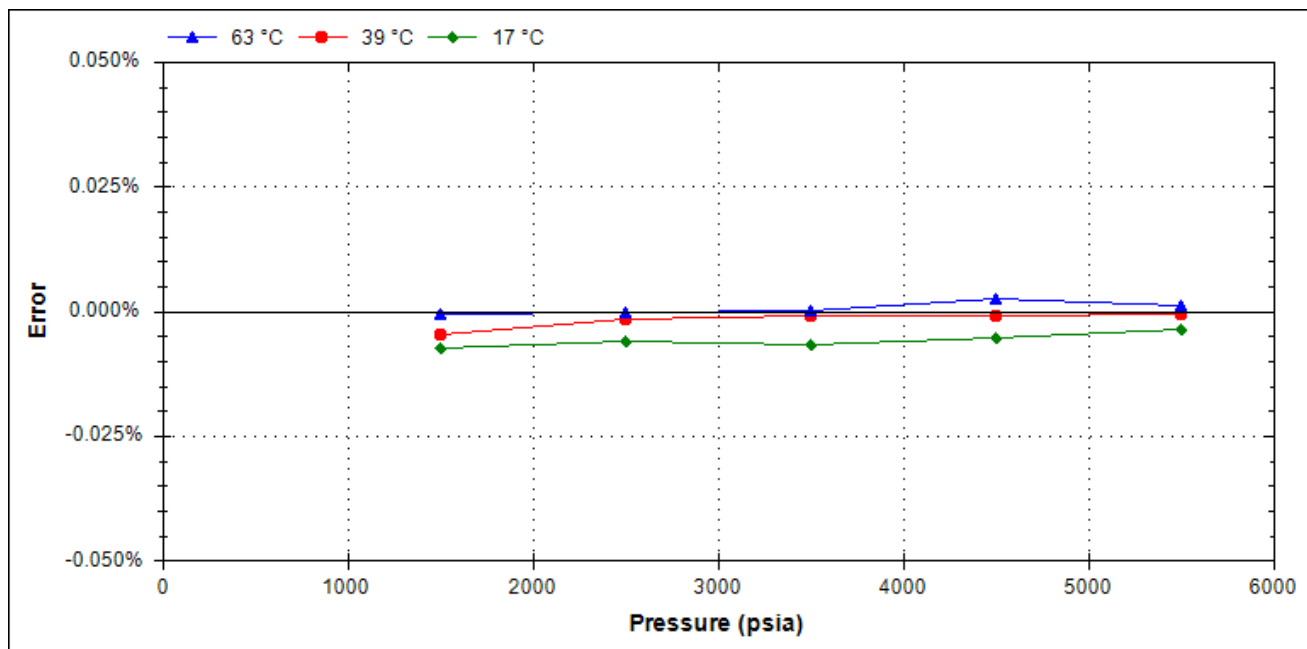


<b>Calibration Date:</b>	29-Mar-21	<b>Calibration System:</b>	CALIBRATION04
<b>Max Pressure Error:</b>	0.007% F.S.	<b>Batch Number:</b>	20210325.160414
<b>Max Temperature Error:</b>	0.135 °C		
<b>Part Number:</b>	108931		
<b>Serial Number:</b>	DC5193		

## 0.75 OD\_Multi-Gauge\_Piezo\_Bottom\_1/4 Wire\_SS

Max Pressure		Max Temperature	
psi	kPa	°F	°C
6,000	41,369	185	85

**Accuracy:** As shown in the graph below, this DataCan Pressure gauge conforms to within +/- 0.030% F.S. of the pressure standard used in calibration, which is accurate to within +/- 0.01% of reading.

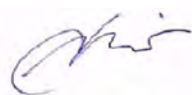


### Working Standards

Sun Electronic Systems Environmental Chamber, Model: EC127, Serial: EC0180  
DHI Instruments Pressure Controller, Model: PPCH-200M (30,000psi Reference), Serial: 3171

### Traceability Statement

All working standards are traceable to nationally or internationally recognized standards.



Approved By:  
DataCan Services Corp.

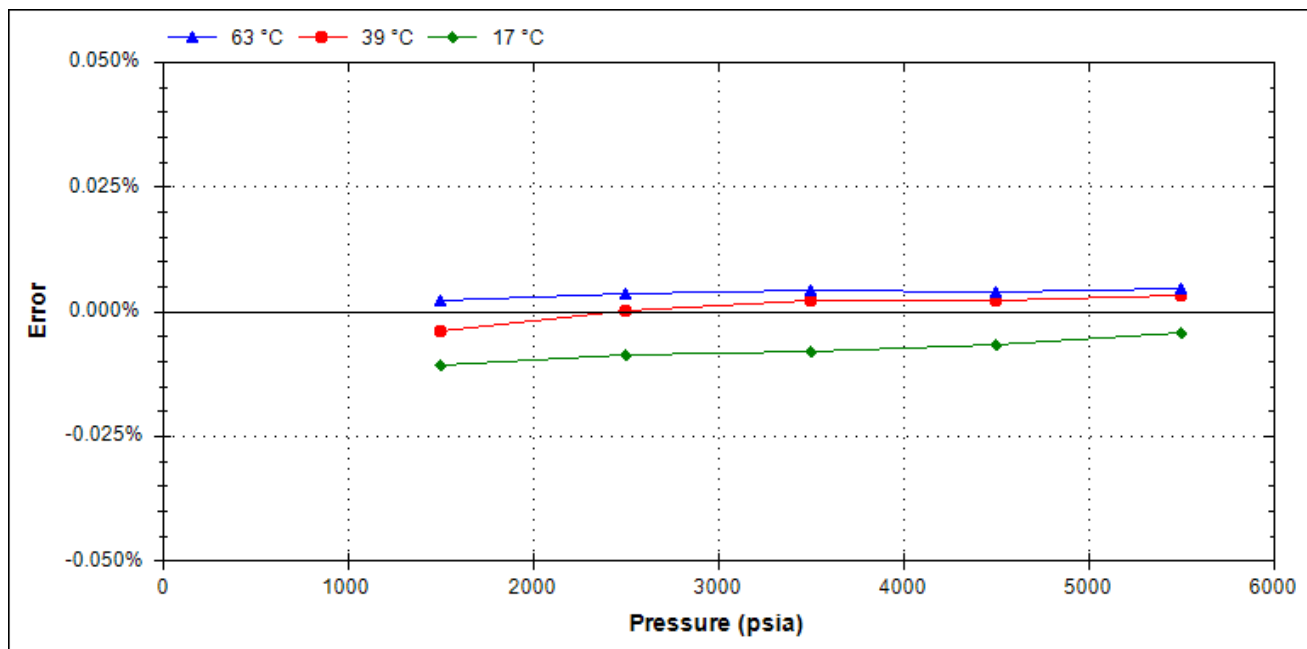
Calibrated By:  
Angelo Pulido

<b>Calibration Date:</b>	29-Mar-21	<b>Calibration System:</b>	CALIBRATION04
<b>Max Pressure Error:</b>	0.011% F.S.	<b>Batch Number:</b>	20210325.160414
<b>Max Temperature Error:</b>	0.126 °C		
<b>Part Number:</b>	108931		
<b>Serial Number:</b>	DC5194		

## 0.75 OD\_Multi-Gauge\_Piezo\_Bottom\_1/4 Wire\_SS

Max Pressure		Max Temperature	
psi	kPa	°F	°C
6,000	41,369	185	85

**Accuracy:** As shown in the graph below, this DataCan Pressure gauge conforms to within +/- 0.030% F.S. of the pressure standard used in calibration, which is accurate to within +/- 0.01% of reading.

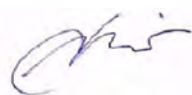


### Working Standards

Sun Electronic Systems Environmental Chamber, Model: EC127, Serial: EC0180  
DHI Instruments Pressure Controller, Model: PPCH-200M (30,000psi Reference), Serial: 3171

### Traceability Statement

All working standards are traceable to nationally or internationally recognized standards.



Approved By:  
DataCan Services Corp.

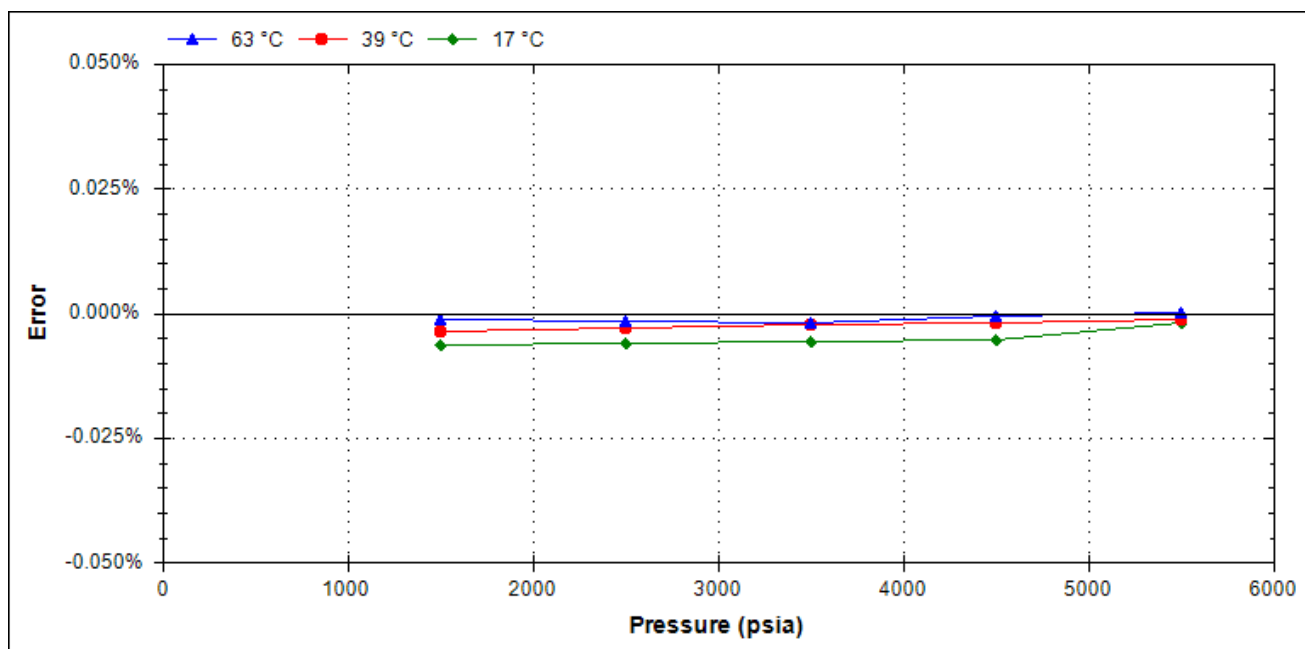
Calibrated By:  
Angelo Pulido

<b>Calibration Date:</b>	29-Mar-21	<b>Calibration System:</b>	CALIBRATION04
<b>Max Pressure Error:</b>	0.006% F.S.	<b>Batch Number:</b>	20210325.160414
<b>Max Temperature Error:</b>	0.129 °C		
<b>Part Number:</b>	108931		
<b>Serial Number:</b>	DC5195		

## 0.75 OD\_Multi-Gauge\_Piezo\_Bottom\_1/4 Wire\_SS

Max Pressure		Max Temperature	
psi	kPa	°F	°C
6,000	41,369	185	85

**Accuracy:** As shown in the graph below, this DataCan Pressure gauge conforms to within +/- 0.030% F.S. of the pressure standard used in calibration, which is accurate to within +/- 0.01% of reading.

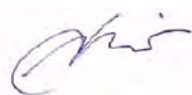


### Working Standards

Sun Electronic Systems Environmental Chamber, Model: EC127, Serial: EC0180  
DHI Instruments Pressure Controller, Model: PPCH-200M (30,000psi Reference), Serial: 3171

### Traceability Statement

All working standards are traceable to nationally or internationally recognized standards.



Approved By:  
DataCan Services Corp.

Calibrated By:  
Angelo Pulido

**Wescan Calibration**  
9-12240 Horseshoe Way  
Richmond, BC V7A 4X9

Page 1 of 1

## CERTIFICATE OF CALIBRATION

<b>Description</b>	<b>PRESSURE GAUGE, DIGITAL</b>	<b>Work Order</b>	<b>R0920140</b>
<b>Model Number</b>	<b>DPG4000</b>	<b>Serial Number</b>	<b>4645403</b>
<b>Instrument Id</b>	<b>N/A</b>	<b>Cal Procedure</b>	<b>33K6-4-314-1</b>
<b>Manufacturer</b>	<b>OMEGA</b>	<b>Cal Date</b>	<b>26 Mar 2021</b>
<b>Customer Name</b>	<b>GOLDER ASSOCIATES LTD.</b>	<b>Recall Cycle</b>	<b>52 Weeks</b>
	<b>300 - 3811 NORTH FRASER WAY</b>	<b>Next Cal Date</b>	<b>26 Mar 2022</b>
	<b>BURNABY, BC V5J 5J2</b>	<b>Purchase Order</b>	<b>PENDING</b>

**Calibration Environment:** Temperature **21.0°C** Relative Humidity **35.0 %RH**

**Received Condition:** **Not Within Tolerance**

**Completed Condition:** **Within Tolerance**

**Remarks:** **Adjusted**

### Standards Used to Establish Traceability

<u>Instrument Type</u>	<u>Model</u>	<u>Asset #</u>	<u>Cal Due Date</u>
<b>PRESSURE CALIBRATOR</b>	<b>6270A/PM600-A7M/P</b>	<b>102018</b>	<b>28 Feb 2022</b>

Wescan certifies that, at the time of calibration, the above listed instrument meets or exceeds all of the specifications defined on the Test Data Sheet (TDS), otherwise indicated. The Certificate received and completed conditions and the TDS specifications are based on the procedure(s) and/or specification(s) referenced on the TDS unless otherwise indicated. Any statement of compliance is made without taking measurement uncertainty into account and is based on the instrument's performance against the test limits documented on the test data sheet.

Wescan has been independently assessed and accredited to ISO/IEC 17025:2017. The above listed instrument has been calibrated using standards that are traceable to the International System of Units (SI) through a National Metrological Institute (such as NRC or NIST) and in compliance with ISO/IEC 17025:2017. The reported expanded uncertainty is a normal distribution with a coverage factor of K=2, corresponding to a coverage of approximately 95% and conforms with the recommendations of the ISO Guide to the Expression of Uncertainty in Measurement. This certificate may contain data that is not included in the Scope of Accreditation or where measurement uncertainty is not applicable. Unaccredited results, including uncertainties reported as N/A, and functional or binary (such as Pass / Fail, True / False) are clearly defined within the test data.

This report consists of two parts with separate page numbering schemes; the Certificate of Calibration and the Test Data Sheet (TDS). Copyright of this report is owned by the issuing laboratory and may not be reproduced, other than in full, except with the prior written permission of the issuing laboratory.

Test data As Found and Final (as left) results are the same unless reported otherwise. Certificate remarks identify if adjustments were performed.

**Metrologist :** **R007**

**Quality Assurance:** **R001**

**Date of Issue:** **26 Mar 2021**

F083 Rev 16  
pyleent

HALIFAX

MONTREAL

OTTAWA

TORONTO

EDMONTON

CALGARY

Calibration procedure 33K6-4-314-1  
 Item type Pressure gauge  
 Range 2000.0 psi  
 Accuracy 0.05 % of full scale  
 Test item resolution 0.1 psi



Note: this data sheet applies to calibrations where the standard is set to an exact gauge marking

#### As found

	Nominal	Standard	Lower limit	Test item	Upper limit	% limits used	Uncertainty	TUR if<4:1
	% of range	psi	psi	psi	psi		psi	
increasing	10%	200.000	199.000	199.7	201.000	-30.0%	0.065	
	20%	400.000	399.000	399.6	401.000	-40.0%	0.070	
	30%	600.000	599.000	599.4	601.000	-60.0%	0.083	
	40%	800.000	799.000	799.3	801.000	-70.0%	0.099	
	50%	1000.000	999.000	999.3	1001.000	-70.0%	0.12	
	60%	1200.000	1199.000	1199.2	1201.000	-80.0%	0.13	
	70%	1400.000	1399.000	1399.2	1401.000	-80.0%	0.15	
	80%	1600.000	1599.000	1599.1	1601.000	-90.0%	0.17	
	90%	1800.000	1799.000	1798.9	1801.000	-110.0%	0.19	
	100%	2000.000	1999.000	1998.8	2001.000	-120.0%	0.21	
decreasing	90%	1800.000	1799.000	1799.0	1801.000	-100.0%	0.19	
	80%	1600.000	1599.000	1599.2	1601.000	-80.0%	0.17	
	70%	1400.000	1399.000	1399.3	1401.000	-70.0%	0.15	
	60%	1200.000	1199.000	1199.3	1201.000	-70.0%	0.13	
	50%	1000.000	999.000	999.4	1001.000	-60.0%	0.12	
	40%	800.000	799.000	799.3	801.000	-70.0%	0.099	
	30%	600.000	599.000	599.4	601.000	-60.0%	0.083	
	20%	400.000	399.000	399.6	401.000	-40.0%	0.070	
	10%	200.000	199.000	199.8	201.000	-20.0%	0.065	

#### As left

	Nominal	Standard	Lower limit	Test item	Upper limit	% limits used	Uncertainty	TUR if<4:1
	% of range	psi	psi	psi	psi		psi	
increasing	10%	200.000	199.000	200.0	201.000	0.0%	0.065	
	20%	400.000	399.000	399.9	401.000	-10.0%	0.070	
	30%	600.000	599.000	599.9	601.000	-10.0%	0.083	
	40%	800.000	799.000	799.9	801.000	-10.0%	0.099	
	50%	1000.000	999.000	1000.0	1001.000	0.0%	0.12	
	60%	1200.000	1199.000	1199.9	1201.000	-10.0%	0.13	
	70%	1400.000	1399.000	1399.9	1401.000	-10.0%	0.15	
	80%	1600.000	1599.000	1599.9	1601.000	-10.0%	0.17	
	90%	1800.000	1799.000	1799.9	1801.000	-10.0%	0.19	
	100%	2000.000	1999.000	2000.0	2001.000	0.0%	0.21	
decreasing	90%	1800.000	1799.000	1800.0	1801.000	0.0%	0.19	
	80%	1600.000	1599.000	1599.9	1601.000	-10.0%	0.17	
	70%	1400.000	1399.000	1399.9	1401.000	-10.0%	0.15	
	60%	1200.000	1199.000	1199.9	1201.000	-10.0%	0.13	
	50%	1000.000	999.000	1000.0	1001.000	0.0%	0.12	
	40%	800.000	799.000	800.0	801.000	0.0%	0.099	
	30%	600.000	599.000	600.0	601.000	0.0%	0.083	
	20%	400.000	399.000	400.0	401.000	0.0%	0.070	
	10%	200.000	199.000	200.0	201.000	0.0%	0.065	

End of calibration data

Highlighted data are outside acceptance limits

# CALIBRATION REPORT

Instrument type      Memory Gauge  
 Calibration Date    2020-09-02              Due date: 2021-09-02  
 Model Number        LevelTroll 700  
 Pressure Range      1000 PSI  
 Manufacturer        In-Situ Inc.  
 Serial number              373153

---

**Pressure Test Data Sheet**


---

Applied Pressure (PSI)	Reported Pressure (PSI)	Deviation (PSI)	FS Error %
0.5	0.503	0.0	0.00
103.5	103.600	0.1	0.01
202.4	202.300	-0.1	-0.01
307.1	307.200	0.1	0.01
405.0	405.200	0.2	0.02
502.0	502.500	0.5	0.05
599.0	599.600	0.6	0.06
700.0	700.800	0.8	0.08
816.4	817.200	0.8	0.08
903.0	903.770	0.8	0.08
998.3	999.400	1.1	0.11
Maximum Value:		1.10	0.11

**End of calibration data**

Performed by              A.Brugger

**Calibration and Equipment used:**

Instrument type      DPG4000-2K  
 Calibration Date      2019-06-24  
 Manufacturer        Omega

Equipment used is traceable to the National Institute of Standards and Technology

Pressure Range:      0-2000 psi  
 Accuracy               +/- 0.1%  
 Serial Number        4645403





**Pioneer Petrotech Services Inc.**

#1, 1431 - 40 Ave. NE  
Calgary, AB, Canada, T2E 8N6

Tel: +1 (403)282-7669

Fax: +1 (403)282-0509

[www.pioneerps.com](http://www.pioneerps.com)

## Calibration Certificate

---

<b>Model:</b>	<b>PPS25</b>	<b>Pressure Range:</b>	<b>6,000 psi</b>
<b>Serial Number:</b>	<b>5231</b>	<b>Calibration Date:</b>	<b>Apr 07, 2021</b>

---

### Specifications

Pressure Range:	Minimum:	13 psia	Maximum:	6,000 psia
Temperature Range:	Minimum:	0 °C	Maximum:	150 °C
Pressure Accuracy:			±	0.03 %F.S.
Temperature Accuracy:			±	0.5 °C

Housing Material:	SS 17-4
Housing OD	0.75"

### Calibration Summary

Calibration Pressure Range:	Minimum:	15.03 psia	Maximum:	6,001 psia
Calibration Temperature Range:	Minimum:	0.77 °C	Maximum:	151 °C
Pressure Accuracy (Maximum Error):			—	1.70 psi
Temperature Accuracy (Maximum Error):			—	0.26 °C

---

### Working Standards

Pressure:	Fluke DH Instruments piston-cylinder, 30kpsi (±0.01% of reading)
Temperature:	Fluke Hart Scientific RTD (±0.05°C)

### Traceability Statement

All working standards are traceable to nationally or internationally recognized standards.

\_\_\_\_\_  
Pioneer Petrotech Services Inc.

\_\_\_\_\_  
Apr 30, 2021

Date



## Instrument:

Manufacturer:	Solinst Canada
Product:	3001 LT Barologger
Model Number:	M1.5
Serial Number:	2110133
Pressure Range:	0-1.5 m H2O
Resolution:	0.03 mm H2O
Temperature Range:	-20 - +80 °C
Temperature Resolution:	0.003 °C

## Method of Calibration:

The Levellogger is calibrated against a range of set reference points, with units of pressure in pounds per square inch. The conversion factor for pounds per square inch relates to pressure in bars and meters of water column is as follows: 1 pound per square inch = 0.0689476 bar = 0.703070 m H2O @ 4°C.

During the calibration procedure, the Levellogger is fully submerged in a highly accurate water bath, set to 6°C. The pressure is then calibrated to six separate pressure points covering the entire range for that particular Levellogger, to check for any non-linearity. This process is repeated at 18°C and then 36°C to check for temperature effects. The Levellogger is approved after all specifications for accuracy, precision, stability and hysteresis have been met.

## Traceability:

Pressure standard: ISO/IEC 17025:2005, ANSI/NCSL Z540-1-1994, NIST  
Temperature standard: ISO/IEC 17025:2005, NVLAP LAB CODE: 200348-0

## Uncertainty:

The standard deviation of the temperature was calculated from the contributions of uncertainties originating from the measurement standard, the bath homogeneity, and from any short term contribution from the instrument being calibrated. The standard deviation of the pressure was calculated from the contributions of the uncertainties originating from the measurement standard, any short term contribution from the instrument, and the uncertainty resulting from the uncertainty in temperature compensation. The reported uncertainty is stated as the standard deviation multiplied by a factor of two.

Serial Number: 2110133

Model Number: M1.5

**Test Results:**

Calibration Date: 8/2/2019

**Pressure Tests**

Pressure	Reading (6 °C)	Level	Reading	Error (%FS)
12.5 psi	12.4995 psi	-0.7116 m	-0.7120 m	0.003%
13.2 psi	13.1496 psi	-0.2546 m	-0.2549 m	0.003%
13.8 psi	13.8005 psi	0.2024 m	0.2027 m	-0.003%
14.5 psi	14.4496 psi	0.6594 m	0.6591 m	0.003%
15.1 psi	15.0996 psi	1.1164 m	1.1161 m	0.003%
15.8 psi	15.7503 psi	1.5734 m	1.5736 m	-0.002%

Hysteresis:

Standard Deviation: 0.0028%

**Temperature Tests**

Temperature	Reading	Error (%FS)
6 °C	5.9997 °C	0.000%
18 °C	17.9998 °C	0.000%
36 °C	35.9998 °C	0.000%

Standard Deviation: 0.0001%

**Conclusion: This instrument fulfils the specifications**

Uncertainty temperature standard: 0.003 °C

Overall uncertainty temperature:  $\pm 1.002$ Uncertainty pressure standard:  $<0.003\%$ 

Overall uncertainty pressure: 0.01%

Calibration Manager: *Ken Shah*

## Instrument:

Manufacturer:	Solinst Canada
Product:	3001 LT Barologger
Model Number:	M1.5
Serial Number:	2110146
Pressure Range:	0-1.5 m H2O
Resolution:	0.03 mm H2O
Temperature Range:	-20 - +80 °C
Temperature Resolution:	0.003 °C

## Method of Calibration:

The Levellogger is calibrated against a range of set reference points, with units of pressure in pounds per square inch. The conversion factor for pounds per square inch relates to pressure in bars and meters of water column is as follows: 1 pound per square inch = 0.0689476 bar = 0.703070 m H2O @ 4°C.

During the calibration procedure, the Levellogger is fully submerged in a highly accurate water bath, set to 6°C. The pressure is then calibrated to six separate pressure points covering the entire range for that particular Levellogger, to check for any non-linearity. This process is repeated at 18°C and then 36°C to check for temperature effects. The Levellogger is approved after all specifications for accuracy, precision, stability and hysteresis have been met.

## Traceability:

Pressure standard: ISO/IEC 17025:2005, ANSI/NCSL Z540-1-1994, NIST  
Temperature standard: ISO/IEC 17025:2005, NVLAP LAB CODE: 200348-0

## Uncertainty:

The standard deviation of the temperature was calculated from the contributions of uncertainties originating from the measurement standard, the bath homogeneity, and from any short term contribution from the instrument being calibrated. The standard deviation of the pressure was calculated from the contributions of the uncertainties originating from the measurement standard, any short term contribution from the instrument, and the uncertainty resulting from the uncertainty in temperature compensation. The reported uncertainty is stated as the standard deviation multiplied by a factor of two.

Serial Number: 2110146

Model Number: M1.5

**Test Results:**

Calibration Date: 8/2/2019

**Pressure Tests**

Pressure	Reading (6 °C)	Level	Reading	Error (%FS)
12.5 psi	12.5006 psi	-0.7116 m	-0.7112 m	-0.004%
13.2 psi	13.1506 psi	-0.2546 m	-0.2542 m	-0.004%
13.8 psi	13.8005 psi	0.2024 m	0.2027 m	-0.003%
14.5 psi	14.4504 psi	0.6594 m	0.6596 m	-0.002%
15.1 psi	15.0995 psi	1.1164 m	1.1160 m	0.003%
15.8 psi	15.7502 psi	1.5734 m	1.5735 m	-0.002%

Hysteresis:

Standard Deviation: 0.0027%

**Temperature Tests**

Temperature	Reading	Error (%FS)
6 °C	5.9997 °C	0.000%
18 °C	17.9997 °C	0.000%
36 °C	35.9998 °C	0.000%

Standard Deviation: 0.0001%

**Conclusion: This instrument fulfils the specifications**

Uncertainty temperature standard: 0.003 °C

Overall uncertainty temperature:  $\pm 1.002$ Uncertainty pressure standard:  $< 0.003\%$ 

Overall uncertainty pressure: 0.01%

Calibration Manager: *Ken Shah*

**APPENDIX C**

# Test Results

## 1.0 HT001 (87.00 – 107.02 M)

HT001 was selected to test a shallow fractured interval. 5 broken fractures were observed in the core. A loss of drilling fluid was observed in this interval during drilling. An indication of flow was recorded during FFEC logging post-drilling.

The test was initiated with a shut-in pressure recovery phase (PSR). A pulse withdrawal test (PW) with a shut-in recovery followed by a slug withdrawal (SW) phase was completed after the PSR phase.

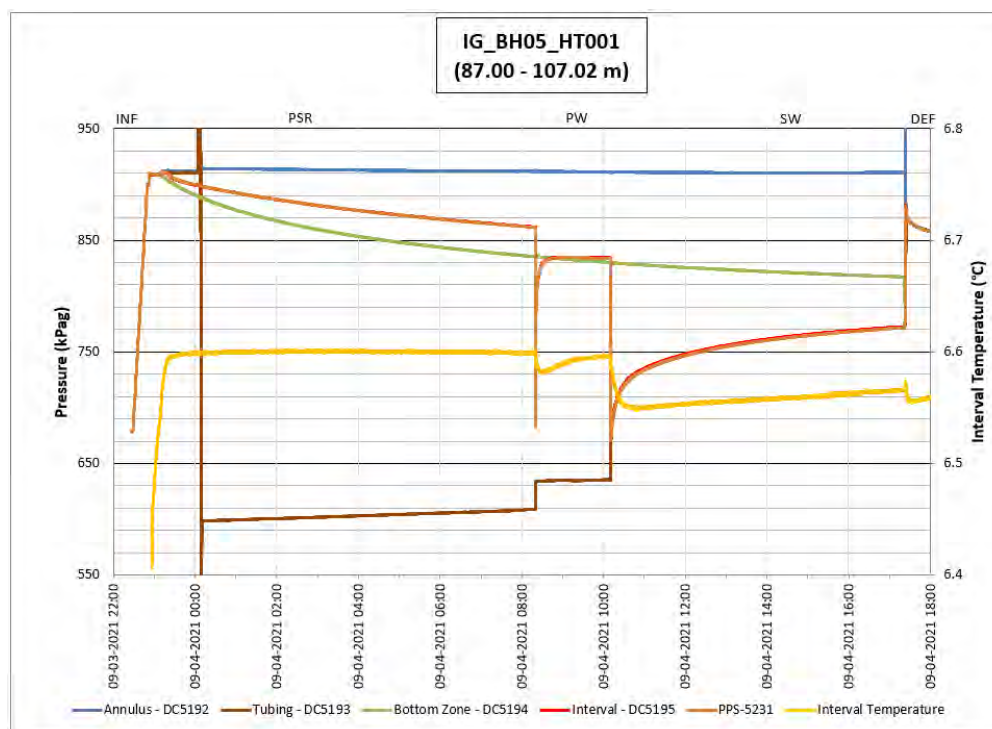
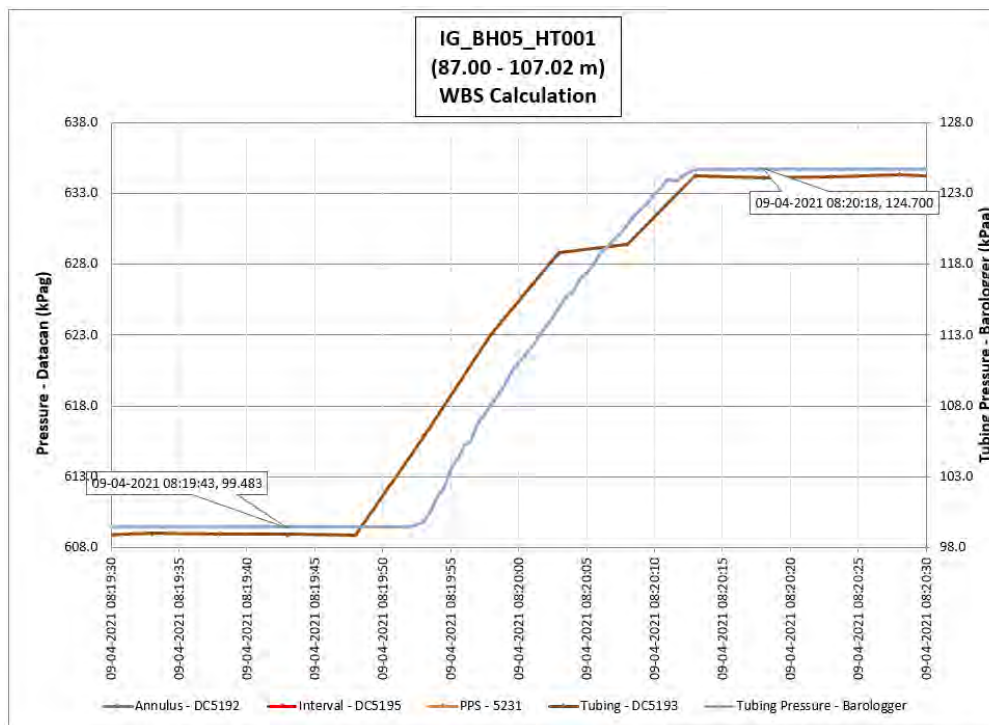


Figure 1: HT001 Annotated test plot showing monitored zone pressure and interval temperature.



**Figure 2: HT001 Tubing pressure during DHSIV activation. DHSIV Closed Wellbore Storage Estimate =  $3\text{E}-8$  m<sup>3</sup>/Pa**

**Table 1: Summary of Analysis Results – HT001**

	Formation conductivity	Skin zone conductivity	Static formation pressure	Formation specific storage	Radial thickness of skin	Flow dimension
	[m/s]	[m/s]	[kPa]	[1/m]	[m]	[–]
Best Fit	8E-10	3E-07	809	3E-07	6.33E+01	1.7
Minimum	6E-12	1E-08	786	5E-09	8E+00	1.6
Maximum	6E-09	3E-07	860	7E-07	9E+01	2.5
Mean	4E-10	9E-08	830	1E-07	3E+01	1.9
Median	2E-10	7E-08	836	1E-07	3E+01	1.9
Geometric mean	2E-10	7E-08	829	1E-07	3E+01	1.9



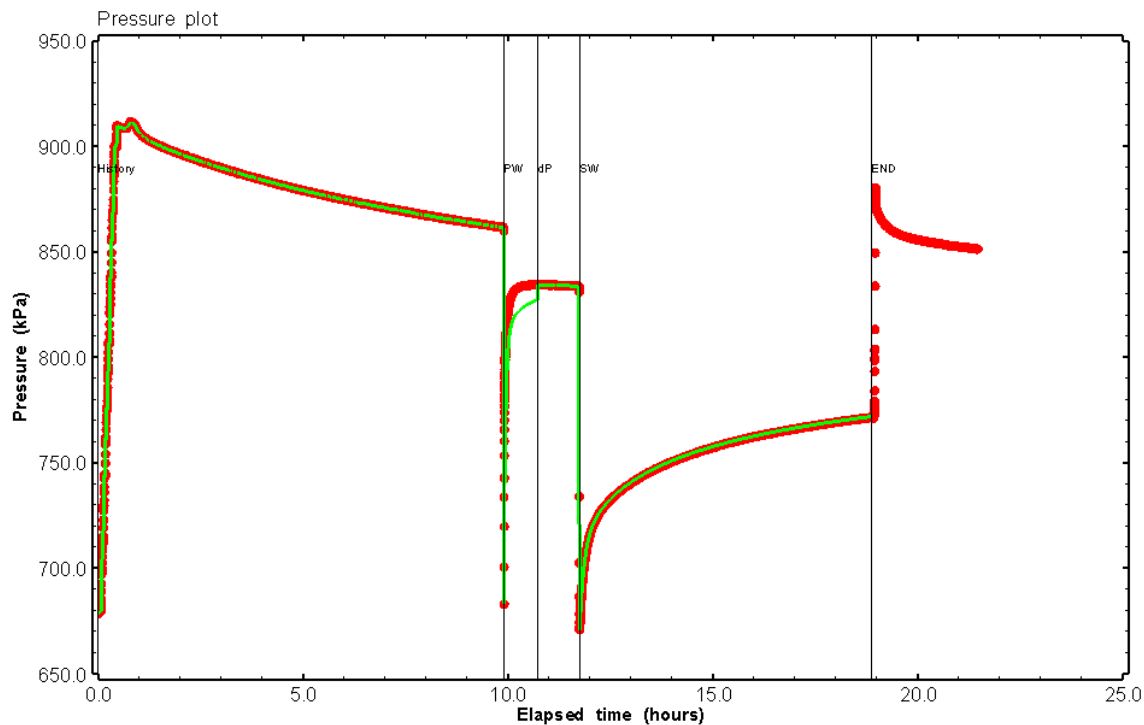


Figure 3: HT001 Pressure plot showing best-fit simulation and best fit results

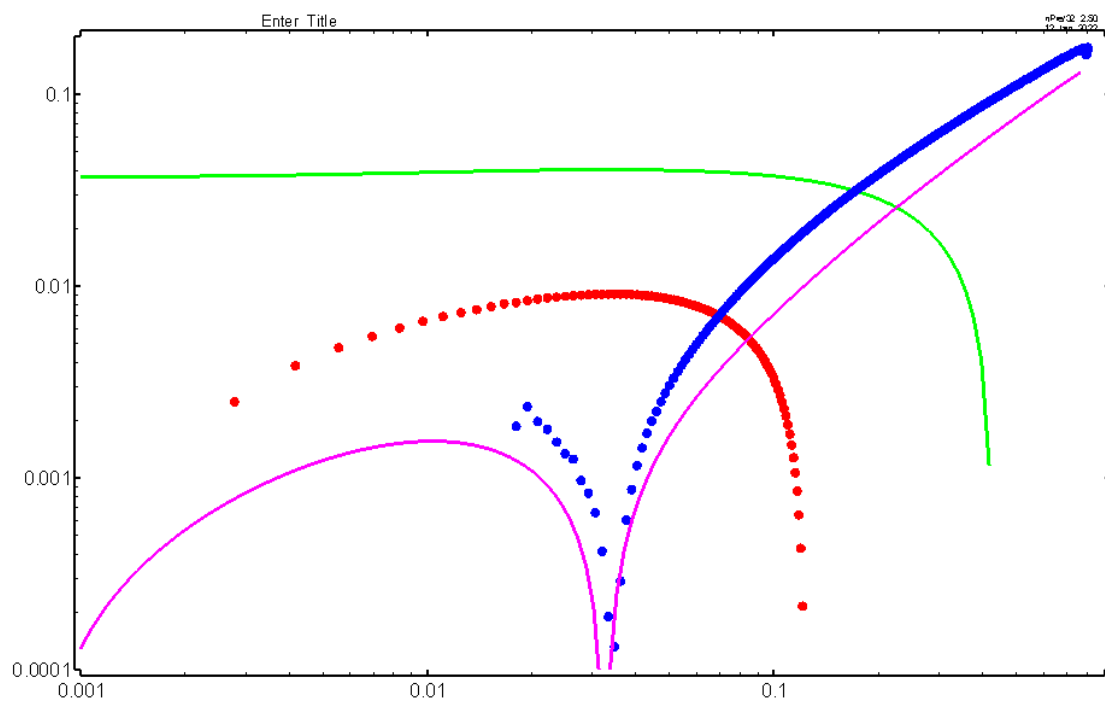


Figure 4: HT001 Deconvolved pressure change and derivative plot of the PW sequence showing best-fit simulation

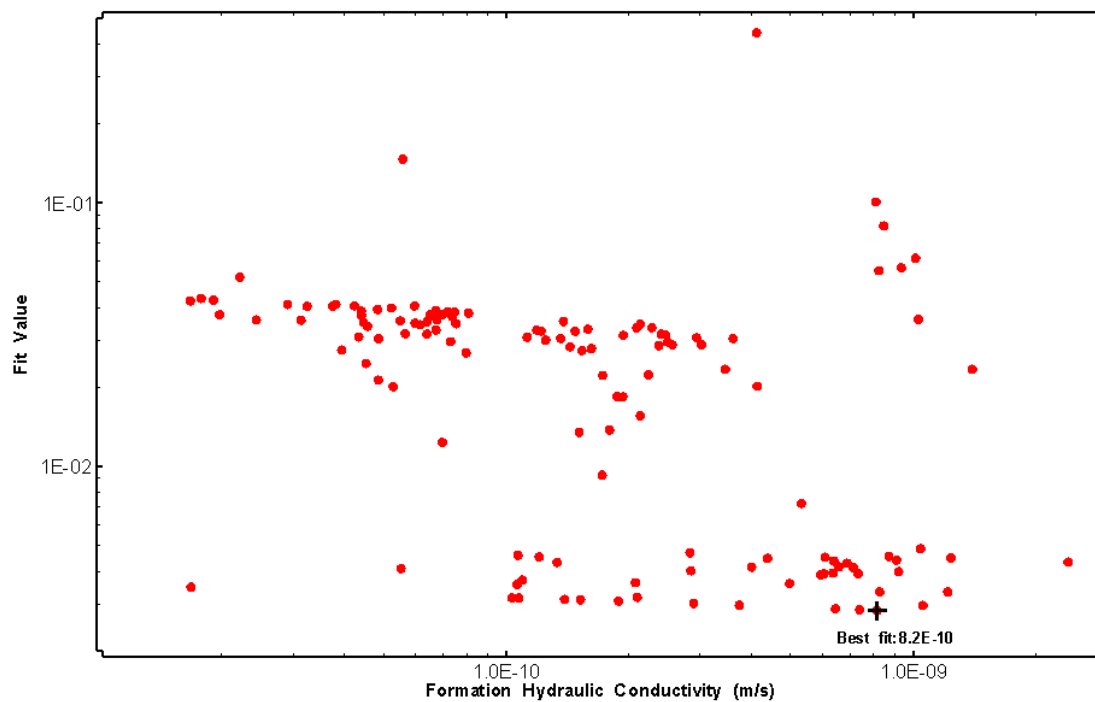


Figure 5: HT001 XY-scatter plot of formation hydraulic conductivity vs. fit value

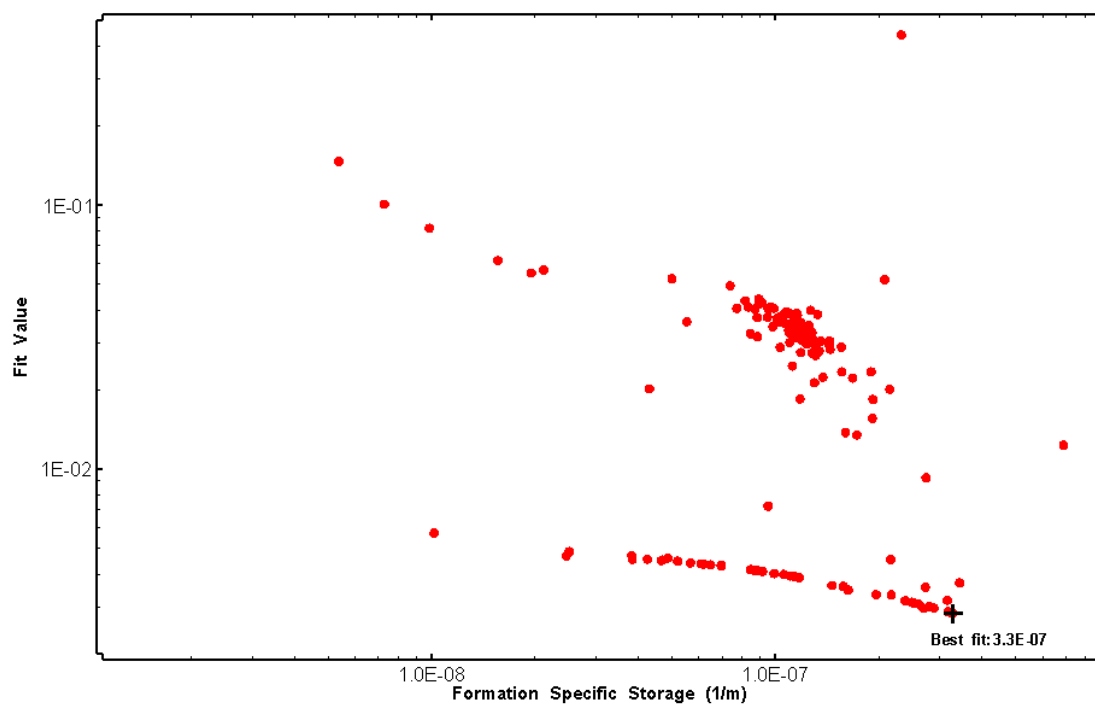


Figure 6: HT001 XY-scatter plot of formation specific storage vs. fit value

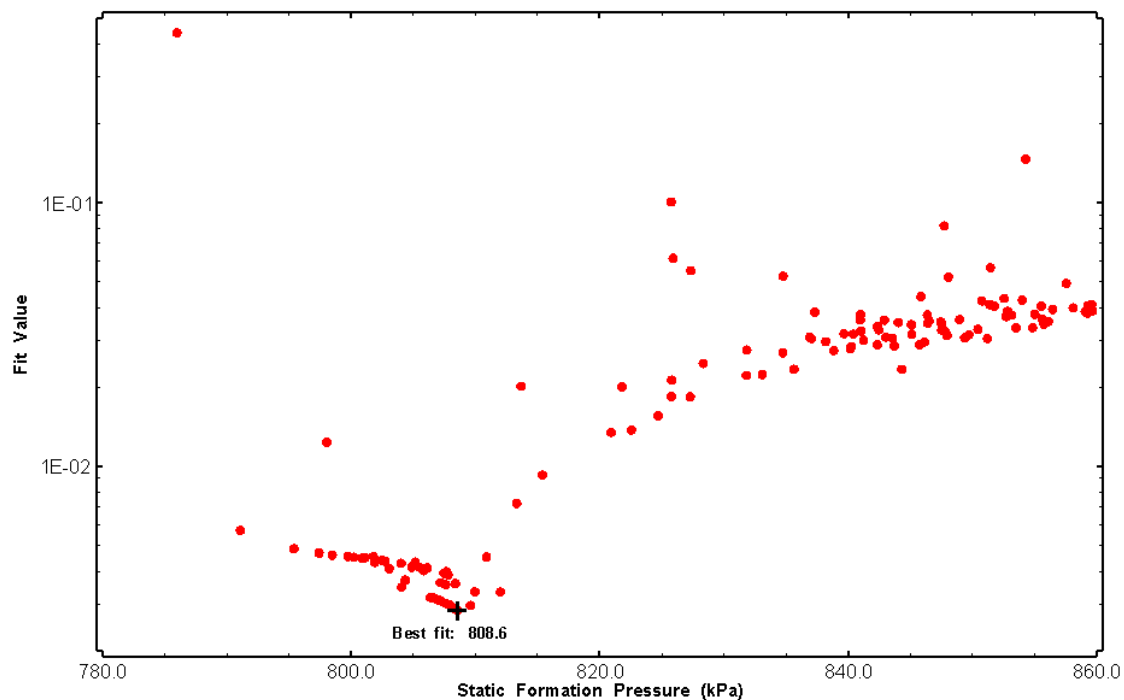


Figure 7: HT001 XY-scatter plot of static formation pressure vs. fit value

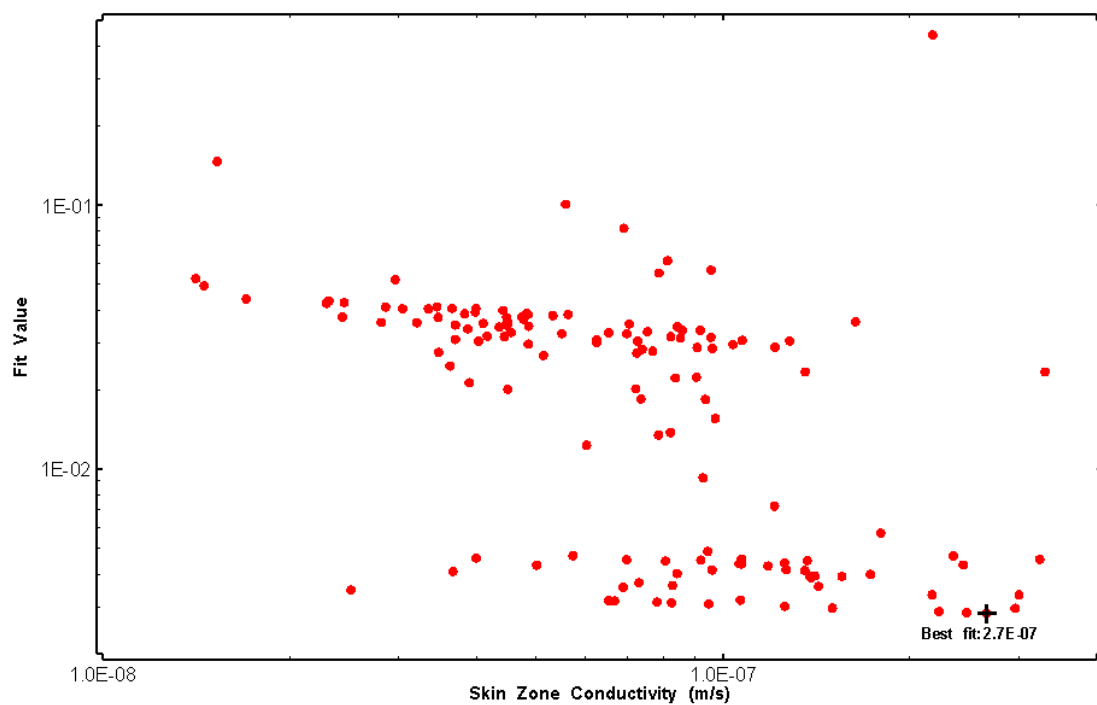


Figure 8: HT001 XY-scatter plot of skin zone conductivity vs. fit value

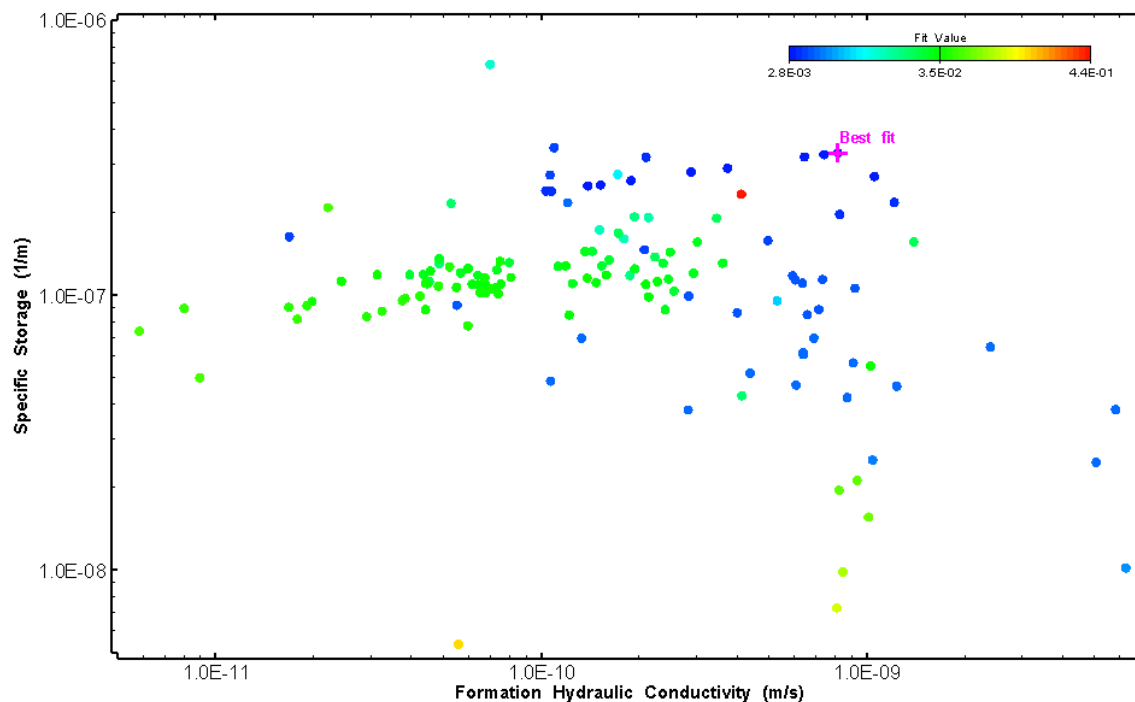


Figure 9: HT001 XY-scatter plot showing estimates of formation hydraulic conductivity and specific storage from perturbation analysis

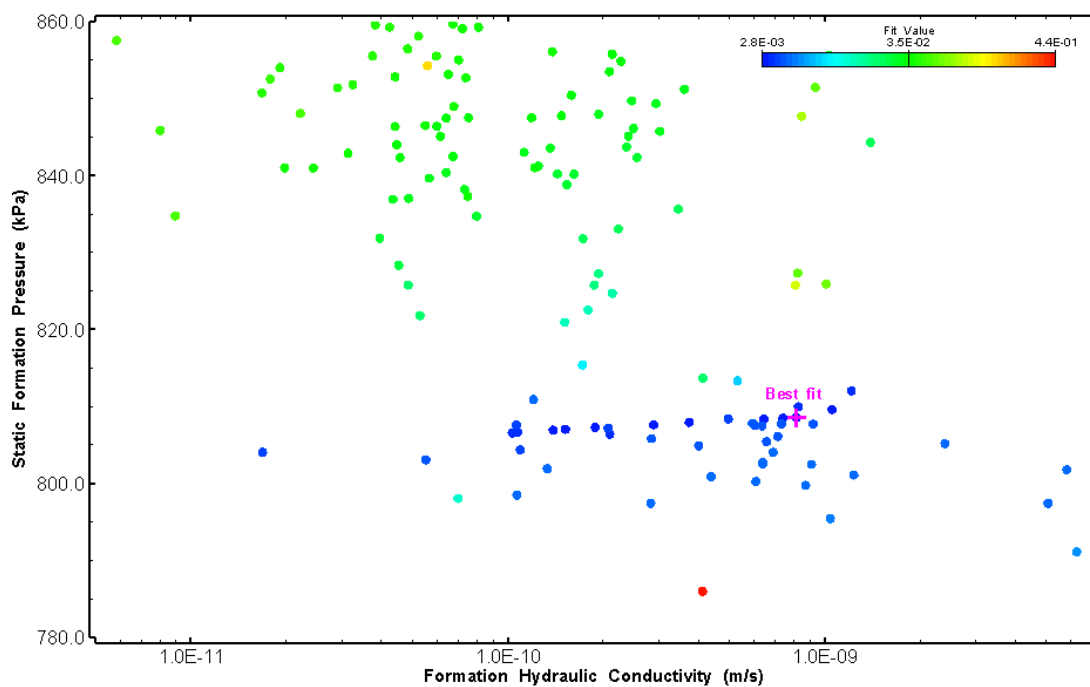


Figure 10: HT001 XY-scatter plot showing estimates of formation hydraulic conductivity and static formation pressure from perturbation analysis

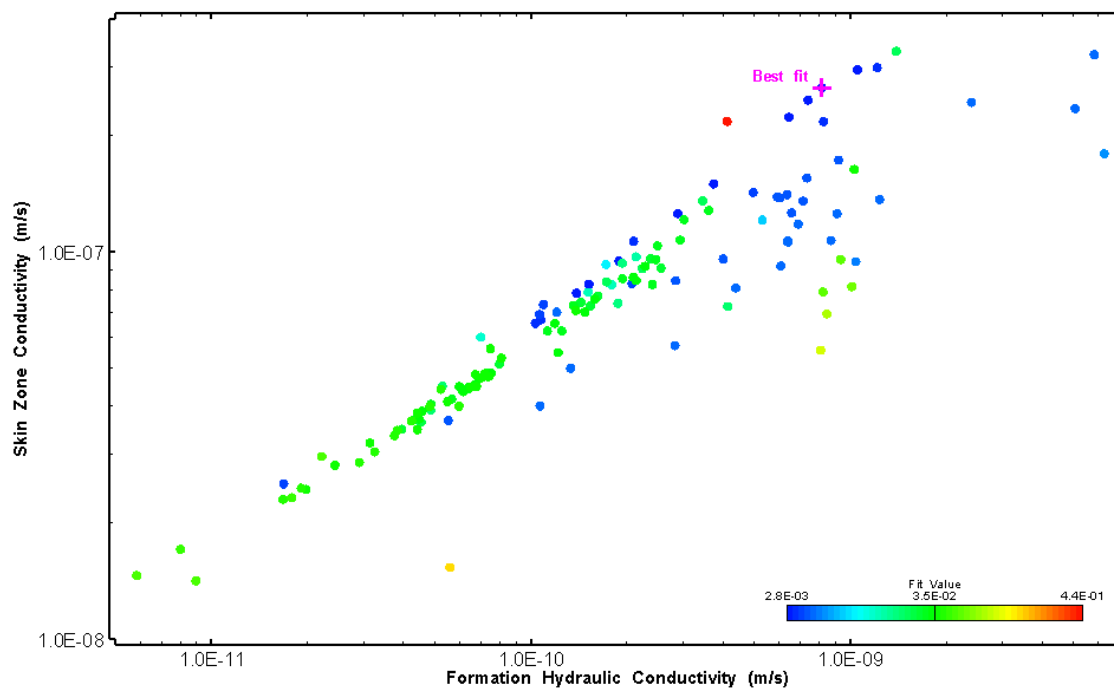


Figure 11: HT001 XY-scatter plot showing estimates of formation hydraulic conductivity and skin zone conductivity from perturbation analysis

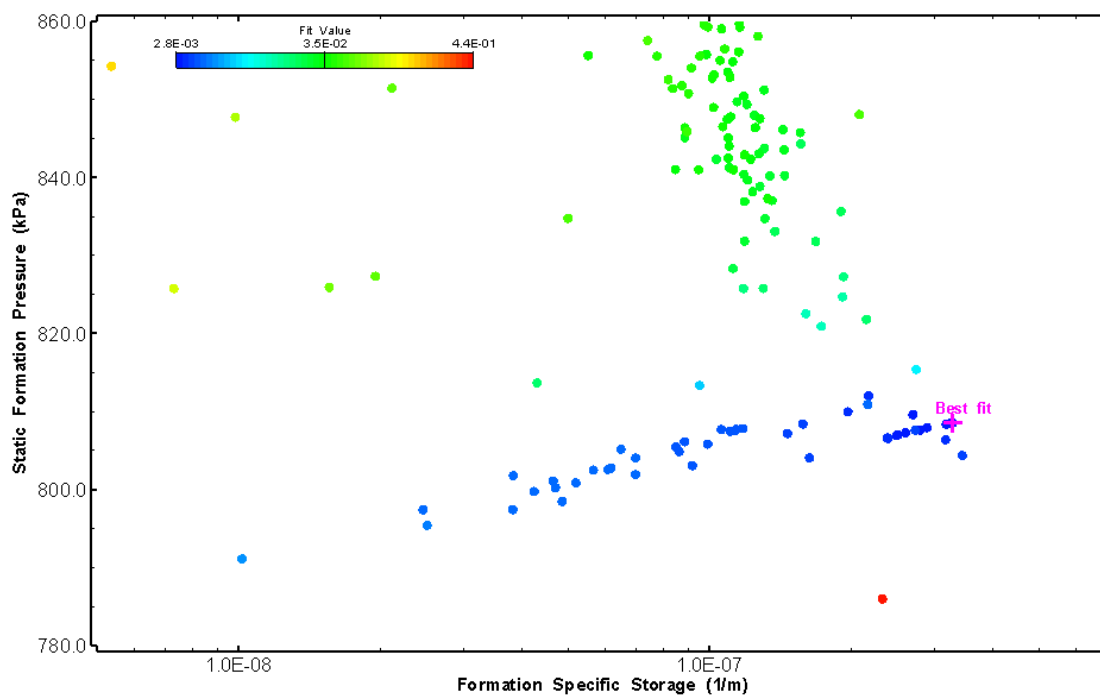


Figure 12: HT001 XY-scatter plot showing estimates of specific storage and static formation pressure from perturbation analysis

## 2.0 HT002 (157.37 – 177.39 M)

HT002 was selected to test a shallow fractured interval. 47 broken fractures were observed in the core. A loss of drilling fluid was observed in this interval during drilling. An indication of flow was recorded during FFEC logging post-drilling.

The test was initiated with a shut-in pressure recovery phase (PSR). A pulse withdrawal test (PW) with a shut-in recovery followed by a slug withdrawal (SW) phase was completed after the PSR phase.

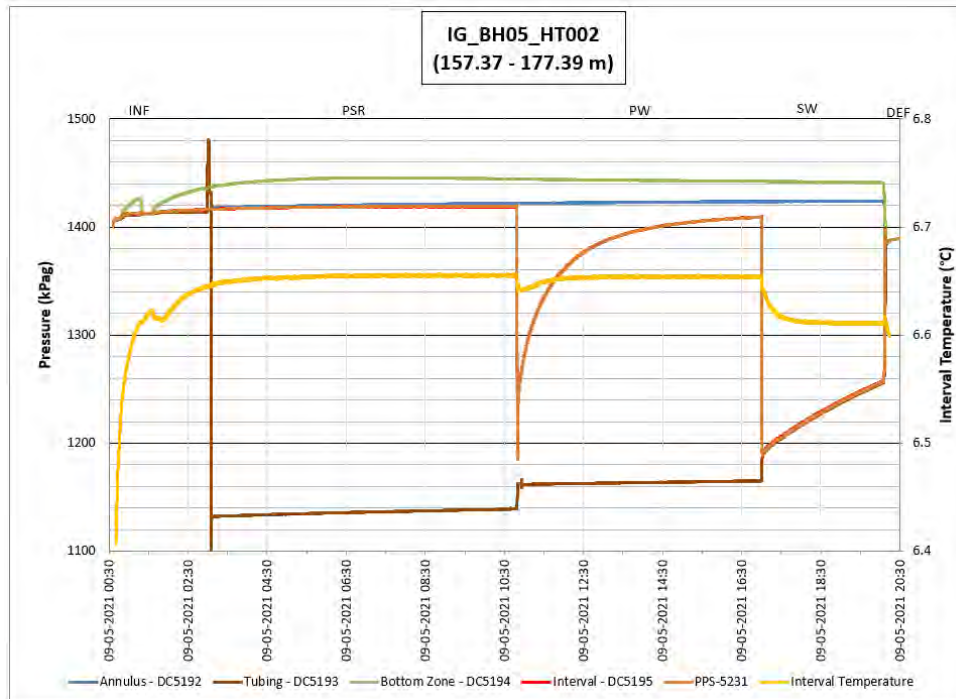


Figure 13: HT002 Annotated test plot showing monitored zone pressure and interval temperature.

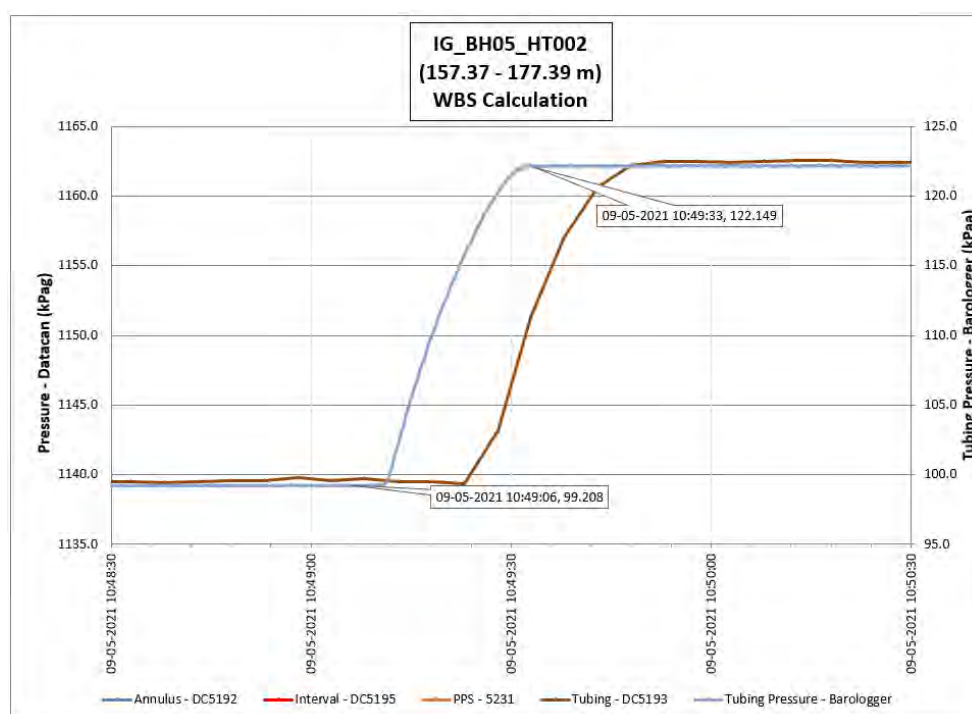


Figure 14: HT002 Tubing pressure during DHSIV activation. DHSIV Closed Wellbore Storage Estimate =  $2\text{E-}8 \text{ m}^3/\text{Pa}$

Table 2: Summary of Analysis Results – HT002

	Formation conductivity	Skin zone conductivity	Static formation pressure	Formation specific storage	Radial thickness of skin	Flow dimension
	[m/s]	[m/s]	[kPa]	[1/m]	[m]	[–]
Best Fit	2E-08	1E-07	1449	3E-08	1.97E+01	1.5
Minimum	1E-11	2E-09	1416	1E-10	2E-01	1.3
Maximum	8E-08	9E-07	1450	1E-05	3E+01	3.0
Mean	5E-09	4E-08	1436	4E-07	6E+00	2.2
Median	4E-10	1E-08	1434	6E-08	4E+00	2.1
Geometric mean	3E-10	1E-08	1436	4E-08	4E+00	2.2



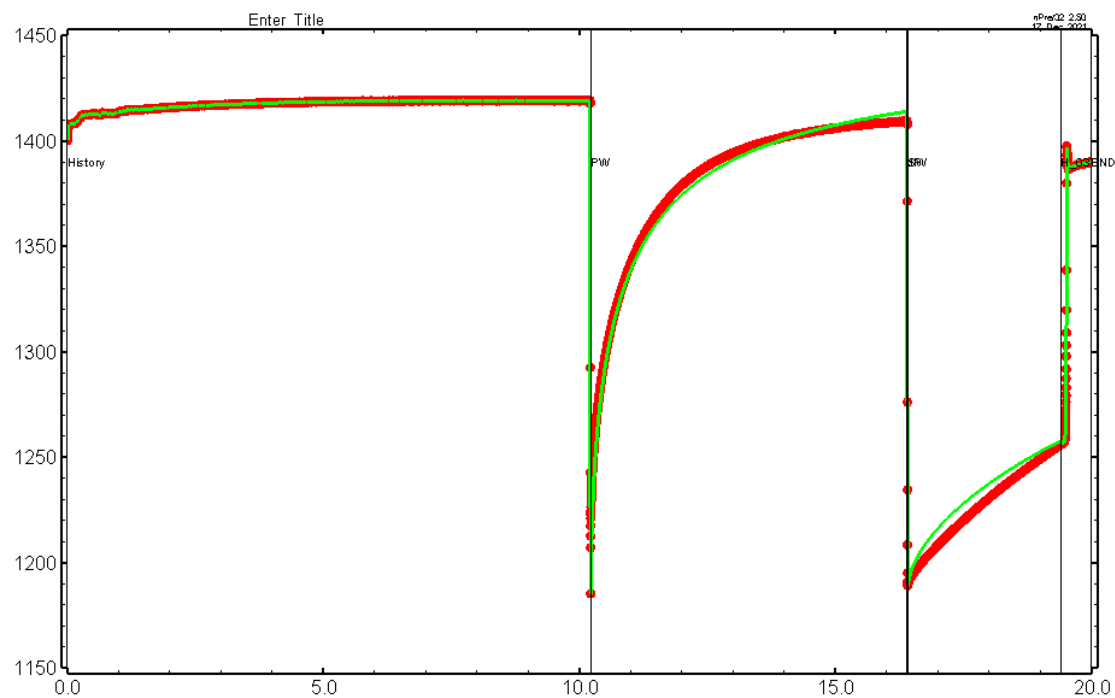


Figure 15: HT002 Pressure plot showing best-fit simulation and best fit results

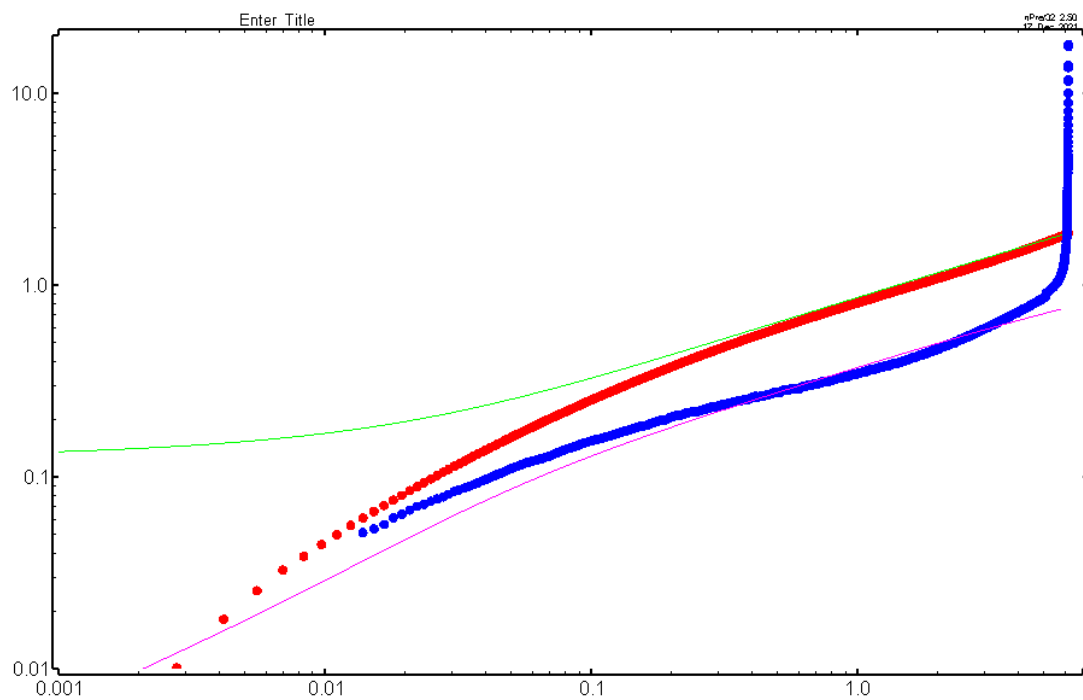


Figure 16: HT002 Deconvolved pressure change and derivative plot of the PW sequence showing best-fit simulation

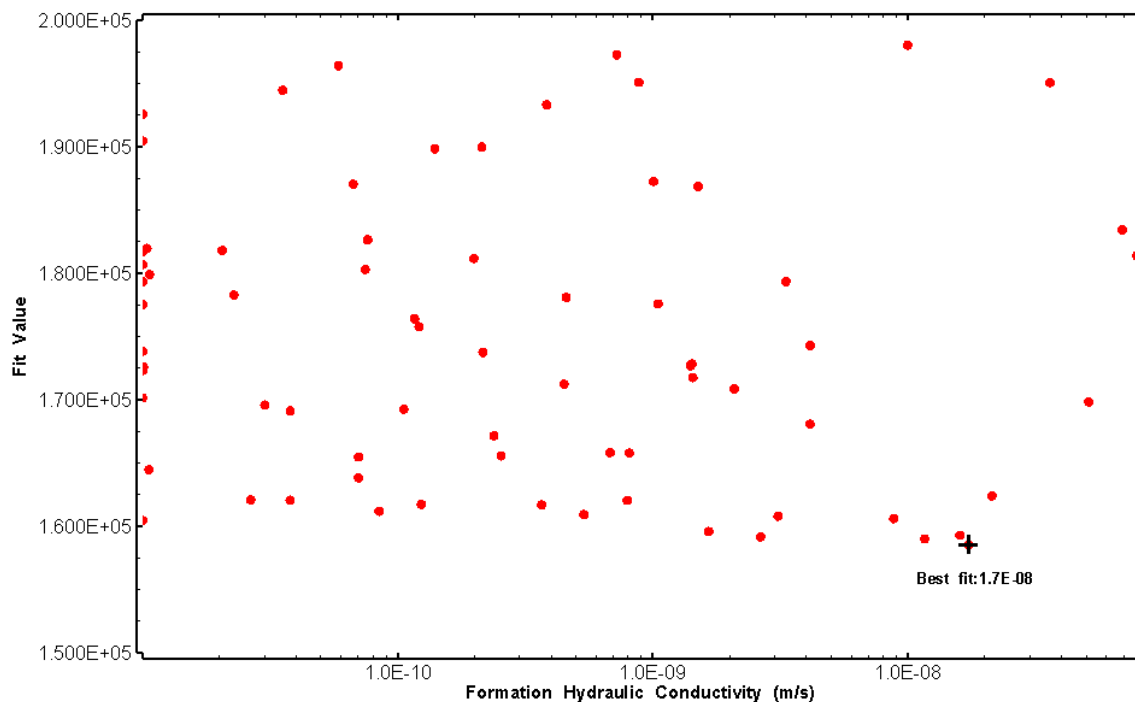


Figure 17: HT002 XY-scatter plot of formation hydraulic conductivity vs. fit value

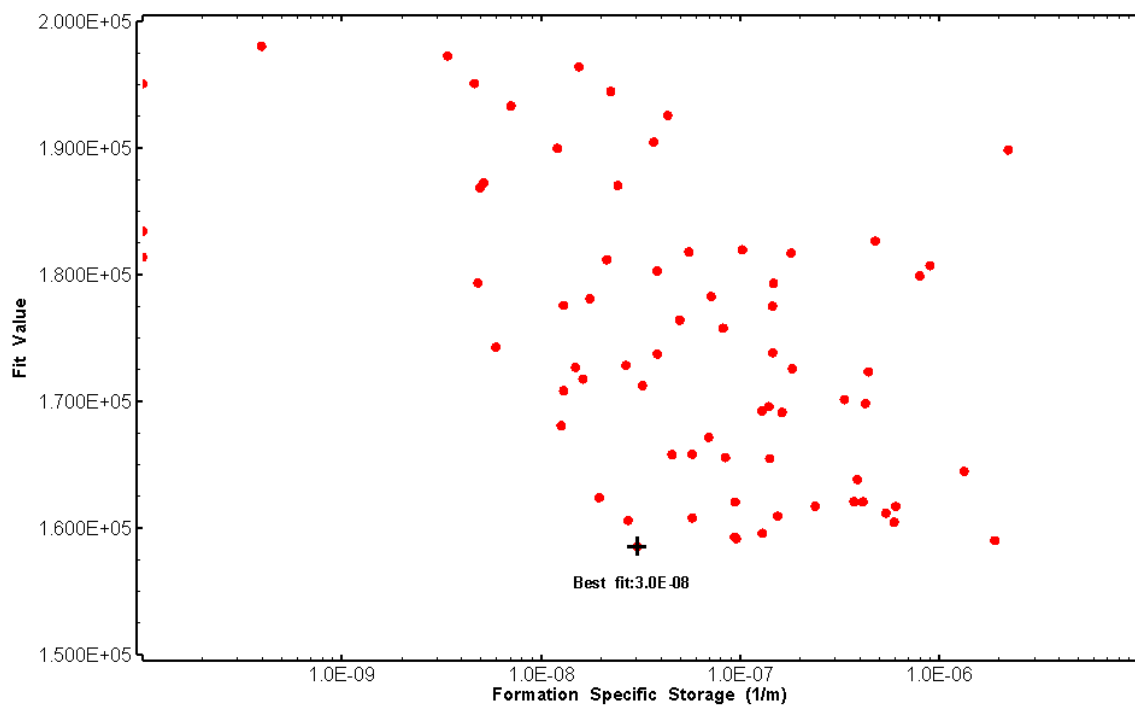


Figure 18: HT002 XY-scatter plot of formation specific storage vs. fit value

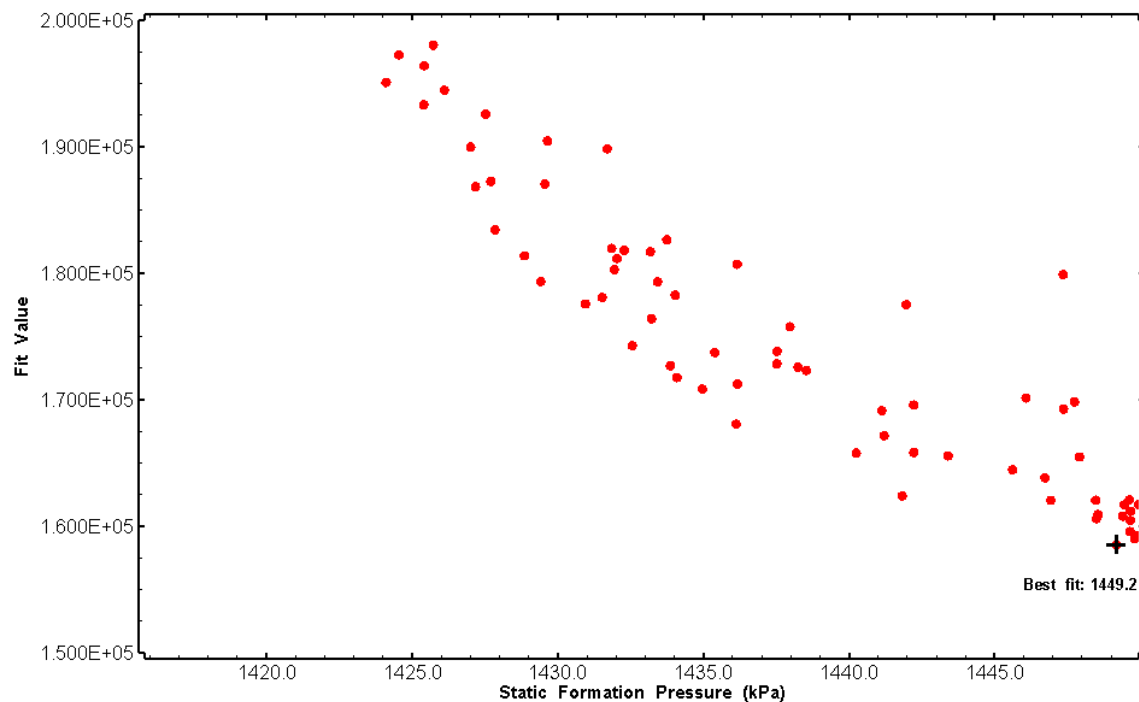


Figure 19: HT002 XY-scatter plot of static formation pressure vs. fit value

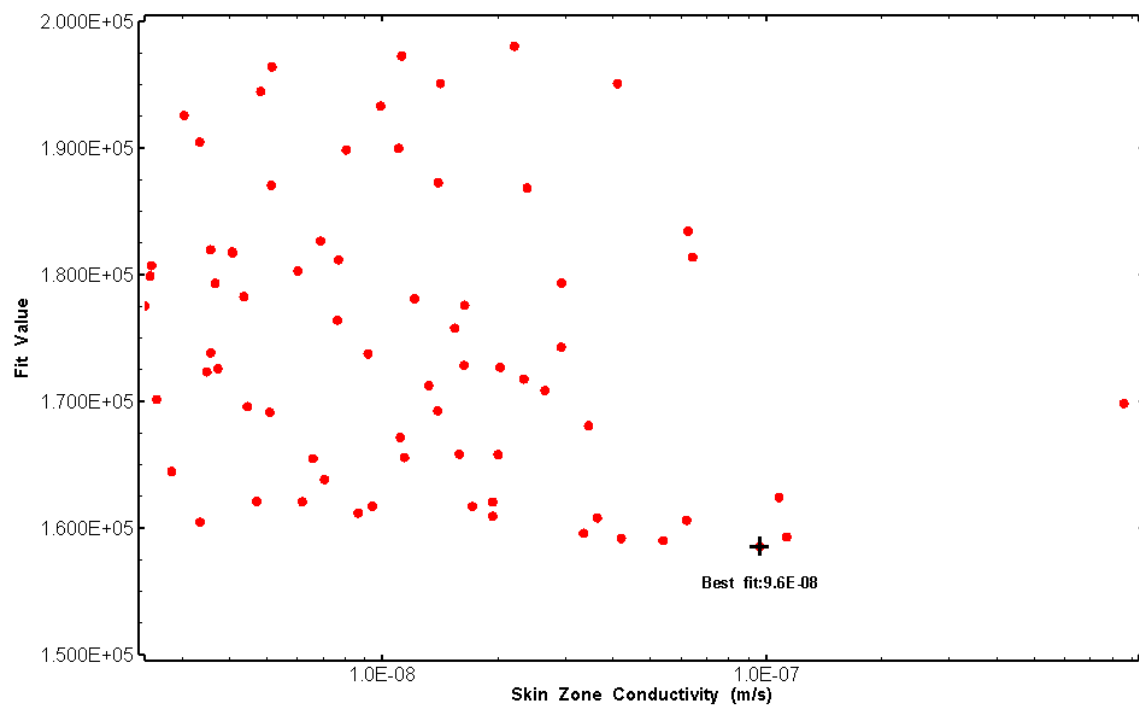


Figure 20: HT002 XY-scatter plot of skin zone conductivity vs. fit value

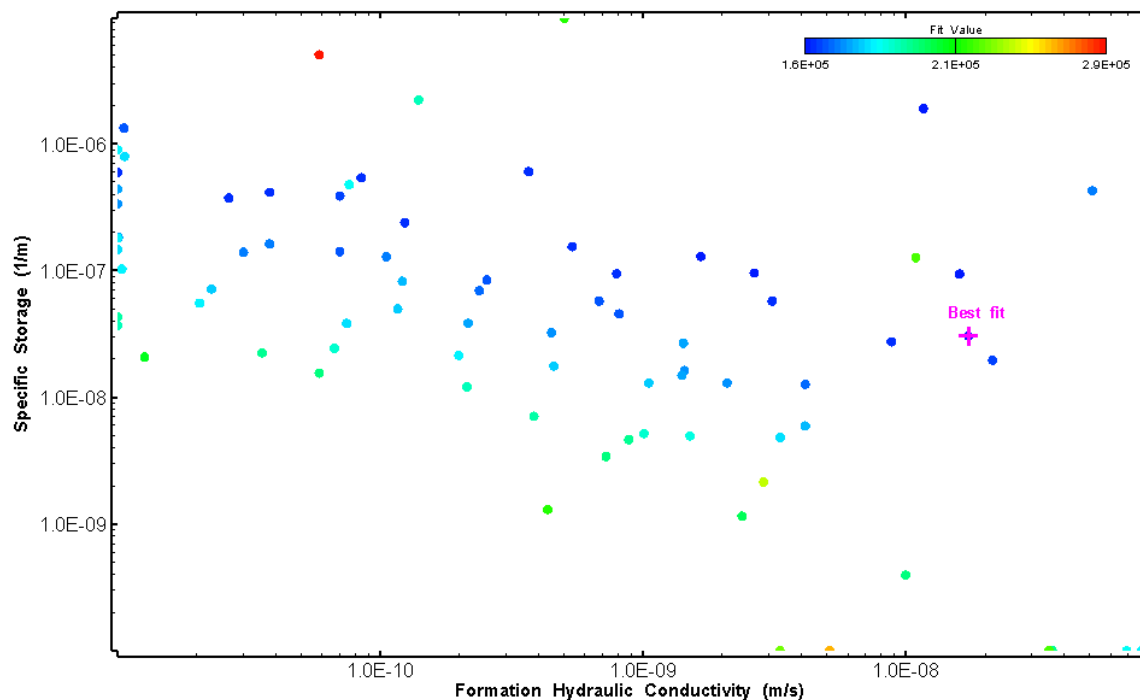


Figure 21: HT002 XY-scatter plot showing estimates of formation hydraulic conductivity and specific storage from perturbation analysis

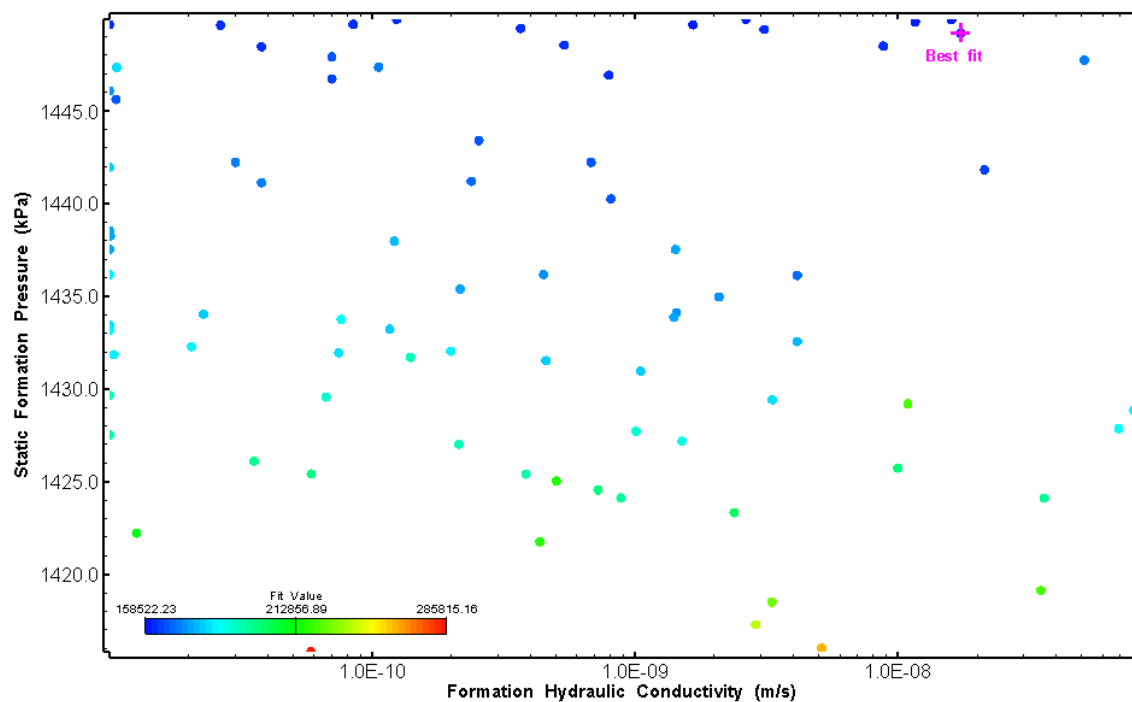


Figure 22: HT002 XY-scatter plot showing estimates of formation hydraulic conductivity and static formation pressure from perturbation analysis

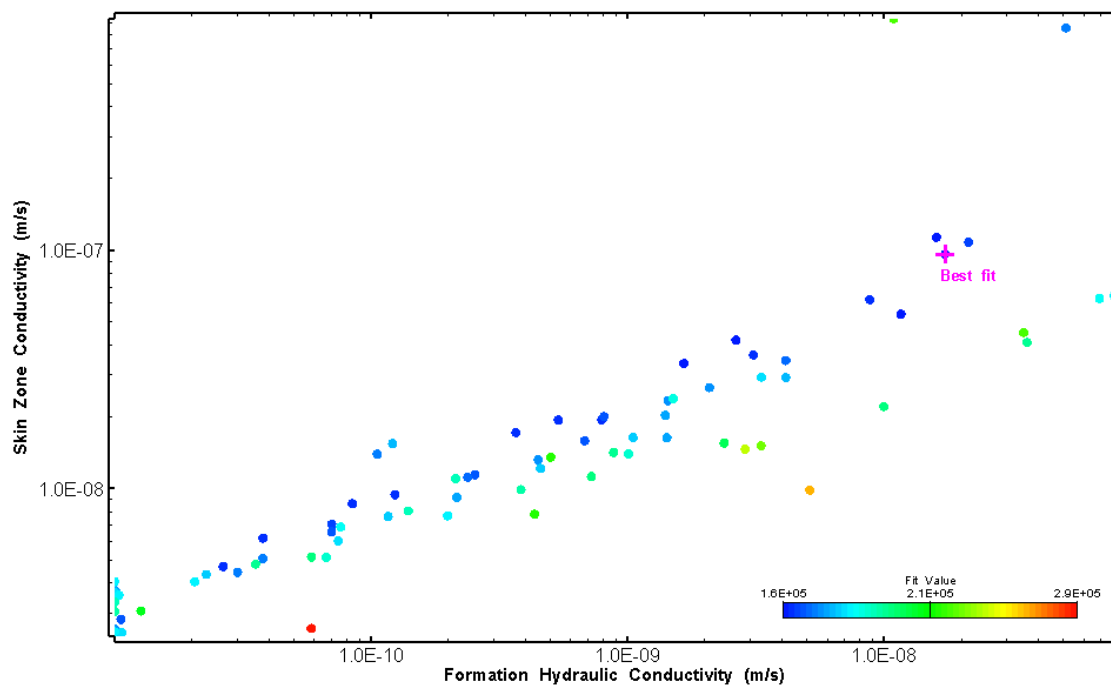


Figure 23: HT002 XY-scatter plot showing estimates of formation hydraulic conductivity and skin zone conductivity from perturbation analysis

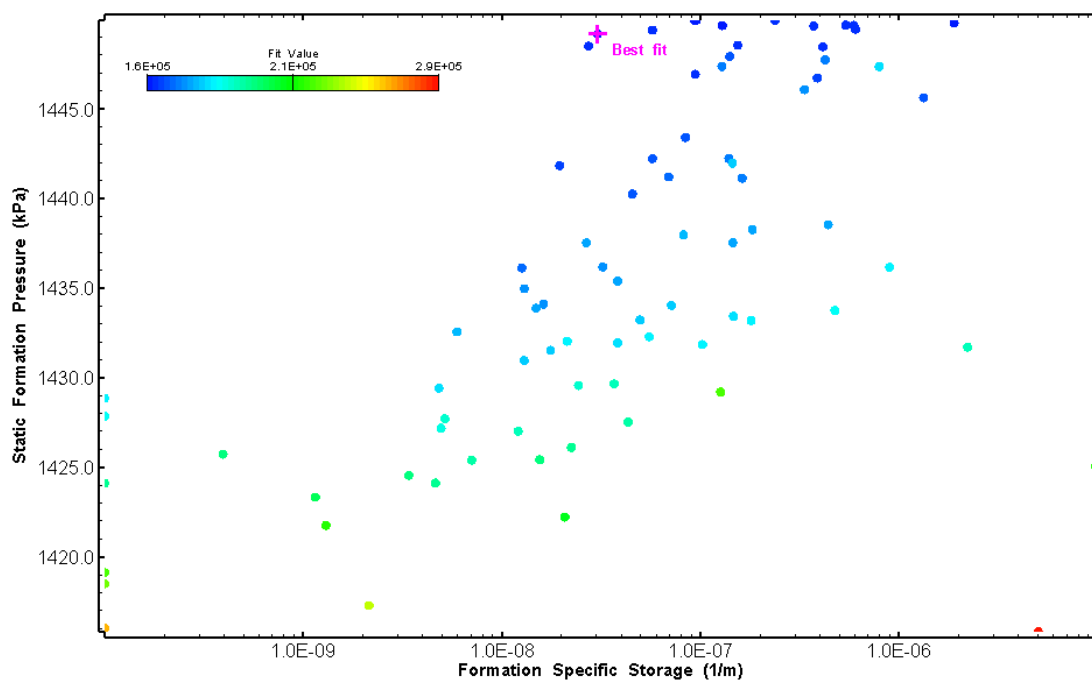


Figure 24: HT002 XY-scatter plot showing estimates of specific storage and static formation pressure from perturbation analysis

3.0 HT003 (222.00 – 242.02 M)

HT003 was selected to test a shallow fractured interval. 12 broken fractures were observed in the core. No drill fluid parameter triggers were reached during drilling. An indication of flow was recorded during FFEC logging post-drilling.

The test was initiated with a shut-in pressure recovery phase (PSR). A pulse withdrawal test (PW) with a shut-in recovery was completed after the PSR phase.

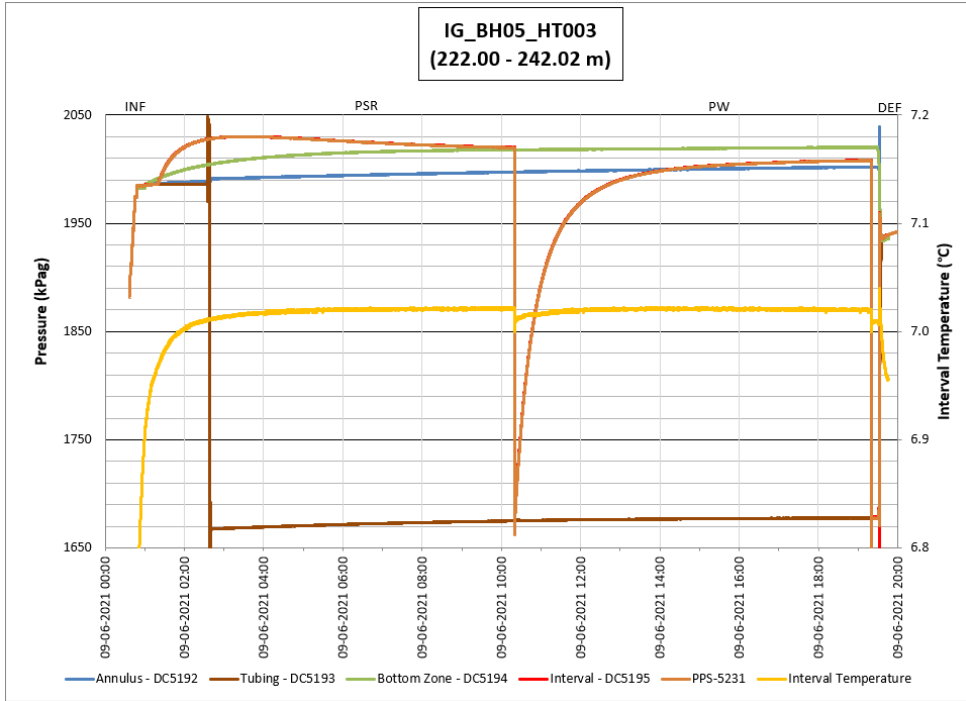
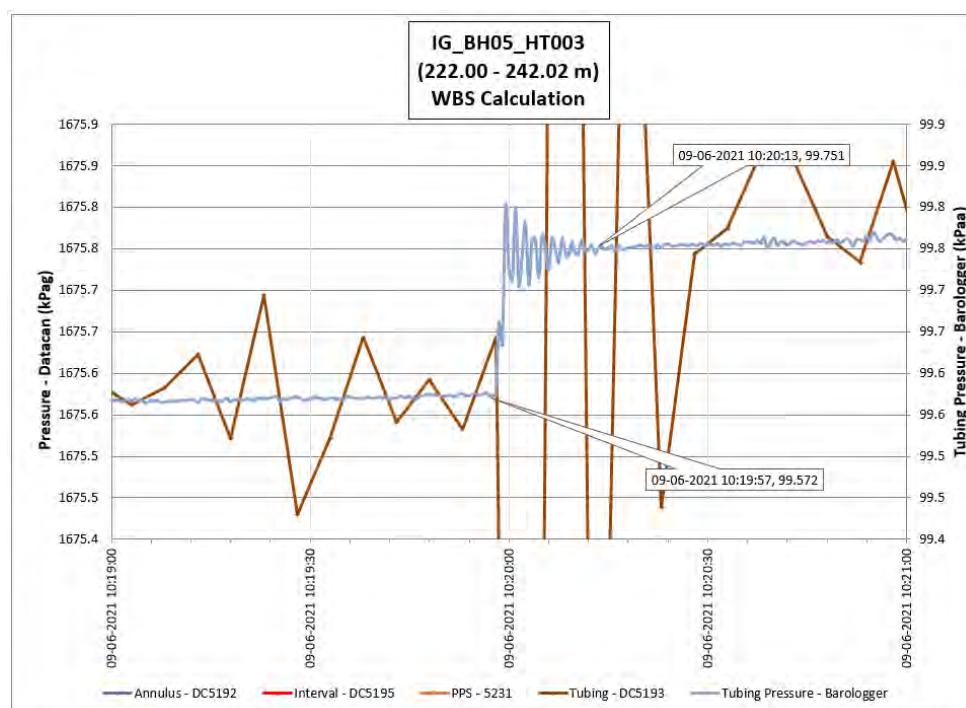


Figure 25: HT003 Annotated test plot showing monitored zone pressure and interval temperature.



**Figure 26: HT003 Tubing pressure during DHSIV activation. DHSIV Closed Wellbore Storage Estimate =  $9\text{E-}11 \text{ m}^3/\text{Pa}$**

**Table 3: Summary of Analysis Results – HT003**

	Formation conductivity	Skin zone conductivity	Static formation pressure	Formation specific storage	Radial thickness of skin	Flow dimension
	[m/s]	[m/s]	[kPa]	[1/m]	[m]	[–]
Best Fit	3E-13	3E-12	2017	1E-05	1.00E-01	3.0
Minimum	1E-14	3E-12	2007	1.E-09	1E-01	1.0
Maximum	6E-11	9E-08	2050	1E-05	7E+00	3.0
Mean	5E-12	9E-10	2014	1E-06	2E+00	2.5
Median	7E-13	4E-12	2009	9E-08	1E+00	2.5
Geometric mean	8E-13	5E-12	2014	1E-07	1E+00	2.5



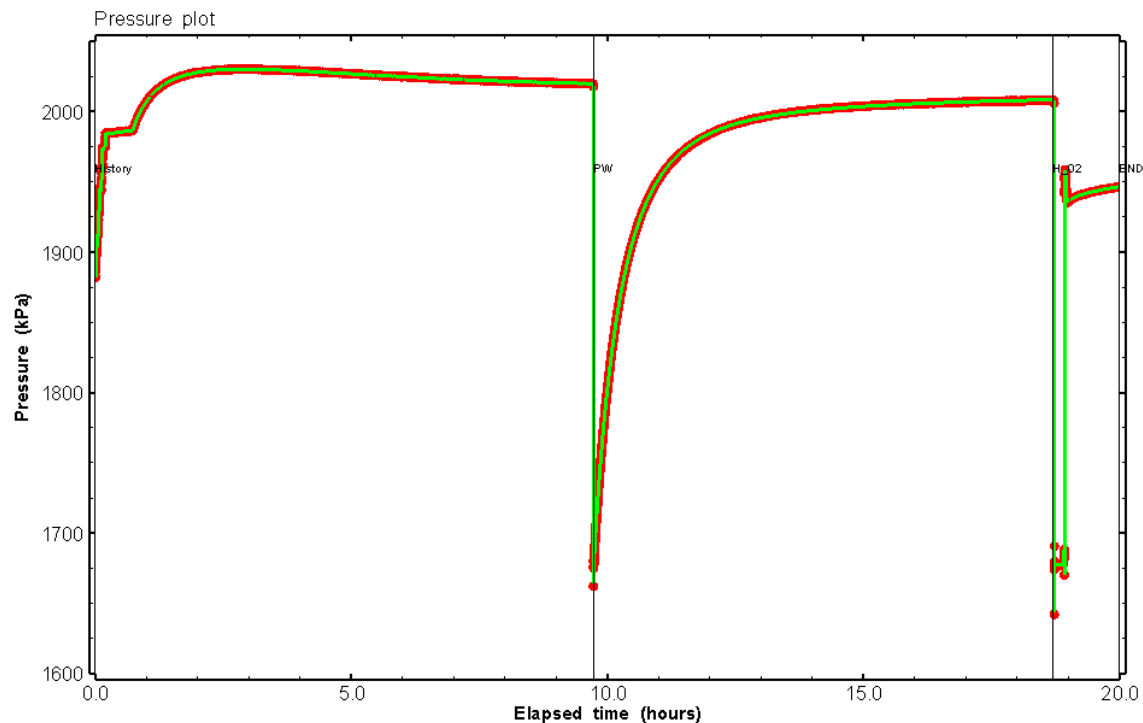


Figure 27: HT003 Pressure plot showing best-fit simulation and best fit results

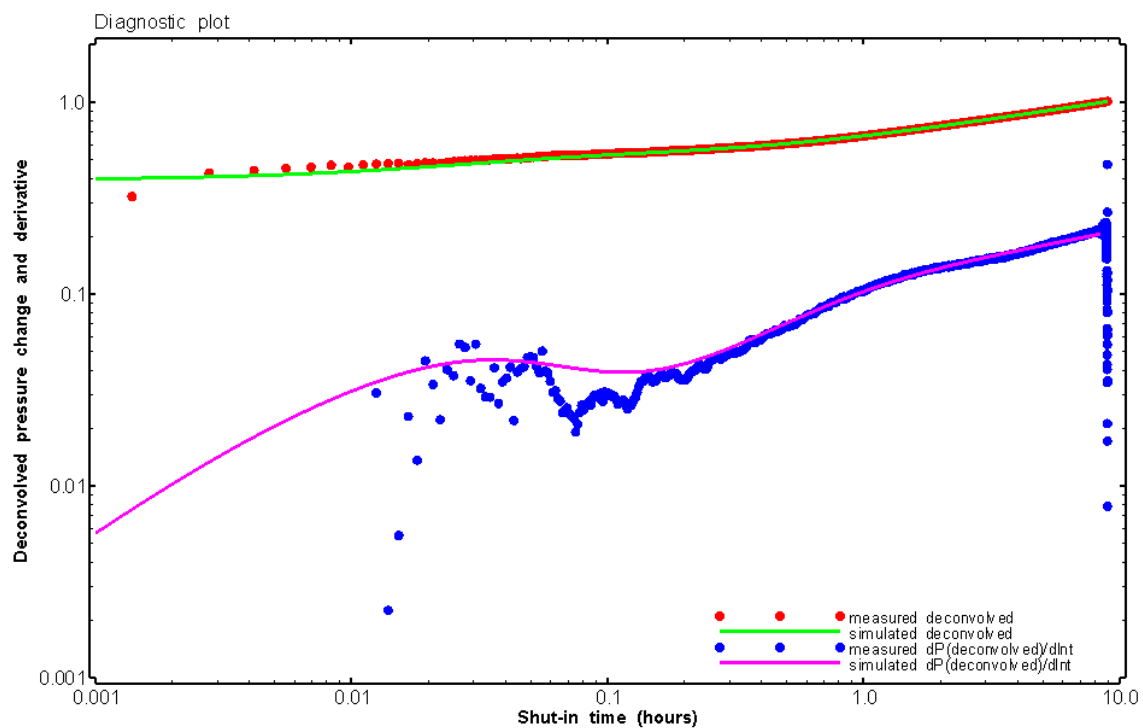


Figure 28: HT003 Deconvolved pressure change and derivative plot of the PW sequence showing best-fit simulation

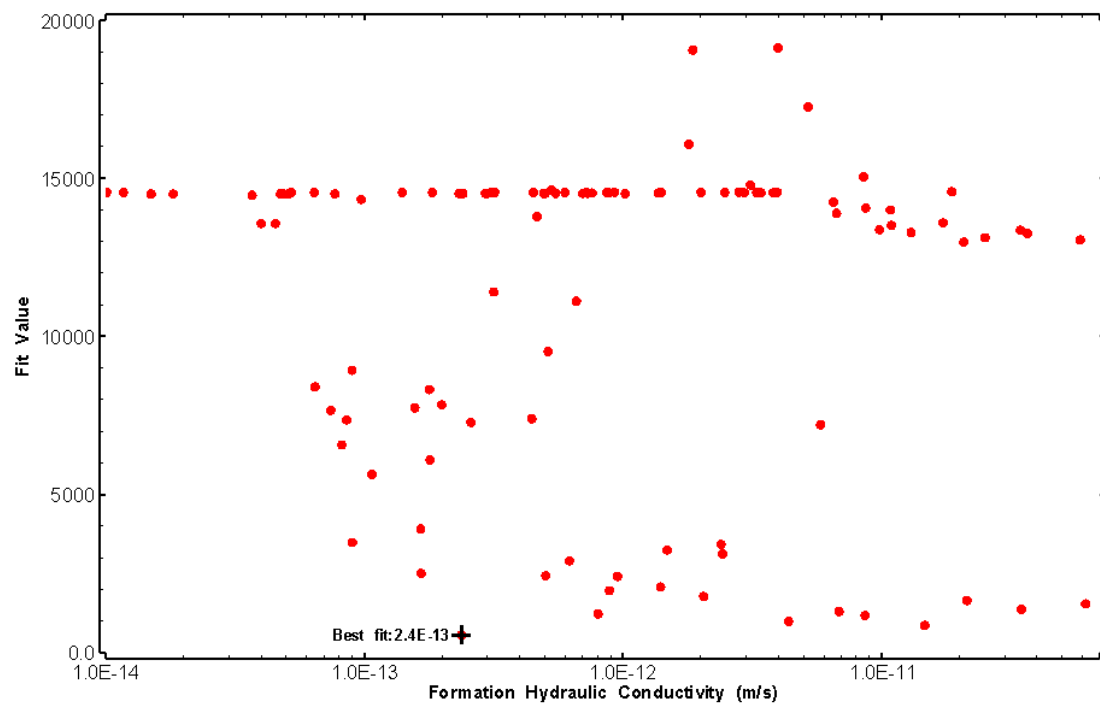


Figure 29: HT003 XY-scatter plot of formation hydraulic conductivity vs. fit value

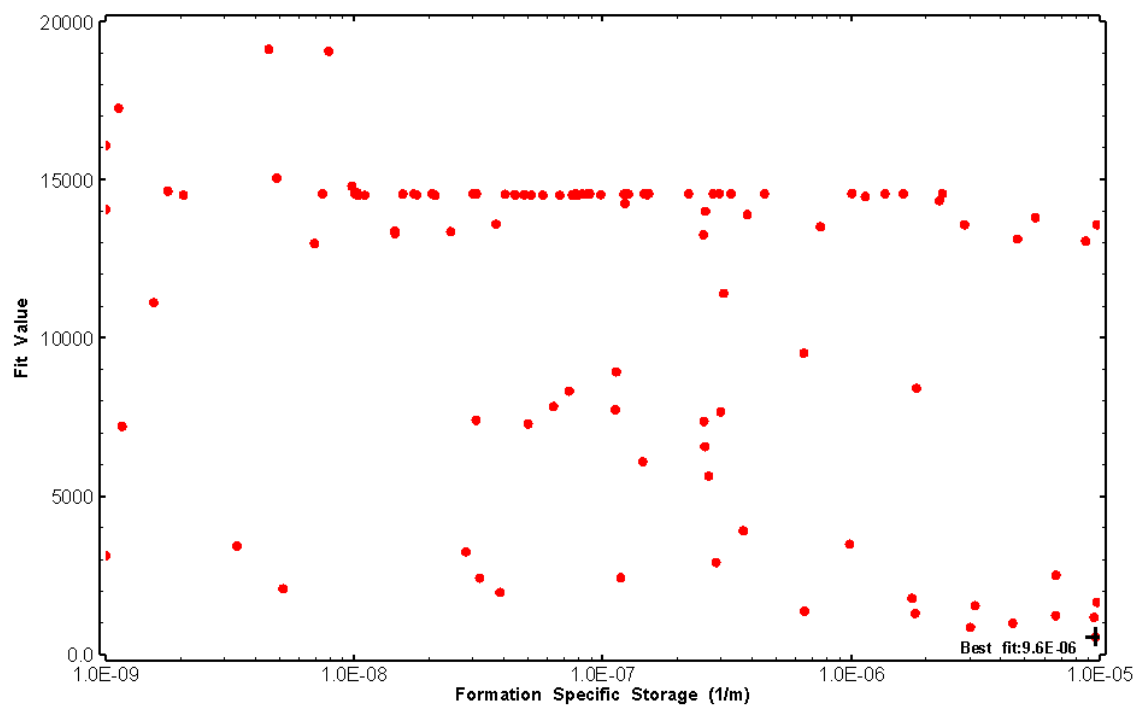


Figure 30: HT003 XY-scatter plot of formation specific storage vs. fit value

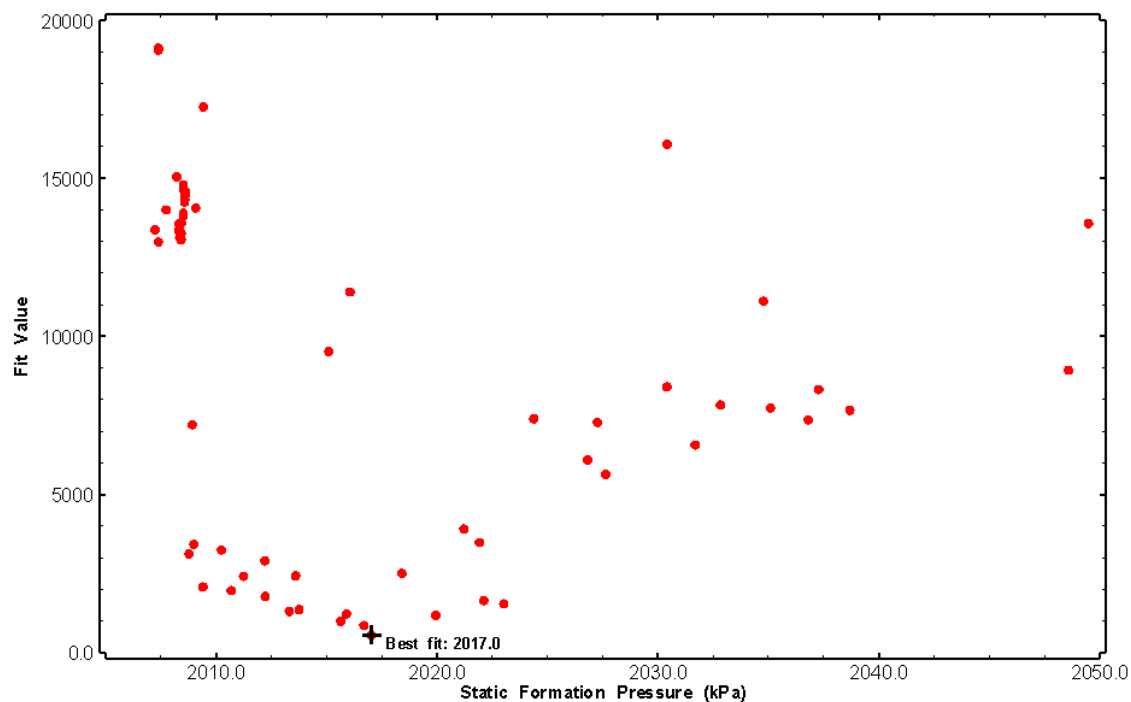


Figure 31: HT003 XY-scatter plot of static formation pressure vs. fit value

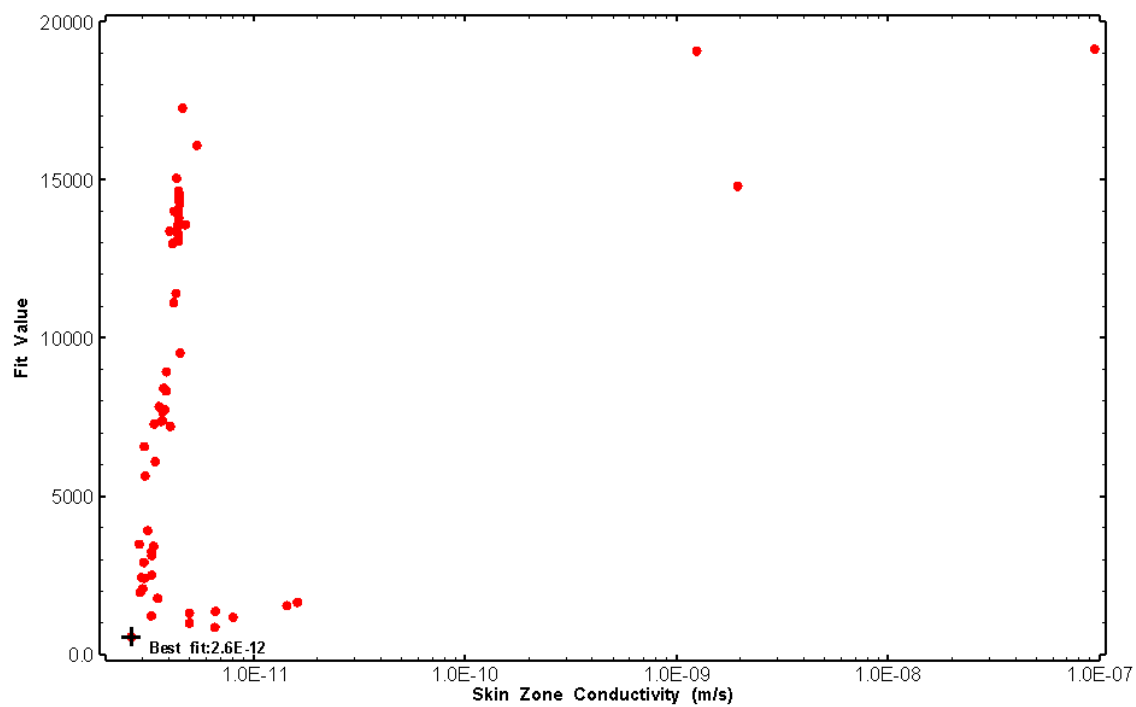


Figure 32: HT003 XY-scatter plot of skin zone conductivity vs. fit value

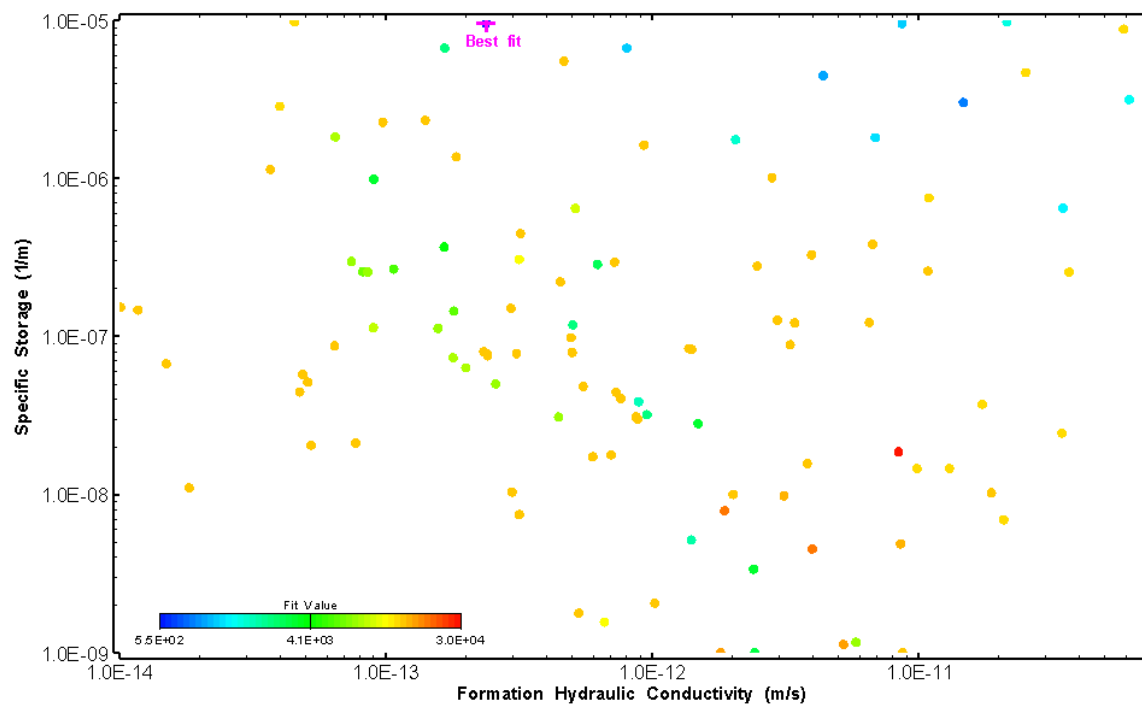


Figure 33: HT003 XY-scatter plot showing estimates of formation hydraulic conductivity and specific storage from perturbation analysis

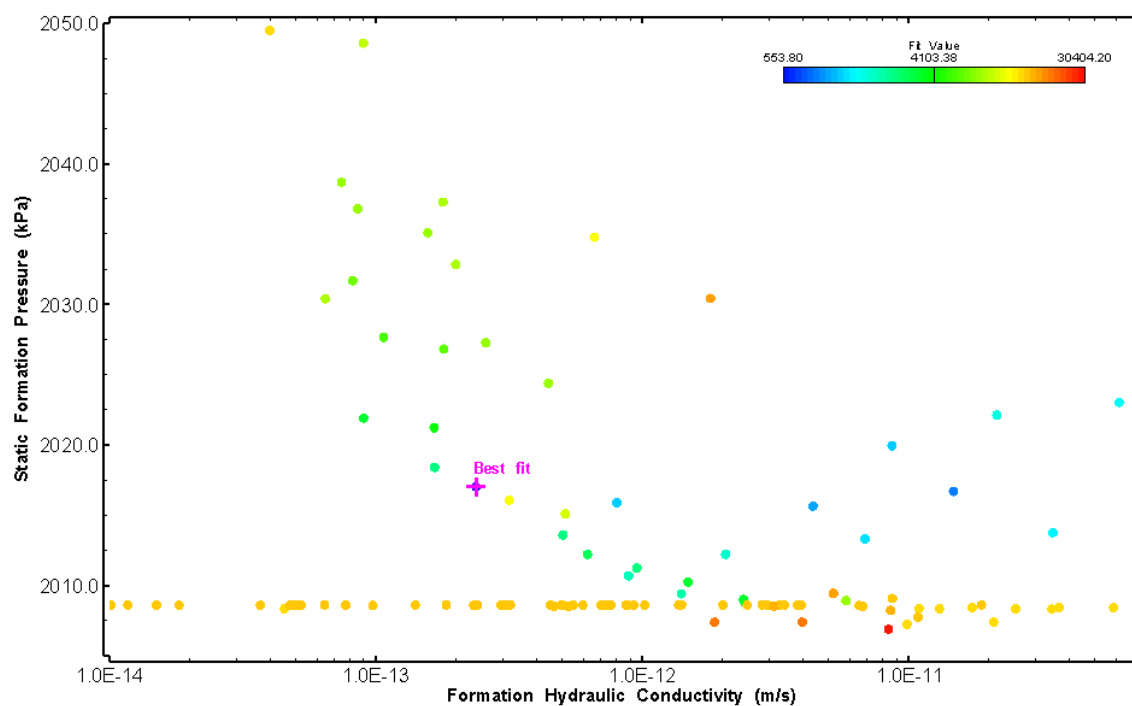


Figure 34: HT003 XY-scatter plot showing estimates of formation hydraulic conductivity and static formation pressure from perturbation analysis

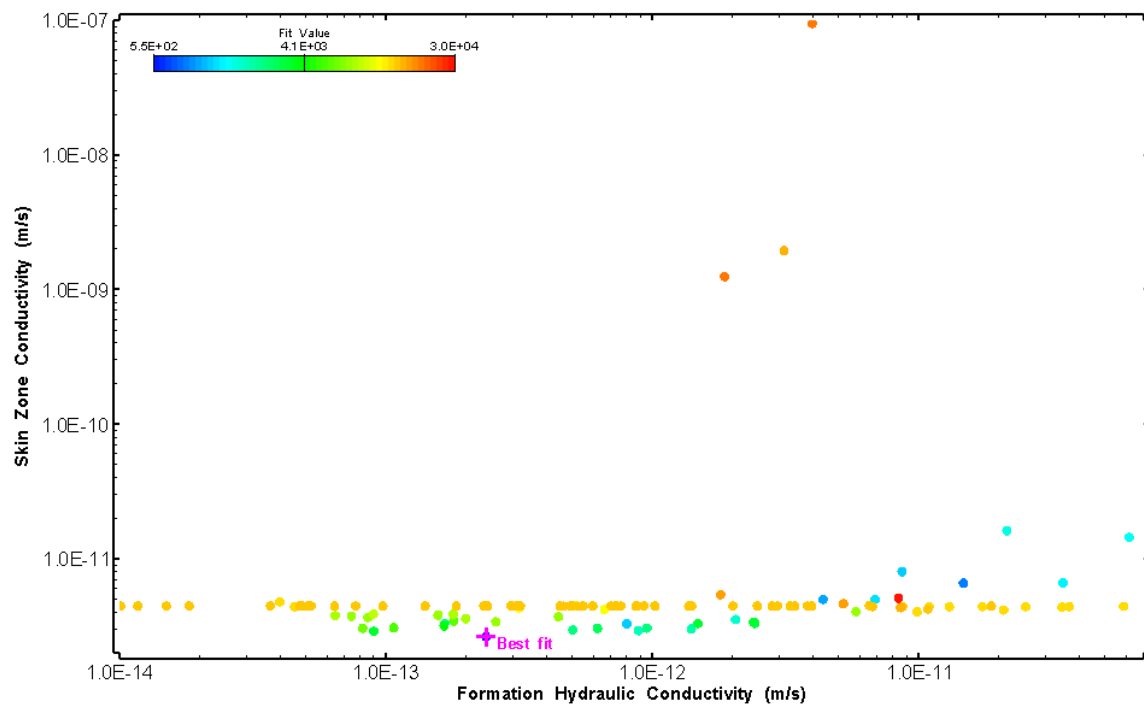


Figure 35: HT003 XY-scatter plot showing estimates of formation hydraulic conductivity and skin zone conductivity from perturbation analysis

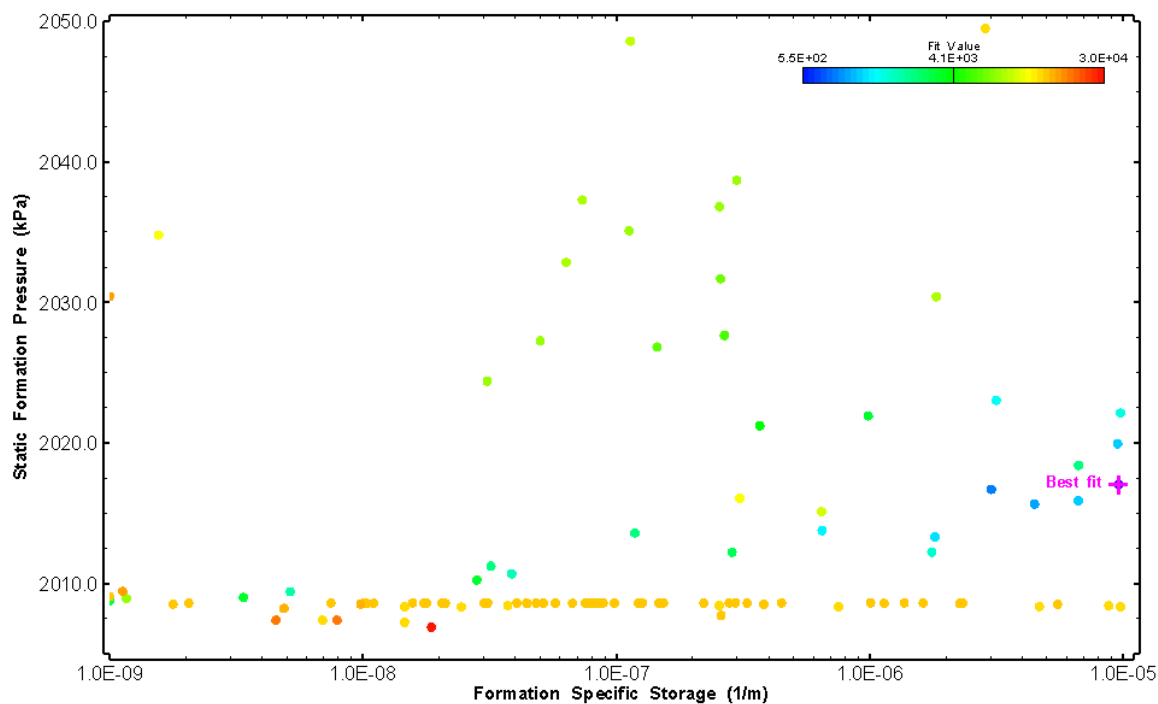


Figure 36: HT003 XY-scatter plot showing estimates of specific storage and static formation pressure from perturbation analysis

## 4.0 HT004 (260.00 – 280.02 M)

HT004 was selected to test a shallow fractured interval. 12 broken fractures were observed in the core. No drill fluid parameter triggers were reached during drilling. No indication of flow was recorded during FFEC logging post-drilling.

The test was initiated with a shut-in pressure recovery phase (PSR). A pulse withdrawal test (PW) with a shut-in recovery was completed after the PSR phase.

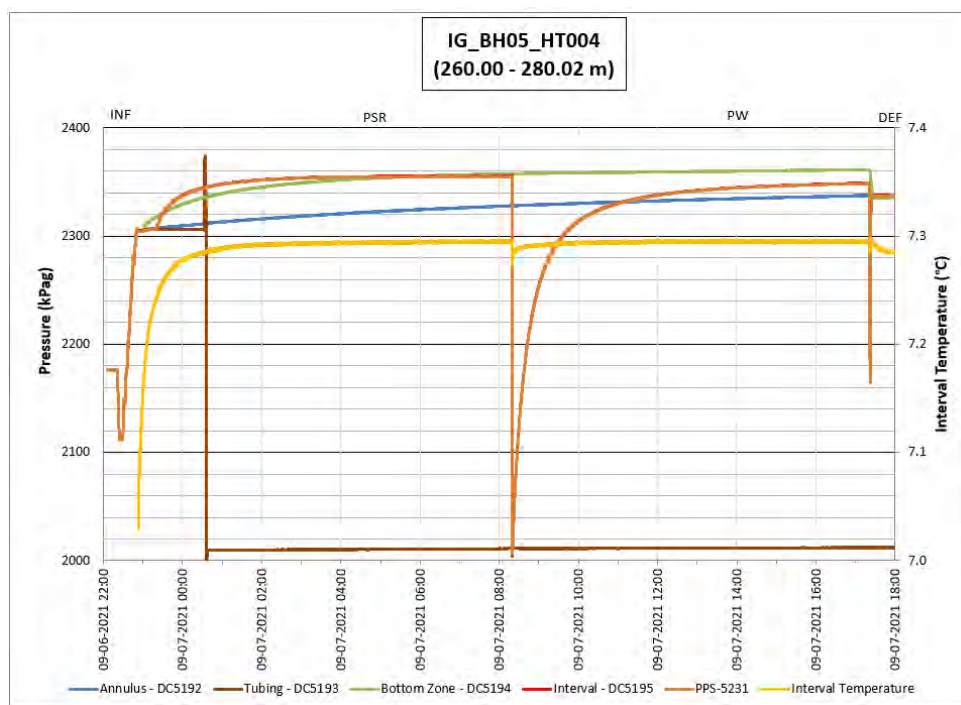
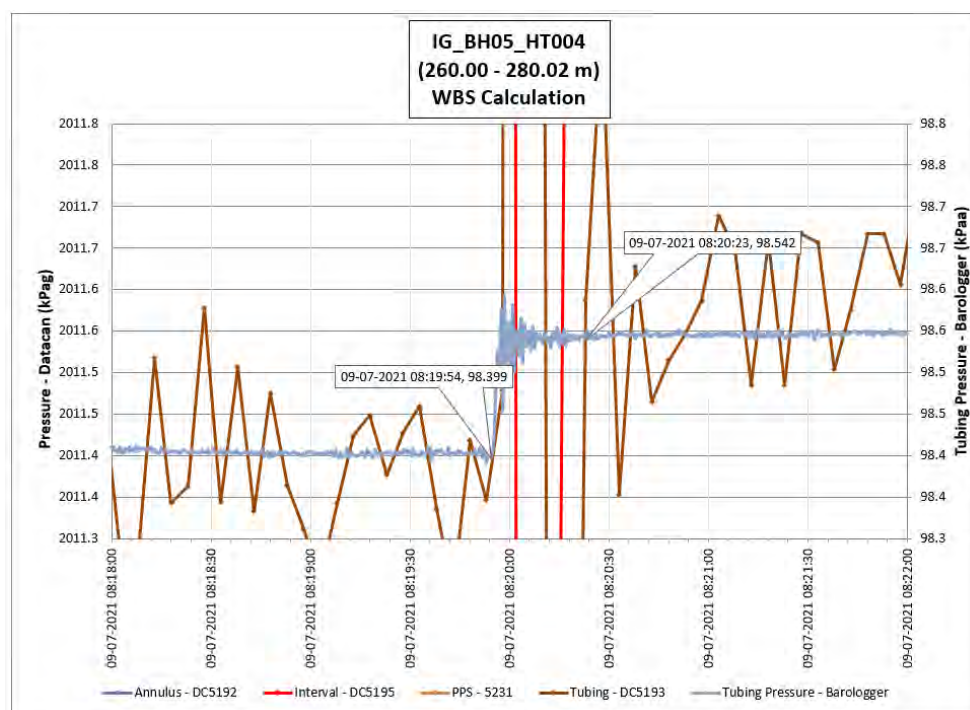


Figure 37: HT004 Annotated test plot showing monitored zone pressure and interval temperature.



**Figure 38: HT004 Tubing pressure during DHSIV activation. DHSIV Closed Wellbore Storage Estimate =  $7\text{E-}11 \text{ m}^3/\text{Pa}$**

**Table 4: Summary of Analysis Results – HT004**

	Formation conductivity	Skin zone conductivity	Static formation pressure	Formation specific storage	Radial thickness of skin	Flow dimension
	[m/s]	[m/s]	[kPa]	[1/m]	[m]	[–]
Best Fit	1E-12	2E-12	2356	7E-06	1.98E-02	3.0
Minimum	2E-13	2E-12	2348	1E-09	1E-02	1.3
Maximum	1E-9	9E-08	2370	1E-05	8E+00	3.0
Mean	3E-11	2E-09	2357	2E-06	6E-01	2.1
Median	8E-12	4.E-12	2357	7E-07	6E-02	2.1
Geometric mean	8E-12	6E-12	2357	3E-07	9E-02	2.0



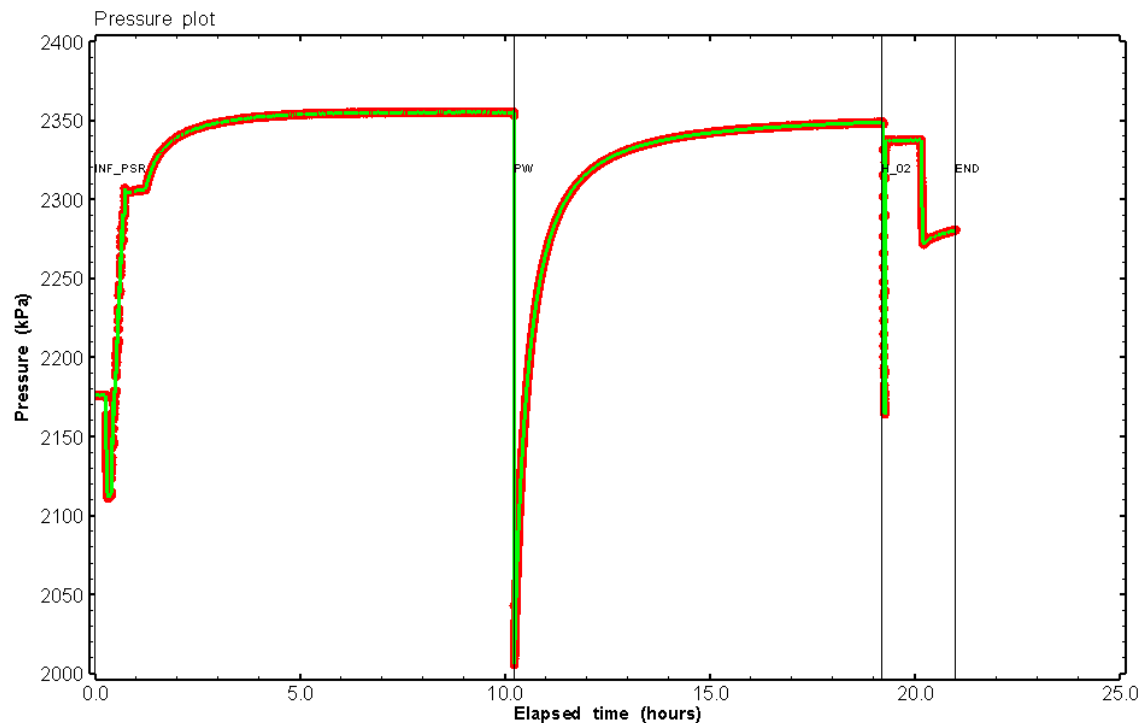


Figure 39: HT004 Pressure plot showing best-fit simulation and best fit results

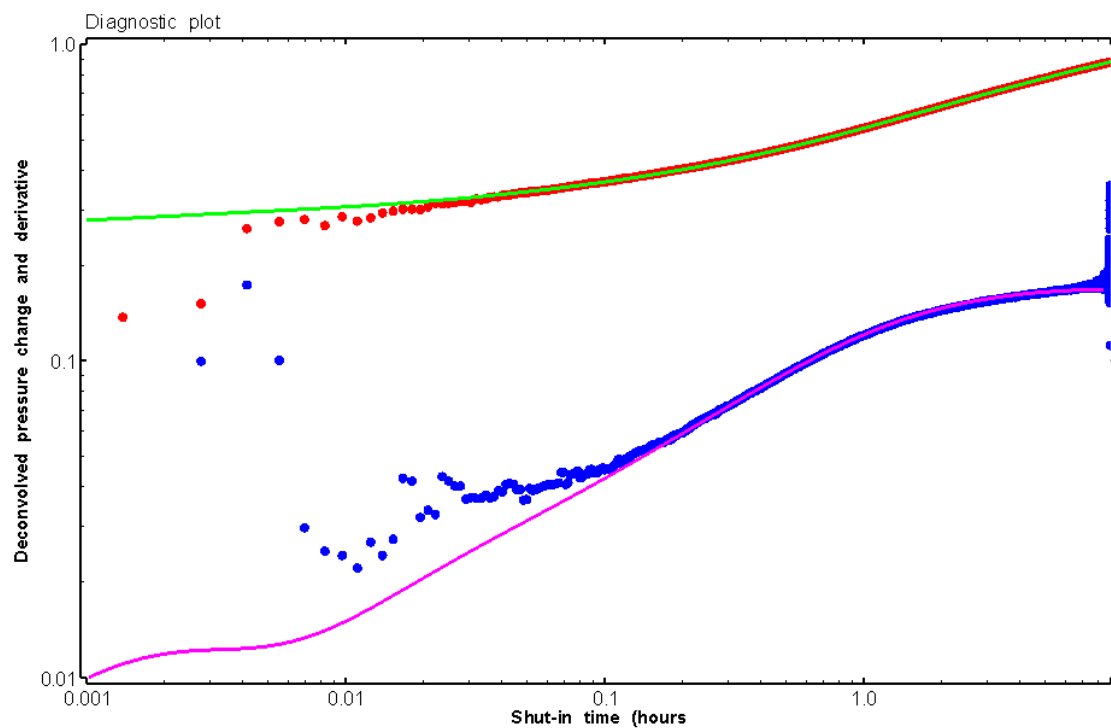


Figure 40: HT004 Deconvolved pressure change and derivative plot of the PW sequence showing best-fit simulation

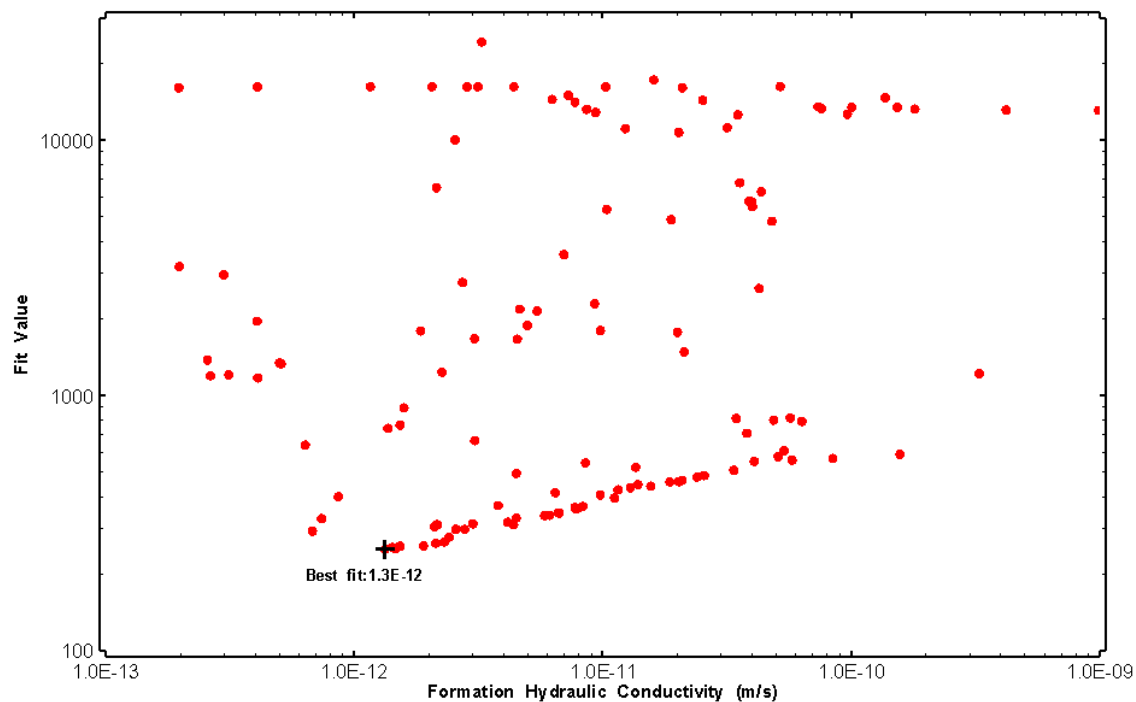


Figure 41: HT004 XY-scatter plot of formation hydraulic conductivity vs. fit value

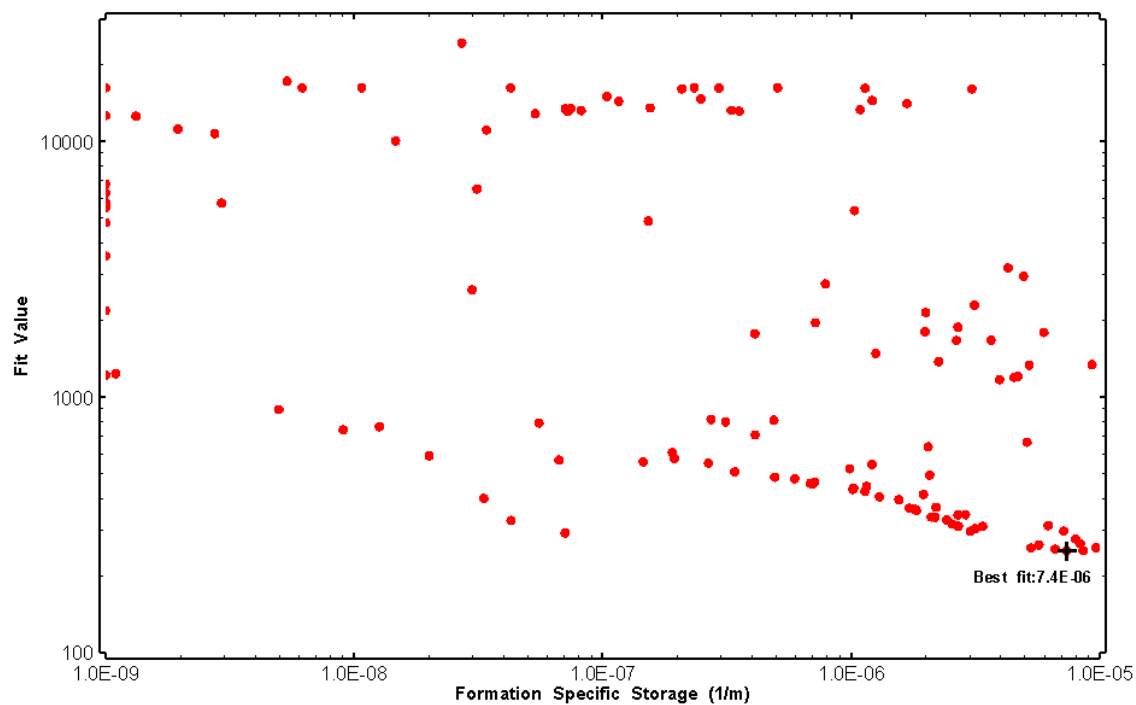


Figure 42: HT004 XY-scatter plot of formation specific storage vs. fit value

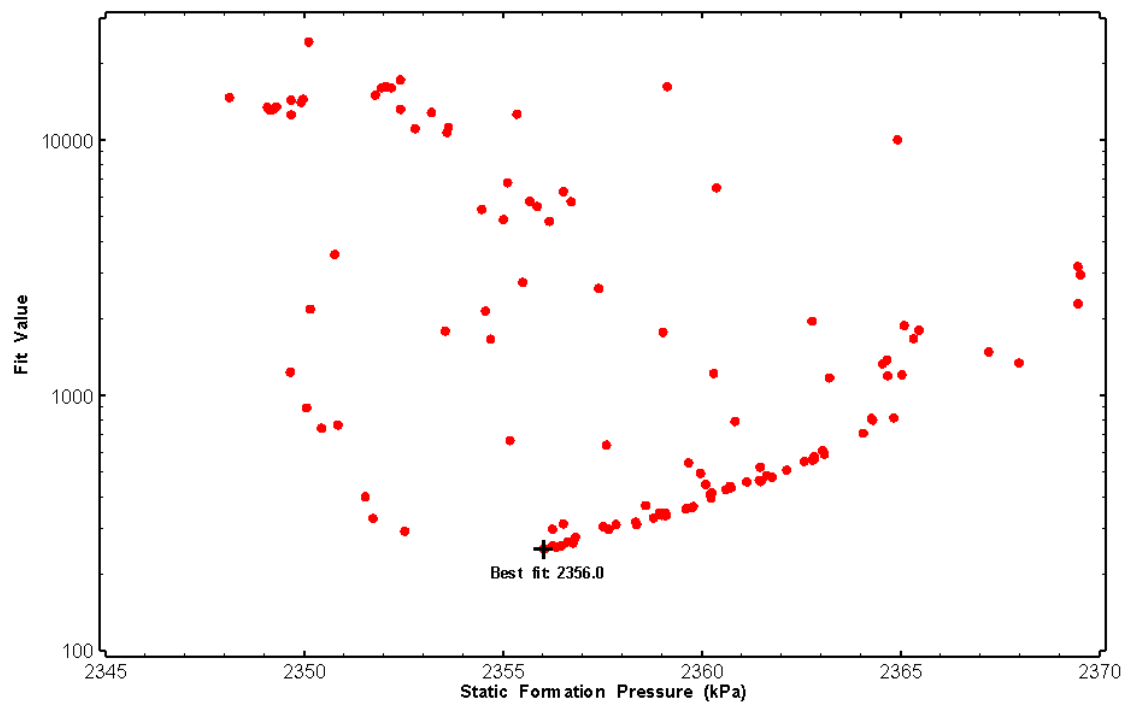


Figure 43: HT004 XY-scatter plot of static formation pressure vs. fit value

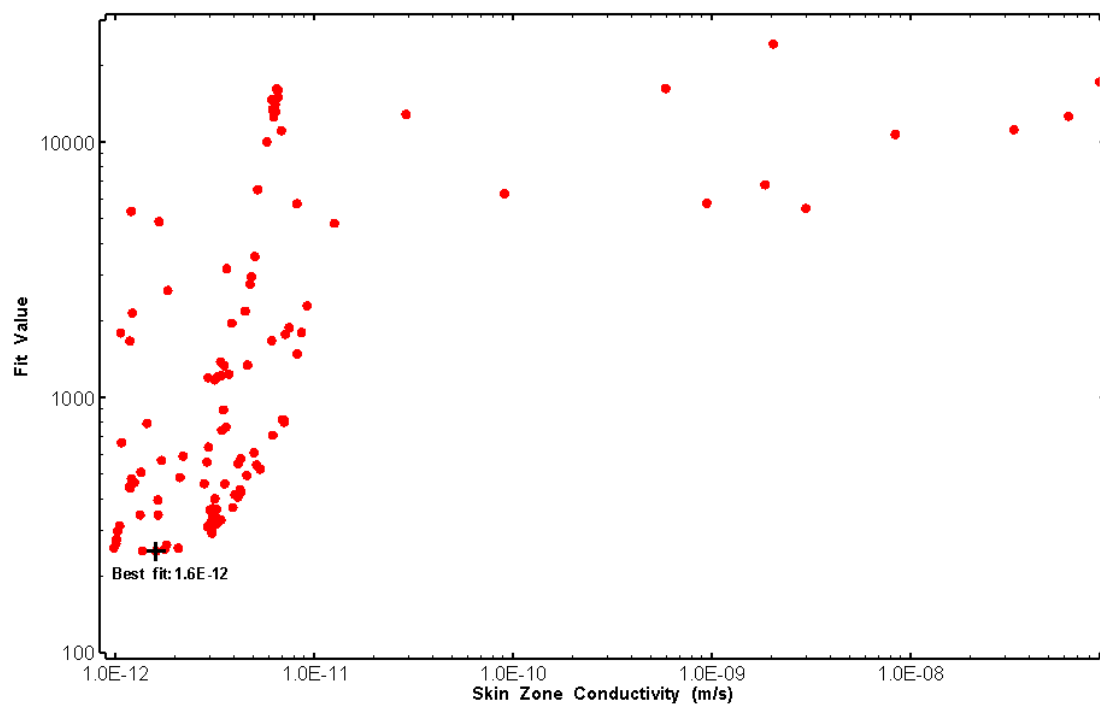


Figure 44: HT004 XY-scatter plot of skin zone conductivity vs. fit value

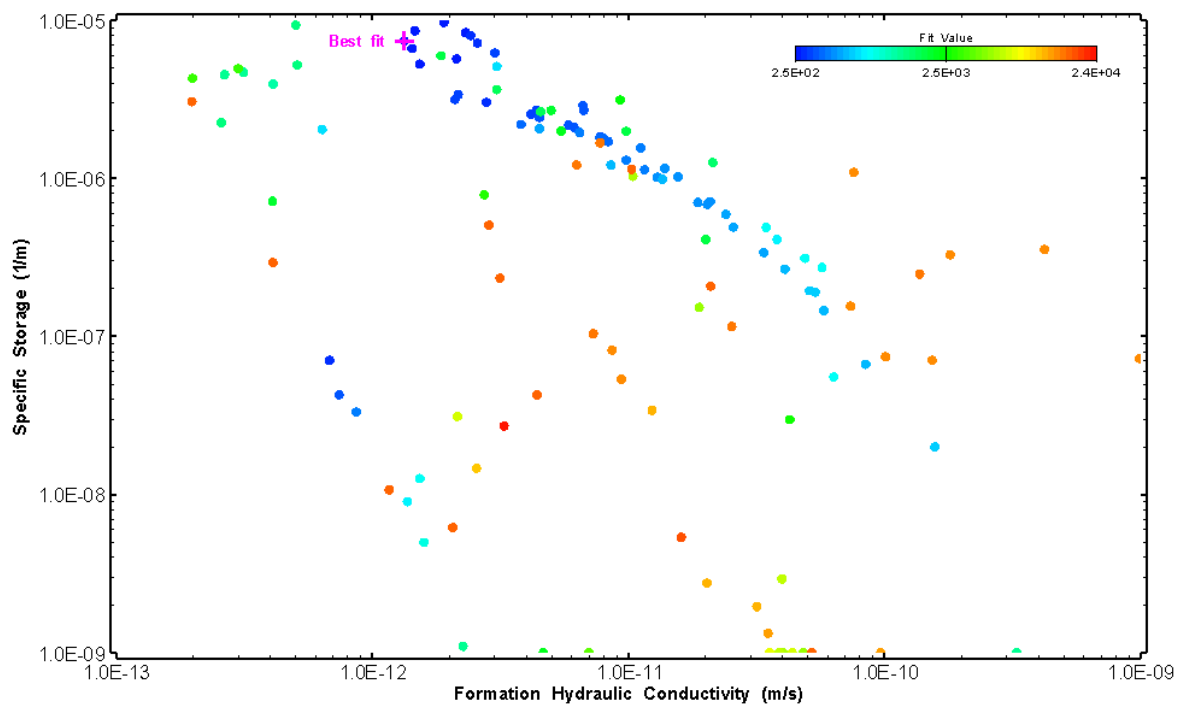


Figure 45: HT004 XY-scatter plot showing estimates of formation hydraulic conductivity and specific storage from perturbation analysis

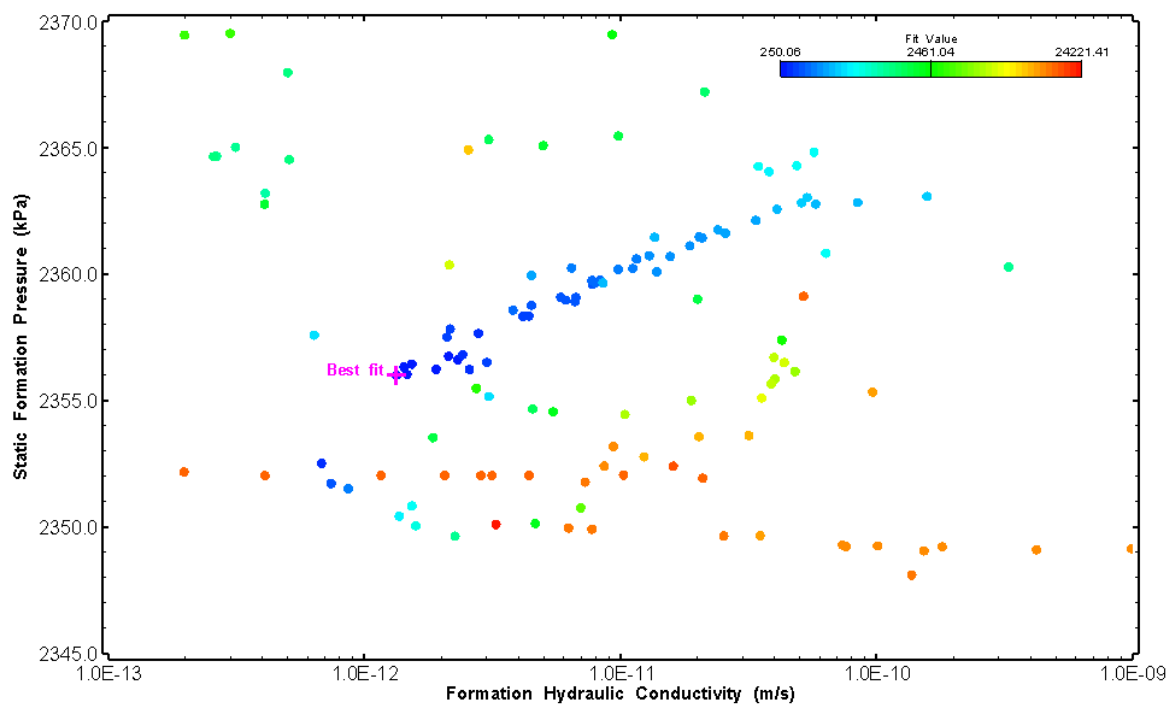


Figure 46: HT004 XY-scatter plot showing estimates of formation hydraulic conductivity and static formation pressure from perturbation analysis

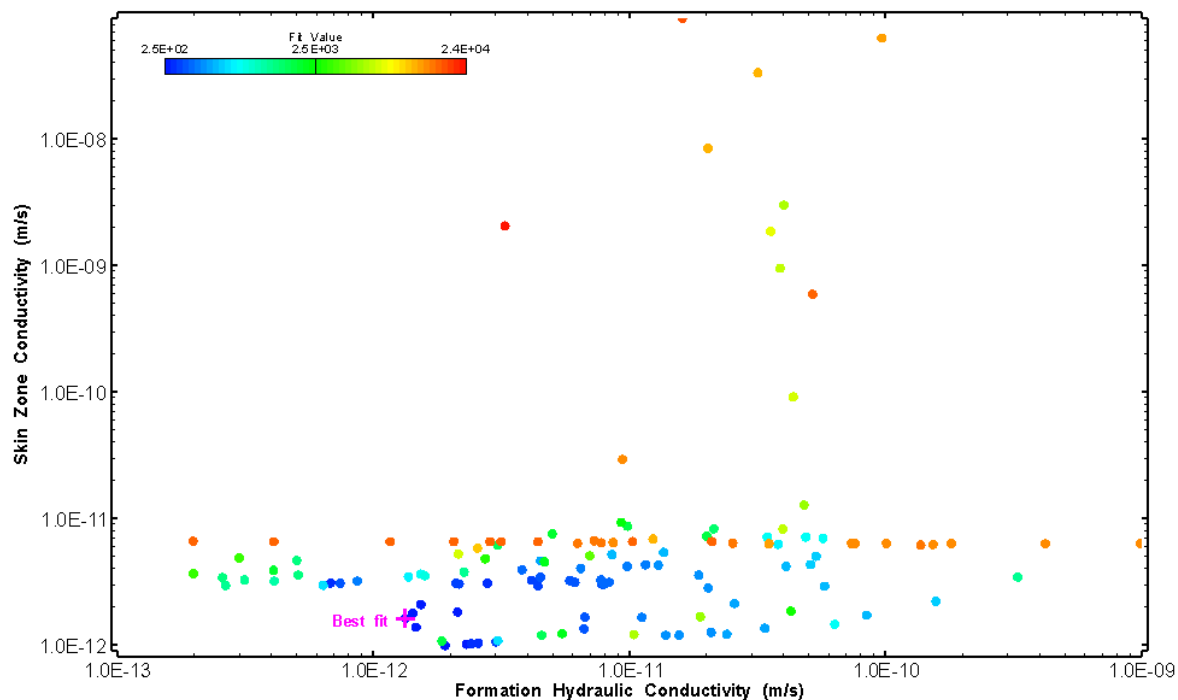


Figure 47: HT004 XY-scatter plot showing estimates of formation hydraulic conductivity and skin zone conductivity from perturbation analysis

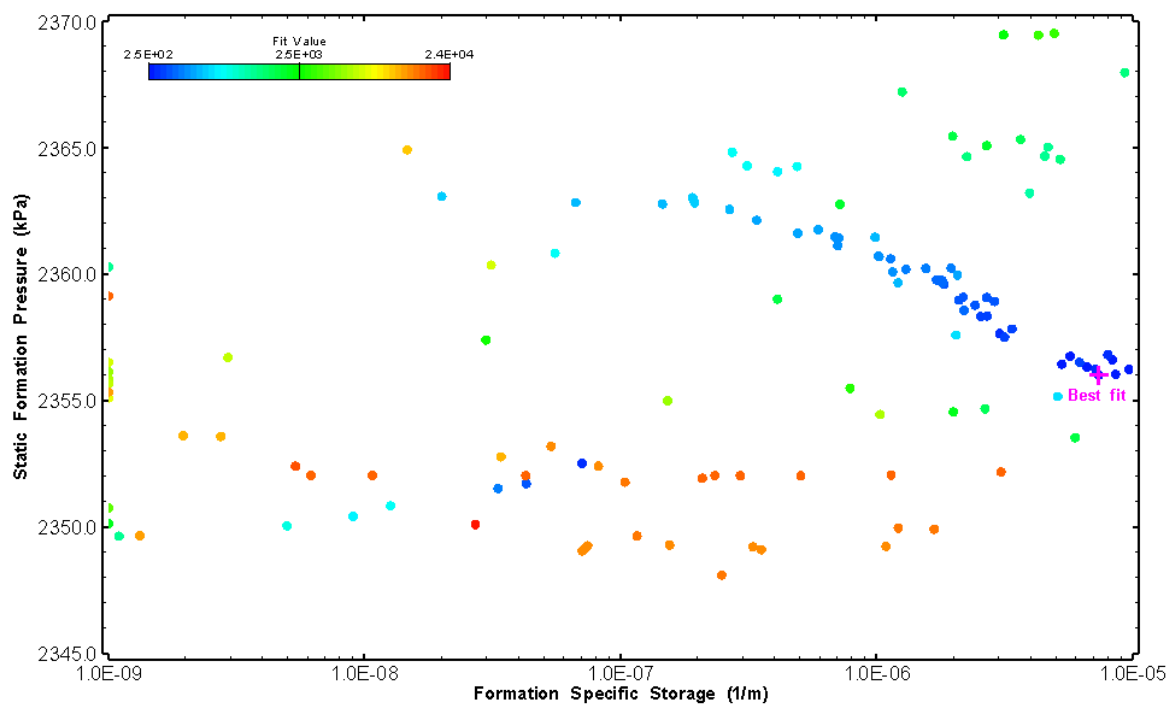


Figure 48: HT004 XY-scatter plot showing estimates of specific storage and static formation pressure from perturbation analysis

## 5.0 HT005 (280.70 – 300.72 M)

HT005 was selected to test a shallow fractured interval containing a dyke. 33 broken fractures were observed in the core. No drill fluid parameter triggers were reached during drilling. No indication of flow was recorded during FFEC logging post-drilling.

The test was initiated with a shut-in pressure recovery phase (PSR). A pulse withdrawal test (PW) with a shut-in recovery was completed after the PSR phase.

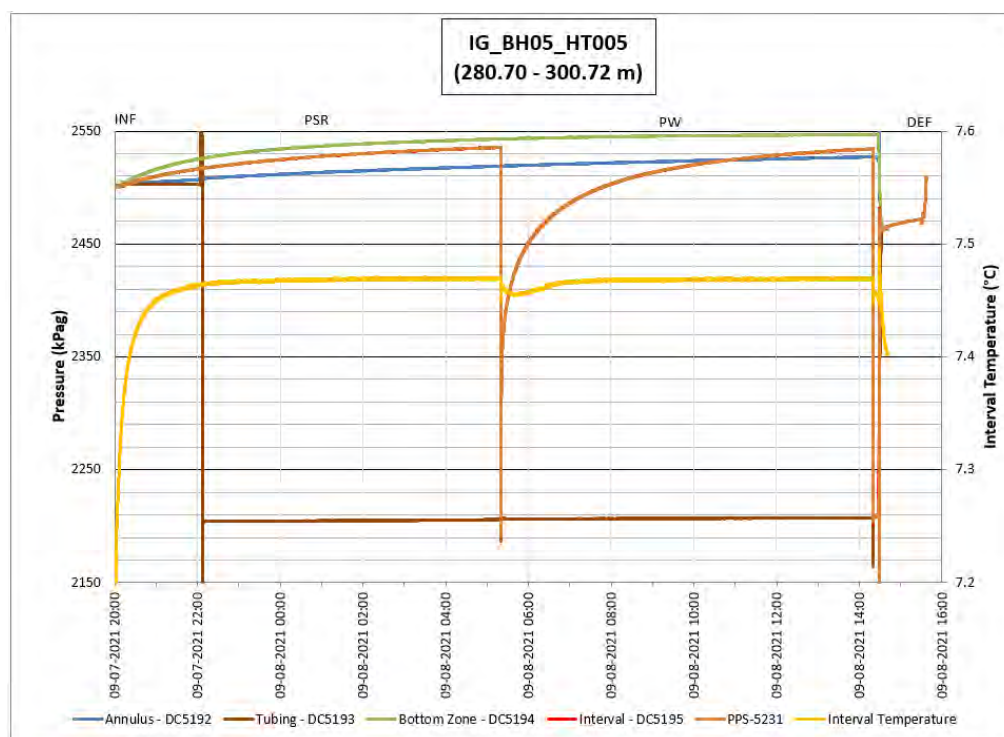
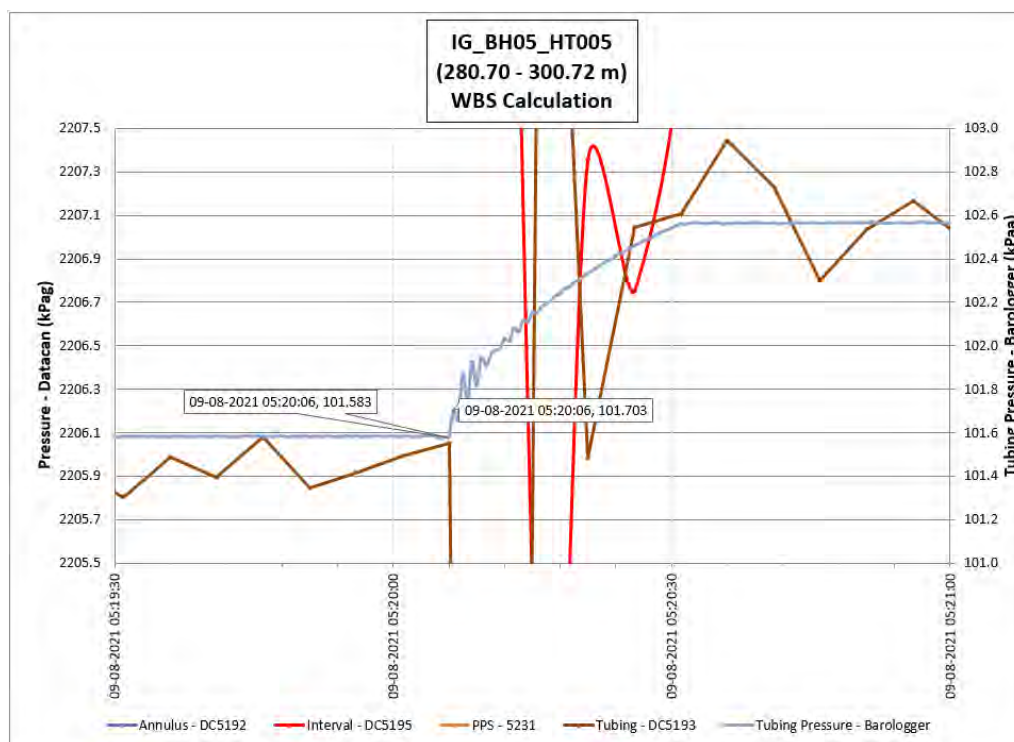


Figure 49: HT005 Annotated test plot showing monitored zone pressure and interval temperature.



**Figure 50: HT005 Tubing pressure during DHSIV activation. DHSIV Closed Wellbore Storage Estimate =  $2\text{E-}10 \text{ m}^3/\text{Pa}$**

**Table 5: Summary of Analysis Results – HT005**

	Formation conductivity	Skin zone conductivity	Static formation pressure	Formation specific storage	Radial thickness of skin	Flow dimension
	[m/s]	[m/s]	[kPa]	[1/m]	[m]	[–]
Best Fit	5E-12	1E-09	2558	2E-07	5.03E-01	2.2
Minimum	1E-13	5E-11	2539	1E-09	1E-02	1.1
Maximum	1E-09	6E-08	2600	1E-05	1E+01	3.0
Mean	6E-11	3E-09	2562	6E-07	9E-01	2.0
Median	9E-12	2E-09	2560	1E-07	6E-01	2.0
Geometric mean	1E-11	2E-09	2562	1E-07	7E-01	2.0



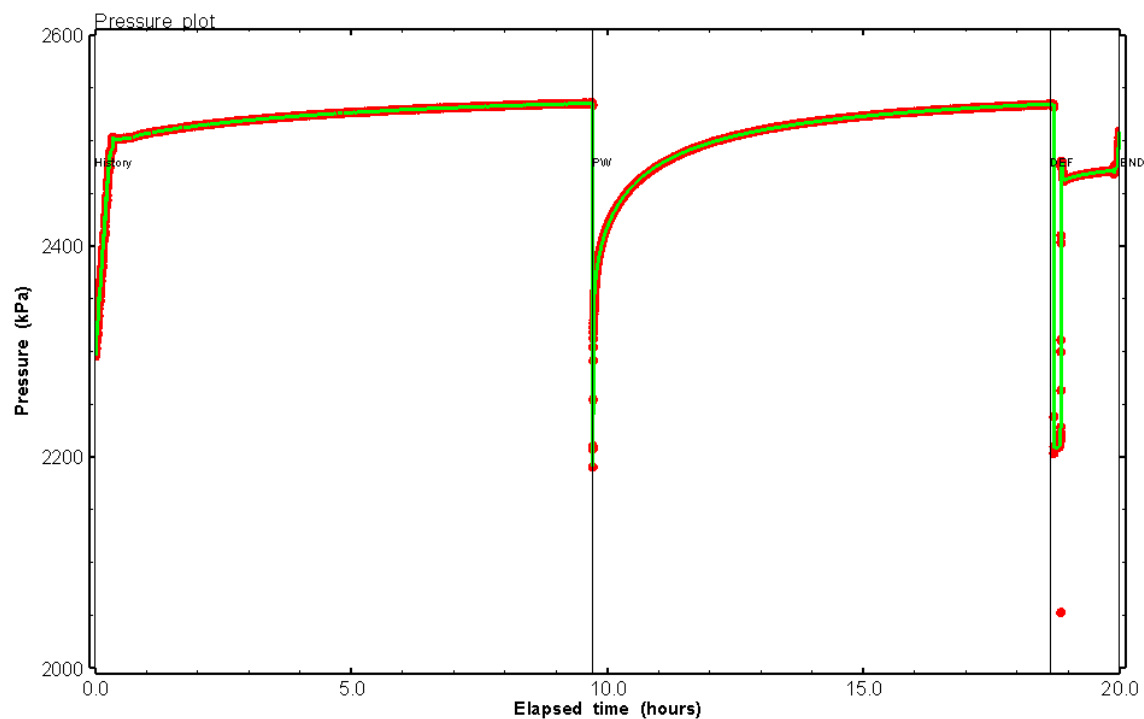


Figure 51: HT005 Pressure plot showing best-fit simulation and best fit results

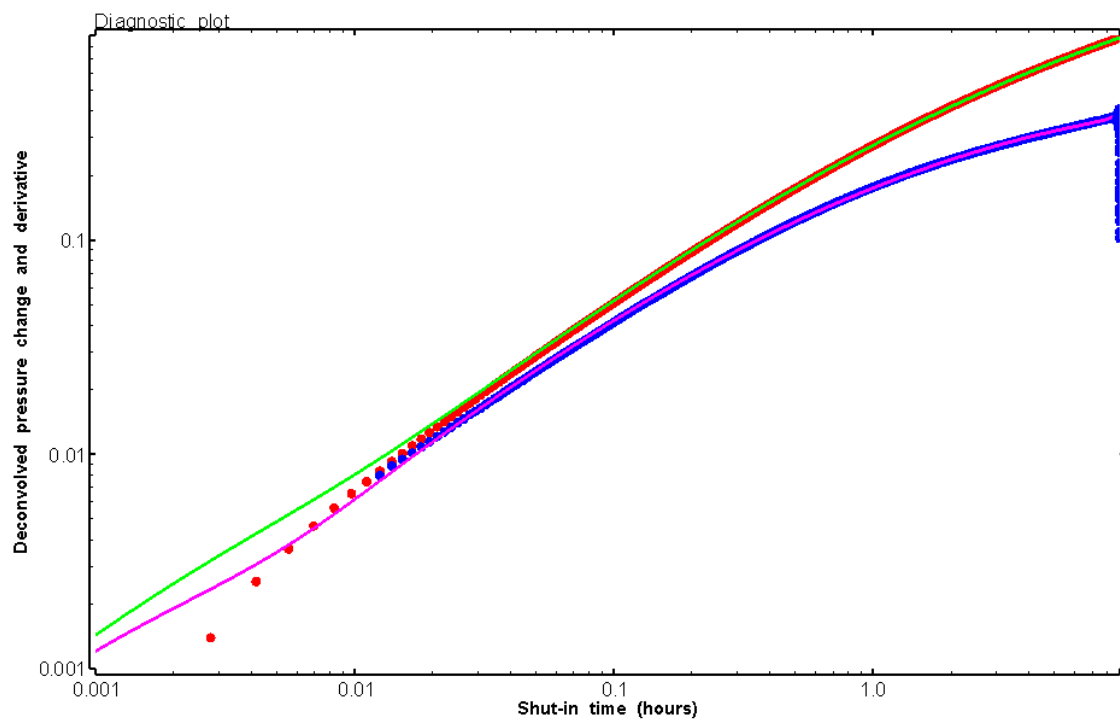


Figure 52: HT005 Deconvolved pressure change and derivative plot of the PW sequence showing best-fit simulation

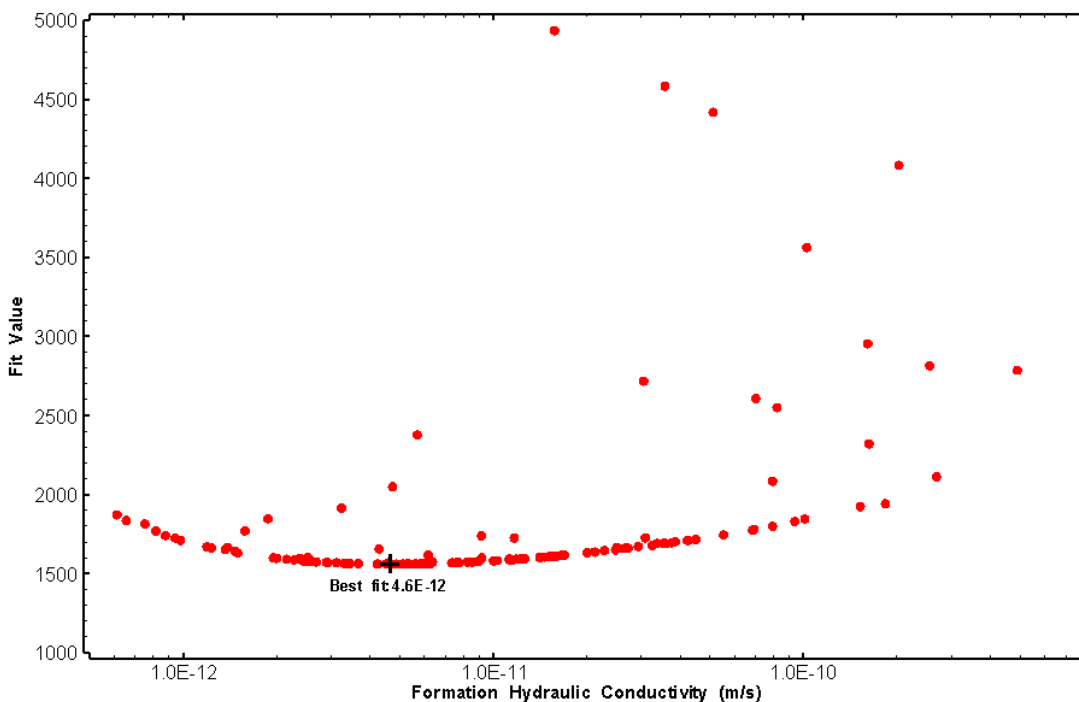


Figure 53: HT005 XY-scatter plot of formation hydraulic conductivity vs. fit value

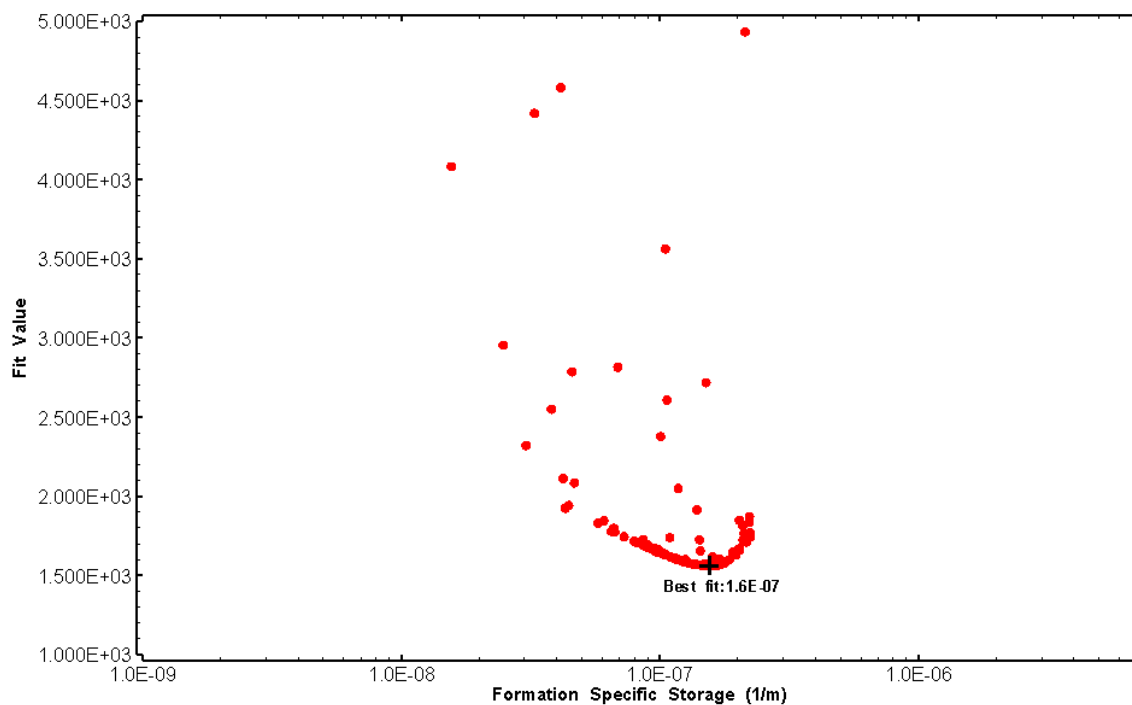


Figure 54: HT005 XY-scatter plot of formation specific storage vs. fit value

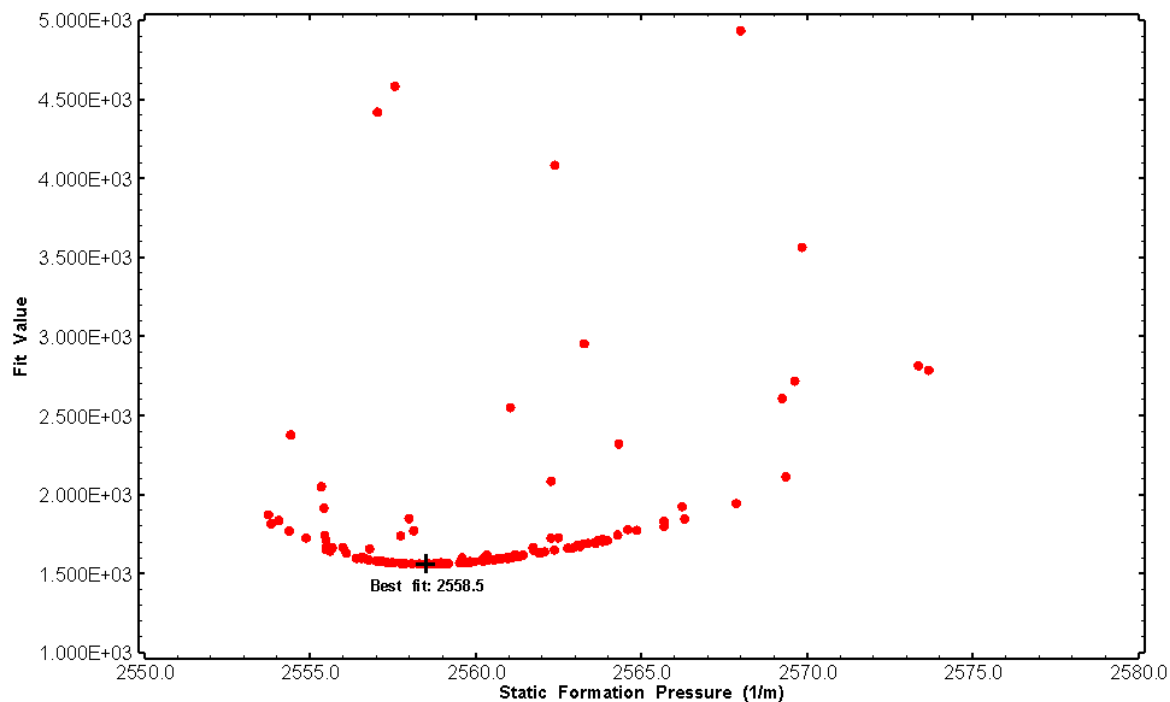


Figure 55: HT005 XY-scatter plot of static formation pressure vs. fit value

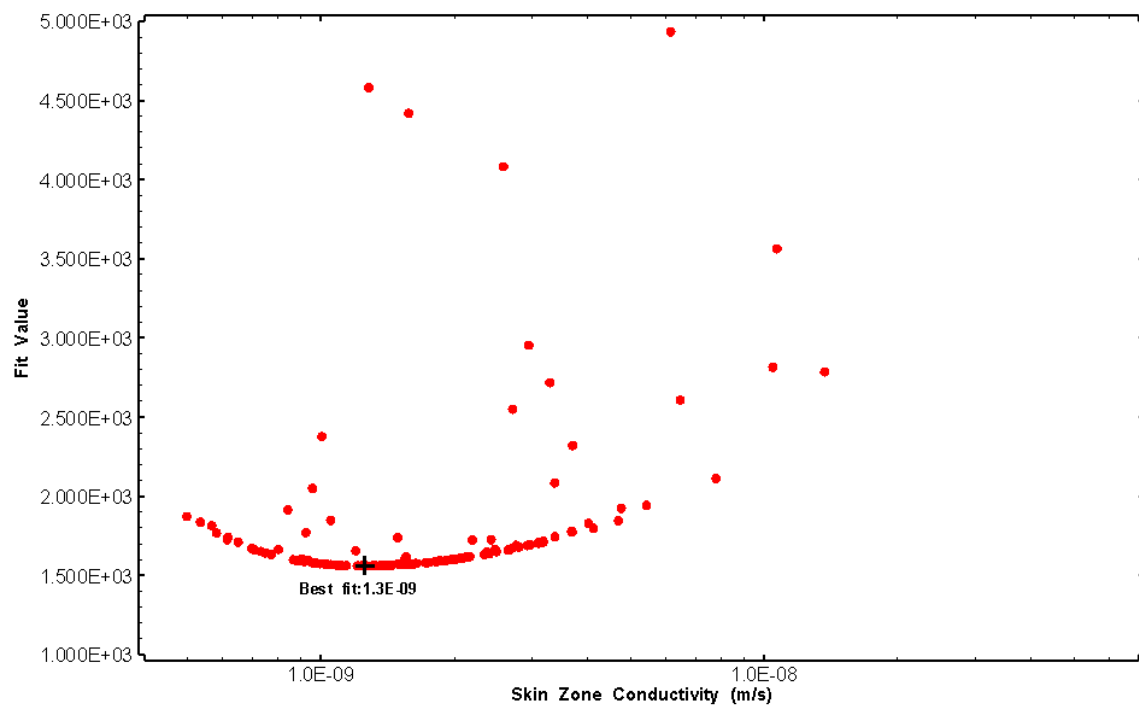


Figure 56: HT005 XY-scatter plot of skin zone conductivity vs. fit value

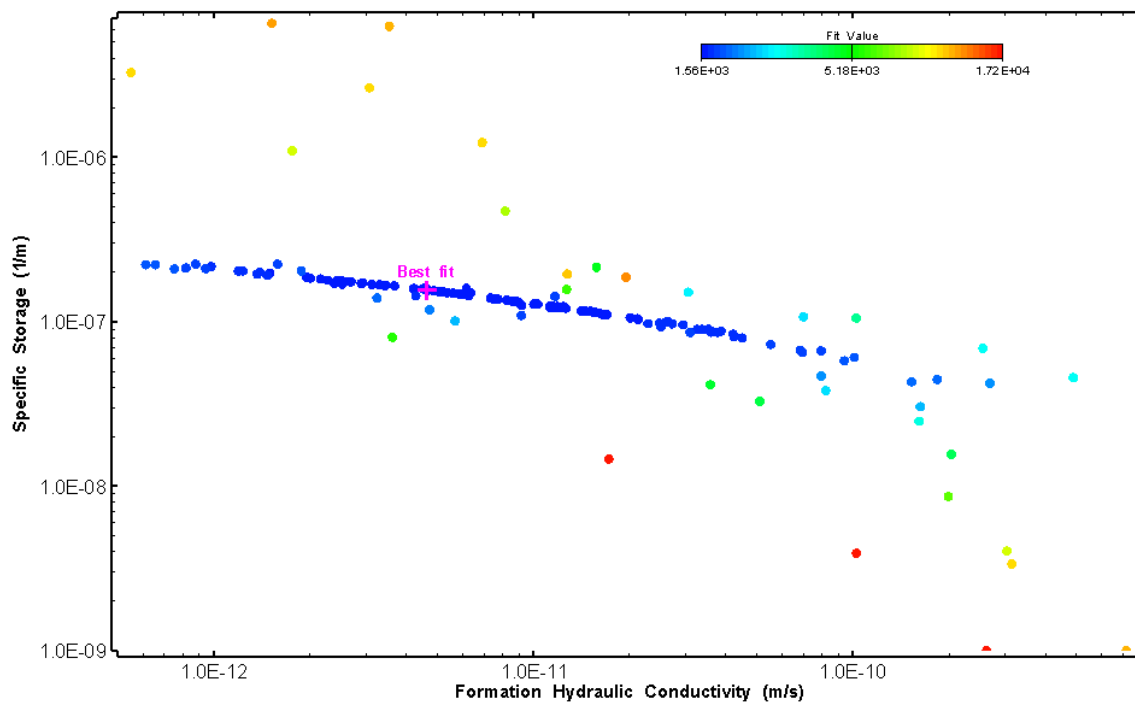


Figure 57: HT005 XY-scatter plot showing estimates of formation hydraulic conductivity and specific storage from perturbation analysis

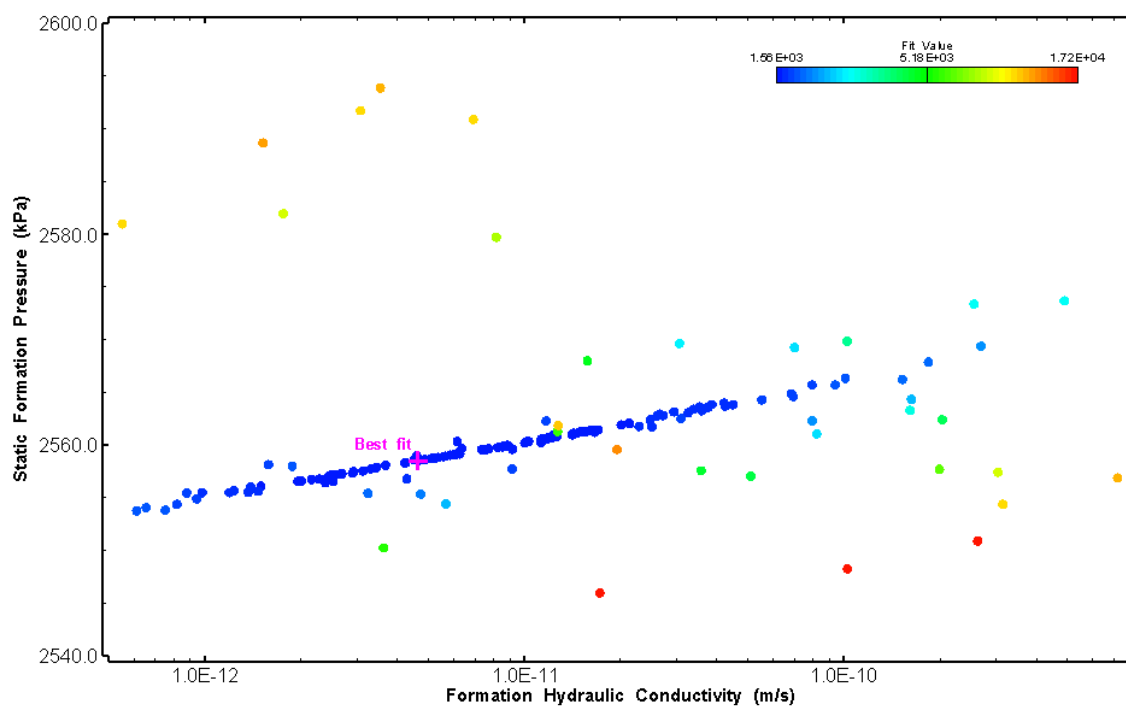


Figure 58: HT005 XY-scatter plot showing estimates of formation hydraulic conductivity and static formation pressure from perturbation analysis

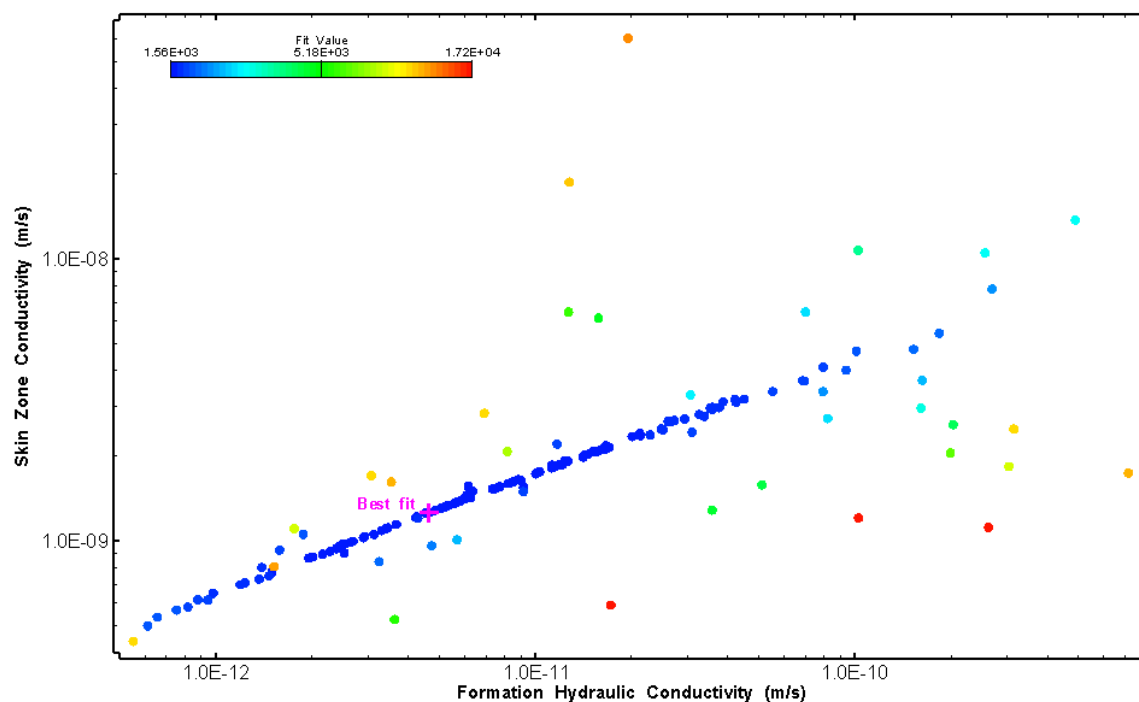


Figure 59: HT005 XY-scatter plot showing estimates of formation hydraulic conductivity and skin zone conductivity from perturbation analysis

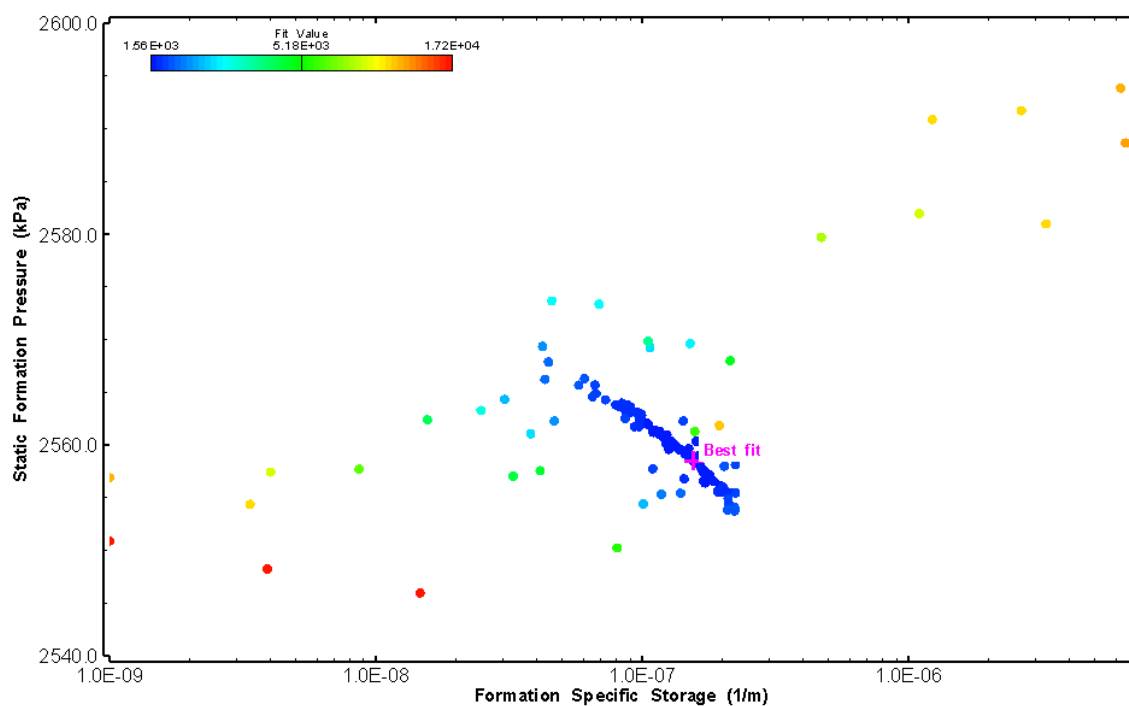


Figure 60: HT005 XY-scatter plot showing estimates of specific storage and static formation pressure from perturbation analysis

## 6.0 HT006 (309.00 – 329.02 M)

HT006 was selected to test a shallow fractured interval containing a dyke. 19 broken fractures were observed in the core. An indication of flow was recorded during FFEC logging post-drilling.

The test was initiated with a shut-in pressure recovery phase (PSR). A pulse withdrawal test (PW) with a shut-in recovery was completed after the PSR phase.

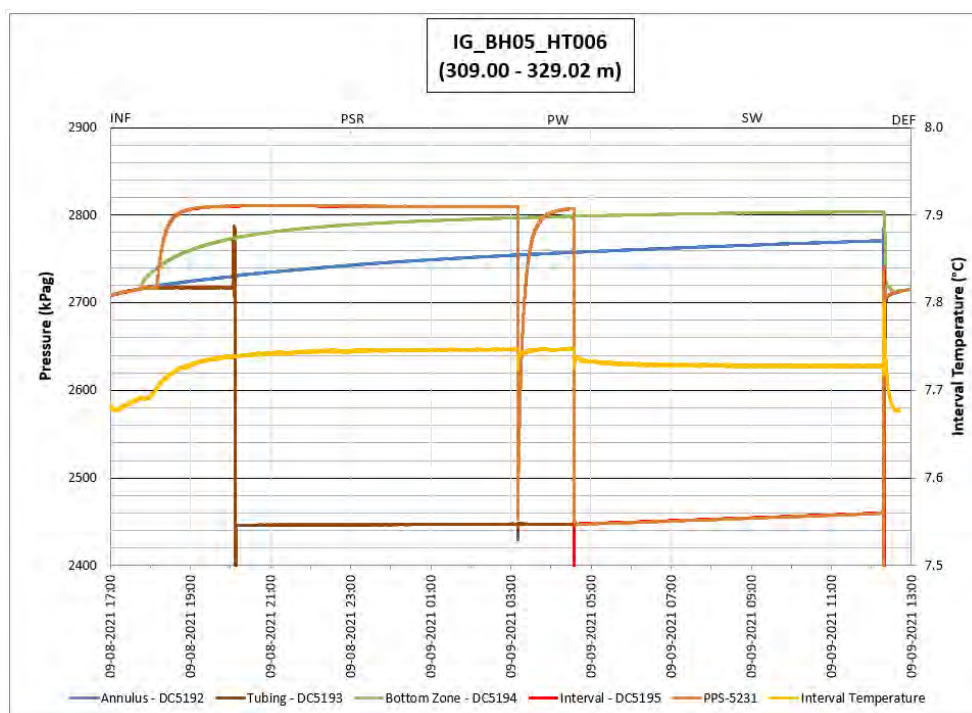
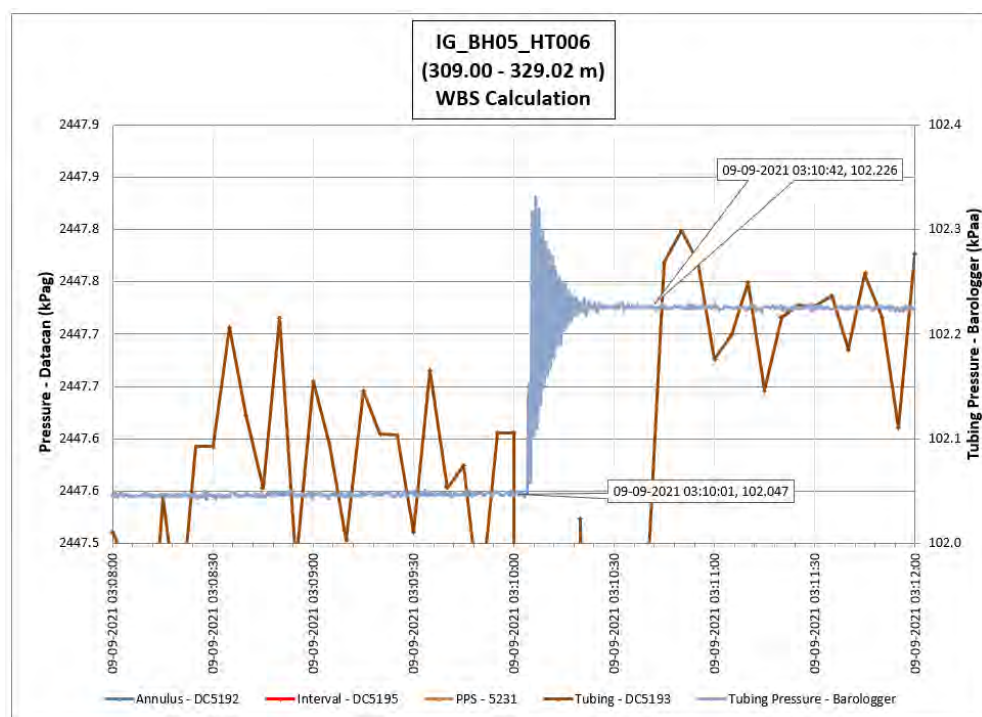


Figure 61: HT006 Annotated test plot showing monitored zone pressure and interval temperature.



**Figure 62: HT006 Tubing pressure during DHSIV activation. DHSIV Closed Wellbore Storage Estimate =  $9\text{E-}11 \text{ m}^3/\text{Pa}$**

**Table 6: Summary of Analysis Results – HT006**

	Formation conductivity	Skin zone conductivity	Static formation pressure	Formation specific storage	Radial thickness of skin	Flow dimension
	[m/s]	[m/s]	[kPa]	[1/m]	[m]	[–]
Best Fit	1E-11	1E-09	2808	4E-09	8.83E-02	2.8
Minimum	1E-11	1E-13	2804	1E-09	1E-04	1.4
Maximum	1E-08	1E-9	2811	1E-05	4E-01	3.0
Mean	8E-10	5E-11	2806	3E-07	2E-01	2.3
Median	2E-10	2E-11	2806	5E-08	2E-01	2.3
Geometric mean	2E-10	2E-11	2806	5E-08	1E-01	2.3



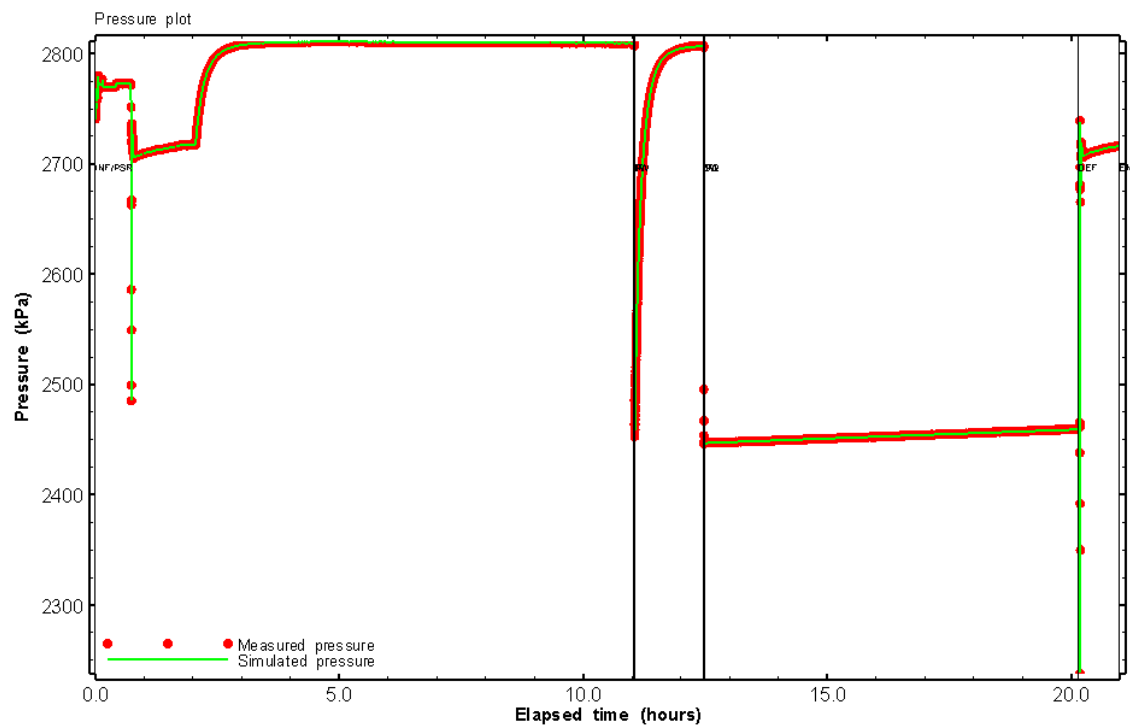


Figure 63: HT006 Pressure plot showing best-fit simulation and best fit results

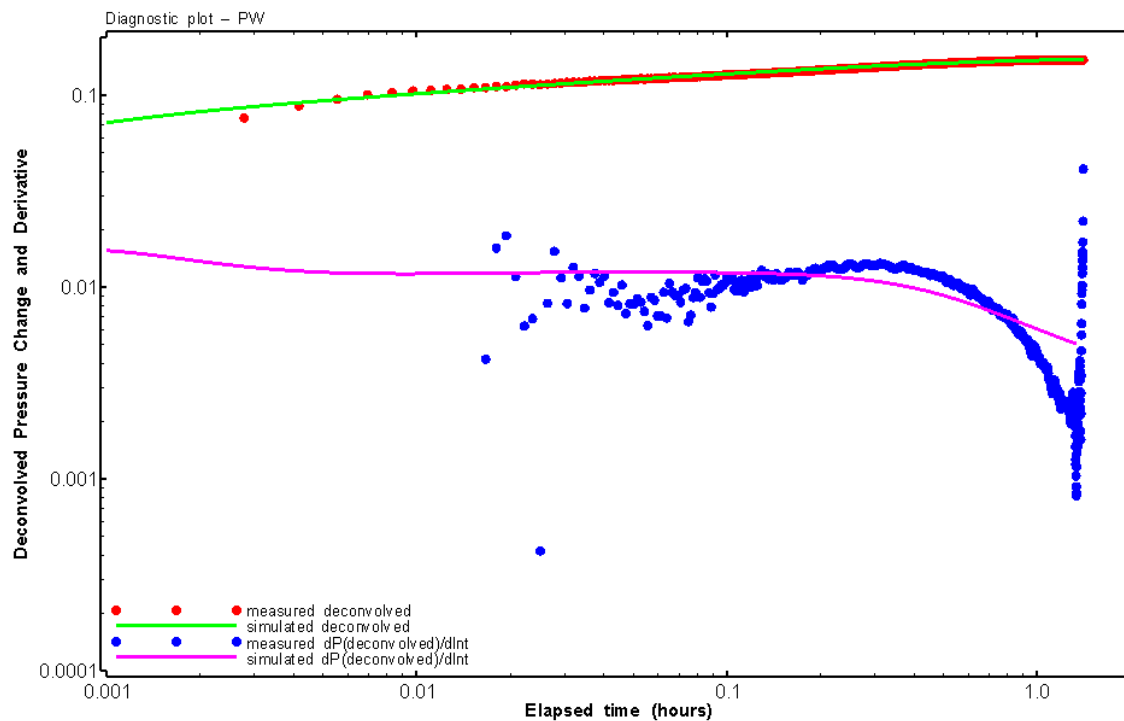


Figure 64: HT006 Deconvolved pressure change and derivative plot of the PW sequence showing best-fit simulation

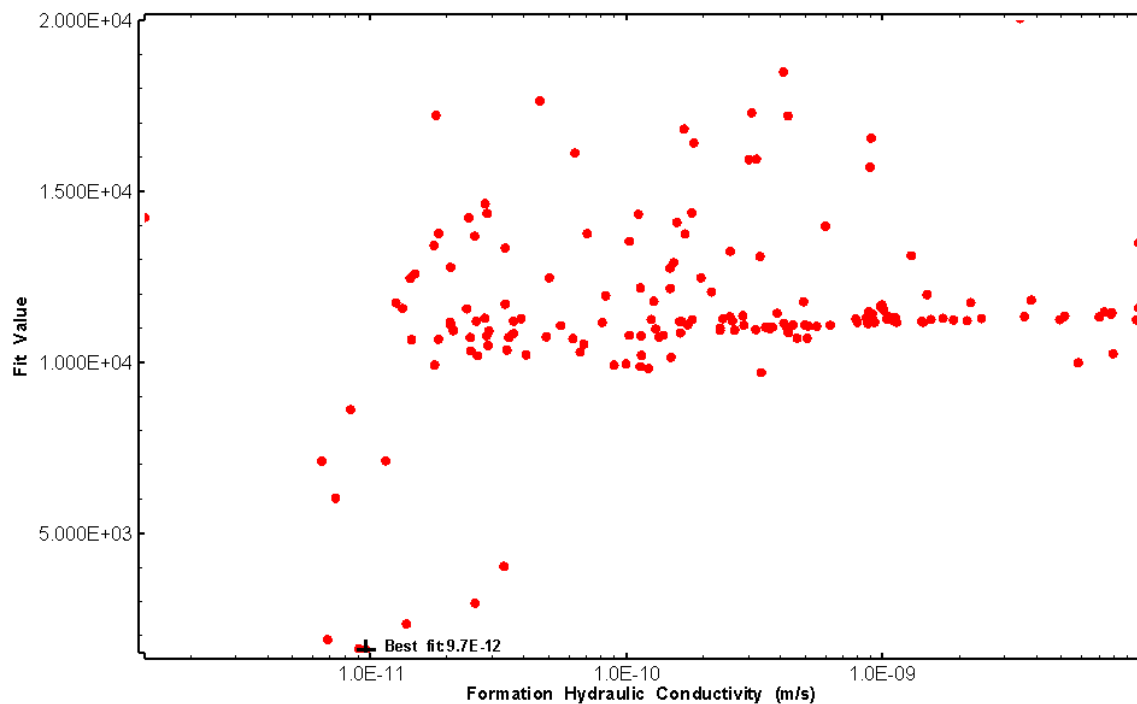


Figure 65: HT006 XY-scatter plot of formation hydraulic conductivity vs. fit value

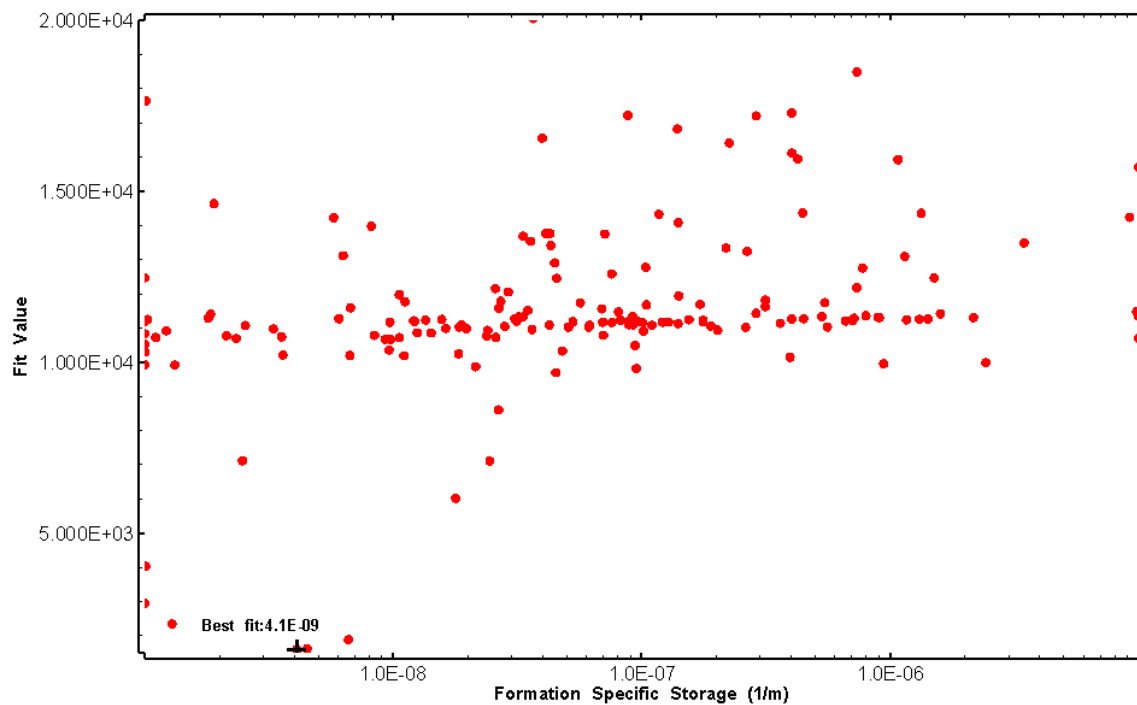


Figure 66: HT006 XY-scatter plot of formation specific storage vs. fit value

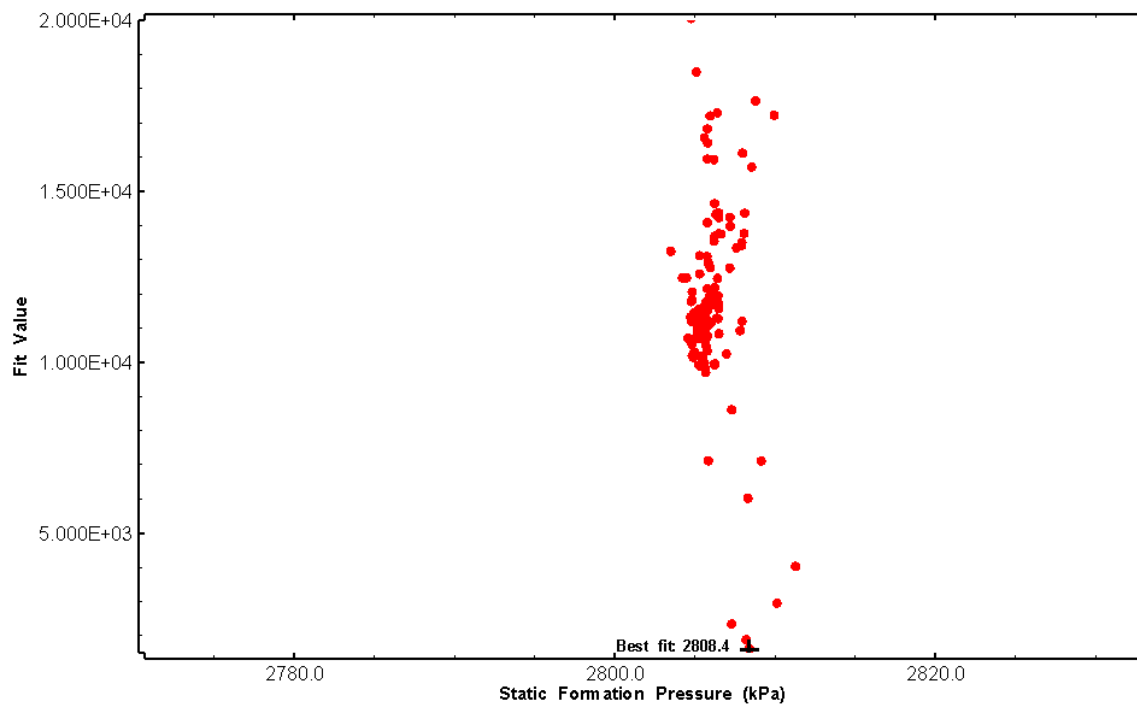


Figure 67: HT006 XY-scatter plot of static formation pressure vs. fit value

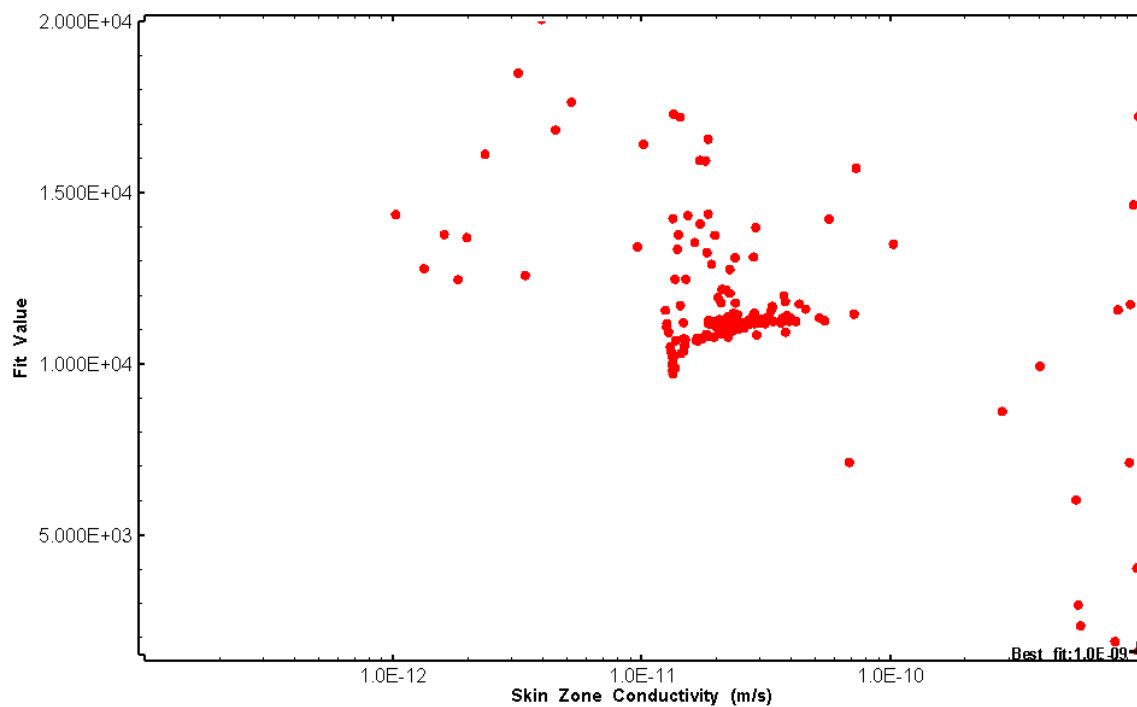


Figure 68: HT006 XY-scatter plot of skin zone conductivity vs. fit value

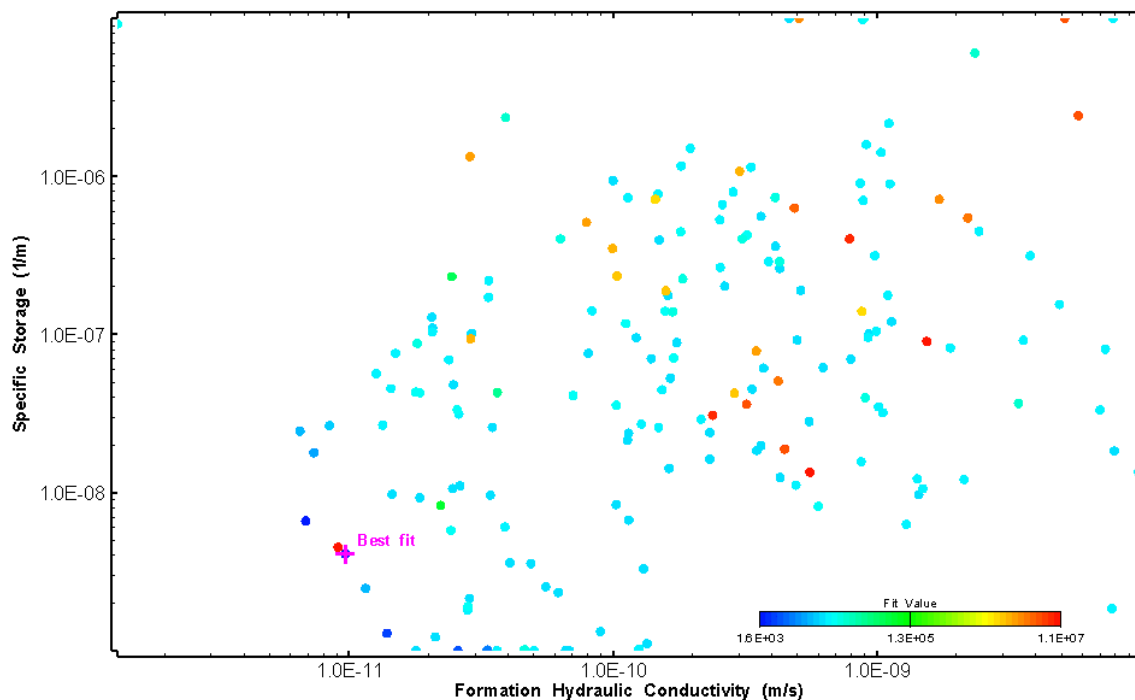


Figure 69: HT006 XY-scatter plot showing estimates of formation hydraulic conductivity and specific storage from perturbation analysis

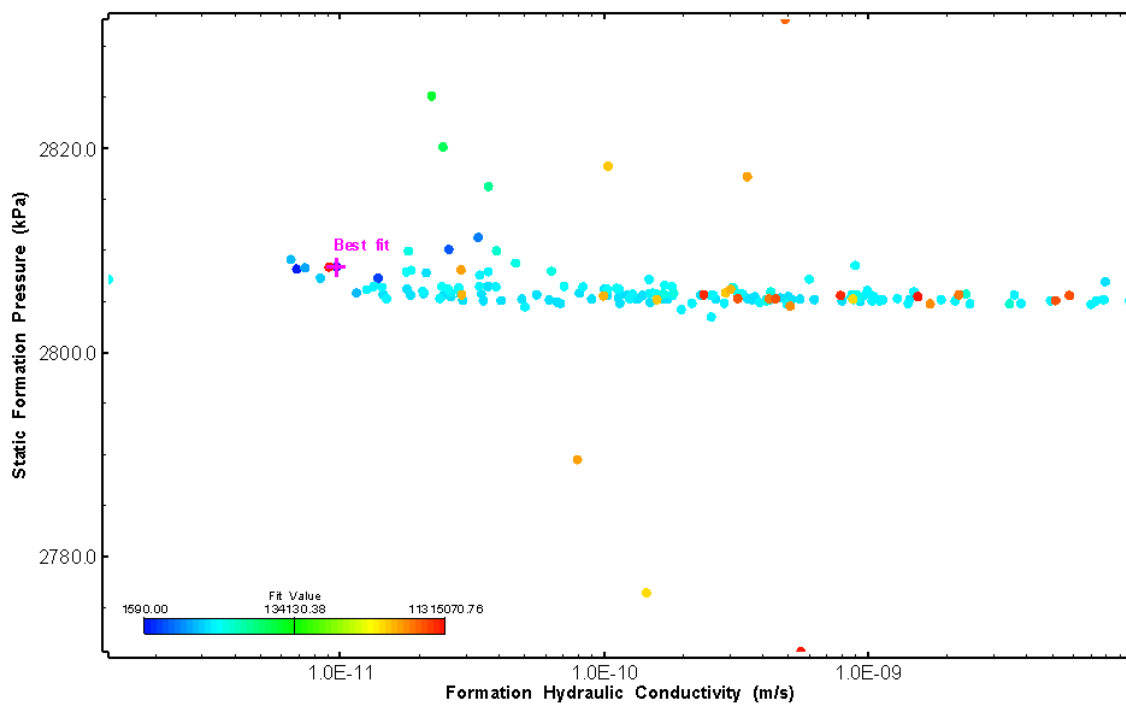


Figure 70: HT006 XY-scatter plot showing estimates of formation hydraulic conductivity and static formation pressure from perturbation analysis

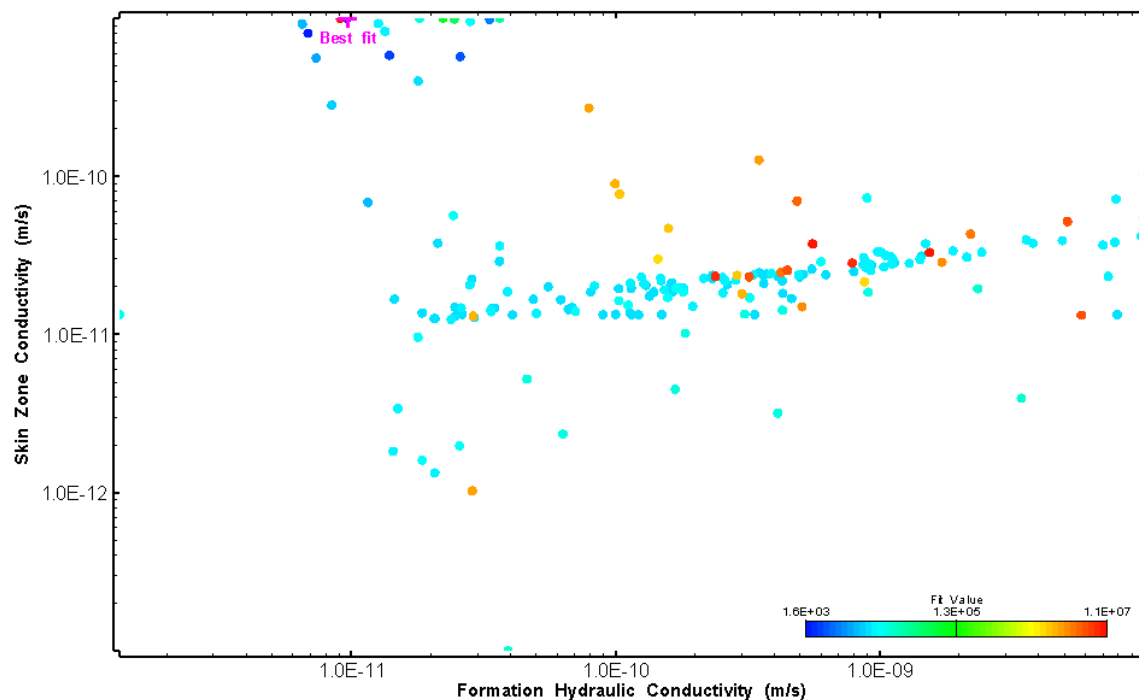


Figure 71: HT006 XY-scatter plot showing estimates of formation hydraulic conductivity and skin zone conductivity from perturbation analysis

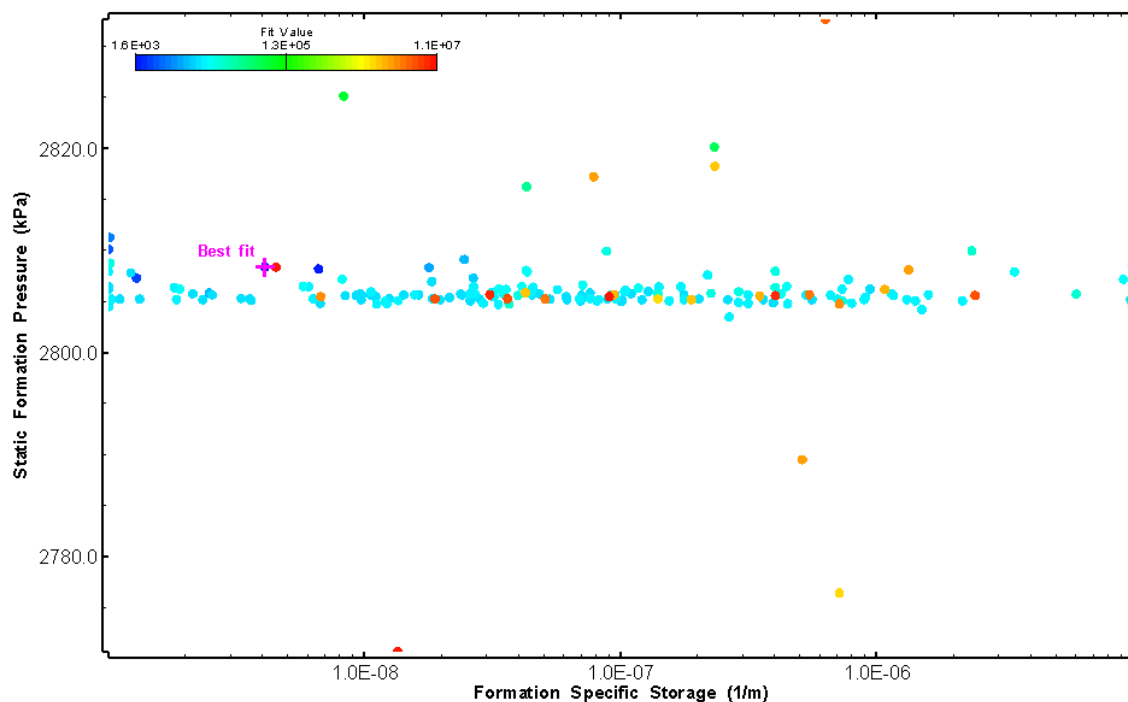


Figure 72: HT006 XY-scatter plot showing estimates of specific storage and static formation pressure from perturbation analysis

## 7.0 HT007 (347.05 – 367.07 M)

HT007 was selected to test a fractured interval with a dyke. 19 broken fractures were observed in the core. No drill fluid parameter triggers were reached during drilling. No indication of flow was recorded during FFEC logging post-drilling.

The test was initiated with a shut-in pressure recovery phase (PSR). A pulse withdrawal test (PW) with a shut-in recovery was completed after the PSR phase.

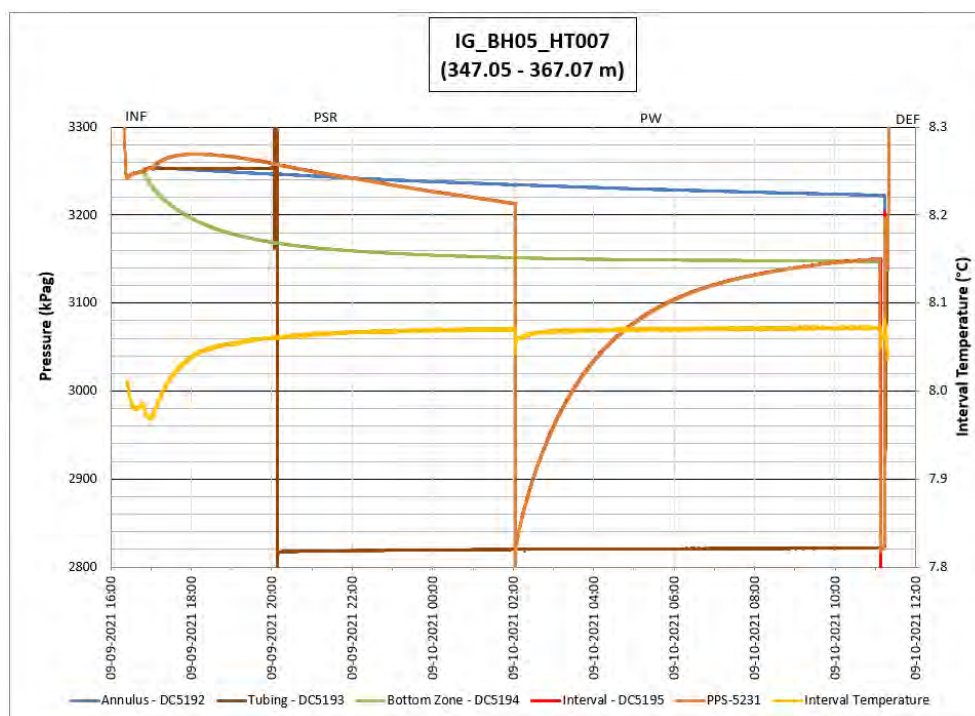
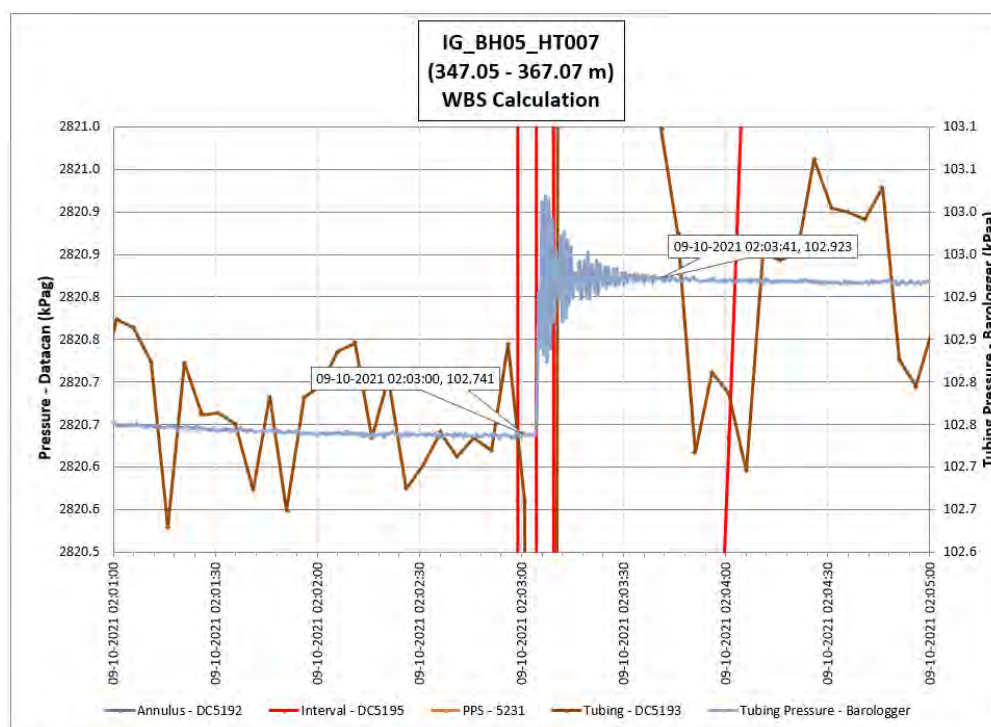


Figure 73: HT007 Annotated test plot showing monitored zone pressure and interval temperature.



**Figure 74: HT007 Tubing pressure during DHSIV activation. DHSIV Closed Wellbore Storage Estimate =  $8\text{E-}11 \text{ m}^3/\text{Pa}$**

**Table 7: Summary of Analysis Results – HT007**

	Formation conductivity	Skin zone conductivity	Static formation pressure	Formation specific storage	Radial thickness of skin	Flow dimension
	[m/s]	[m/s]	[kPa]	[1/m]	[m]	[–]
Best Fit	8E-13	1E-12	3170	4E-06	9.43E-02	2.0
Minimum	4E-13	3E-14	3153	1E-09	1E-03	1.0
Maximum	1E-10	4E-11	3220	8E-06	3E-01	3.0
Mean	6E-12	2E-12	3165	6E-07	5E-02	2.1
Median	3E-12	1E-12	3163	2E-07	4E-02	2.1
Geometric mean	3.E-12	9E-13	3165	2E-07	3E-02	2.0

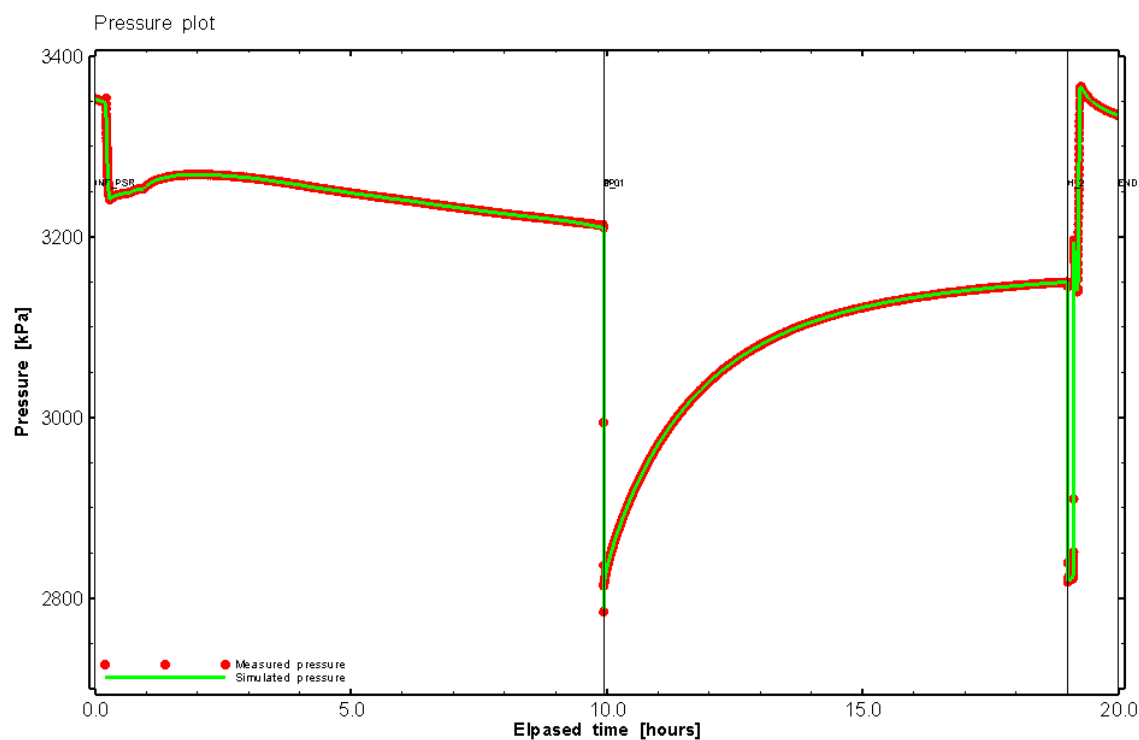


Figure 75: HT007 Pressure plot showing best-fit simulation and best fit results

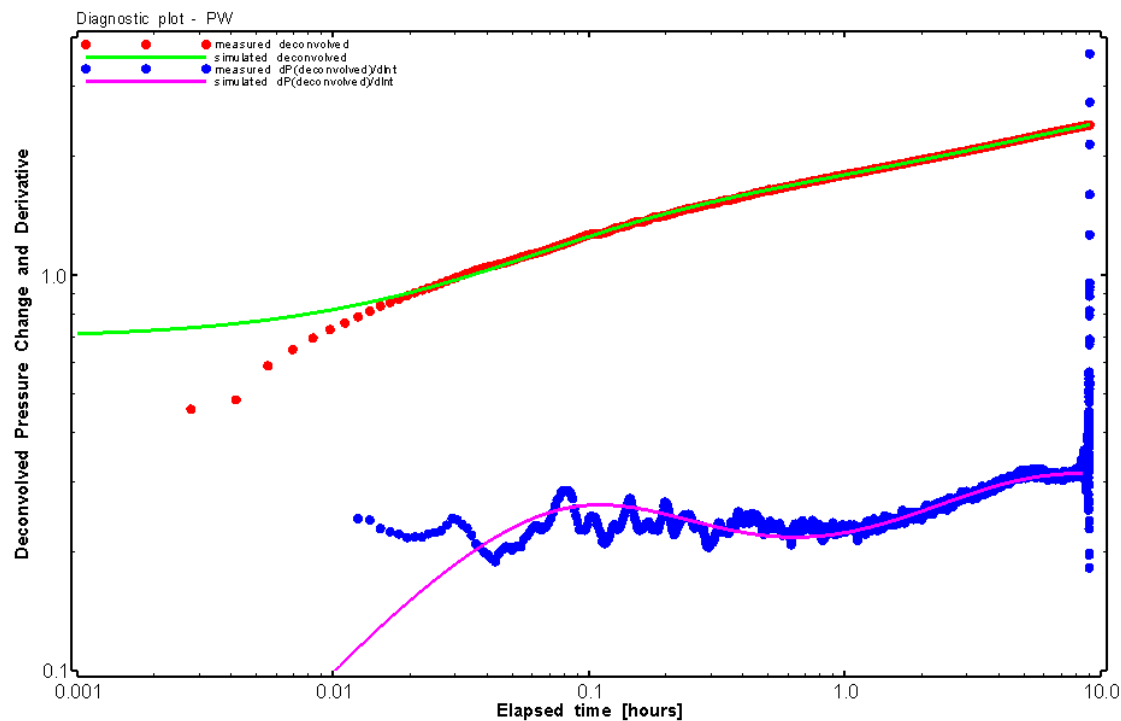


Figure 76: HT007 Deconvolved pressure change and derivative plot of the PW sequence showing best-fit simulation



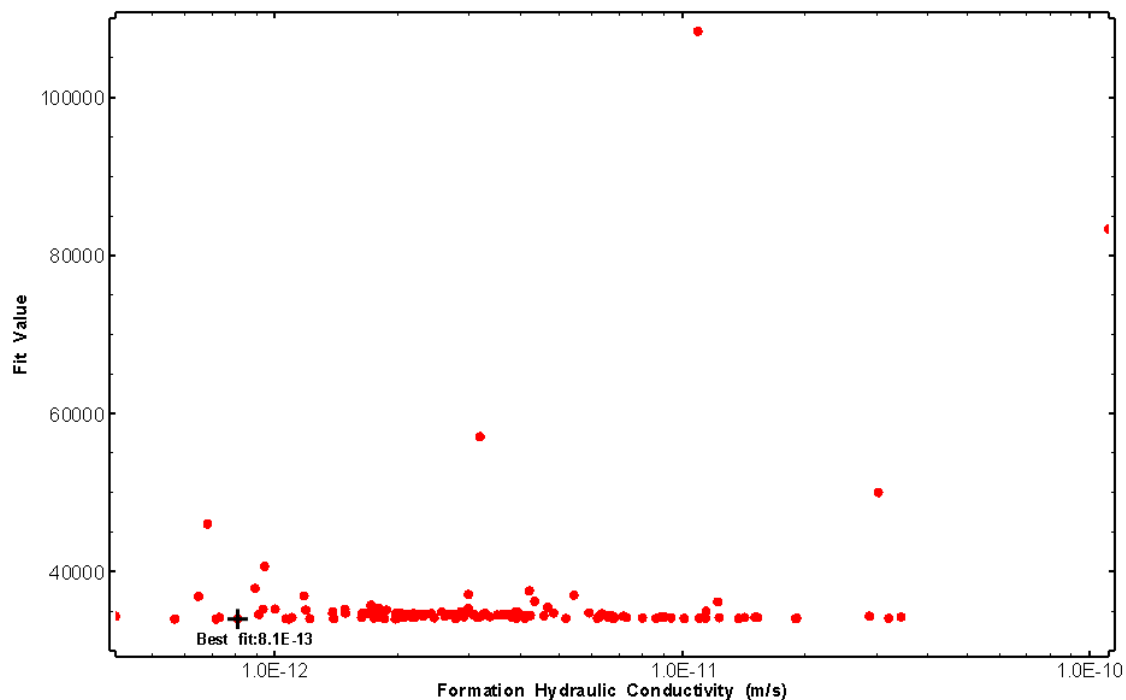


Figure 77: HT007 XY-scatter plot of formation hydraulic conductivity vs. fit value

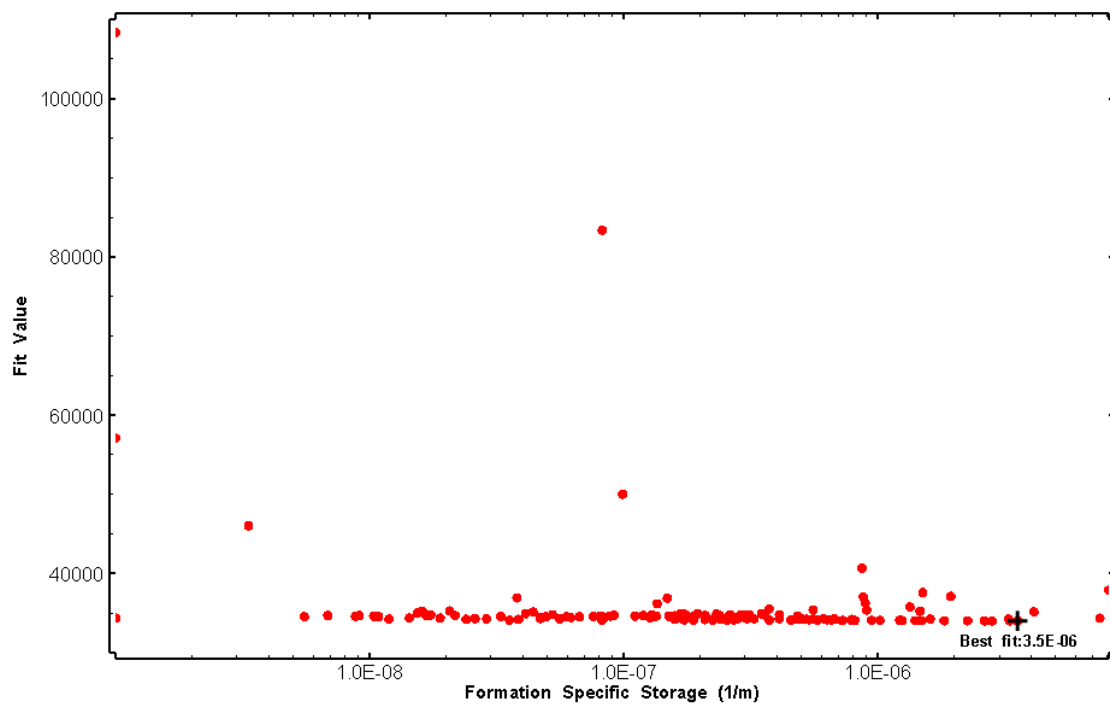


Figure 78: HT007 XY-scatter plot of formation specific storage vs. fit value

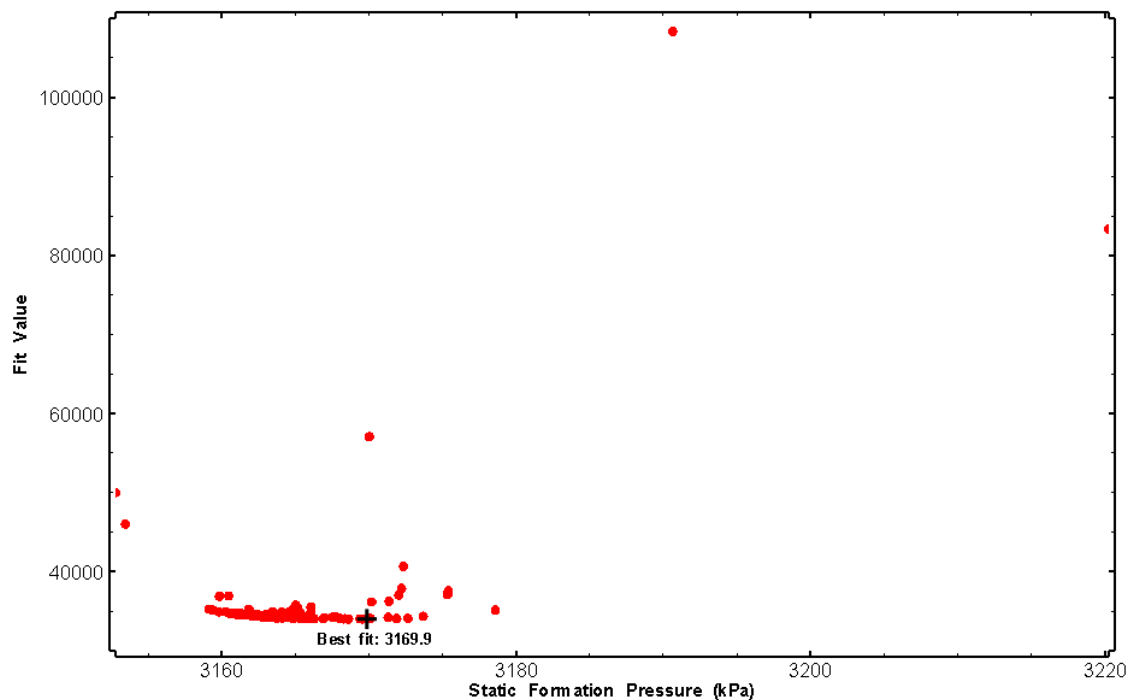


Figure 79: HT007 XY-scatter plot of static formation pressure vs. fit value

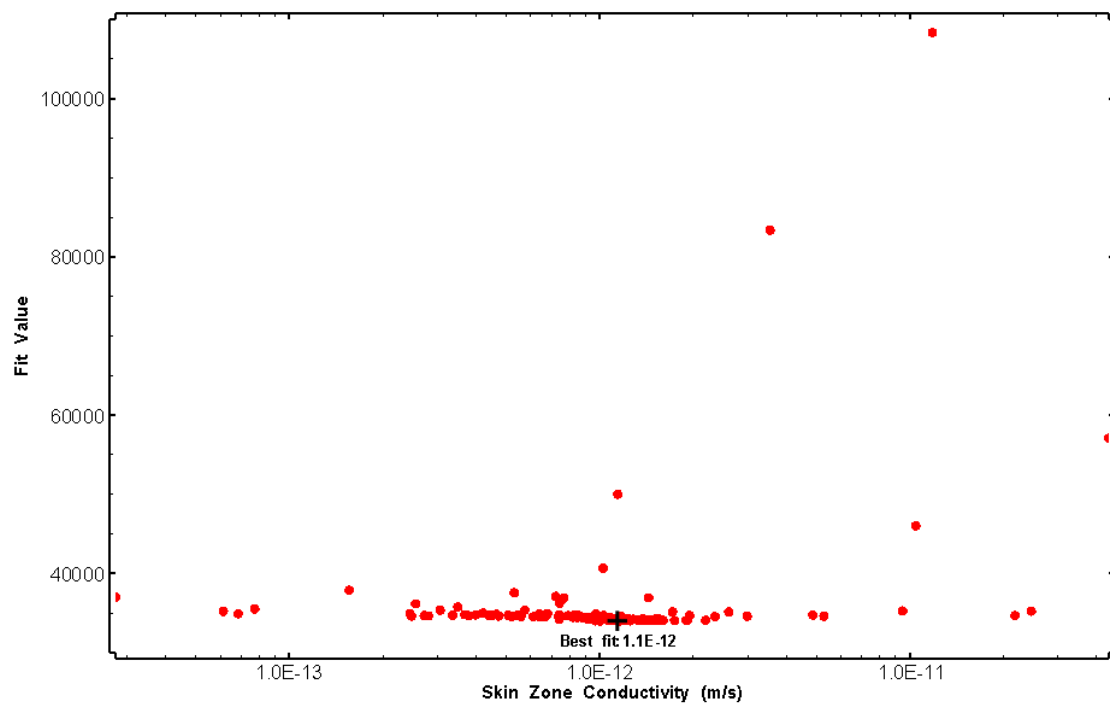


Figure 80: HT007 XY-scatter plot of skin zone conductivity vs. fit value

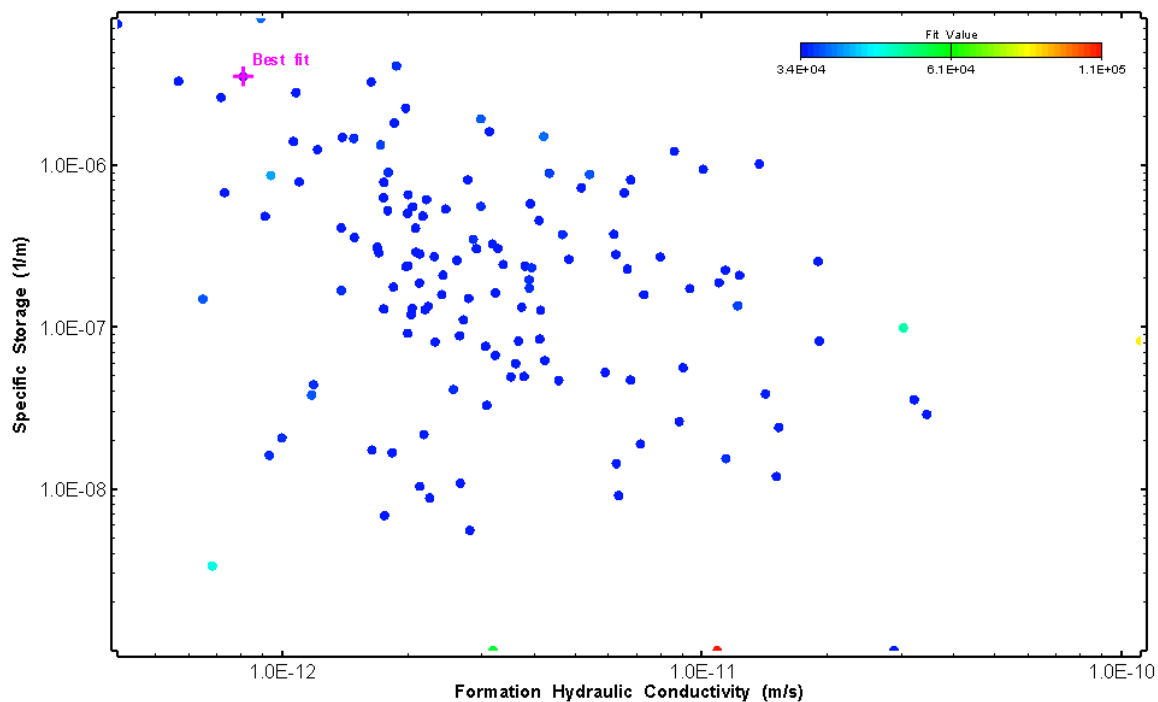


Figure 81: HT007 XY-scatter plot showing estimates of formation hydraulic conductivity and specific storage from perturbation analysis

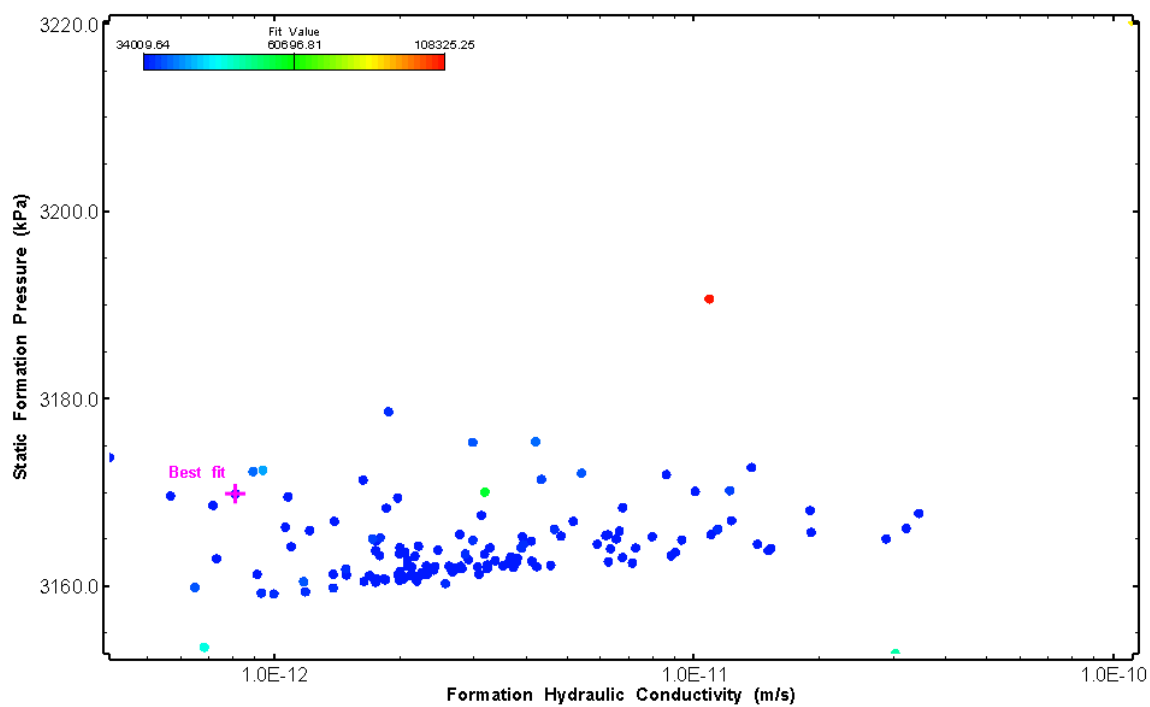


Figure 82: HT007 XY-scatter plot showing estimates of formation hydraulic conductivity and static formation pressure from perturbation analysis

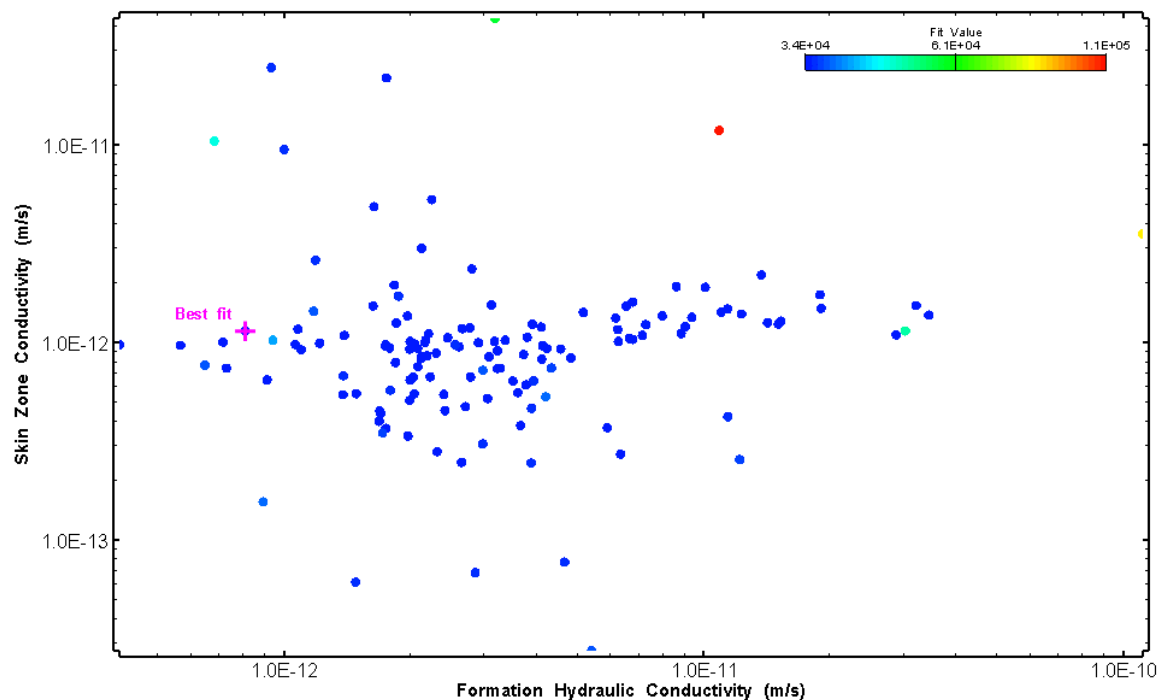


Figure 83: HT007 XY-scatter plot showing estimates of formation hydraulic conductivity and skin zone conductivity from perturbation analysis

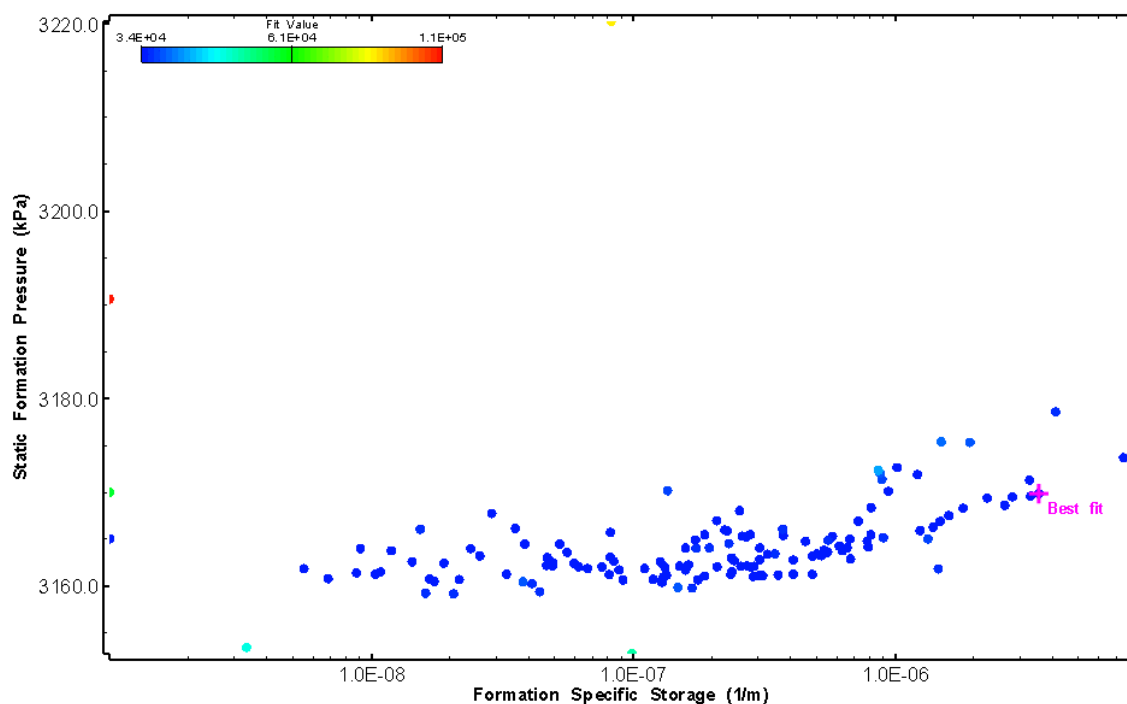


Figure 84: HT007 XY-scatter plot showing estimates of specific storage and static formation pressure from perturbation analysis

## 8.0 HT008 (383.00 – 403.02 M)

HT008 was selected to test a fractured interval containing dykes. 12 broken fractures were observed in the core. A loss of drilling fluid was observed in this interval during drilling. An indication of flow was recorded during FFEC logging post-drilling.

The test was initiated with a shut-in pressure recovery phase (PSR). A pulse withdrawal test (PW) with a shut-in recovery was completed after the PSR phase.

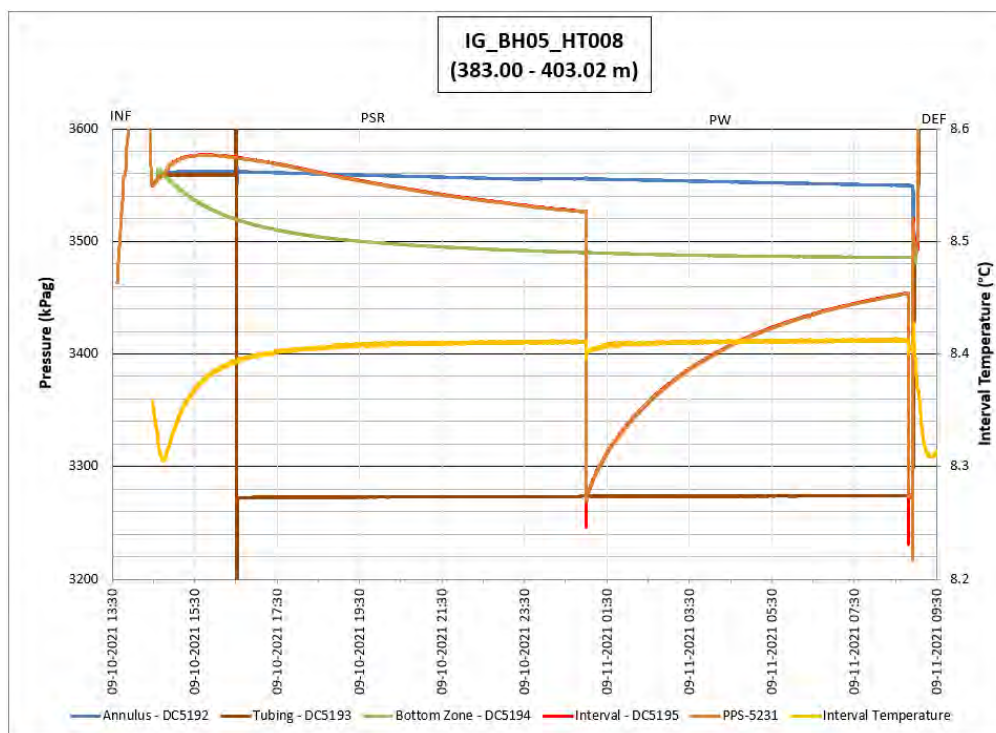
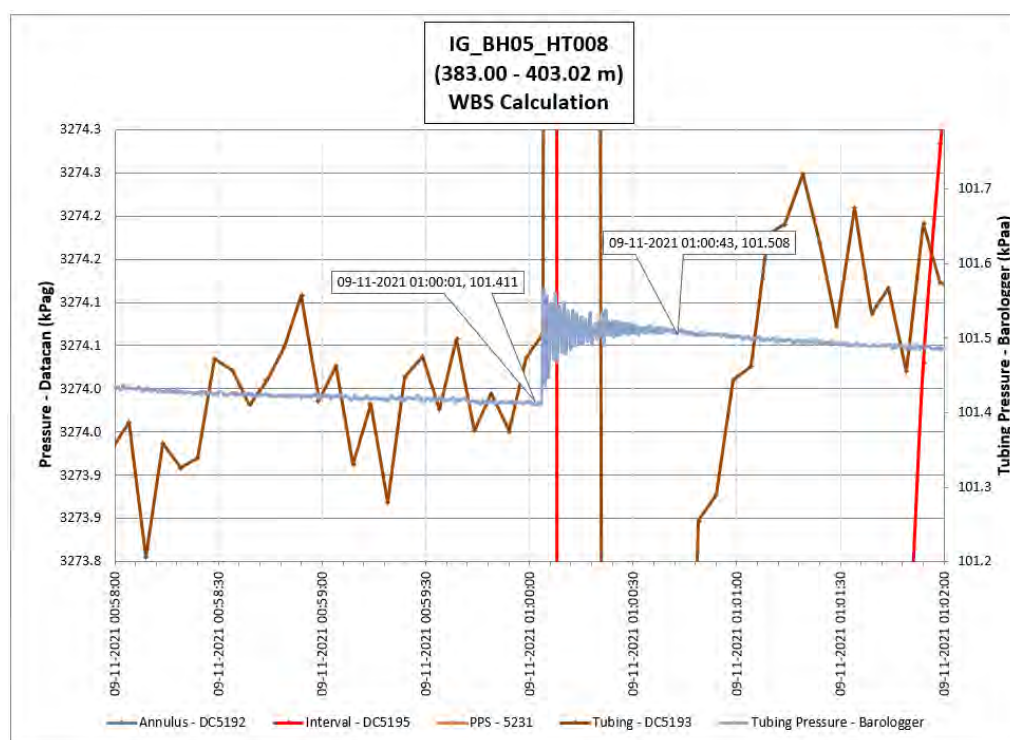


Figure 85: HT008 Annotated test plot showing monitored zone pressure and interval temperature.



**Figure 86: HT008 Tubing pressure during DHSIV activation. DHSIV Closed Wellbore Storage Estimate =  $7\text{E-}11 \text{ m}^3/\text{Pa}$**

**Table 8: Summary of Analysis Results – HT008**

	Formation conductivity	Skin zone conductivity	Static formation pressure	Formation specific storage	Radial thickness of skin	Flow dimension
	[m/s]	[m/s]	[kPa]	[1/m]	[m]	[–]
Best Fit	6E-13	8E-14	3488	2E-07	2.8E-03	2.5
Minimum	1E-14	8E-14	3458	1E-09	1E-03	1.1
Maximum	6E-11	4E-12	3550	1E-05	1E+00	3.0
Mean	2E-12	4E-13	3502	1E-06	1E-01	2.1
Median	9E-13	3E-13	3497	3E-07	3E-02	2.0
Geometric mean	7E-13	3E-13	3501	3E-07	4E-02	2.0

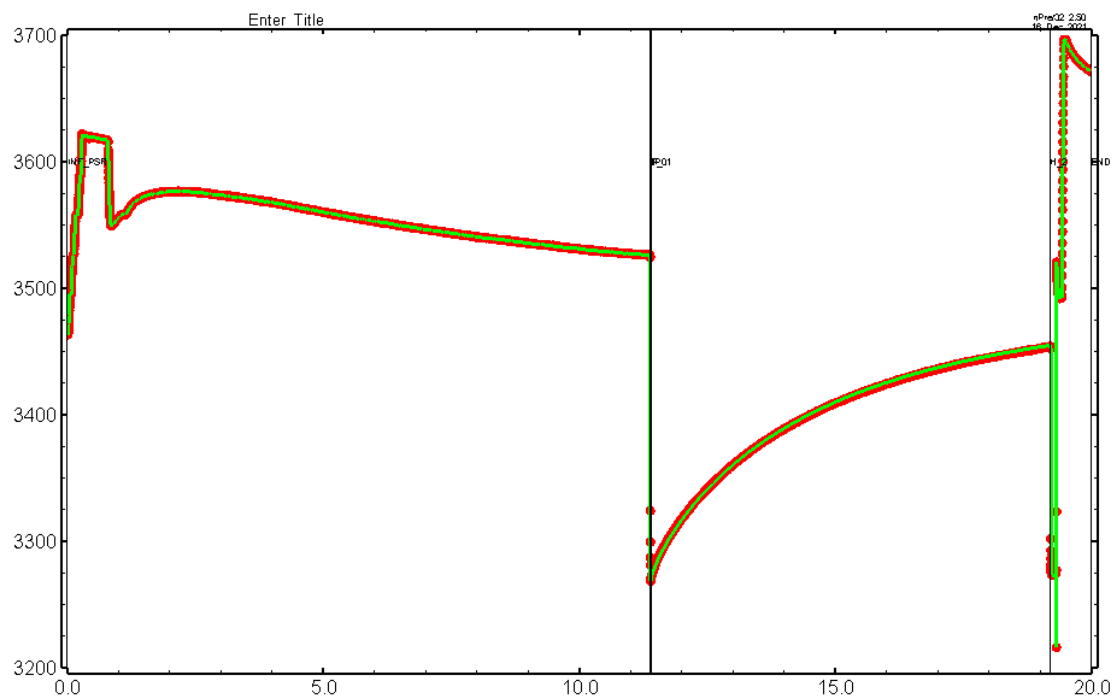


Figure 87: HT008 Pressure plot showing best-fit simulation and best fit results

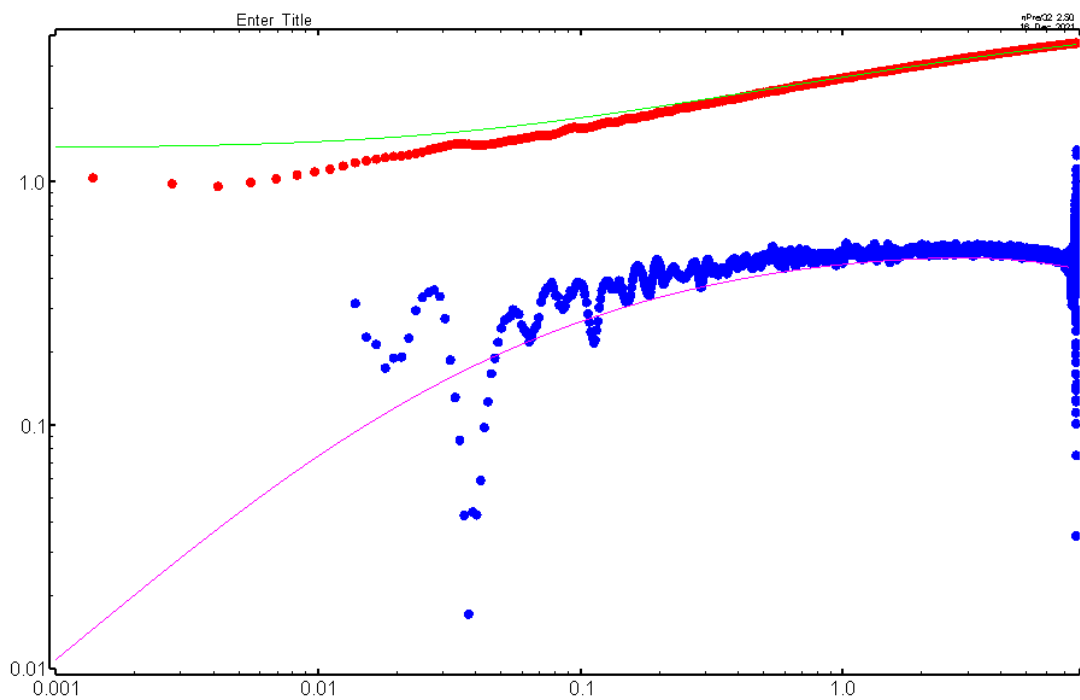


Figure 88: HT008 Deconvolved pressure change and derivative plot of the PW sequence showing best-fit simulation

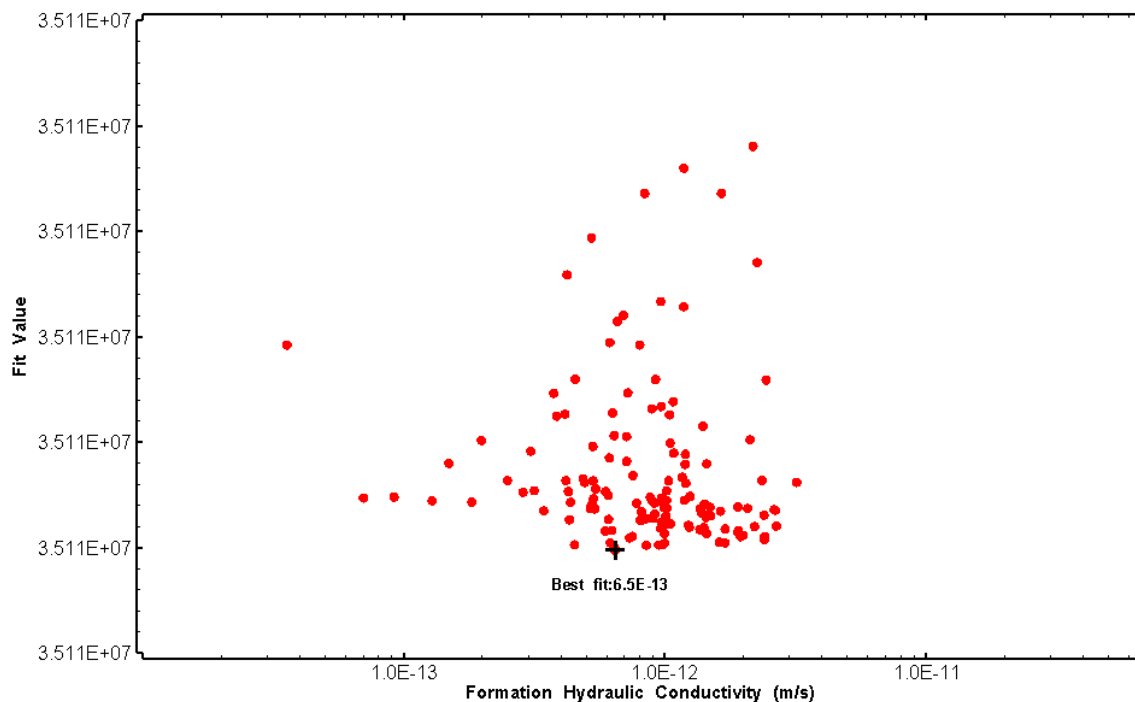


Figure 89: HT008 XY-scatter plot of formation hydraulic conductivity vs. fit value

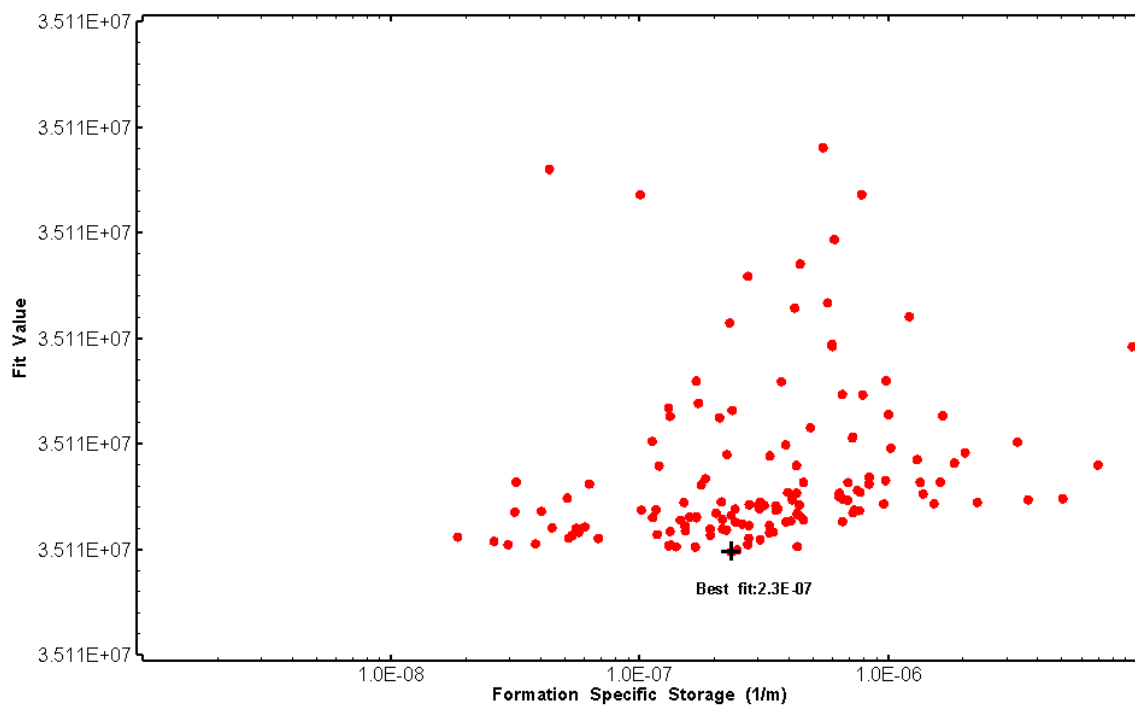


Figure 90: HT008 XY-scatter plot of formation specific storage vs. fit value



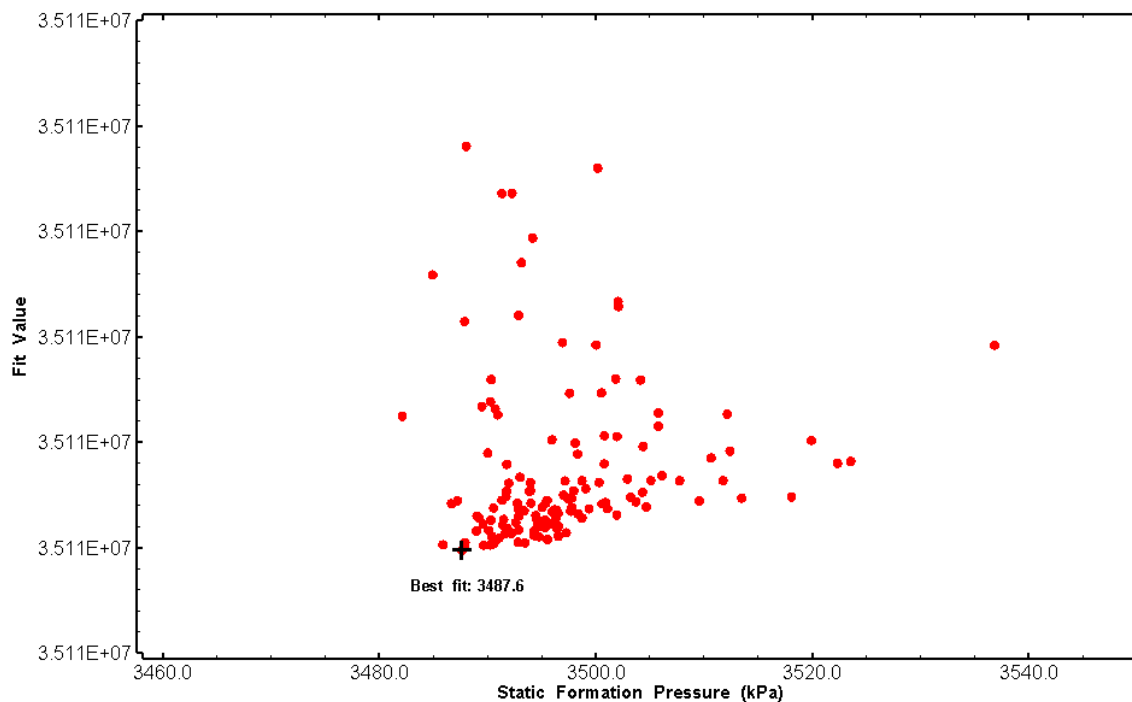


Figure 91: HT008 XY-scatter plot of static formation pressure vs. fit value

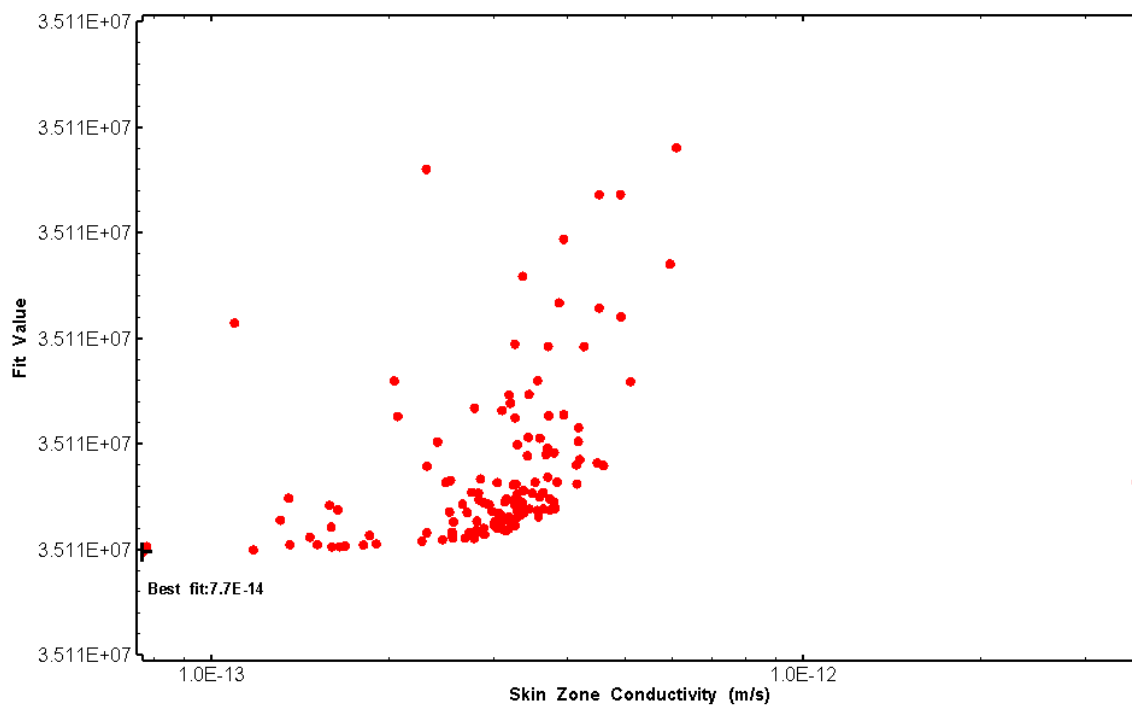


Figure 92: HT008 XY-scatter plot of skin zone conductivity vs. fit value

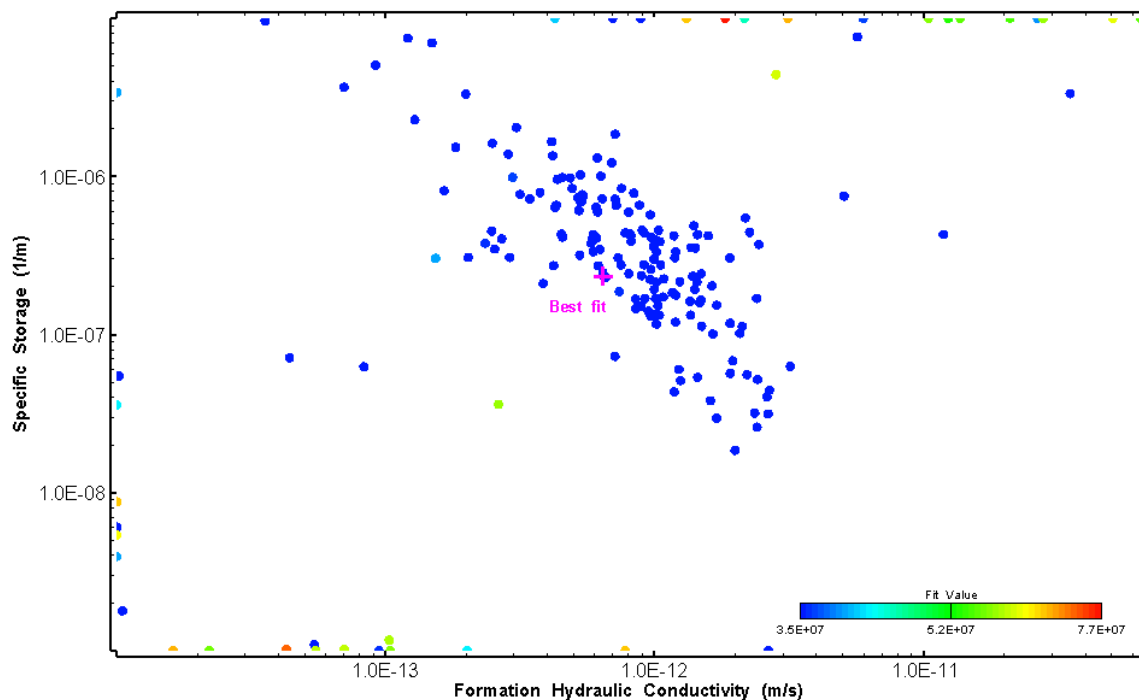


Figure 93: HT008 XY-scatter plot showing estimates of formation hydraulic conductivity and specific storage from perturbation analysis

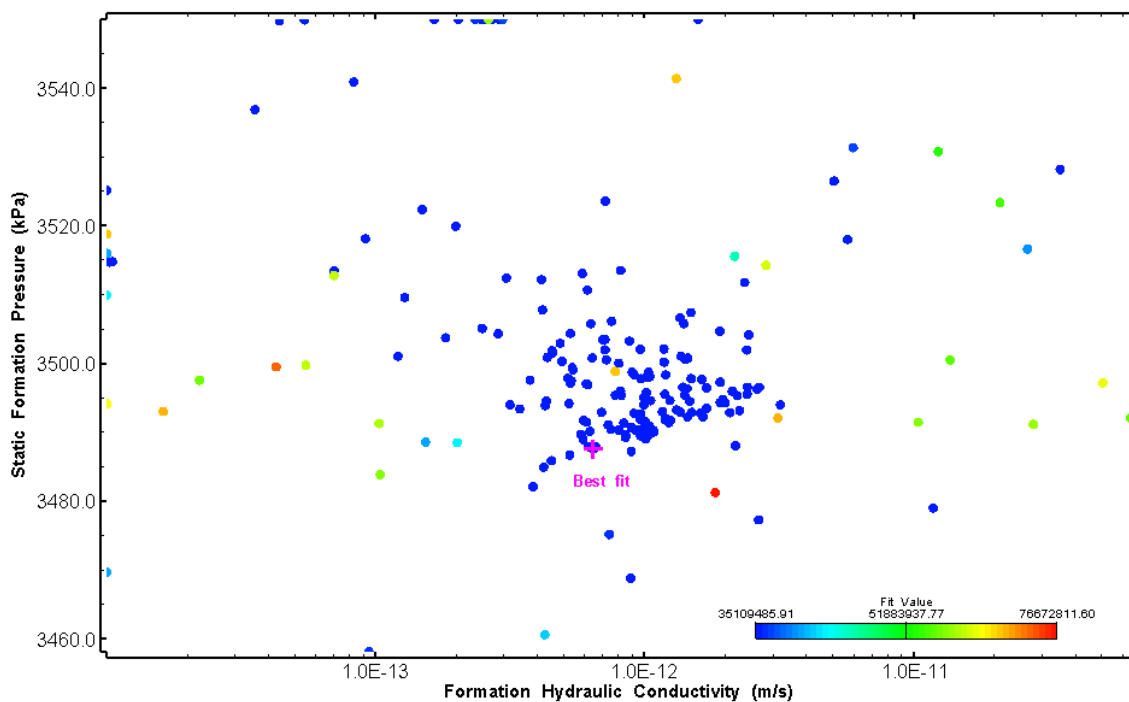


Figure 94: HT008 XY-scatter plot showing estimates of formation hydraulic conductivity and static formation pressure from perturbation analysis

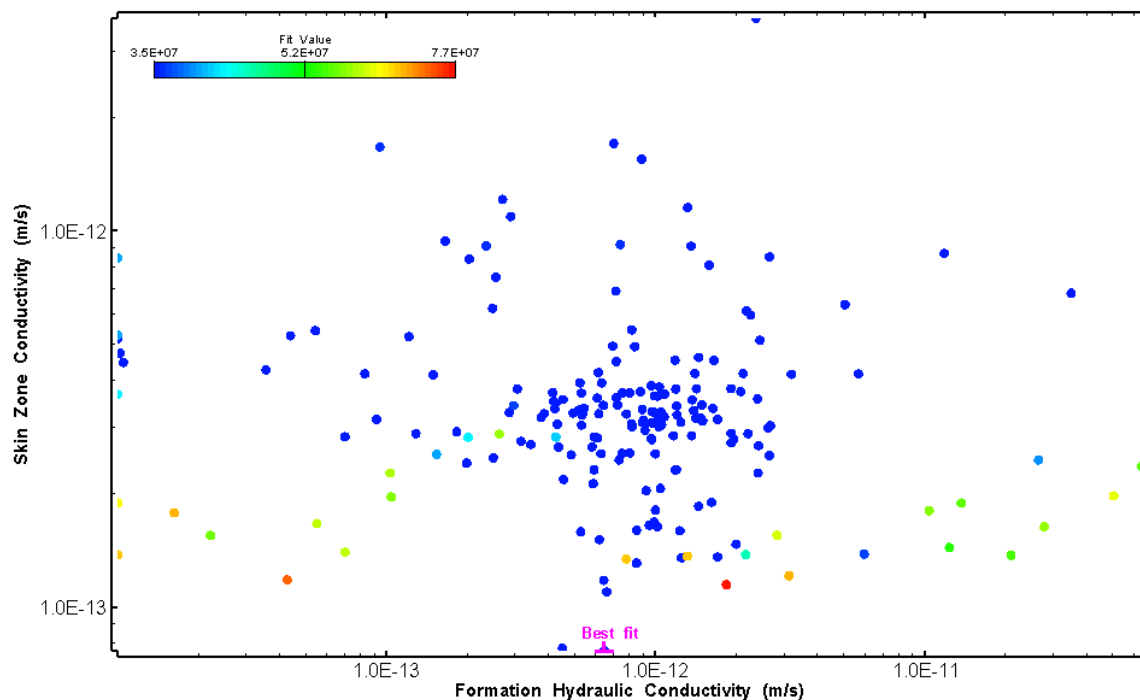


Figure 95: HT008 XY-scatter plot showing estimates of formation hydraulic conductivity and skin zone conductivity from perturbation analysis

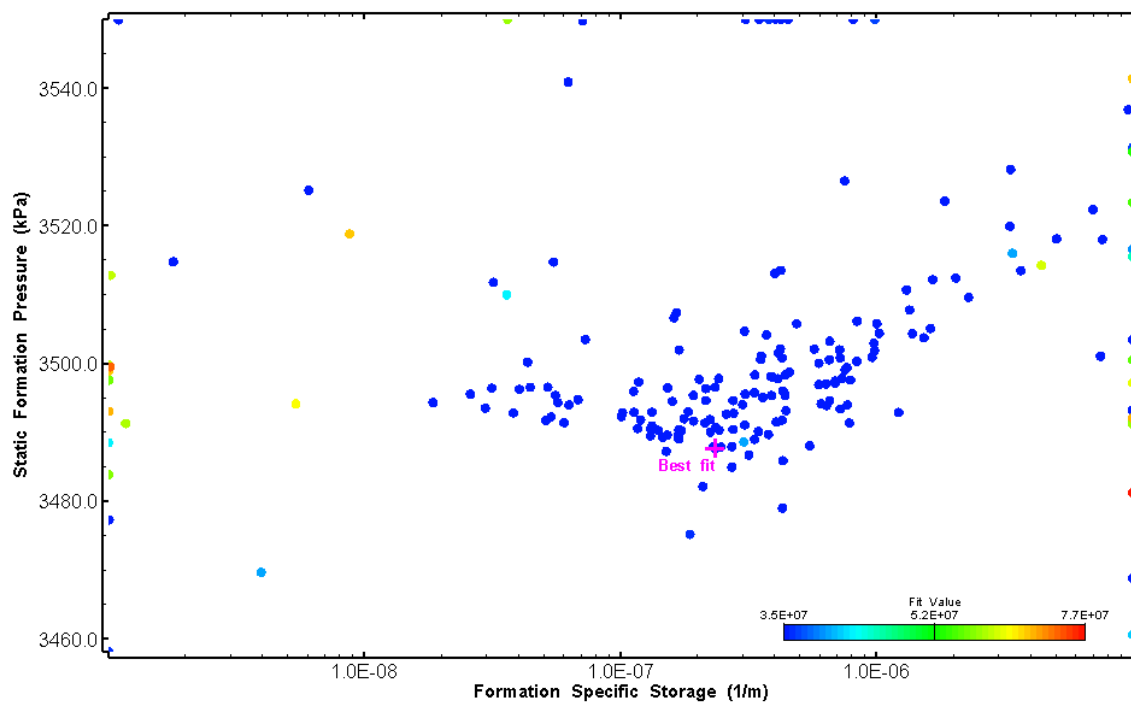


Figure 96: HT008 XY-scatter plot showing estimates of specific storage and static formation pressure from perturbation analysis

## 9.0 HT009 (404.00 – 424.02 M)

HT009 was selected to test a fractured interval containing dykes. 25 broken fractures were observed in the core. No indication of flow was recorded during FFEC logging post-drilling.

The test was initiated with a shut-in pressure recovery phase (PSR). A pulse withdrawal test (PW) with a shut-in recovery was completed after the PSR phase.

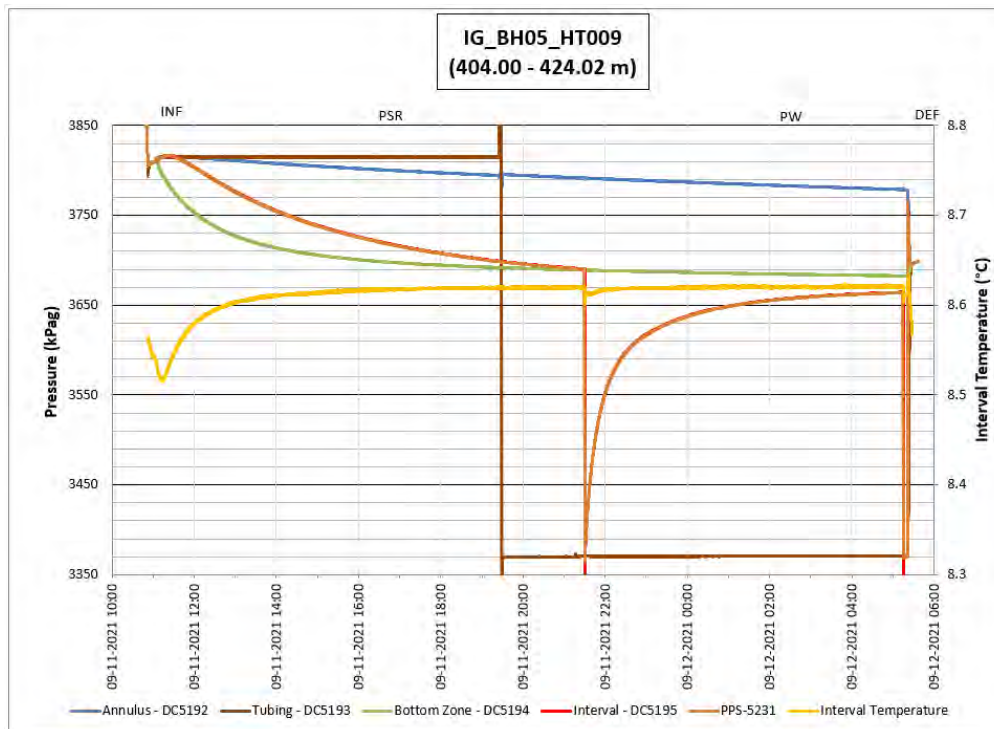
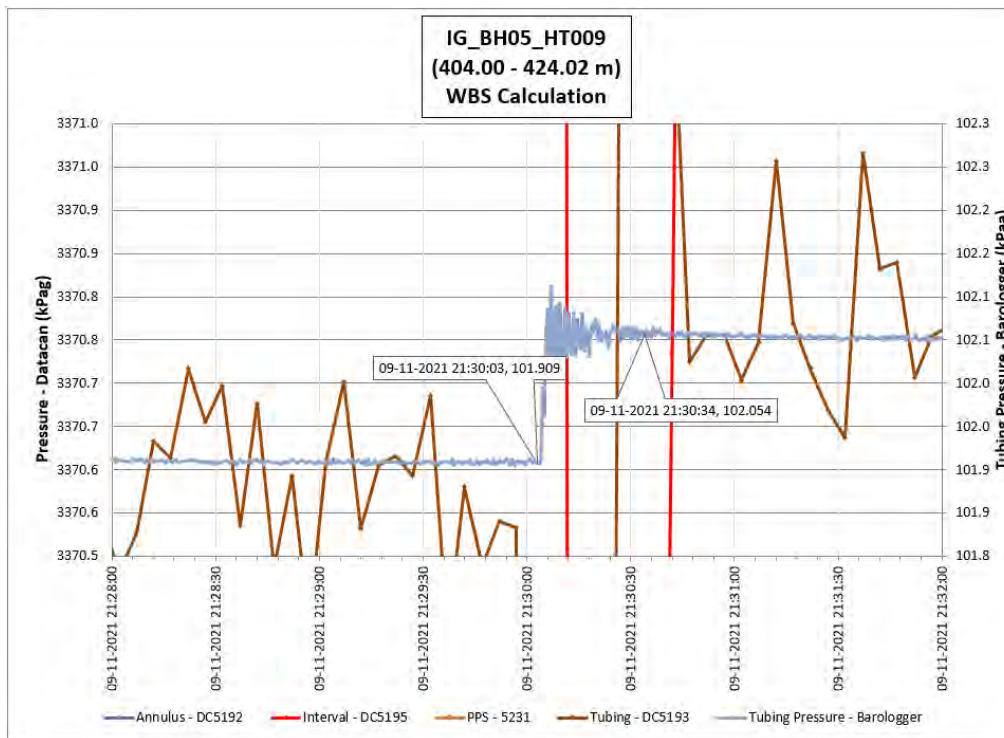


Figure 97: HT009 Annotated test plot showing monitored zone pressure and interval temperature.



**Figure 98: HT009 Tubing pressure during DHSIV activation. DHSIV Closed Wellbore Storage Estimate =  $8\text{E-}11 \text{ m}^3/\text{Pa}$**

**Table 9: Summary of Analysis Results – HT009**

	Formation conductivity	Skin zone conductivity	Static formation pressure	Formation specific storage	Radial thickness of skin	Flow dimension
	[m/s]	[m/s]	[kPa]	[1/m]	[m]	[-]
Best Fit	6E-13	3E-12	3668	1E-08	1.98E-01	3.0
Minimum	1E-14	1E-13	3615	1E-09	1E-03	1.1
Maximum	5E-11	1E-11	3724	1E-05	1E+00	3.0
Mean	3E-12	5E-12	3677	2E-06	2E-01	2.1
Median	2E-12	4E-12	3678	3E-07	1E-01	2.1
Geometric mean	1E-12	4E-12	3677	2E-07	8E-02	2.1

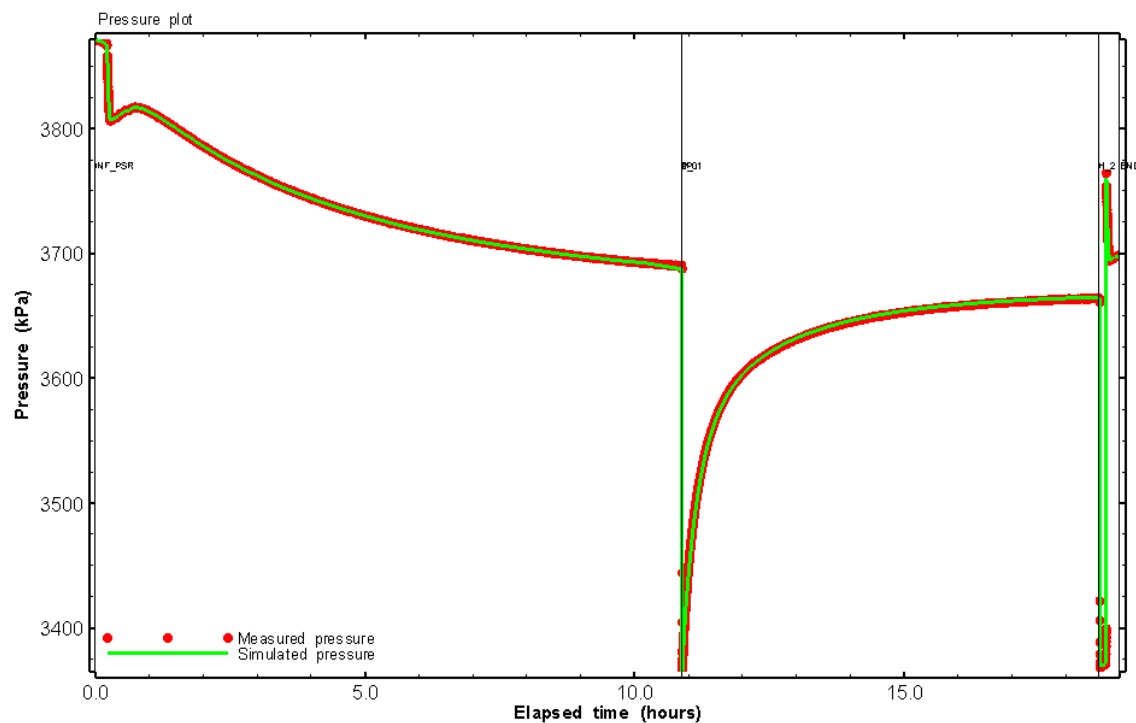


Figure 99: HT009 Pressure plot showing best-fit simulation and best fit results

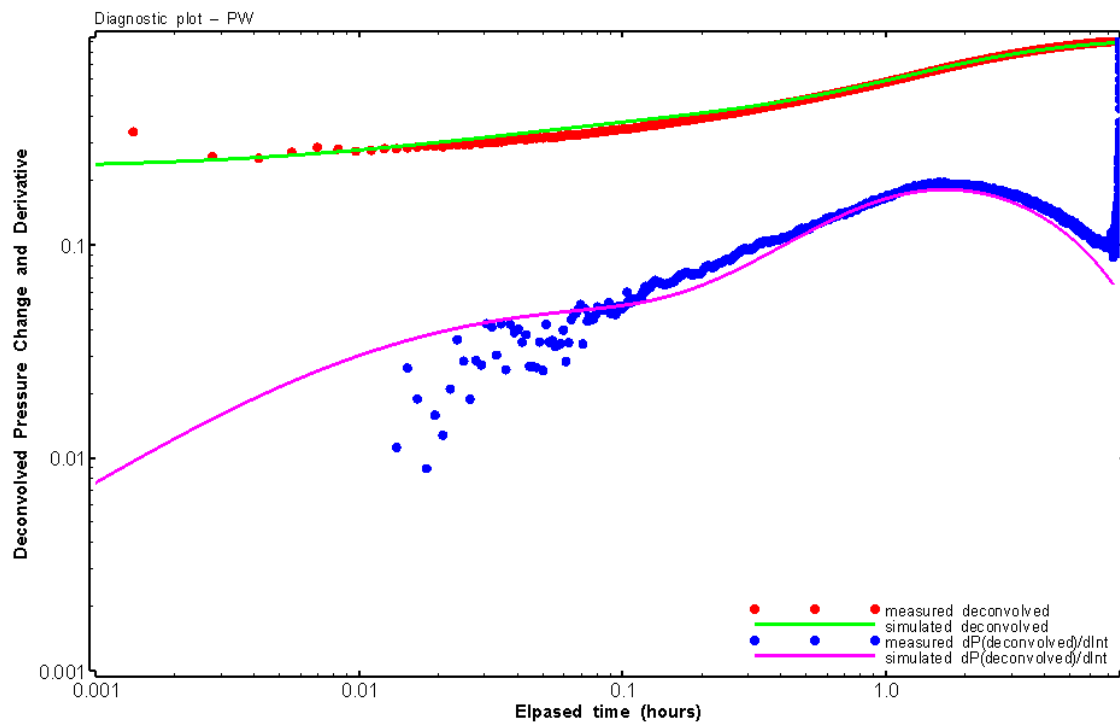


Figure 100: HT009 Deconvolved pressure change and derivative plot of the PW sequence showing best-fit simulation

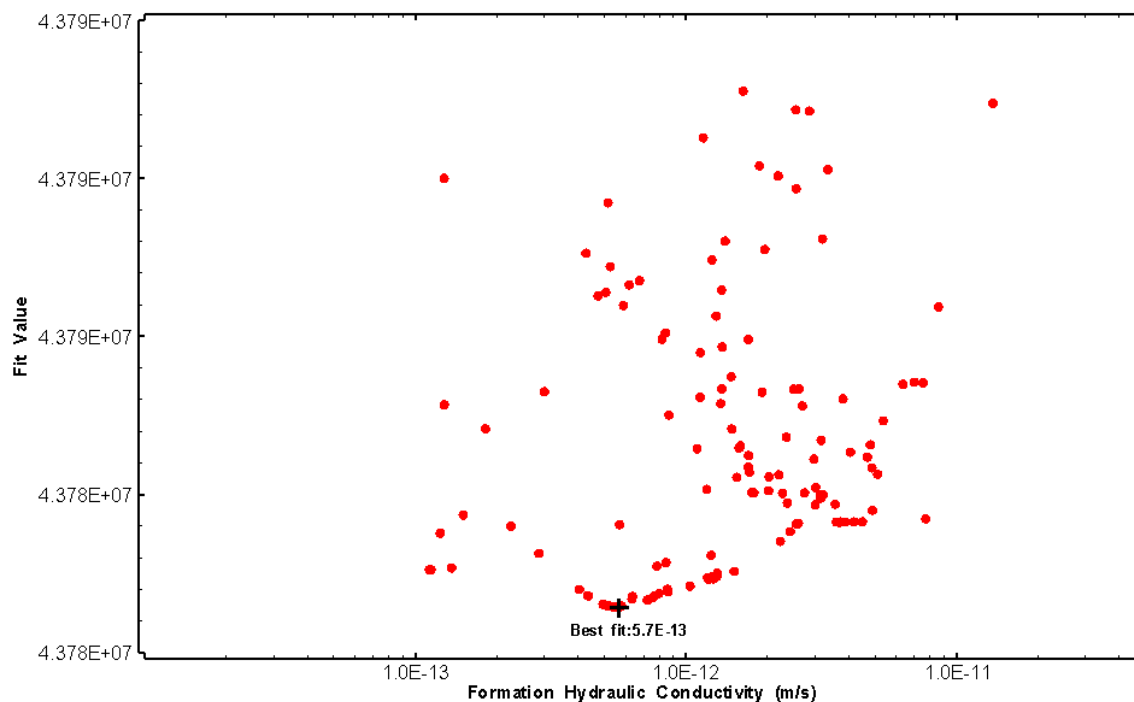


Figure 101: HT009 XY-scatter plot of formation hydraulic conductivity vs. fit value

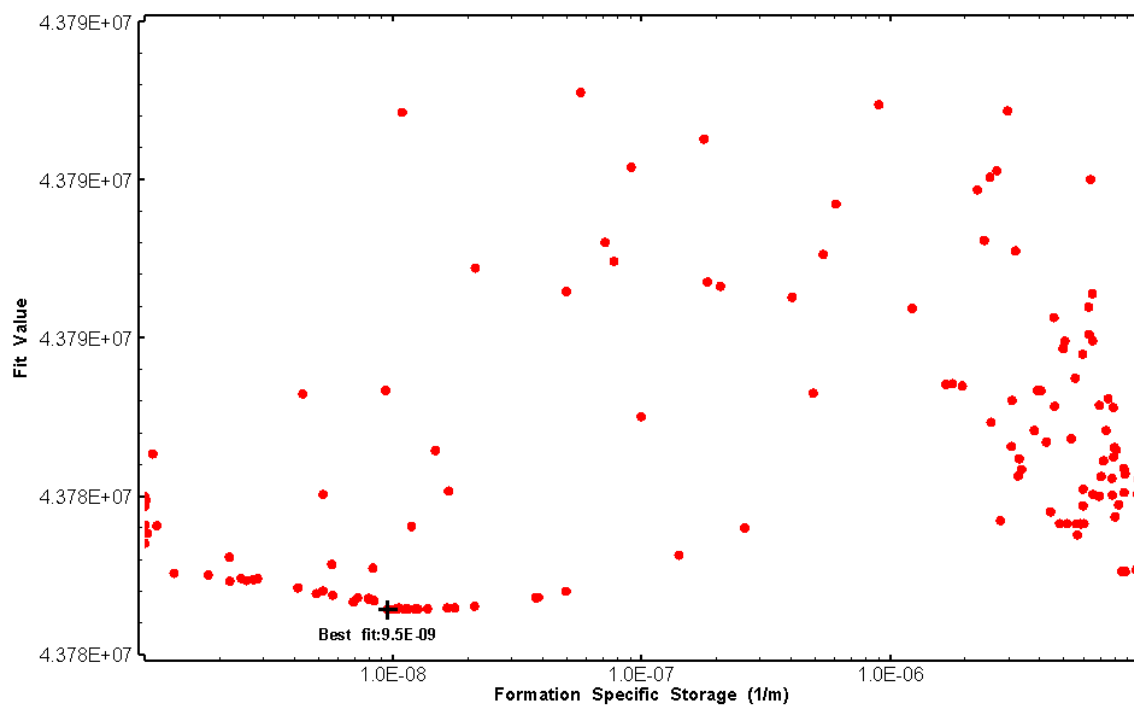


Figure 102: HT009 XY-scatter plot of formation specific storage vs. fit value

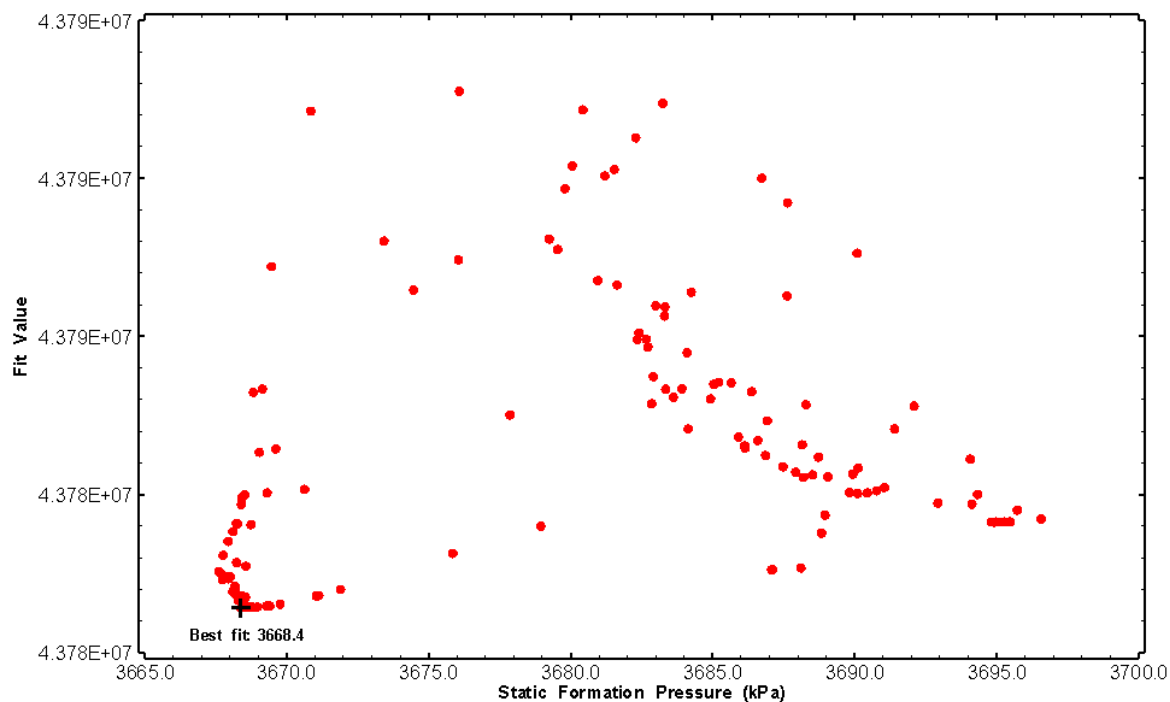


Figure 103: HT009 XY-scatter plot of static formation pressure vs. fit value

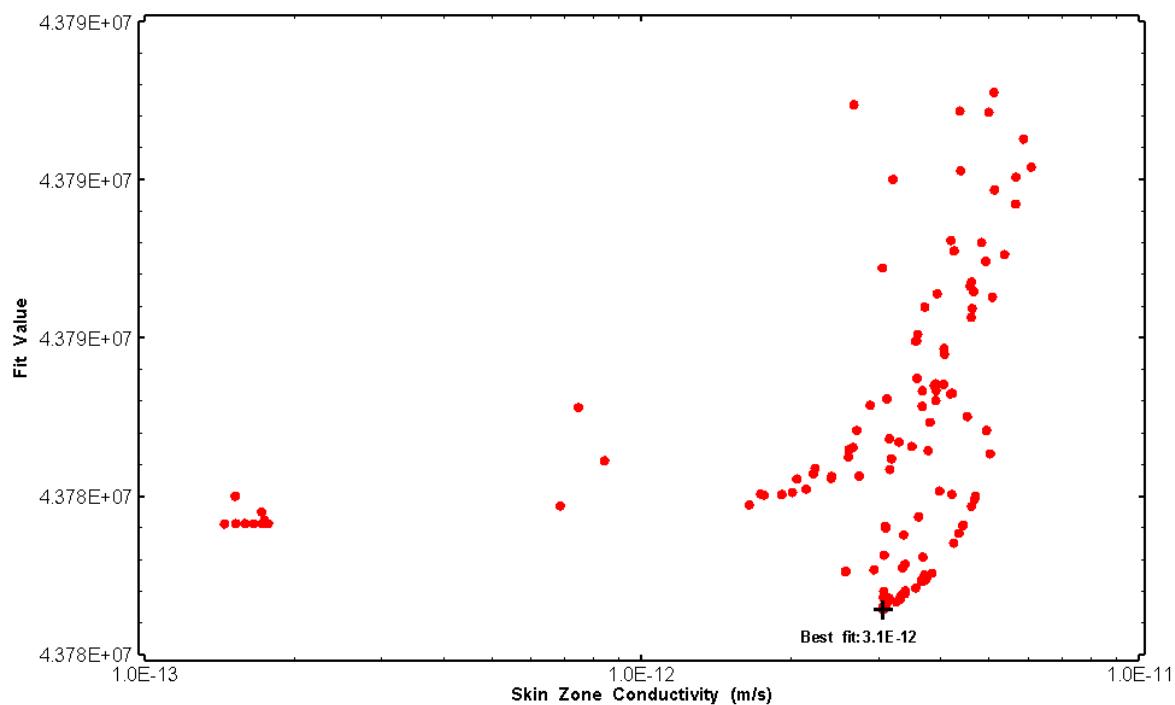


Figure 104: HT009 XY-scatter plot of skin zone conductivity vs. fit value



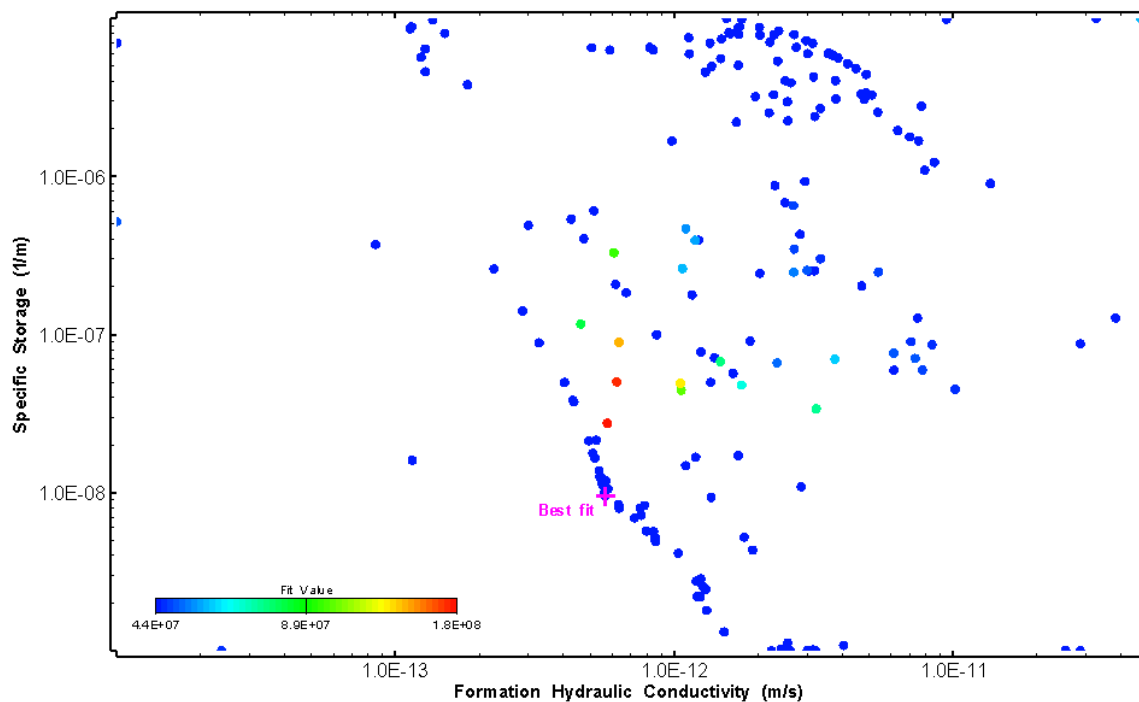


Figure 105: HT009 XY-scatter plot showing estimates of formation hydraulic conductivity and specific storage from perturbation analysis

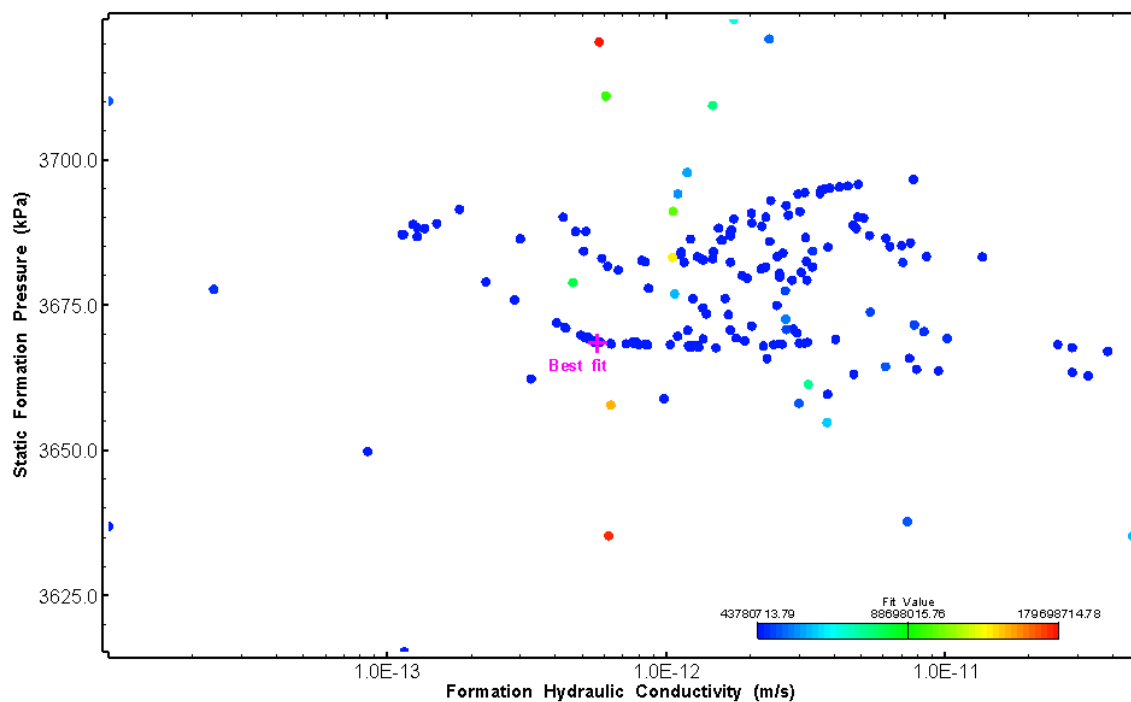


Figure 106: HT009 XY-scatter plot showing estimates of formation hydraulic conductivity and static formation pressure from perturbation analysis

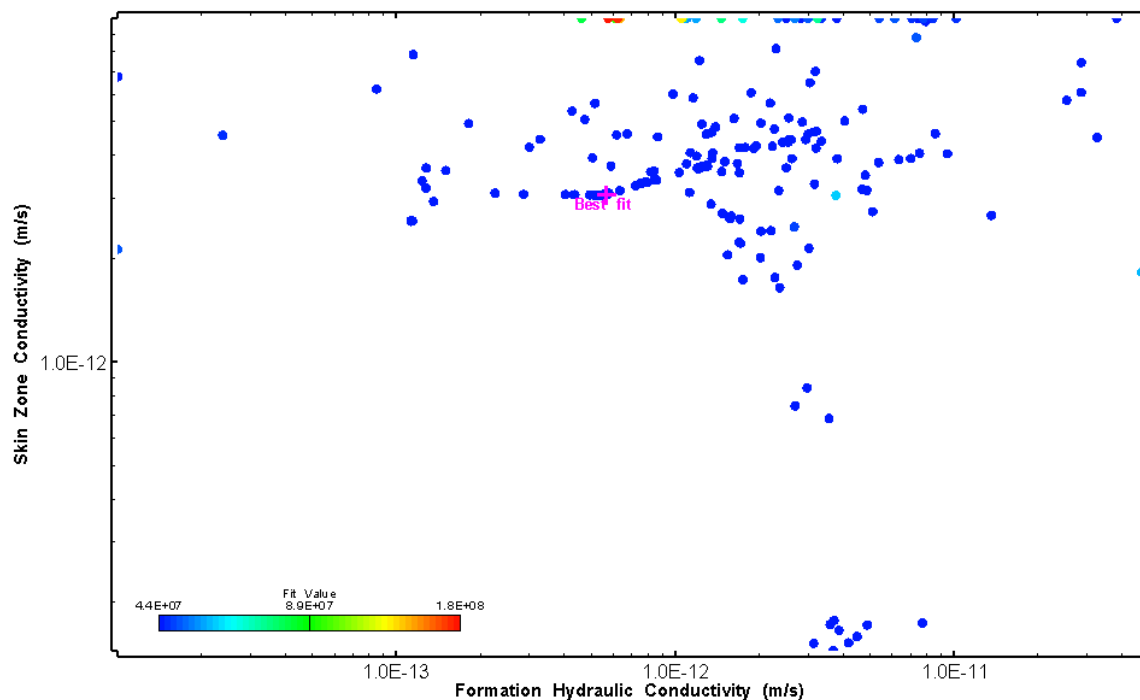


Figure 107: HT009 XY-scatter plot showing estimates of formation hydraulic conductivity and skin zone conductivity from perturbation analysis

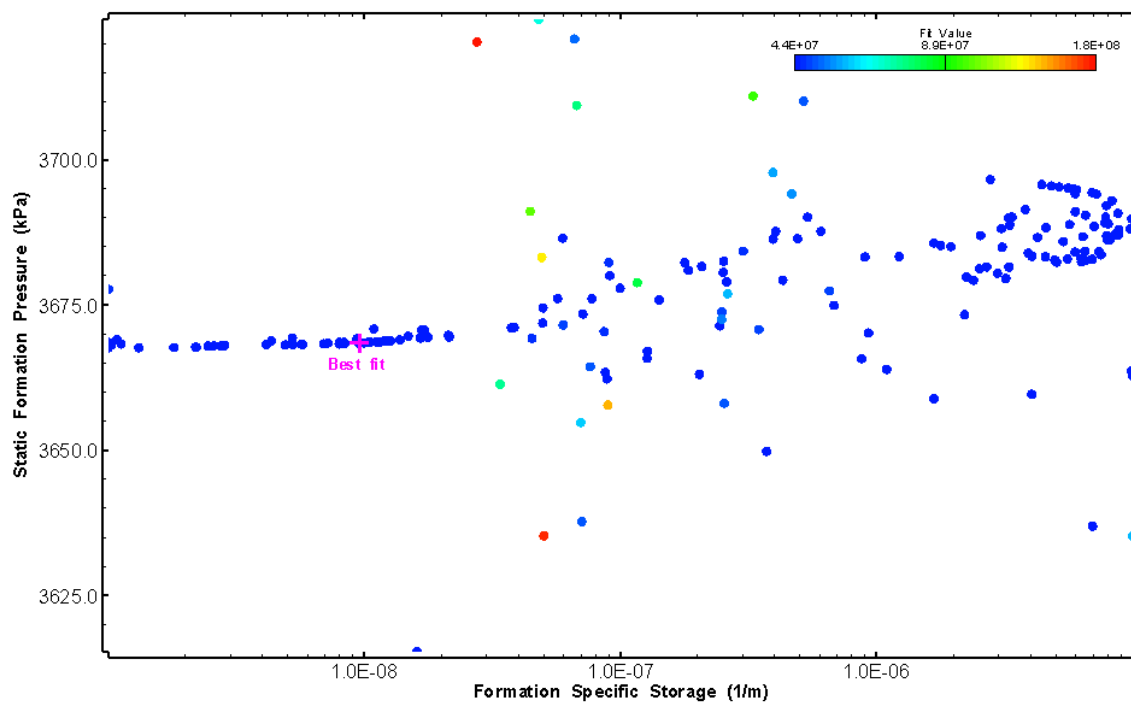


Figure 108: HT009 XY-scatter plot showing estimates of specific storage and static formation pressure from perturbation analysis

## 10.0 HT010 (429.02 – 449.04 M)

HT010 was selected to test an intact interval. Zero broken fractures were observed in the core. No drill fluid parameter triggers were reached during drilling. No indication of flow was recorded during FFEC logging post-drilling.

The test was initiated with a shut-in pressure recovery phase (PSR). A pulse withdrawal test (PW) with a shut-in recovery was completed after the PSR phase.

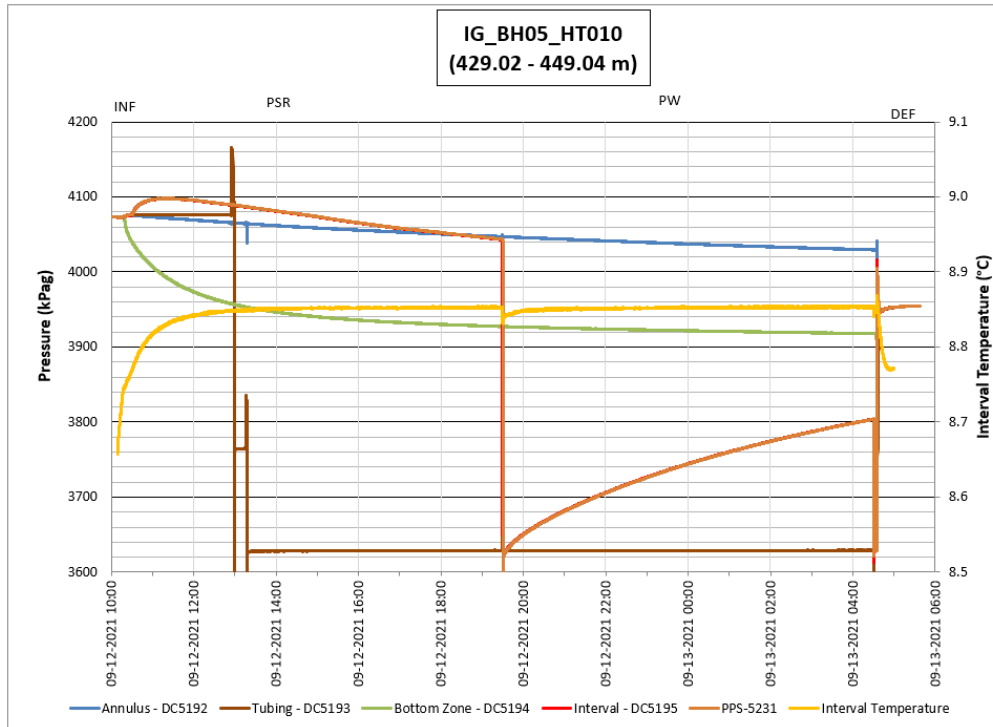
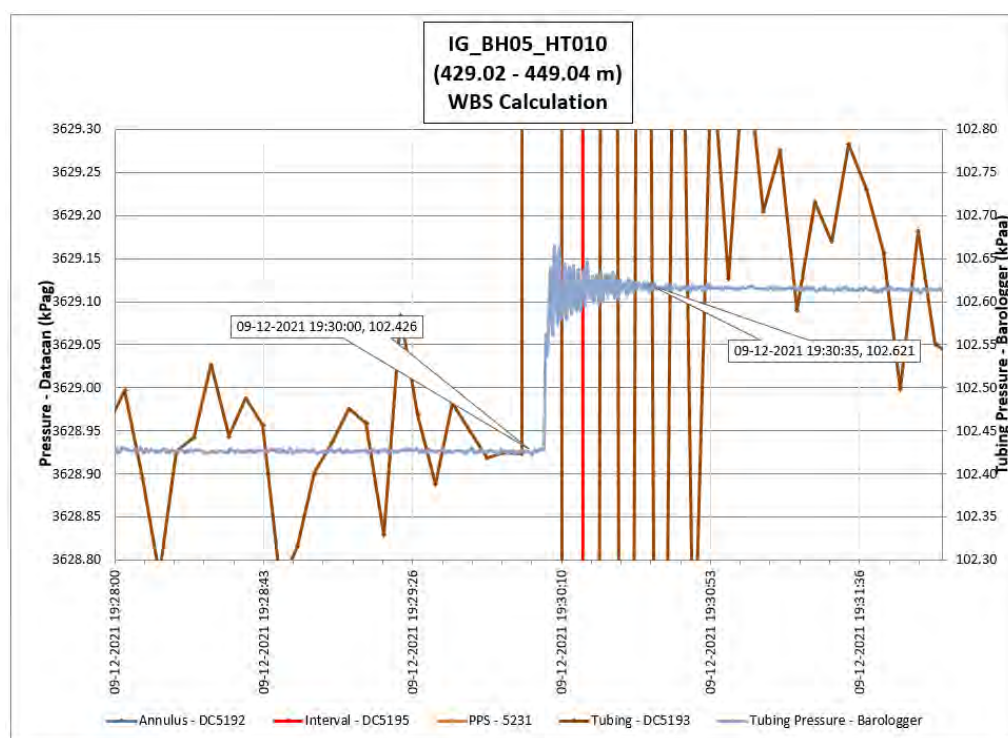


Figure 109: HT010 Annotated test plot showing monitored zone pressure and interval temperature.



**Figure 110: HT010 Tubing pressure during DHSIV activation. DHSIV Closed Wellbore Storage Estimate =  $8\text{E-}11 \text{ m}^3/\text{Pa}$**

**Table 10: Summary of Analysis Results – HT010**

	Formation conductivity	Skin zone conductivity	Static formation pressure	Formation specific storage	Radial thickness of skin	Flow dimension
	[m/s]	[m/s]	[kPa]	[1/m]	[m]	[–]
Best Fit	2E-14	1E-13	3932	3E-06	2.08E-01	2.9
Minimum	1E-15	4E-14	3850	1E-09	1E-03	1.4
Maximum	1E-11	1E-12	4050	1E-05	9E-01	3.0
Mean	1E-12	2E-13	3970	1E-06	2E-01	2.2
Median	2E-13	2E-13	3966	1E-07	7E-02	2.1
Geometric mean	1E-13	2E-13	3969	1E-07	8E-02	2.1

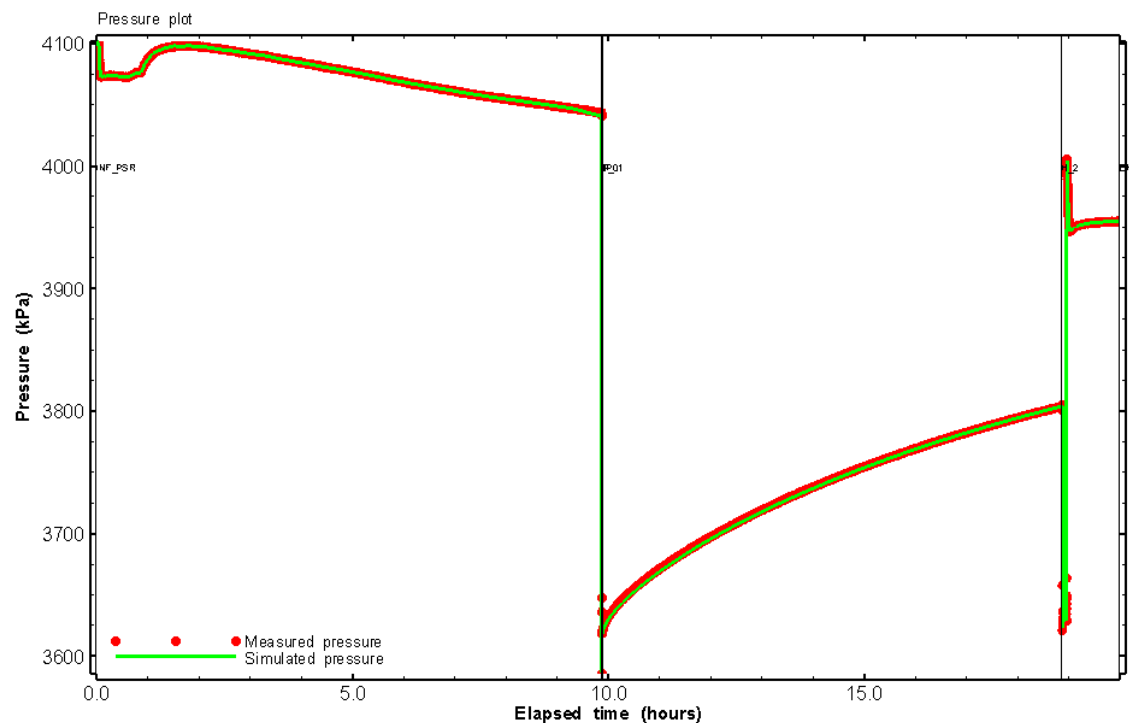


Figure 111: HT010 Pressure plot showing best-fit simulation and best fit results

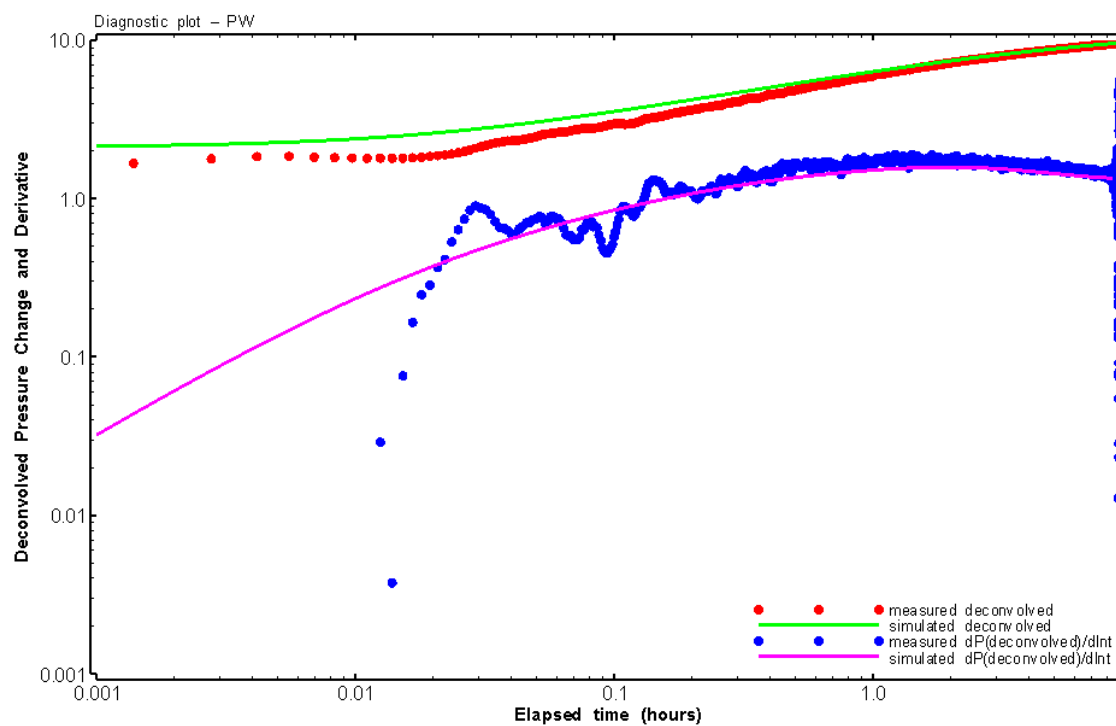


Figure 112: HT010 Deconvolved pressure change and derivative plot of the PW sequence showing best-fit simulation

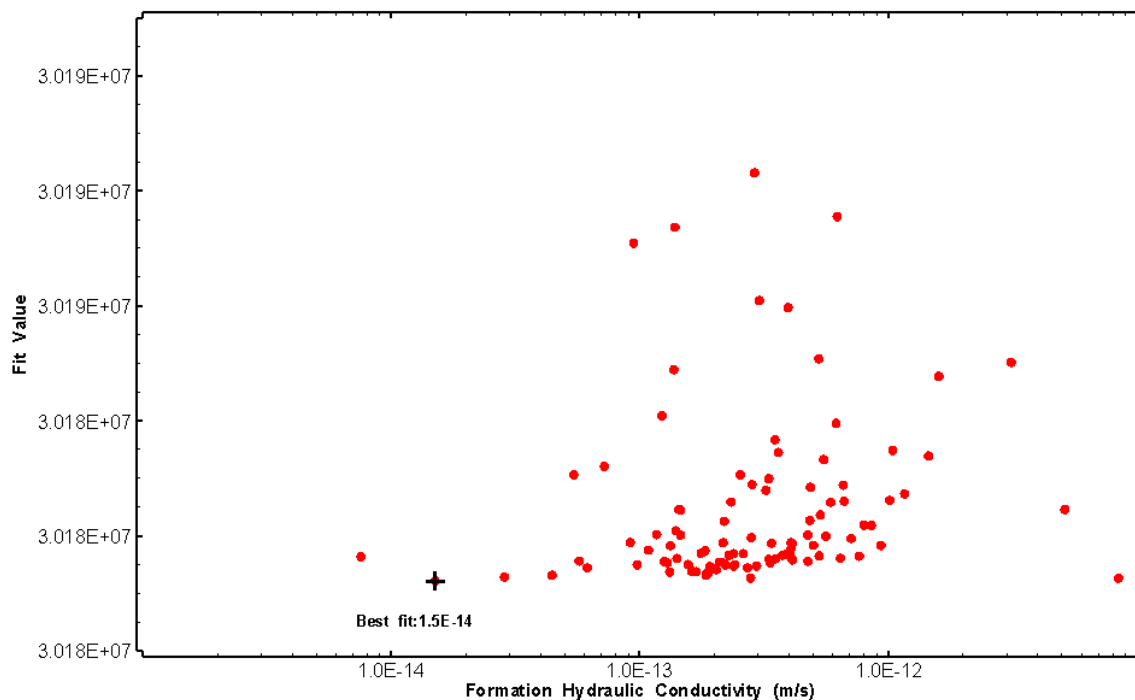


Figure 113: HT010 XY-scatter plot of formation hydraulic conductivity vs. fit value

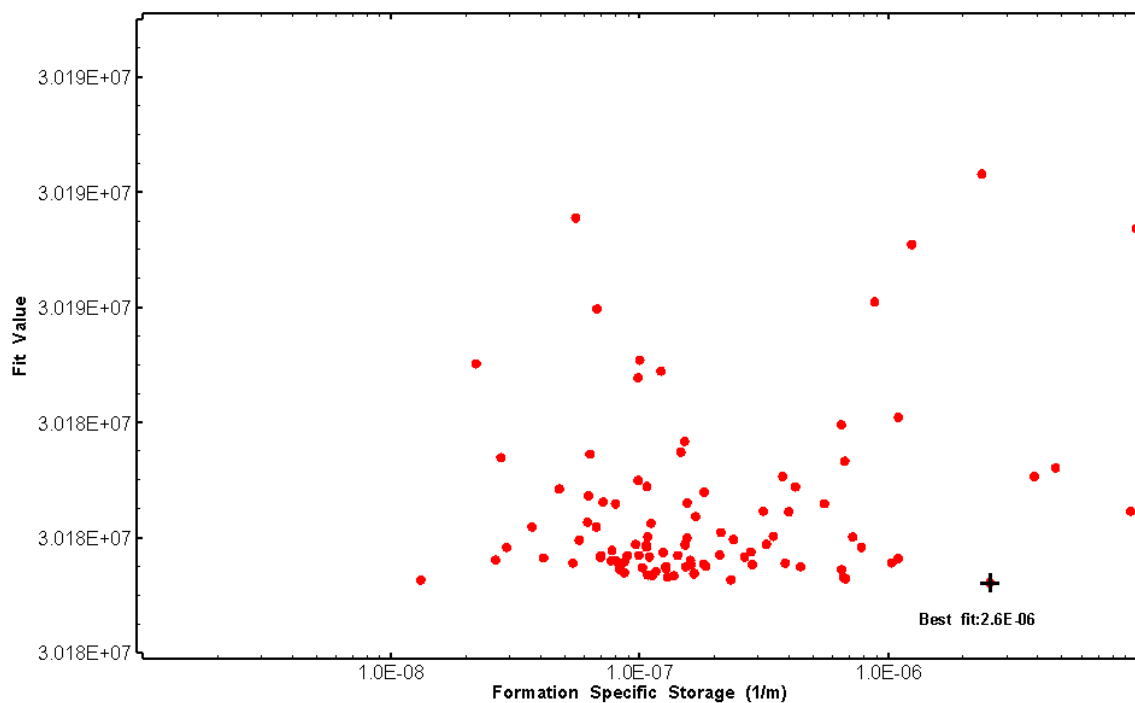


Figure 114: HT010 XY-scatter plot of formation specific storage vs. fit value

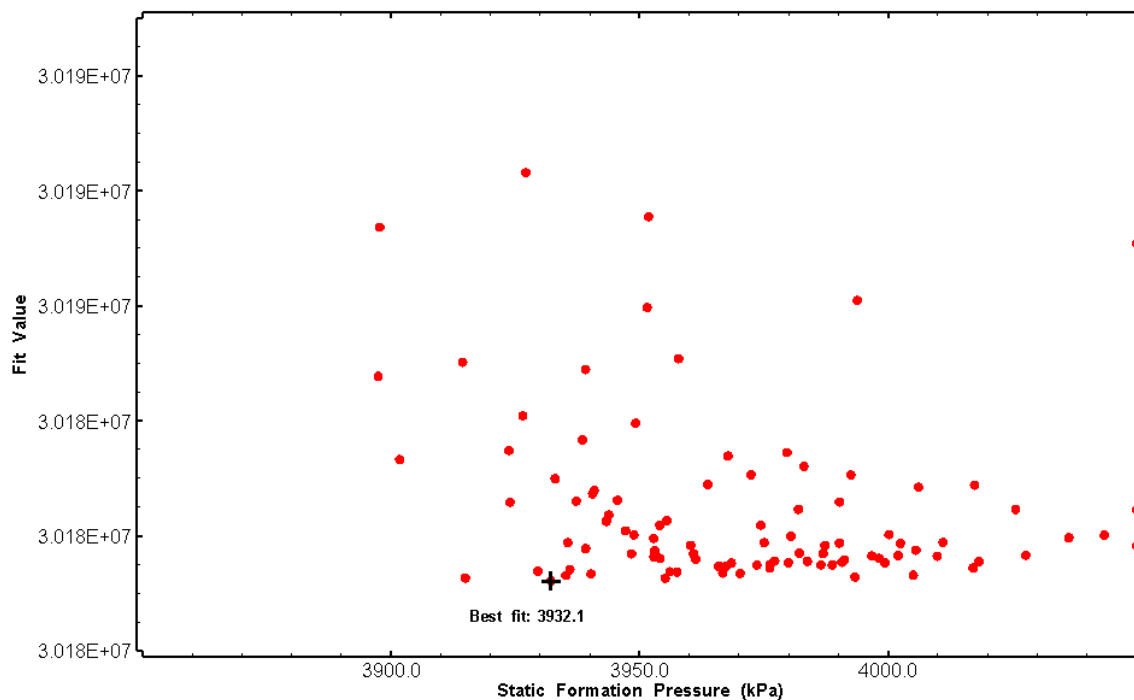


Figure 115: HT010 XY-scatter plot of static formation pressure vs. fit value

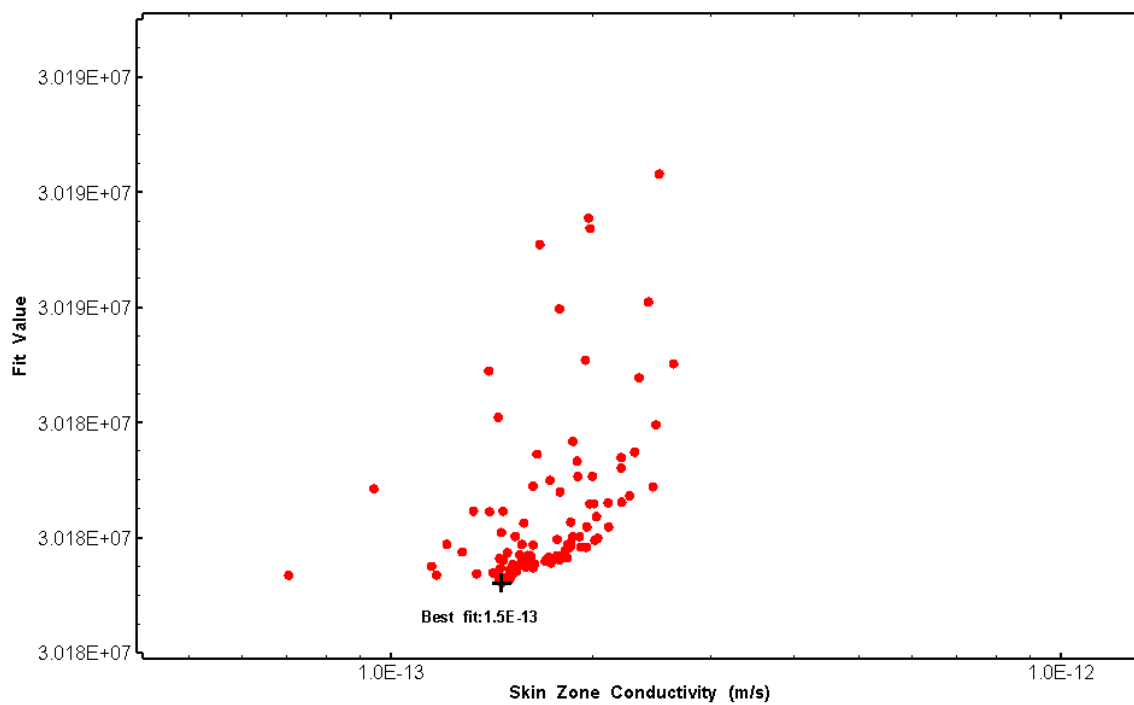


Figure 116: HT010 XY-scatter plot of skin zone conductivity vs. fit value

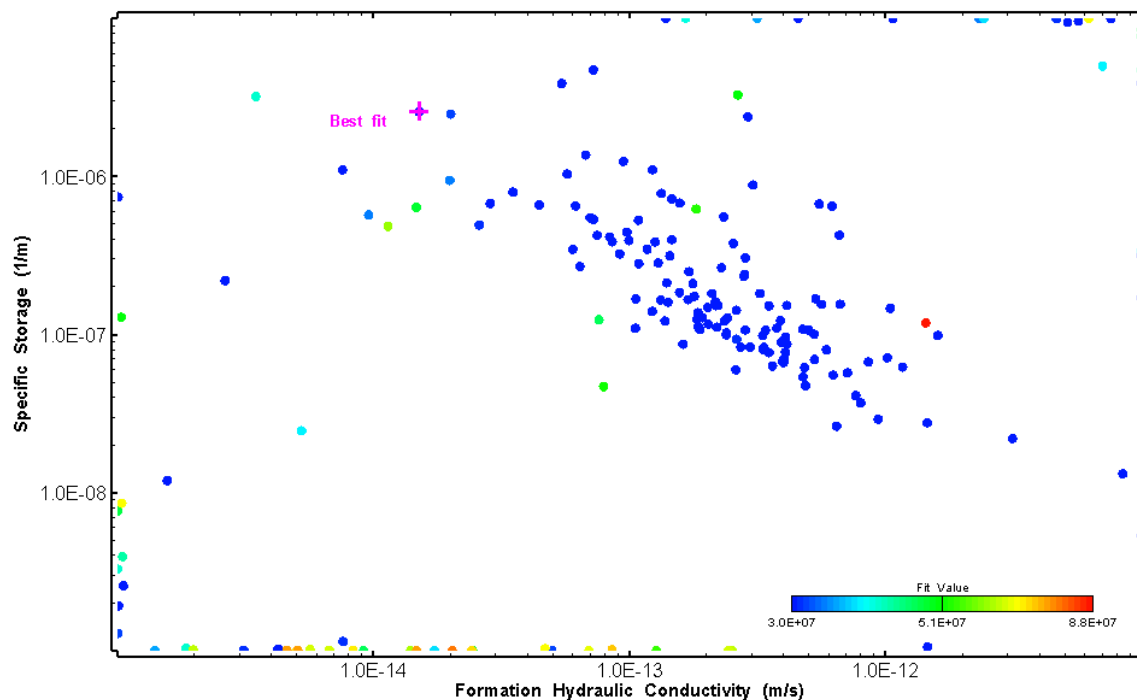


Figure 117: HT010 XY-scatter plot showing estimates of formation hydraulic conductivity and specific storage from perturbation analysis

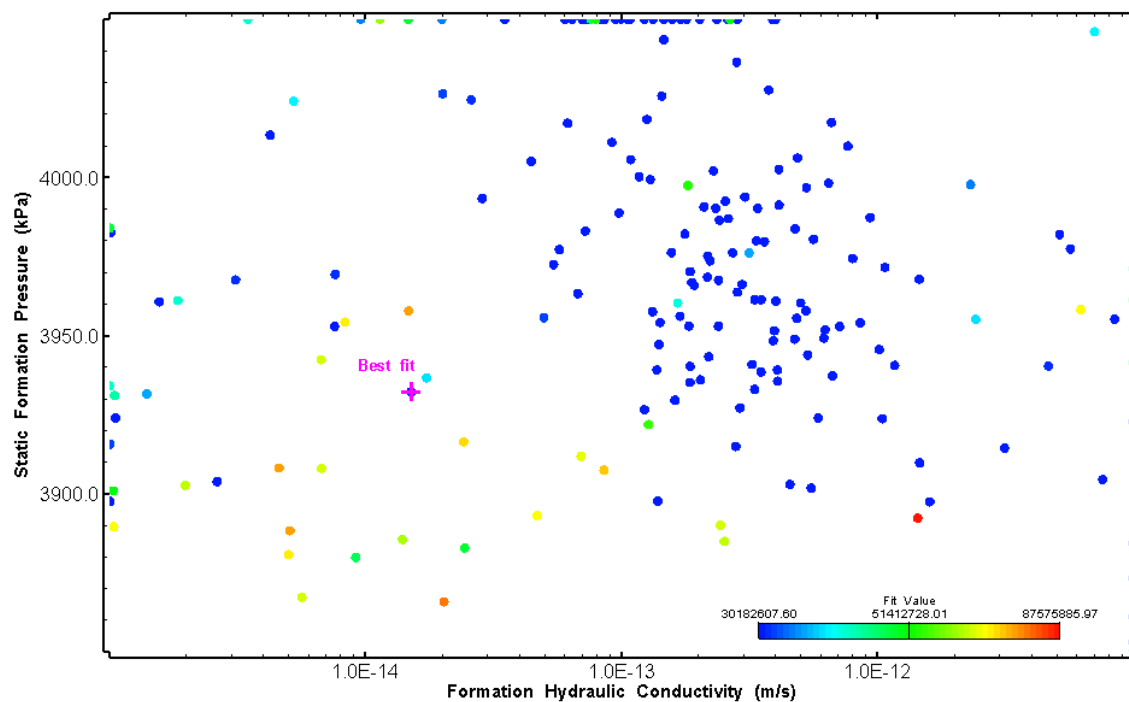


Figure 118: HT010 XY-scatter plot showing estimates of formation hydraulic conductivity and static formation pressure from perturbation analysis



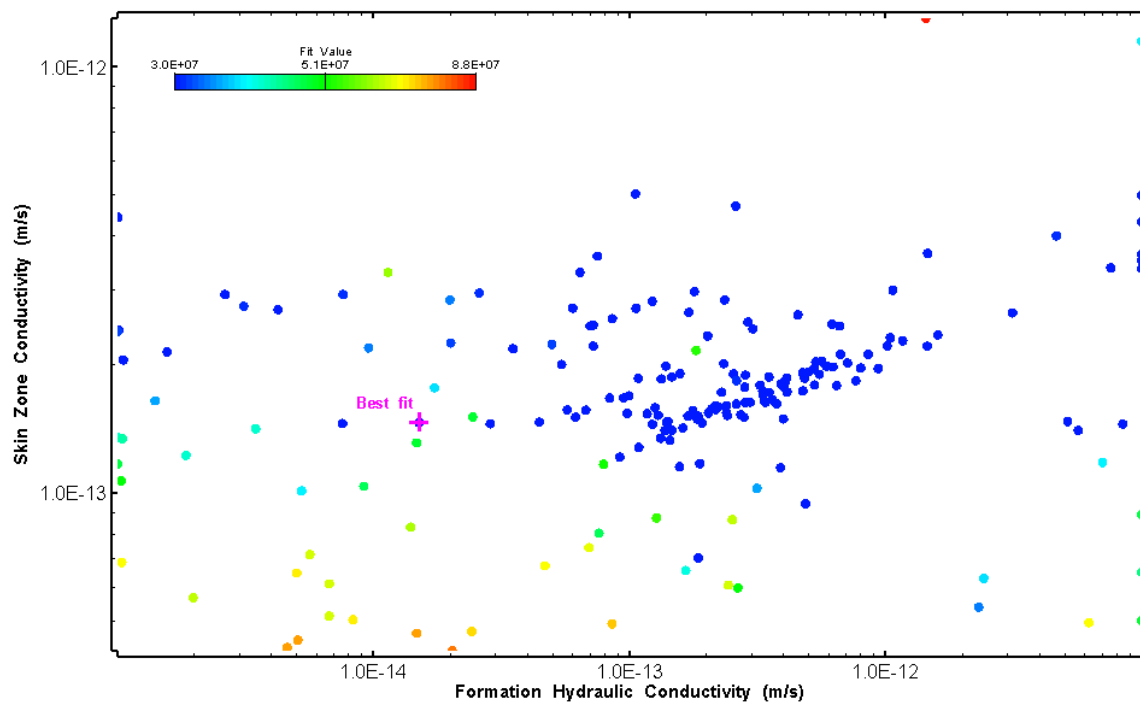


Figure 119: HT010 XY-scatter plot showing estimates of formation hydraulic conductivity and skin zone conductivity from perturbation analysis

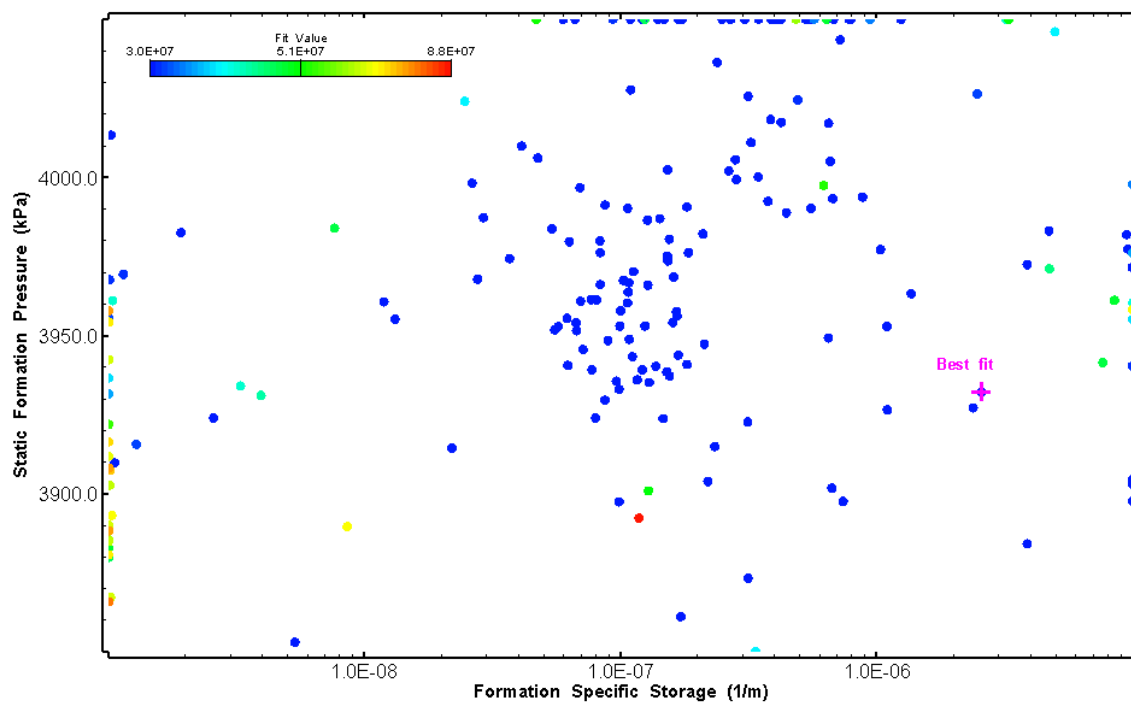


Figure 120: HT010 XY-scatter plot showing estimates of specific storage and static formation pressure from perturbation analysis

## 11.0 HT011 (462.00 – 482.02 M)

HT011 was selected to test a fractured interval containing a dyke. Four broken fractures were observed in the core. No drill fluid parameter triggers were reached during drilling. No indication of flow was recorded during FFEC logging post-drilling.

The test was initiated with a shut-in pressure recovery phase (PSR). A pulse withdrawal test (PW) with a shut-in recovery was completed after the PSR phase.

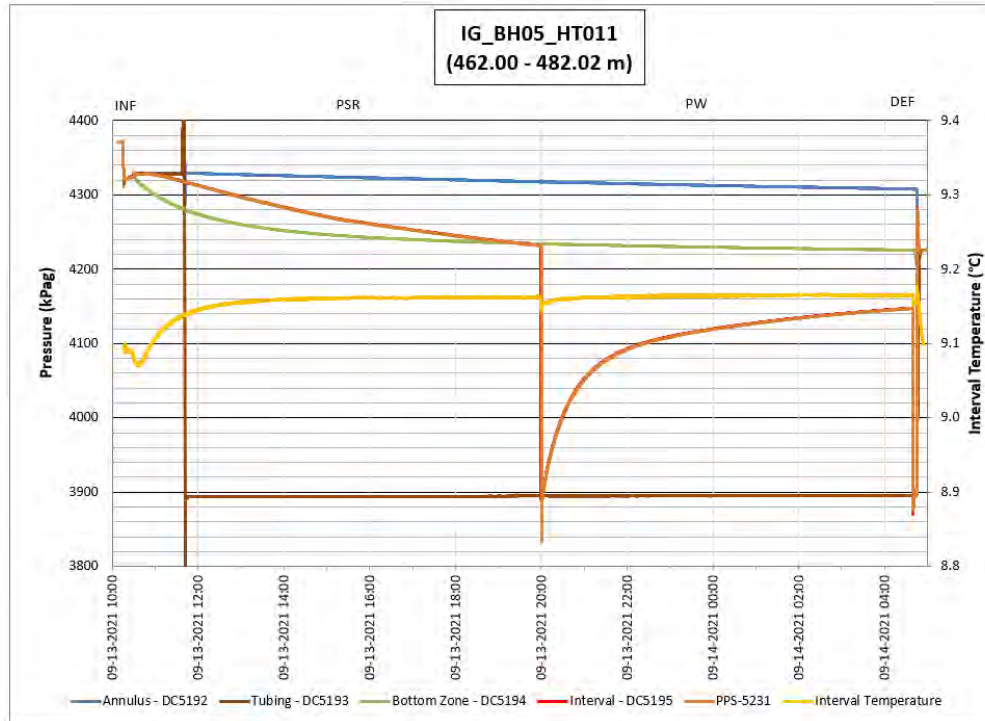
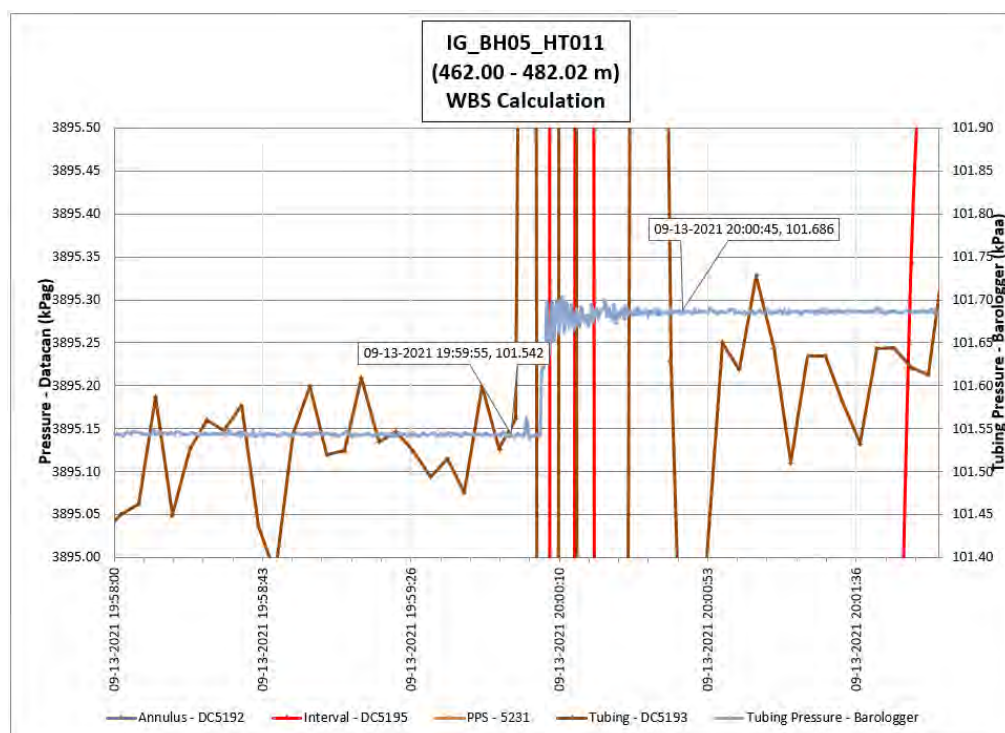


Figure 121: HT011 Annotated test plot showing monitored zone pressure and interval temperature.



**Figure 122: HT011 Tubing pressure during DHSIV activation. DHSIV Closed Wellbore Storage Estimate =  $8\text{E-}11 \text{ m}^3/\text{Pa}$**

**Table 11: Summary of Analysis Results – HT011**

	Formation conductivity	Skin zone conductivity	Static formation pressure	Formation specific storage	Radial thickness of skin	Flow dimension
	[m/s]	[m/s]	[kPa]	[1/m]	[m]	[–]
Best Fit	5E-14	1E-12	4209	2E-08	1.54E-01	3.0
Minimum	1E-14	1E-12	4140	1E-10	8E-03	1.1
Maximum	2E-11	9E-11	4230	1E-05	9E-01	3.0
Mean	7E-13	2E-12	4198	1E-06	2E-01	2.4
Median	2E-13	1E-12	4201	6E-09	2E-01	2.4
Geometric mean	2E-13	2E-12	4198	1E-08	2E-01	2.3

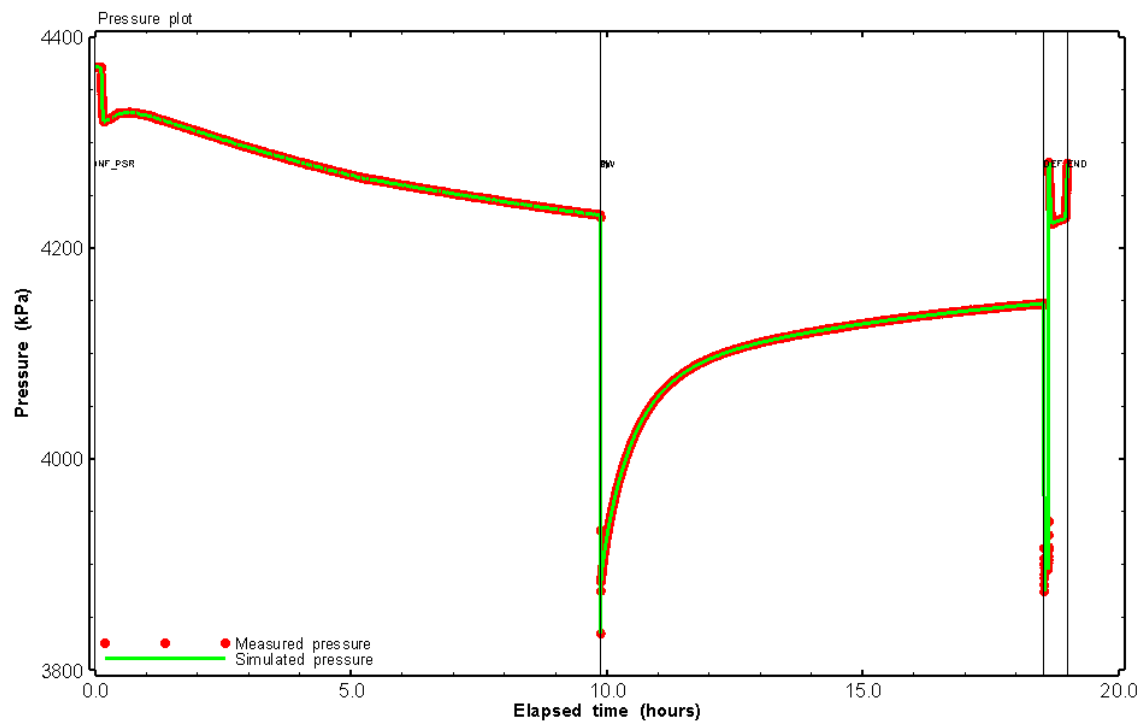


Figure 123: HT011 Pressure plot showing best-fit simulation and best fit results

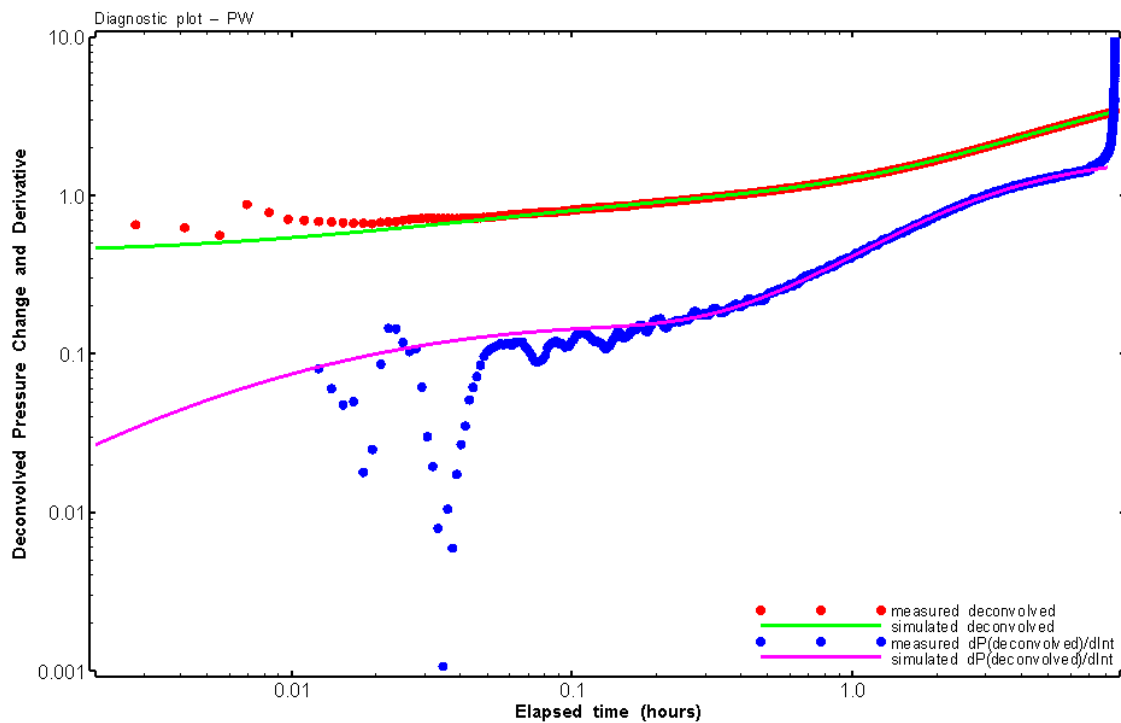


Figure 124: HT011 Deconvolved pressure change and derivative plot of the PW sequence showing best-fit simulation

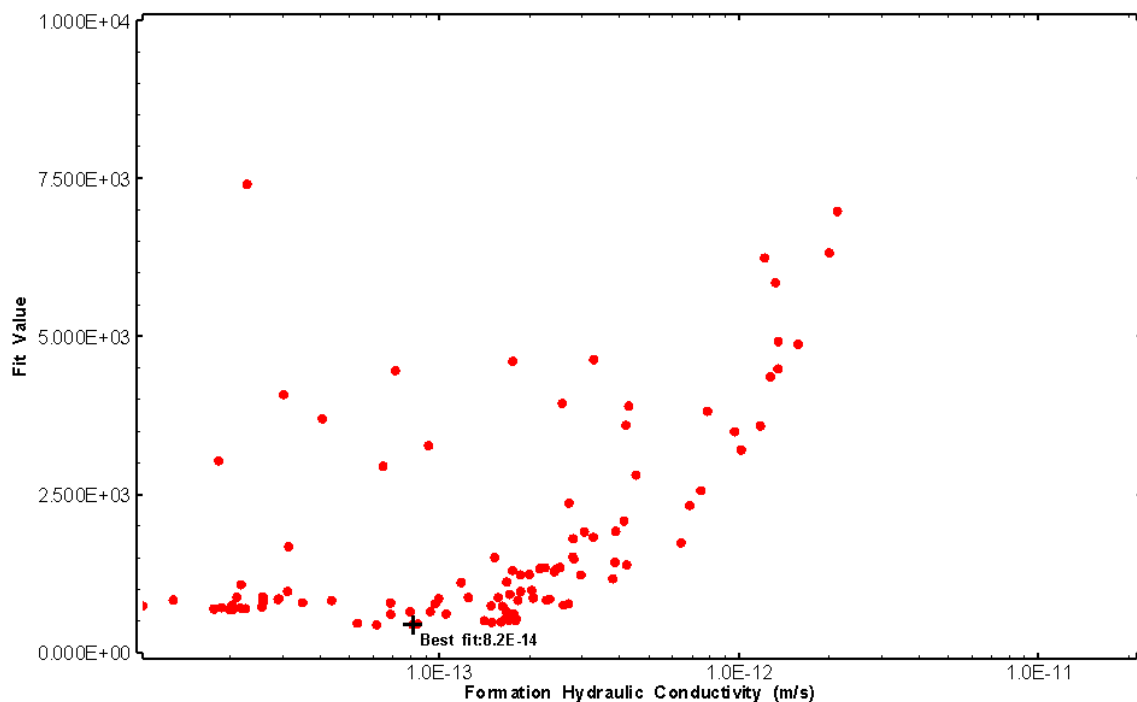


Figure 125: HT011 XY-scatter plot of formation hydraulic conductivity vs. fit value

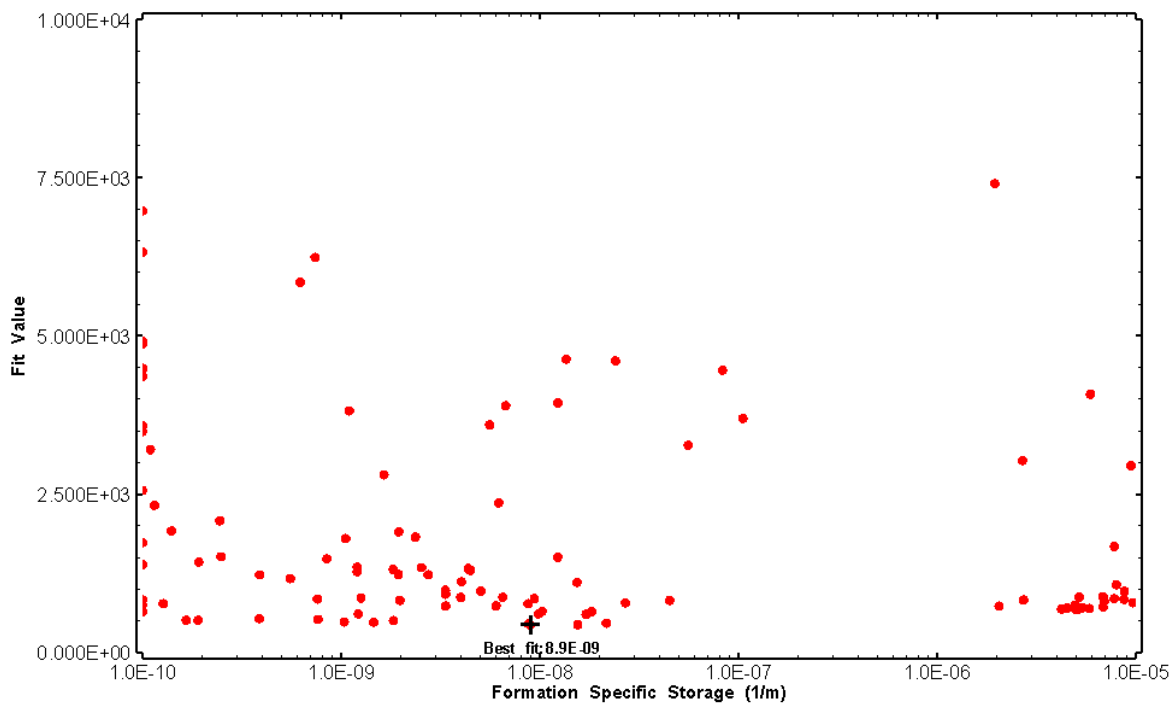


Figure 126: HT011 XY-scatter plot of formation specific storage vs. fit value

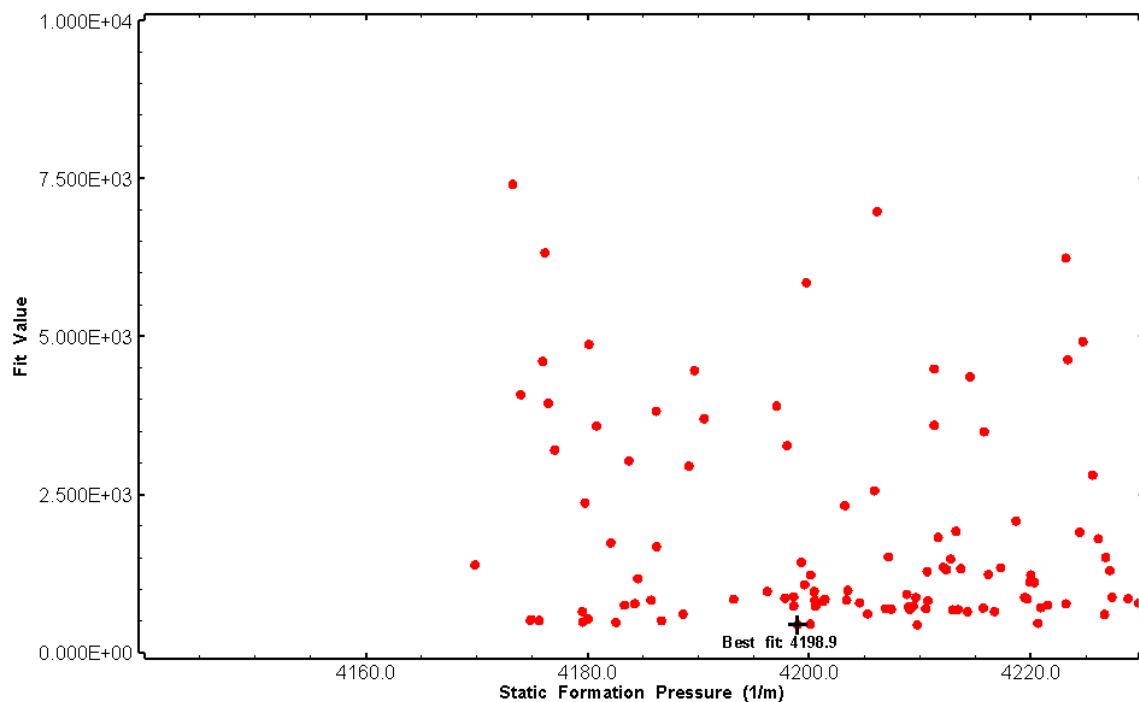


Figure 127: HT011 XY-scatter plot of static formation pressure vs. fit value

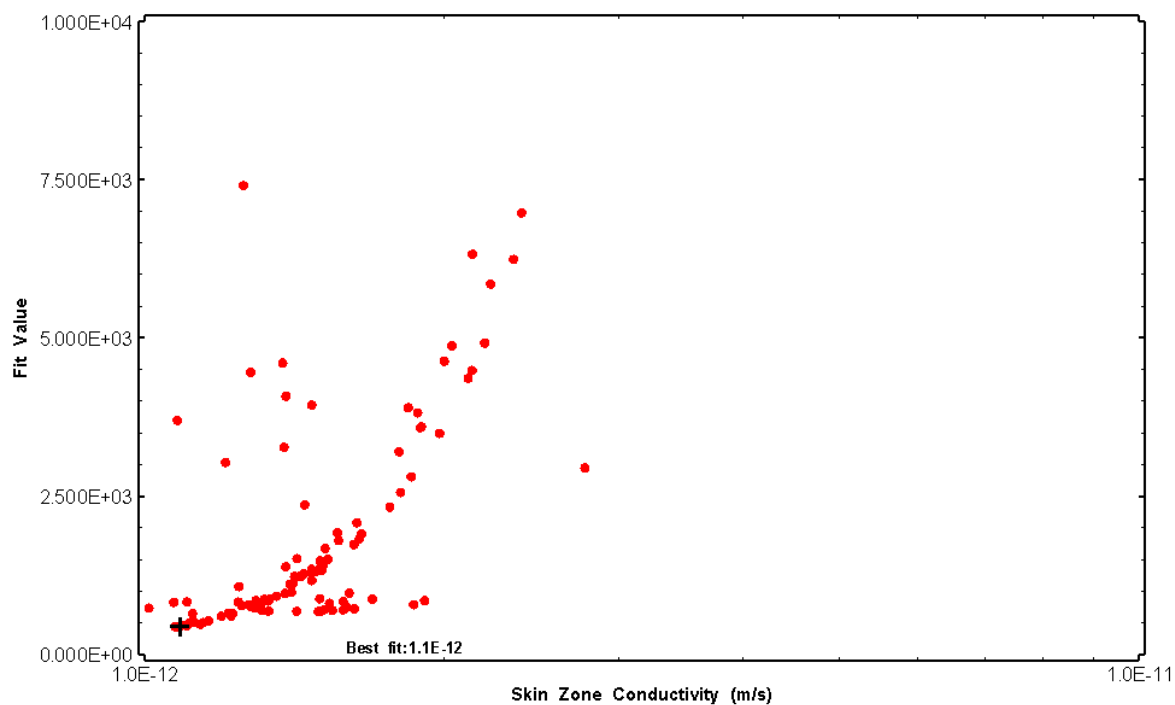


Figure 128: HT011 XY-scatter plot of skin zone conductivity vs. fit value

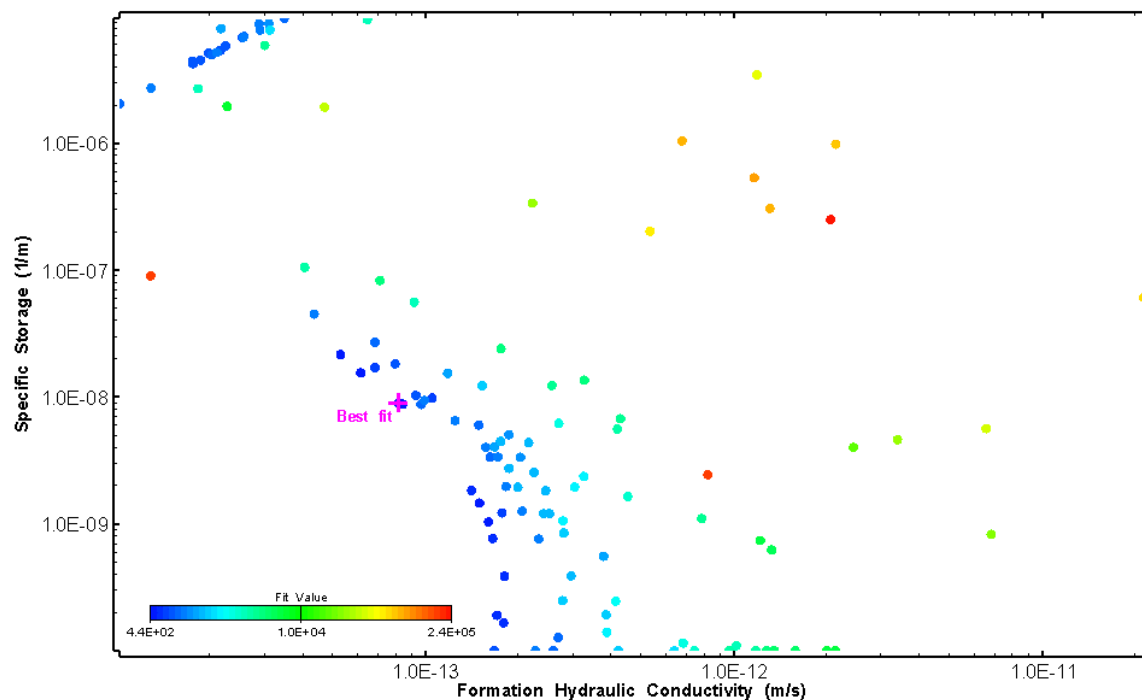


Figure 129: HT011 XY-scatter plot showing estimates of formation hydraulic conductivity and specific storage from perturbation analysis

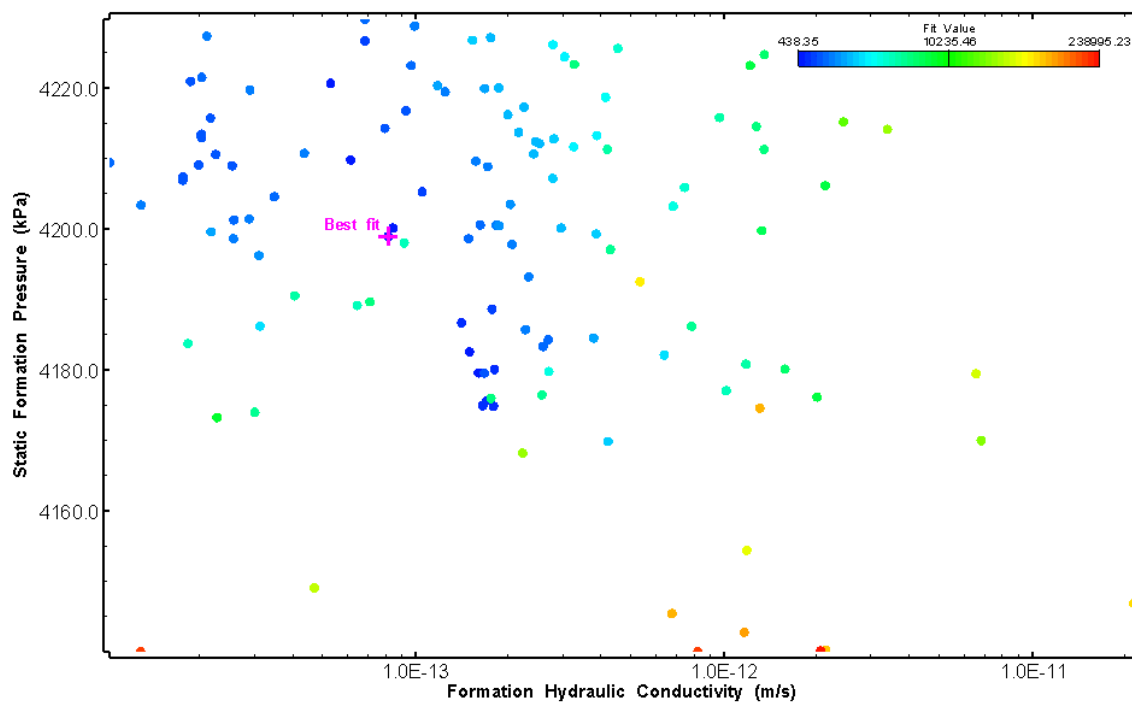


Figure 130: HT011 XY-scatter plot showing estimates of formation hydraulic conductivity and static formation pressure from perturbation analysis

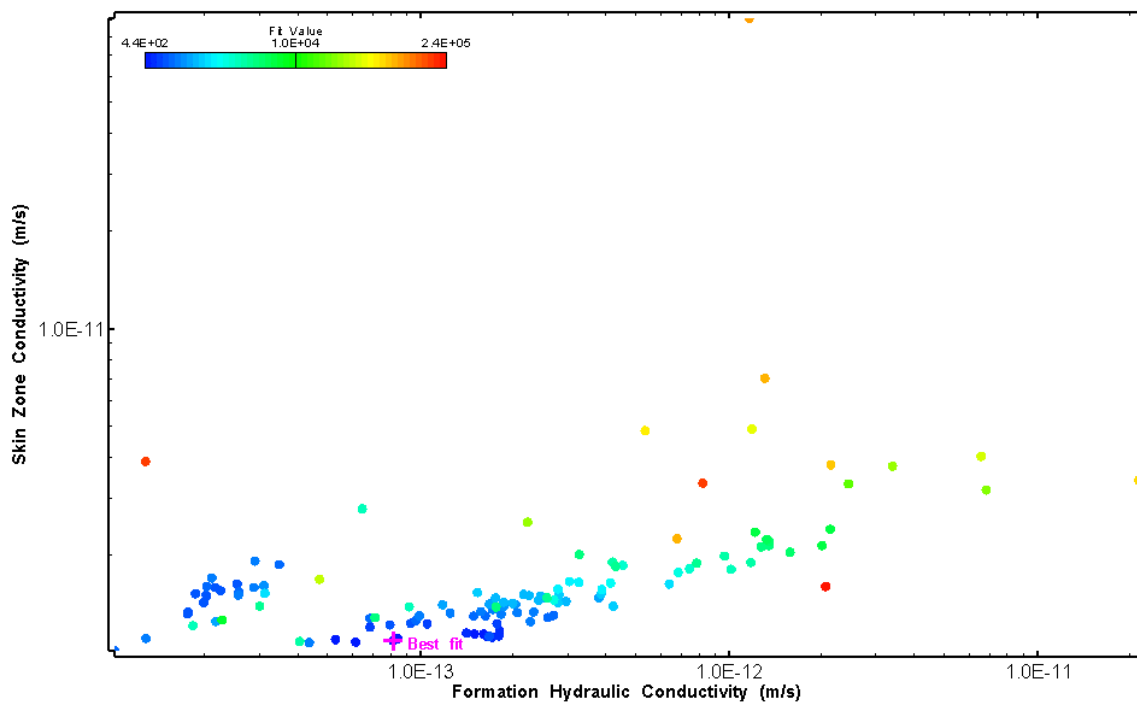


Figure 131: HT011 XY-scatter plot showing estimates of formation hydraulic conductivity and skin zone conductivity from perturbation analysis

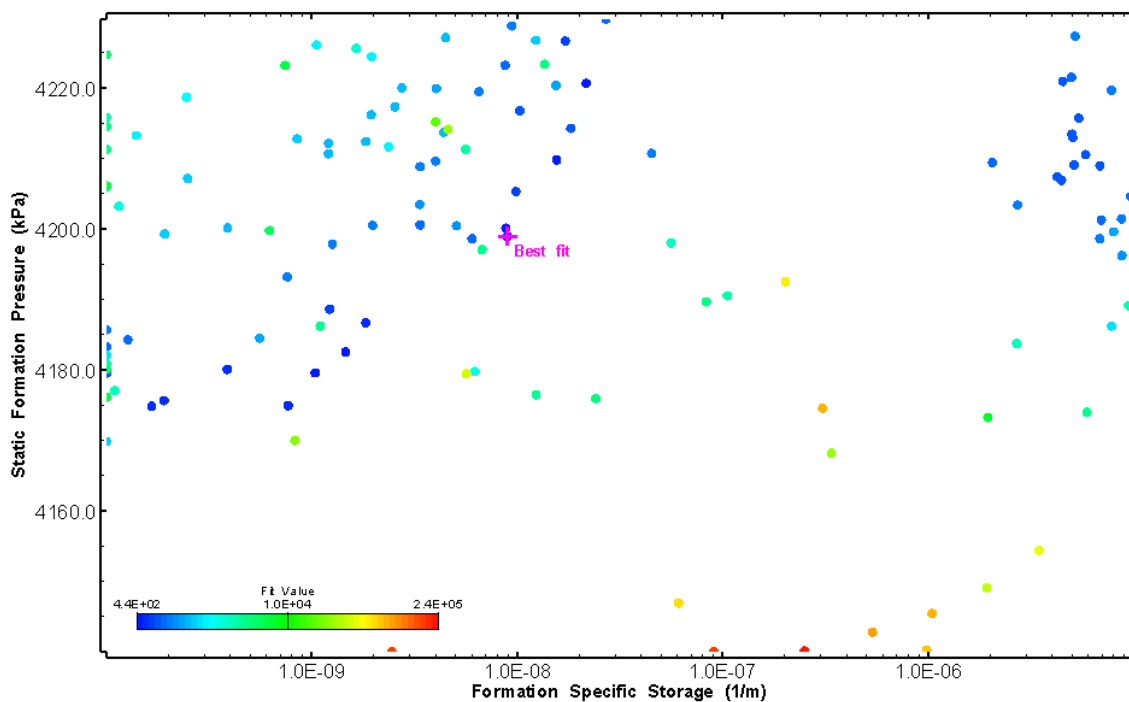


Figure 132: HT011 XY-scatter plot showing estimates of specific storage and static formation pressure from perturbation analysis



## 12.0 HT012 (518.00 – 538.02 M)

HT012 was selected to test an intact interval. Zero broken fractures were observed in the core. No drill fluid parameter triggers were reached during drilling. No indication of flow was recorded during FFEC logging post-drilling.

The test was initiated with a shut-in pressure recovery phase (PSR). A pulse withdrawal test (PW) with a shut-in recovery was completed after the PSR phase.

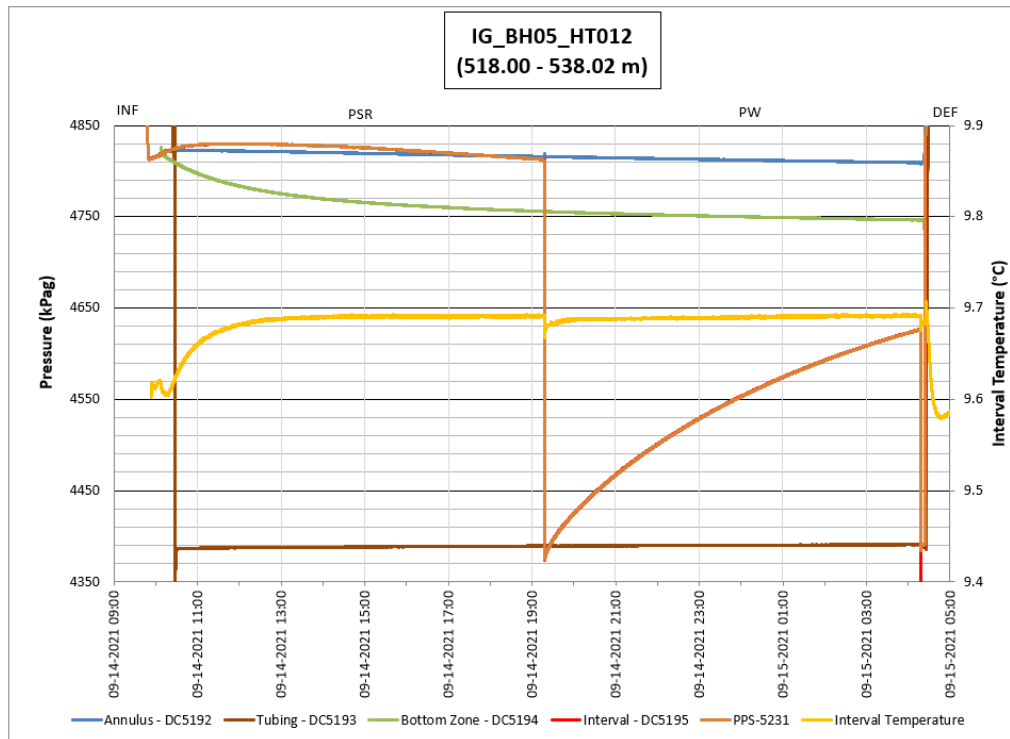
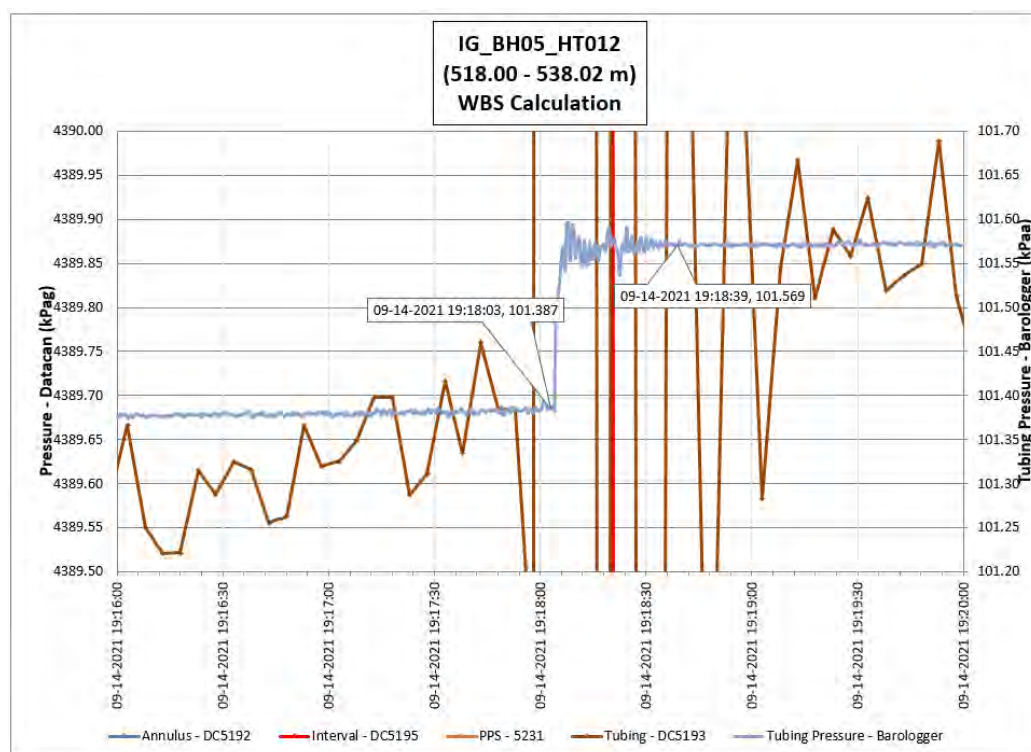


Figure 133: HT012 Annotated test plot showing monitored zone pressure and interval temperature.



**Figure 134: HT012 Tubing pressure during DHSIV activation. DHSIV Closed Wellbore Storage Estimate =  $8\text{E-}11 \text{ m}^3/\text{Pa}$**

**Table 12: Summary of Analysis Results – HT012**

	Formation conductivity	Skin zone conductivity	Static formation pressure	Formation specific storage	Radial thickness of skin	Flow dimension
	[m/s]	[m/s]	[kPa]	[1/m]	[m]	[–]
Best Fit	3E-13	2E-13	4758	2E-07	1.03E-01	2.7
Minimum	1E-15	1E-13	4714	1E-10	1E-02	1.4
Maximum	9E-12	1E-11	4849	1E-05	1E-00	3.0
Mean	9E-13	3E-13	4789	7E-07	2E-01	2.3
Median	4E-13	2E-13	4790	1E-07	1E-01	2.3
Geometric mean	3E-13	2E-13	4789	8E-08	1E-01	2.3

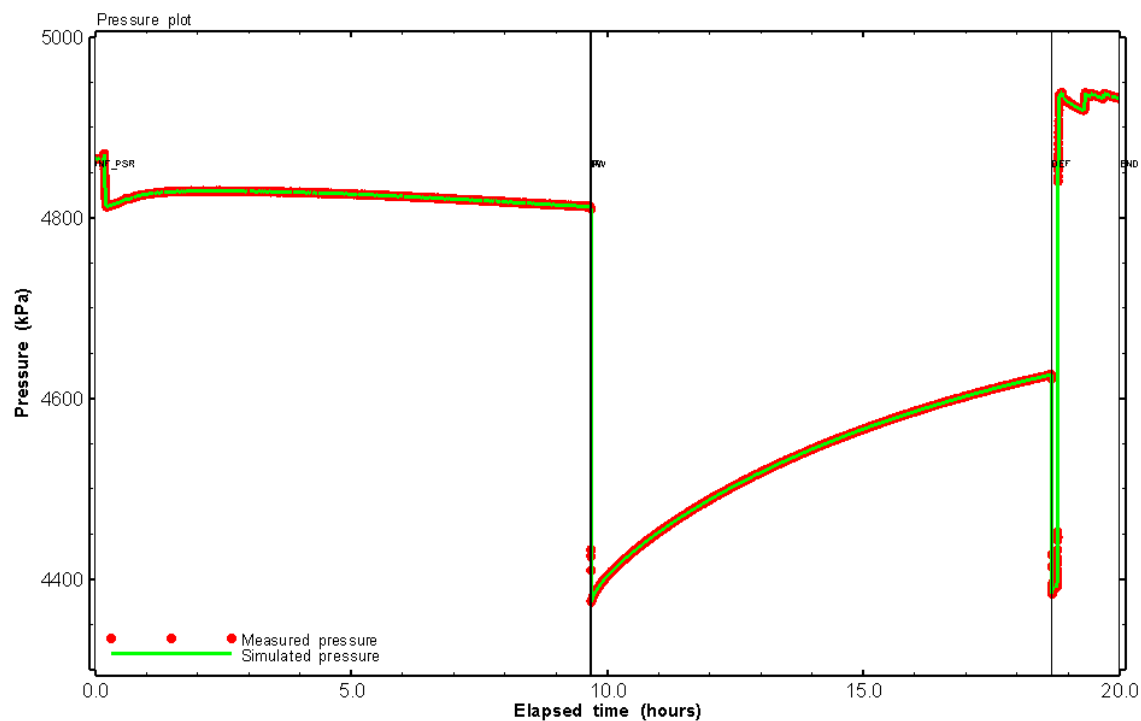


Figure 135: HT012 Pressure plot showing best-fit simulation and best fit results

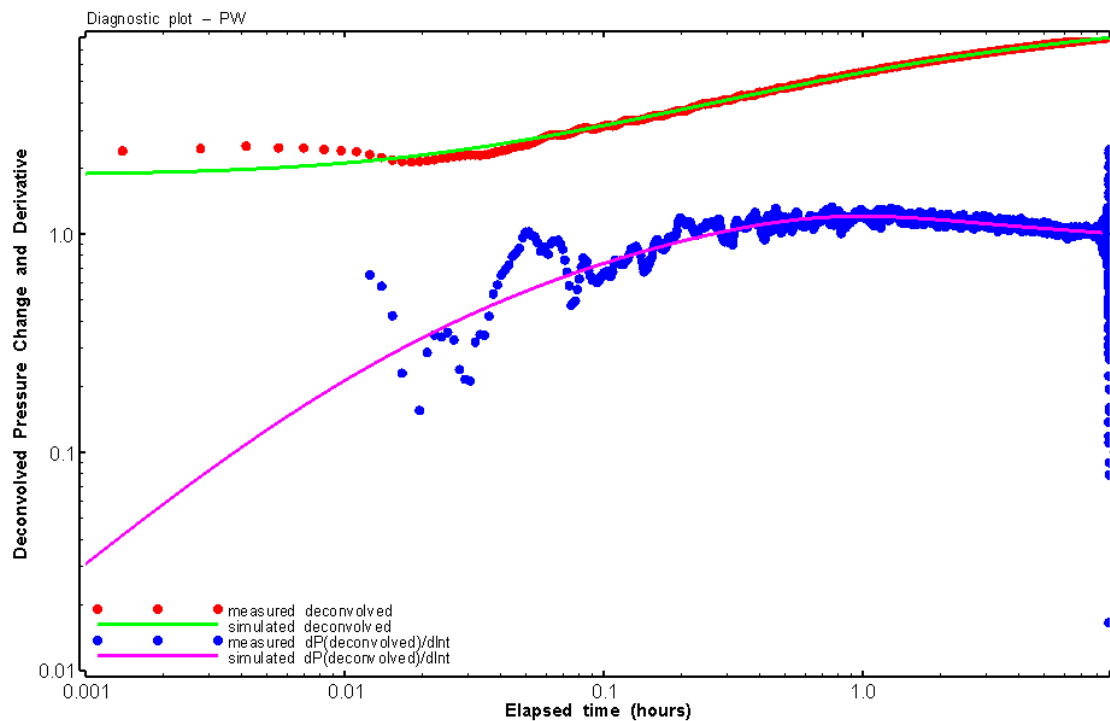


Figure 136: HT012 Deconvolved pressure change and derivative plot of the PW sequence showing best-fit simulation

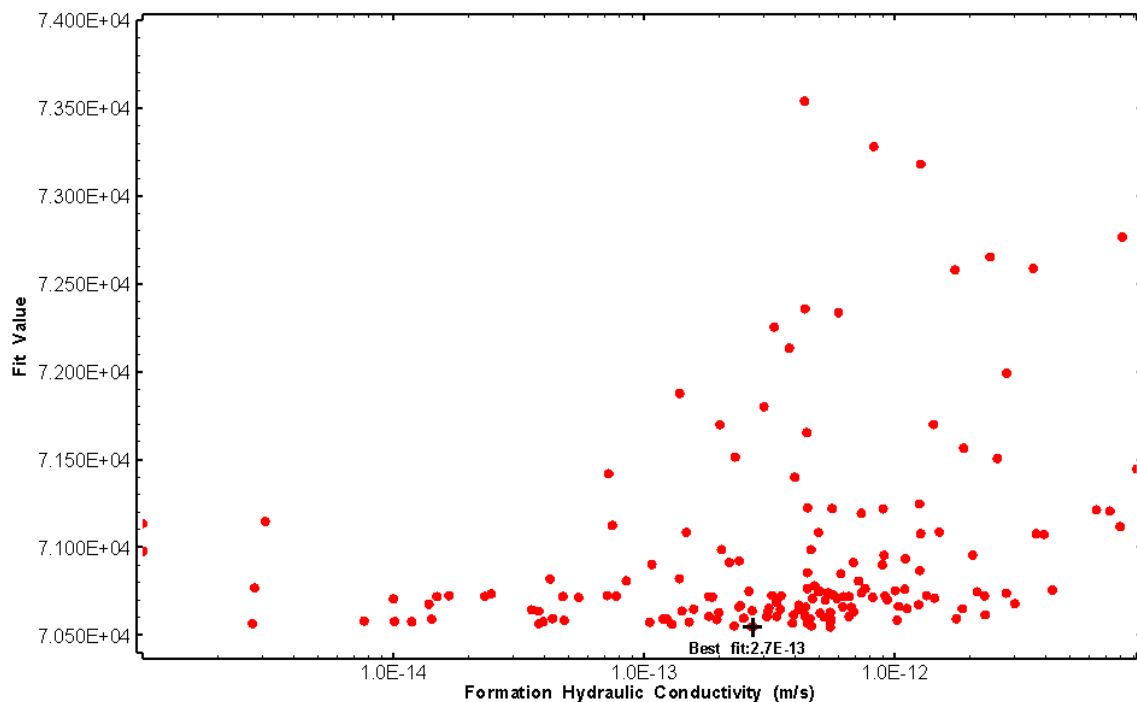


Figure 137: HT012 XY-scatter plot of formation hydraulic conductivity vs. fit value

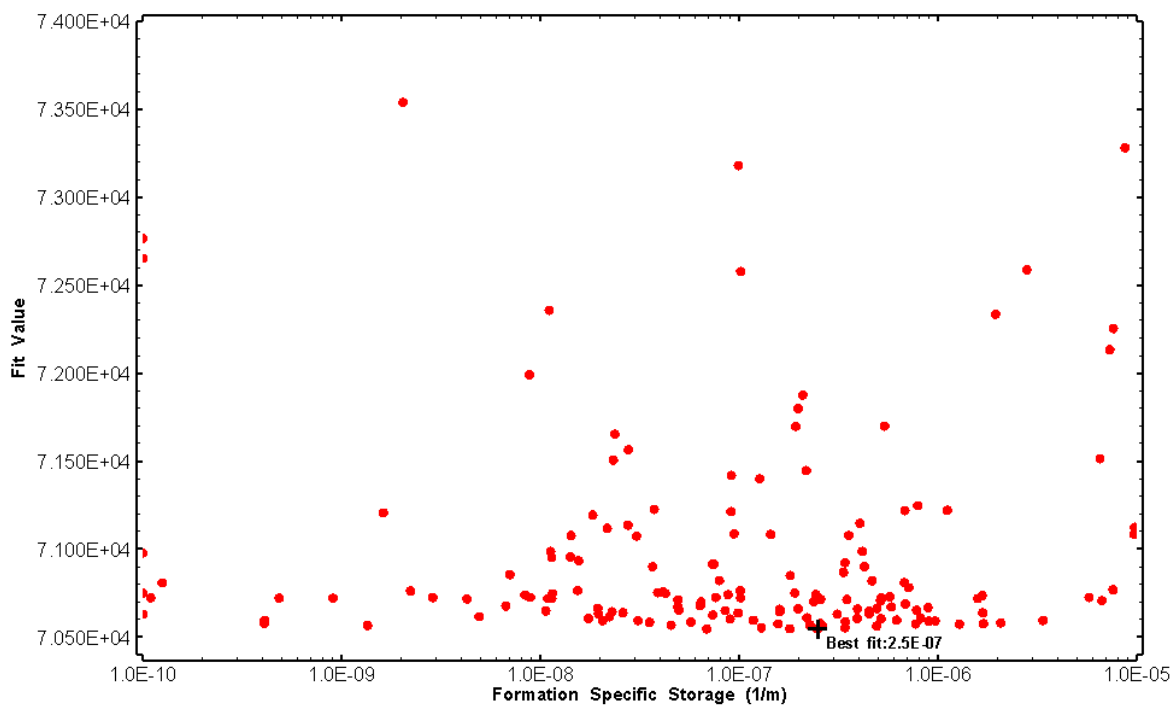


Figure 138: HT012 XY-scatter plot of formation specific storage vs. fit value

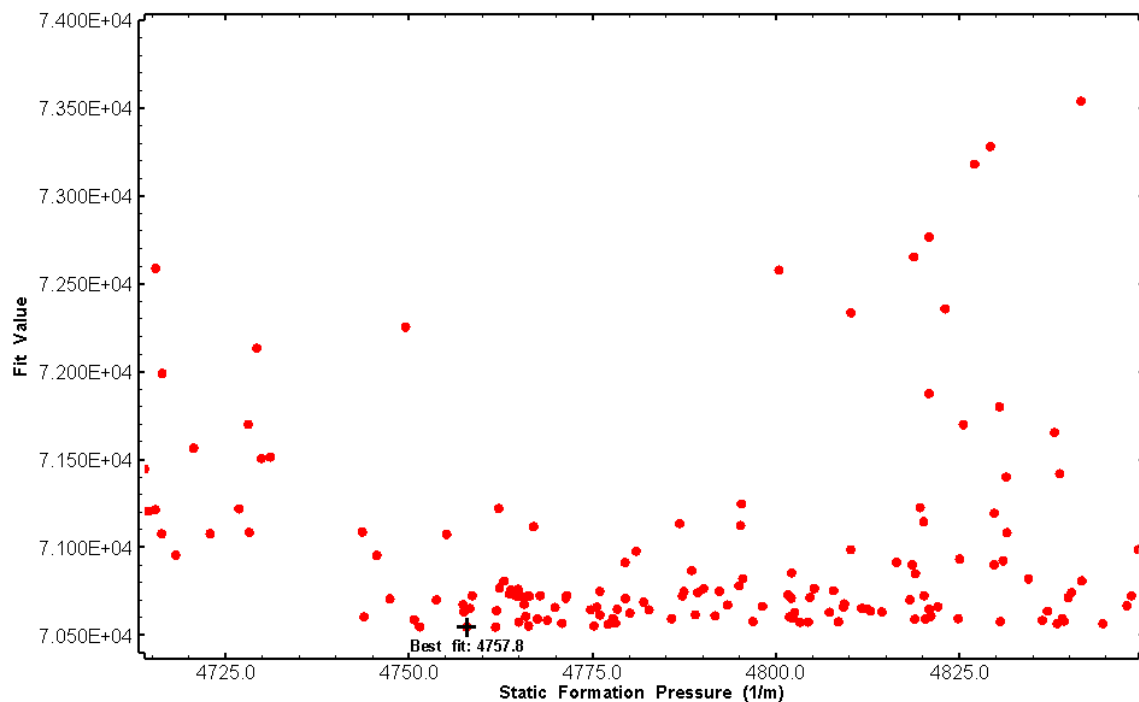


Figure 139: HT012 XY-scatter plot of static formation pressure vs. fit value

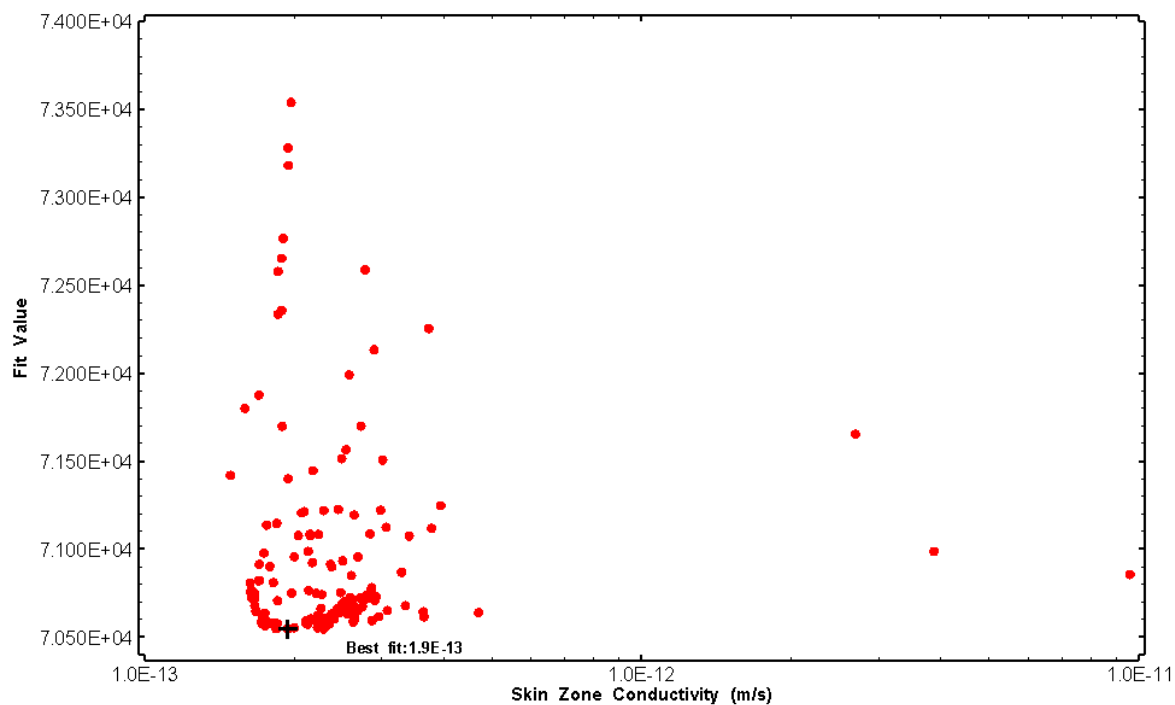


Figure 140: HT012 XY-scatter plot of skin zone conductivity vs. fit value

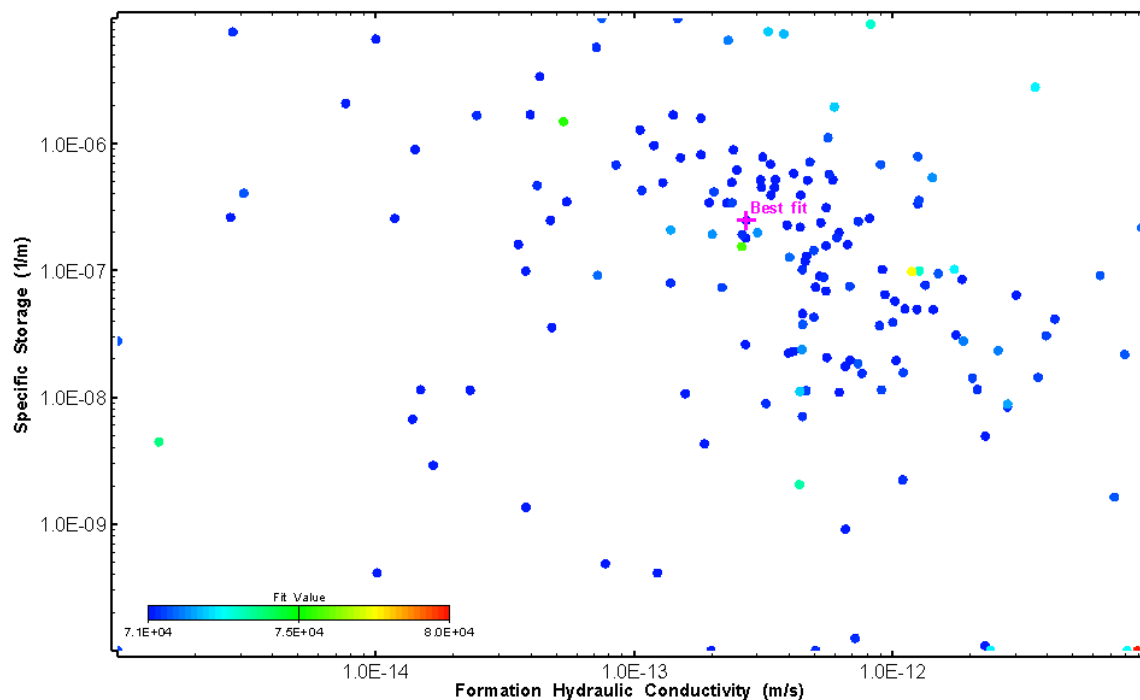


Figure 141: HT012 XY-scatter plot showing estimates of formation hydraulic conductivity and specific storage from perturbation analysis

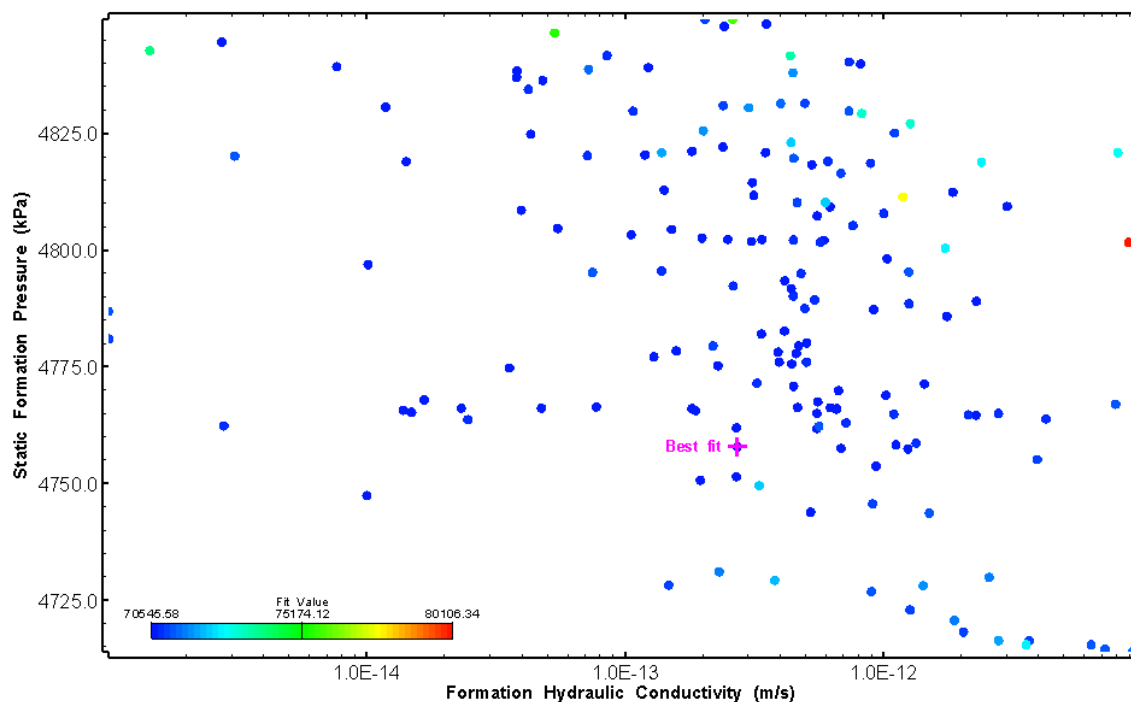


Figure 142: HT012 XY-scatter plot showing estimates of formation hydraulic conductivity and static formation pressure from perturbation analysis

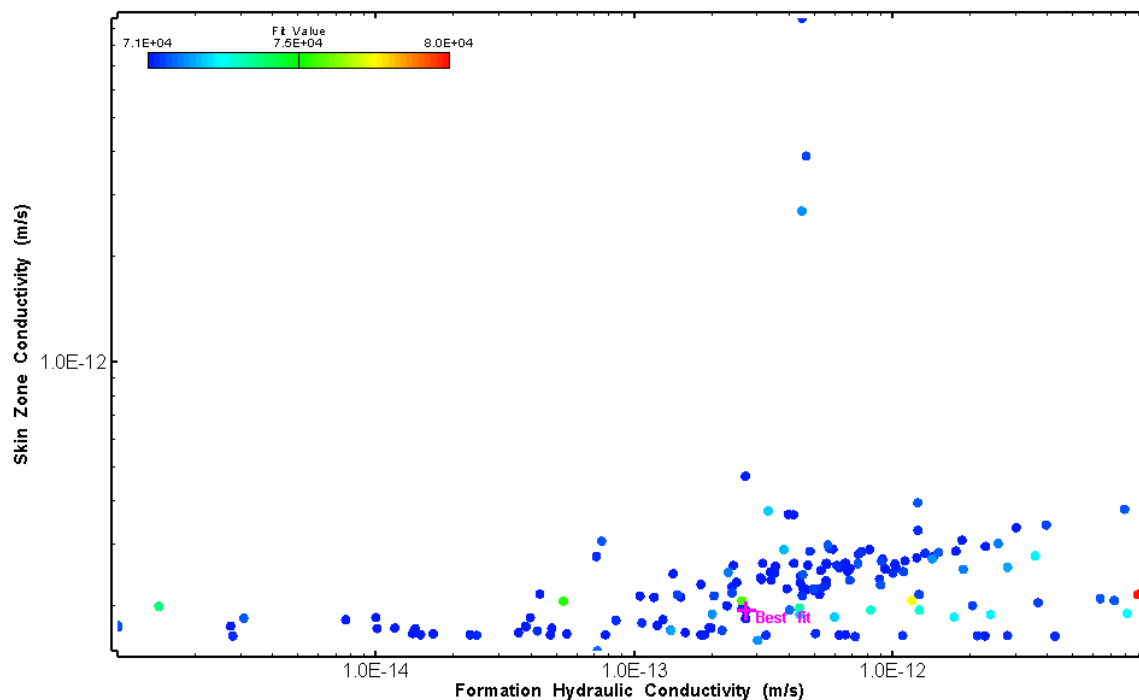


Figure 143: HT012 XY-scatter plot showing estimates of formation hydraulic conductivity and skin zone conductivity from perturbation analysis

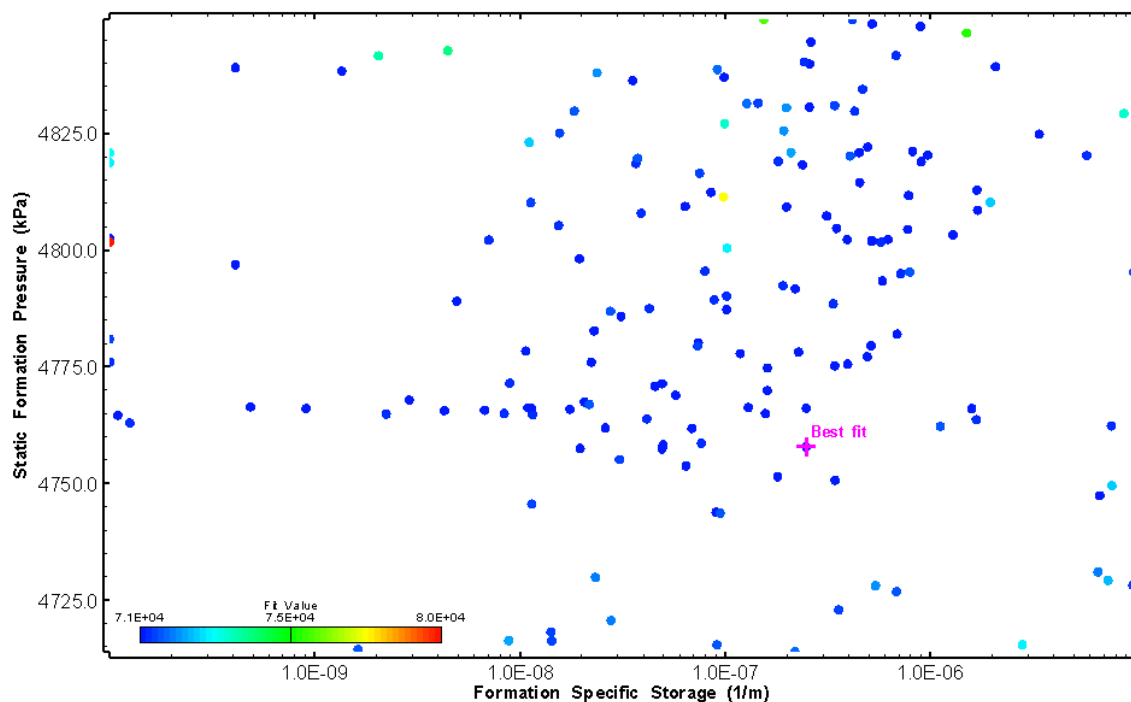


Figure 144: HT012 XY-scatter plot showing estimates of specific storage and static formation pressure from perturbation analysis

### 13.0 HT013 (564.02 – 584.04 M)

HT013 was selected to test an intact zone. Zero broken fractures were observed in the core. No loss of drilling fluid was observed in this interval during drilling. No indication of flow was recorded during FFEC logging post-drilling.

The test was initiated with a shut-in pressure recovery phase (PSR). A pulse withdrawal test (PW) with a shut-in recovery was completed after the PSR phase.

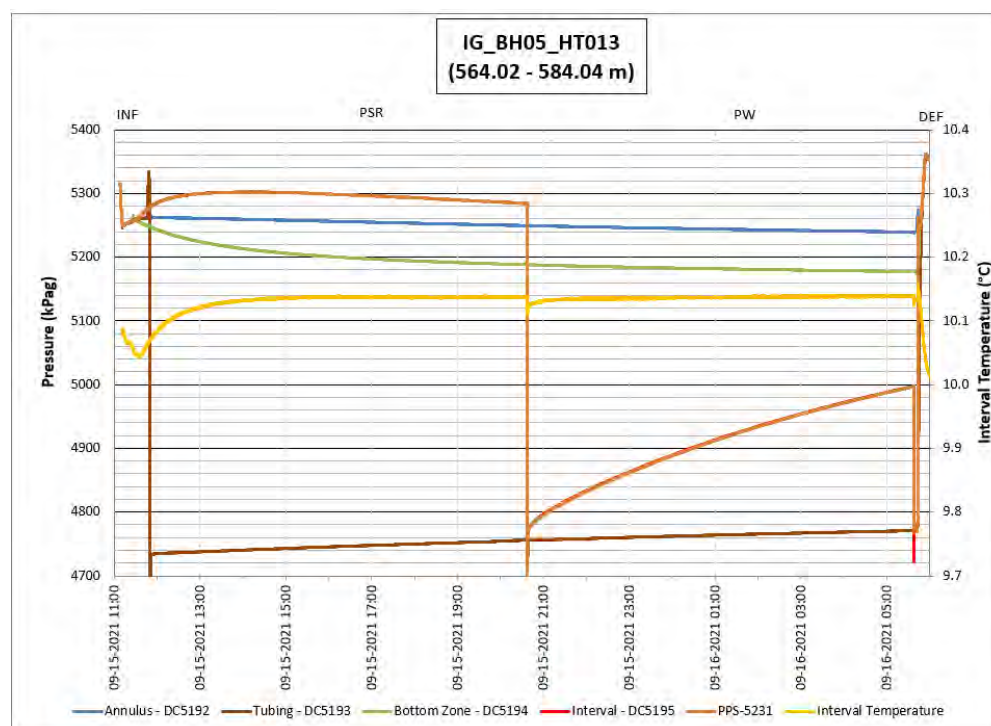
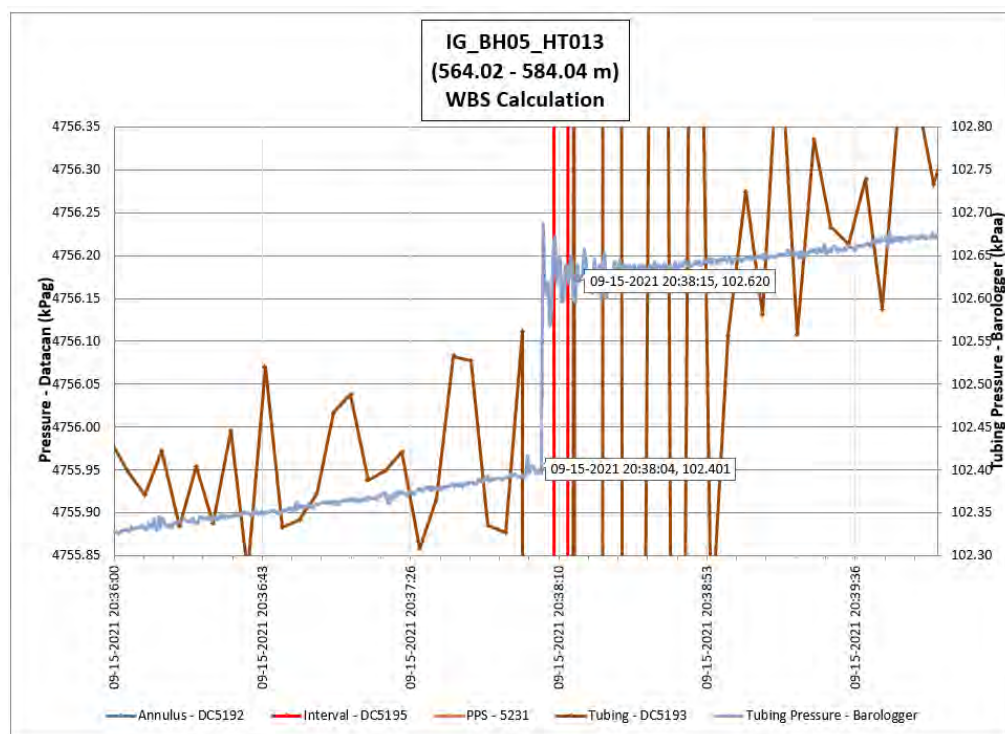


Figure 145: HT013 Annotated test plot showing monitored zone pressure and interval temperature.





**Figure 146: HT013 Tubing pressure during DHSIV activation. DHSIV Closed Wellbore Storage Estimate =  $8\text{E-}11 \text{ m}^3/\text{Pa}$**

**Table 13: Summary of Analysis Results – HT013**

	Formation conductivity	Skin zone conductivity	Static formation pressure	Formation specific storage	Radial thickness of skin	Flow dimension
	[m/s]	[m/s]	[kPa]	[1/m]	[m]	[–]
Best Fit	4E-13	1E-13	5204	1E-06	7.02E-02	2.3
Minimum	1E-14	1E-14	5179	1E-09	6E-04	1.0
Maximum	3E-12	1E-09	5299	8E-06	2E-01	3.0
Mean	3E-13	2E-10	5259	4E-07	5E-02	2.4
Median	1E-13	3E-11	5268	2E-08	4E-02	2.5
Geometric mean	2E-13	1E-11	5259	3E-08	3E-02	2.4

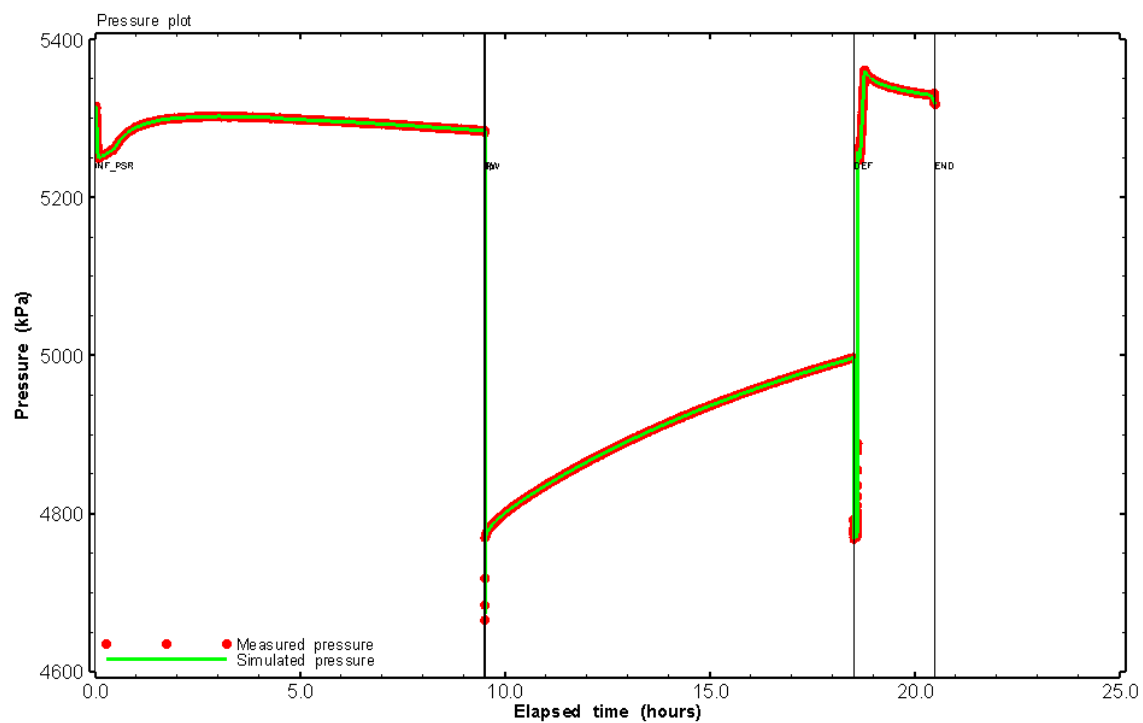


Figure 147: HT013 Pressure plot showing best-fit simulation and best fit results

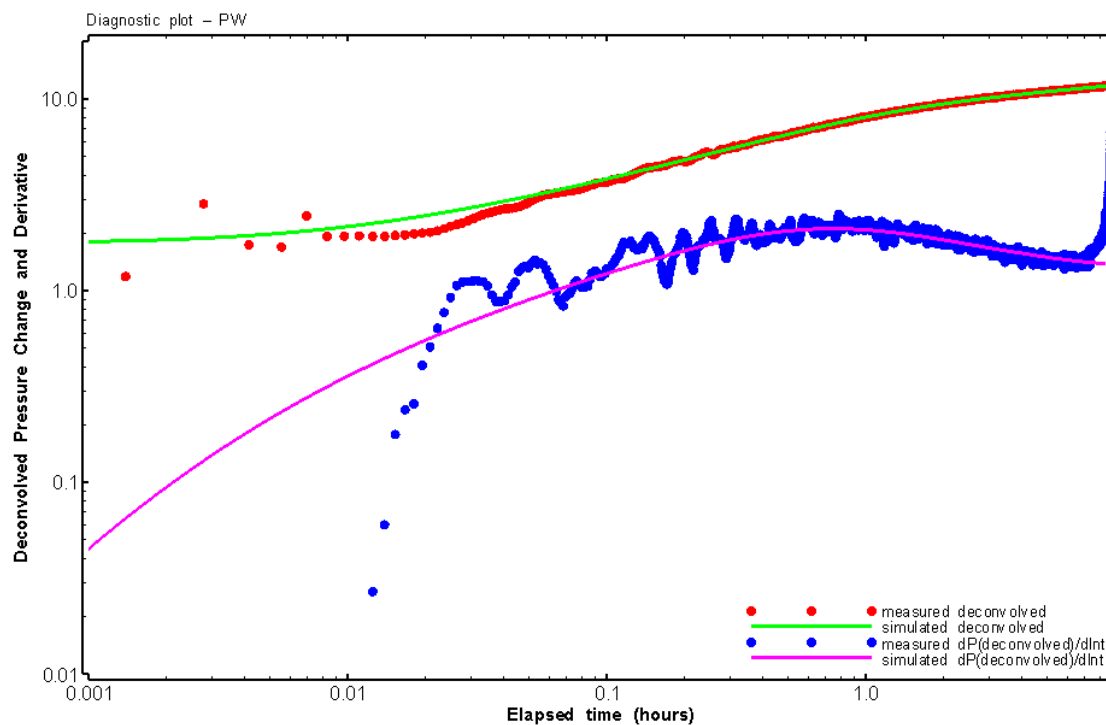


Figure 148: HT013 Deconvolved pressure change and derivative plot of the PW sequence showing best-fit simulation

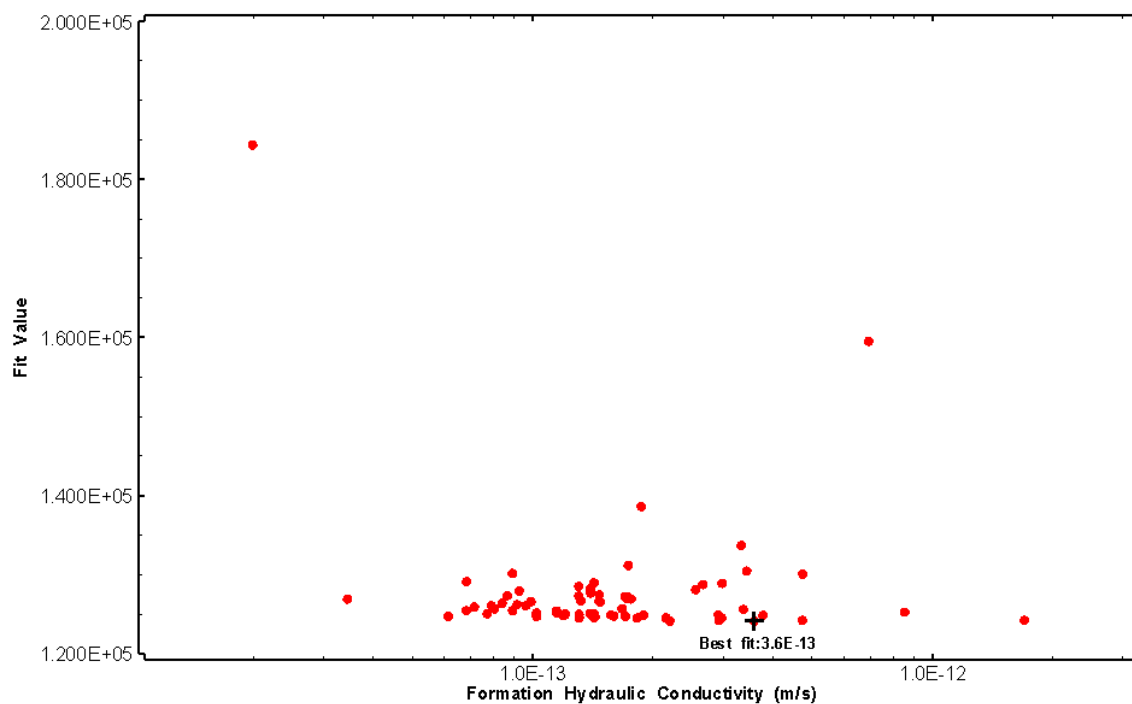


Figure 149: HT013 XY-scatter plot of formation hydraulic conductivity vs. fit value

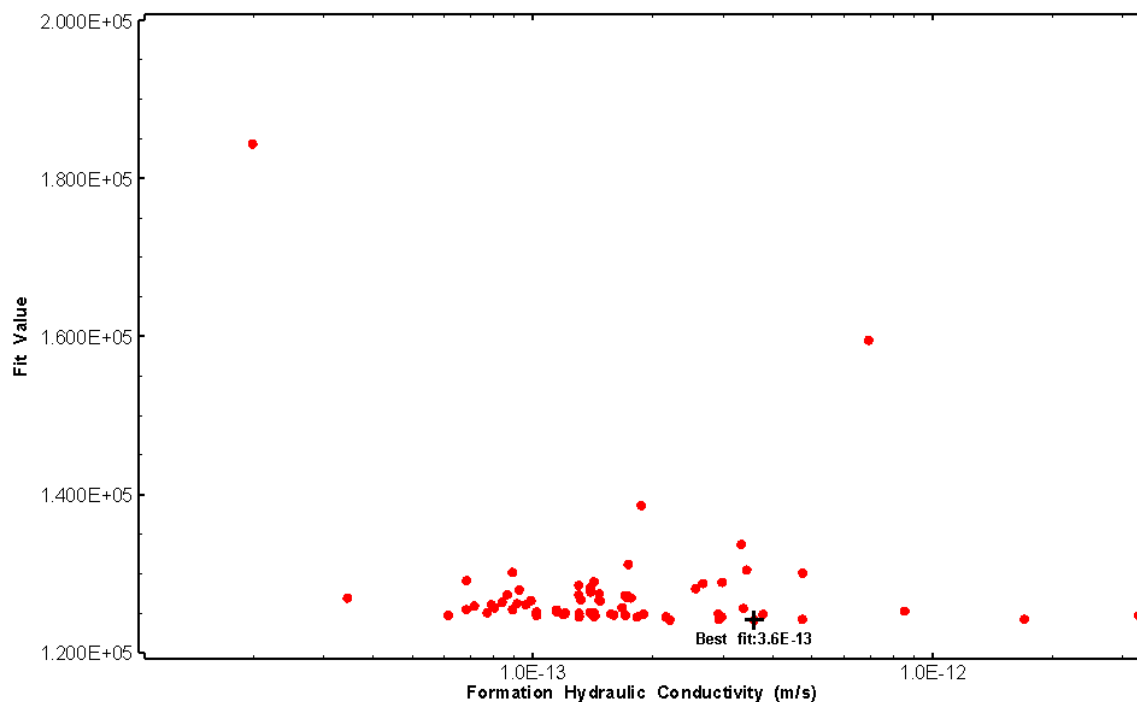


Figure 150: HT013 XY-scatter plot of formation specific storage vs. fit value

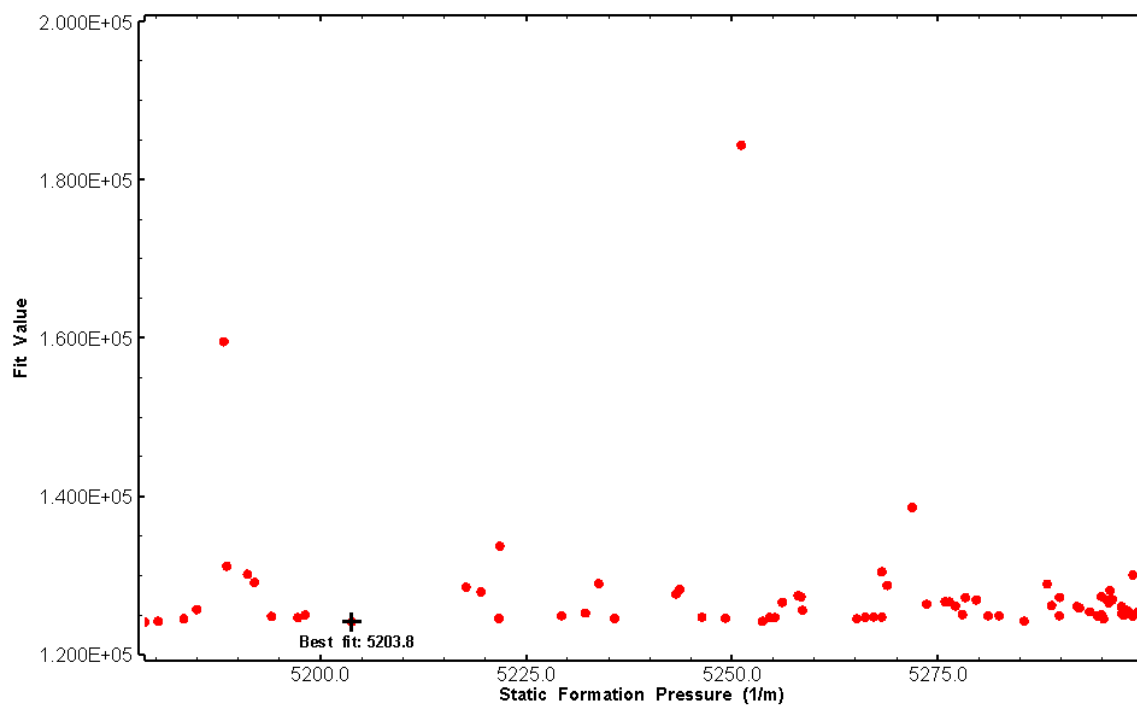


Figure 151: HT013 XY-scatter plot of static formation pressure vs. fit value

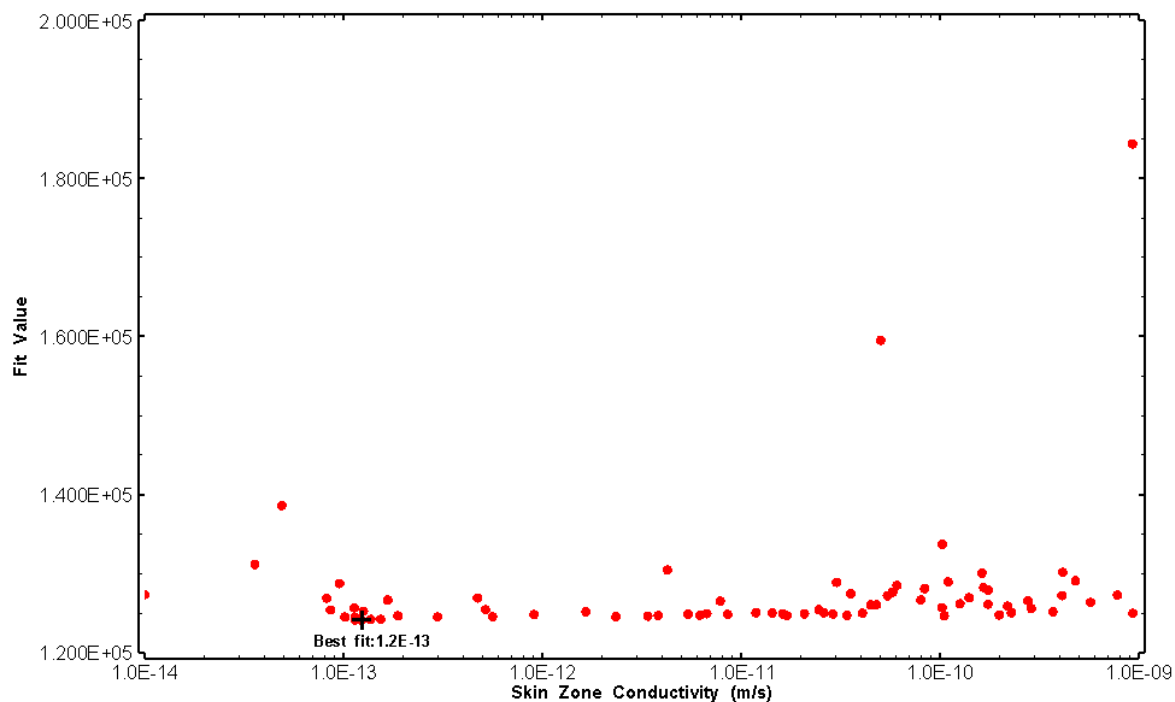


Figure 152: HT013 XY-scatter plot of skin zone conductivity vs. fit value

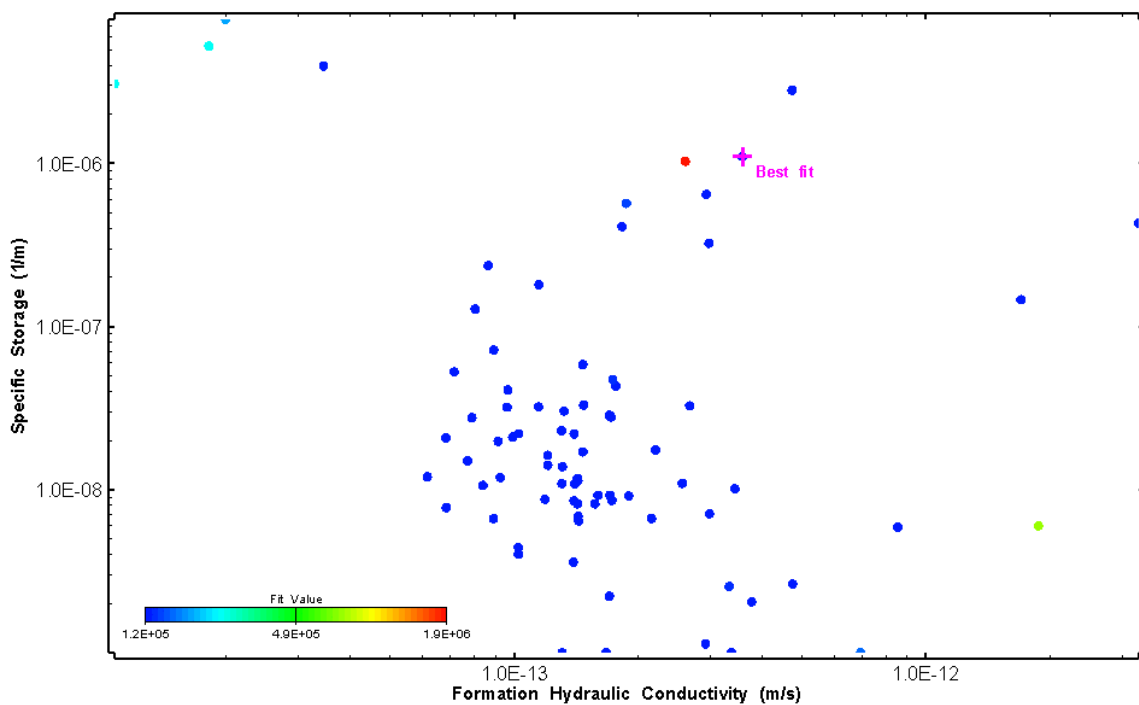


Figure 153: HT013 XY-scatter plot showing estimates of formation hydraulic conductivity and specific storage from perturbation analysis

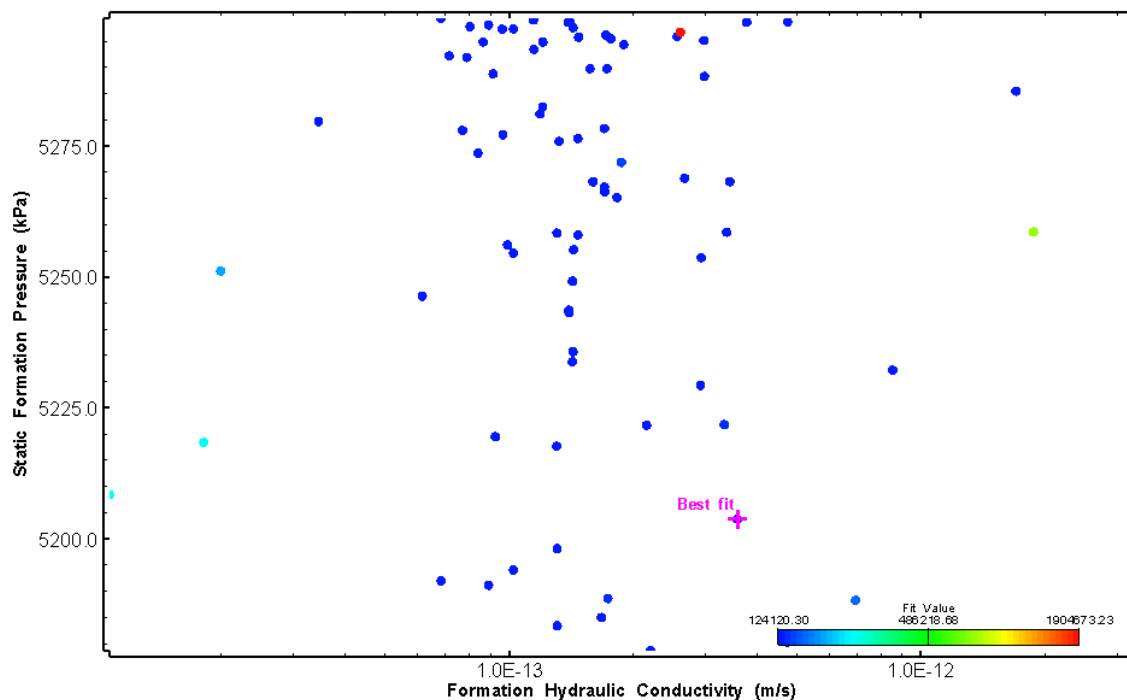


Figure 154: HT013 XY-scatter plot showing estimates of formation hydraulic conductivity and static formation pressure from perturbation analysis

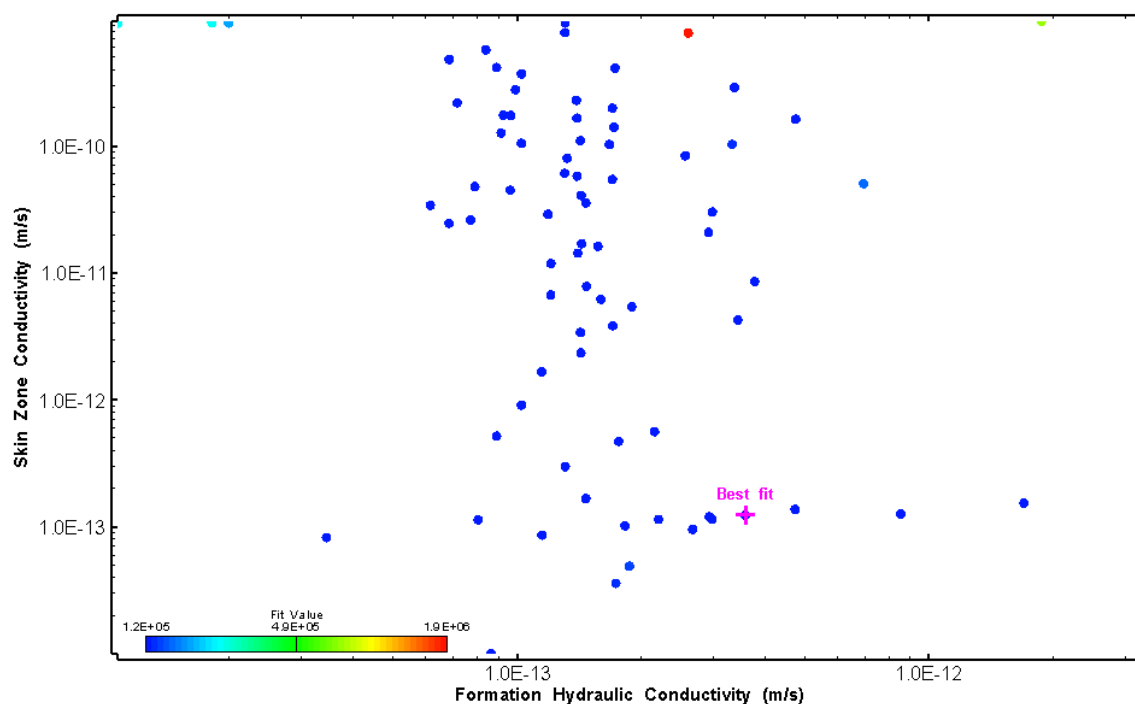
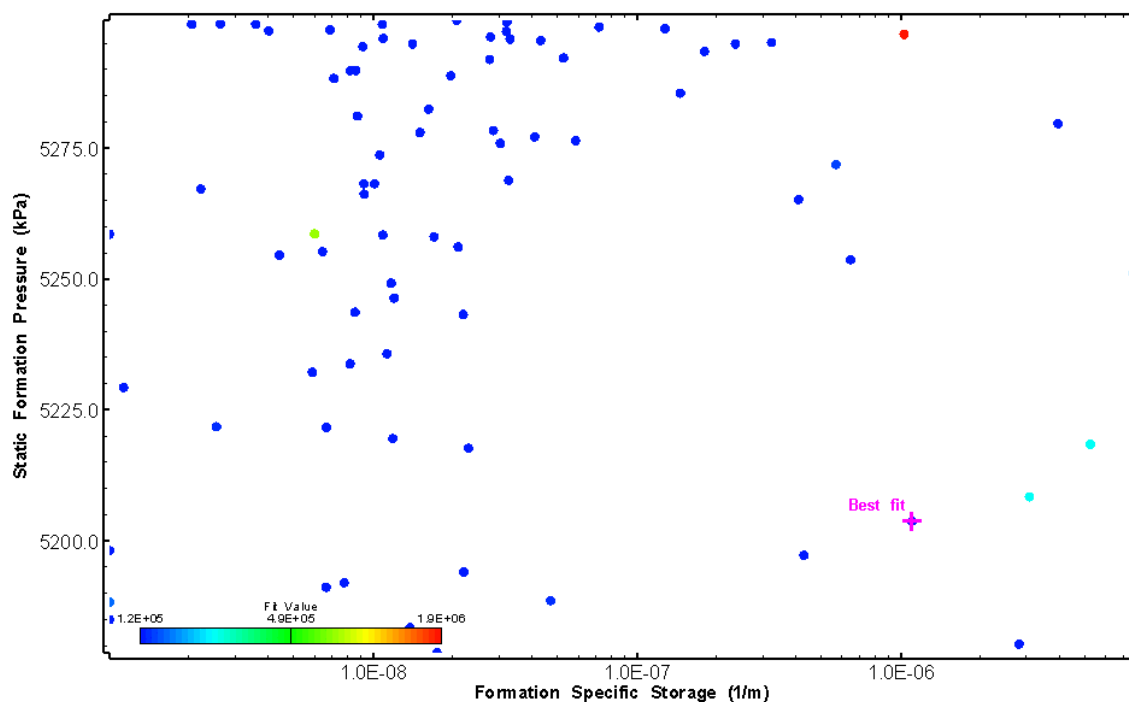


Figure 155: HT013 XY-scatter plot showing estimates of formation hydraulic conductivity and skin zone conductivity from perturbation analysis



**Figure 156: HT013 XY-scatter plot showing estimates of specific storage and static formation pressure from perturbation analysis**

## 14.0 HT014 (594.20 – 614.22 M)

HT014 was selected to obtain continuous testing coverage from 600 to 800 m along hole. 13 broken fractures were observed in the core. No drill fluid parameter triggers were reached during drilling. No indication of flow was recorded during FFEC logging post-drilling.

The test was initiated with a shut-in pressure recovery phase (PSR). A pulse withdrawal test (PW) with a shut-in recovery was completed after the PSR phase.

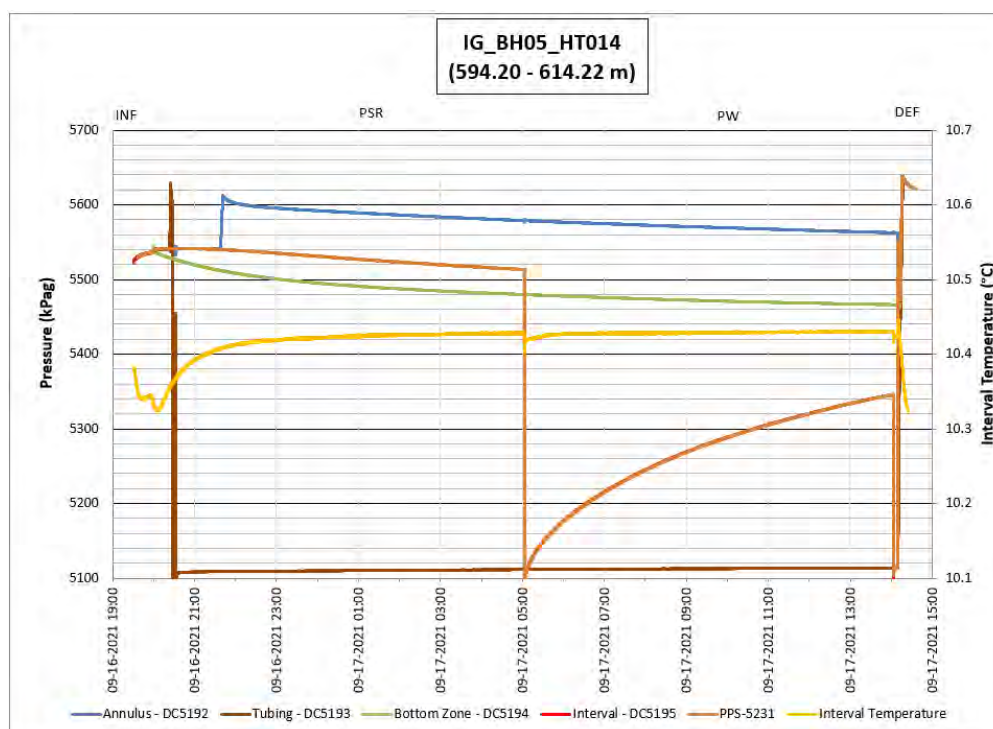


Figure 157: HT014 Annotated test plot showing monitored zone pressure and interval temperature.

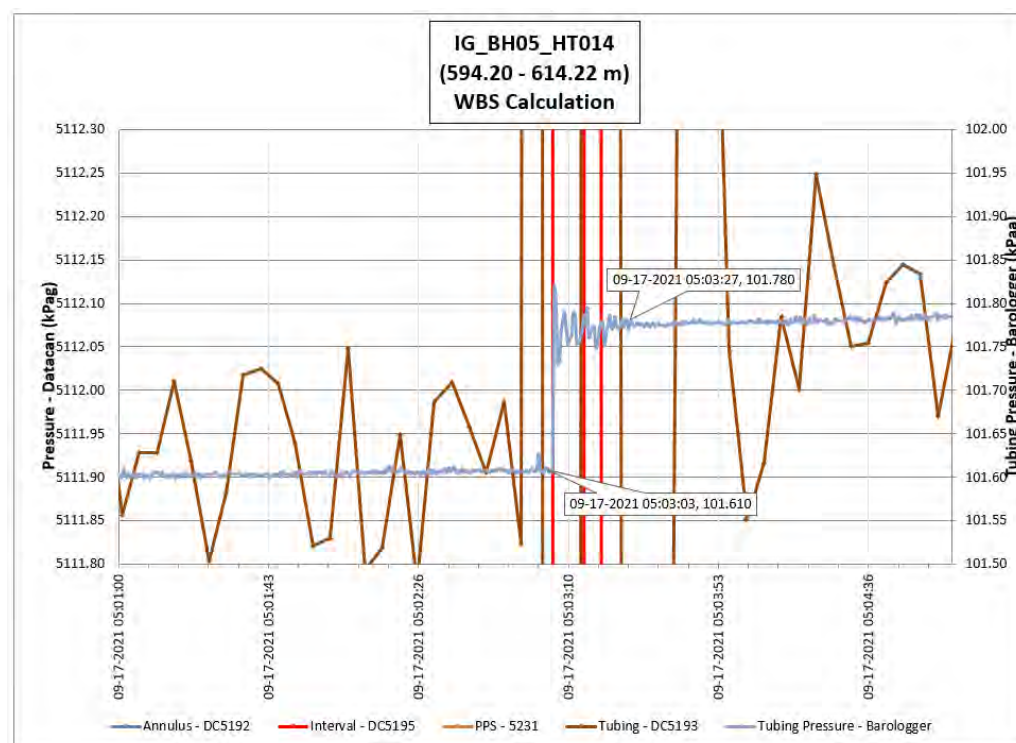


Figure 158: HT014 Tubing pressure during DHSIV activation. DHSIV Closed Wellbore Storage Estimate =  $7E-11 \text{ m}^3/\text{Pa}$



**Table 14: Summary of Analysis Results – HT014**

	Formation conductivity	Skin zone conductivity	Static formation pressure	Formation specific storage	Radial thickness of skin	Flow dimension
	[m/s]	[m/s]	[kPa]	[1/m]	[m]	[–]
Best Fit	2E-13	5E-13	5502	1E-07	4.49E-02	2.2
Minimum	2E-14	8E-14	5432	5E-09	1E-04	1.7
Maximum	3E-12	1E-09	5513	1E-05	3E-01	3.0
Mean	3E-13	2E-10	5496	5E-07	9E-02	2.2
Median	3E-13	7E-11	5501	4E-08	8E-02	2.2
Geometric mean	2E-13	6E-11	5495	5E-08	7E-02	2.2

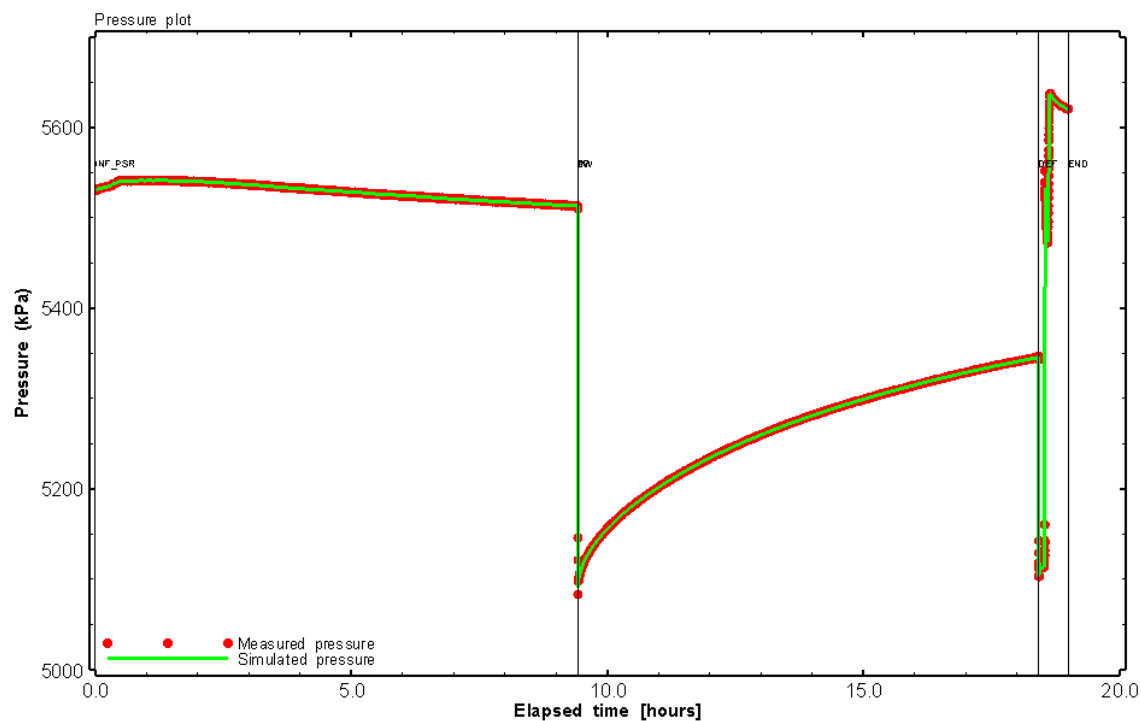


Figure 159: HT014 Pressure plot showing best-fit simulation and best fit results

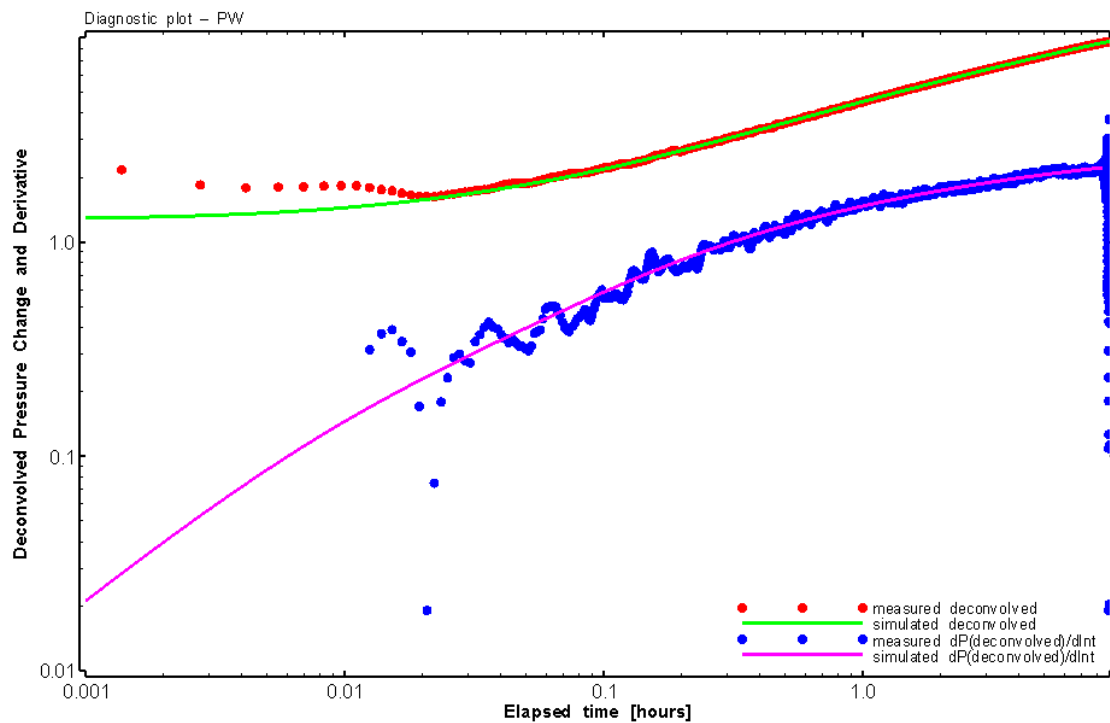


Figure 160: HT014 Deconvolved pressure change and derivative plot of the PW sequence showing best-fit simulation

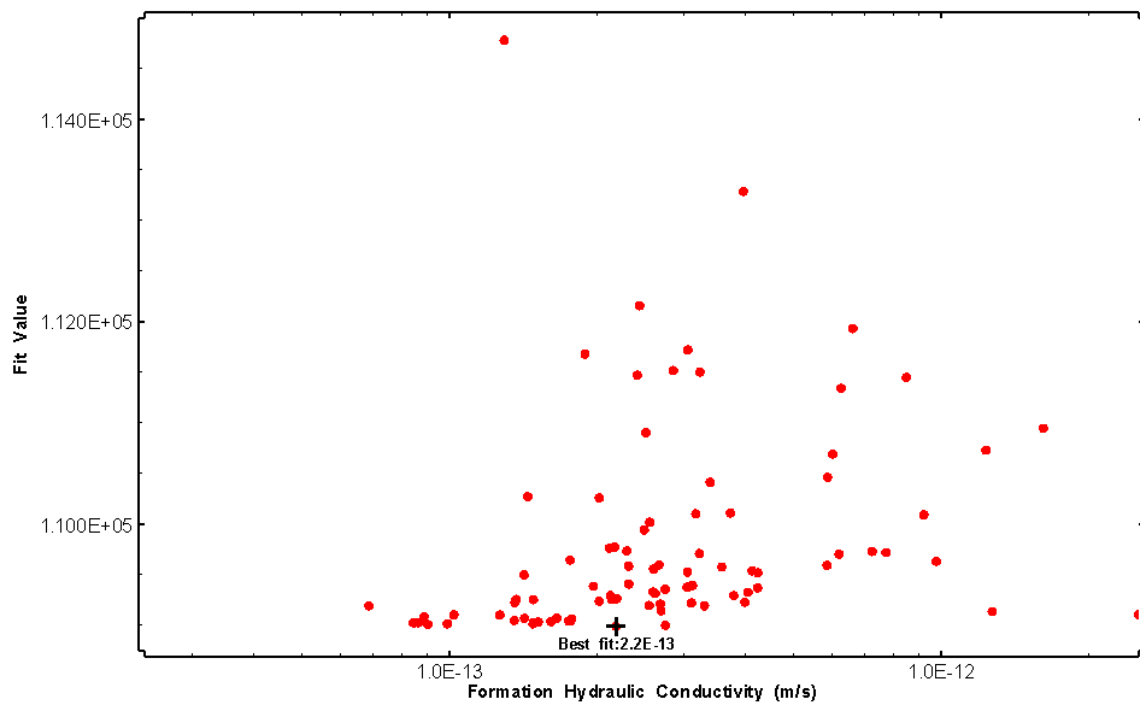


Figure 161: HT014 XY-scatter plot of formation hydraulic conductivity vs. fit value

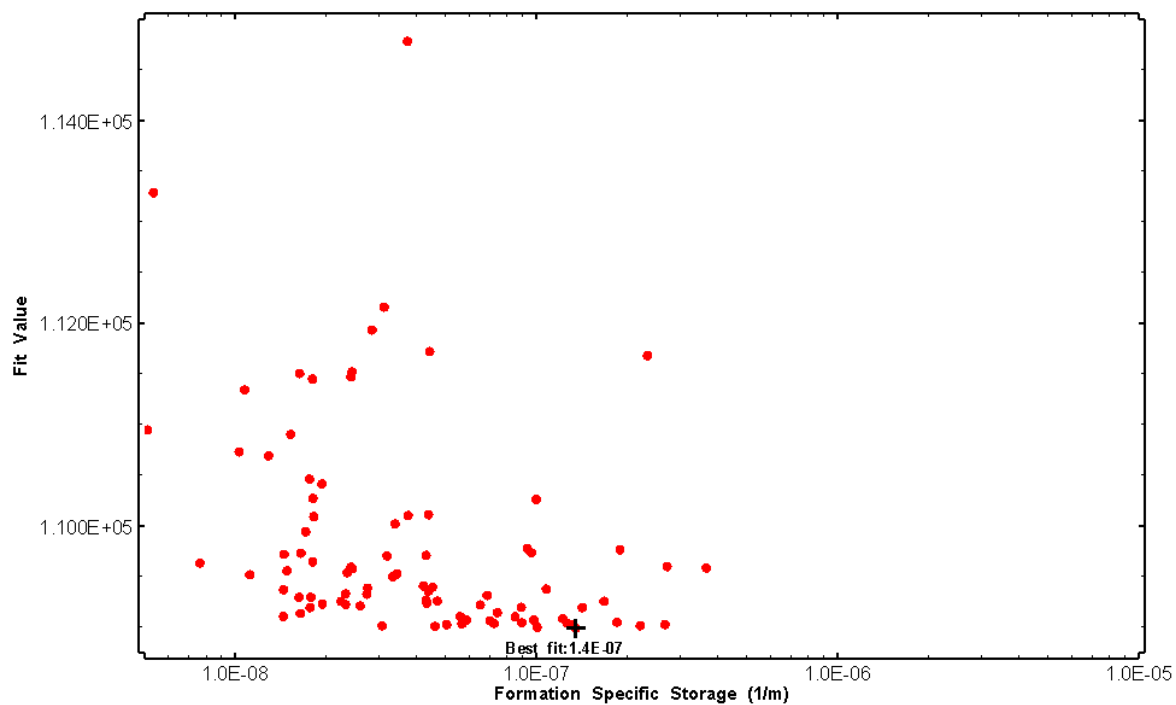


Figure 162: HT014 XY-scatter plot of formation specific storage vs. fit value

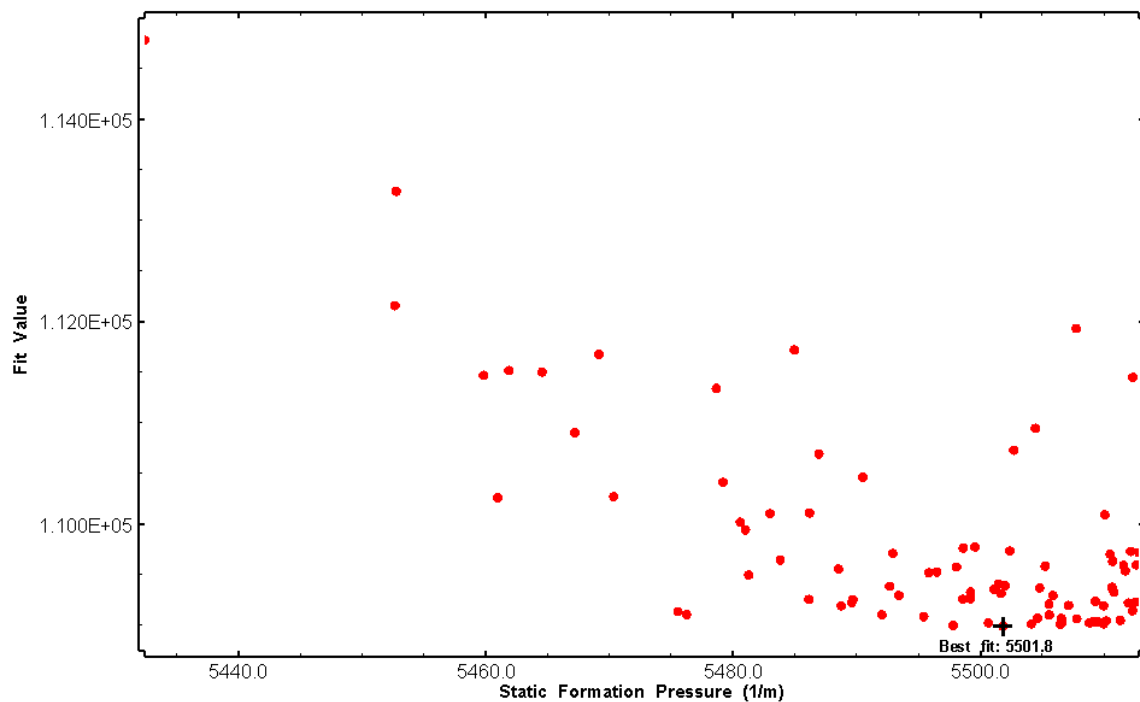


Figure 163: HT014 XY-scatter plot of static formation pressure vs. fit value

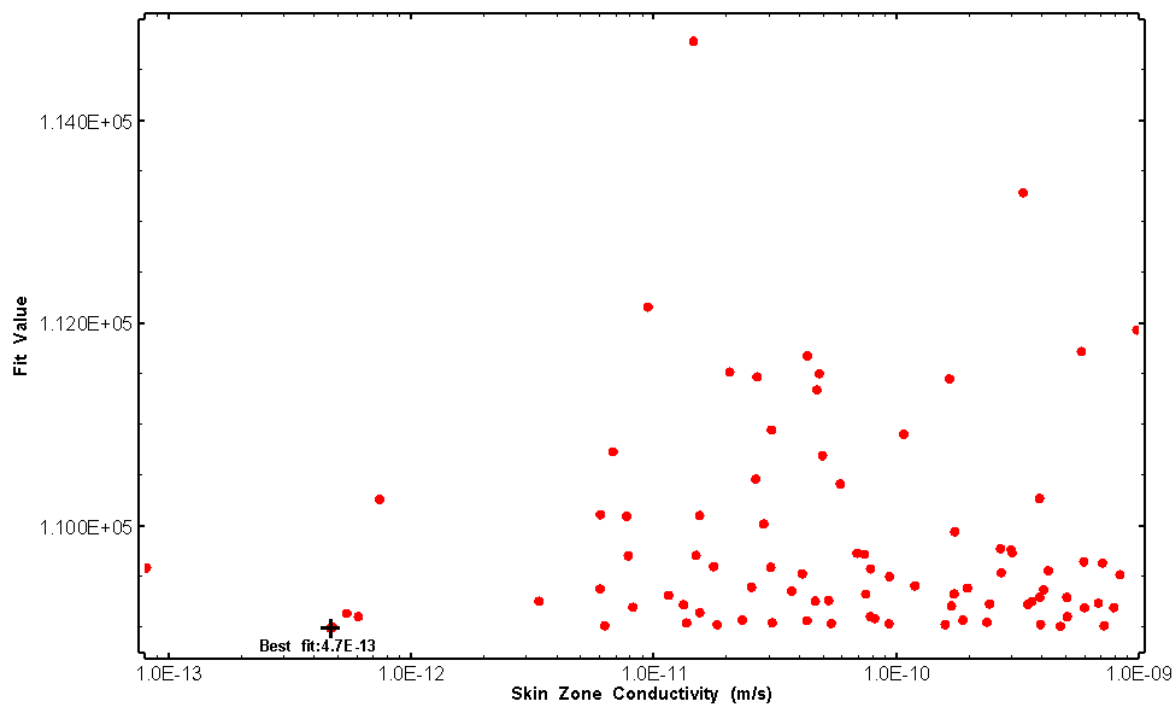


Figure 164: HT014 XY-scatter plot of skin zone conductivity vs. fit value

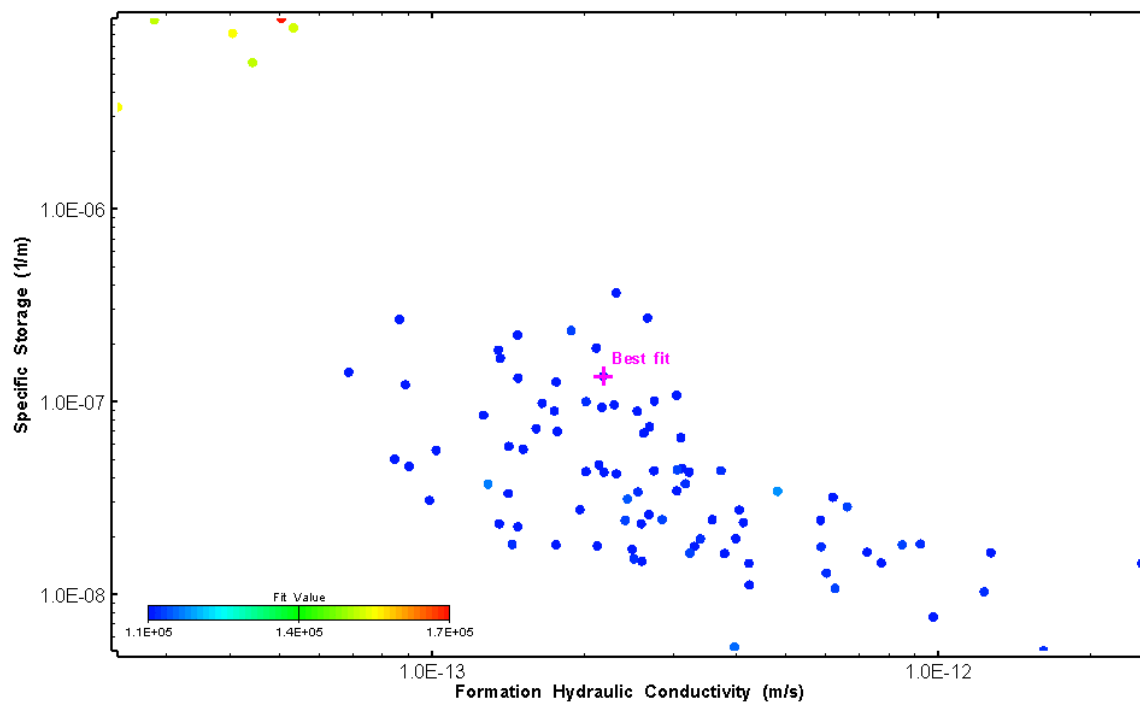


Figure 165: HT014 XY-scatter plot showing estimates of formation hydraulic conductivity and specific storage from perturbation analysis

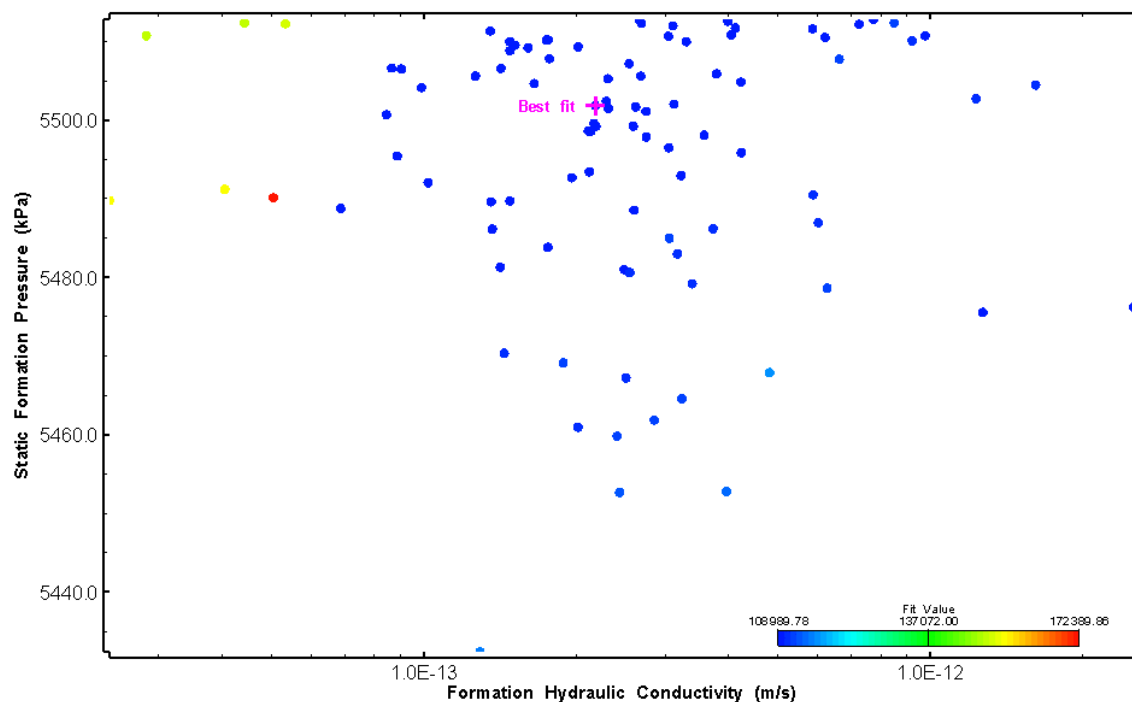
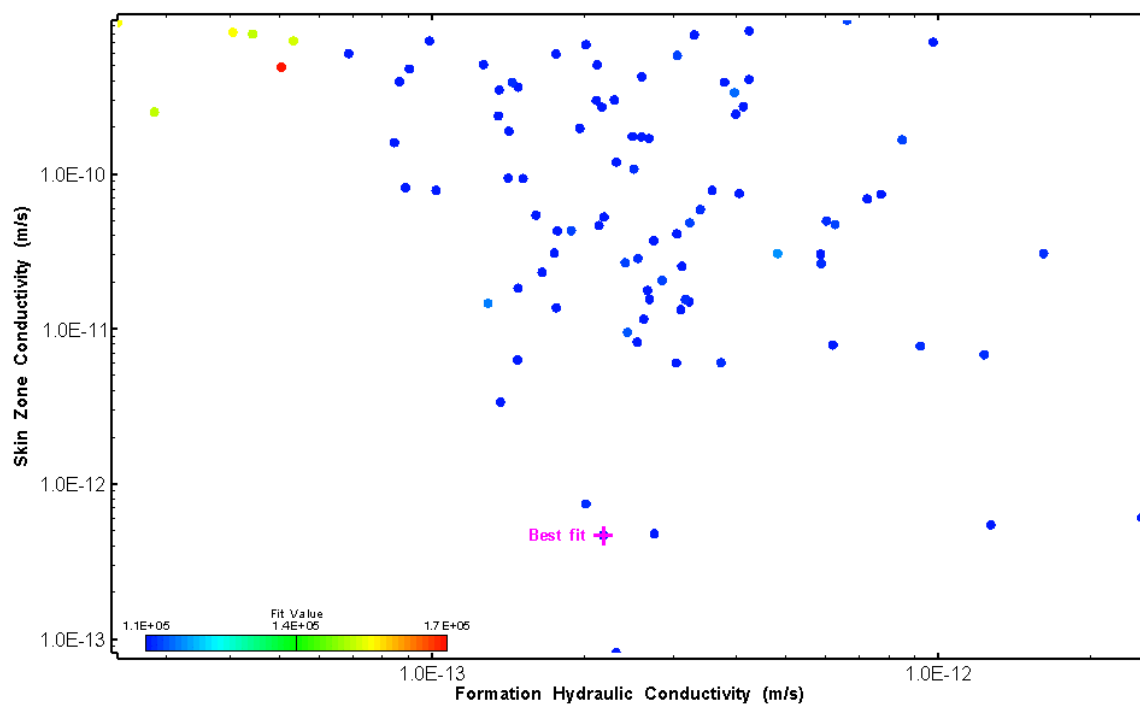
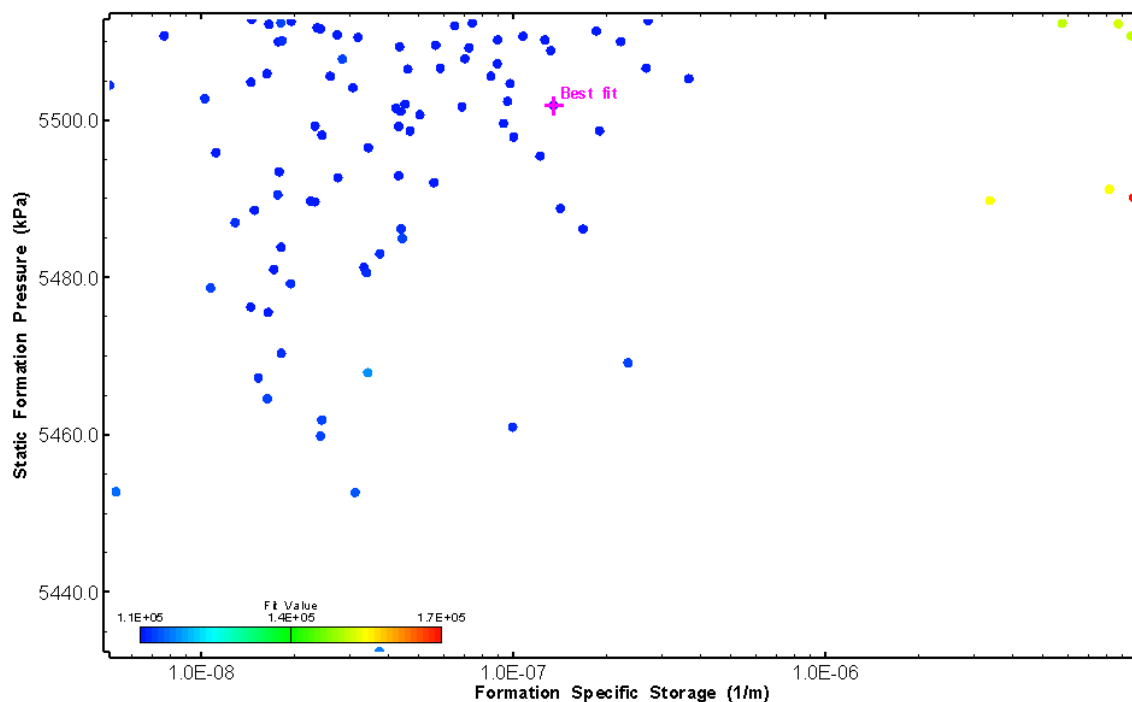


Figure 166: HT014 XY-scatter plot showing estimates of formation hydraulic conductivity and static formation pressure from perturbation analysis



**Figure 167: HT014 XY-scatter plot showing estimates of formation hydraulic conductivity and skin zone conductivity from perturbation analysis**



**Figure 168: HT014 XY-scatter plot showing estimates of specific storage and static formation pressure from perturbation analysis**

## 15.0 HT015 (614.20 – 634.22 M)

HT015 was selected to obtain continuous testing coverage from 600 to 800 m along hole and to target a fractured interval containing a dyke. 23 broken fractures were observed in the core. No drill fluid parameter triggers were reached during drilling. No indication of flow was recorded during FFEC logging post-drilling.

The test was initiated with a shut-in pressure recovery phase (PSR). A pulse withdrawal test (PW) with a shut-in recovery followed by a slug withdrawal (SW) phase was completed after the PSR phase.

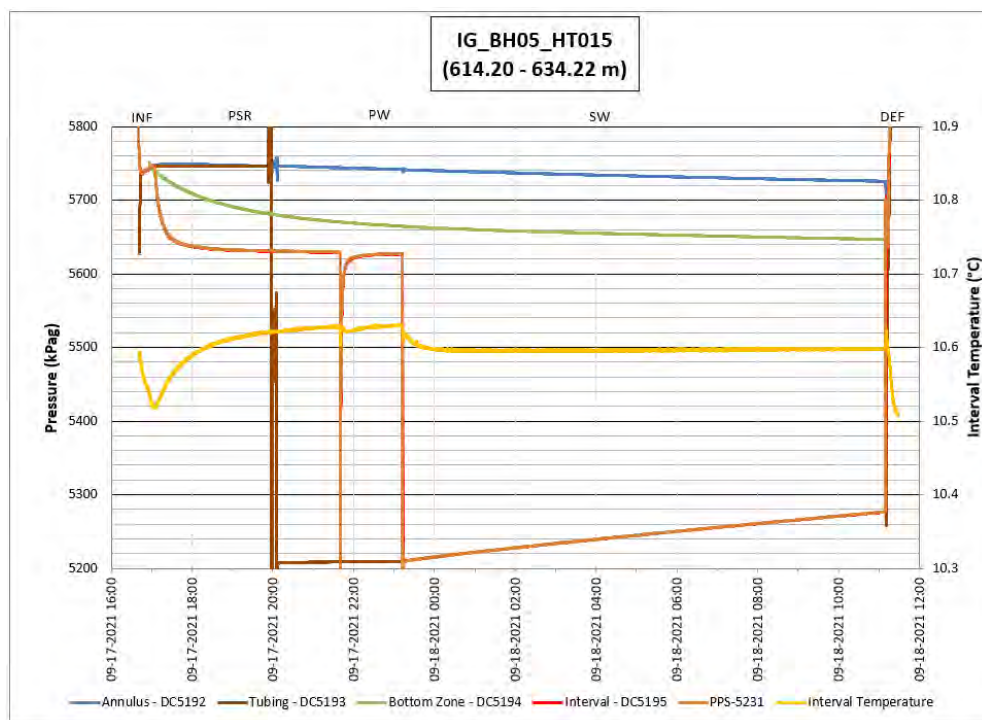
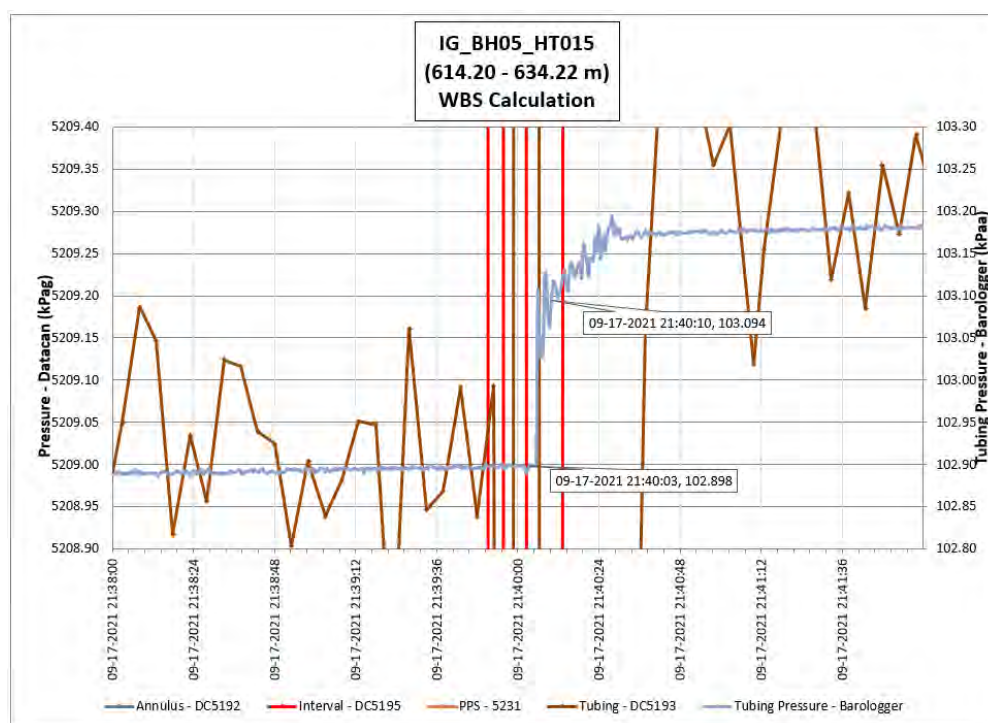


Figure 169: HT015 Annotated test plot showing monitored zone pressure and interval temperature.



**Figure 170: HT015 Tubing pressure during DHSIV activation. DHSIV Closed Wellbore Storage Estimate =  $8\text{E-}11 \text{ m}^3/\text{Pa}$**

**Table 15: Summary of Analysis Results – HT015**

	Formation conductivity	Skin zone conductivity	Static formation pressure	Formation specific storage	Radial thickness of skin	Flow dimension
	[m/s]	[m/s]	[kPa]	[1/m]	[m]	[–]
Best Fit	6E-11	1E-10	5627	2E-07	4.54E-01	2.4
Minimum	3E-11	1E-12	5624	1E-09	1E-04	1.8
Maximum	2E-09	9.E-10	5629	8E-06	9E-01	2.7
Mean	3E-10	2E-10	5627	4E-07	1E-01	2.1
Median	3E-10	1E-10	5627	3E-07	7E-02	2.1
Geometric mean	2E-10	1E-10	5627	2E-07	5E-02	2.1



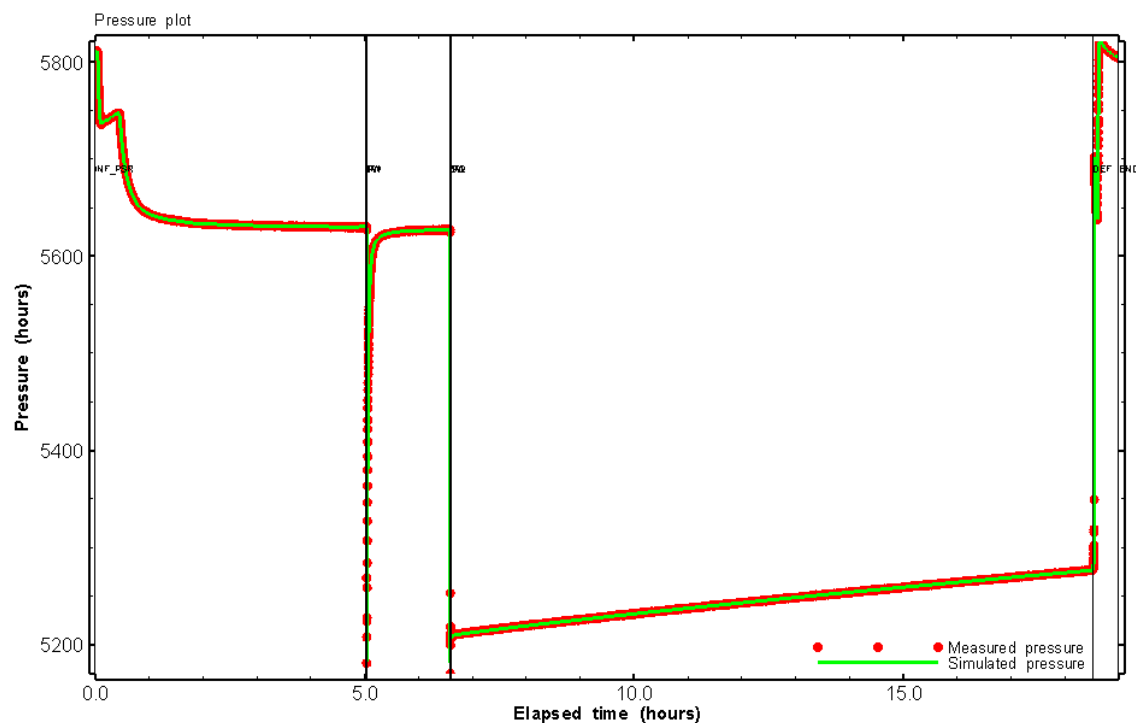


Figure 171: HT015 Pressure plot showing best-fit simulation and best fit results

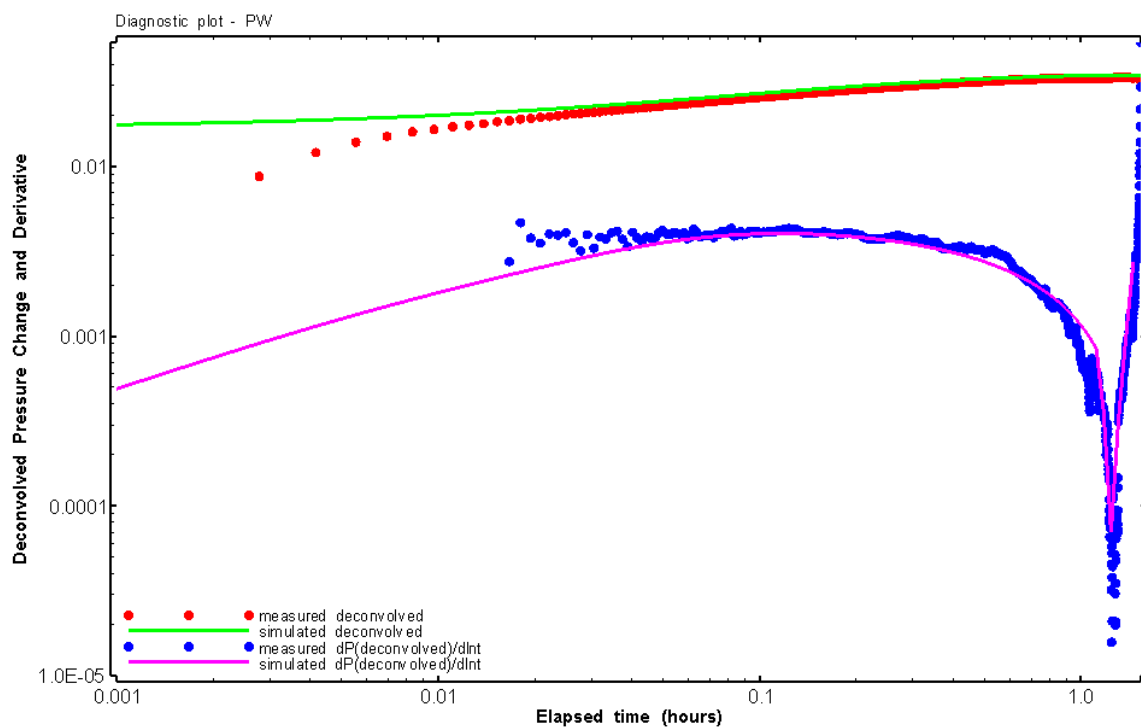


Figure 172: HT015 Deconvolved pressure change and derivative plot of the PW sequence showing best-fit simulation

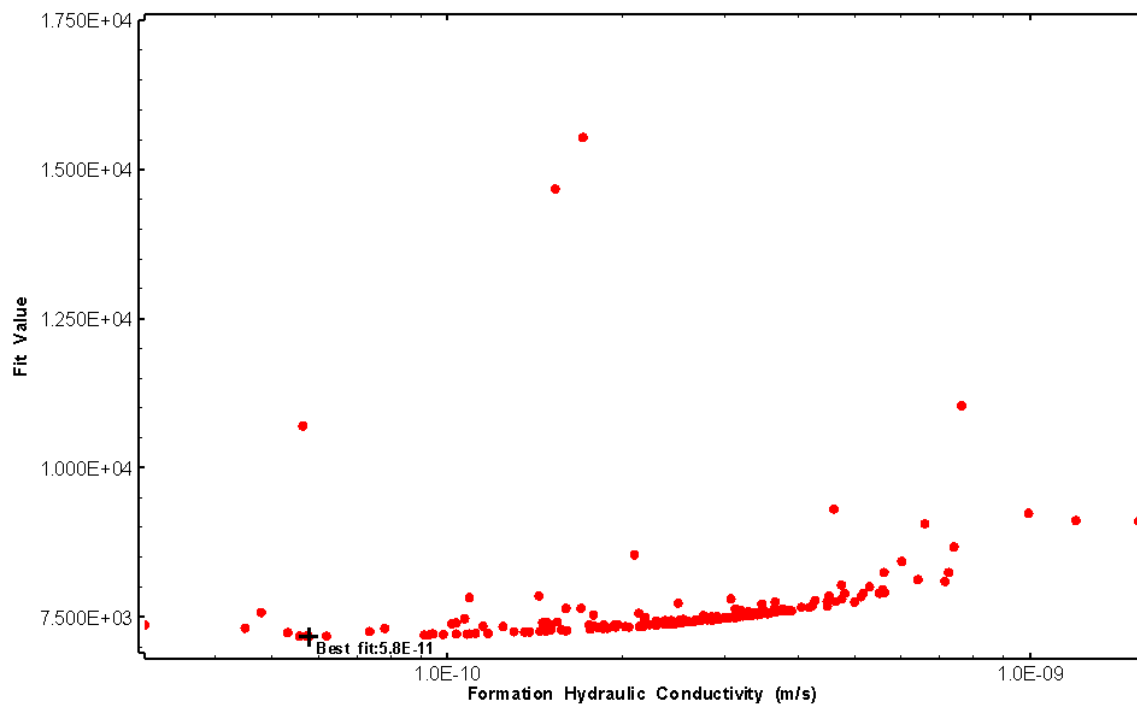


Figure 173: HT015 XY-scatter plot of formation hydraulic conductivity vs. fit value

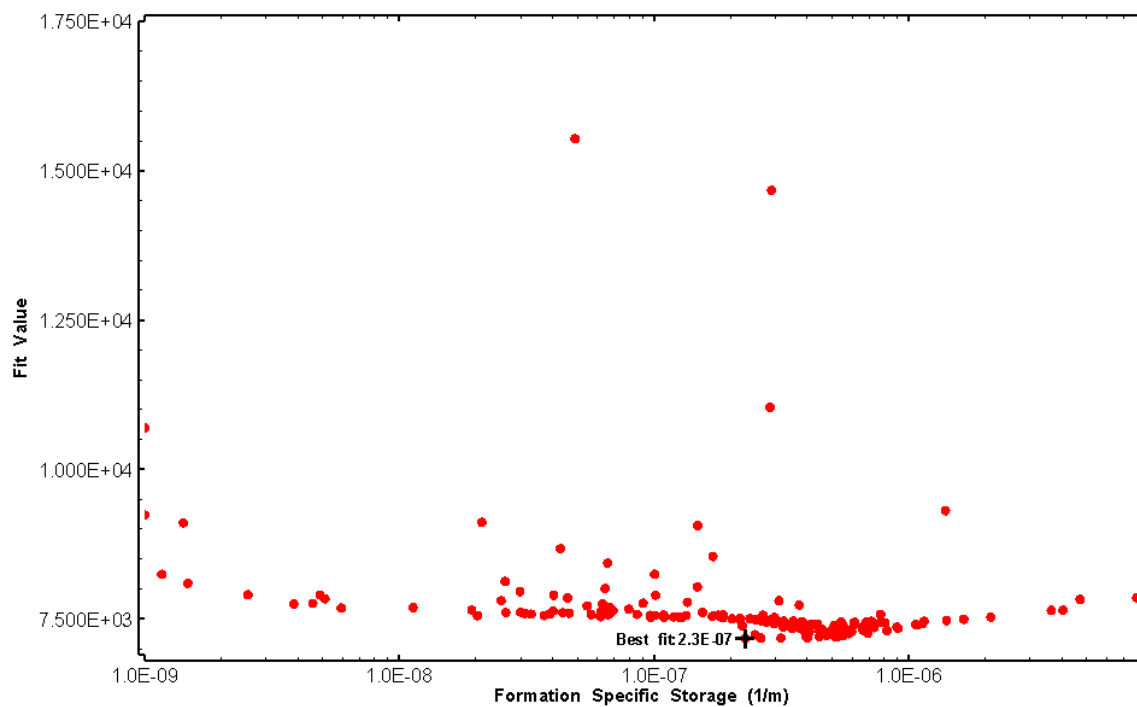


Figure 174: HT015 XY-scatter plot of formation specific storage vs. fit value

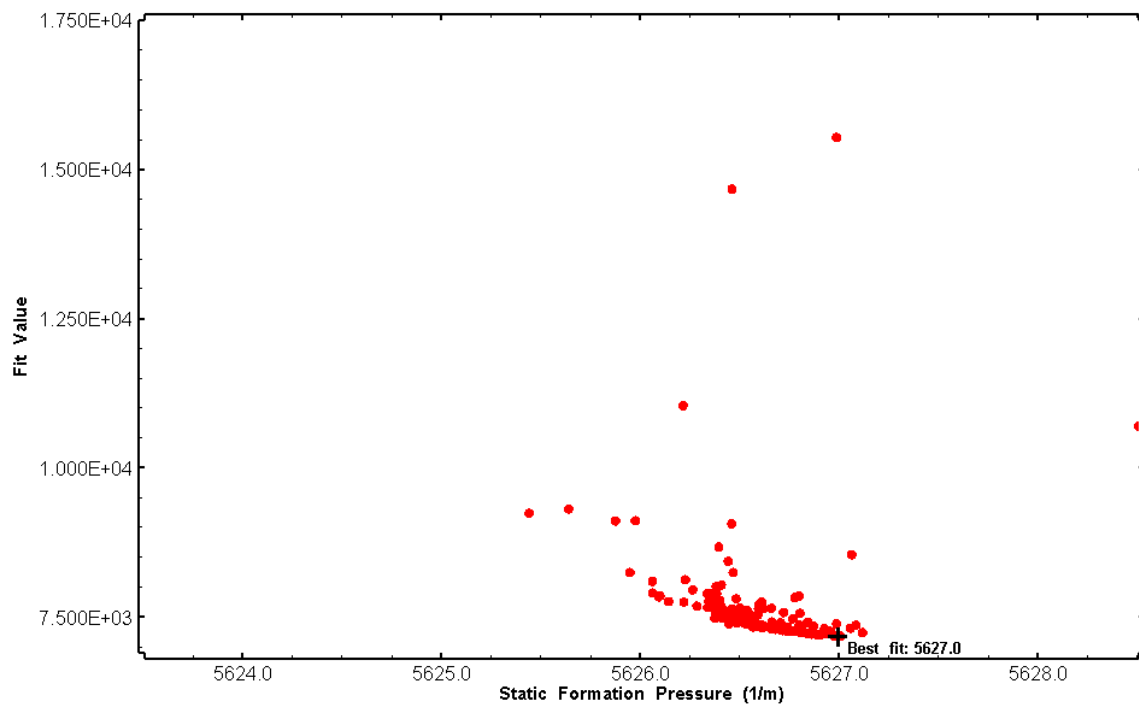


Figure 175: HT015 XY-scatter plot of static formation pressure vs. fit value

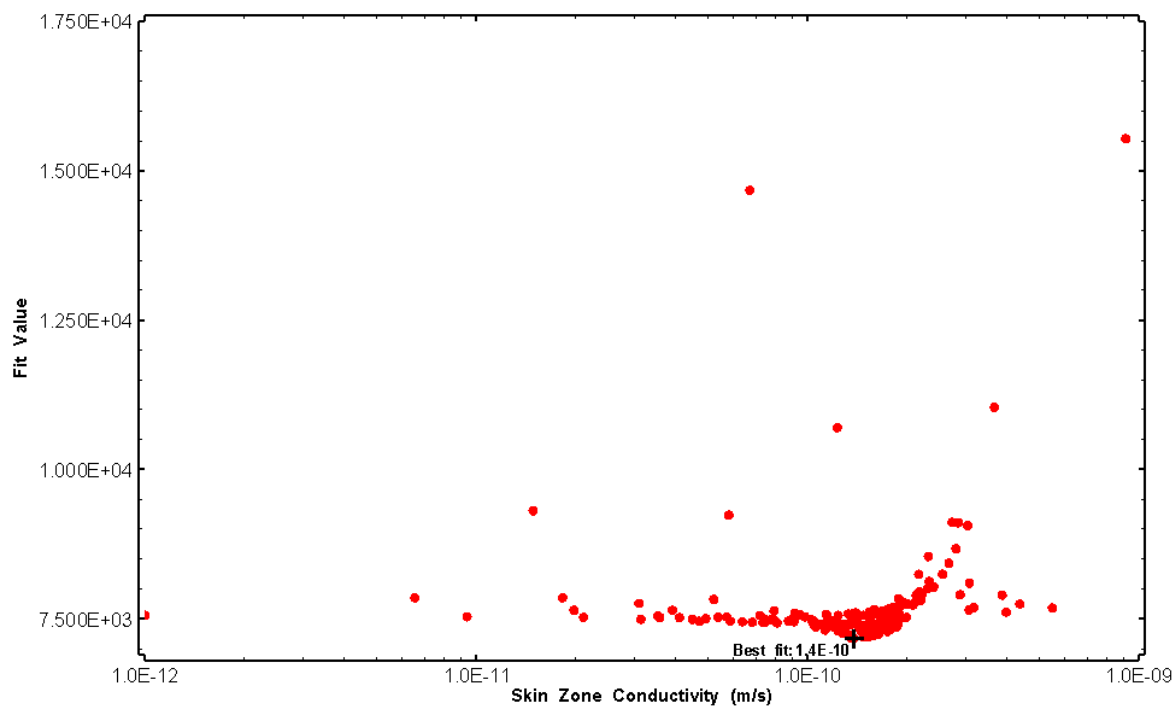


Figure 176: HT015 XY-scatter plot of skin zone conductivity vs. fit value

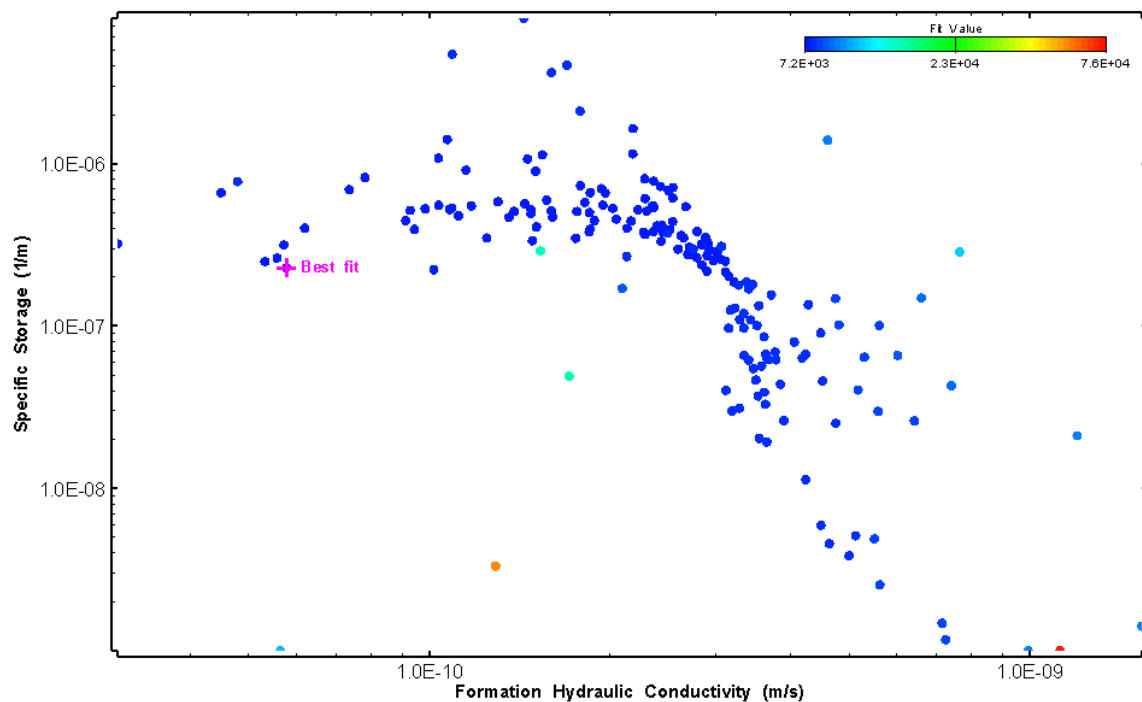


Figure 177: HT015 XY-scatter plot showing estimates of formation hydraulic conductivity and specific storage from perturbation analysis

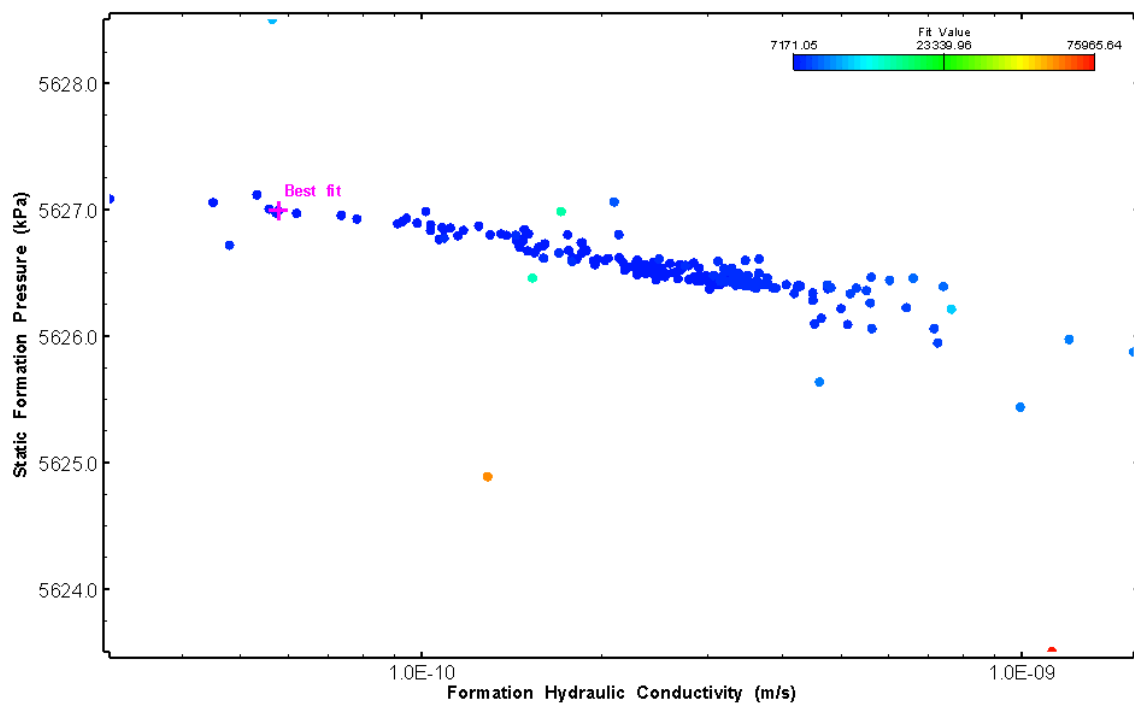


Figure 178: HT015 XY-scatter plot showing estimates of formation hydraulic conductivity and static formation pressure from perturbation analysis

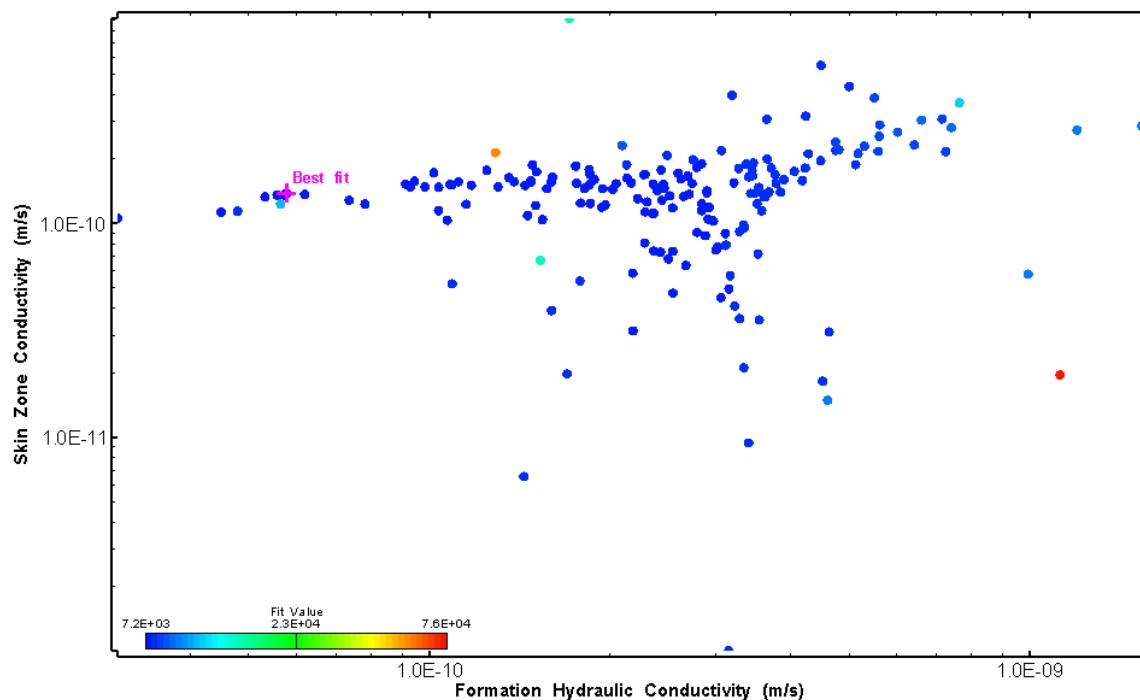


Figure 179: HT015 XY-scatter plot showing estimates of formation hydraulic conductivity and skin zone conductivity from perturbation analysis

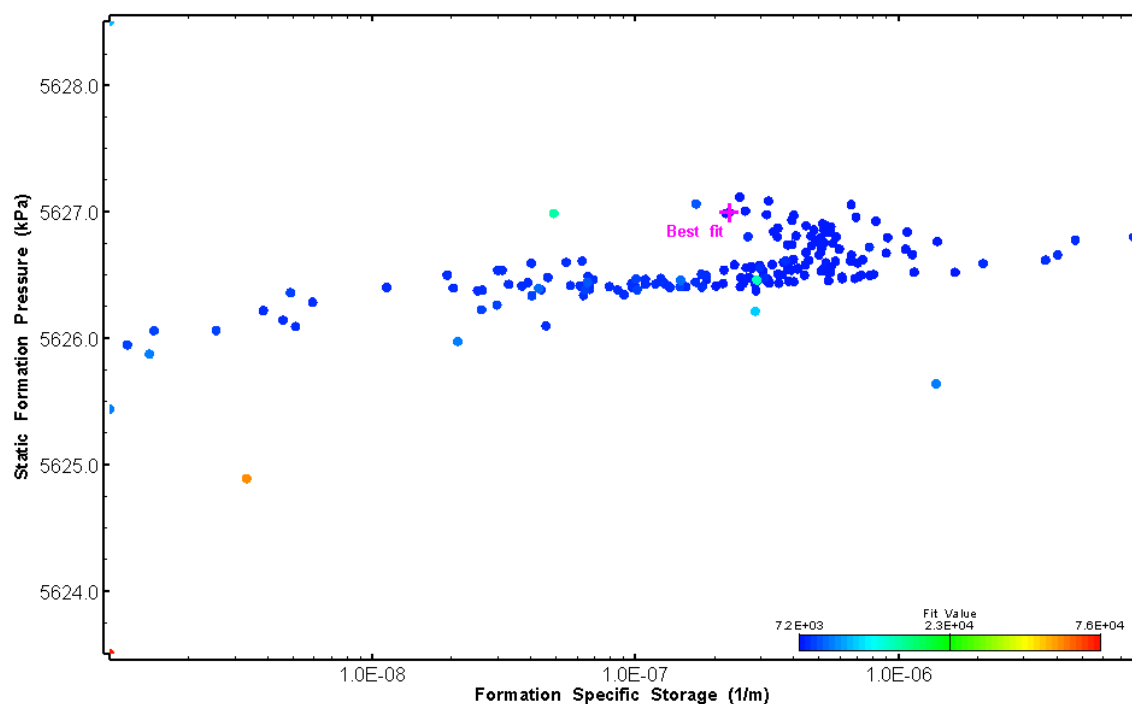


Figure 180: HT015 XY-scatter plot showing estimates of specific storage and static formation pressure from perturbation analysis

## 16.0 HT016 (634.20 – 654.22 M)

HT016 was selected to obtain continuous testing coverage from 600 to 800 m along hole. 17 broken fractures were observed in the core. No drill fluid parameter triggers were reached during drilling. No indication of flow was recorded during FFEC logging post-drilling.

The test was initiated with a shut-in pressure recovery phase (PSR). A pulse withdrawal test (PW) with a shut-in recovery was completed after the PSR phase.

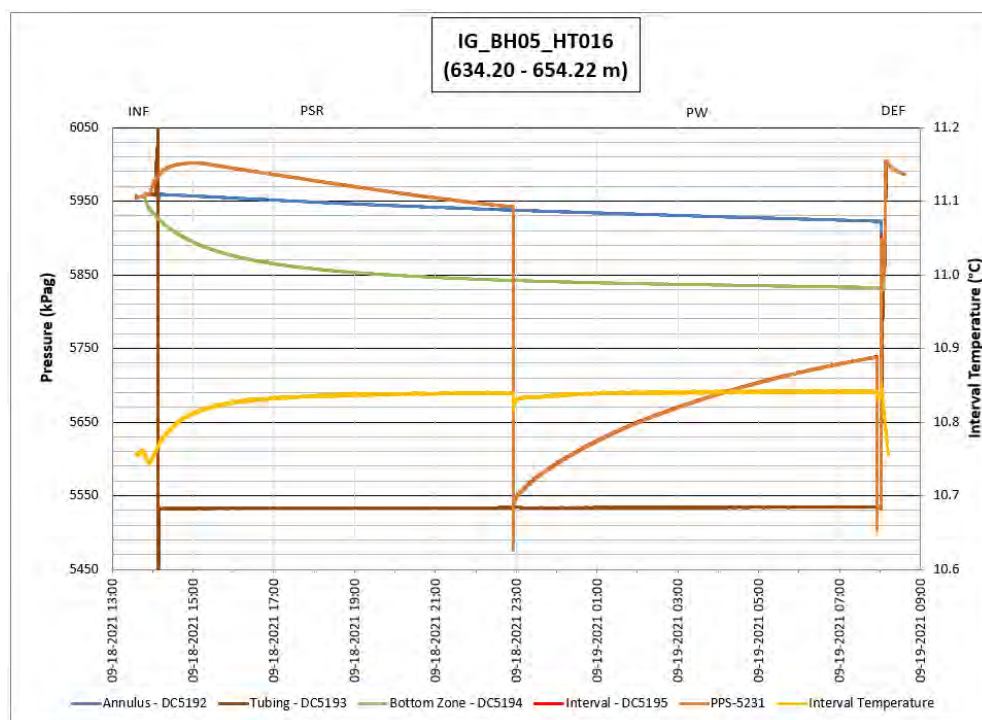
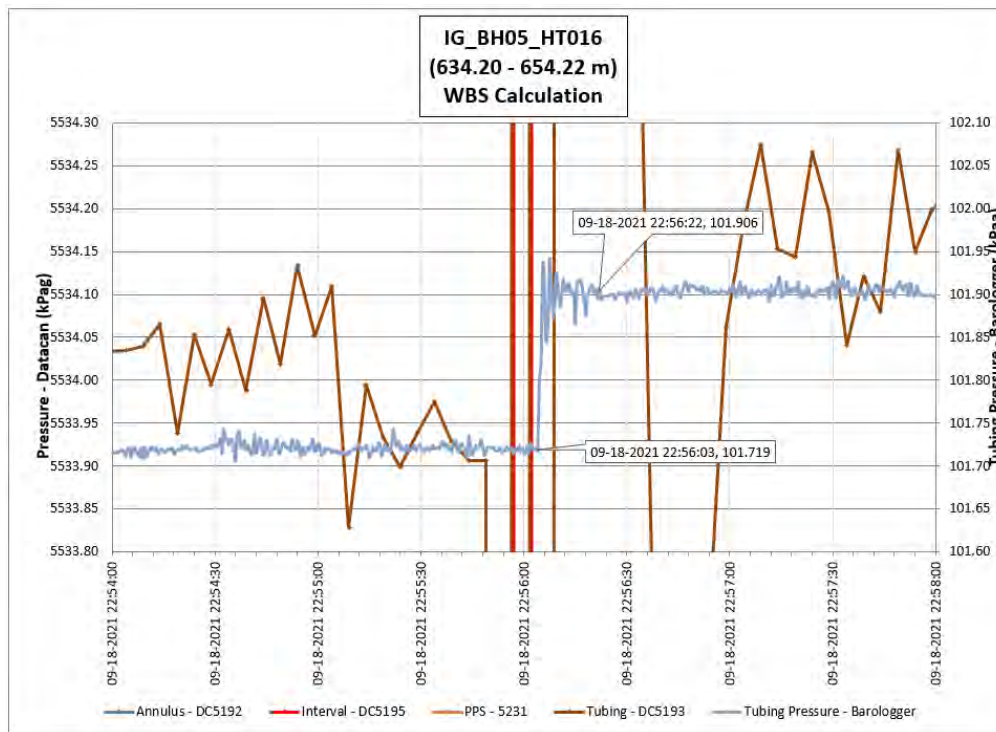


Figure 181: HT016 Annotated test plot showing monitored zone pressure and interval temperature.



**Figure 182: HT016 Tubing pressure during DHSIV activation. DHSIV Closed Wellbore Storage Estimate =  $8\text{E-}11 \text{ m}^3/\text{Pa}$**

**Table 16: Summary of Analysis Results – HT016**

	Formation conductivity	Skin zone conductivity	Static formation pressure	Formation specific storage	Radial thickness of skin	Flow dimension
	[m/s]	[m/s]	[kPa]	[1/m]	[m]	[–]
Best Fit	4E-13	2E-12	5847	2E-08	2.14E-02	2.3
Minimum	2E-14	2E-13	5836	1E-09	1E-04	1.0
Maximum	2E-12	1E-09	5940	1E-05	4E-01	3.0
Mean	4E-13	4E-10	5898	1E-06	4E-02	2.1
Median	3E-13	2E-10	5896	3E-08	7E-03	2.1
Geometric mean	3E-13	1E-10	5897	6E-08	4E-03	2.1

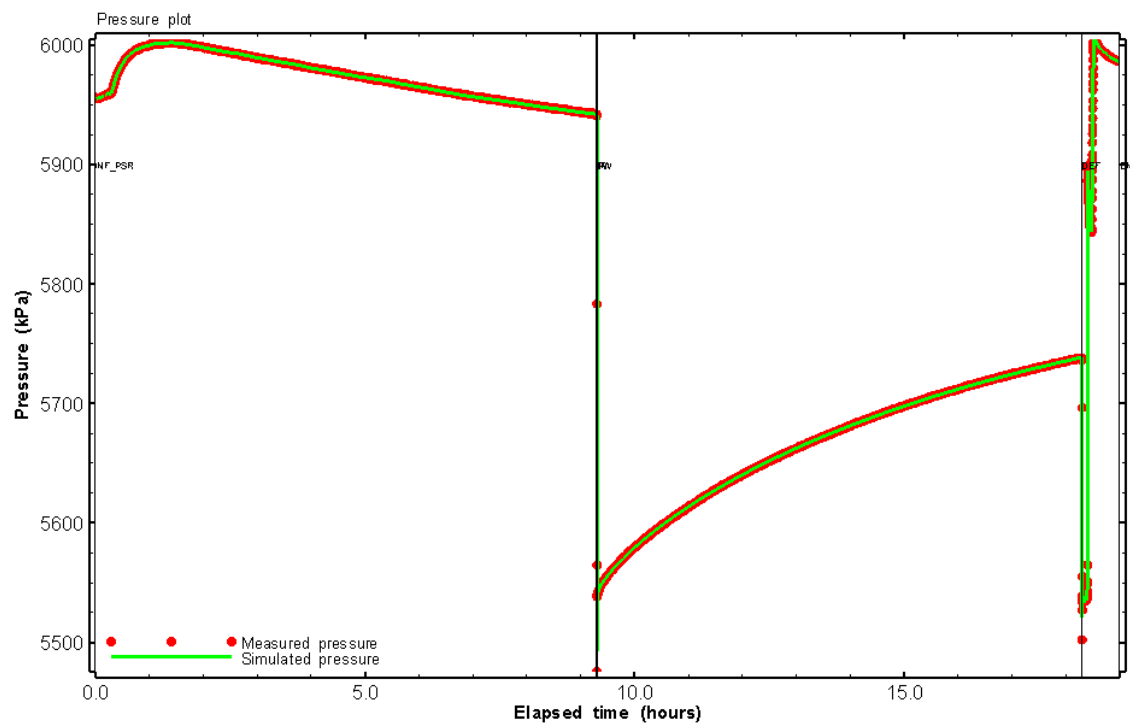


Figure 183: HT016 Pressure plot showing best-fit simulation and best fit results

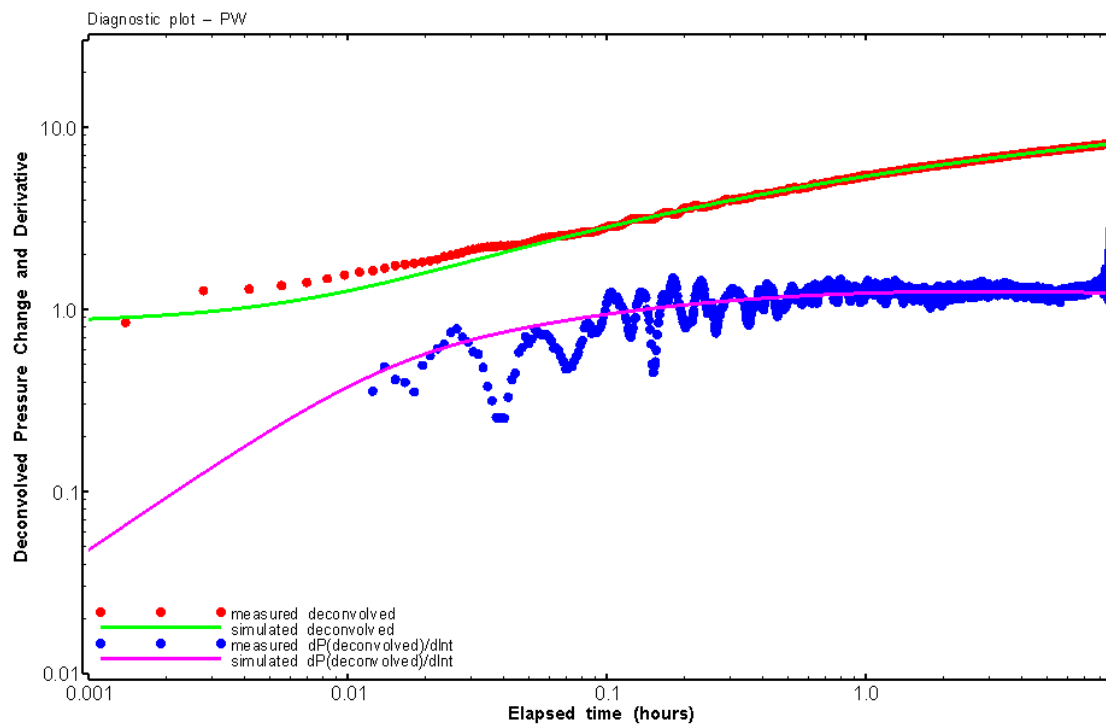


Figure 184: HT016 Deconvolved pressure change and derivative plot of the PW sequence showing best-fit simulation



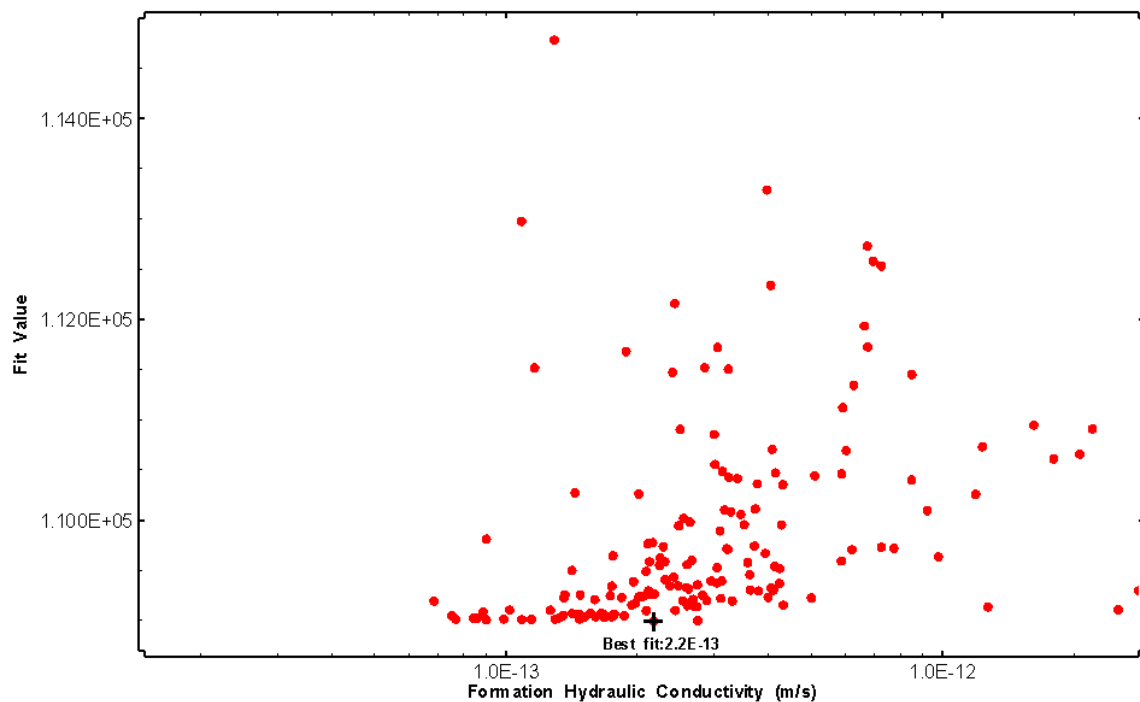


Figure 185: HT016 XY-scatter plot of formation hydraulic conductivity vs. fit value

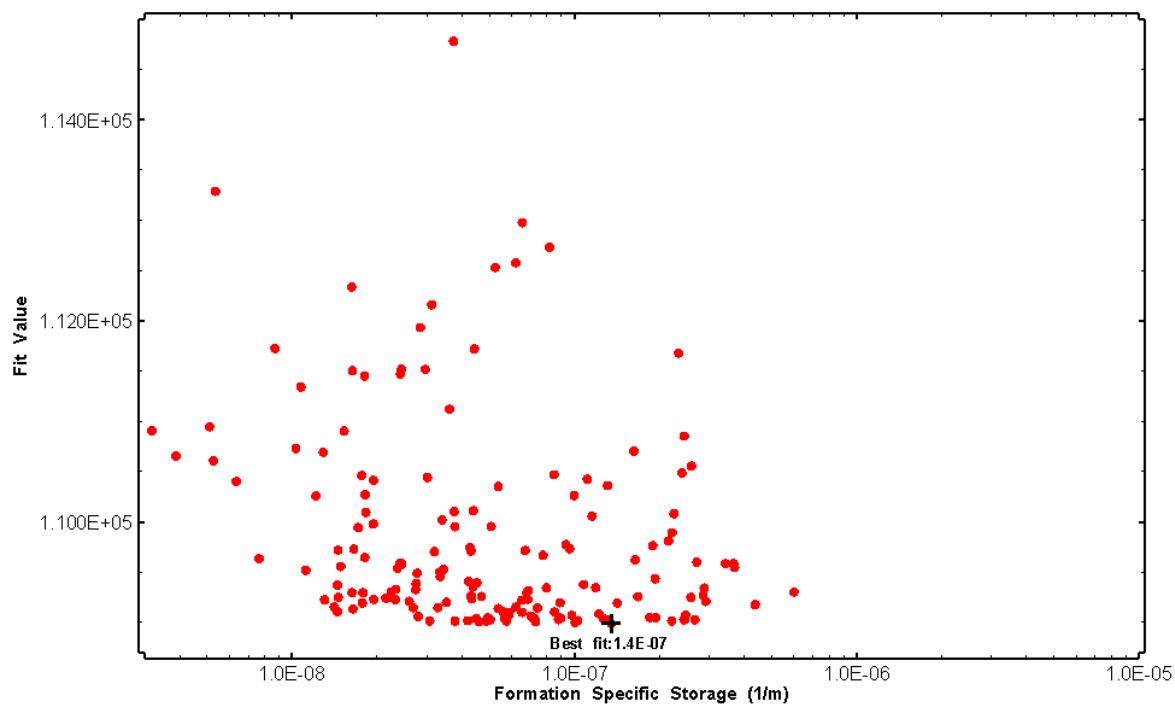


Figure 186: HT016 XY-scatter plot of formation specific storage vs. fit value

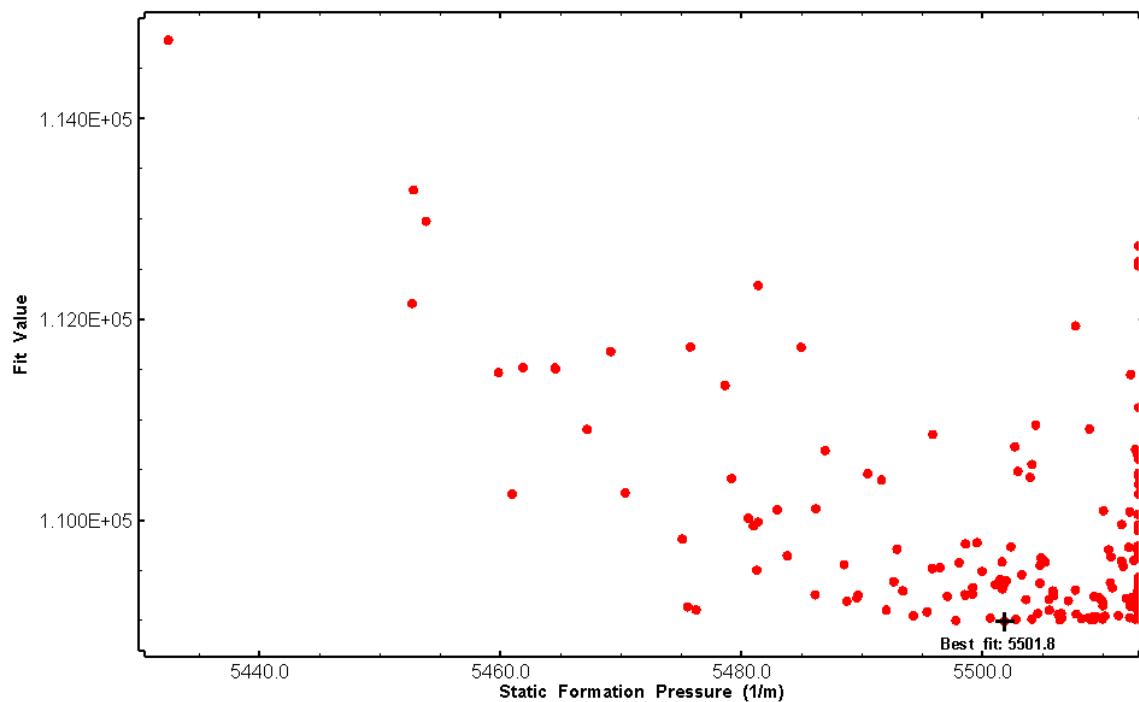


Figure 187: HT016 XY-scatter plot of static formation pressure vs. fit value

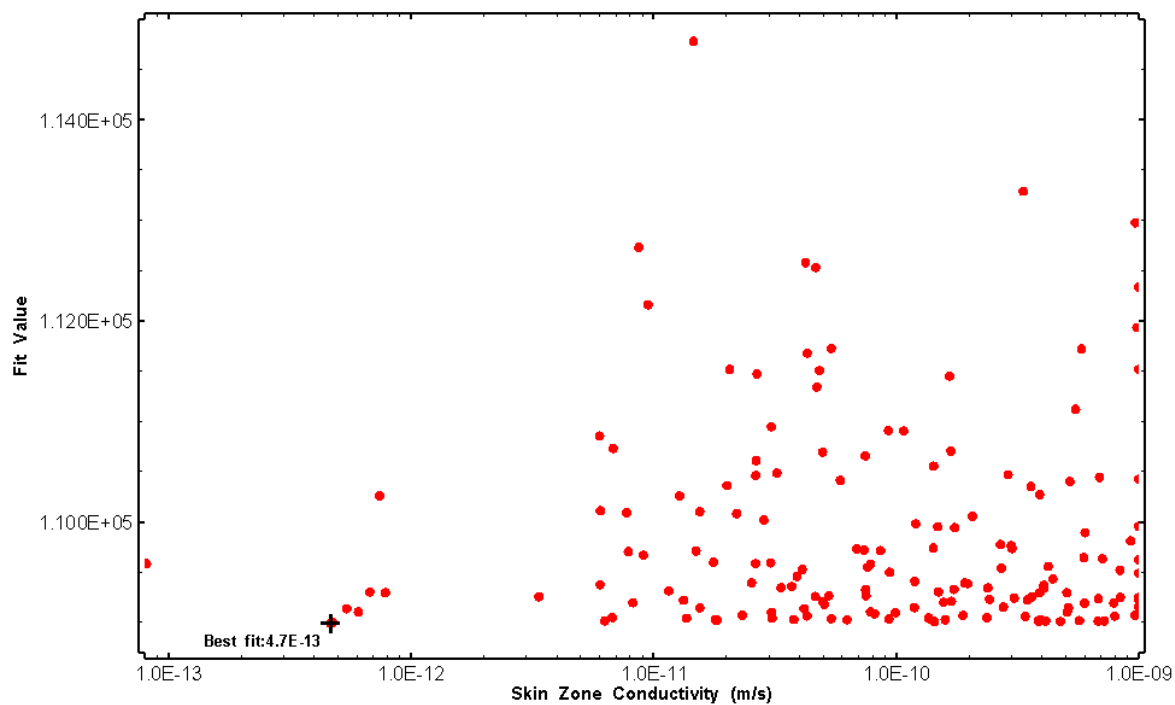


Figure 188: HT016 XY-scatter plot of skin zone conductivity vs. fit value

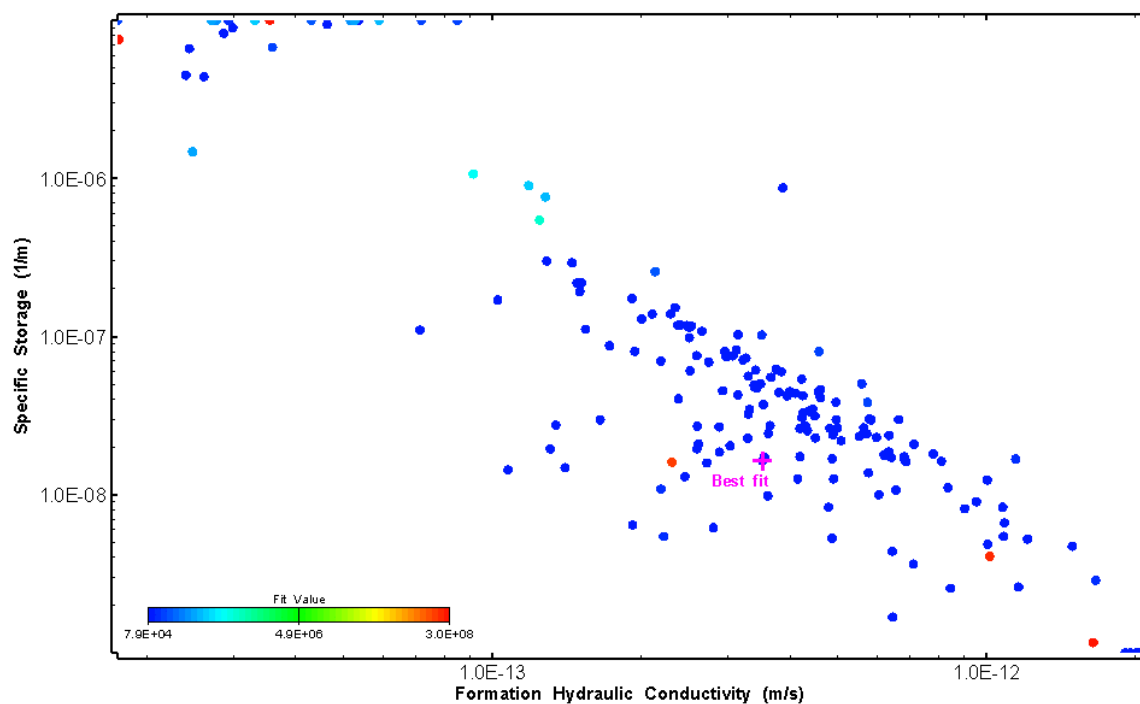


Figure 189: HT016 XY-scatter plot showing estimates of formation hydraulic conductivity and specific storage from perturbation analysis

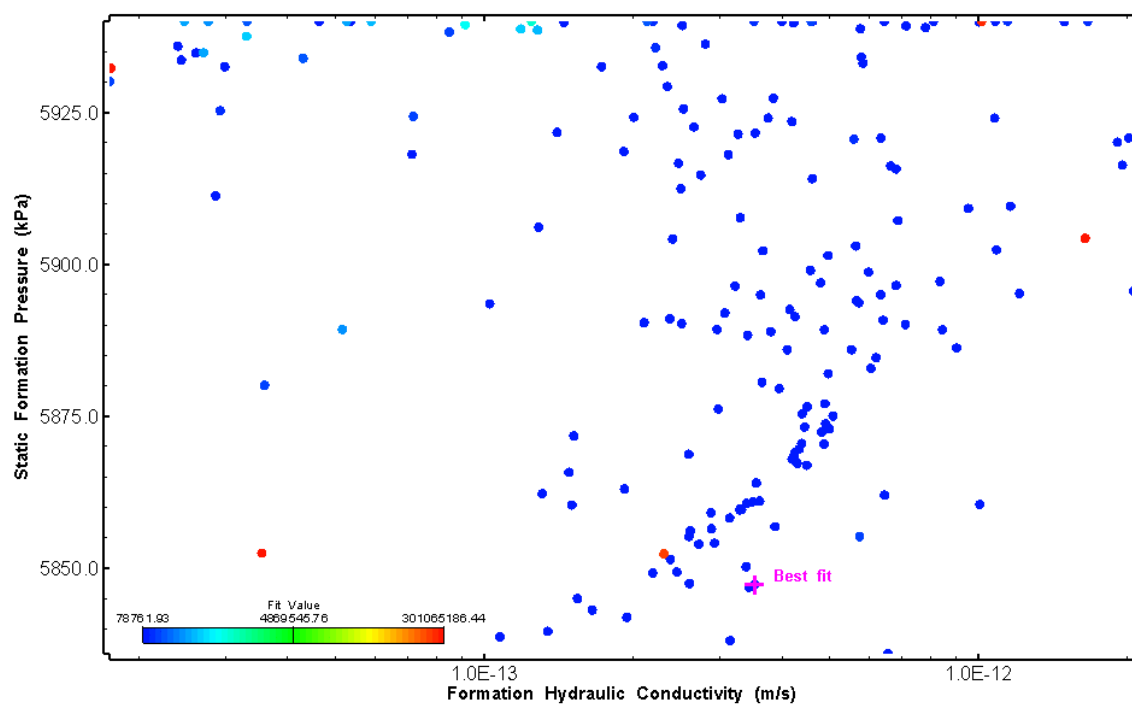


Figure 190: HT016 XY-scatter plot showing estimates of formation hydraulic conductivity and static formation pressure from perturbation analysis

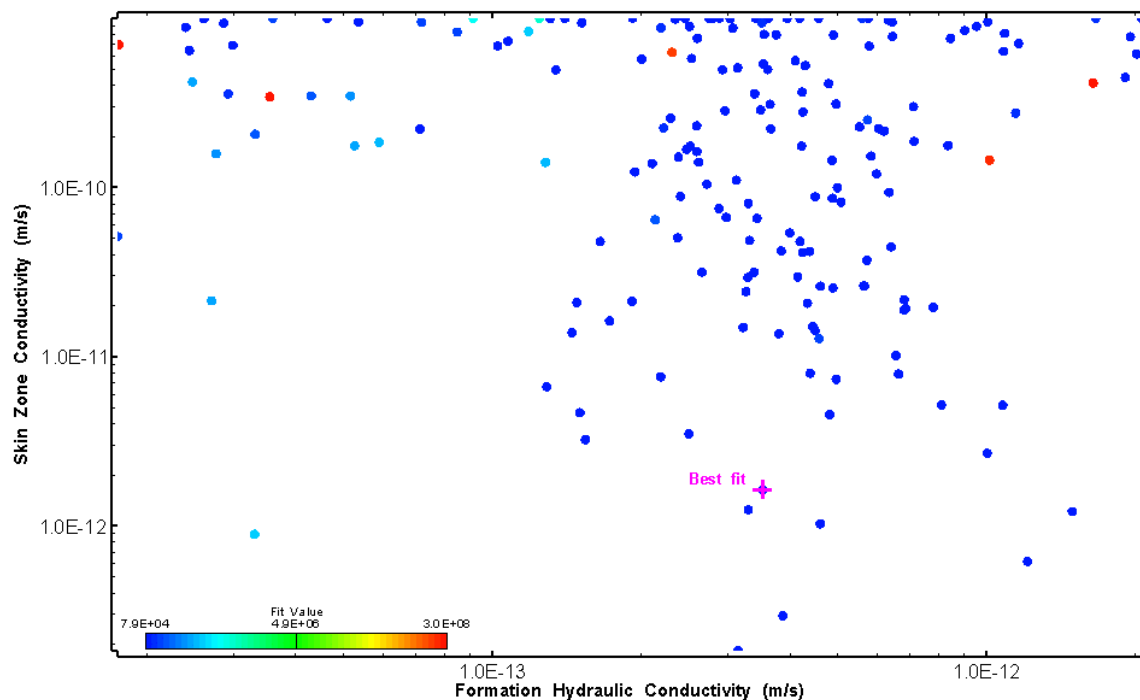


Figure 191: HT016 XY-scatter plot showing estimates of formation hydraulic conductivity and skin zone conductivity from perturbation analysis

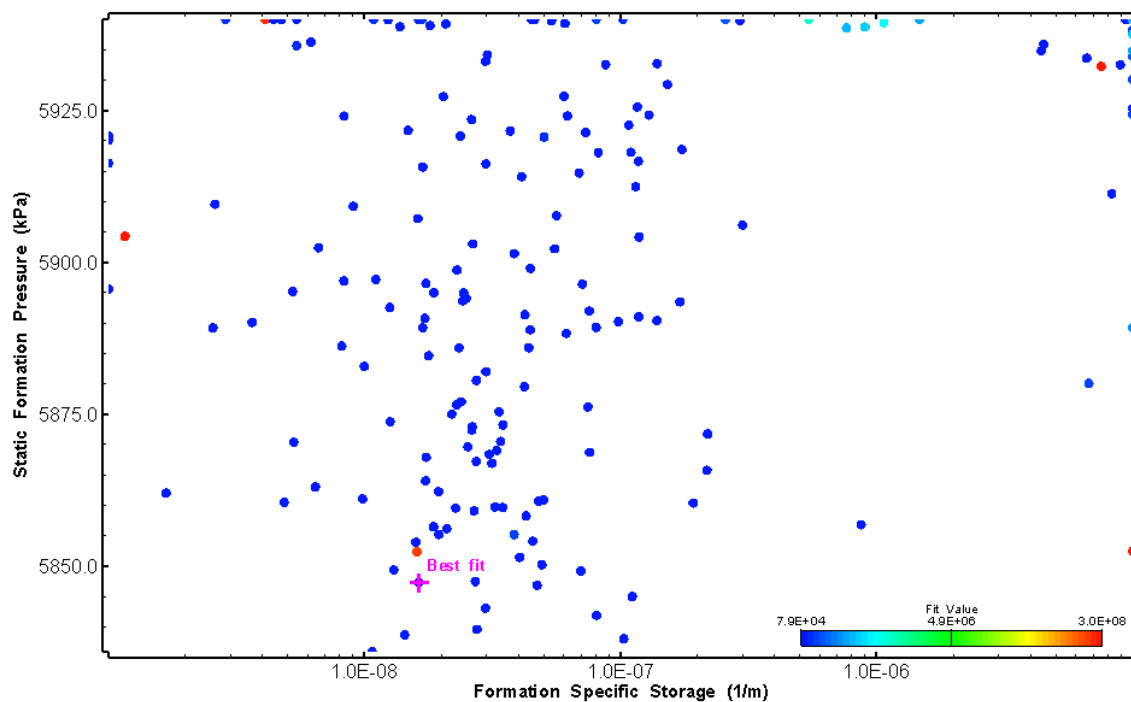


Figure 192: HT016 XY-scatter plot showing estimates of specific storage and static formation pressure from perturbation analysis

## 17.0 HT017 (653.90 – 673.92 M)

HT017 was selected to obtain continuous testing coverage from 600 to 800 m along hole. 14 broken fractures were observed in the core. No indication of flow was recorded during FFEC logging post-drilling.

The test was initiated with a shut-in pressure recovery phase (PSR). A pulse withdrawal test (PW) with a shut-in recovery was completed after the PSR phase.

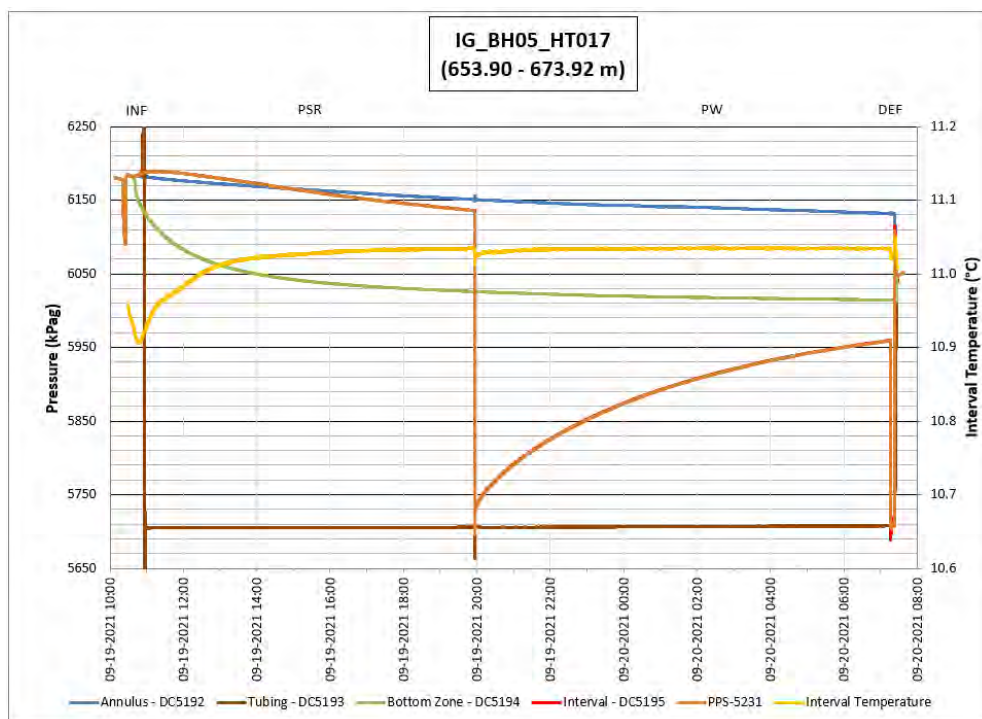
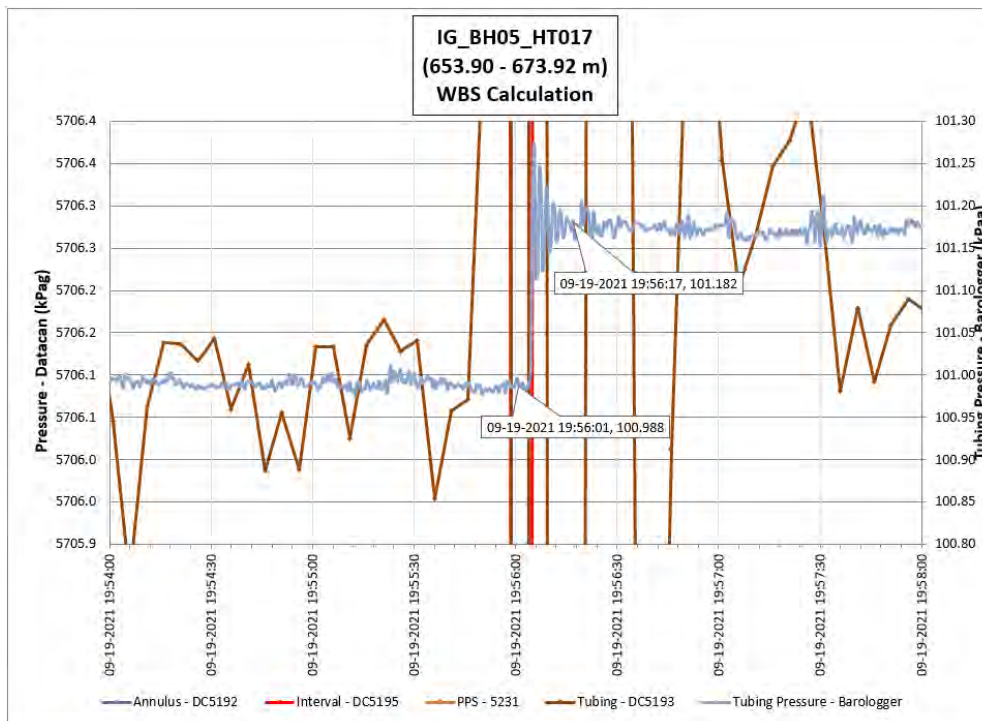


Figure 193: HT017 Annotated test plot showing monitored zone pressure and interval temperature.



**Figure 194: HT017 Tubing pressure during DHSIV activation. DHSIV Closed Wellbore Storage Estimate =  $9\text{E-}11 \text{ m}^3/\text{Pa}$**

**Table 17: Summary of Analysis Results – HT017**

	Formation conductivity	Skin zone conductivity	Static formation pressure	Formation specific storage	Radial thickness of skin	Flow dimension
	[m/s]	[m/s]	[kPa]	[1/m]	[m]	[–]
Best Fit	5E-13	2E-13	6024	6E-08	6.9E-03	2.3
Minimum	1E-15	3E-14	5995	1E-09	1.E-03	1.0
Maximum	1E-11	1E-11	6150	1E-05	1E-00	3.0
Mean	6E-13	4E-13	6078	9E-07	2E-01	2.2
Median	2E-13	3E-13	6083	2E-07	2E-01	2.2
Geometric mean	2E-13	3E-13	6078	2E-07	1E-01	2.2

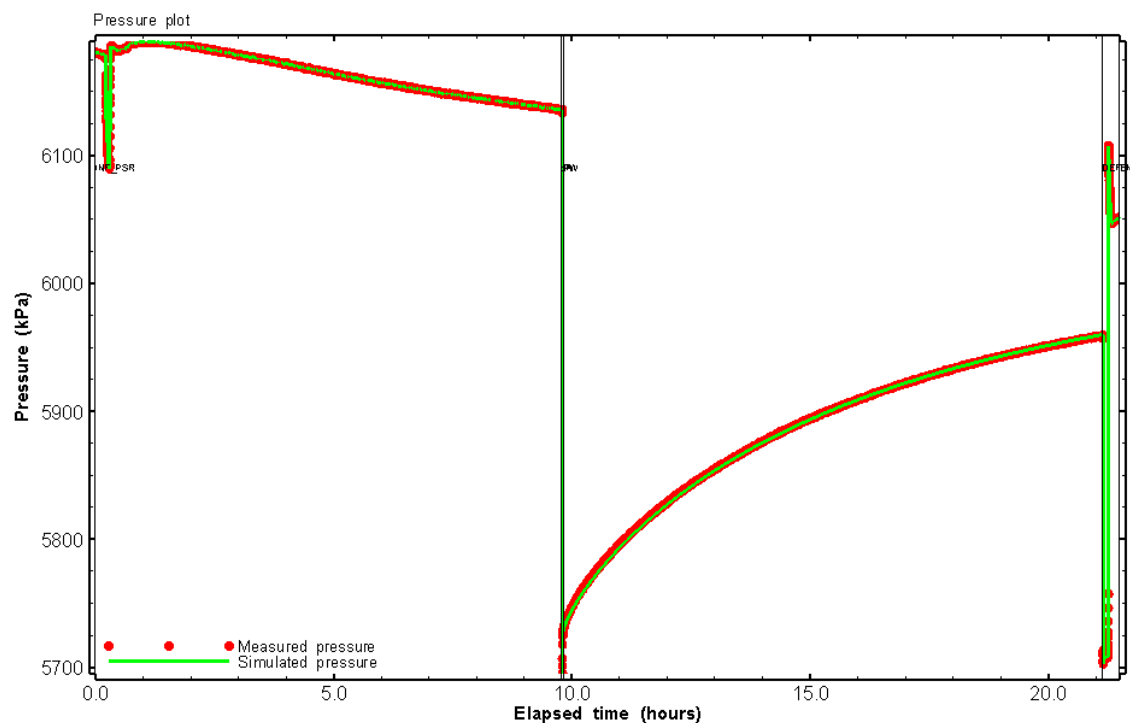


Figure 195: HT017 Pressure plot showing best-fit simulation and best fit results

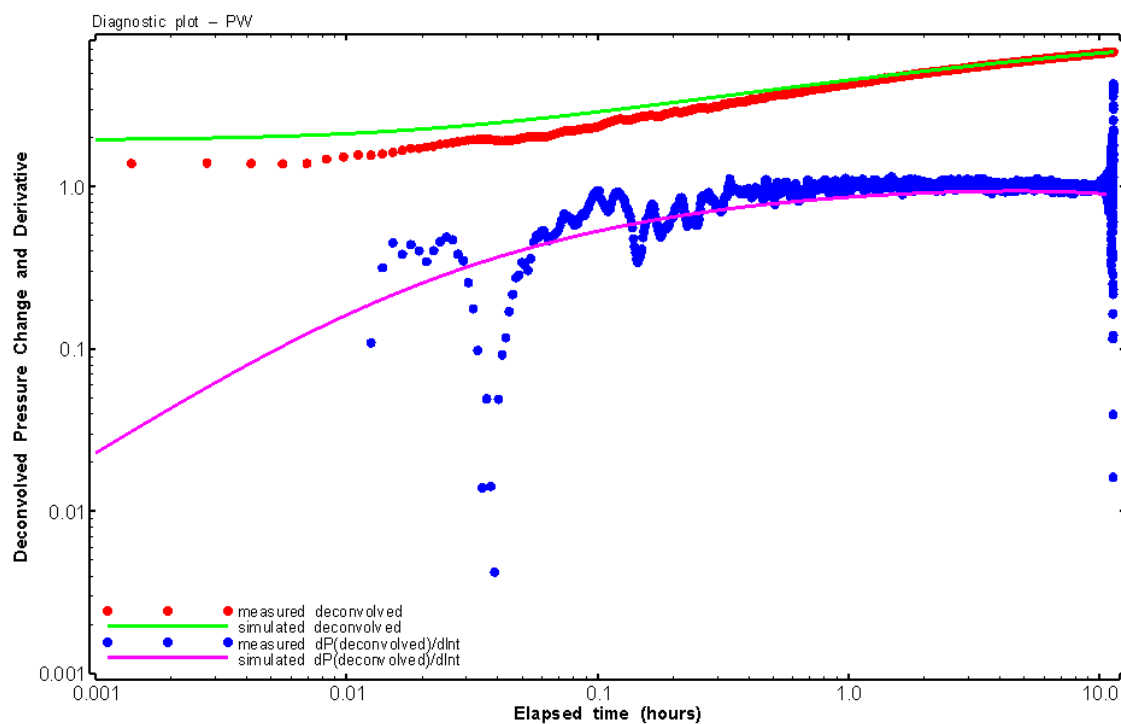


Figure 196: HT017 Deconvolved pressure change and derivative plot of the PW sequence showing best-fit simulation

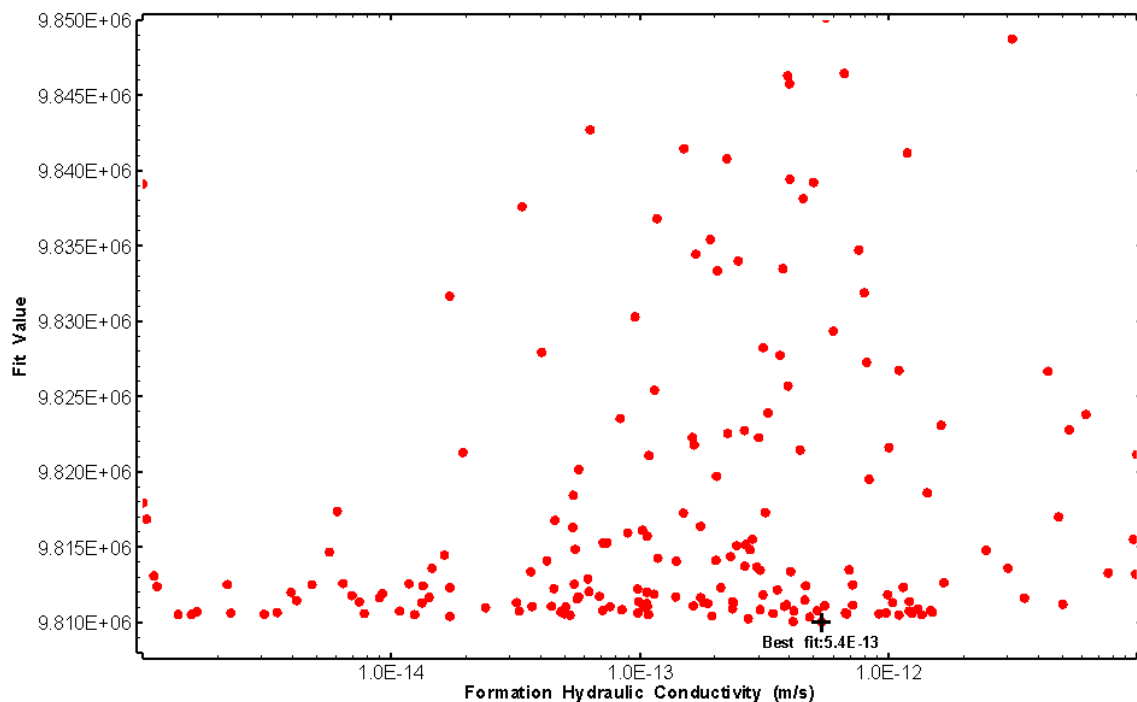


Figure 197: HT017 XY-scatter plot of formation hydraulic conductivity vs. fit value

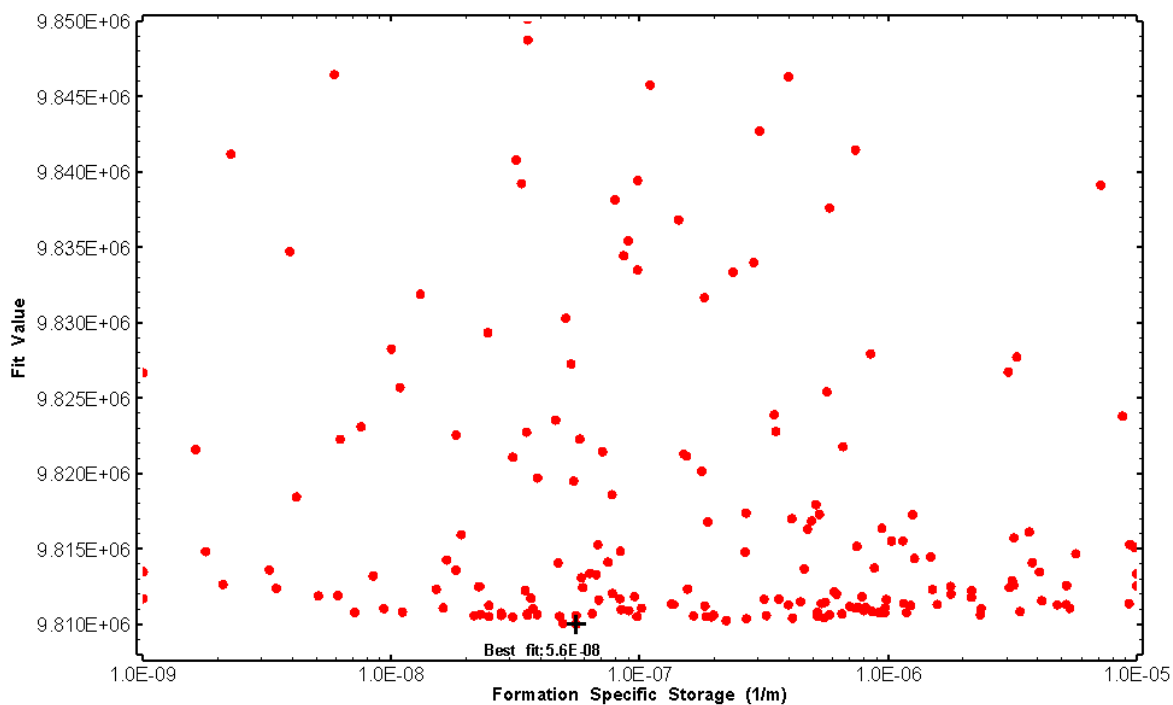


Figure 198: HT017 XY-scatter plot of formation specific storage vs. fit value



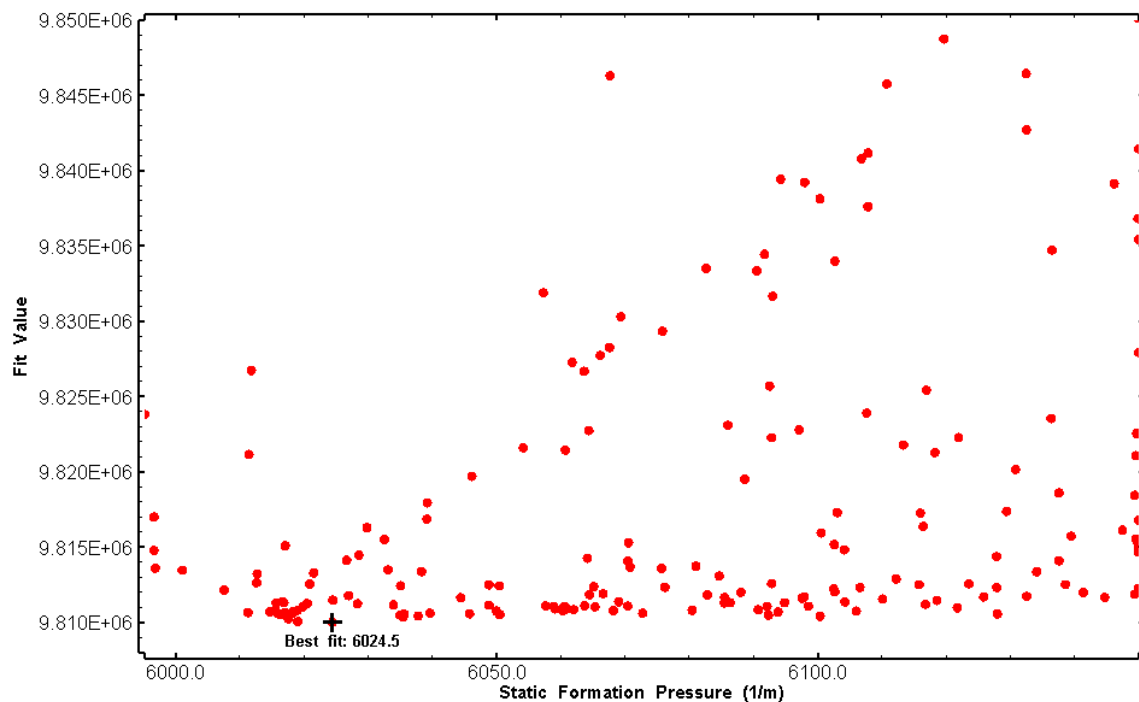


Figure 199: HT017 XY-scatter plot of static formation pressure vs. fit value

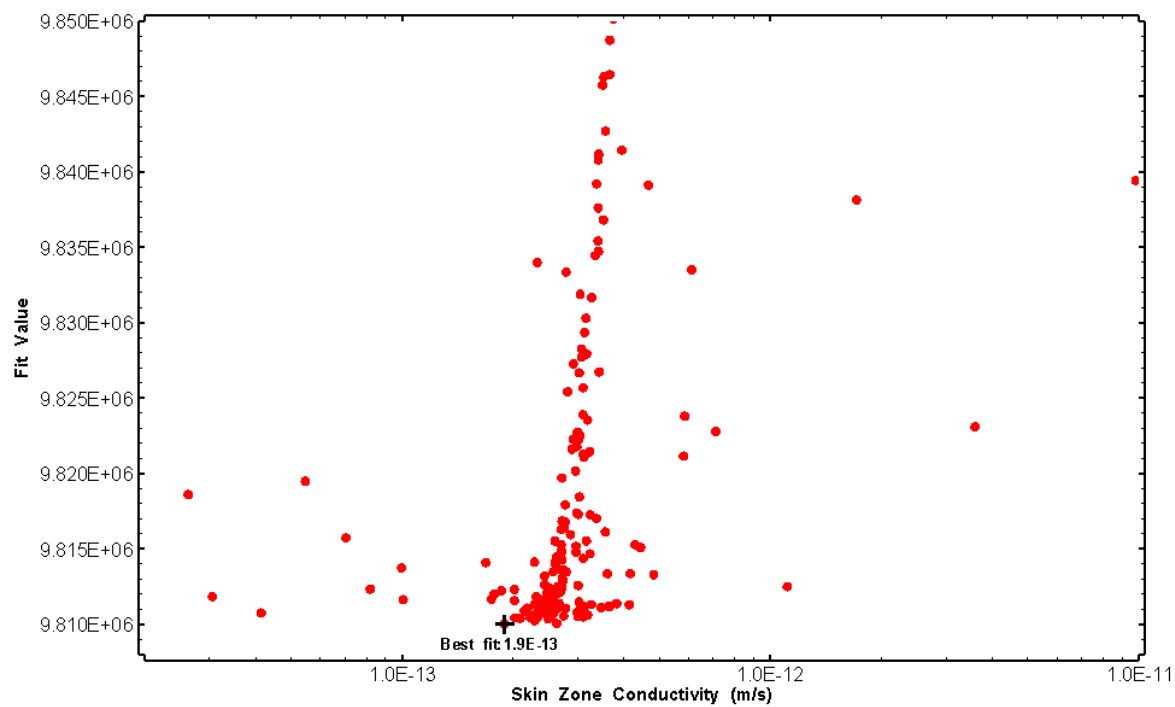


Figure 200: HT017 XY-scatter plot of skin zone conductivity vs. fit value

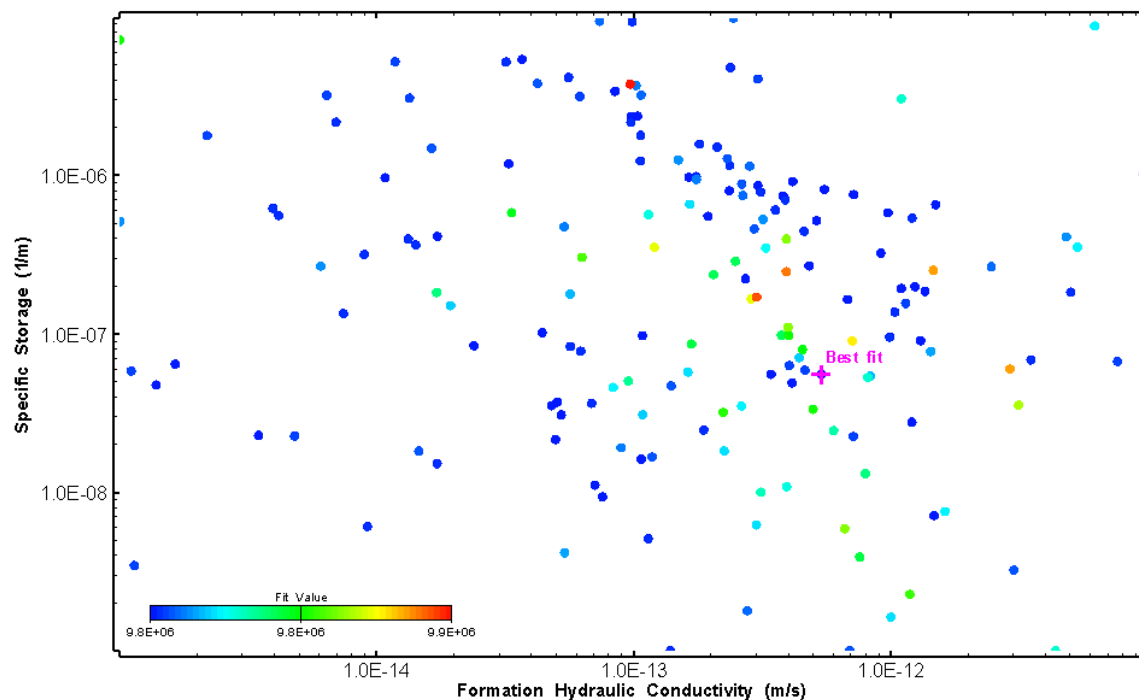


Figure 201: HT017 XY-scatter plot showing estimates of formation hydraulic conductivity and specific storage from perturbation analysis

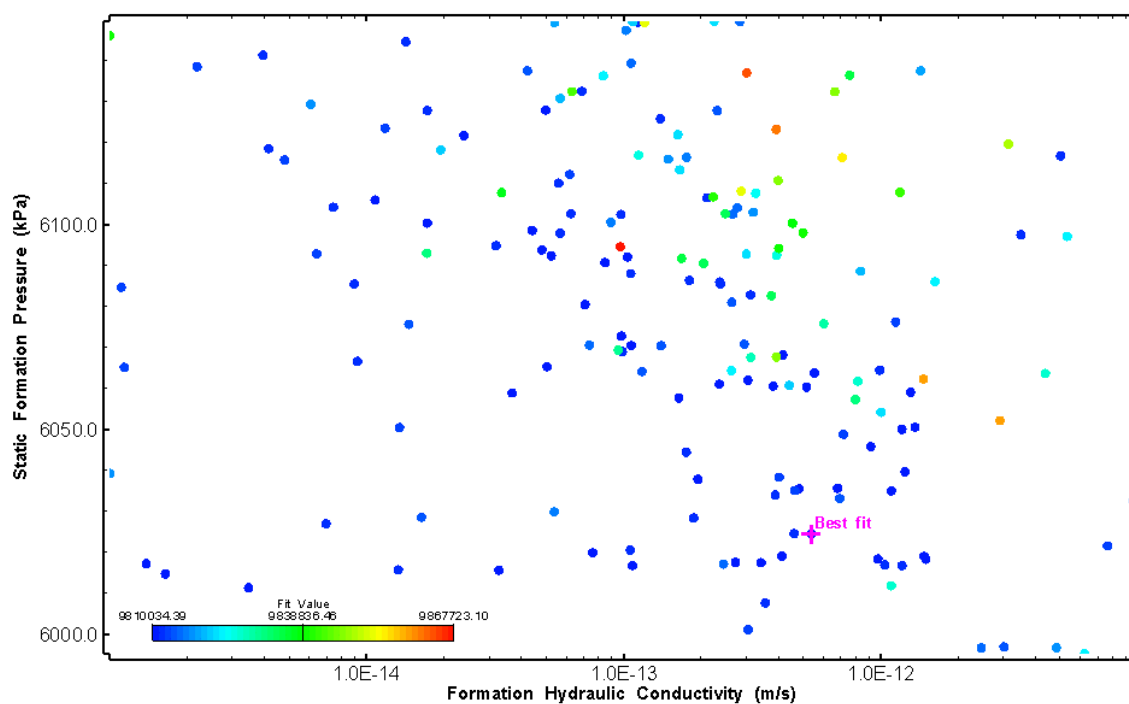


Figure 202: HT017 XY-scatter plot showing estimates of formation hydraulic conductivity and static formation pressure from perturbation analysis

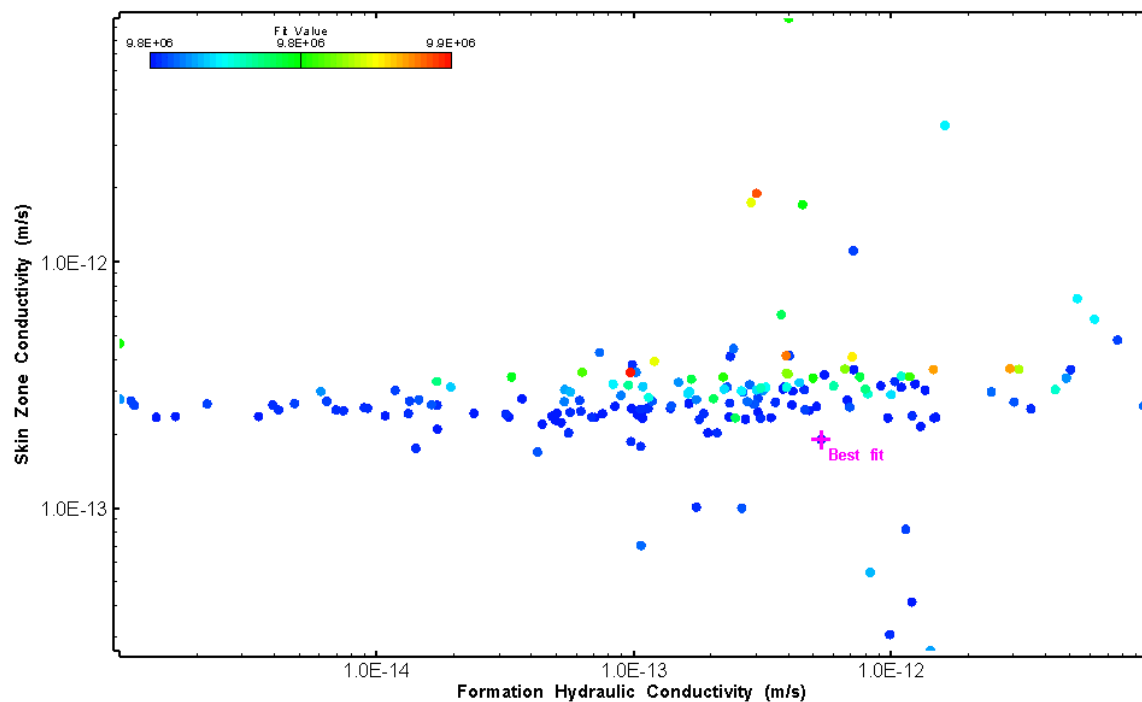


Figure 203: HT017 XY-scatter plot showing estimates of formation hydraulic conductivity and skin zone conductivity from perturbation analysis

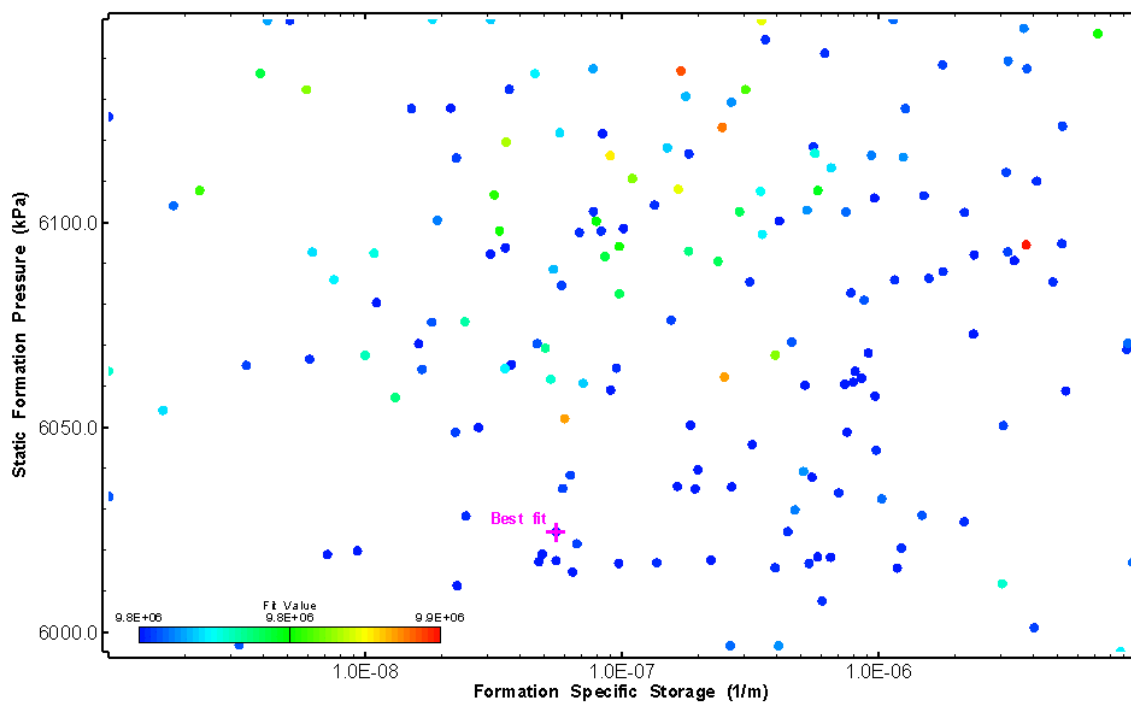


Figure 204: HT017 XY-scatter plot showing estimates of specific storage and static formation pressure from perturbation analysis

## 18.0 HT018 (673.90 – 693.92 M)

HT018 was selected to obtain continuous testing coverage from 600 to 800 m along hole. Eight broken fractures were observed in the core. No indication of flow was recorded during FFEC logging post-drilling.

The test was initiated with a shut-in pressure recovery phase (PSR). A pulse withdrawal test (PW) with a shut-in recovery was completed after the PSR phase.

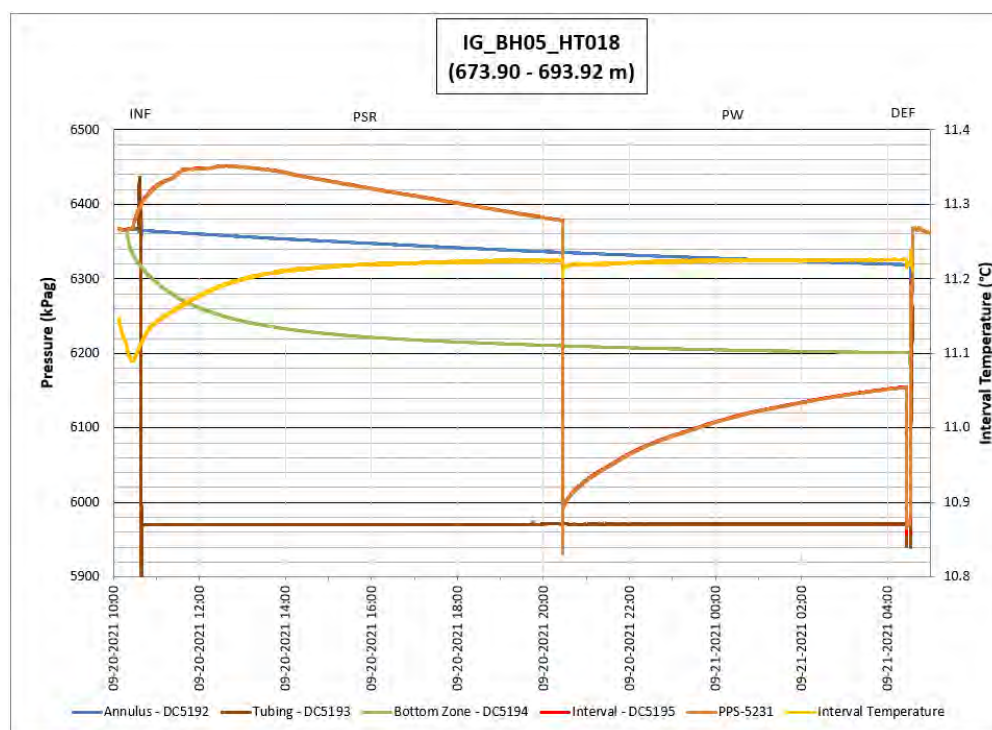
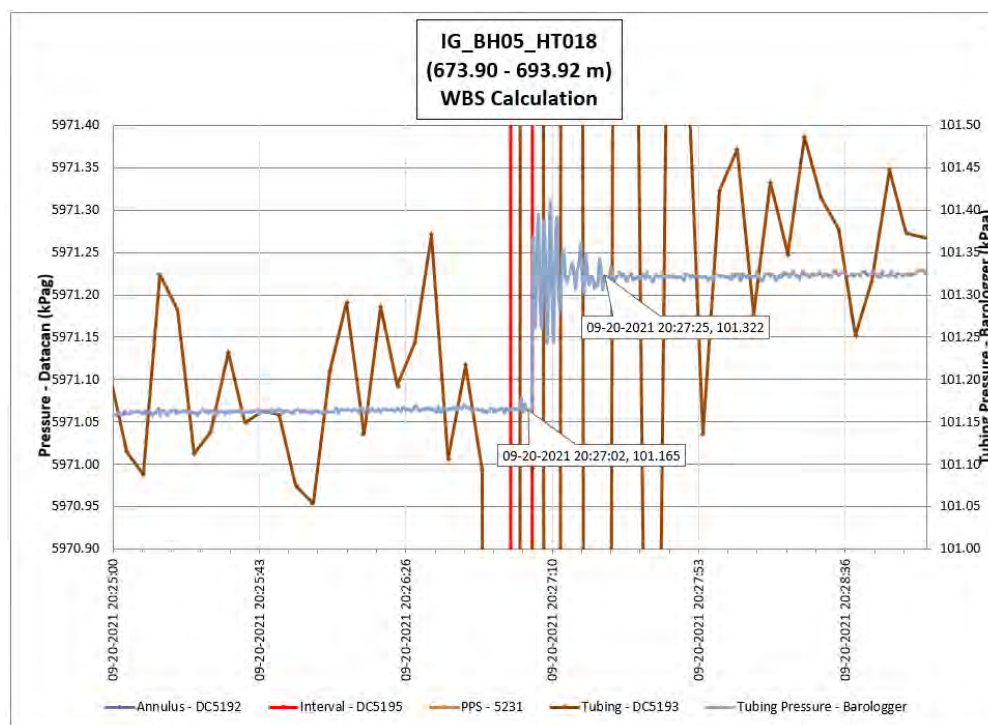


Figure 205: HT018 Annotated test plot showing monitored zone pressure and interval temperature.



**Figure 206: HT018 Tubing pressure during DHSIV activation. DHSIV Closed Wellbore Storage Estimate =  $7\text{E-}11 \text{ m}^3/\text{Pa}$**

**Table 18: Summary of Analysis Results – HT018**

	Formation conductivity	Skin zone conductivity	Static formation pressure	Formation specific storage	Radial thickness of skin	Flow dimension
	[m/s]	[m/s]	[kPa]	[1/m]	[m]	[–]
Best Fit	4E-13	3E-13	6200	3E-07	8.53E-02	2.2
Minimum	1E-15	2E-13	6154	1E-09	1E-04	1.1
Maximum	7E-10	6E-13	6380	5E-05	1E-00	3.0
Mean	7E-12	3E-13	6258	1E-06	3E-01	2.2
Median	7E-14	3E-13	6256	2E-07	2E-01	2.0
Geometric mean	8E-14	3E-13	6258	1E-07	2E-01	2.2

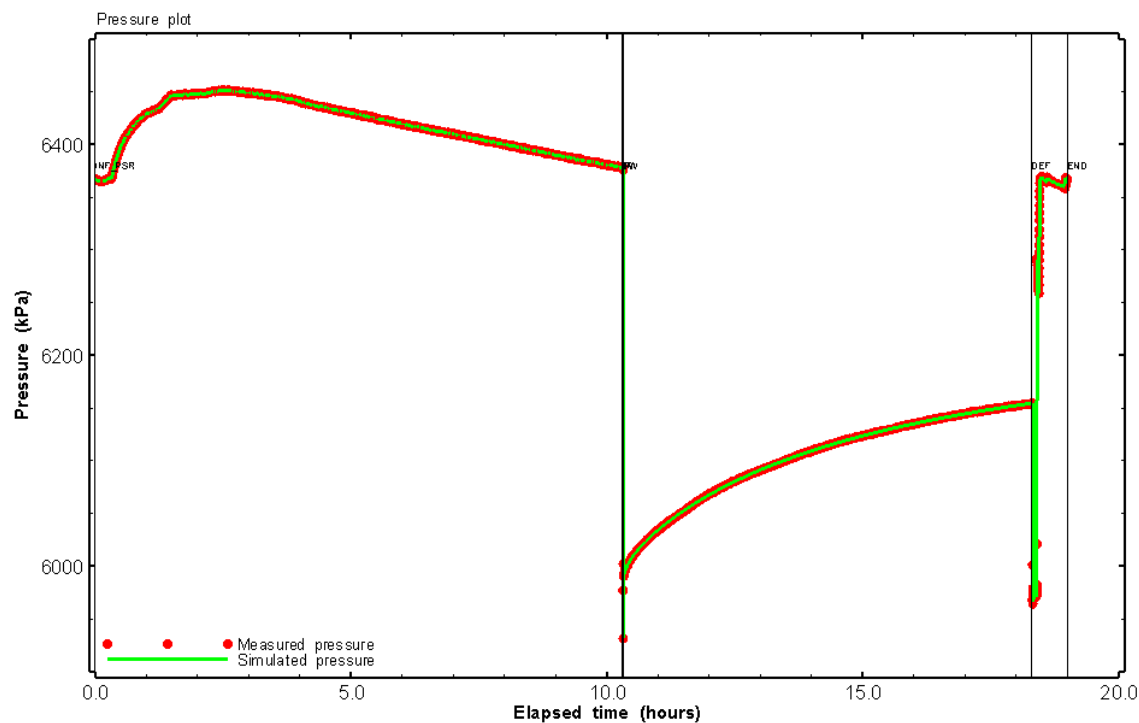


Figure 207: HT018 Pressure plot showing best-fit simulation and best fit results

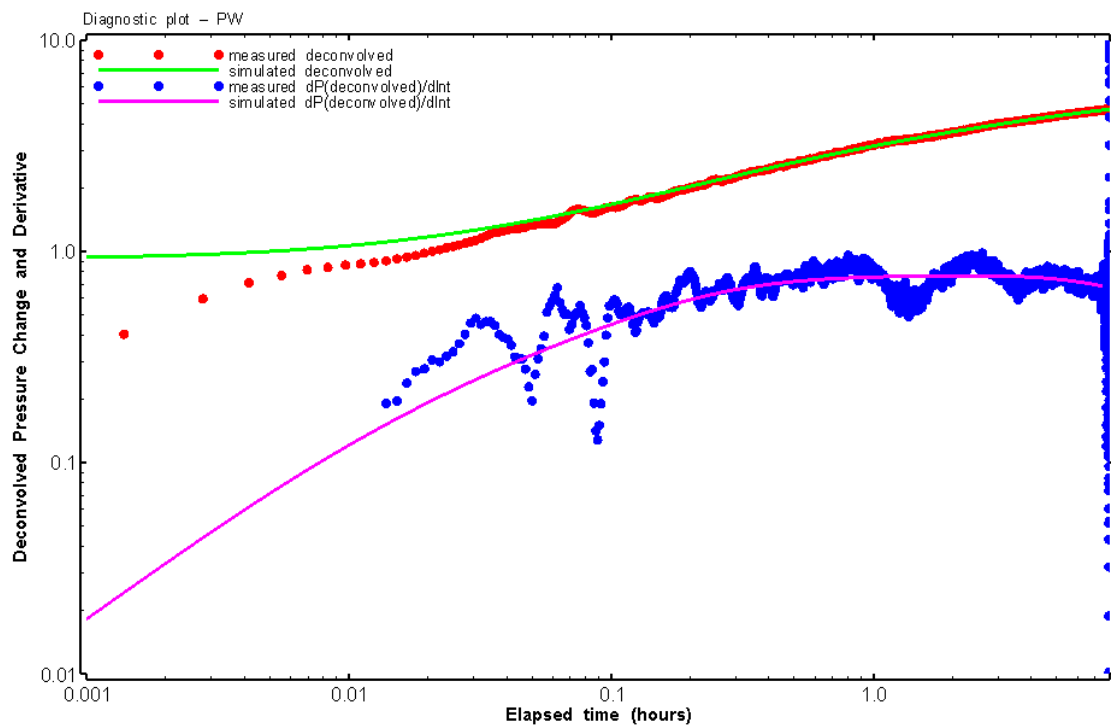


Figure 208: HT018 Deconvolved pressure change and derivative plot of the PW sequence showing best-fit simulation

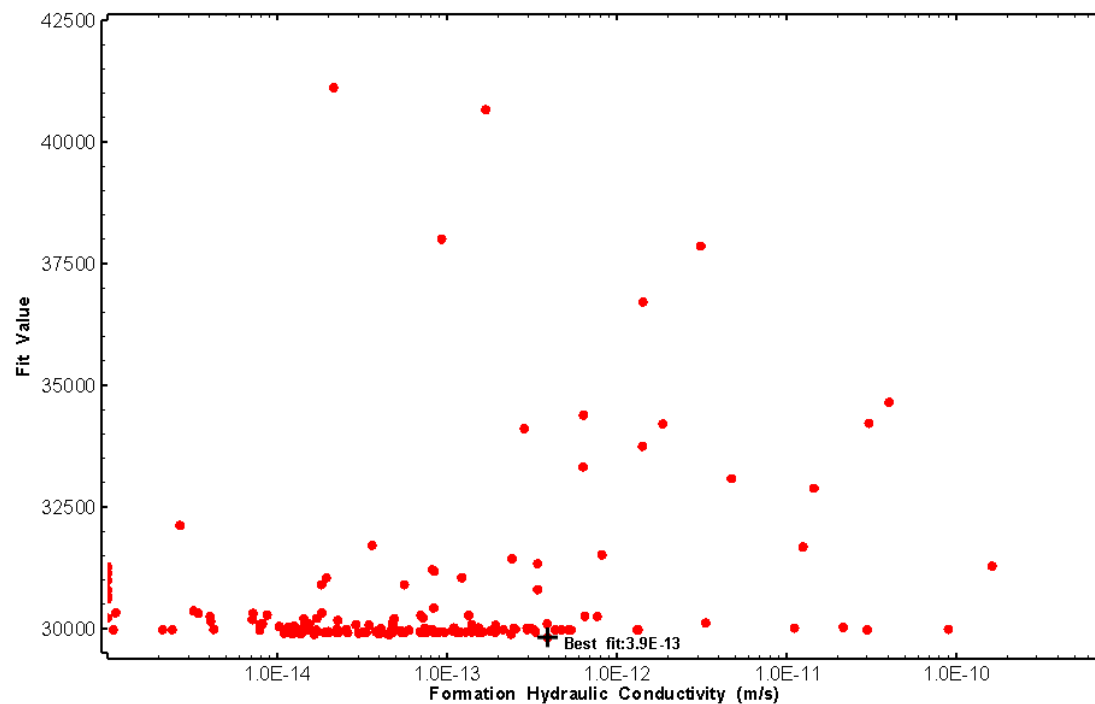


Figure 209: HT018 XY-scatter plot of formation hydraulic conductivity vs. fit value

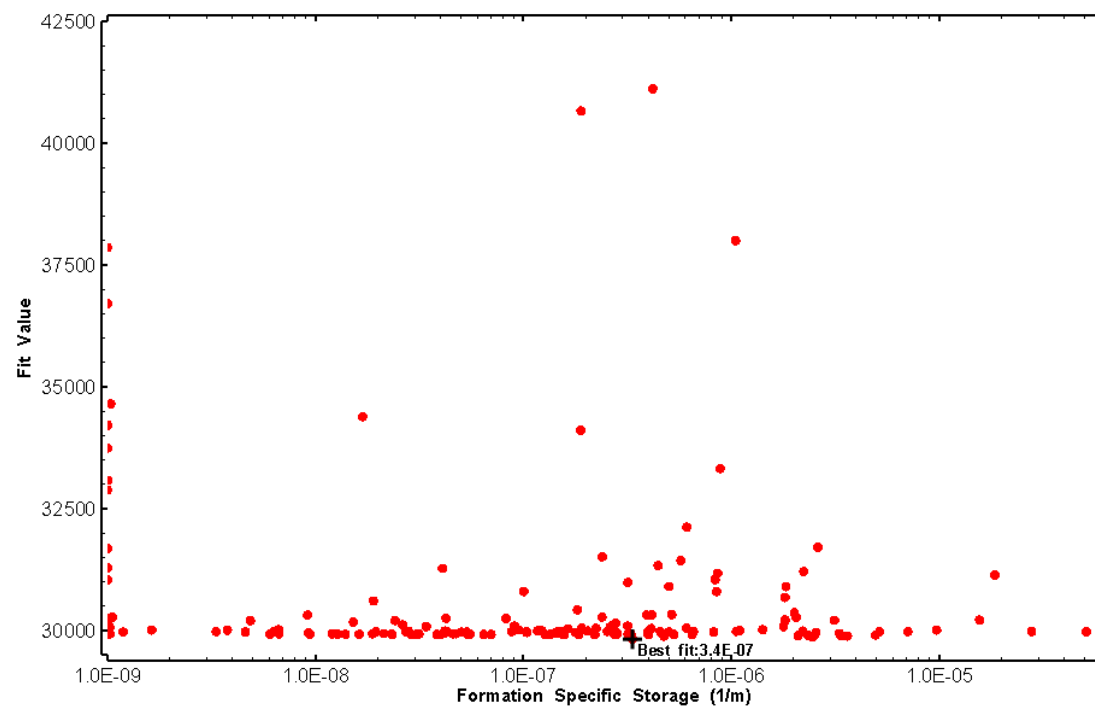


Figure 210: HT018 XY-scatter plot of formation specific storage vs. fit value

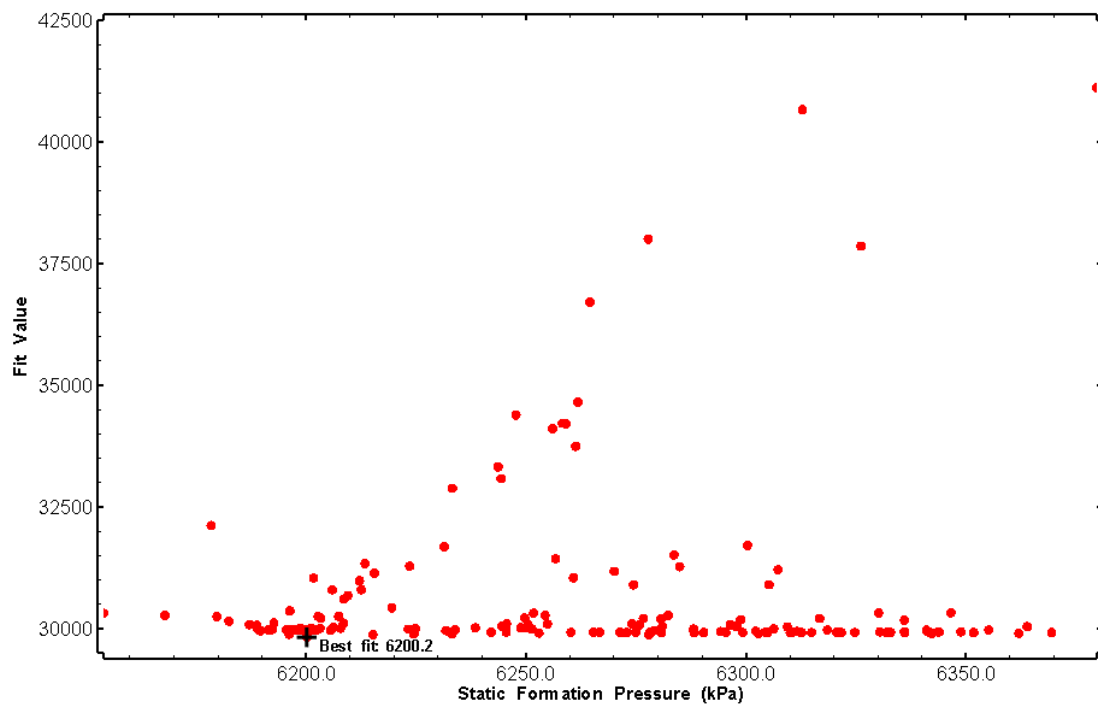


Figure 211: HT018 XY-scatter plot of static formation pressure vs. fit value

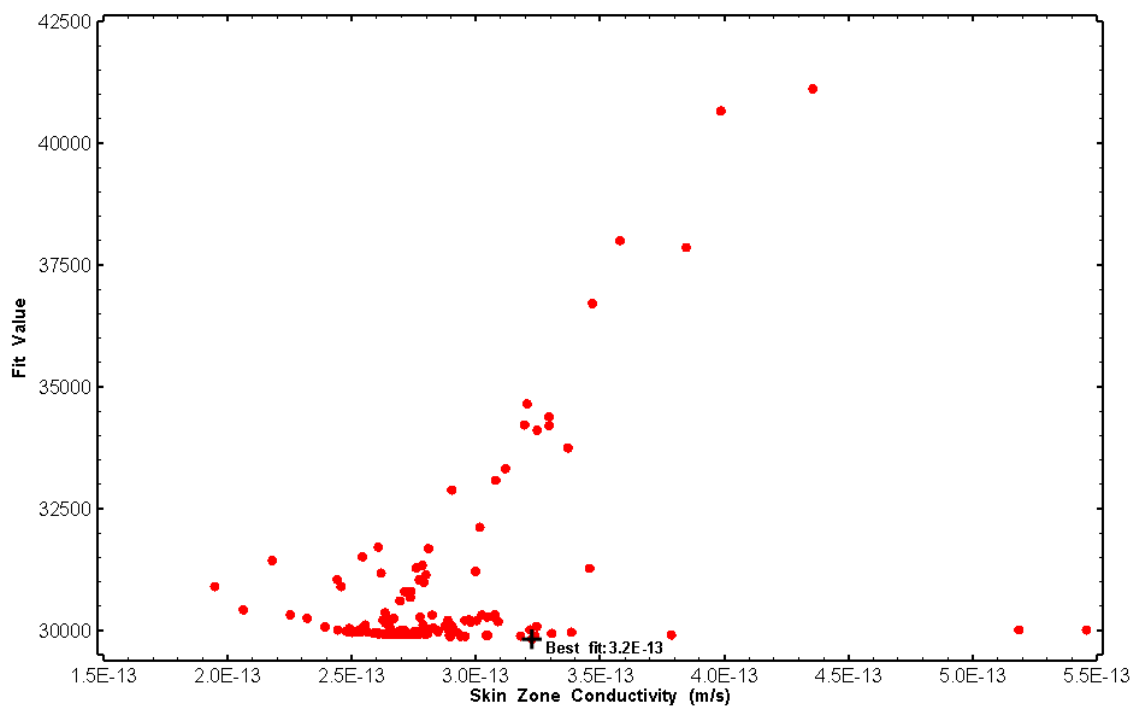


Figure 212: HT018 XY-scatter plot of skin zone conductivity vs. fit value



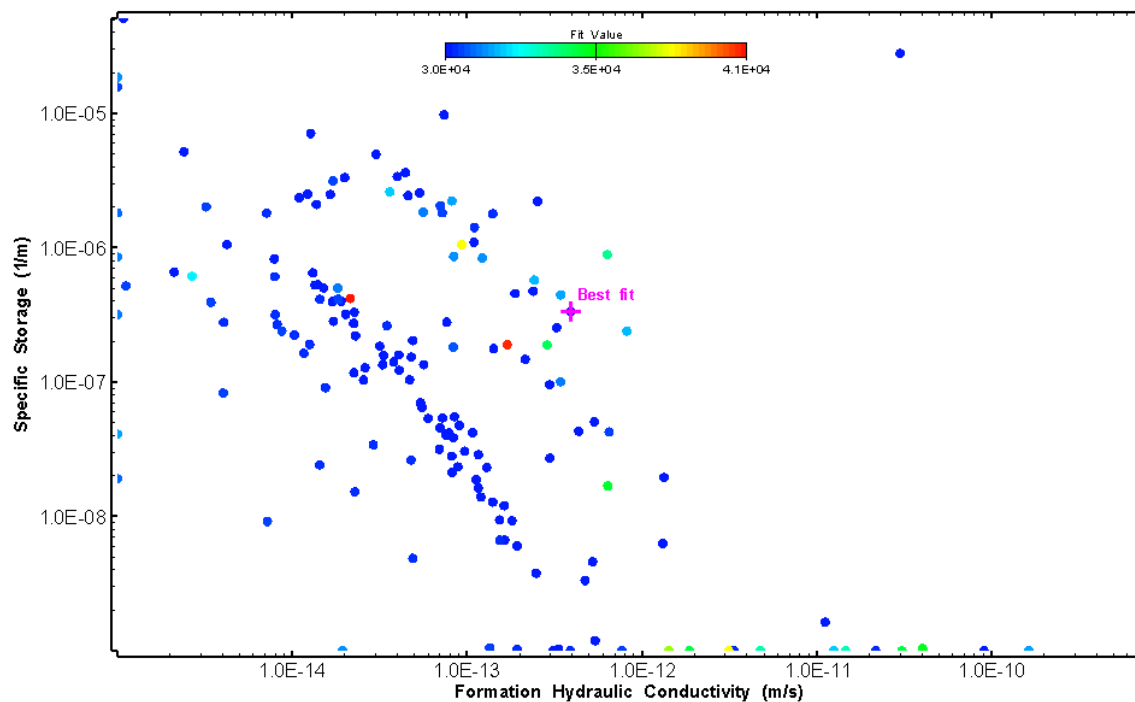


Figure 213: HT018 XY-scatter plot showing estimates of formation hydraulic conductivity and specific storage from perturbation analysis

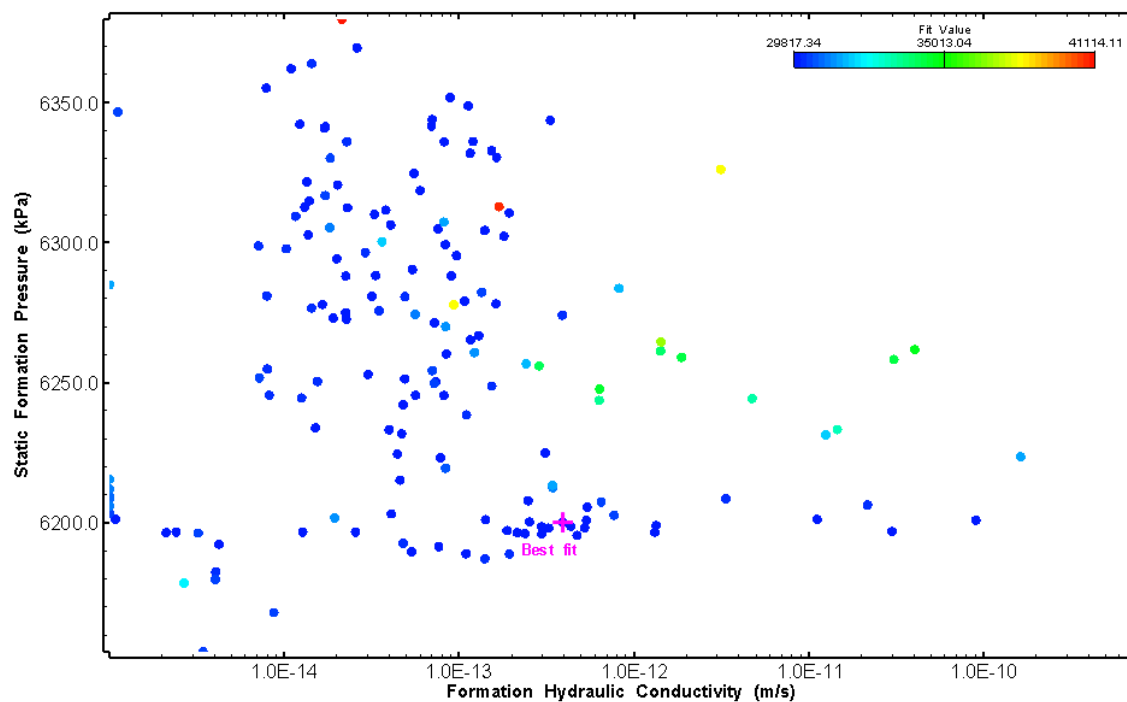


Figure 214: HT018 XY-scatter plot showing estimates of formation hydraulic conductivity and static formation pressure from perturbation analysis

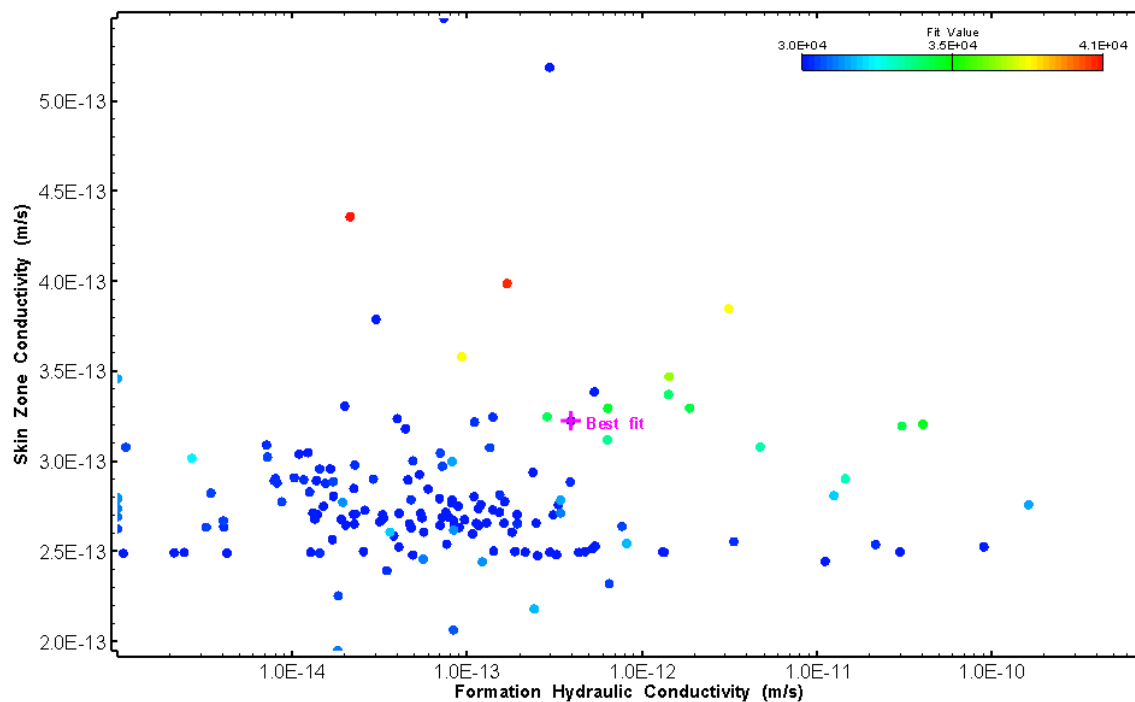


Figure 215: HT018 XY-scatter plot showing estimates of formation hydraulic conductivity and skin zone conductivity from perturbation analysis

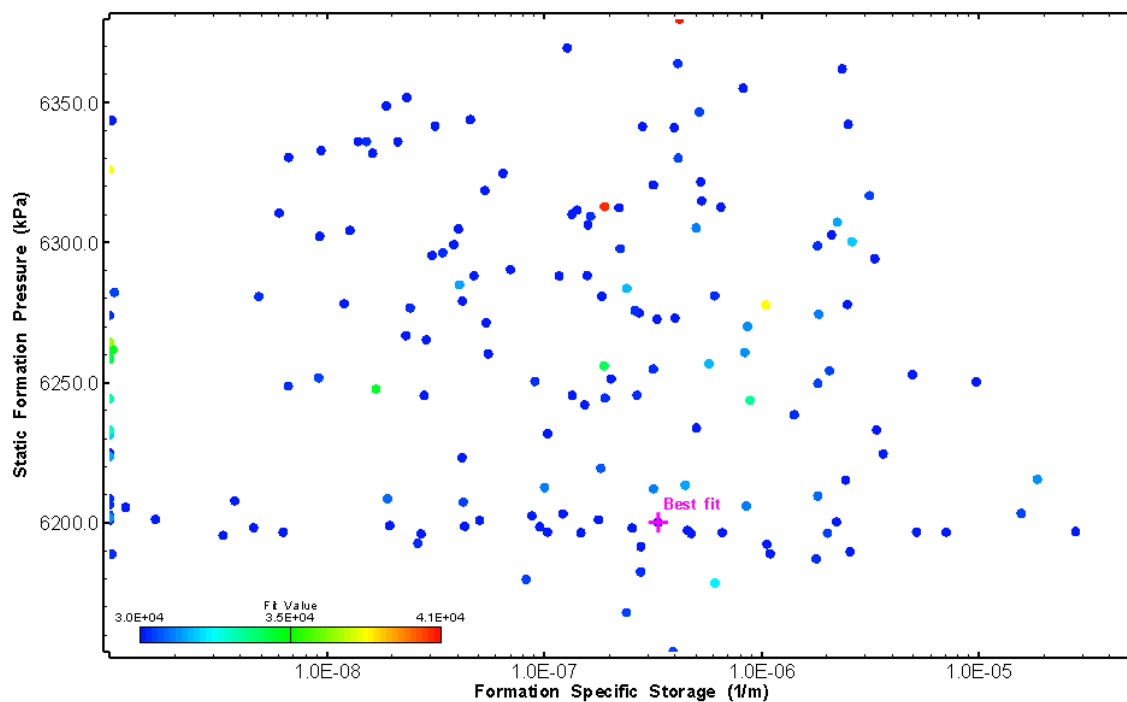


Figure 216: HT018 XY-scatter plot showing estimates of specific storage and static formation pressure from perturbation analysis

## 19.0 HT019 (693.90 – 713.92 M)

HT019 was selected to obtain continuous testing coverage from 600 to 800 m along hole. Three broken fractures were observed in the core. No drill fluid parameter triggers were reached during drilling. No indication of flow was recorded during FFEC logging post-drilling.

The test was initiated with a shut-in pressure recovery phase (PSR). A pulse withdrawal test (PW) with a shut-in recovery was completed after the PSR phase.

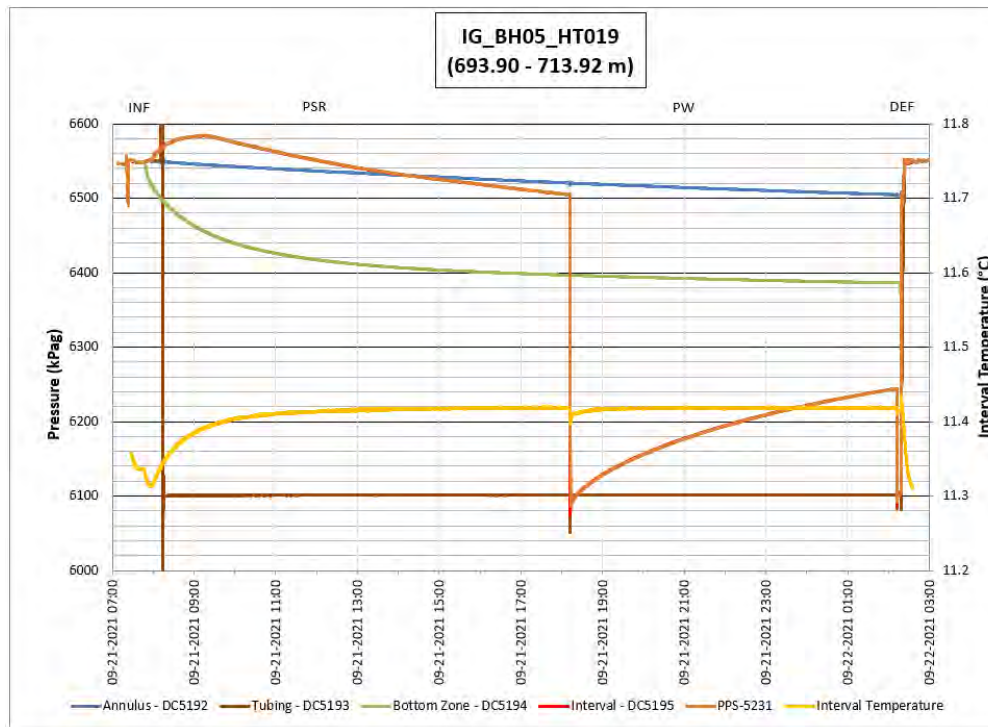
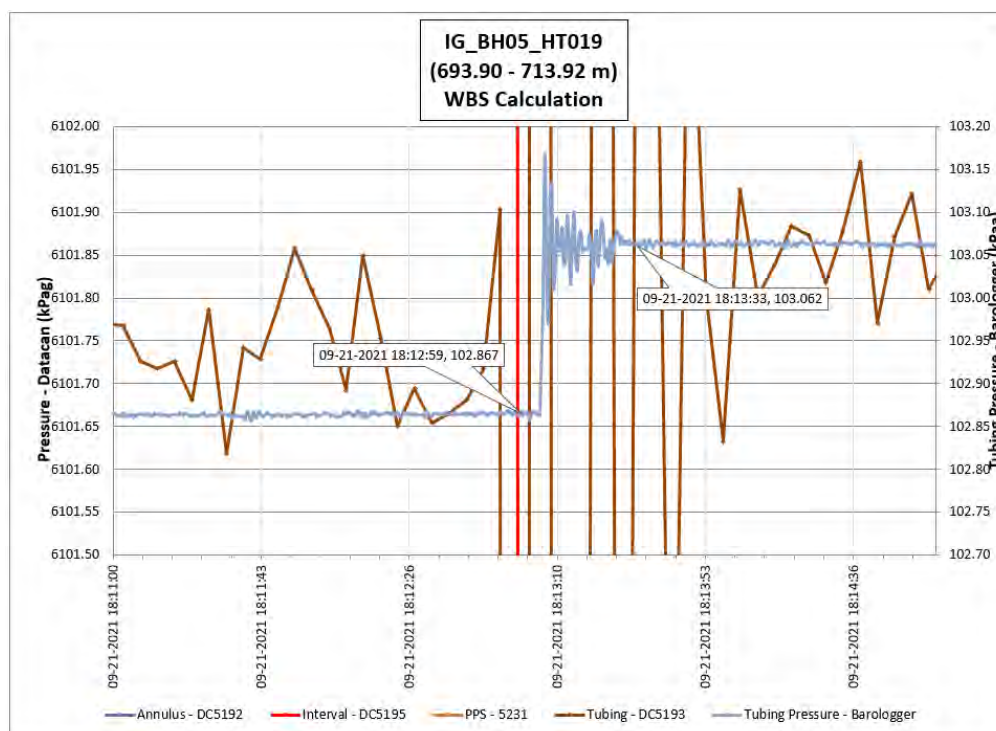


Figure 217: HT019 Annotated test plot showing monitored zone pressure and interval temperature.



**Figure 218: HT019 Tubing pressure during DHSIV activation. DHSIV Closed Wellbore Storage Estimate =  $8\text{E-}11 \text{ m}^3/\text{Pa}$**

**Table 19: Summary of Analysis Results – HT019**

	Formation conductivity	Skin zone conductivity	Static formation pressure	Formation specific storage	Radial thickness of skin	Flow dimension
	[m/s]	[m/s]	[kPa]	[1/m]	[m]	[–]
Best Fit	5E-14	2E-13	6493	7E-08	1.45E-01	2.3
Minimum	7E-15	9E-14	6349	1E-09	2E-04	1.5
Maximum	3E-12	8E-12	6546	3E-06	1E-00	2.5
Mean	3E-13	3E-13	6451	3E-07	2E-01	2.0
Median	2E-13	2E-13	6453	1E-07	2E-01	2.0
Geometric mean	2E-13	2E-13	6451	1E-07	1E-01	2.0

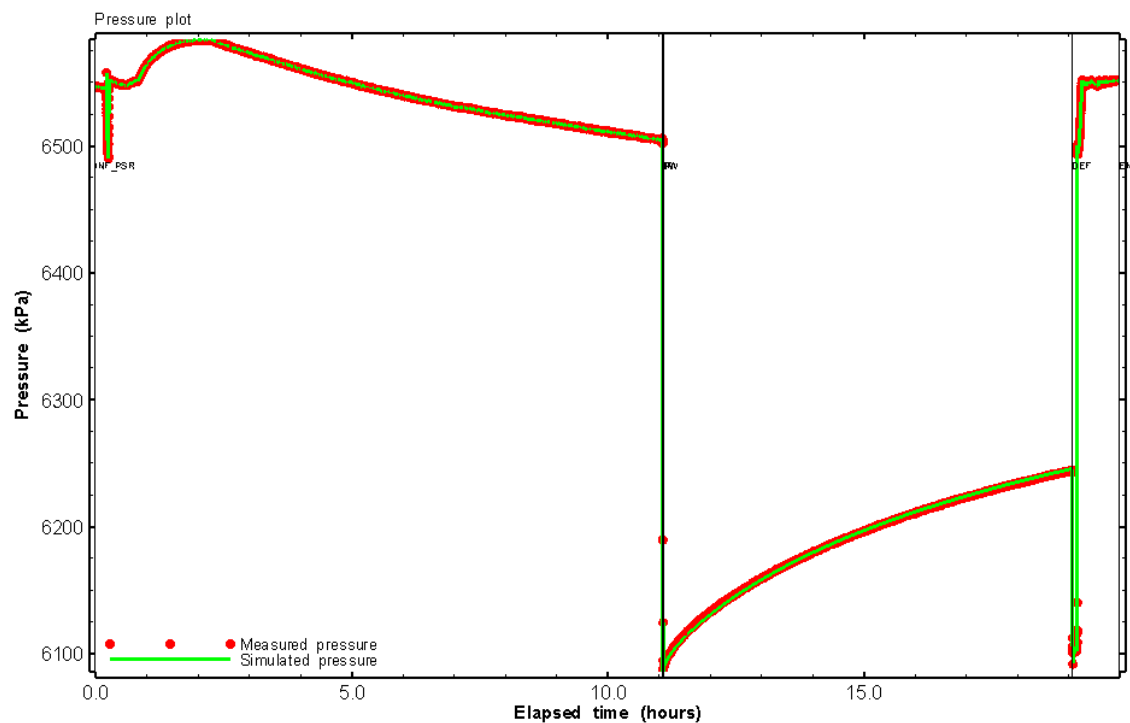


Figure 219: HT019 Pressure plot showing best-fit simulation and best fit results

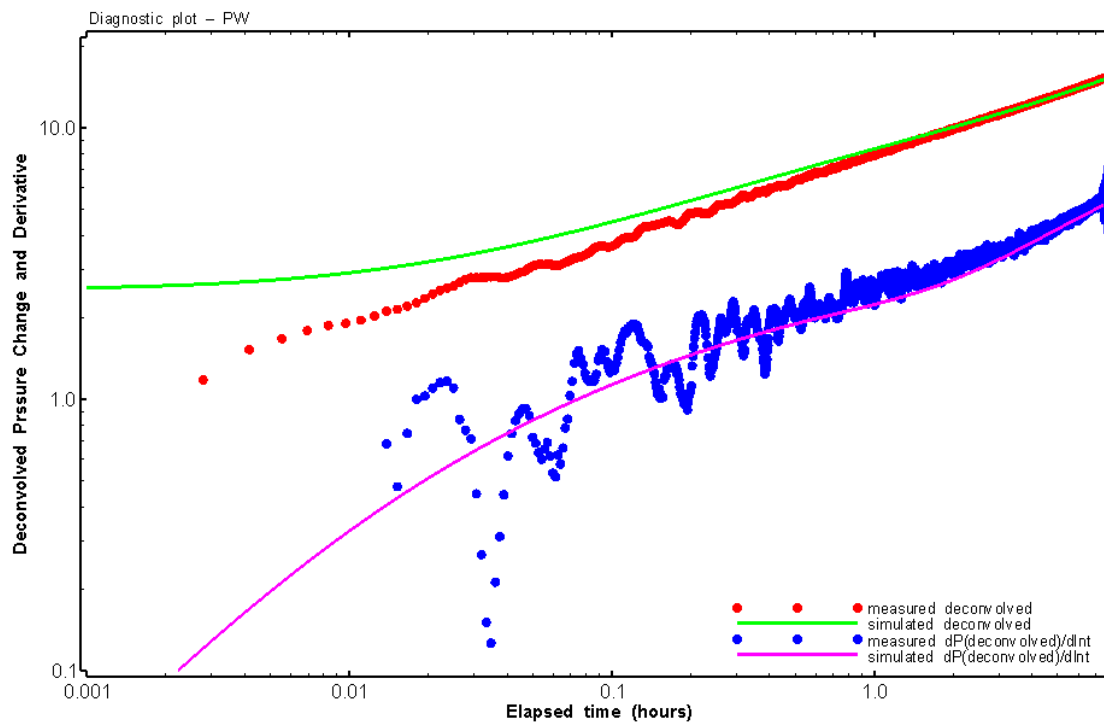


Figure 220: HT019 Deconvolved pressure change and derivative plot of the PW sequence showing best-fit simulation

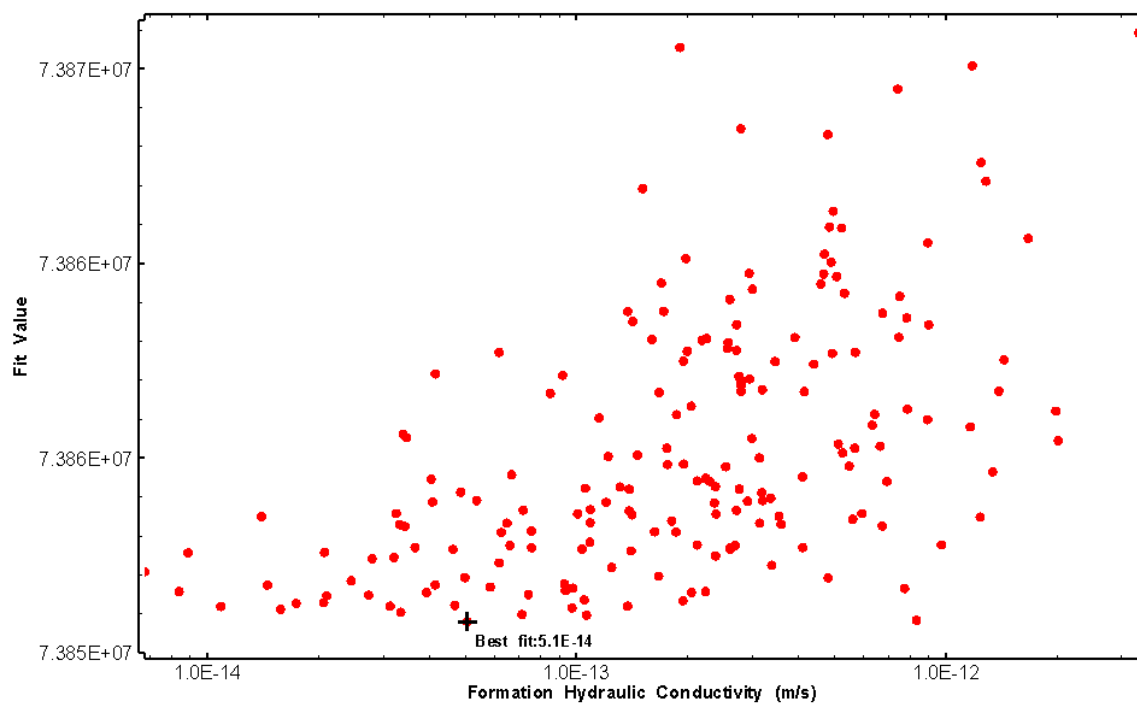


Figure 221: HT019 XY-scatter plot of formation hydraulic conductivity vs. fit value

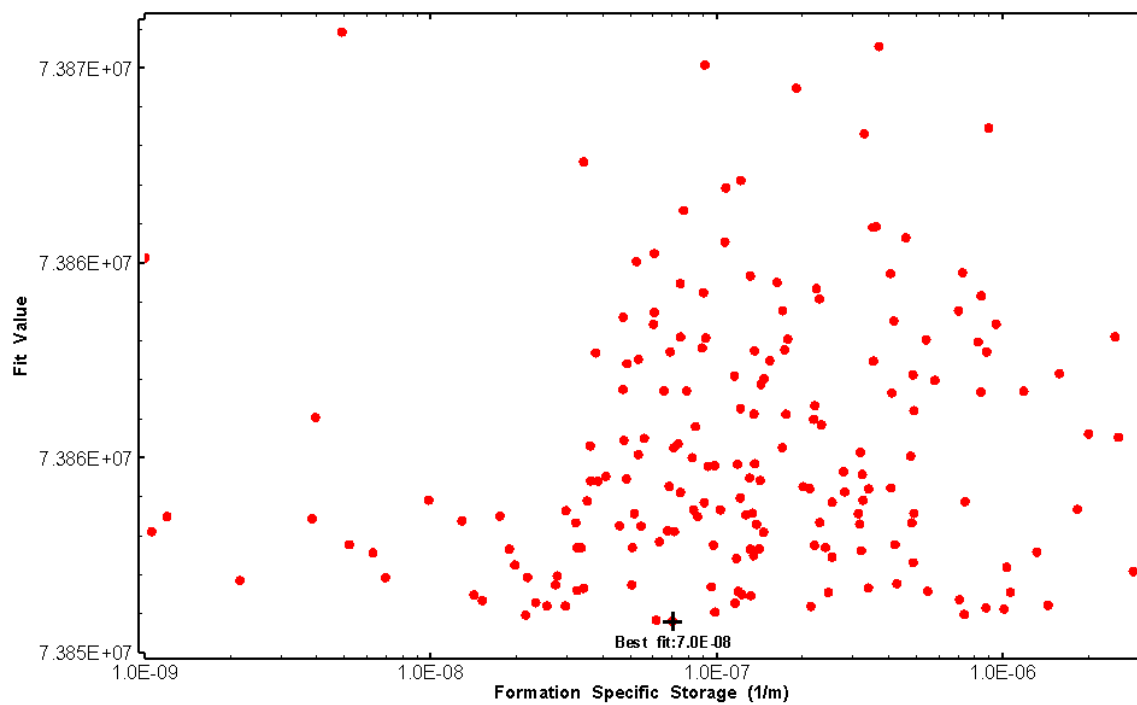


Figure 222: HT019 XY-scatter plot of formation specific storage vs. fit value

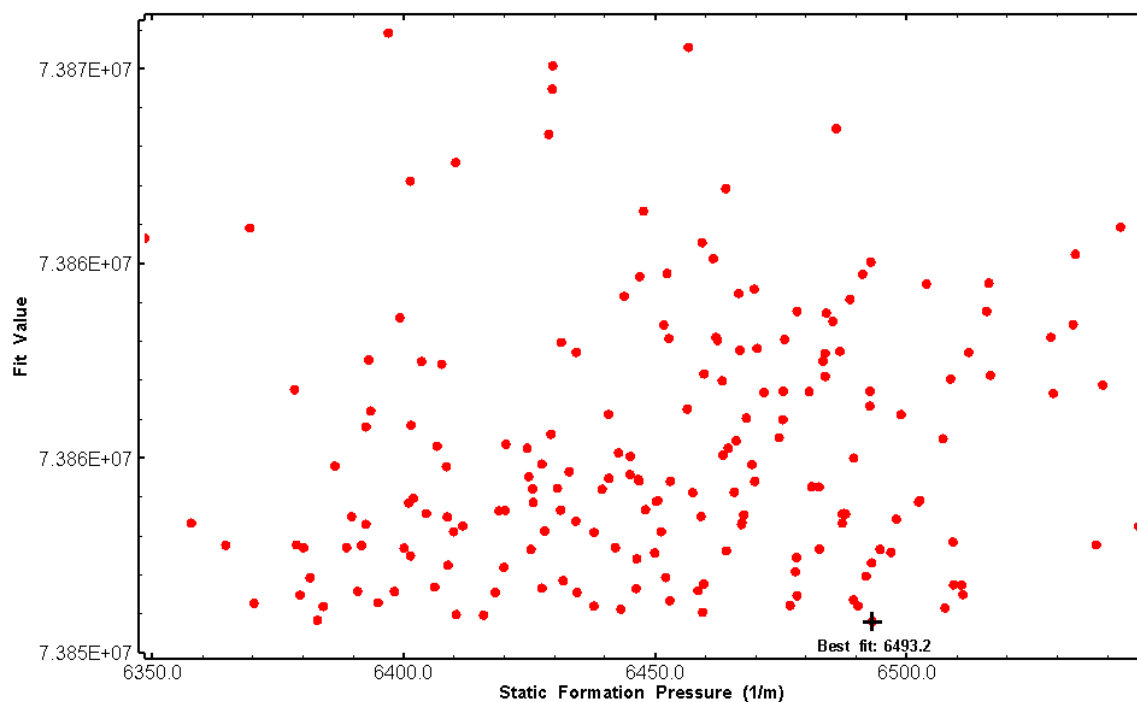


Figure 223: HT019 XY-scatter plot of static formation pressure vs. fit value

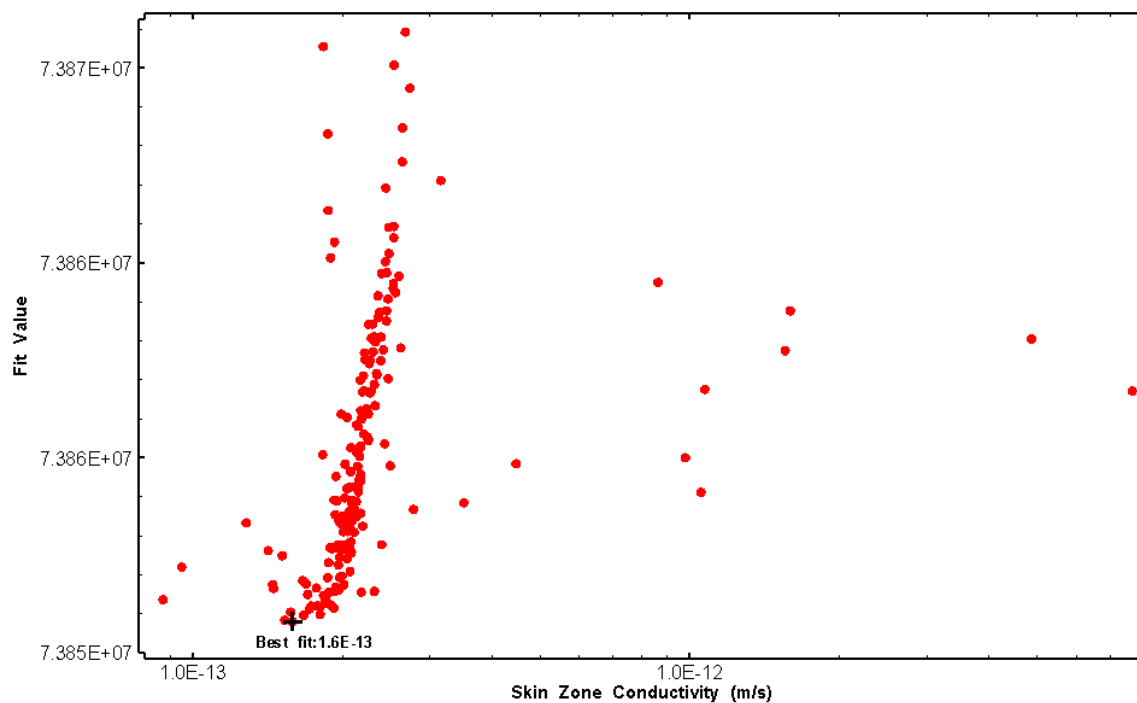


Figure 224: HT019 XY-scatter plot of skin zone conductivity vs. fit value

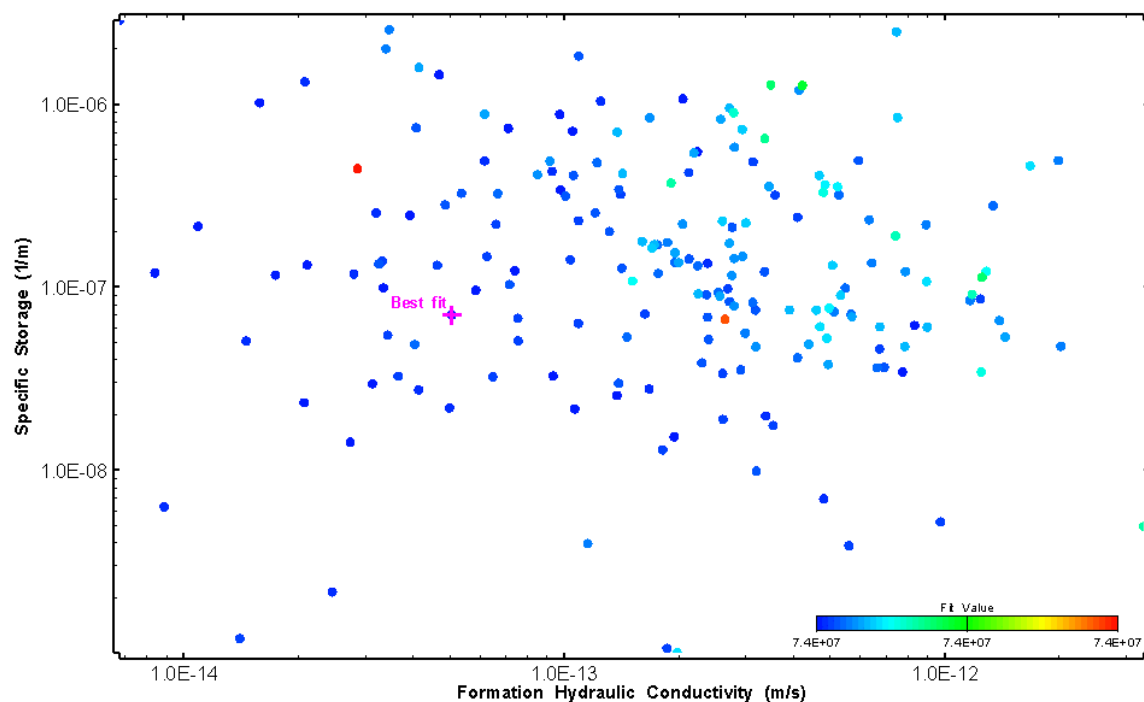


Figure 225: HT019 XY-scatter plot showing estimates of formation hydraulic conductivity and specific storage from perturbation analysis

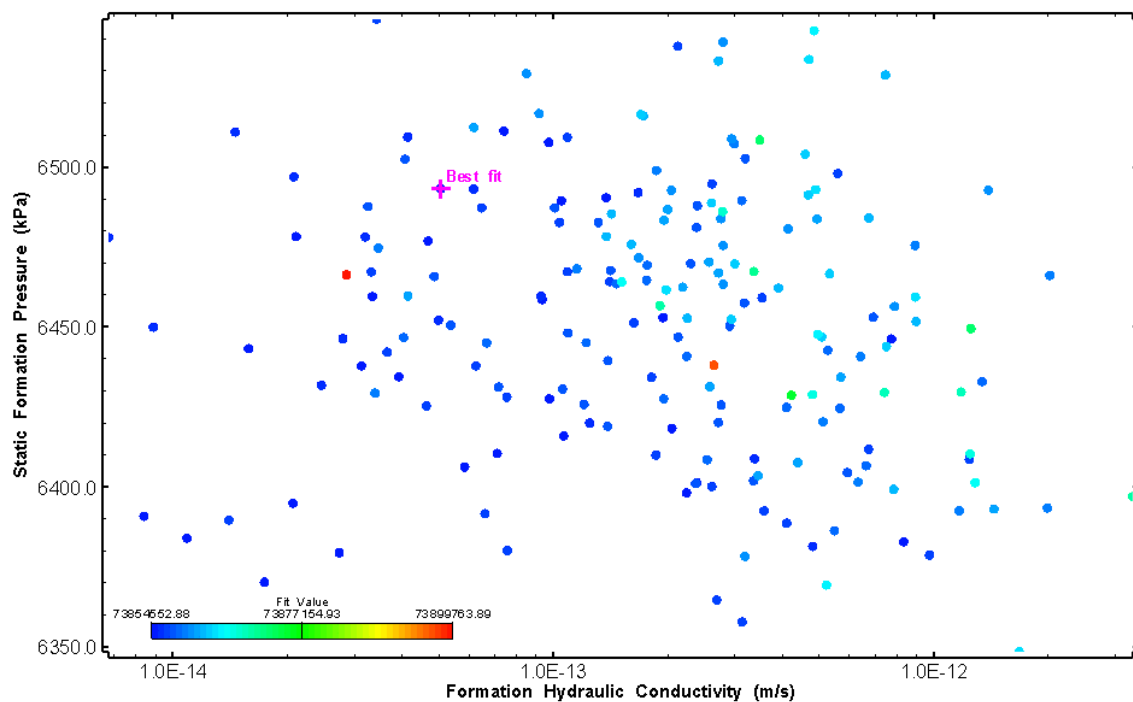


Figure 226: HT019 XY-scatter plot showing estimates of formation hydraulic conductivity and static formation pressure from perturbation analysis



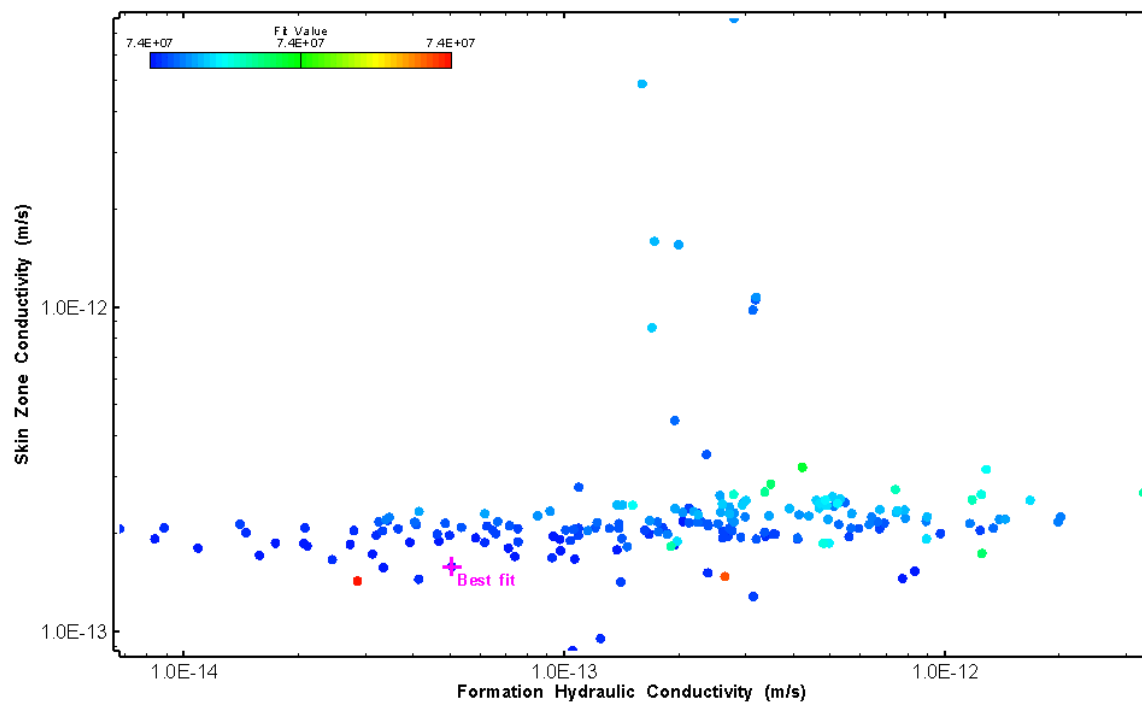


Figure 227: HT019 XY-scatter plot showing estimates of formation hydraulic conductivity and skin zone conductivity from perturbation analysis

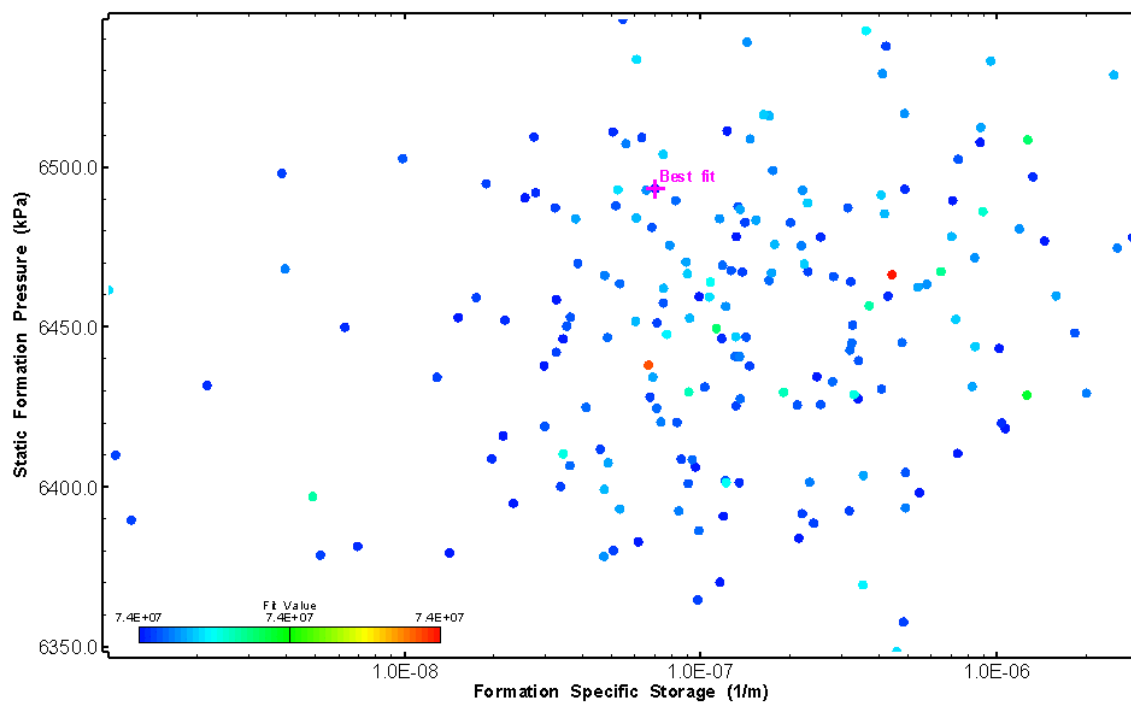


Figure 228: HT019 XY-scatter plot showing estimates of specific storage and static formation pressure from perturbation analysis

## 20.0 HT020 (713.80 – 733.82 M)

HT020 was selected to obtain continuous testing coverage from 600 to 800 m along hole and an interval containing multiple dykes. 17 broken fractures were observed in the core. No indication of flow was recorded during FFEC logging post-drilling.

The test was initiated with a shut-in pressure recovery phase (PSR). A pulse withdrawal test (PW) with a shut-in recovery was completed after the PSR phase.

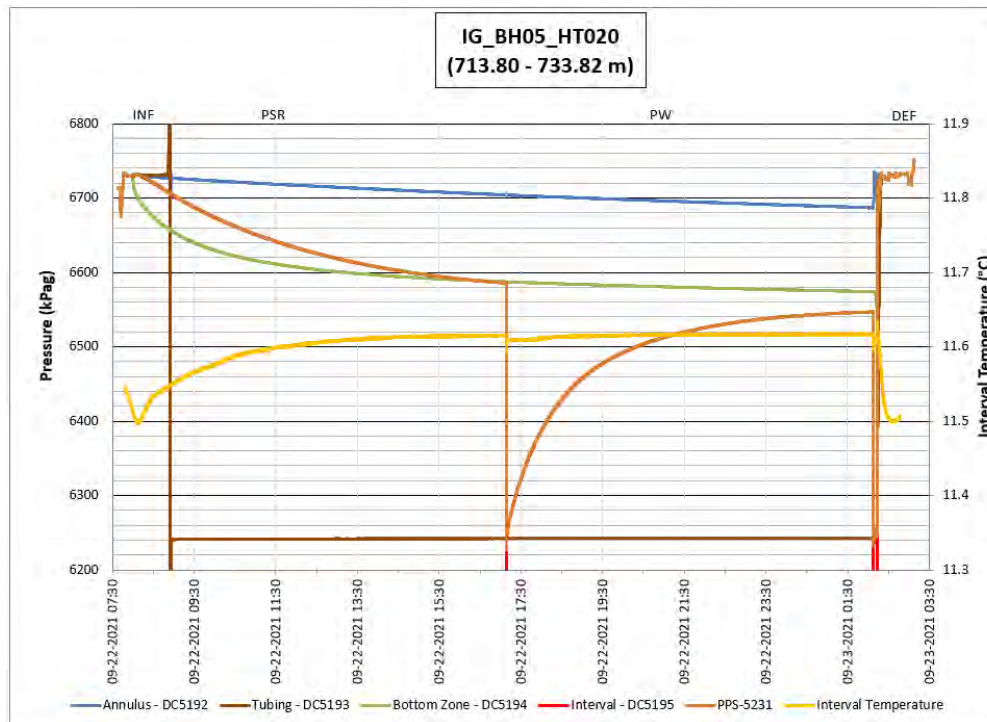
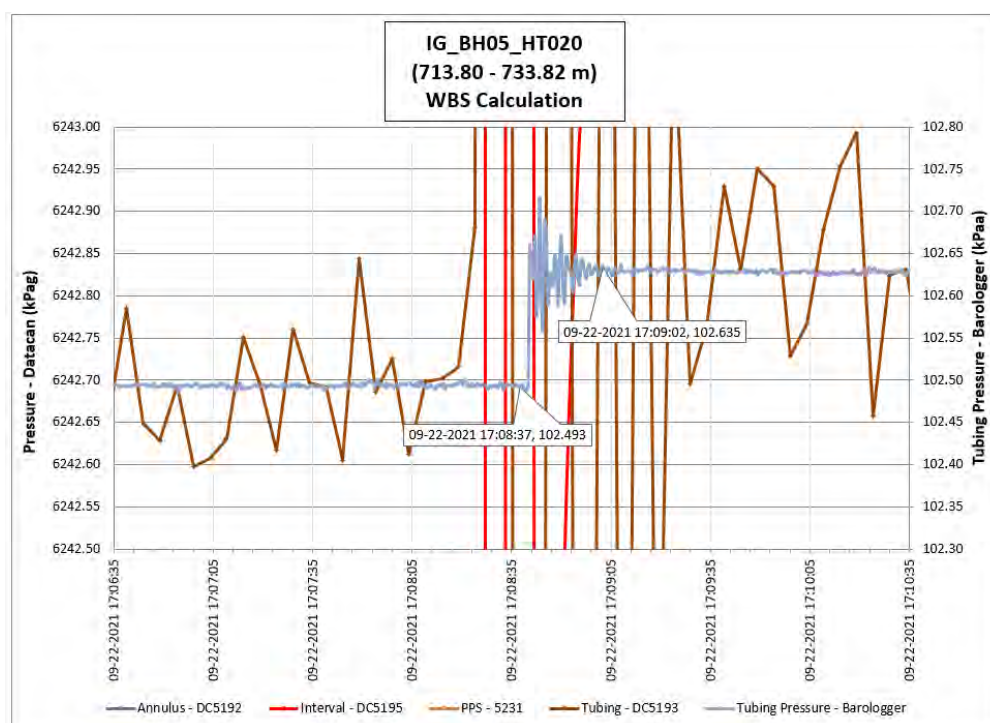


Figure 229: HT020 Annotated test plot showing monitored zone pressure and interval temperature.



**Figure 230: HT020 Tubing pressure during DHSIV activation. DHSIV Closed Wellbore Storage Estimate =  $7\text{E-}11 \text{ m}^3/\text{Pa}$**

**Table 20: Summary of Analysis Results – HT020**

	Formation conductivity	Skin zone conductivity	Static formation pressure	Formation specific storage	Radial thickness of skin	Flow dimension
	[m/s]	[m/s]	[kPa]	[1/m]	[m]	[–]
Best Fit	1E-13	1E-12	6567	6E-06	9.57E-02	2.5
Minimum	4E-14	1E-14	6546	1E-09	1E-04	1.0
Maximum	9E-11	5E-12	6607	9E-06	6E-01	3.0
Mean	9E-12	1E-12	6564	1E-06	8E-02	1.9
Median	2E-12	1E-12	6562	6E-07	5E-02	1.8
Geometric mean	3E-12	1E-12	6564	3E-07	4E-02	1.8

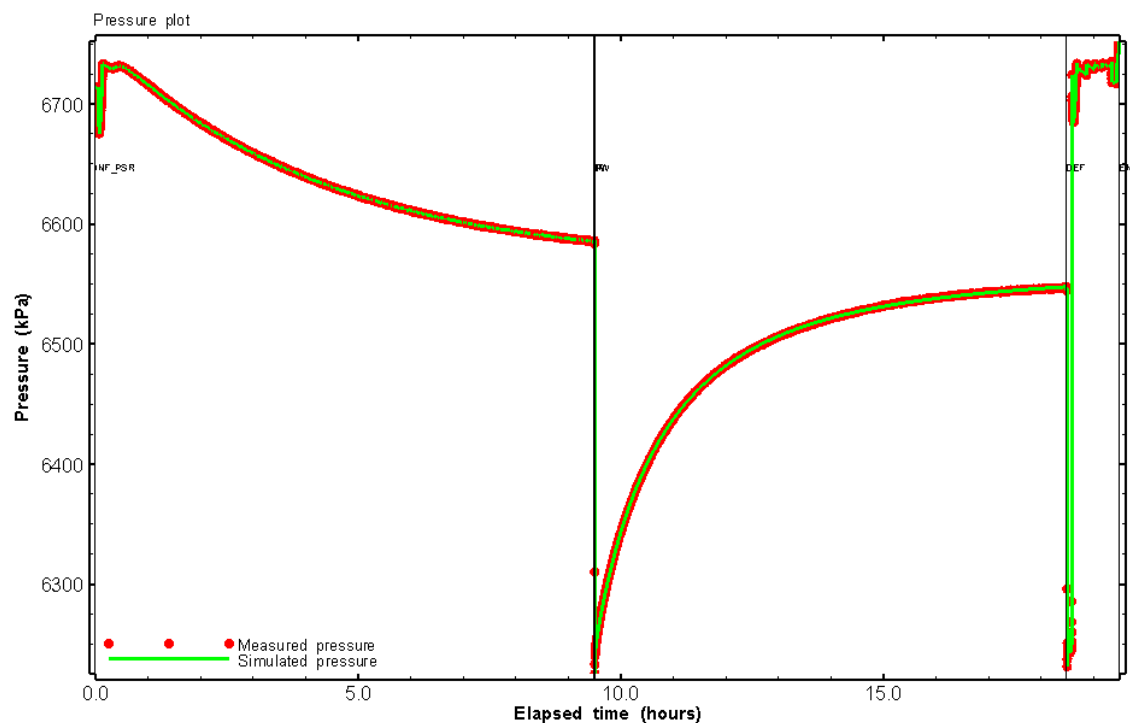


Figure 231: HT020 Pressure plot showing best-fit simulation and best fit results

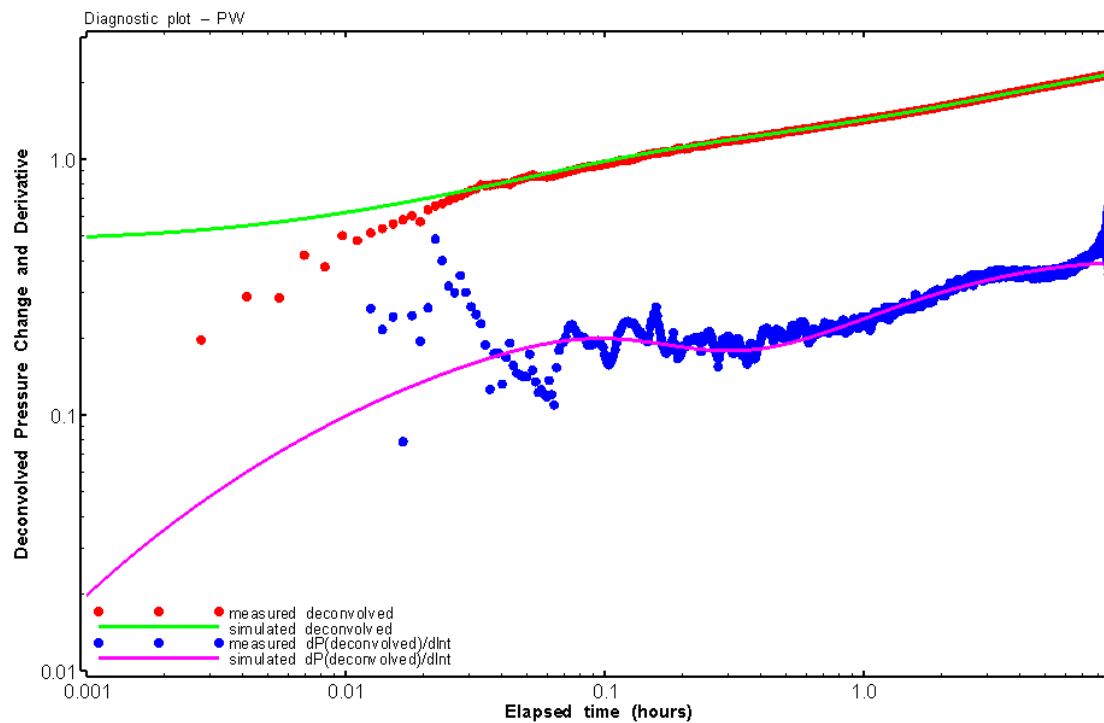


Figure 232: HT020 Deconvolved pressure change and derivative plot of the PW sequence showing best-fit simulation

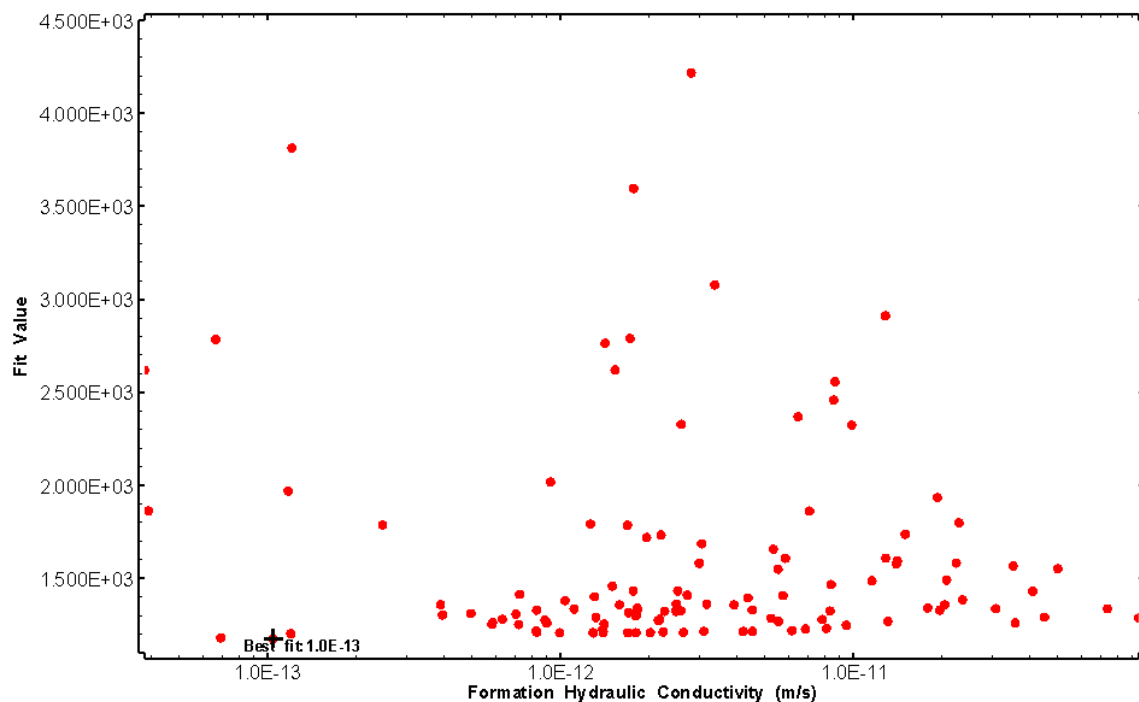


Figure 233: HT020 XY-scatter plot of formation hydraulic conductivity vs. fit value

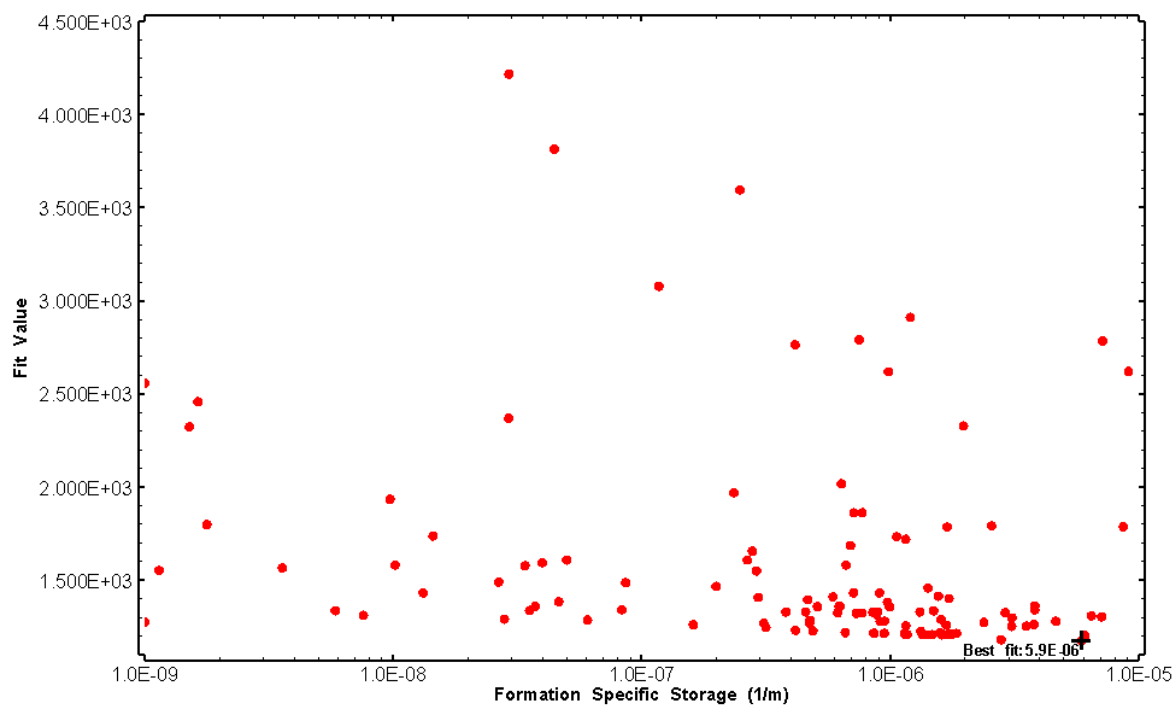


Figure 234: HT020 XY-scatter plot of formation specific storage vs. fit value

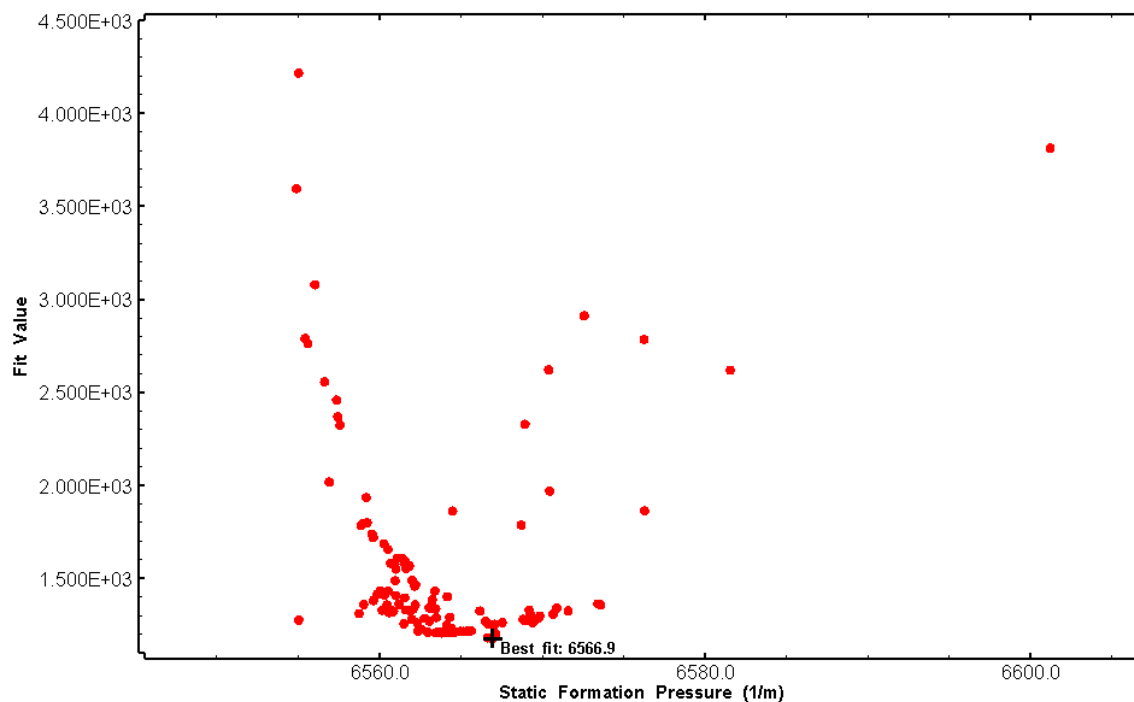


Figure 235: HT020 XY-scatter plot of static formation pressure vs. fit value

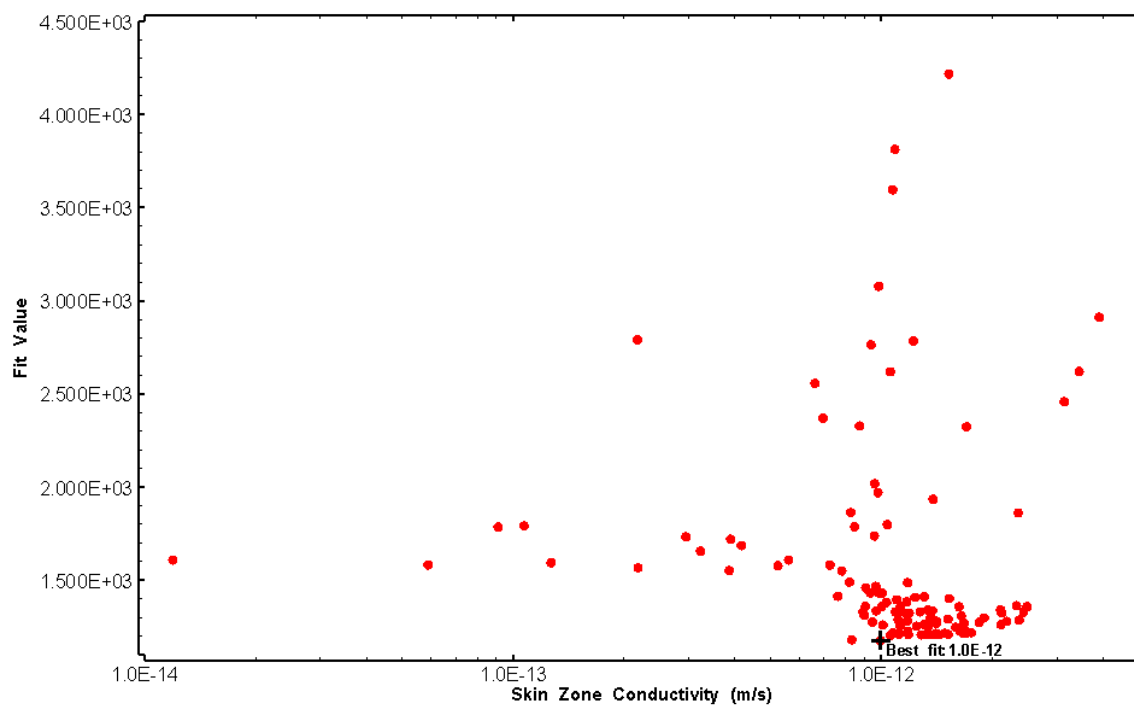


Figure 236: HT020 XY-scatter plot of skin zone conductivity vs. fit value

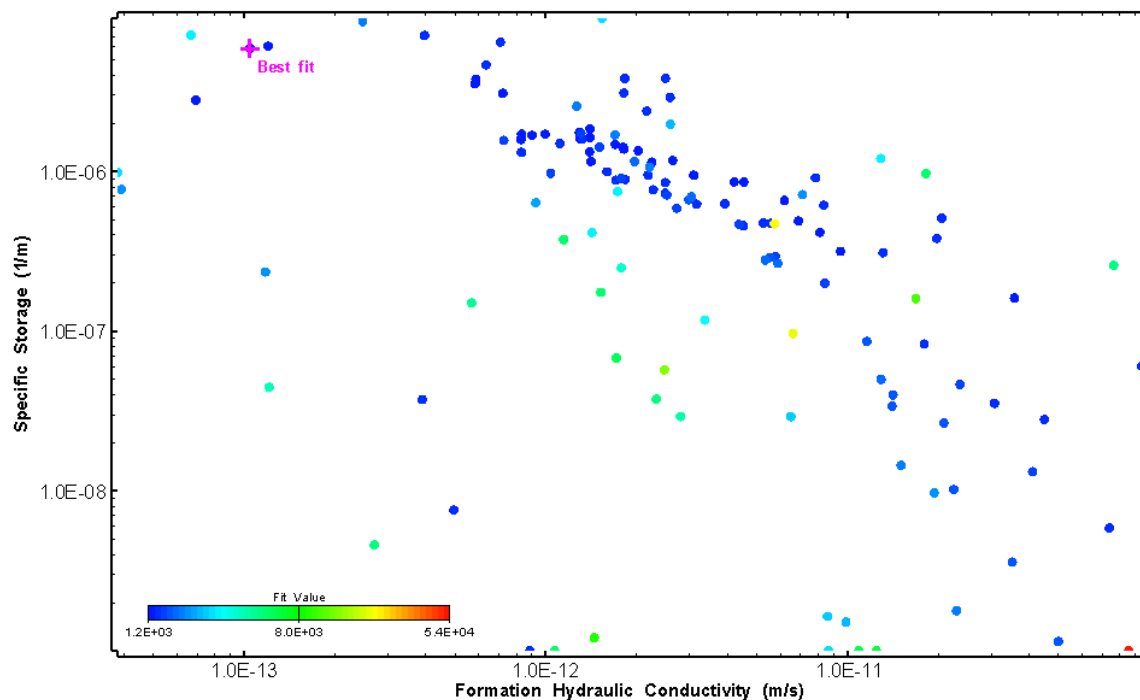


Figure 237: HT020 XY-scatter plot showing estimates of formation hydraulic conductivity and specific storage from perturbation analysis

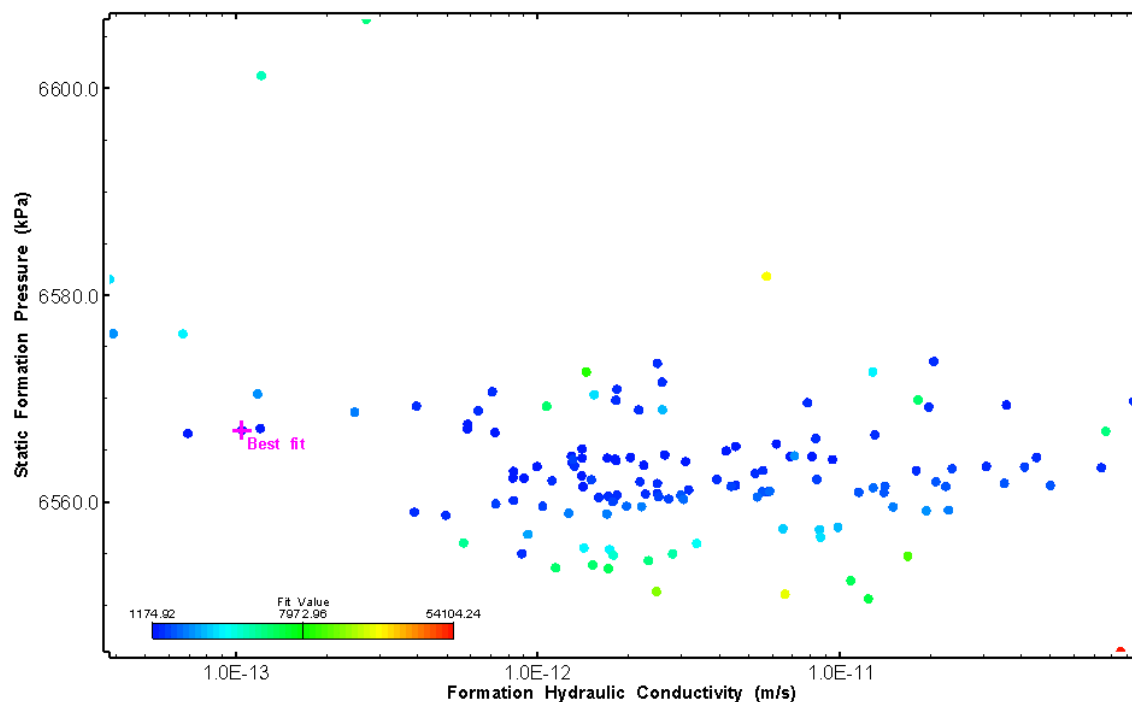


Figure 238: HT020 XY-scatter plot showing estimates of formation hydraulic conductivity and static formation pressure from perturbation analysis

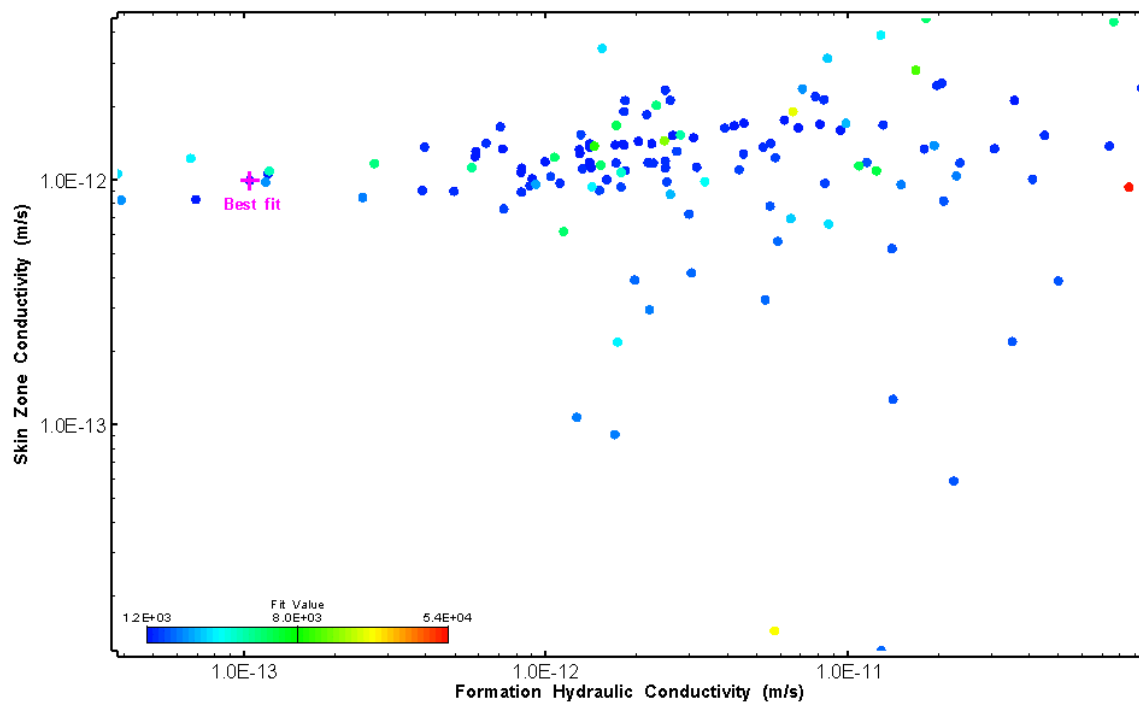


Figure 239: HT020 XY-scatter plot showing estimates of formation hydraulic conductivity and skin zone conductivity from perturbation analysis

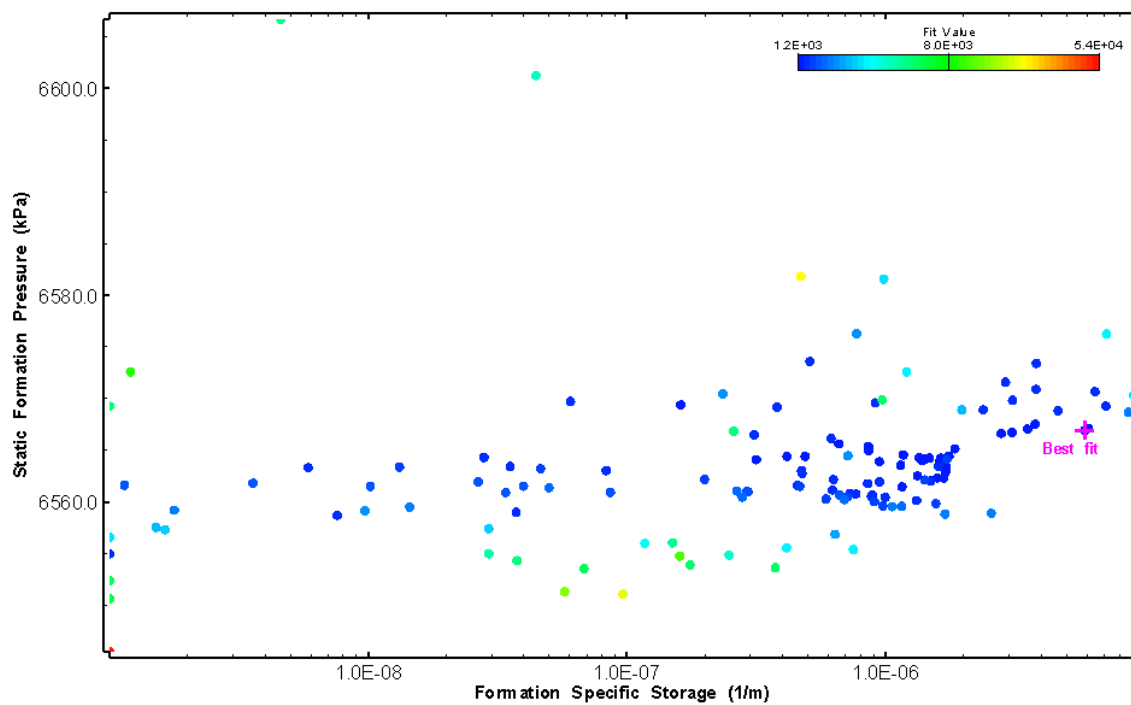


Figure 240: HT020 XY-scatter plot showing estimates of specific storage and static formation pressure from perturbation analysis



## 21.0 HT021 (733.80 – 753.82 M)

HT021 was selected to obtain continuous testing coverage from 600 to 800 m along hole. Four broken fractures were observed in the core. No indication of flow was recorded during FFEC logging post-drilling.

The test was initiated with a shut-in pressure recovery phase (PSR). A pulse withdrawal test (PW) with a shut-in recovery was completed after the PSR phase.

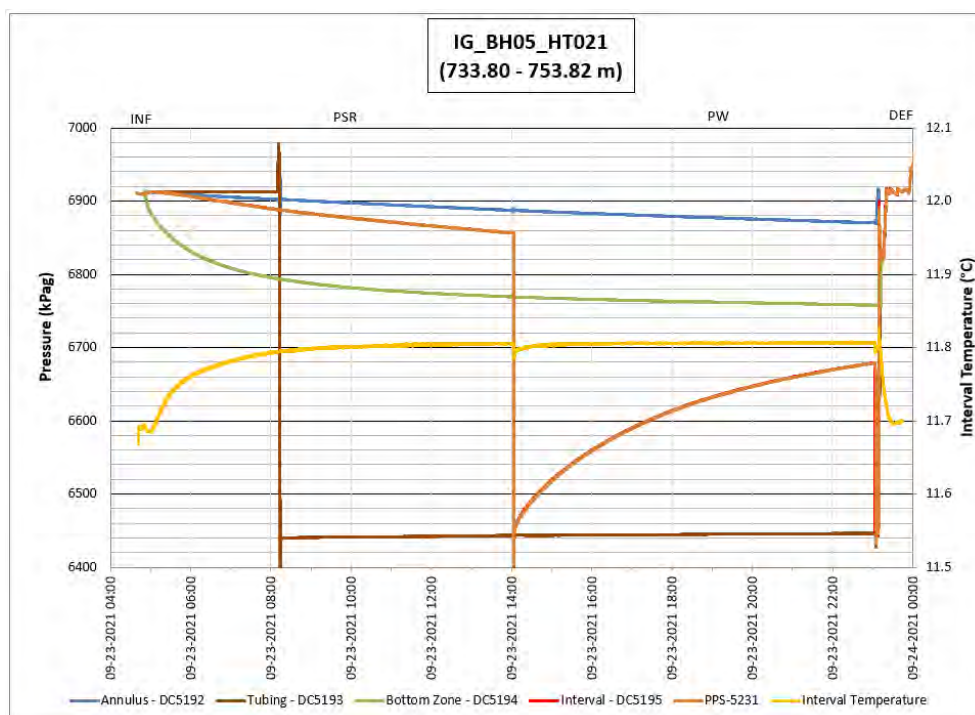
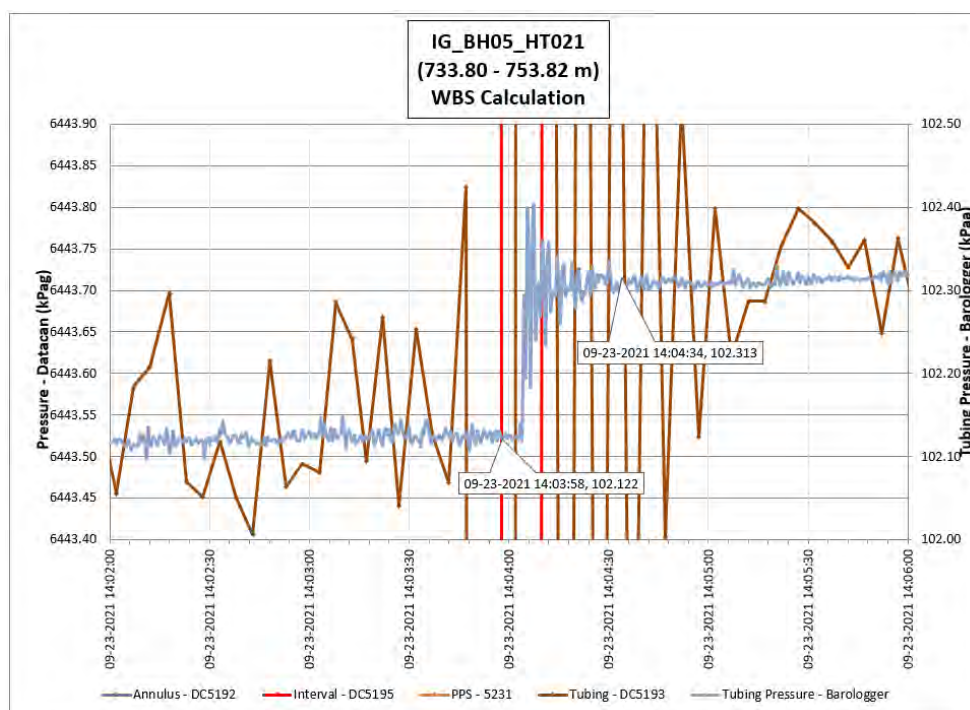


Figure 241: HT021 Annotated test plot showing monitored zone pressure and interval temperature.



**Figure 242: HT021 Tubing pressure during DHSIV activation. DHSIV Closed Wellbore Storage Estimate =  $9\text{E-}11 \text{ m}^3/\text{Pa}$**

**Table 21: Summary of Analysis Results – HT021**

	Formation conductivity	Skin zone conductivity	Static formation pressure	Formation specific storage	Radial thickness of skin	Flow dimension
	[m/s]	[m/s]	[kPa]	[1/m]	[m]	[–]
Best Fit	2E-13	3E-13	6756	2E-06	4.42E-02	2.6
Minimum	1E-15	6E-14	6718	1E-09	5E-03	1.2
Maximum	1E-12	6E-13	6853	1E-05	1E-00	3.0
Mean	1E-13	3E-13	6773	1E-06	3E-01	2.5
Median	1E-14	3E-13	6768	3E-08	3E-01	2.5
Geometric mean	1E-14	3E-13	6773	6E-08	3E-01	2.5

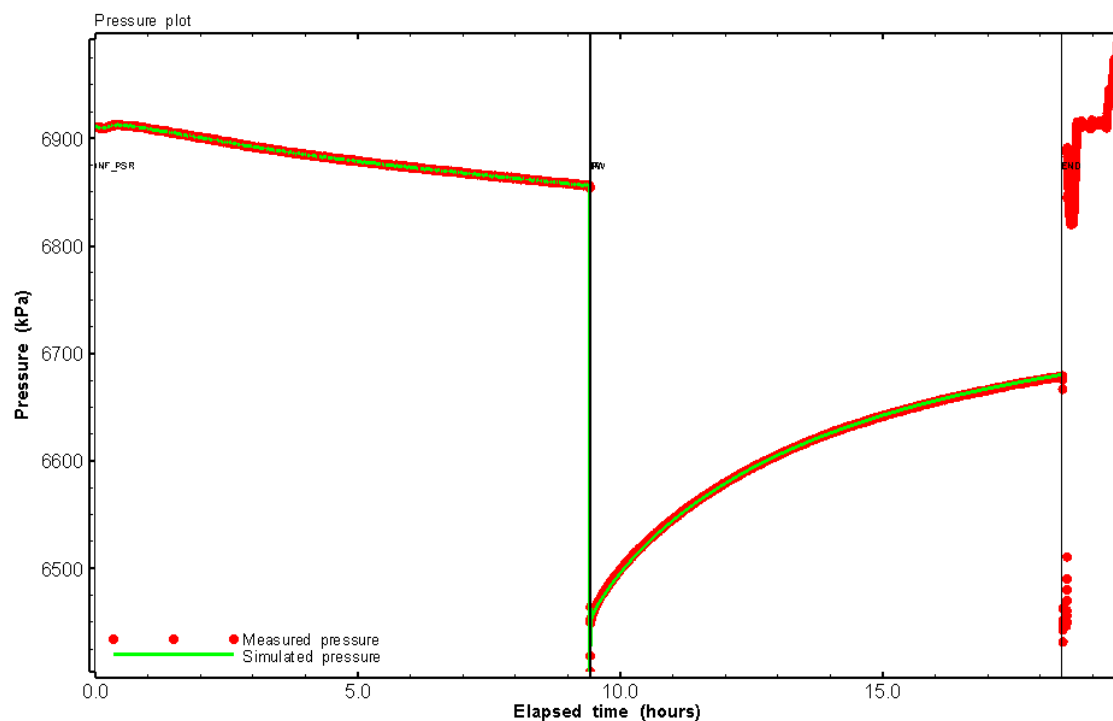


Figure 243: HT021 Pressure plot showing best-fit simulation and best fit results

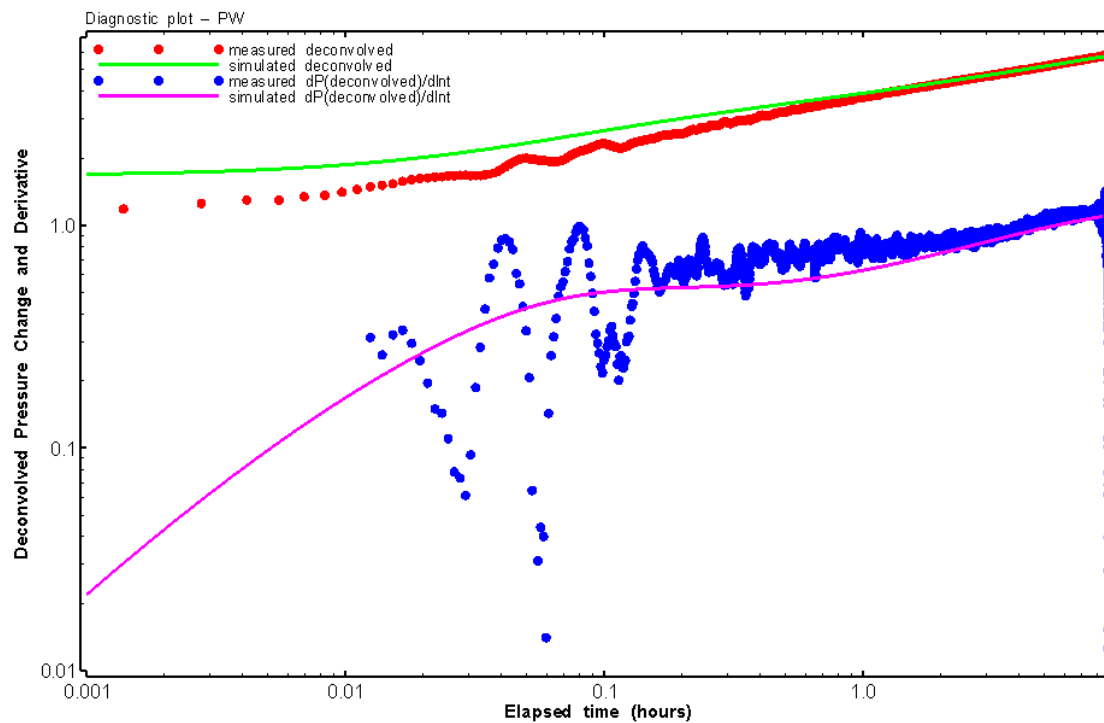


Figure 244: HT021 Deconvolved pressure change and derivative plot of the PW sequence showing best-fit simulation

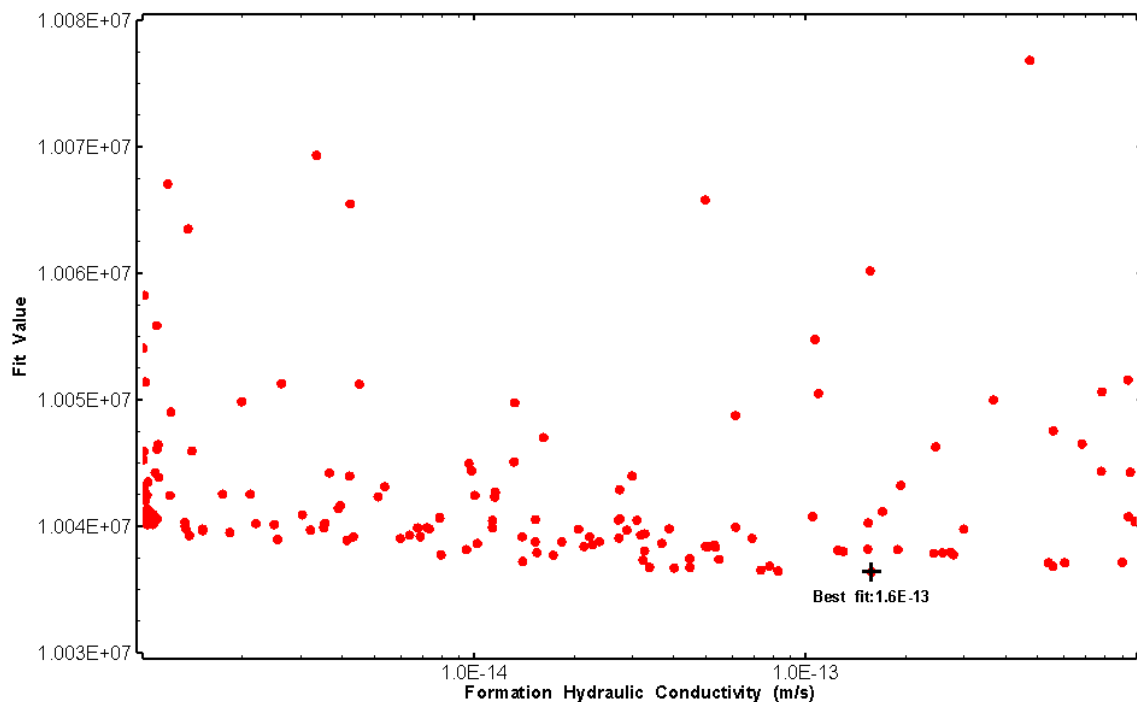


Figure 245: HT021 XY-scatter plot of formation hydraulic conductivity vs. fit value

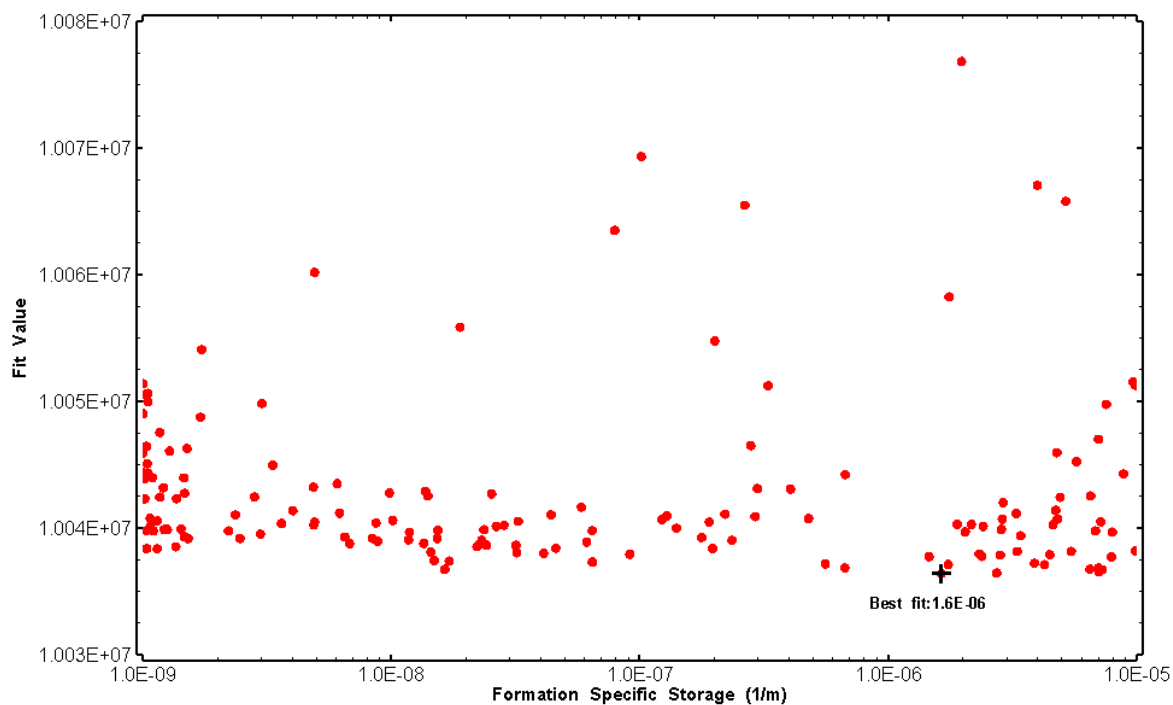


Figure 246: HT021 XY-scatter plot of formation specific storage vs. fit value

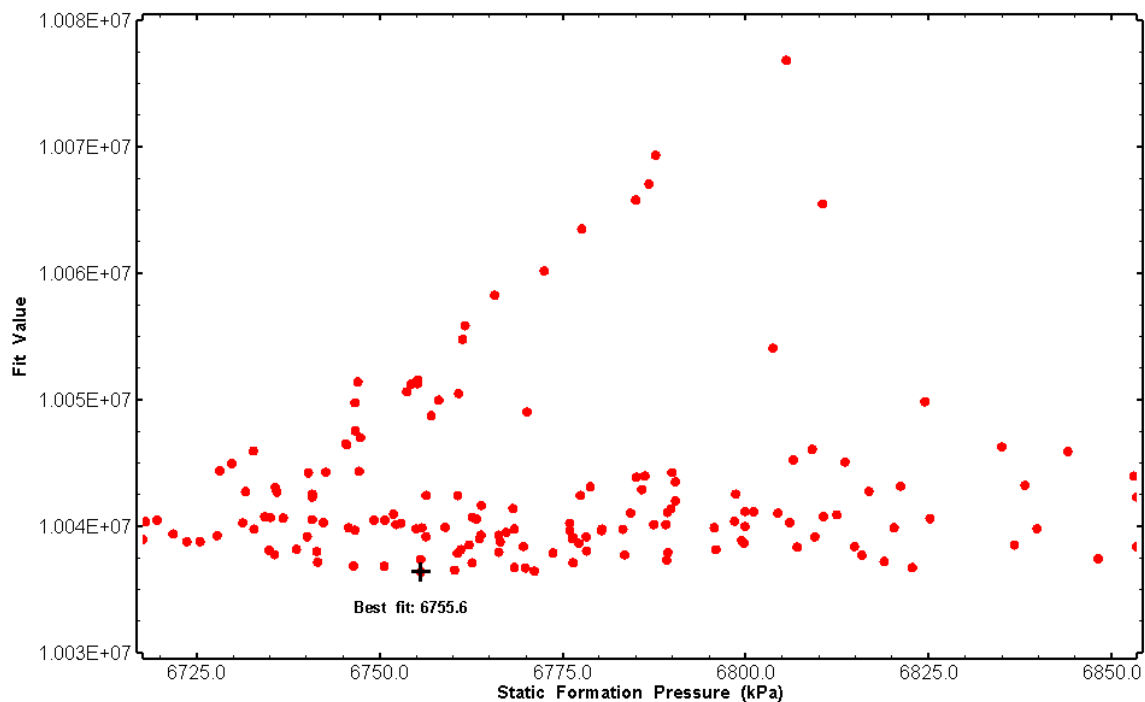


Figure 247: HT021 XY-scatter plot of static formation pressure vs. fit value

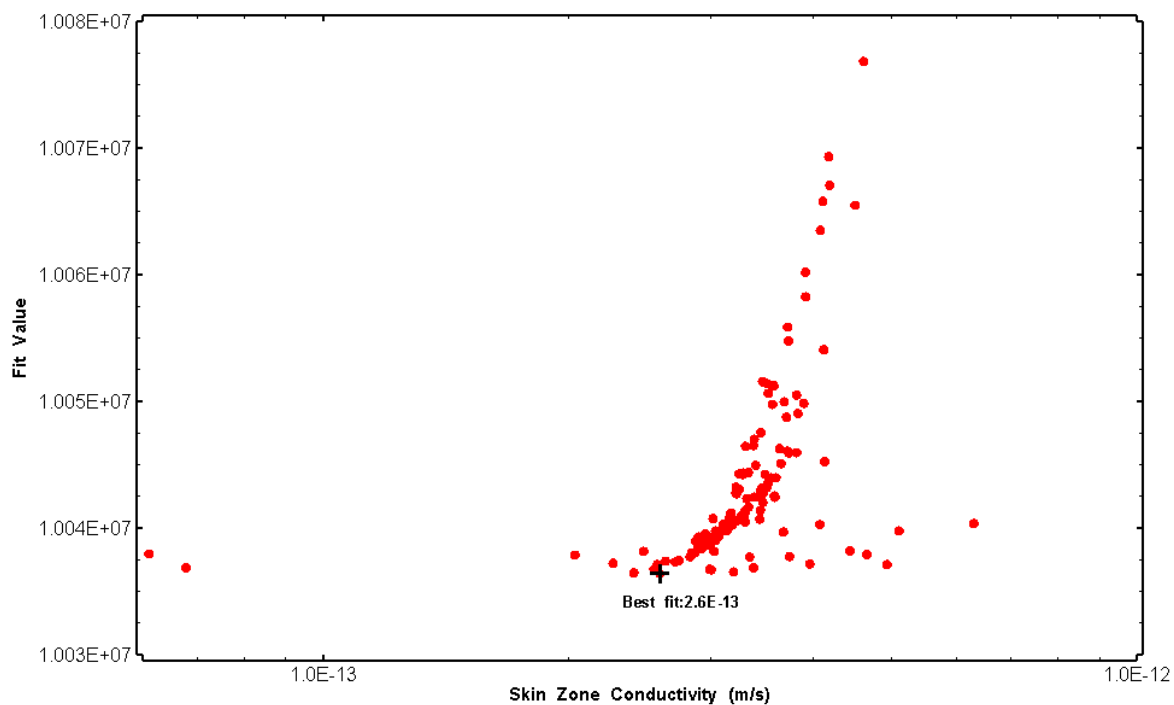


Figure 248: HT021 XY-scatter plot of skin zone conductivity vs. fit value

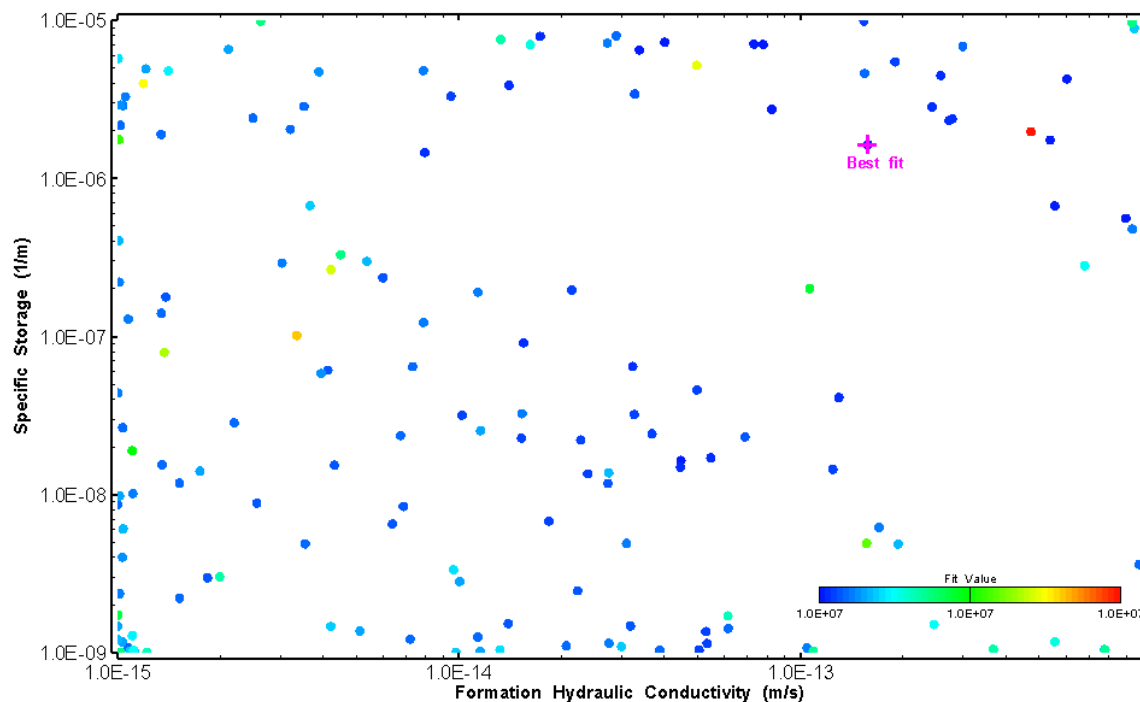


Figure 249: HT021 XY-scatter plot showing estimates of formation hydraulic conductivity and specific storage from perturbation analysis

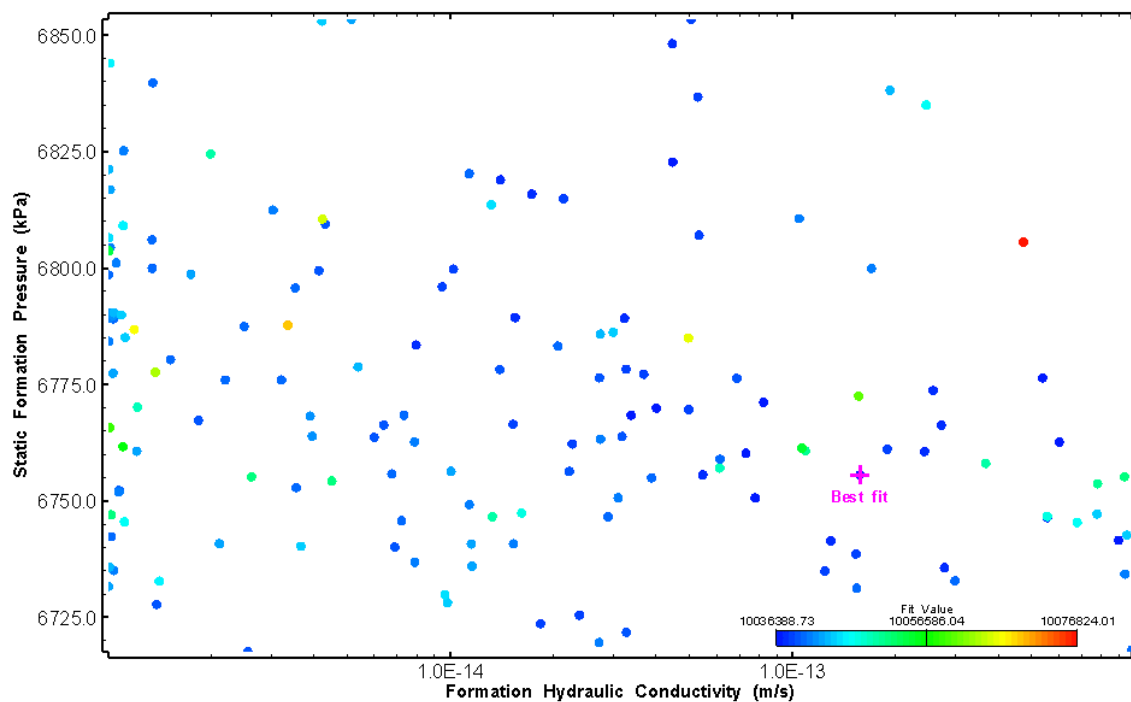


Figure 250: HT021 XY-scatter plot showing estimates of formation hydraulic conductivity and static formation pressure from perturbation analysis

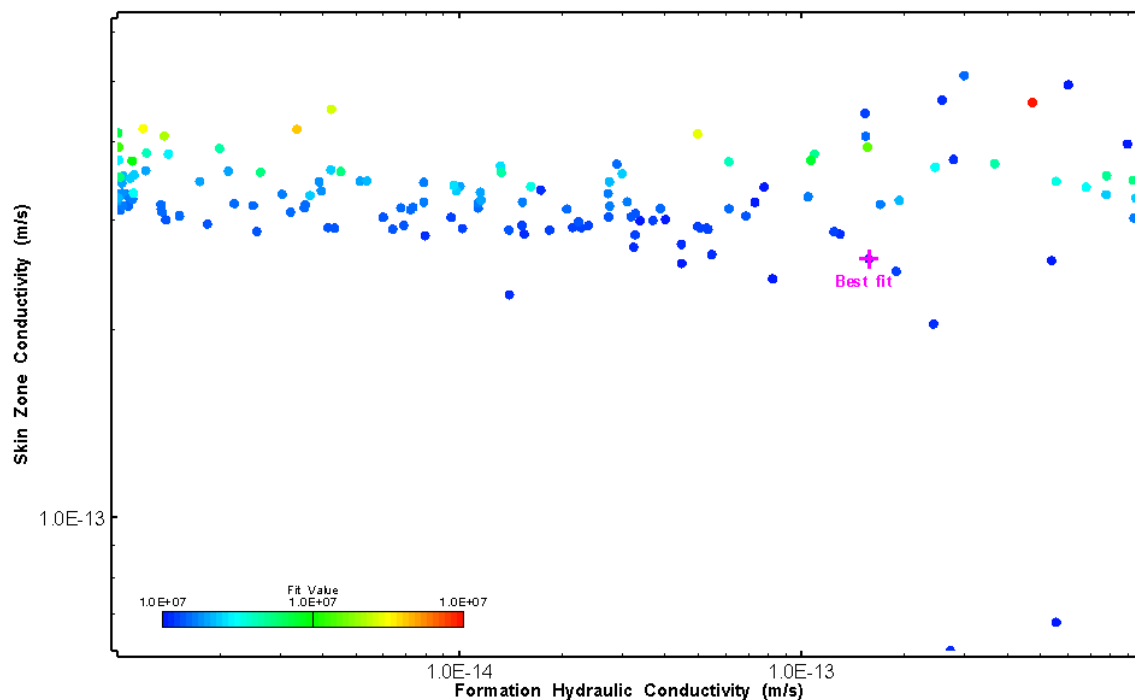


Figure 251: HT021 XY-scatter plot showing estimates of formation hydraulic conductivity and skin zone conductivity from perturbation analysis

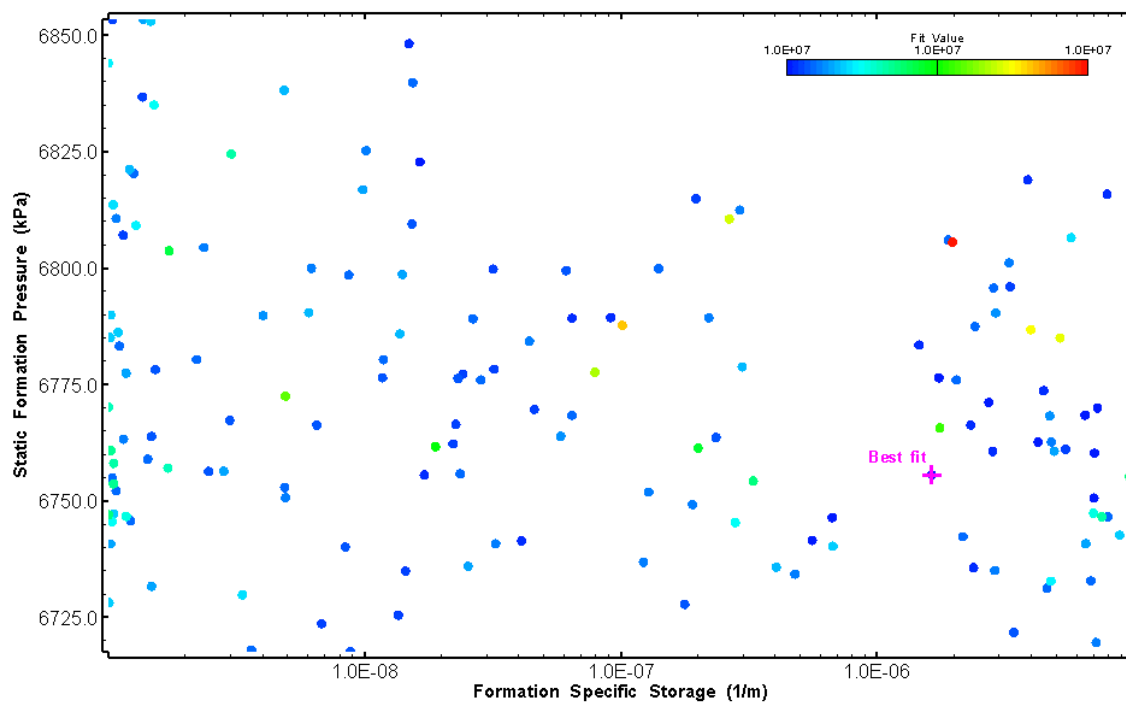


Figure 252: HT021 XY-scatter plot showing estimates of specific storage and static formation pressure from perturbation analysis

## 22.0 HT022 (753.52 – 773.54 M)

HT022 was selected to obtain continuous testing coverage from 600 to 800 m along hole. Two broken fractures were observed in the core. A loss of drilling fluid was observed in this interval during drilling. No indication of flow was recorded during FFEC logging post-drilling.

The test was initiated with a shut-in pressure recovery phase (PSR). A pulse withdrawal test (PW) with a shut-in recovery was completed after the PSR phase.

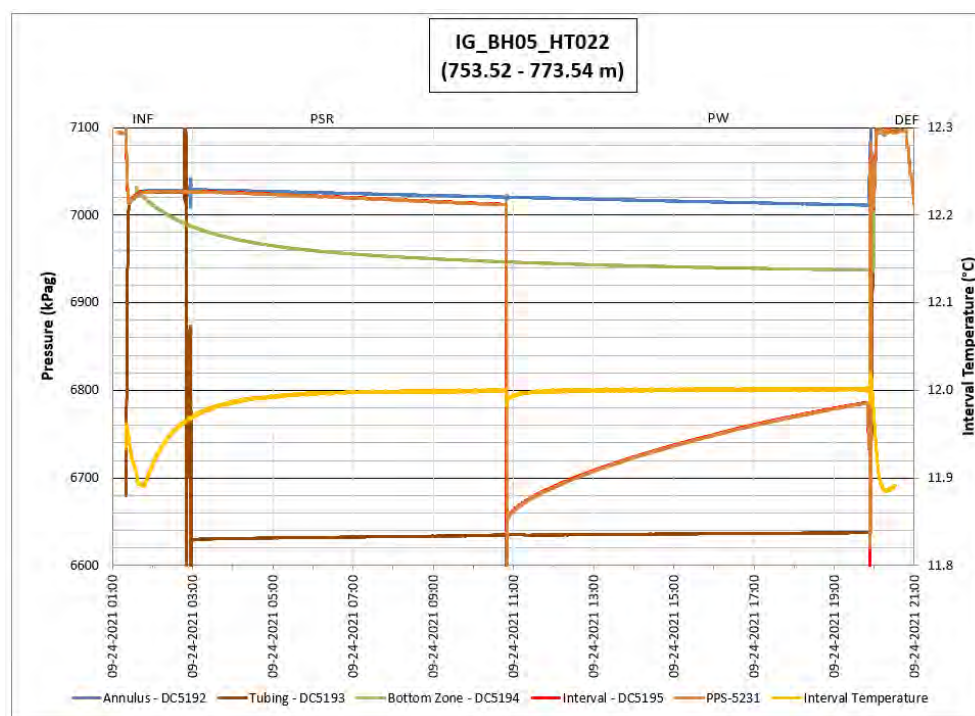
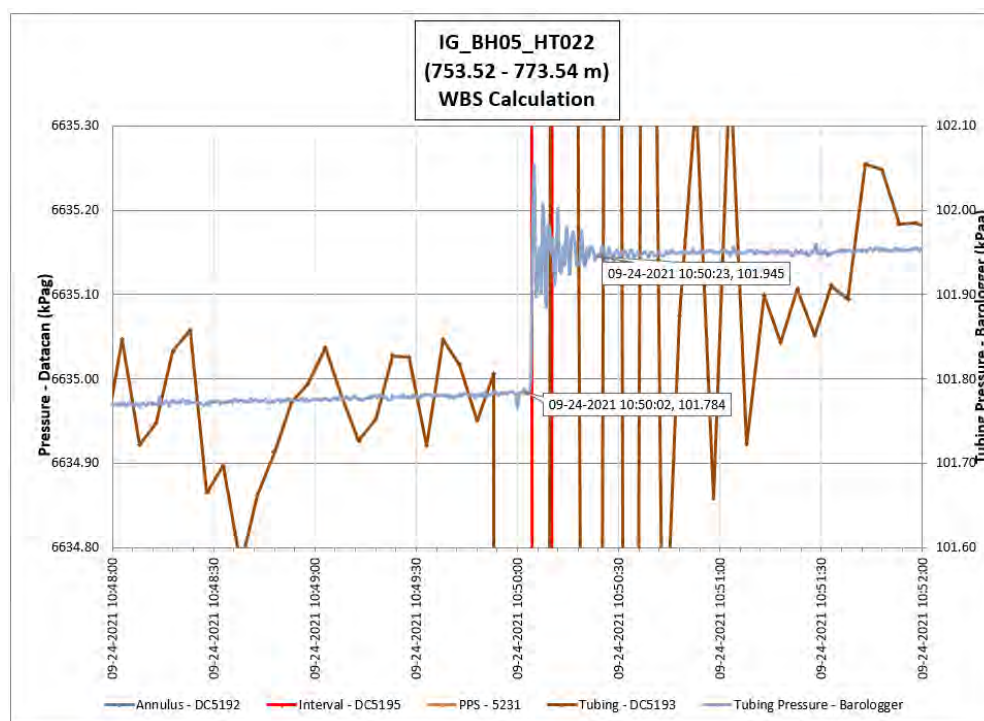


Figure 253: HT022 Annotated test plot showing monitored zone pressure and interval temperature.





**Figure 254: HT022 Tubing pressure during DHSIV activation. DHSIV Closed Wellbore Storage Estimate =  $8\text{E-}11 \text{ m}^3/\text{Pa}$**

**Table 22: Summary of Analysis Results – HT022**

	Formation conductivity	Skin zone conductivity	Static formation pressure	Formation specific storage	Radial thickness of skin	Flow dimension
	[m/s]	[m/s]	[kPa]	[1/m]	[m]	[–]
Best Fit	1E-13	9E-13	6962	5E-08	1.82E-02	2.3
Minimum	1E-14	4E-13	6922	1E-08	1E-03	1.6
Maximum	3E-13	7E-10	7050	1E-05	2E-01	2.5
Mean	1E-13	8E-11	7010	9E-07	5E-02	2.1
Median	1E-13	2E-11	7012	5E-08	4E-02	2.1
Geometric mean	1E-13	2E-11	7010	9E-08	3E-02	2.1

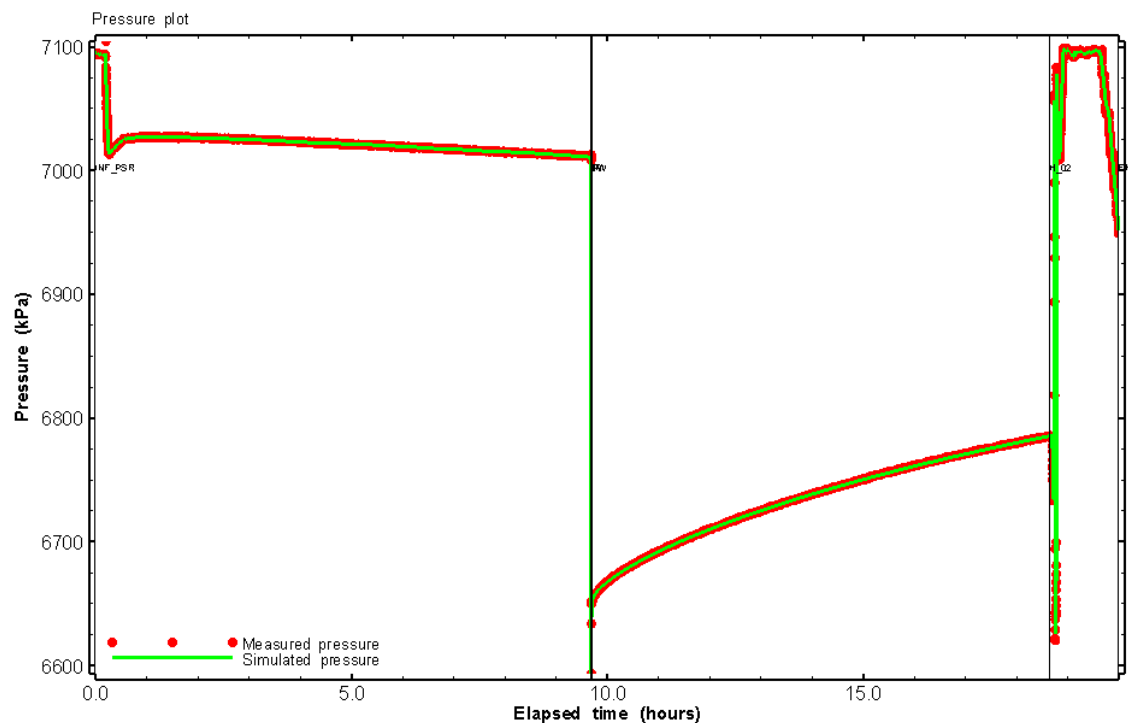


Figure 255: HT022 Pressure plot showing best-fit simulation and best fit results

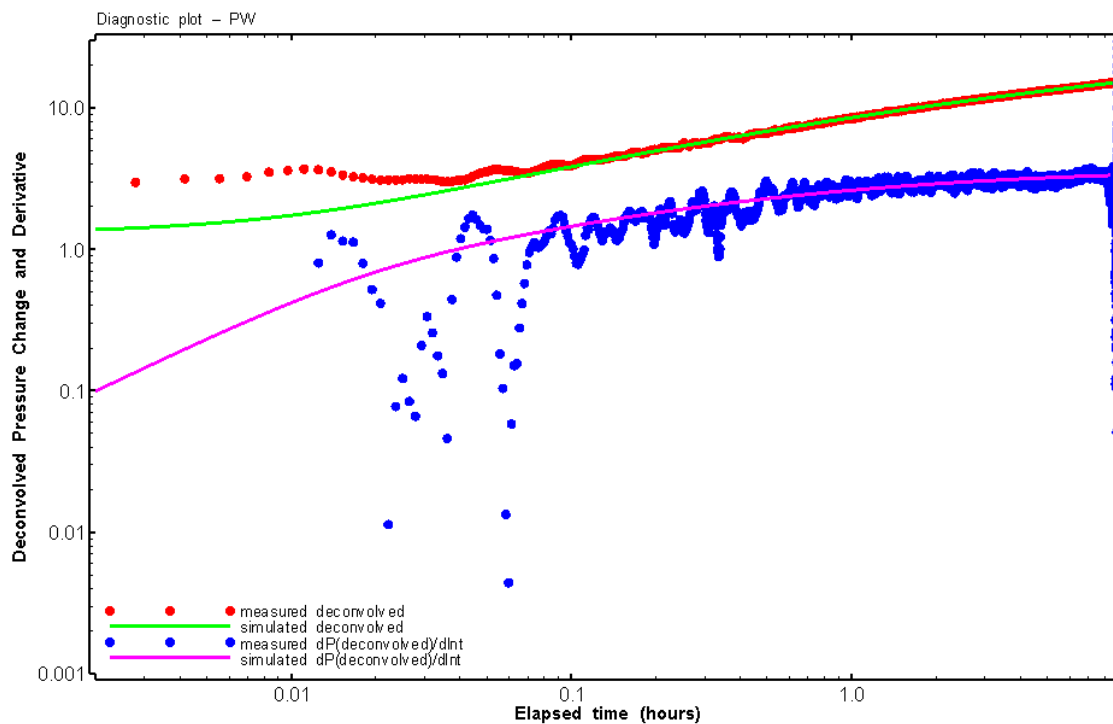


Figure 256: HT022 Deconvolved pressure change and derivative plot of the PW sequence showing best-fit simulation

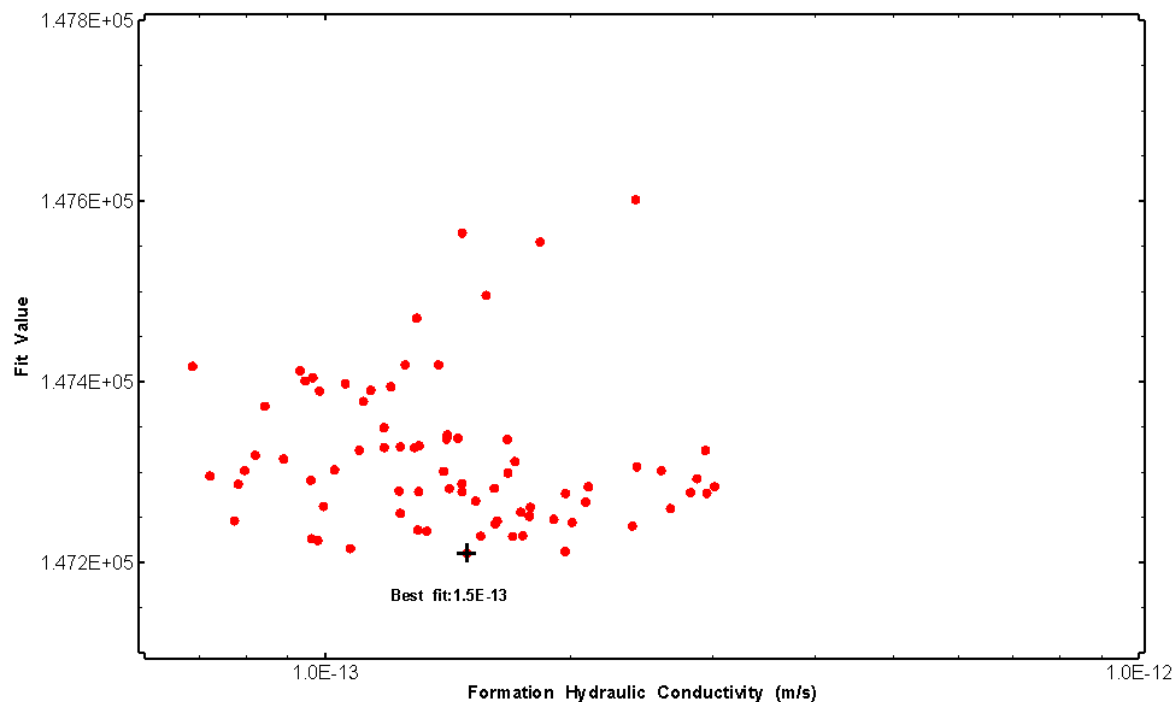


Figure 257: HT022 XY-scatter plot of formation hydraulic conductivity vs. fit value

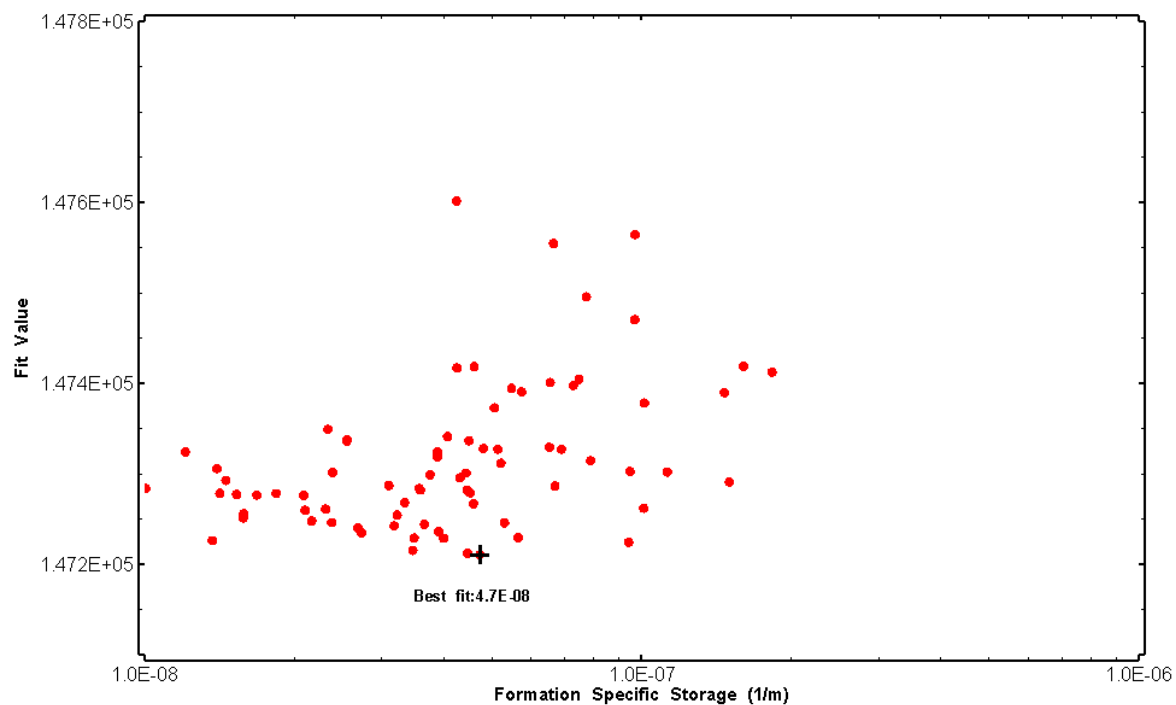


Figure 258: HT022 XY-scatter plot of formation specific storage vs. fit value

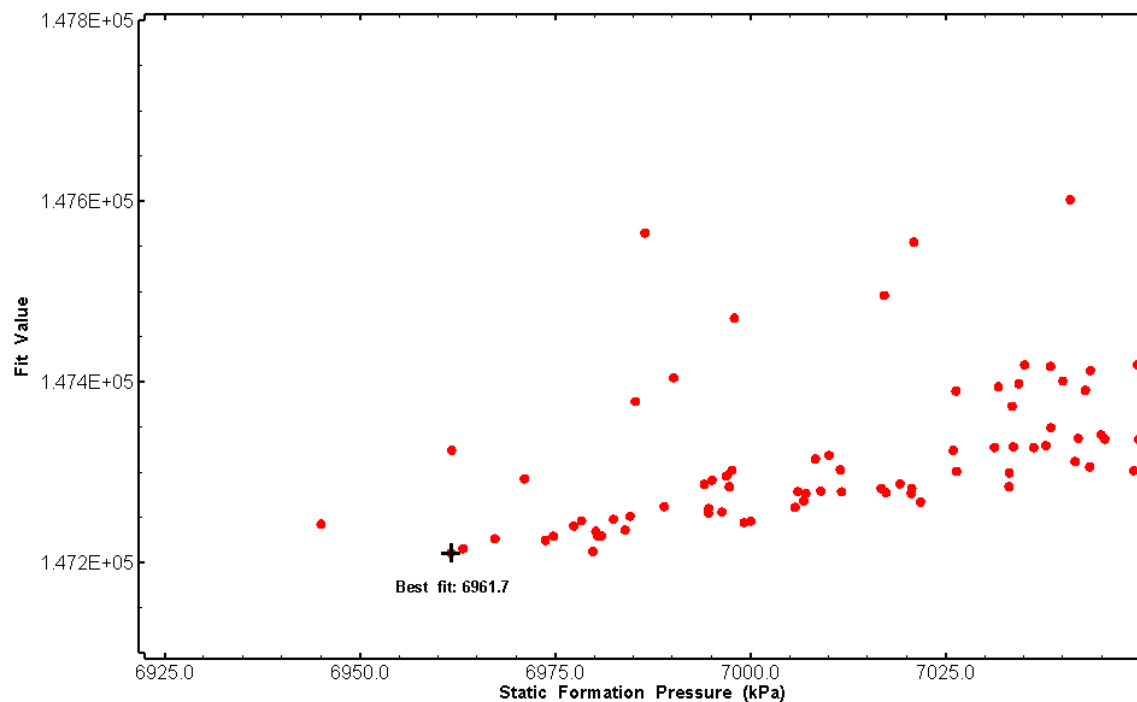


Figure 259: HT022 XY-scatter plot of static formation pressure vs. fit value

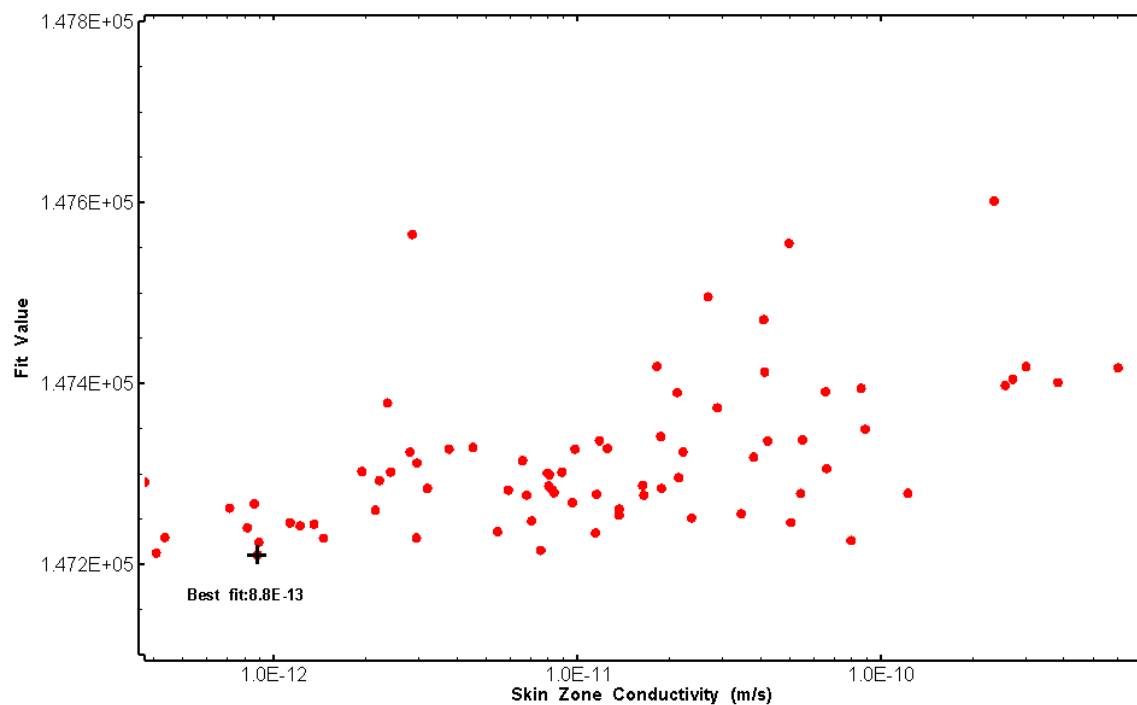


Figure 260: HT022 XY-scatter plot of skin zone conductivity vs. fit value

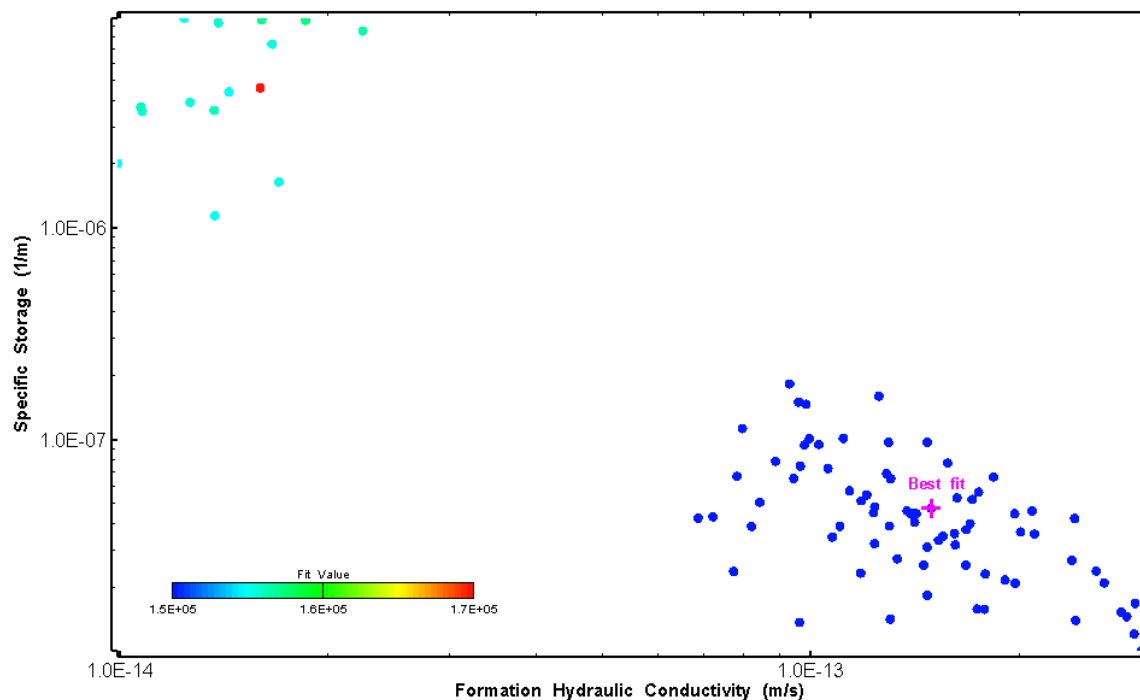


Figure 261: HT022 XY-scatter plot showing estimates of formation hydraulic conductivity and specific storage from perturbation analysis

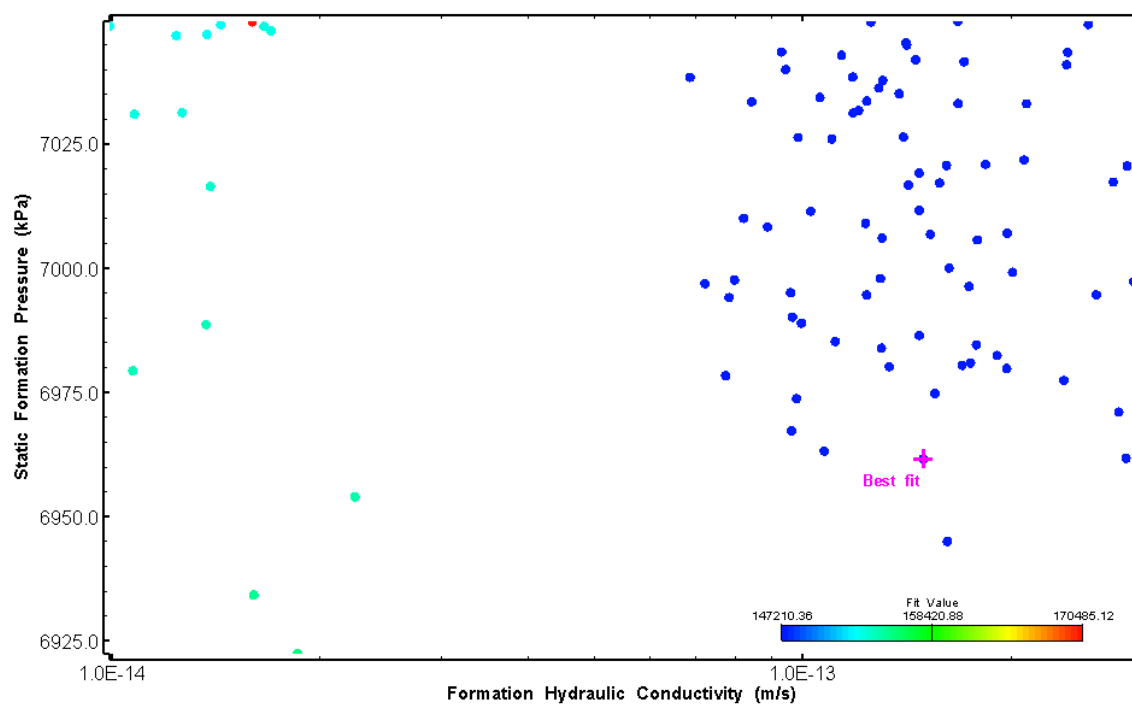


Figure 262: HT022 XY-scatter plot showing estimates of formation hydraulic conductivity and static formation pressure from perturbation analysis

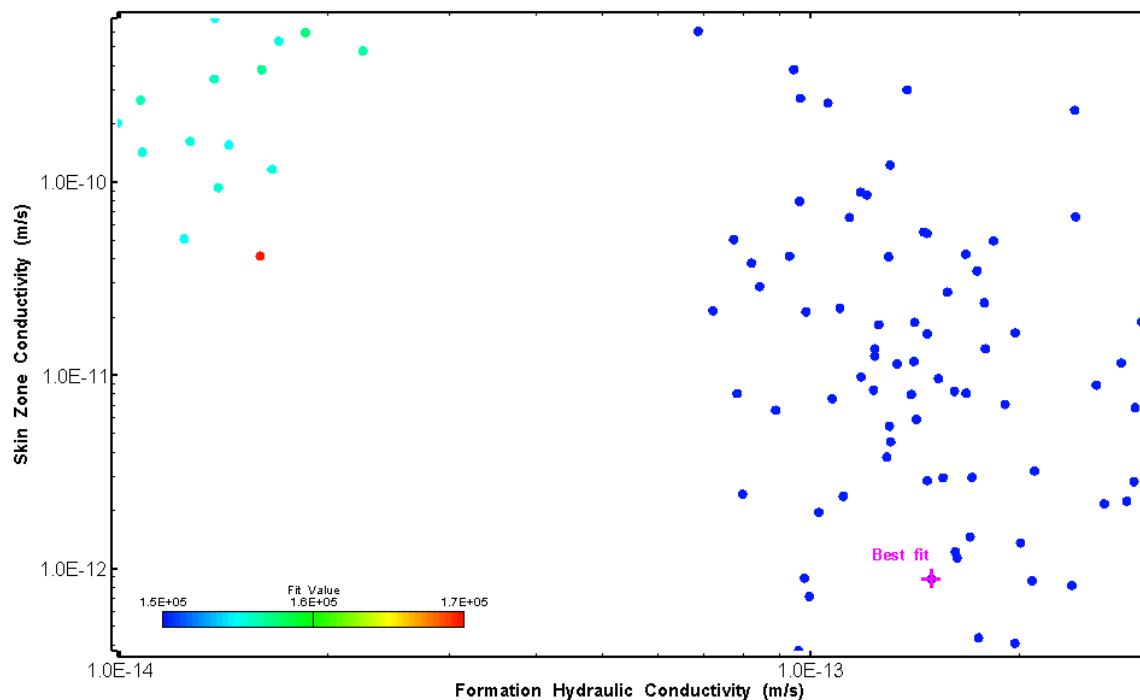


Figure 263: HT022 XY-scatter plot showing estimates of formation hydraulic conductivity and skin zone conductivity from perturbation analysis

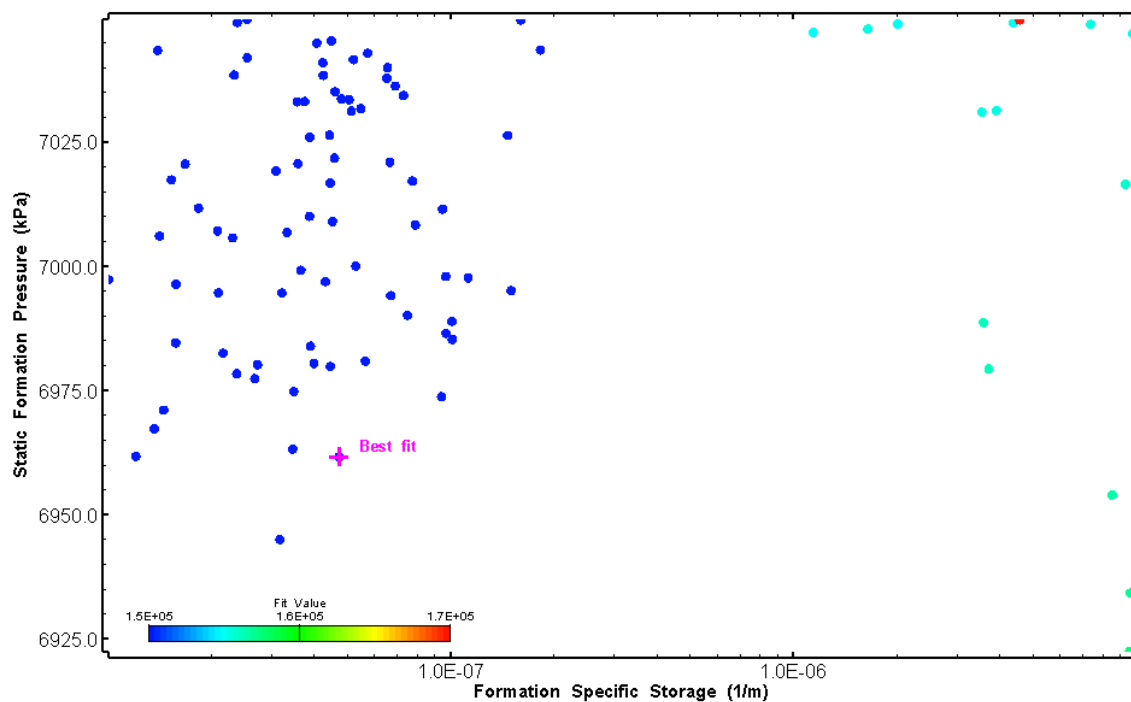


Figure 264: HT022 XY-scatter plot showing estimates of specific storage and static formation pressure from perturbation analysis

## 23.0 HT023 (772.99 – 793.01 M)

HT023 was selected to obtain continuous testing coverage from 600 to 800 m along hole and to target a fractured interval containing multiple dykes. 20 broken fractures were observed in the core. An indication of flow was recorded during FFEC logging post-drilling.

The test was initiated with a shut-in pressure recovery phase (PSR). A pulse withdrawal test (PW) with a shut-in recovery followed by a slug withdrawal (SW) phase was completed after the PSR phase.

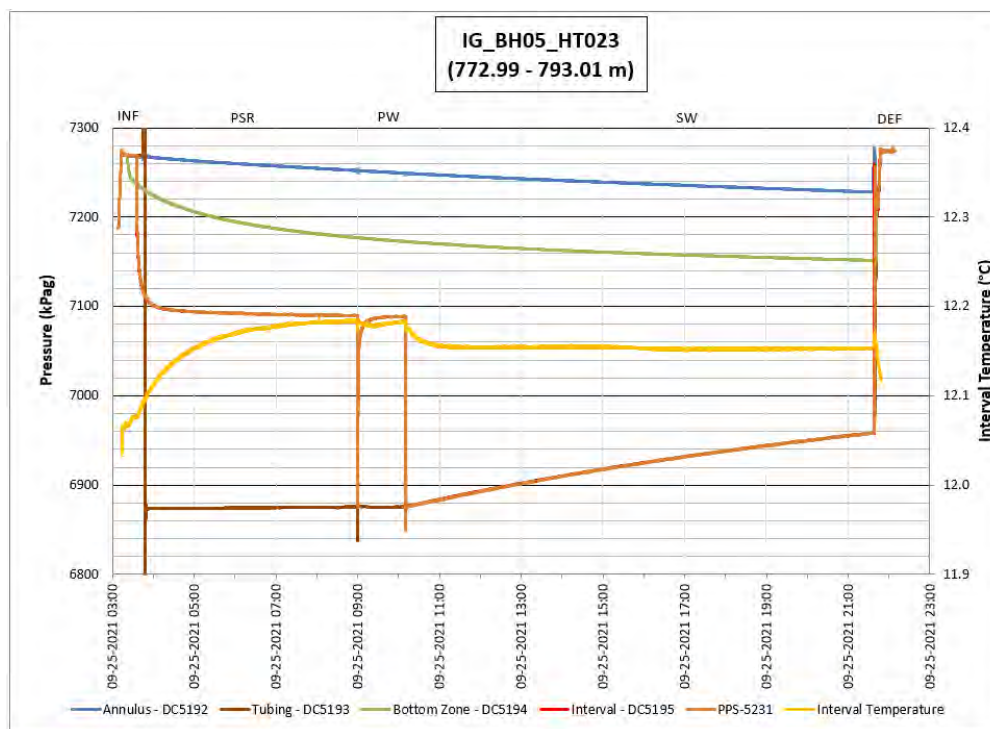
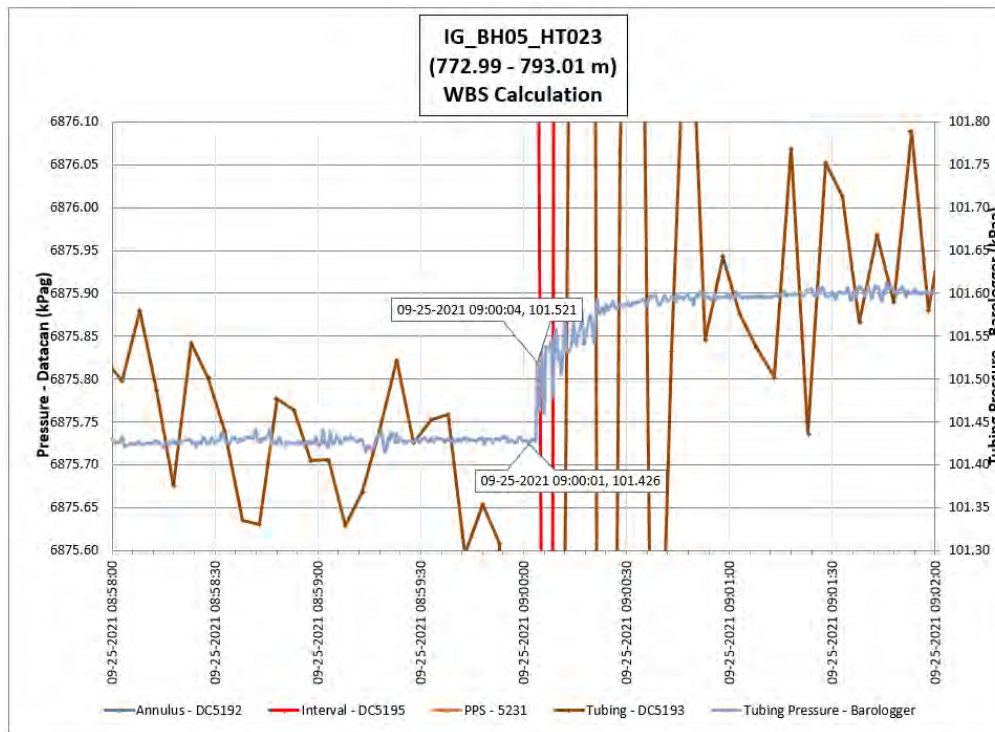


Figure 265: HT023 Annotated test plot showing monitored zone pressure and interval temperature.



**Figure 266: HT023 Tubing pressure during DHSIV activation. DHSIV Closed Wellbore Storage Estimate =  $9\text{E-}11 \text{ m}^3/\text{Pa}$**

**Table 23: Summary of Analysis Results – HT023**

	Formation conductivity	Skin zone conductivity	Static formation pressure	Formation specific storage	Radial thickness of skin	Flow dimension
	[m/s]	[m/s]	[kPa]	[1/m]	[m]	[–]
Best Fit	1E-08	4E-09	7087	8E-06	6.15E+00	1.5
Minimum	8E-11	9E-11	7085	1E-09	1E-03	1.5
Maximum	5E-08	4E-08	7089	1E-05	9E+00	2.9
Mean	9E-09	2E-09	7087	6E-07	2E+00	2.0
Median	3E-09	1E-09	7086	5E-08	2E+00	1.9
Geometric mean	3E-09	1E-09	7087	5E-08	1E+00	1.9



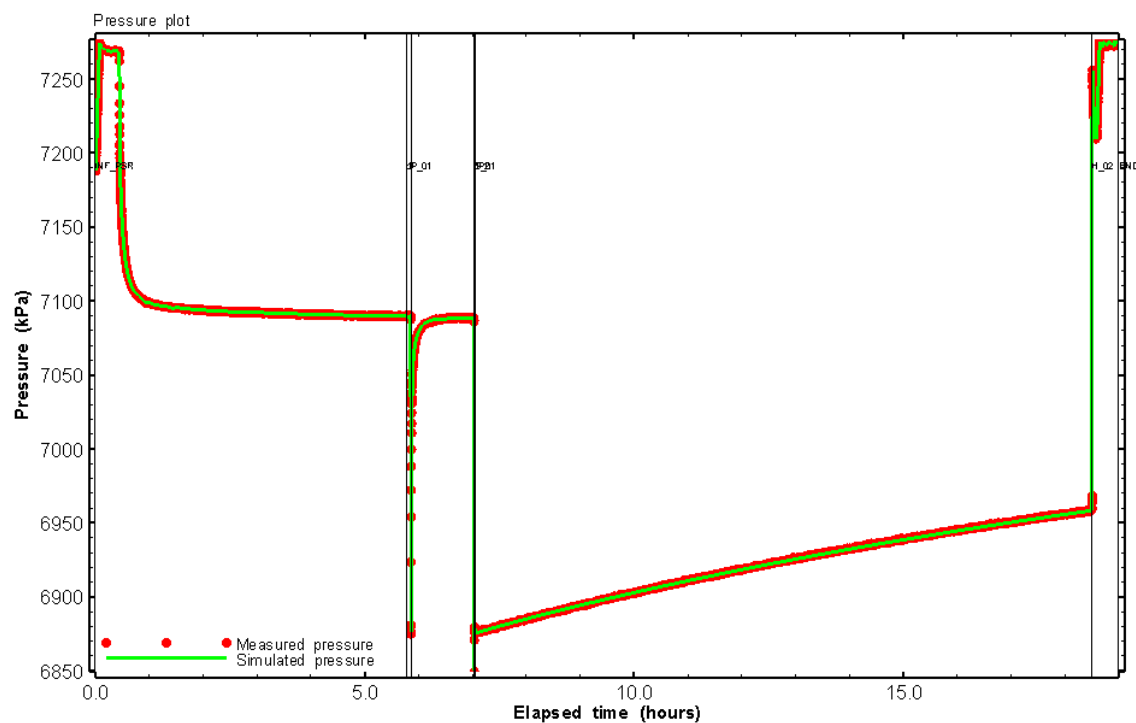


Figure 267: HT023 Pressure plot showing best-fit simulation and best fit results

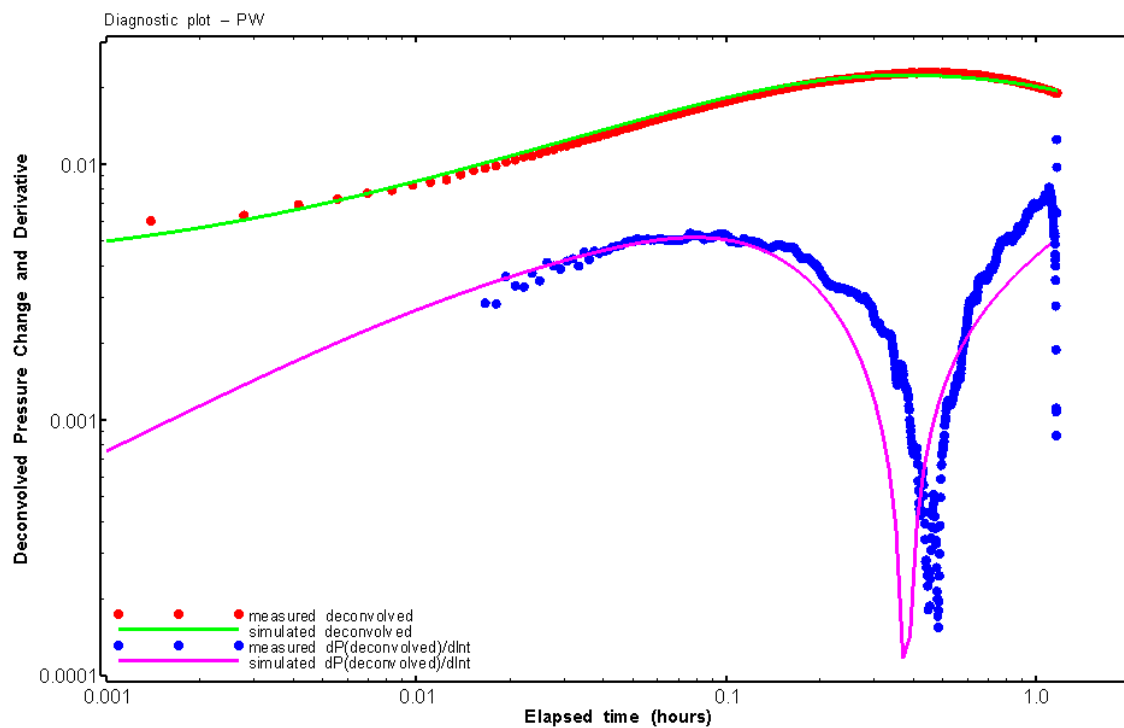


Figure 268: HT023 Deconvolved pressure change and derivative plot of the PW sequence showing best-fit simulation

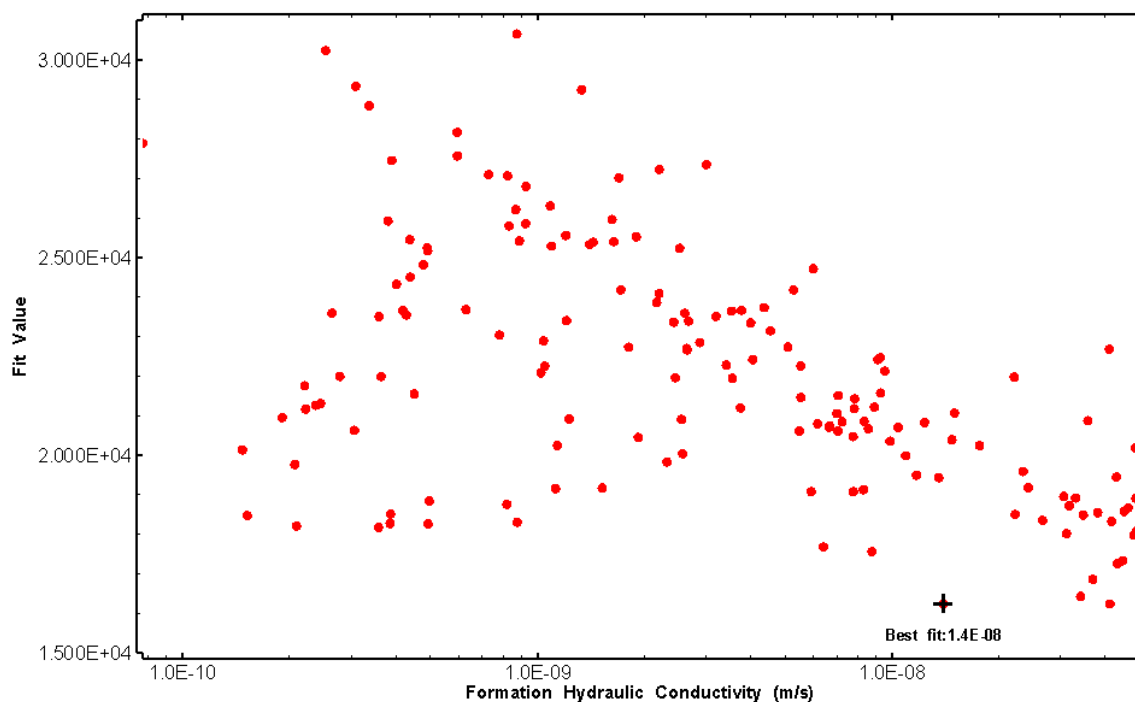


Figure 269: HT023 XY-scatter plot of formation hydraulic conductivity vs. fit value

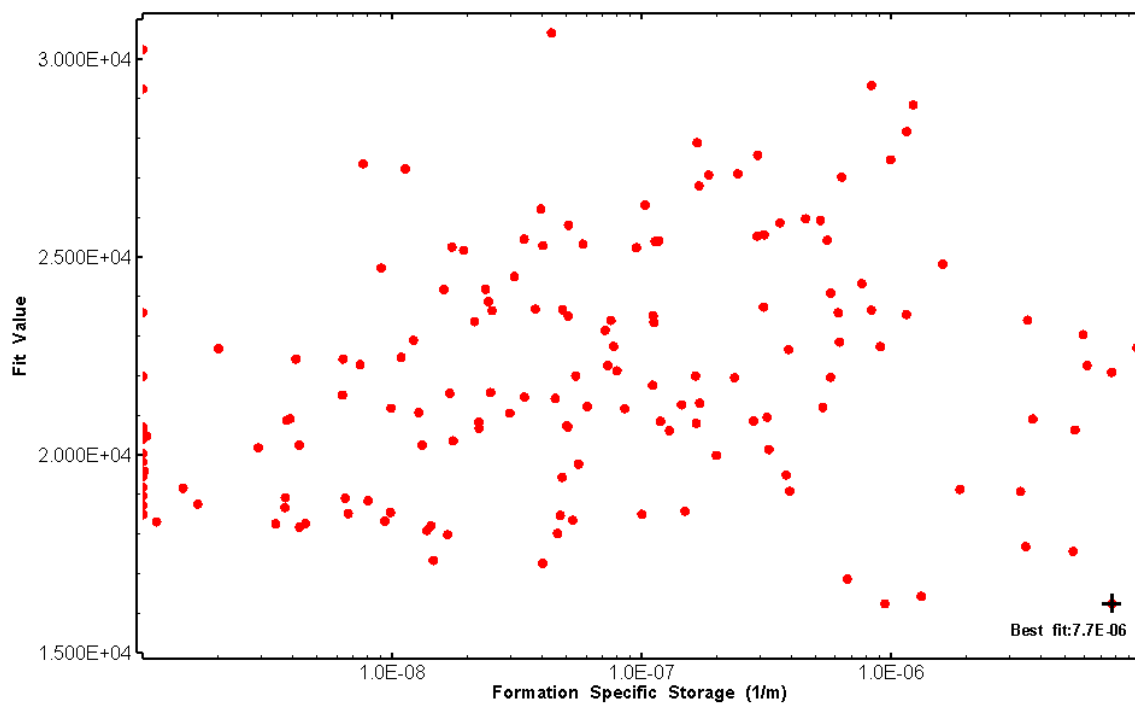


Figure 270: HT023 XY-scatter plot of formation specific storage vs. fit value

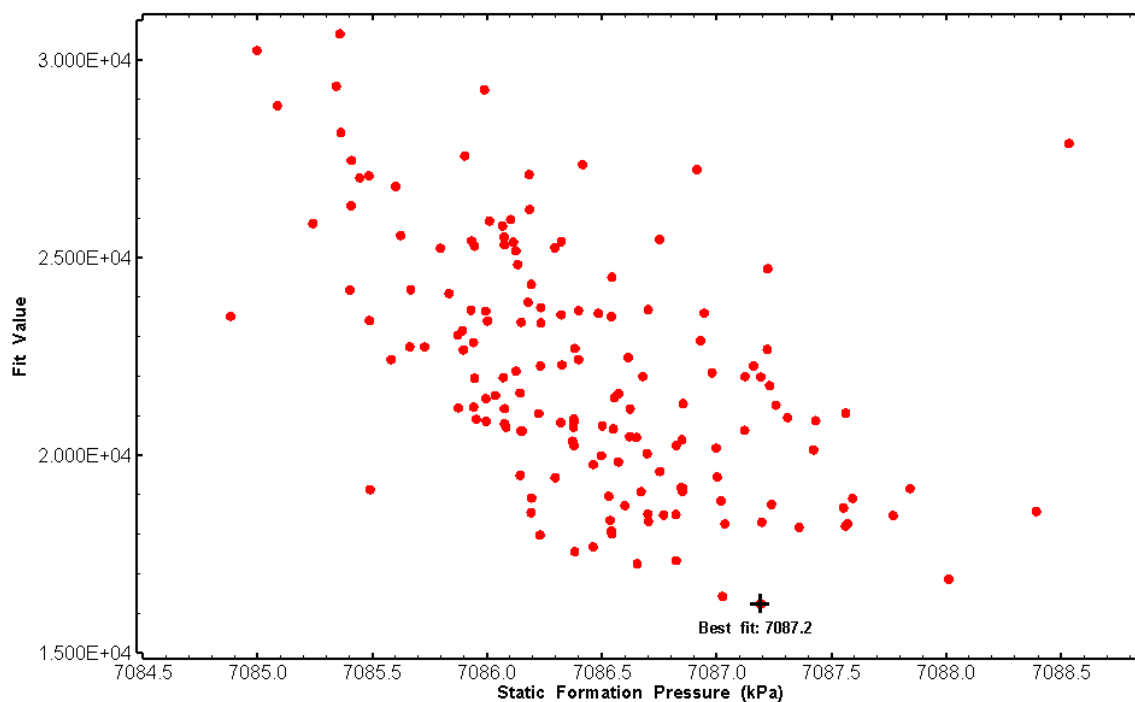


Figure 271: HT023 XY-scatter plot of static formation pressure vs. fit value

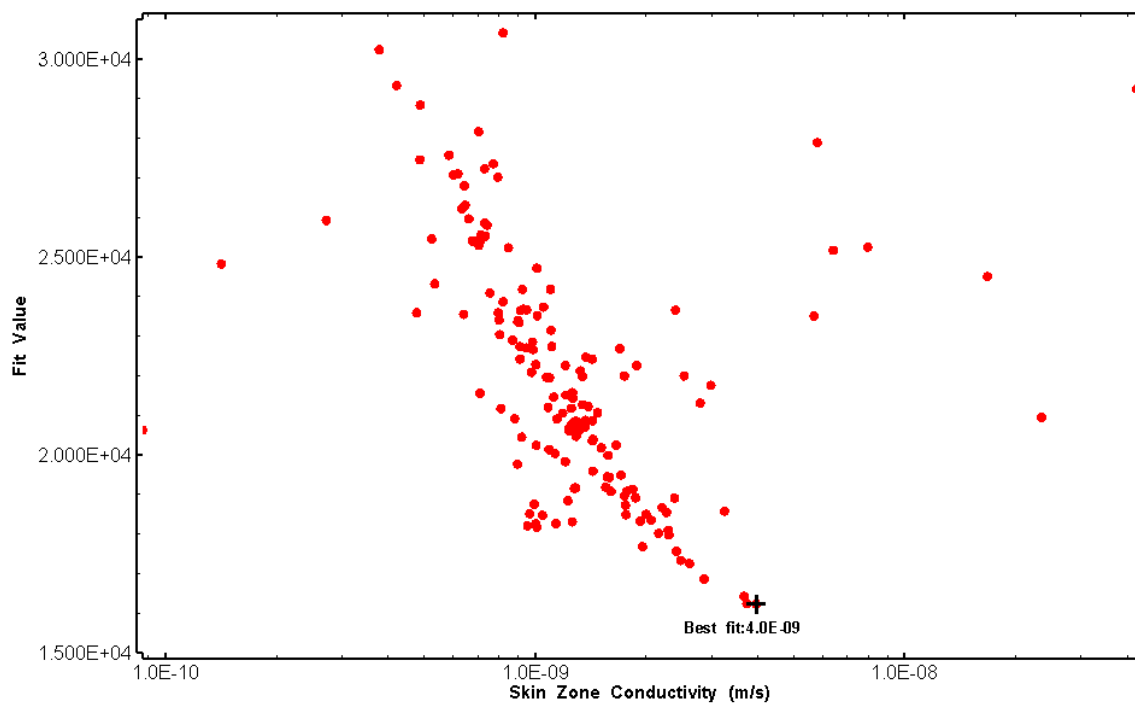


Figure 272: HT023 XY-scatter plot of skin zone conductivity vs. fit value

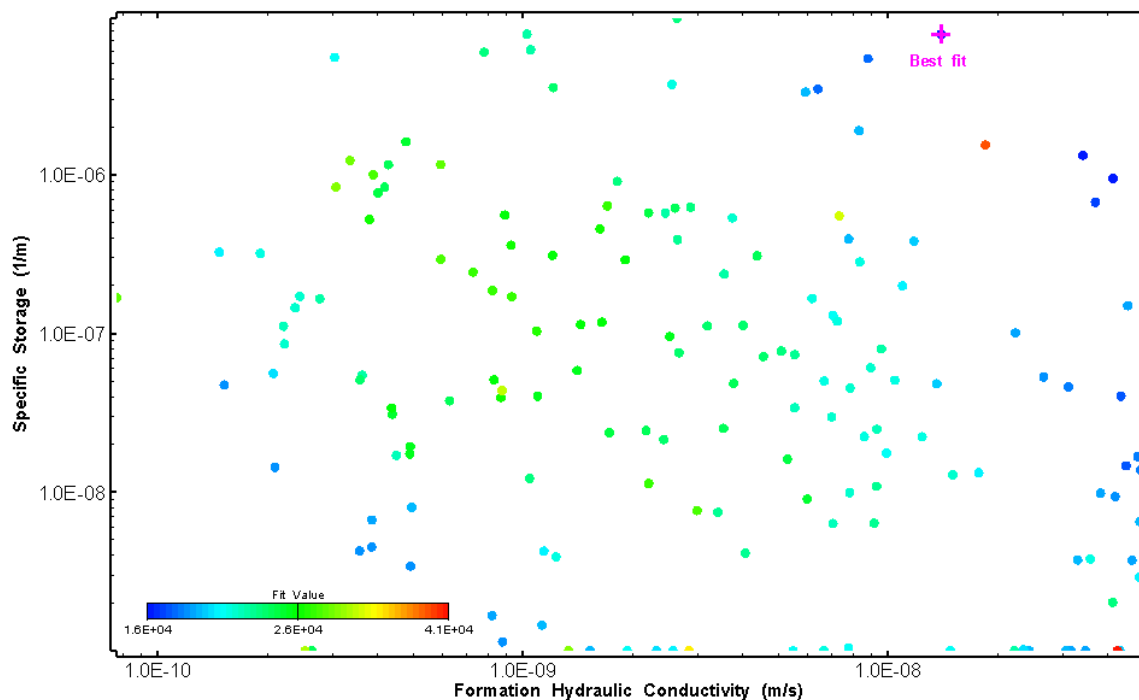


Figure 273: HT023 XY-scatter plot showing estimates of formation hydraulic conductivity and specific storage from perturbation analysis

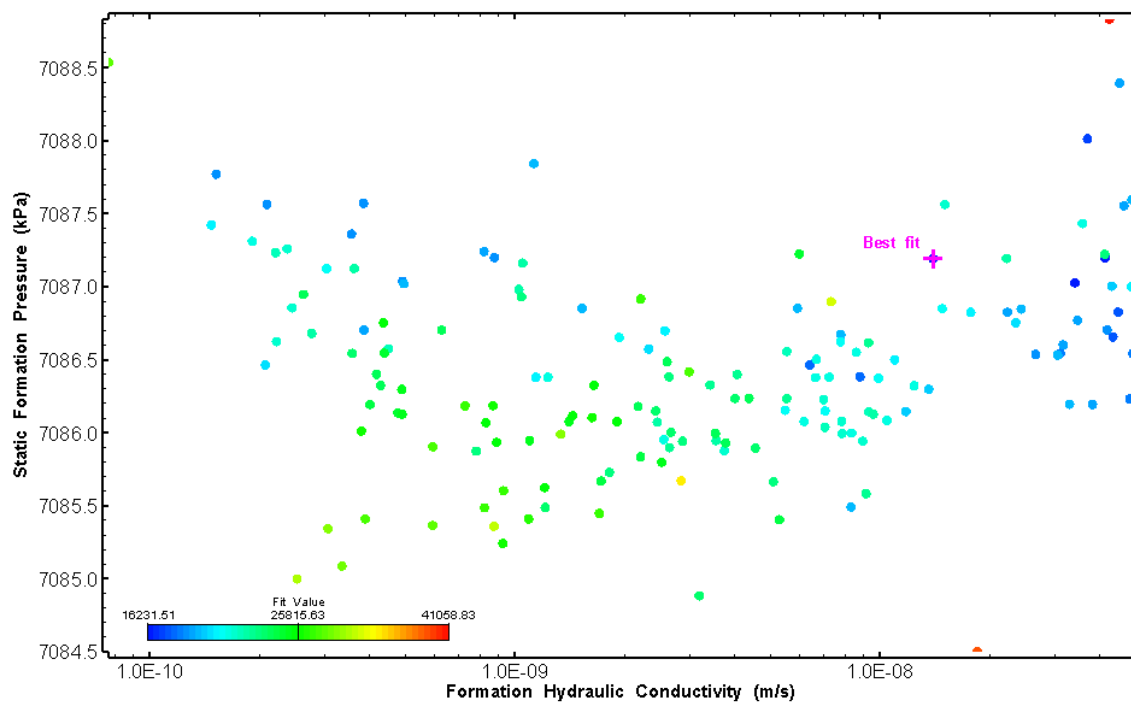


Figure 274: HT023 XY-scatter plot showing estimates of formation hydraulic conductivity and static formation pressure from perturbation analysis

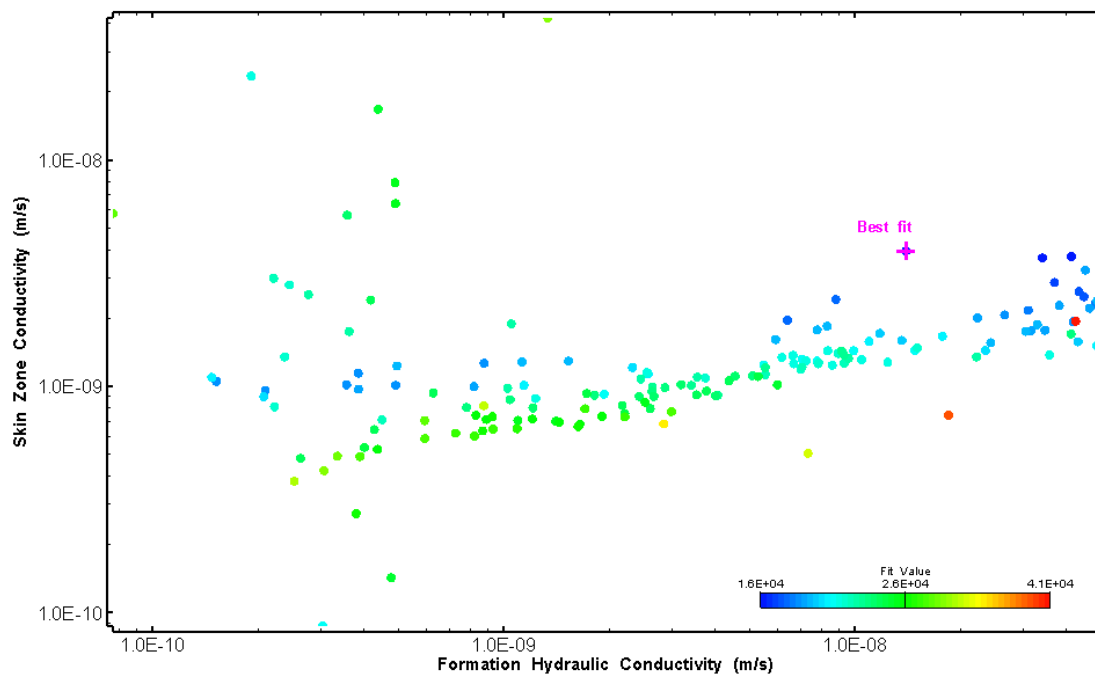


Figure 275: HT023 XY-scatter plot showing estimates of formation hydraulic conductivity and skin zone conductivity from perturbation analysis

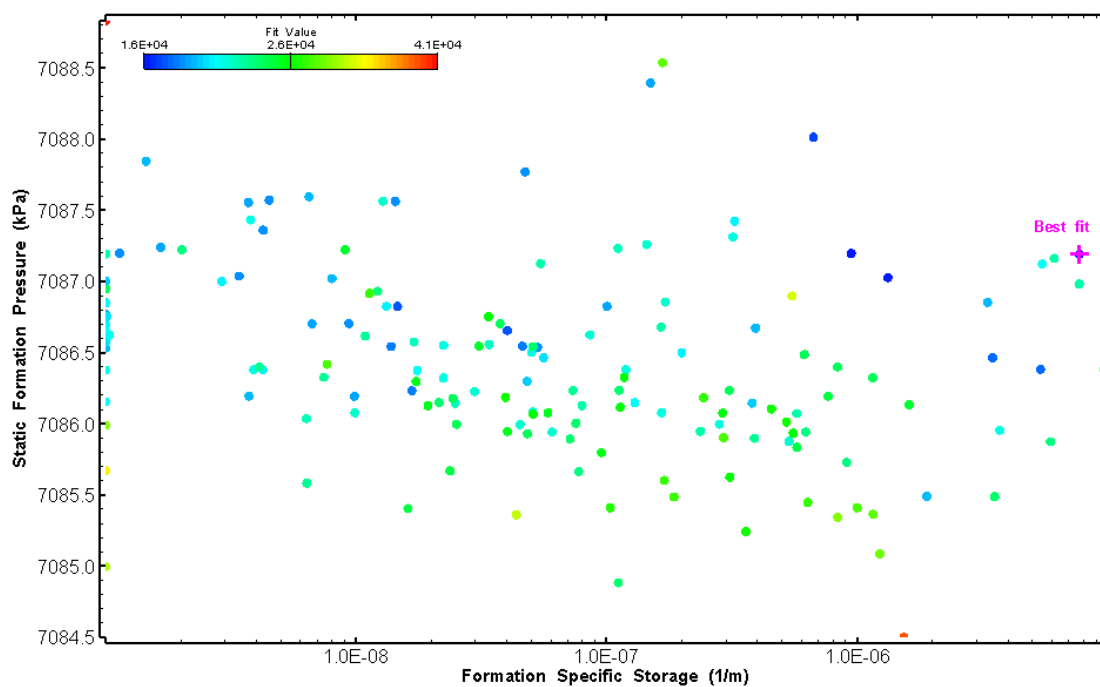


Figure 276: HT023 XY-scatter plot showing estimates of specific storage and static formation pressure from perturbation analysis

## 24.0 HT024 (792.31 – 812.33 M)

HT024 was selected to obtain continuous testing coverage from 600 to 800 m along hole. 16 broken fractures were observed in the core. No indication of flow was recorded during FFEC logging post-drilling.

The test was initiated with a shut-in pressure recovery phase (PSR). A pulse withdrawal test (PW) with a shut-in recovery followed by a slug withdrawal (SW) phase was completed after the PSR phase.

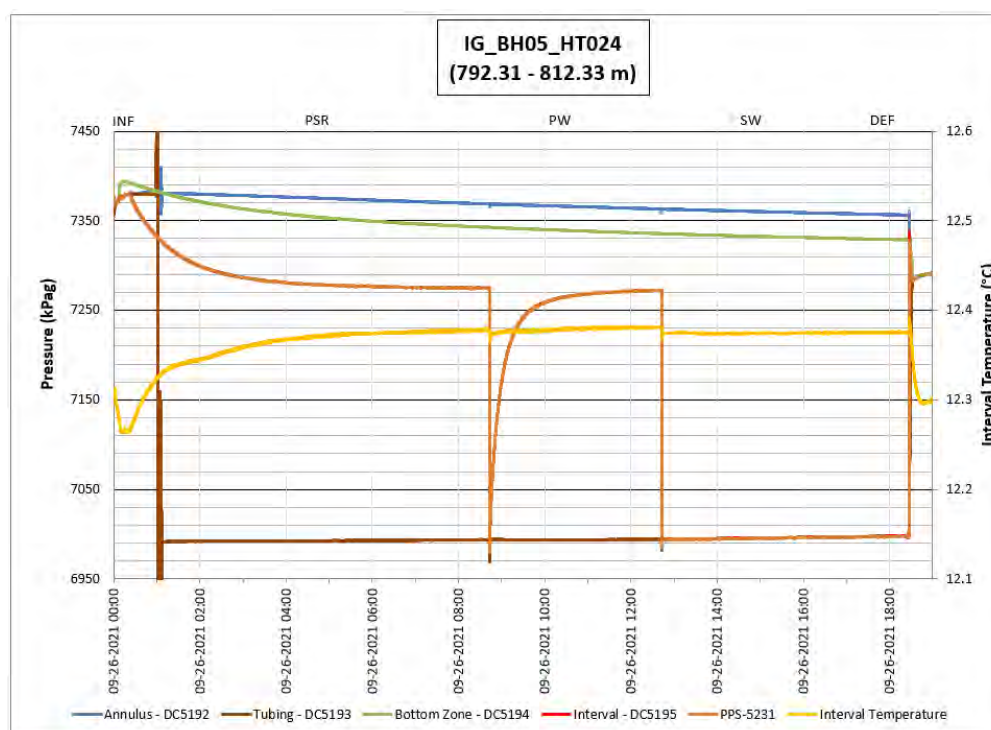
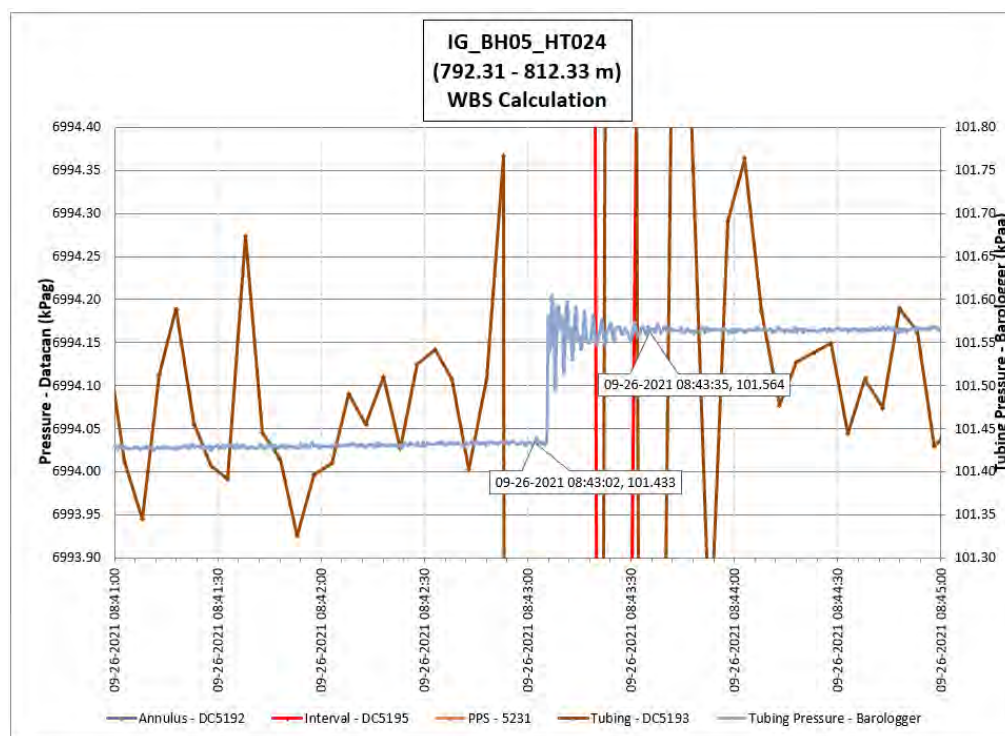


Figure 277: HT024 Annotated test plot showing monitored zone pressure and interval temperature.



**Figure 278: HT024 Tubing pressure during DHSIV activation. DHSIV Closed Wellbore Storage Estimate =  $8\text{E-}11 \text{ m}^3/\text{Pa}$**

**Table 24: Summary of Analysis Results – HT024**

	Formation conductivity	Skin zone conductivity	Static formation pressure	Formation specific storage	Radial thickness of skin	Flow dimension
	[m/s]	[m/s]	[kPa]	[1/m]	[m]	[–]
Best Fit	1E-11	1E-09	7273	6E-09	1.2E-01	2.3
Minimum	5E-13	2E-12	7230	1E-09	1E-03	1.1
Maximum	5E-09	1E-09	7309	1E-05	1E+00	3.0
Mean	7E-11	1E-10	7273	8E-07	2E-01	2.3
Median	1E-11	9E-12	7273	4E-07	9E-02	2.4
Geometric mean	2E-11	2E-11	7273	6E-08	8E-02	2.3

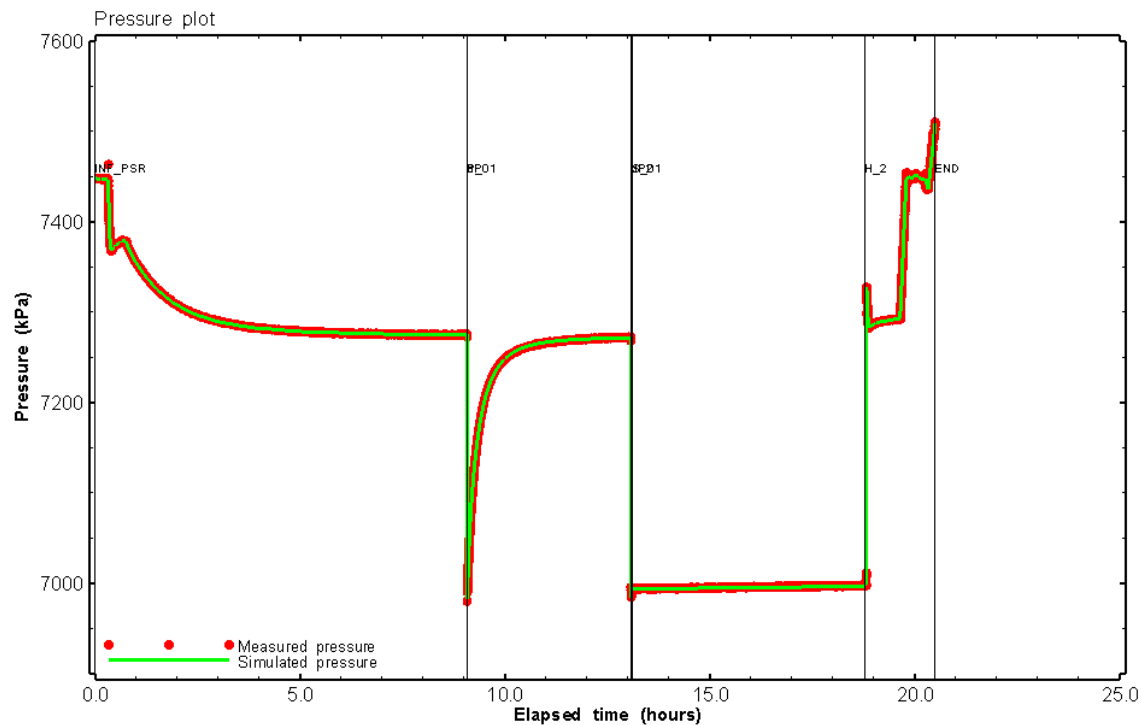


Figure 279: HT024 Pressure plot showing best-fit simulation and best fit results

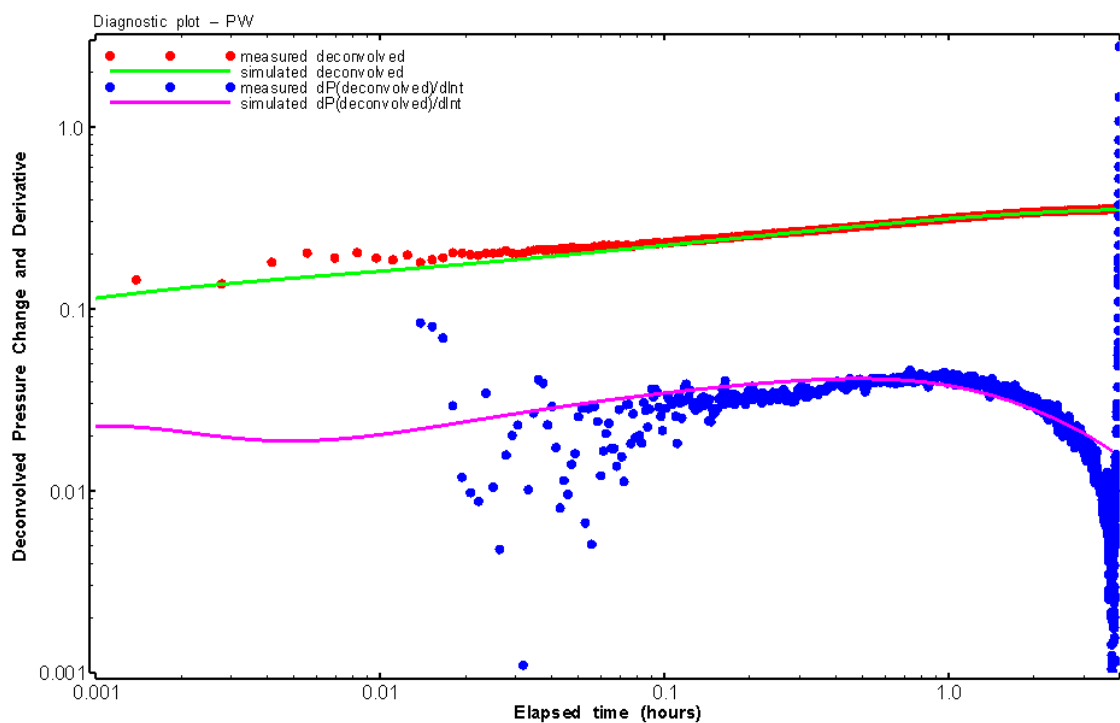


Figure 280: HT024 Deconvolved pressure change and derivative plot of the PW sequence showing best-fit simulation



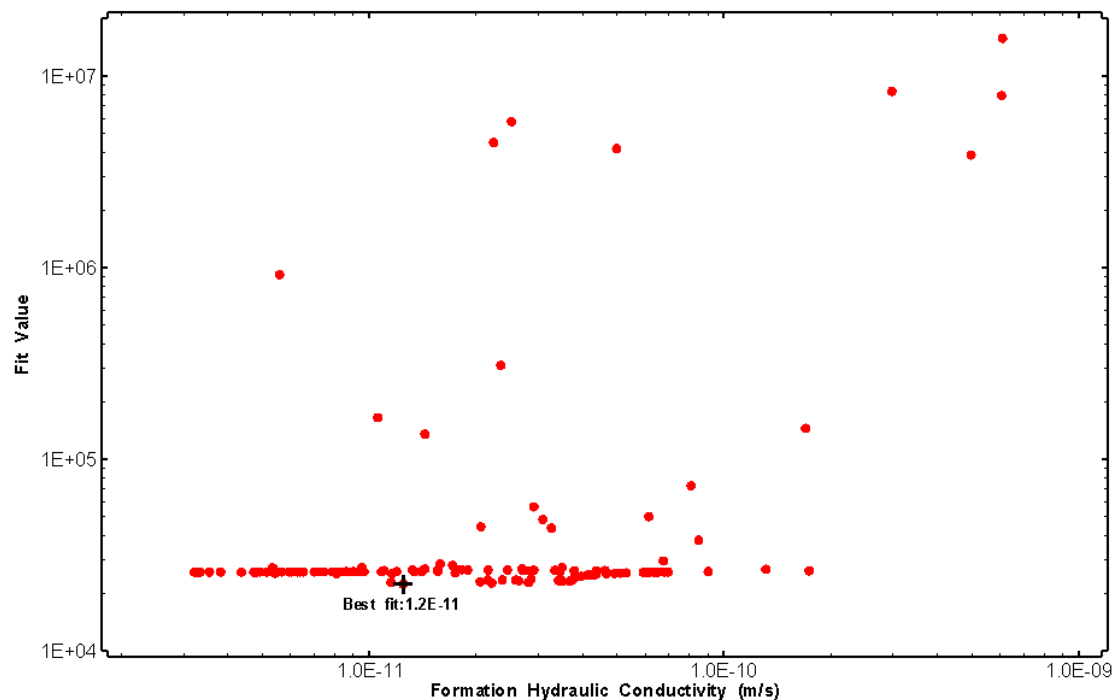


Figure 281: HT024 XY-scatter plot of formation hydraulic conductivity vs. fit value

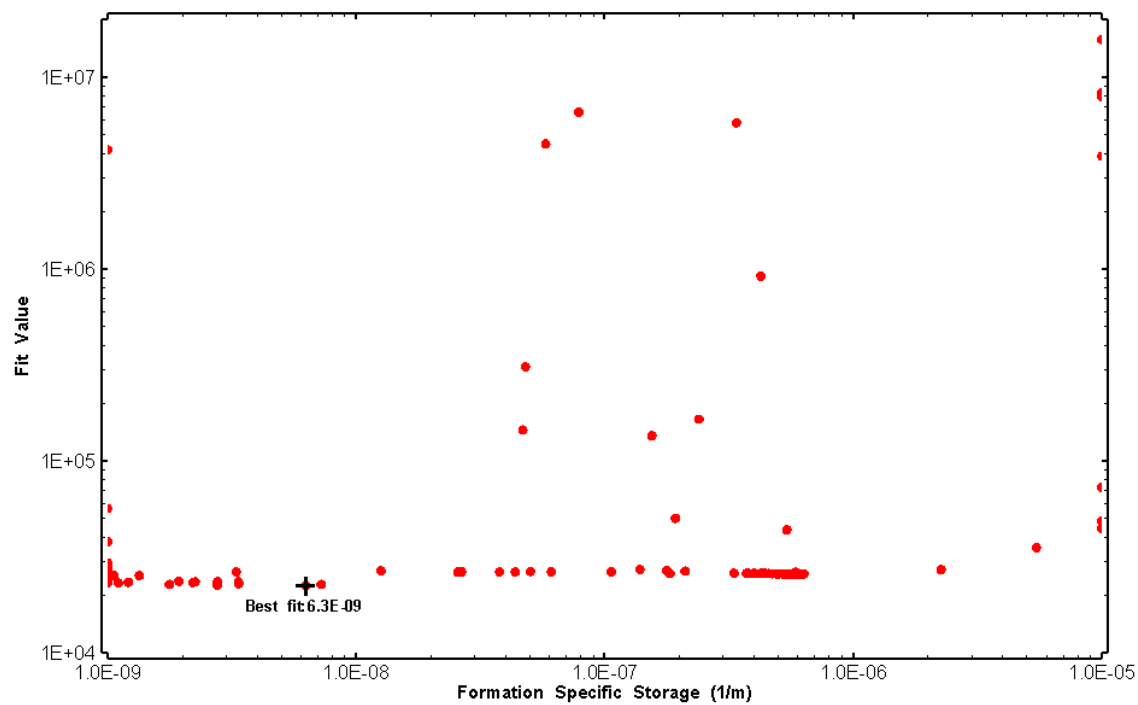


Figure 282: HT024 XY-scatter plot of formation specific storage vs. fit value

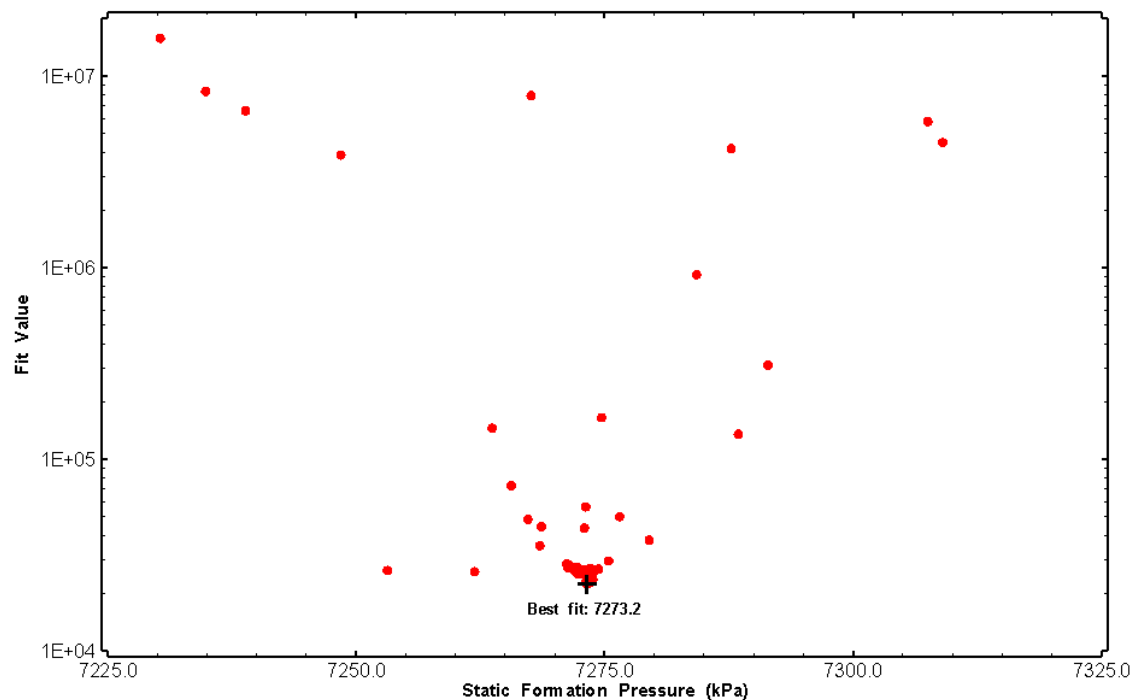


Figure 283: HT024 XY-scatter plot of static formation pressure vs. fit value

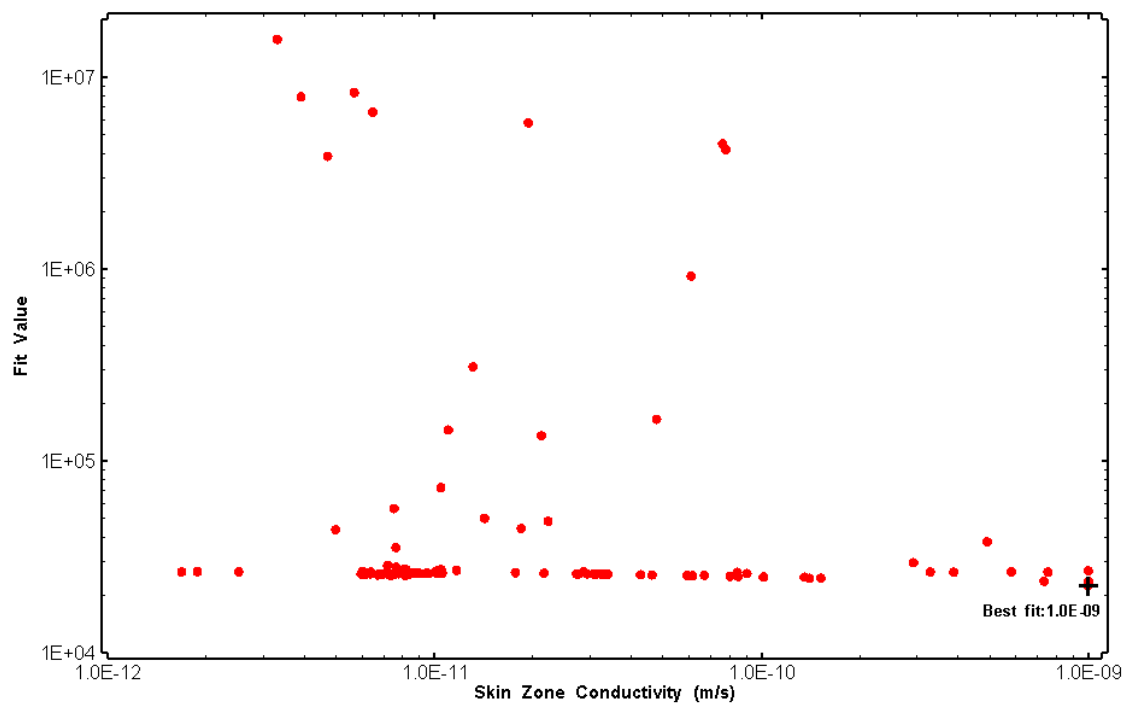


Figure 284: HT024 XY-scatter plot of skin zone conductivity vs. fit value

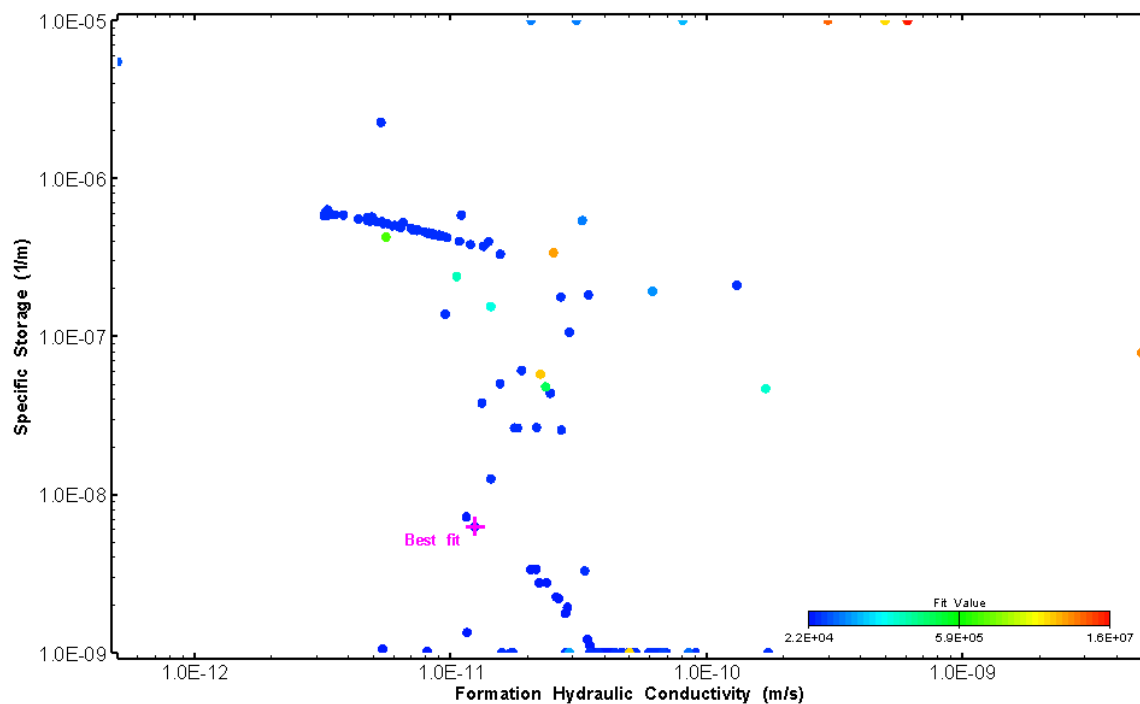


Figure 285: HT024 XY-scatter plot showing estimates of formation hydraulic conductivity and specific storage from perturbation analysis

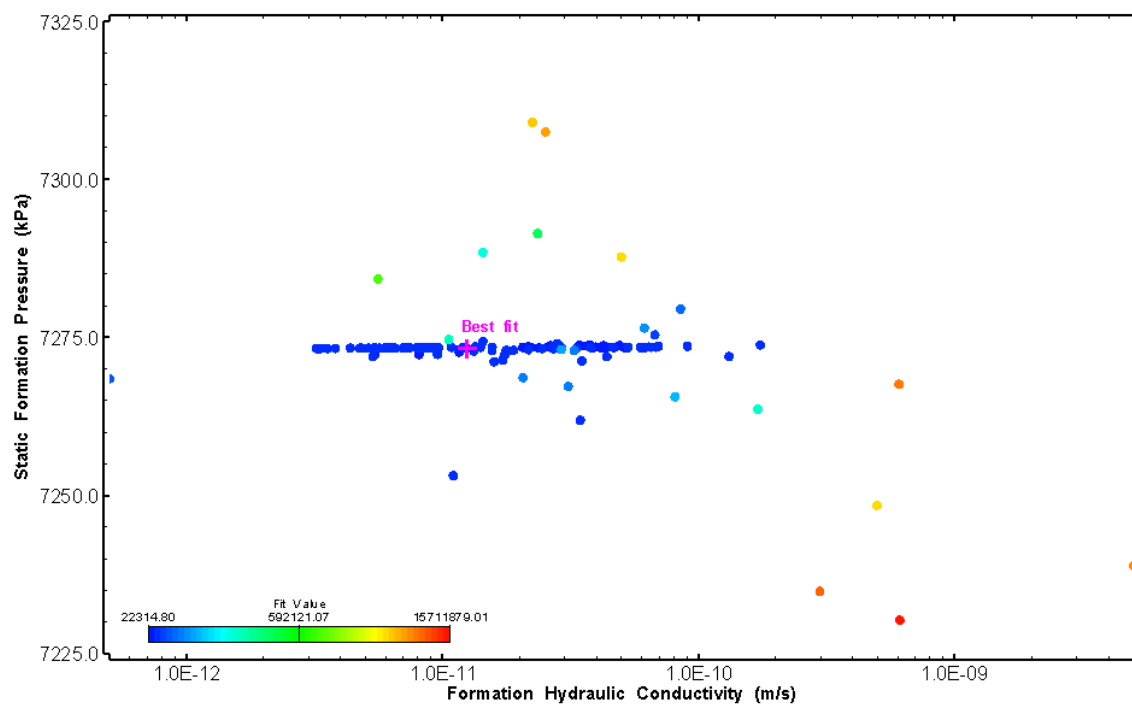


Figure 286: HT024 XY-scatter plot showing estimates of formation hydraulic conductivity and static formation pressure from perturbation analysis

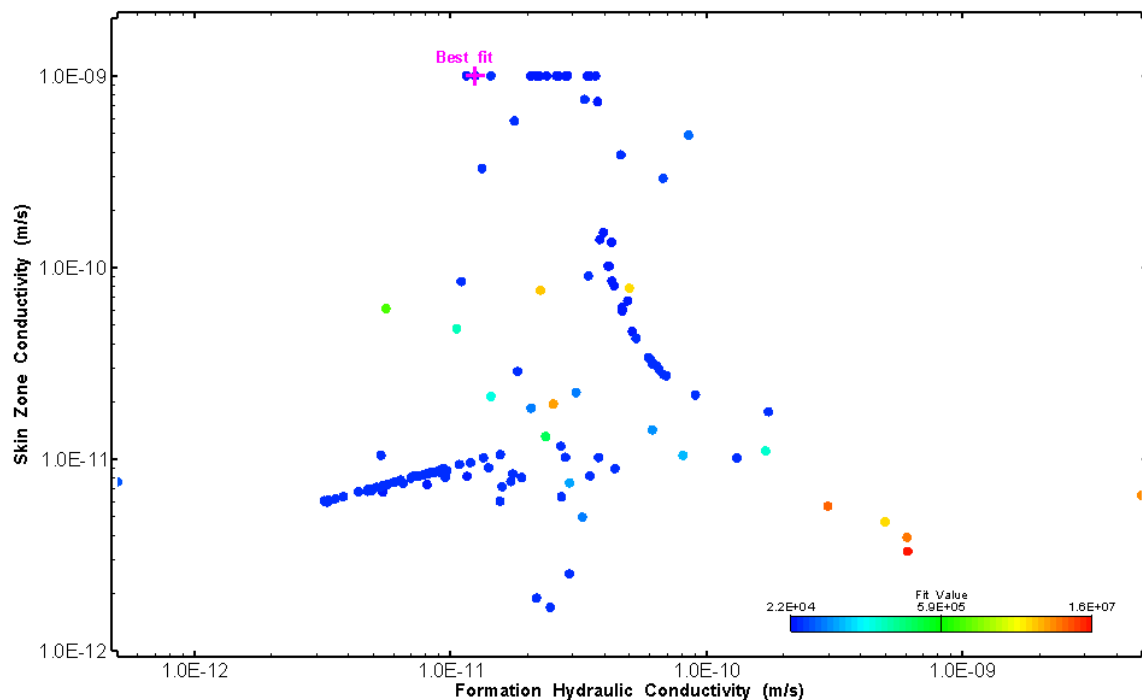


Figure 287: HT024 XY-scatter plot showing estimates of formation hydraulic conductivity and skin zone conductivity from perturbation analysis

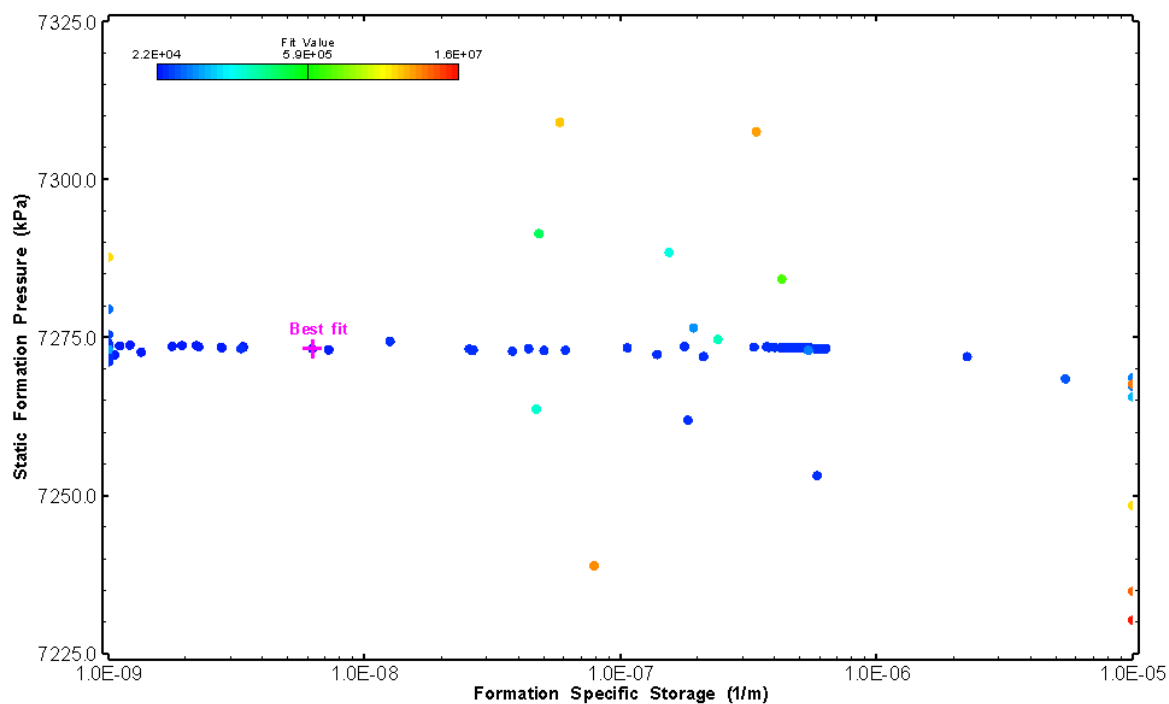


Figure 288: HT024 XY-scatter plot showing estimates of specific storage and static formation pressure from perturbation analysis

## 25.0 HT025 (814.13 – 834.15 M)

HT025 was selected to test a deep fractured interval containing multiple dykes. Seven broken fractures were observed in the core. No indication of flow was recorded during FFEC logging post-drilling.

The test was initiated with a shut-in pressure recovery phase (PSR). A pulse withdrawal test (PW) with a shut-in recovery was completed after the PSR phase.

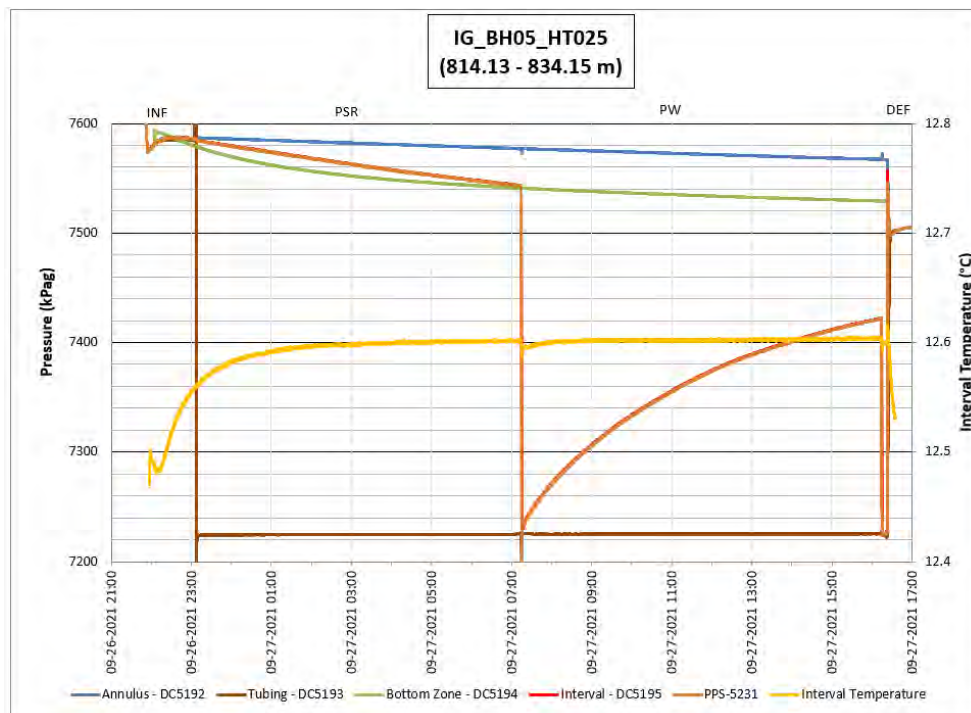
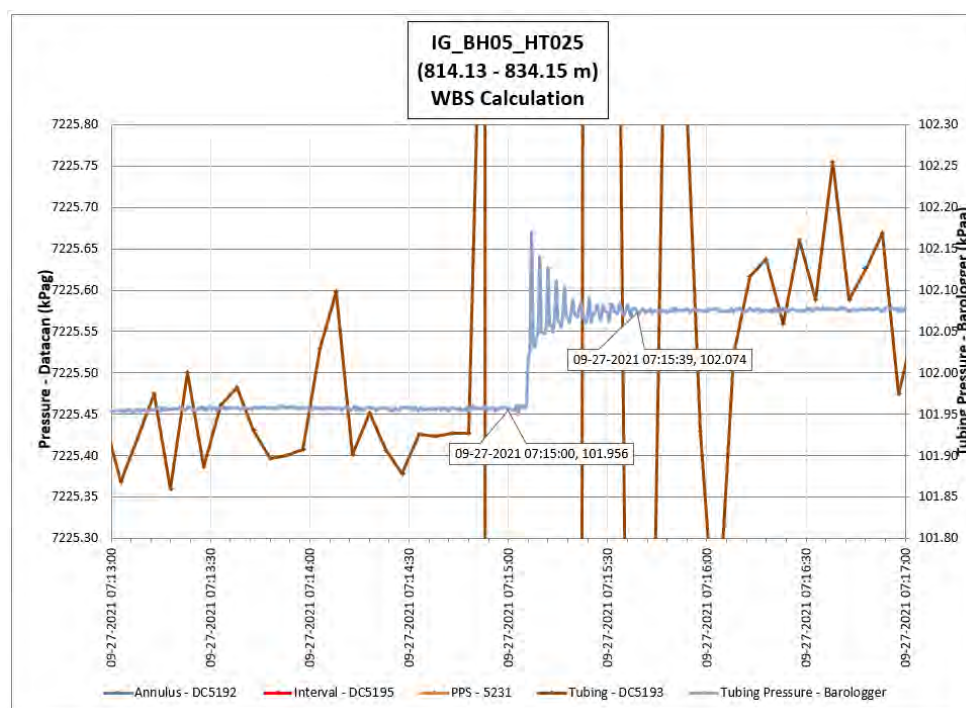


Figure 289: HT025 Annotated test plot showing monitored zone pressure and interval temperature.



**Figure 290: HT025 Tubing pressure during DHSIV activation. DHSIV Closed Wellbore Storage Estimate =  $7\text{E-}11 \text{ m}^3/\text{Pa}$**

**Table 25: Summary of Analysis Results – HT025**

	Formation conductivity	Skin zone conductivity	Static formation pressure	Formation specific storage	Radial thickness of skin	Flow dimension
	[m/s]	[m/s]	[kPa]	[1/m]	[m]	[–]
Best Fit	4E-13	2E-12	7478	2E-08	1E-03	2.5
Minimum	3E-15	8E-15	7451	1E-09	1E-03	1.0
Maximum	3E-11	1E-11	7525	7E-06	7E-01	3.0
Mean	2E-12	6E-13	7479	4E-07	6E-02	2.2
Median	8E-13	2.E-13	7475	5E-08	3E-02	2.3
Geometric mean	8E-13	2E-13	7479	6E-08	2E-02	2.2

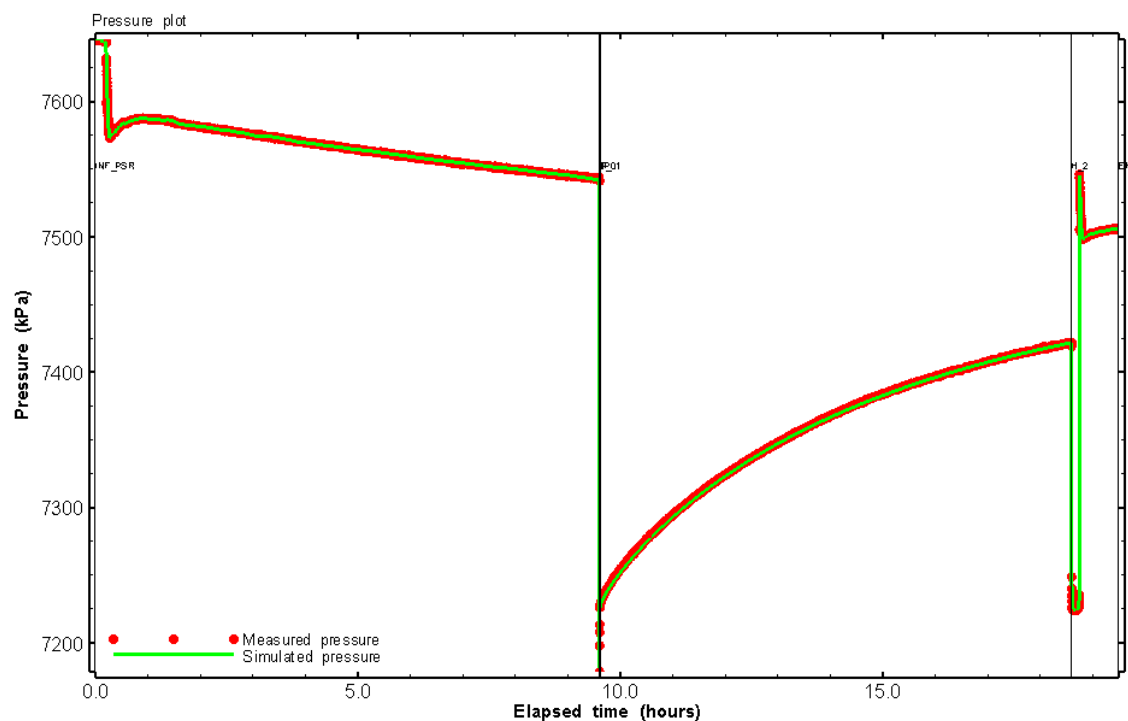


Figure 291: HT025 Pressure plot showing best-fit simulation and best fit results

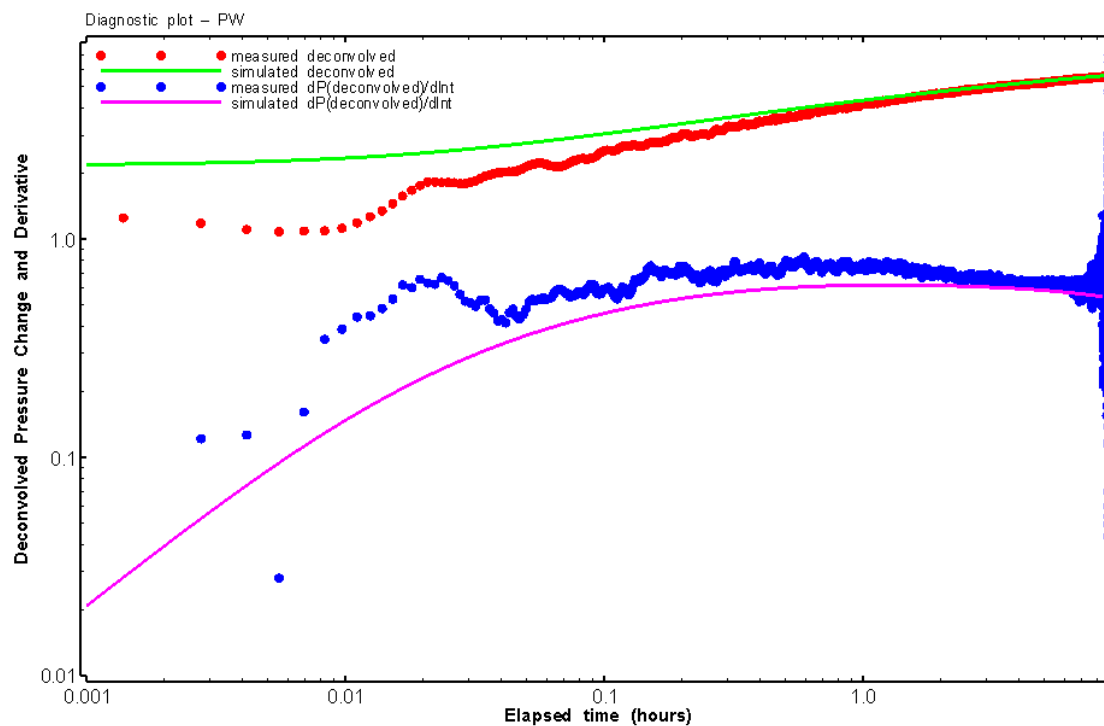


Figure 292: HT025 Deconvolved pressure change and derivative plot of the PW sequence showing best-fit simulation

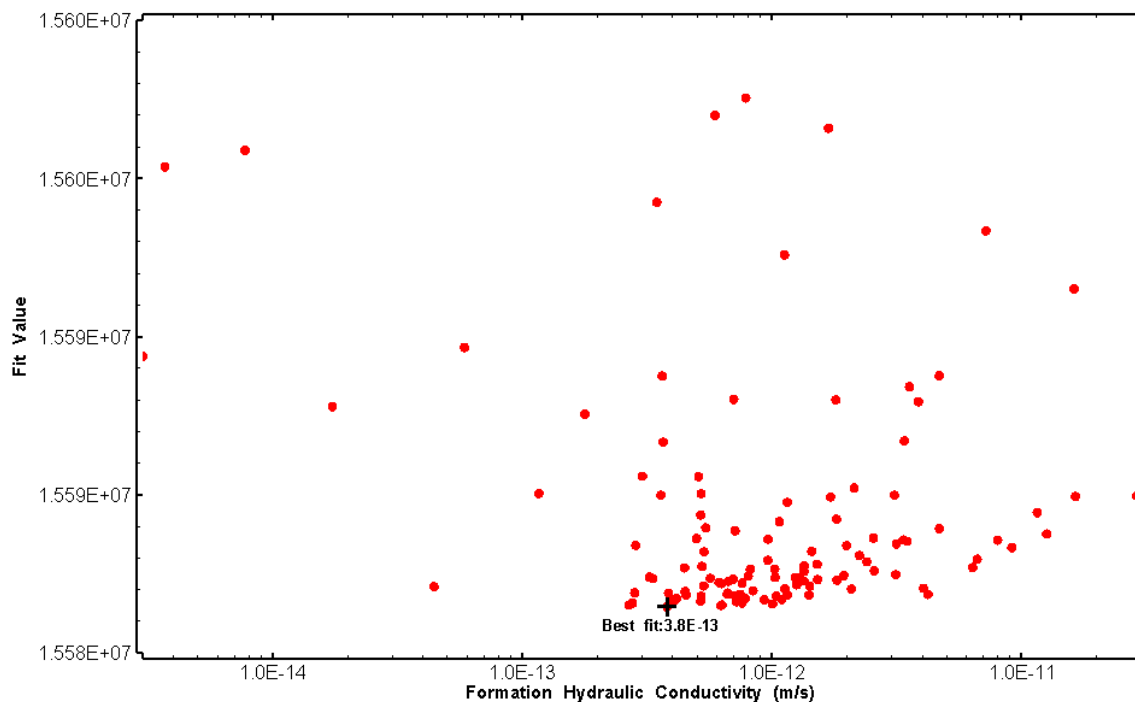


Figure 293: HT025 XY-scatter plot of formation hydraulic conductivity vs. fit value

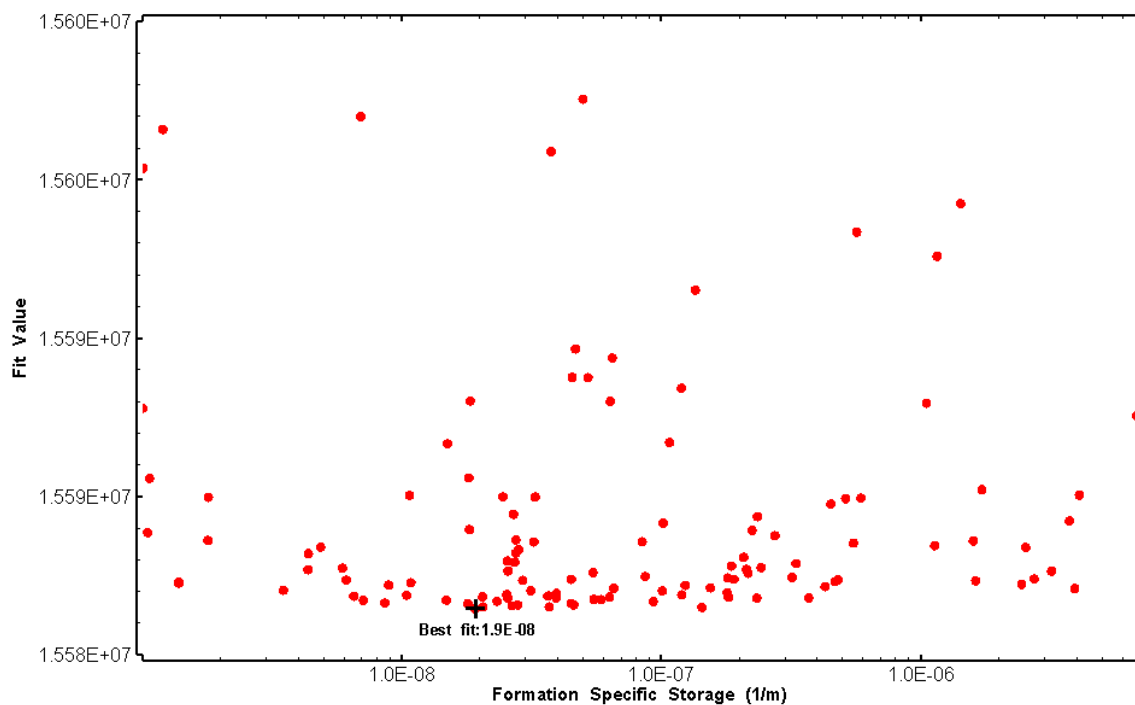


Figure 294: HT025 XY-scatter plot of formation specific storage vs. fit value



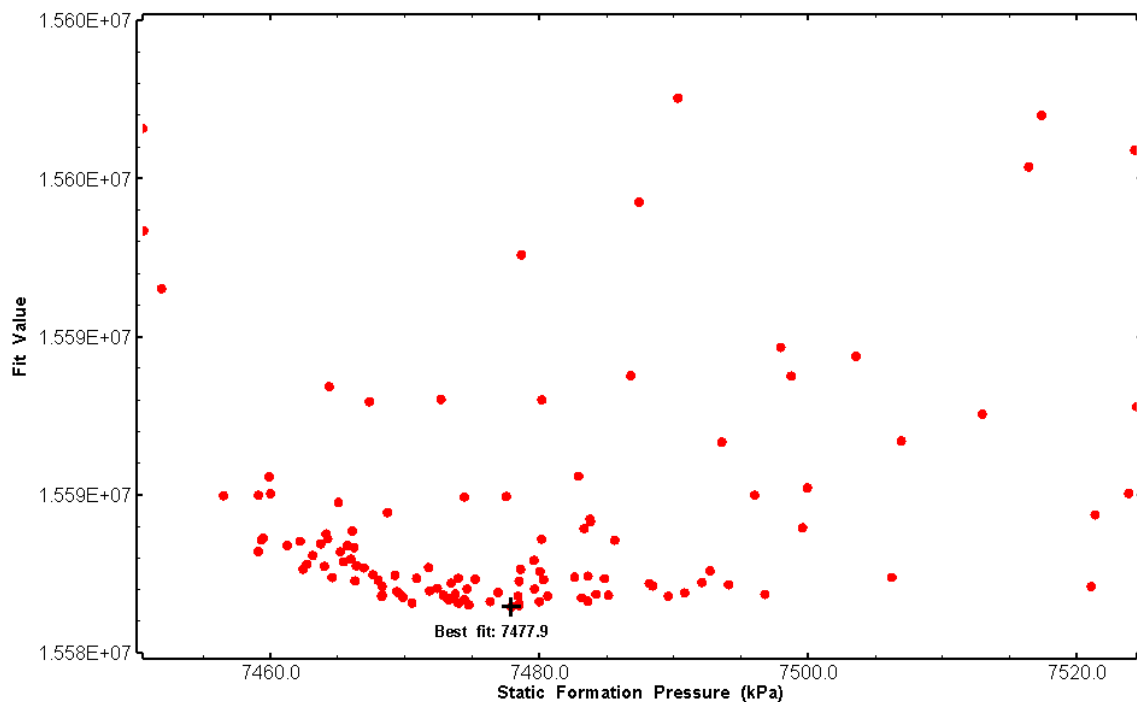


Figure 295: HT025 XY-scatter plot of static formation pressure vs. fit value

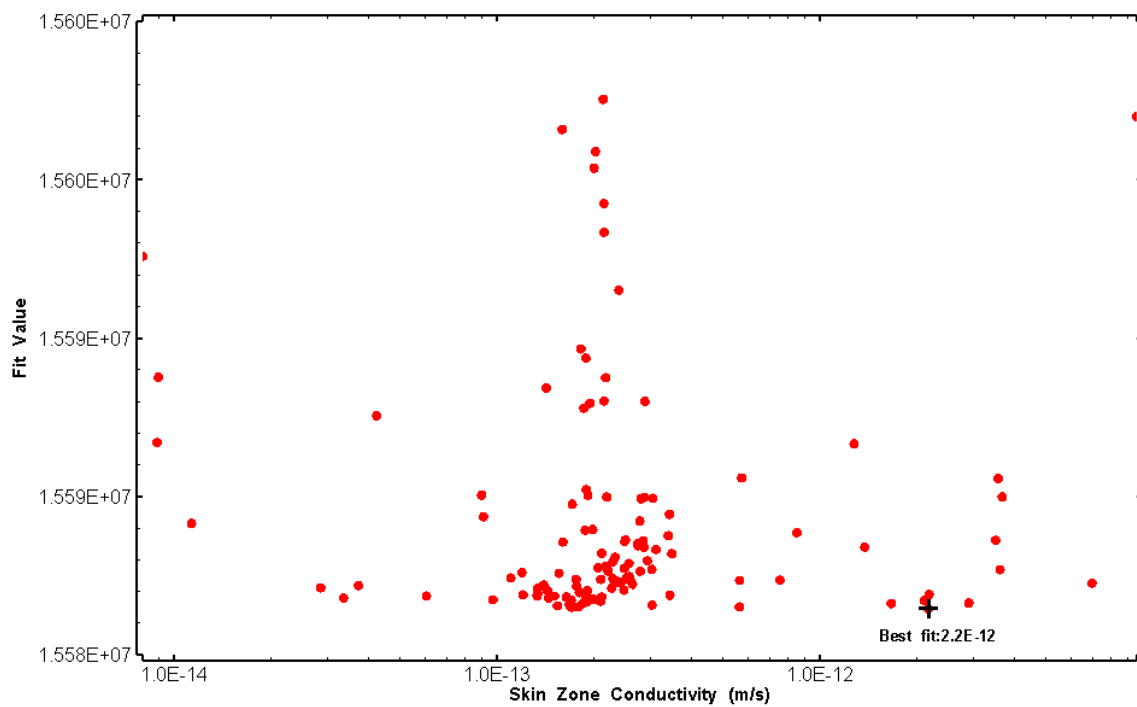
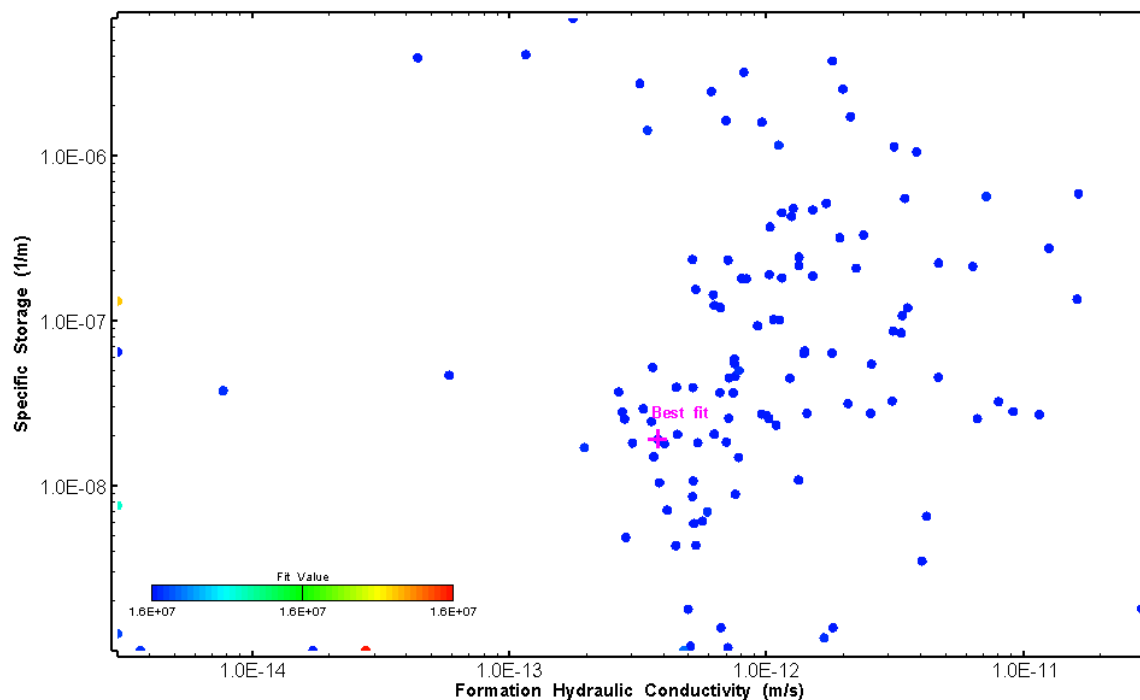
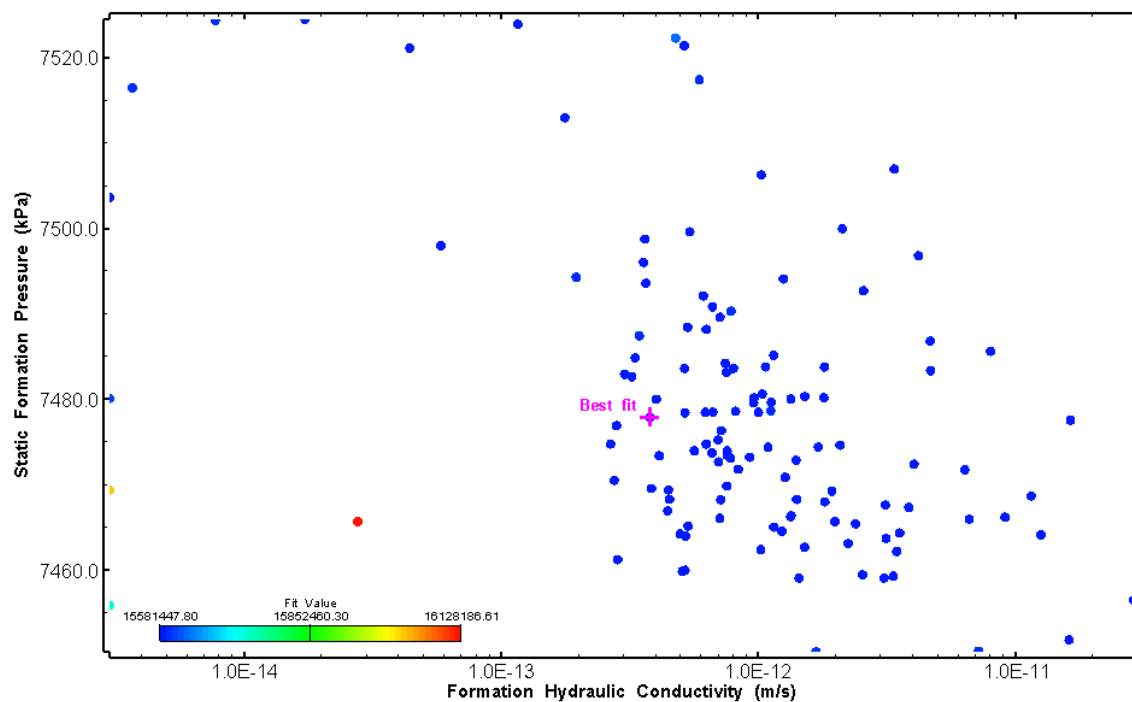


Figure 296: HT025 XY-scatter plot of skin zone conductivity vs. fit value



**Figure 297: HT025 XY-scatter plot showing estimates of formation hydraulic conductivity and specific storage from perturbation analysis**



**Figure 298: HT025 XY-scatter plot showing estimates of formation hydraulic conductivity and static formation pressure from perturbation analysis**

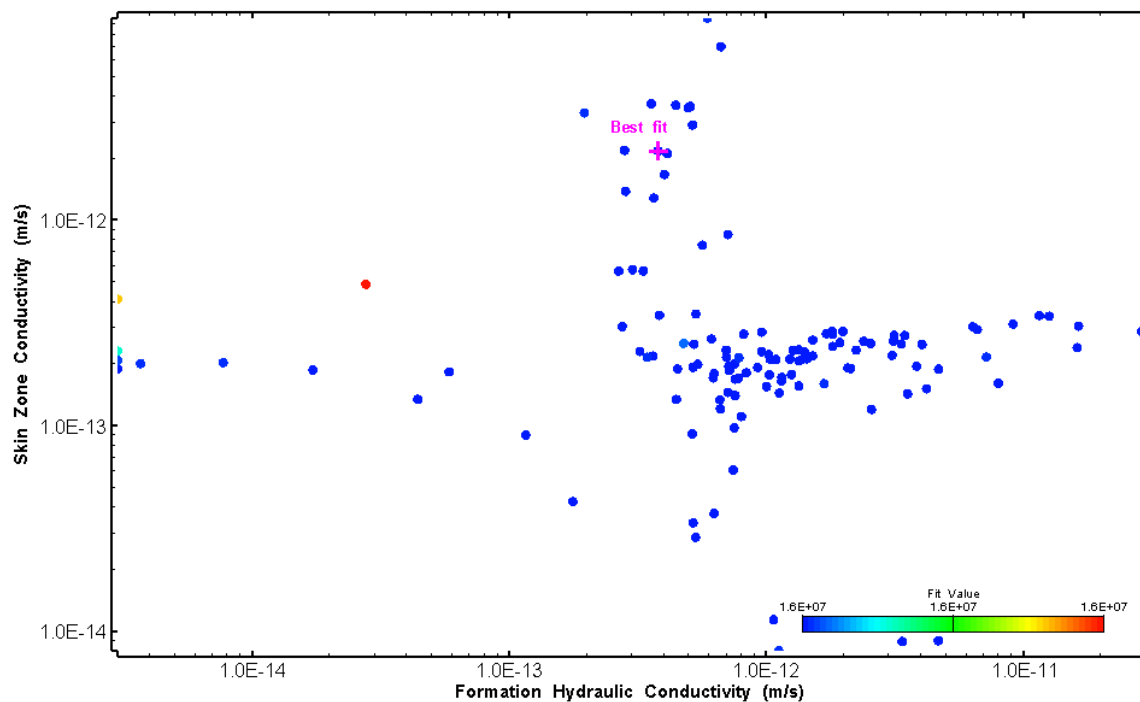


**Figure 299: HT025 XY-scatter plot showing estimates of formation hydraulic conductivity and skin zone conductivity from perturbation analysis**

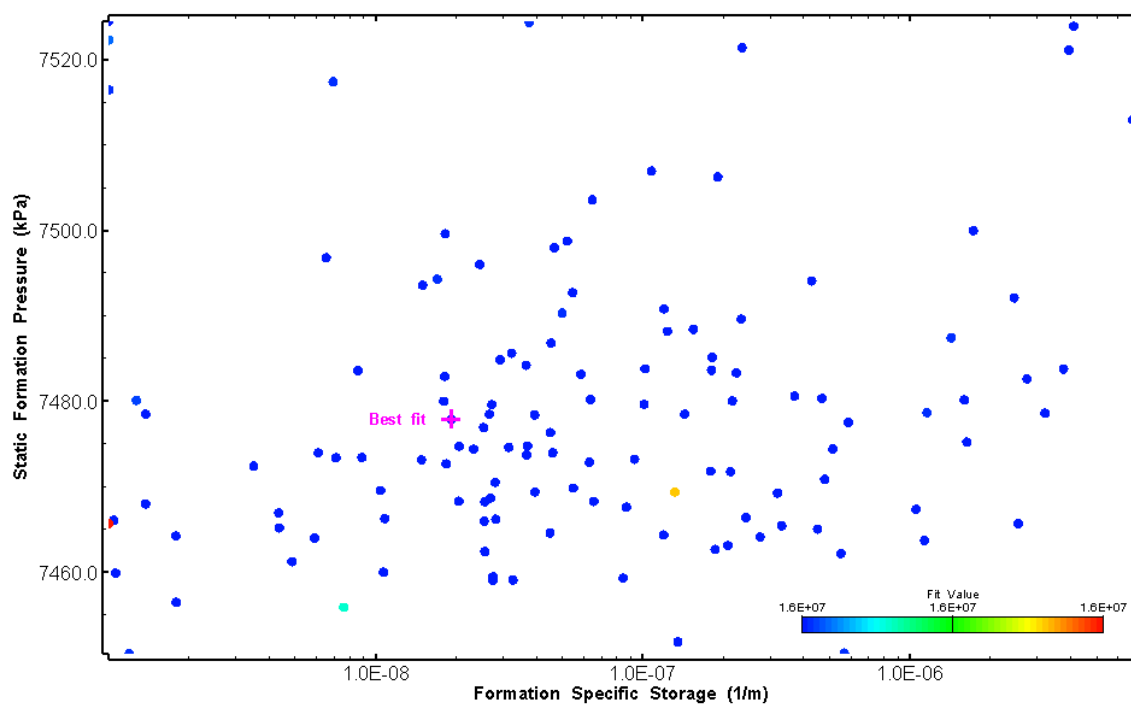


**Figure 300: HT025 XY-scatter plot showing estimates of specific storage and static formation pressure from perturbation analysis**

## 26.0 HT026 (848.70 – 868.72 M)

HT026 was selected to test a deep fractured interval containing a dyke. 11 broken fractures were observed in the core. A loss of drilling fluid was observed in this interval during drilling. An indication of flow was recorded during FFEC logging post-drilling.

The test was initiated with a shut-in pressure recovery phase (PSR). A pulse withdrawal test (PW) with a shut-in recovery followed by a slug withdrawal (SW) phase was completed after the PSR phase.

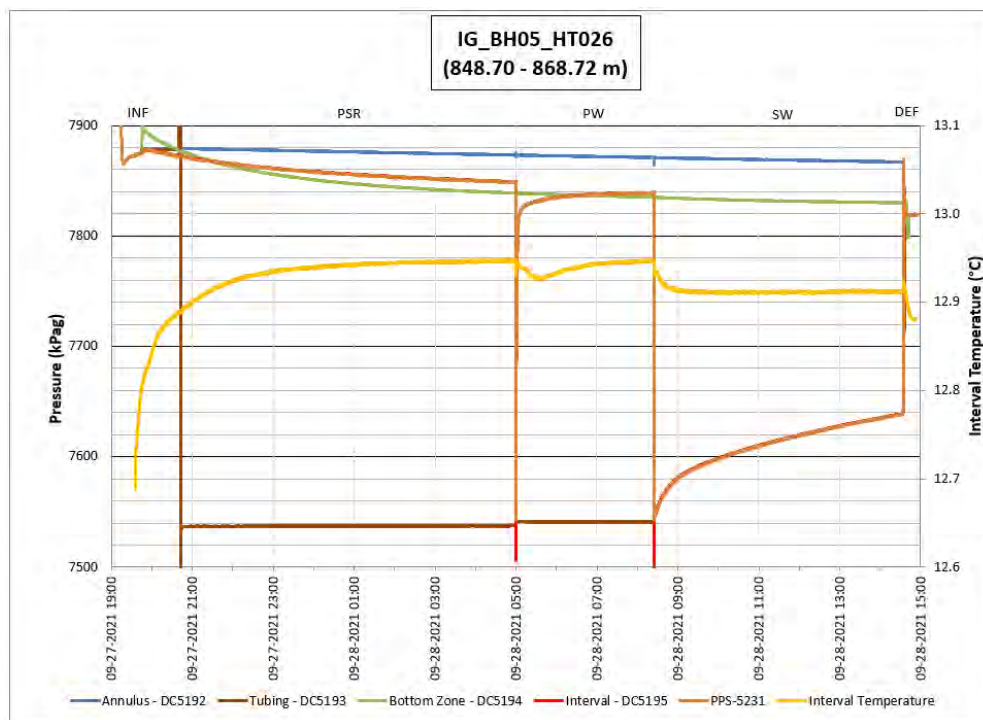


Figure 301: HT026 Annotated test plot showing monitored zone pressure and interval temperature.

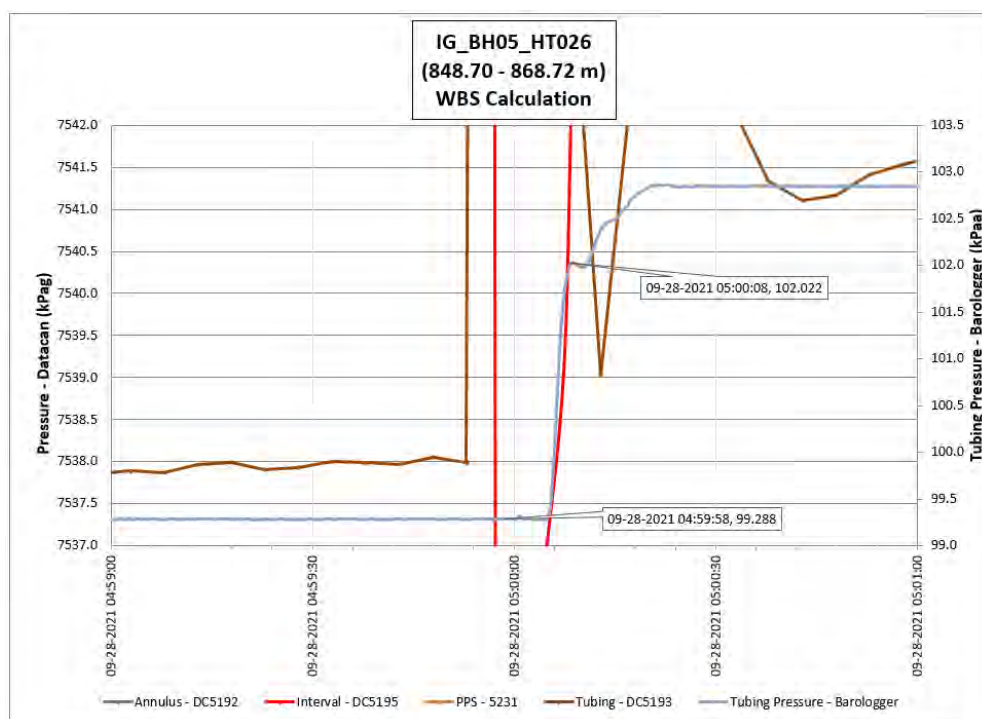


Figure 302: HT026 Tubing pressure during DHSIV activation. DHSIV Closed Wellbore Storage Estimate =  $2\text{E-}09 \text{ m}^3/\text{Pa}$

Table 26: Summary of Analysis Results – HT026

	Formation conductivity	Skin zone conductivity	Static formation pressure	Formation specific storage	Radial thickness of skin	Flow dimension
	[m/s]	[m/s]	[kPa]	[1/m]	[m]	[–]
Best Fit	1E-10	7E-09	7835	4E-07	3.61E+00	2.0
Minimum	2E-11	3E-11	7722	1E-09	1E-03	1.7
Maximum	6E-09	1E-08	7950.	1E-05	1E+01	3.0
Mean	5E-10	5E-09	7845	6E-06	9E-01	2.1
Median	2E-10	5E-09	7838	8E-06	2E-01	2.1
Geometric mean	2E-10	2E-09	7845	3E-06	2E-01	2.1

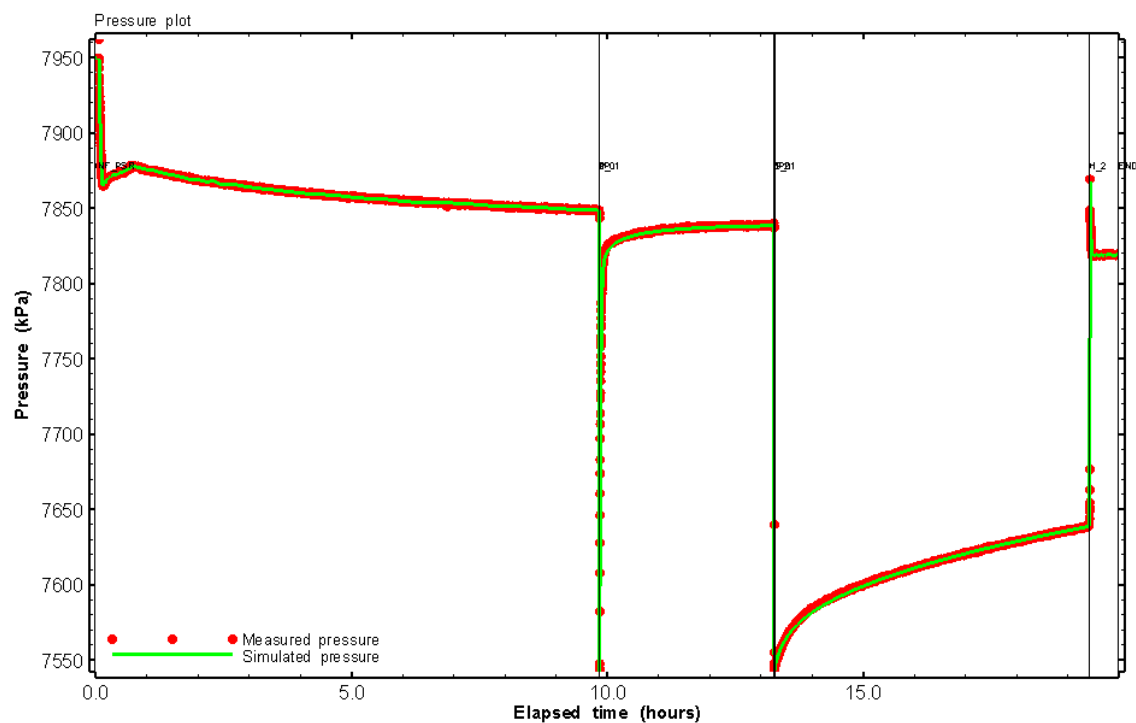


Figure 303: HT026 Pressure plot showing best-fit simulation and best fit results

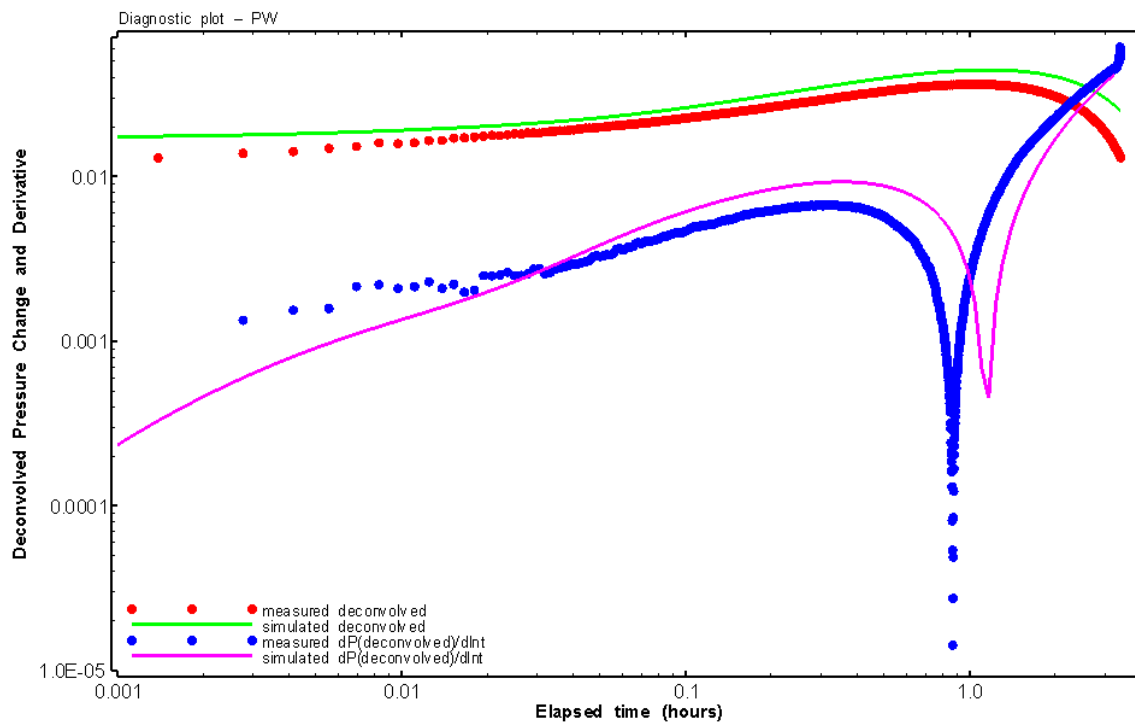


Figure 304: HT026 Deconvolved pressure change and derivative plot of the PW sequence showing best-fit simulation

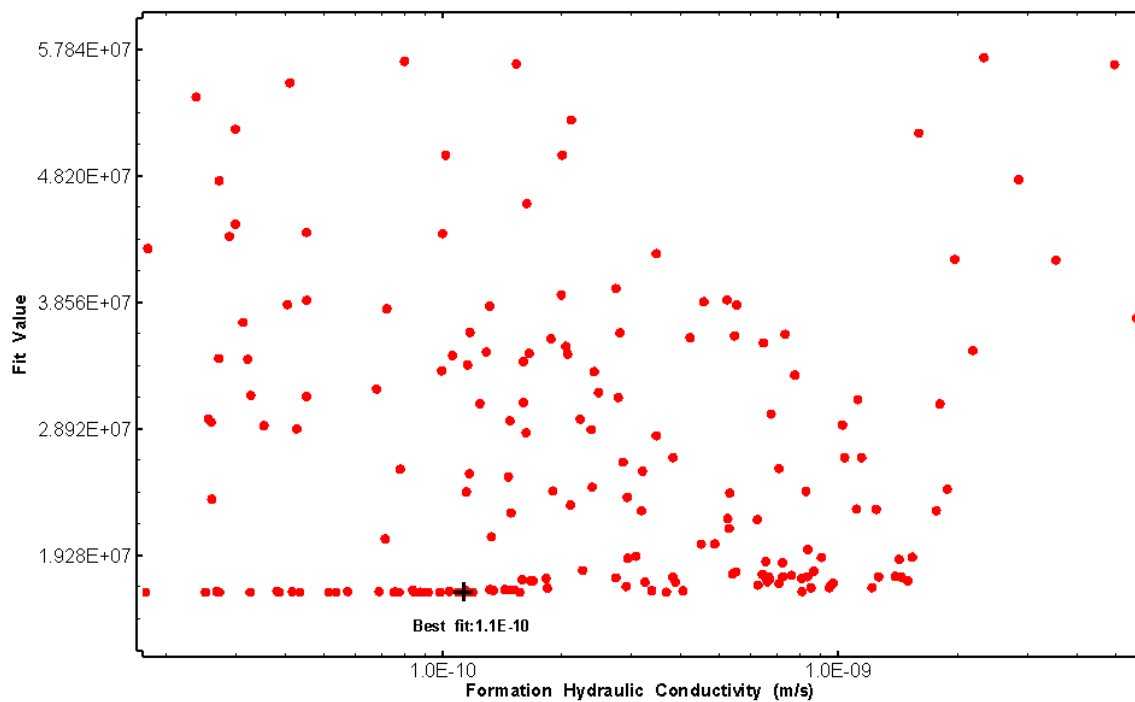


Figure 305: HT026 XY-scatter plot of formation hydraulic conductivity vs. fit value

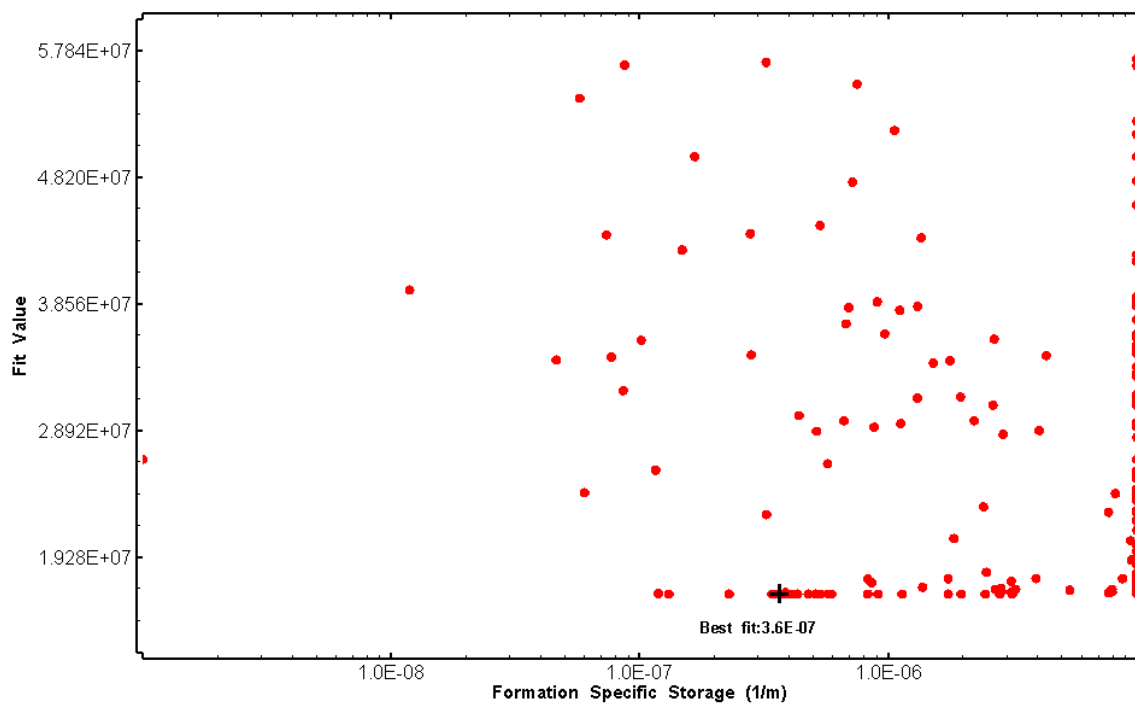


Figure 306: HT026 XY-scatter plot of formation specific storage vs. fit value

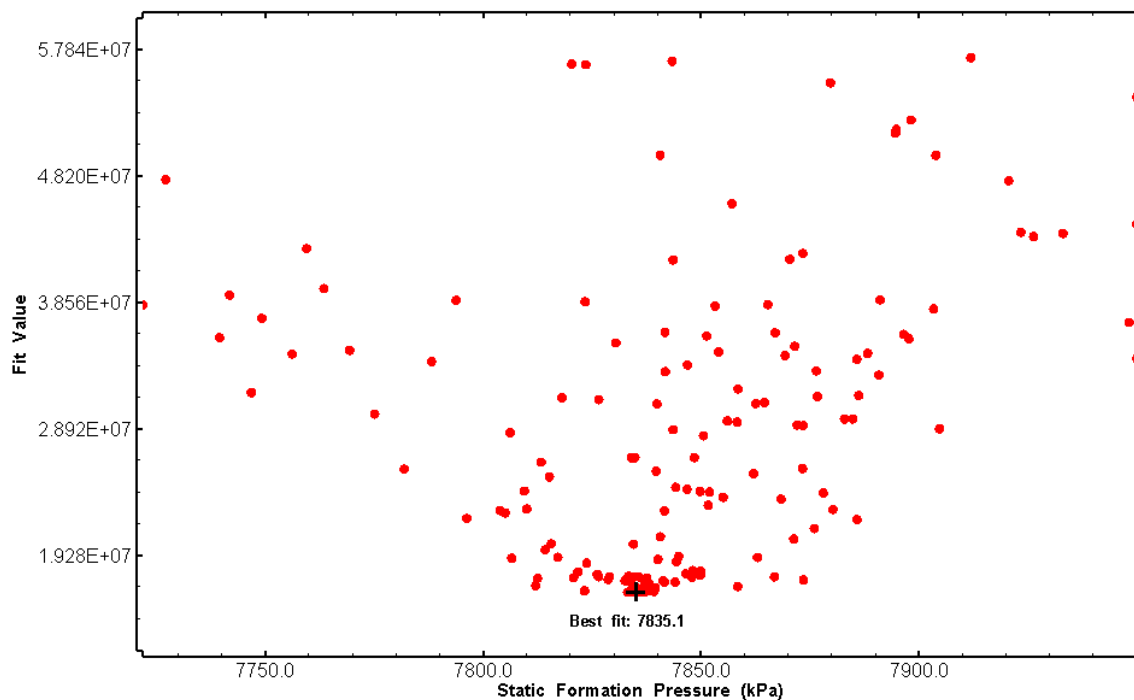


Figure 307: HT026 XY-scatter plot of static formation pressure vs. fit value

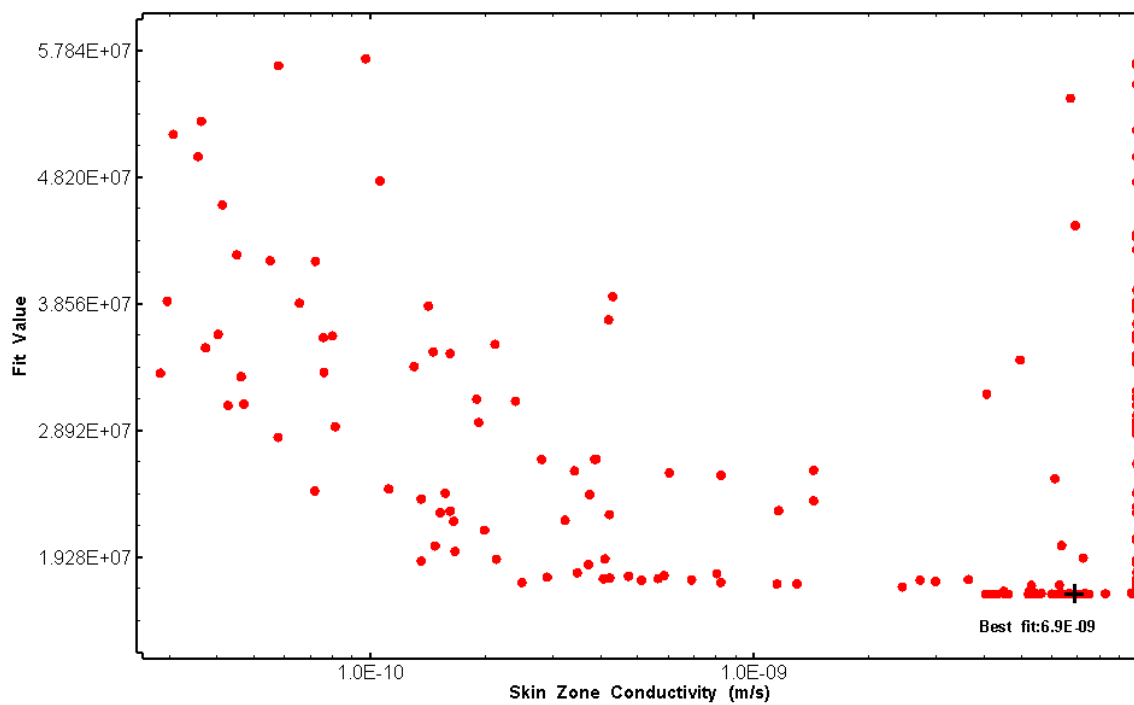


Figure 308: HT026 XY-scatter plot of skin zone conductivity vs. fit value



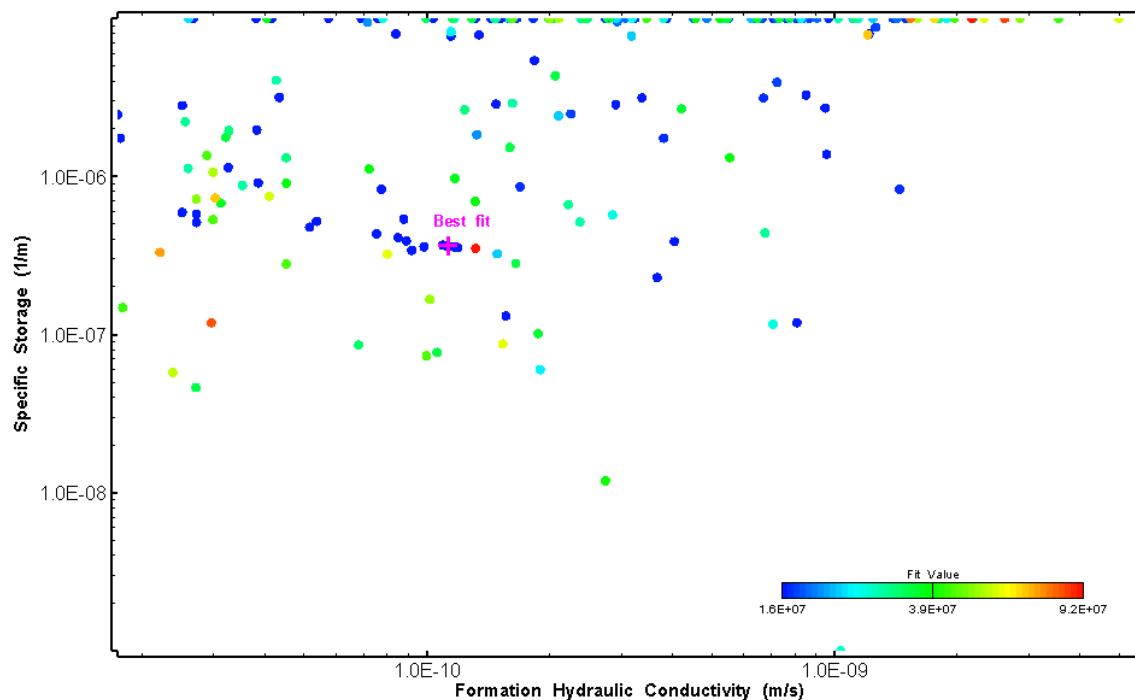


Figure 309: HT026 XY-scatter plot showing estimates of formation hydraulic conductivity and specific storage from perturbation analysis

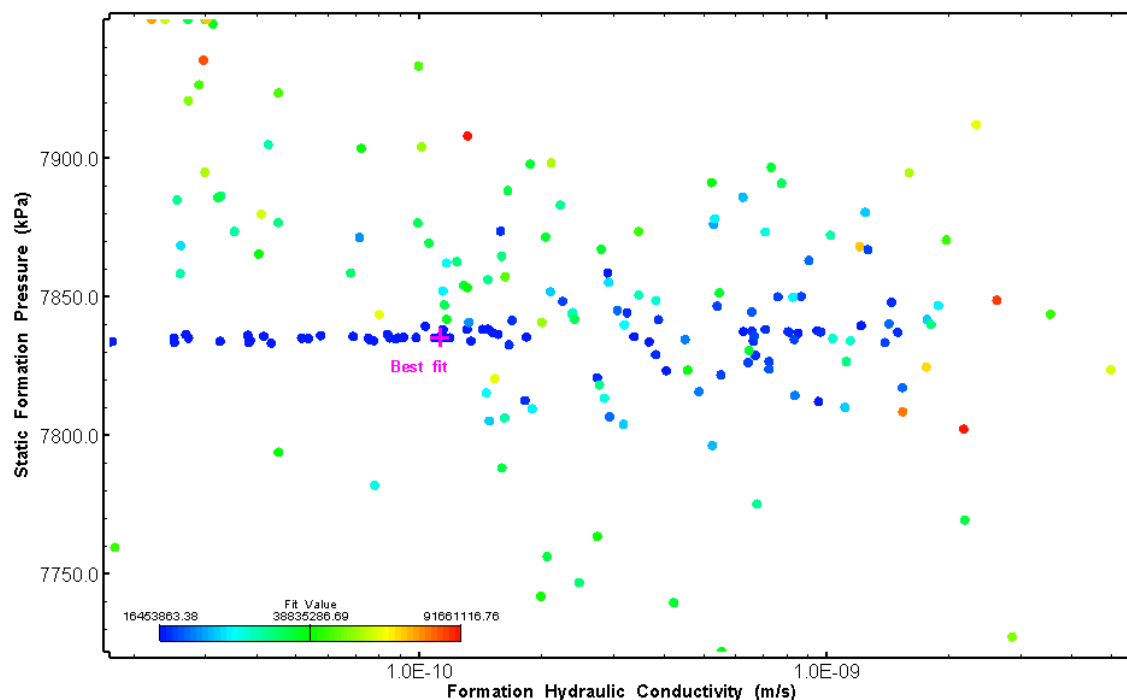


Figure 310: HT026 XY-scatter plot showing estimates of formation hydraulic conductivity and static formation pressure from perturbation analysis

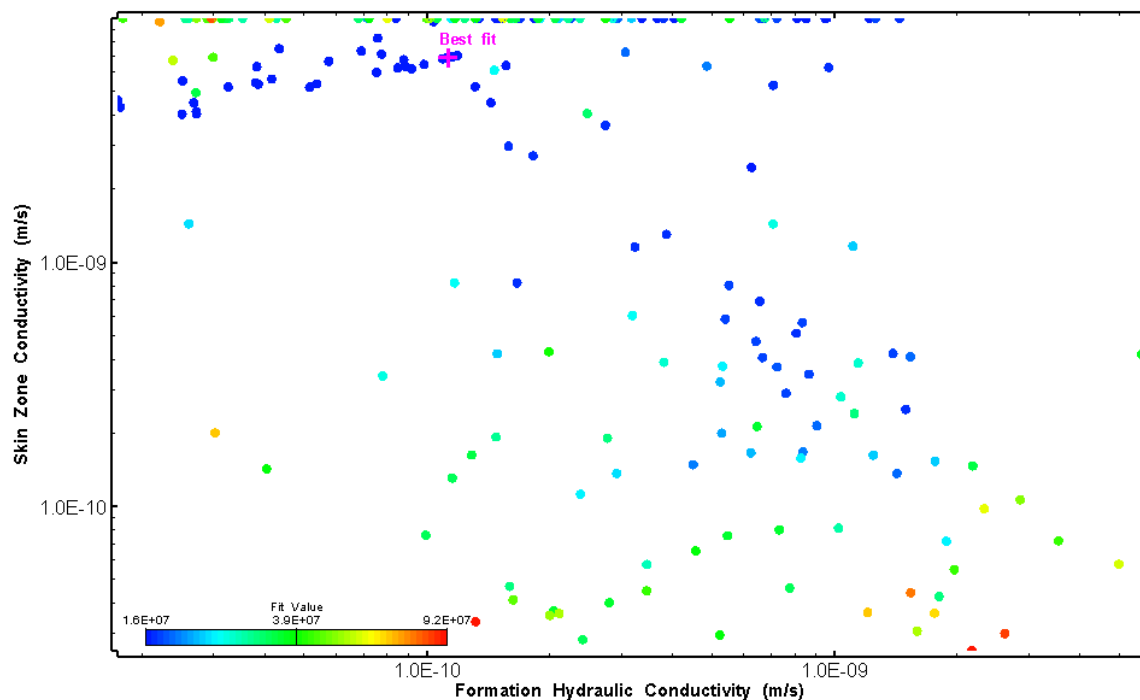


Figure 311: HT026 XY-scatter plot showing estimates of formation hydraulic conductivity and skin zone conductivity from perturbation analysis

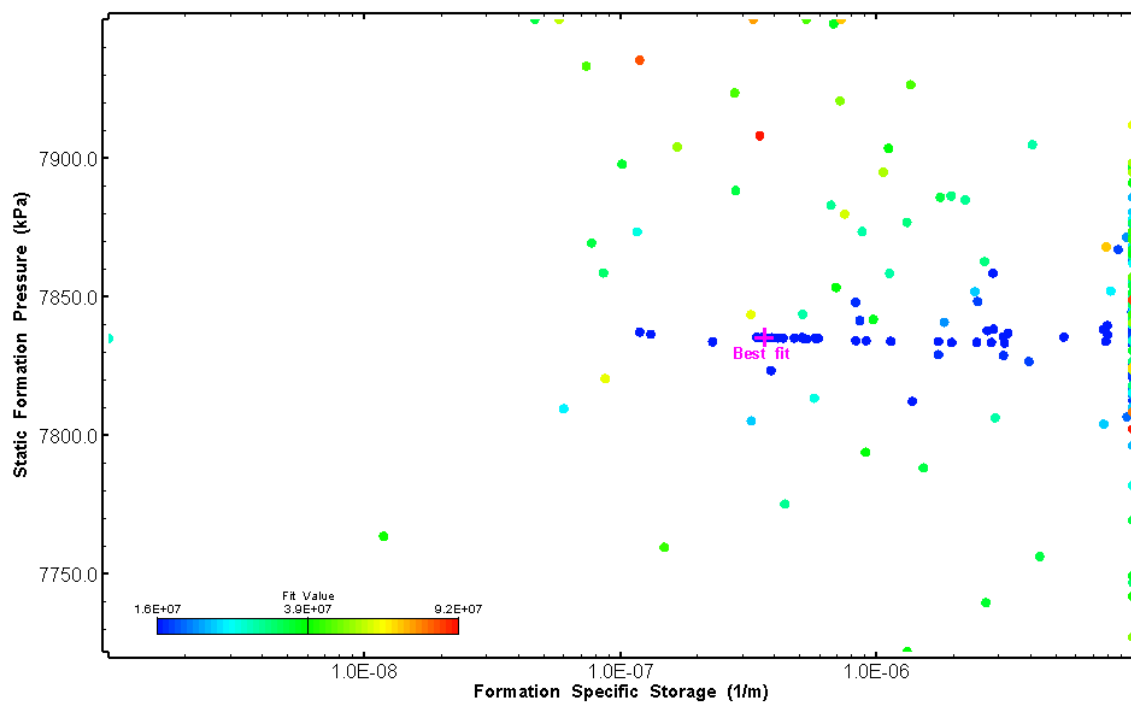


Figure 312: HT026 XY-scatter plot showing estimates of specific storage and static formation pressure from perturbation analysis

27.0 HT027 (907.00 – 927.02 M)

HT027 was selected to test a deep fractured interval containing a dyke. 26 broken fractures were observed in the core. No indication of flow was recorded during FFEC logging post-drilling.

The test was initiated with a shut-in pressure recovery phase (PSR). A pulse withdrawal test (PW) with a shut-in recovery was completed after the PSR phase.

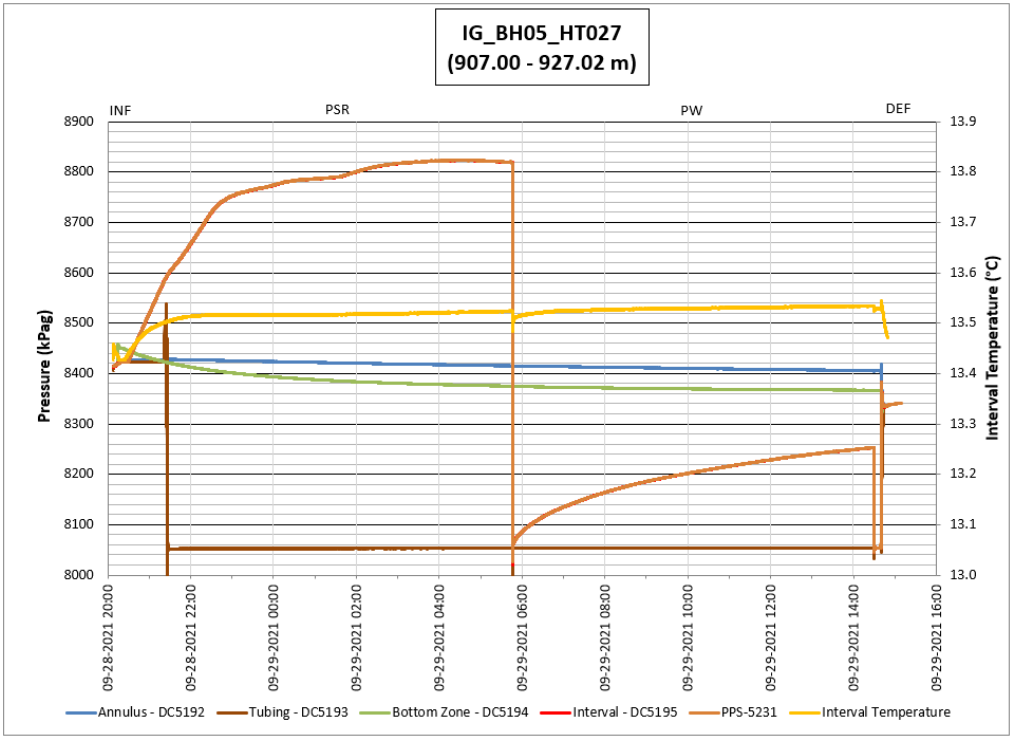
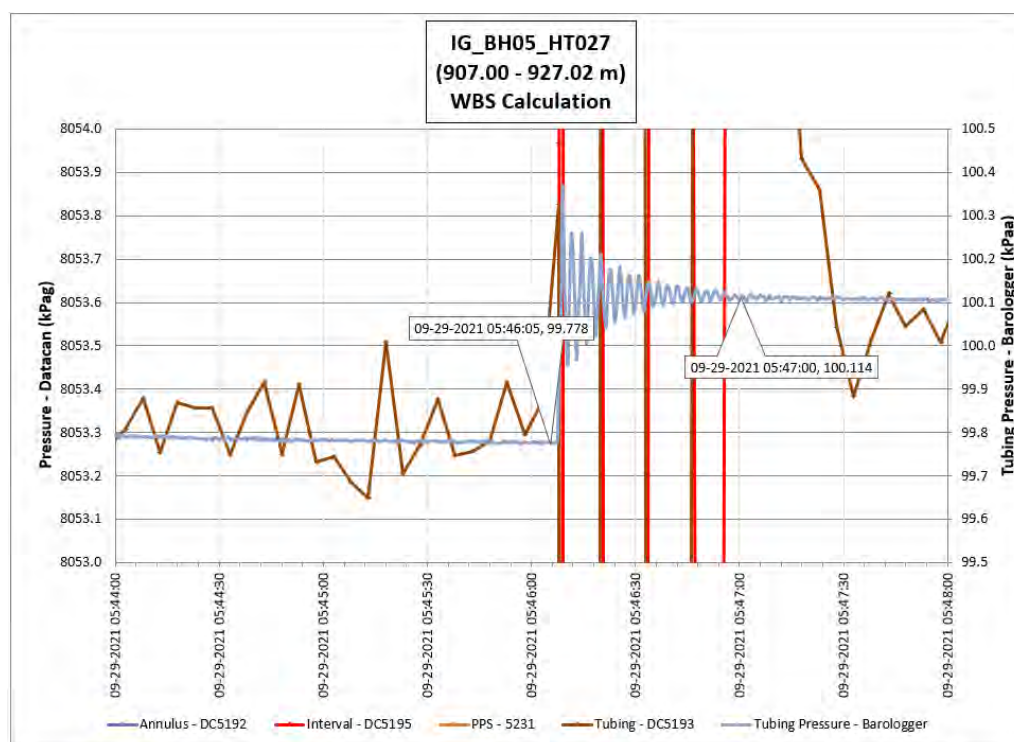


Figure 313: HT027 Annotated test plot showing monitored zone pressure and interval temperature.



**Figure 314: HT027 Tubing pressure during DHSIV activation. DHSIV Closed Wellbore Storage Estimate =  $8\text{E-}11 \text{ m}^3/\text{Pa}$**

**Table 27: Summary of Analysis Results – HT027**

	Formation conductivity	Skin zone conductivity	Static formation pressure	Formation specific storage	Radial thickness of skin	Flow dimension
	[m/s]	[m/s]	[kPa]	[1/m]	[m]	[–]
Best Fit	1E-13	9E-15	8558	7E-07	1.1E-03	1.2
Minimum	1E-15	9E-15	8355	1E-09	1E-03	1.2
Maximum	5E-12	9E-13	8900	1E-05	1E+00	3.0
Mean	1E-12	2E-13	8722	2E-06	3E-01	2.1
Median	7E-14	1E-13	8722	1E-07	1E-01	2.0
Geometric mean	1E-13	2E-13	8721	1E-07	2E-01	2.0

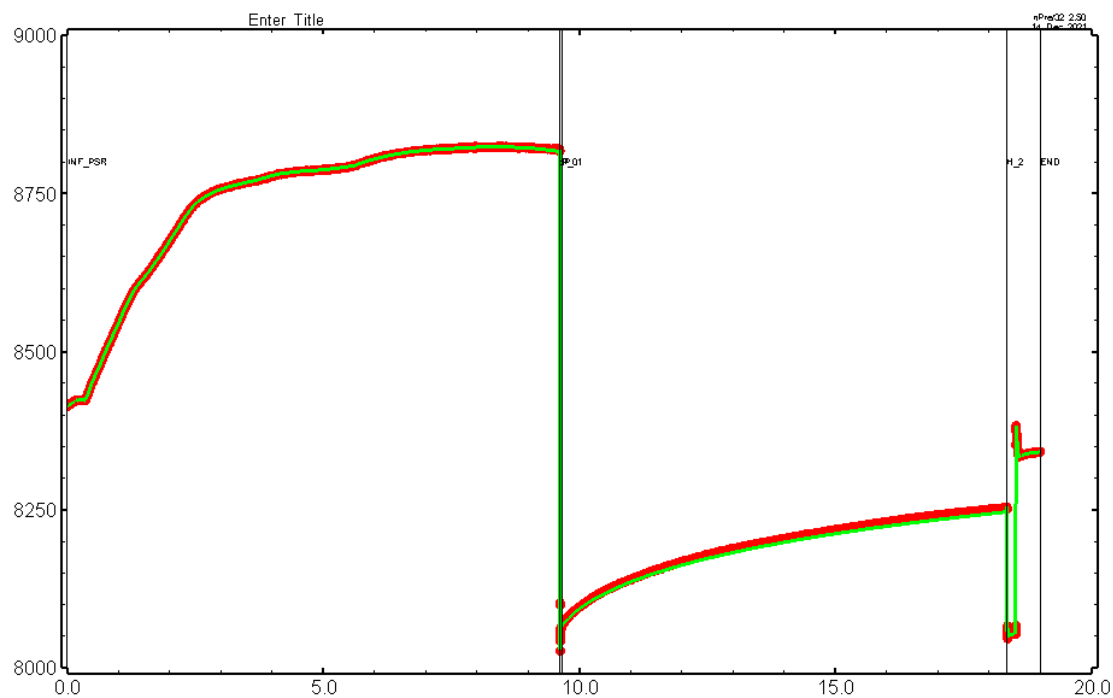


Figure 315: HT027 Pressure plot showing best-fit simulation and best fit results

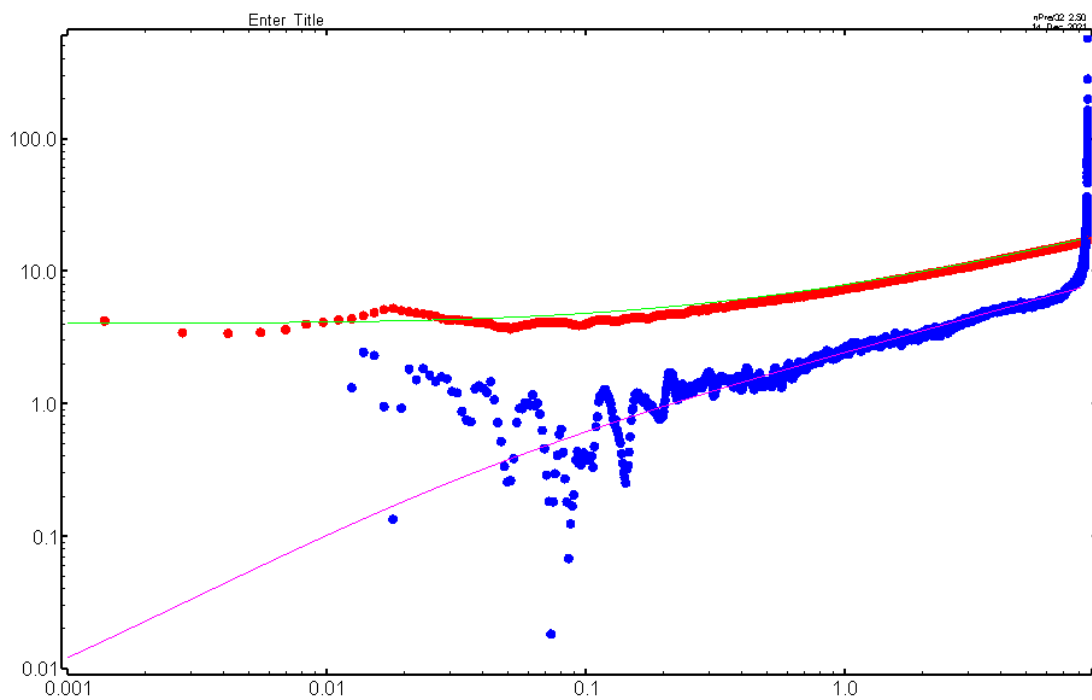


Figure 316: HT027 Deconvolved pressure change and derivative plot of the PW sequence showing best-fit simulation

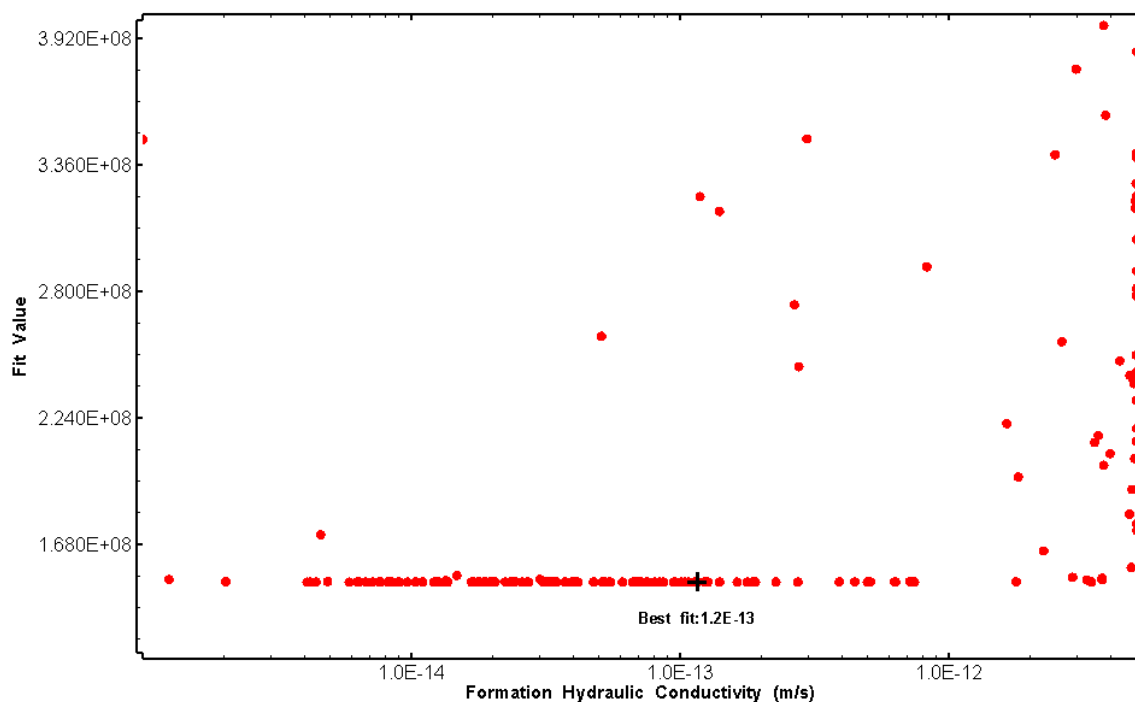


Figure 317: HT027 XY-scatter plot of formation hydraulic conductivity vs. fit value

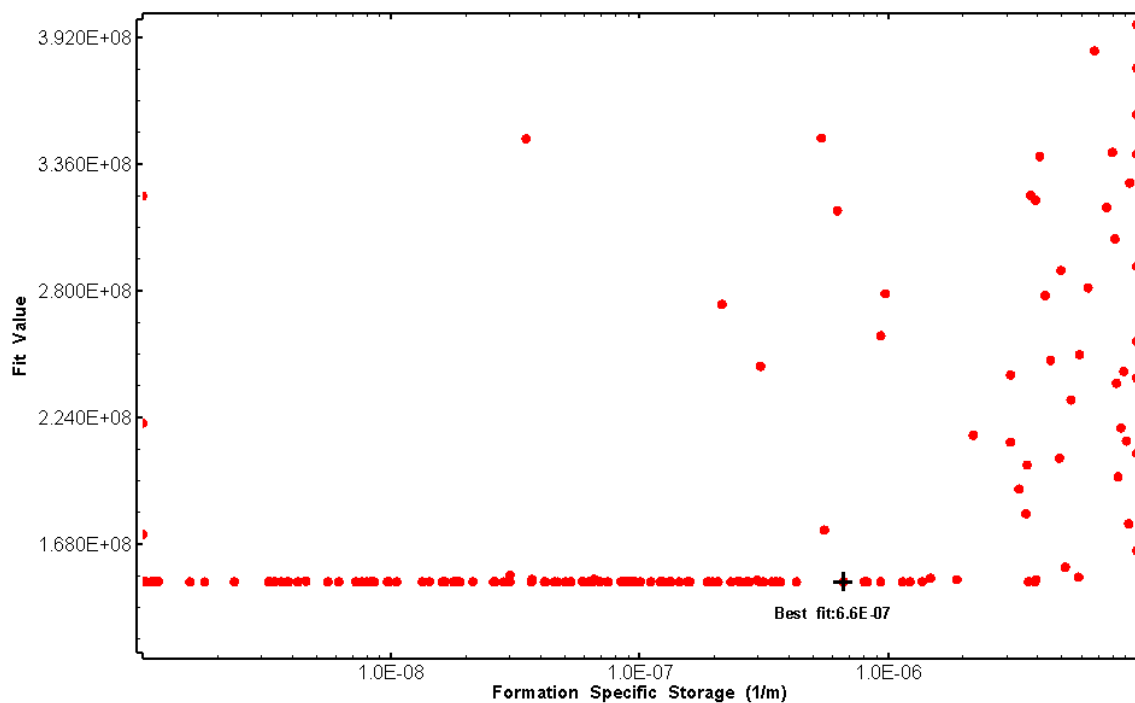


Figure 318: HT027 XY-scatter plot of formation specific storage vs. fit value

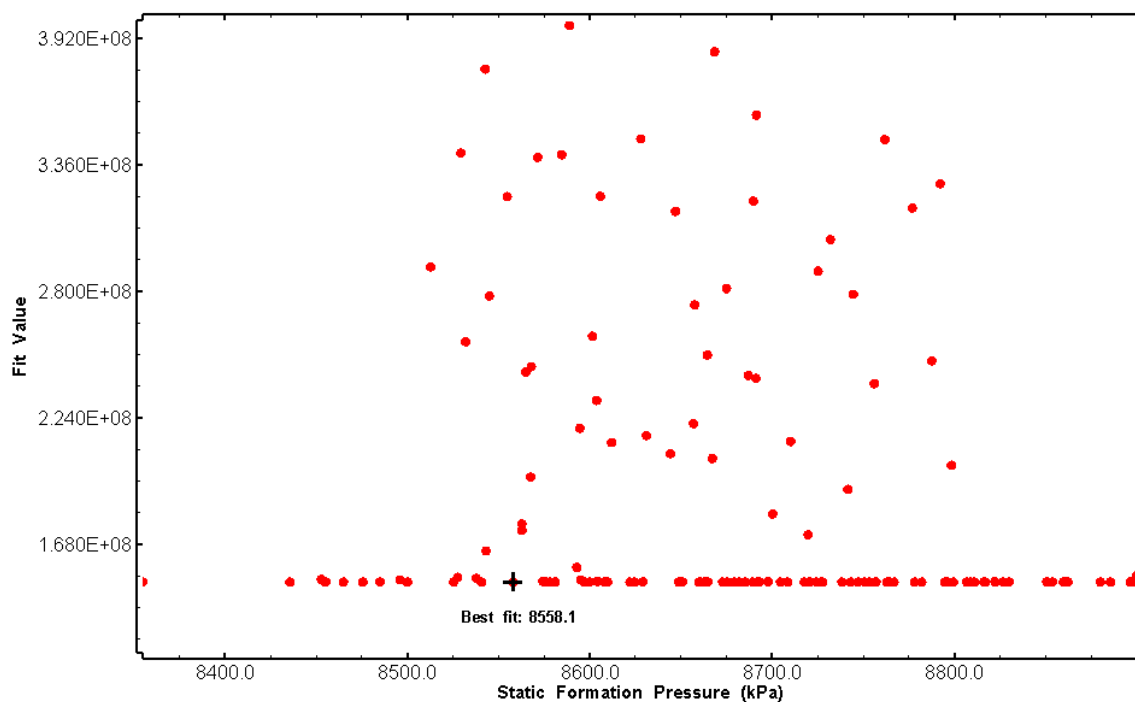


Figure 319: HT027 XY-scatter plot of static formation pressure vs. fit value

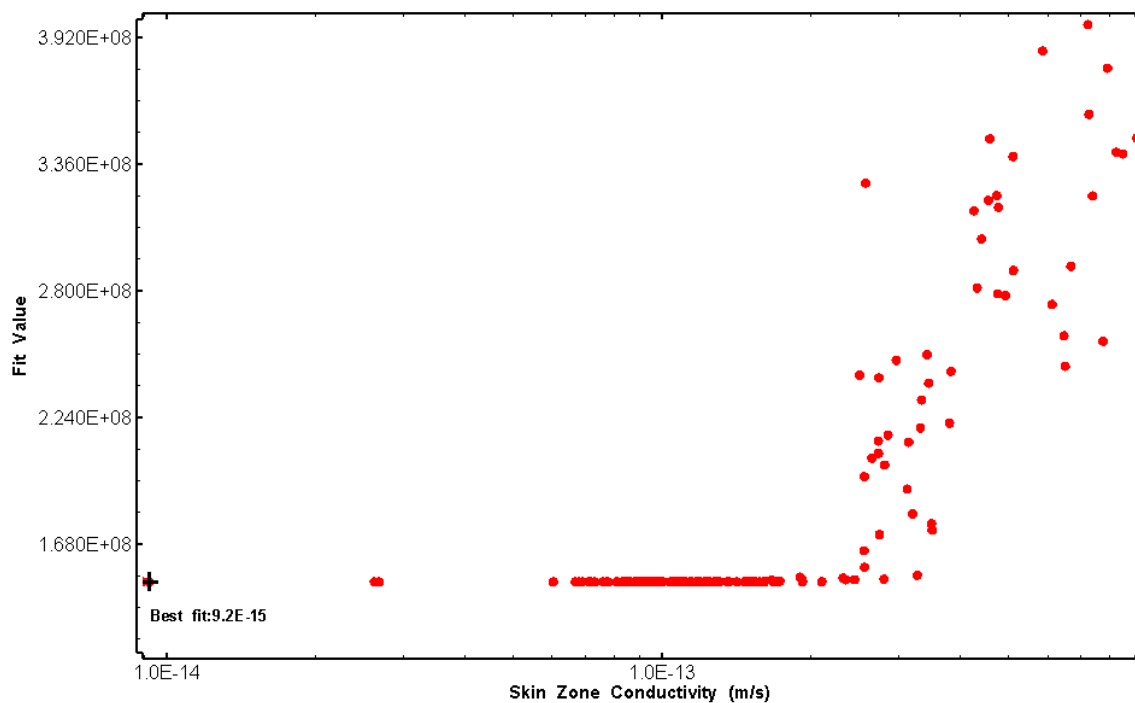


Figure 320: HT027 XY-scatter plot of skin zone conductivity vs. fit value

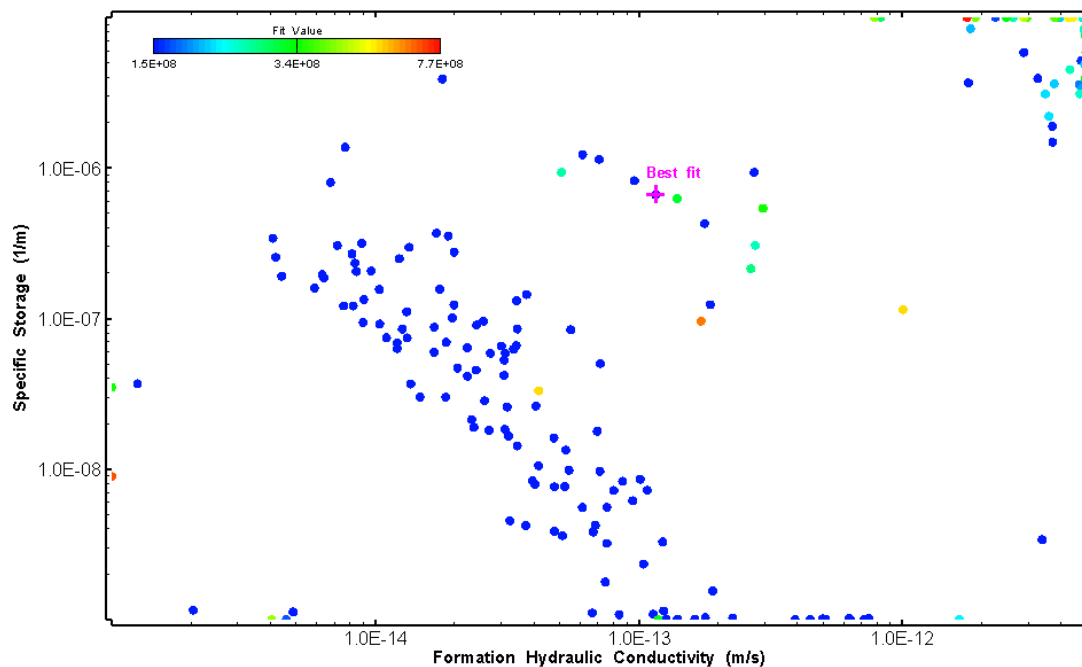


Figure 321: HT027 XY-scatter plot showing estimates of formation hydraulic conductivity and specific storage from perturbation analysis

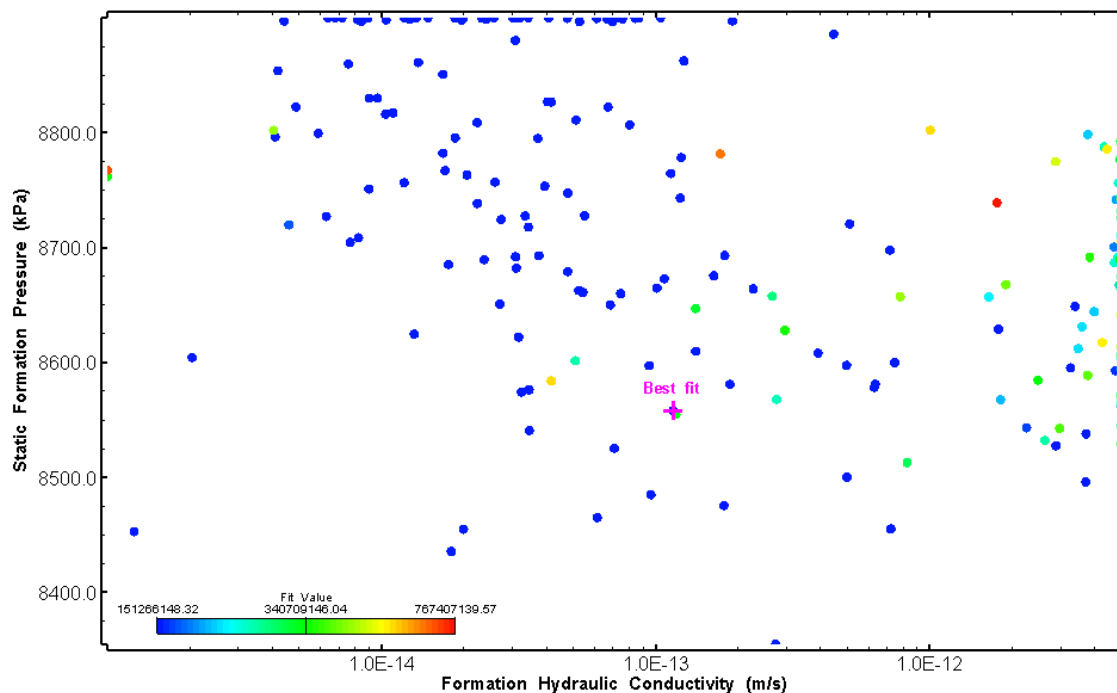


Figure 322: HT027 XY-scatter plot showing estimates of formation hydraulic conductivity and static formation pressure from perturbation analysis



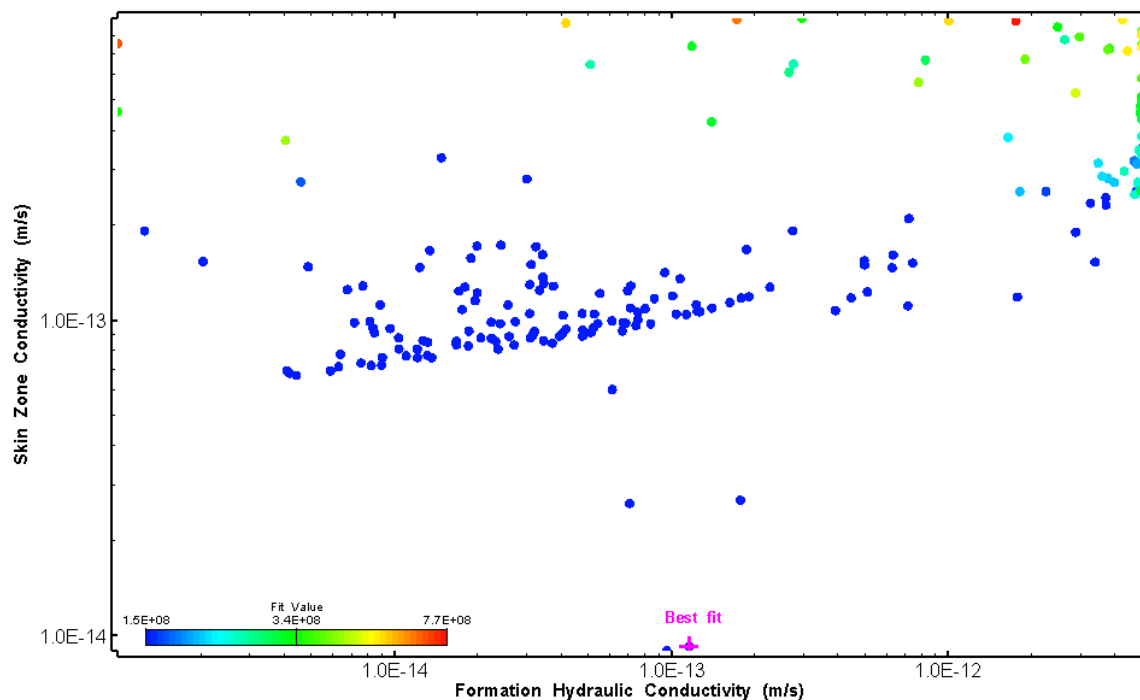


Figure 323: HT027 XY-scatter plot showing estimates of formation hydraulic conductivity and skin zone conductivity from perturbation analysis

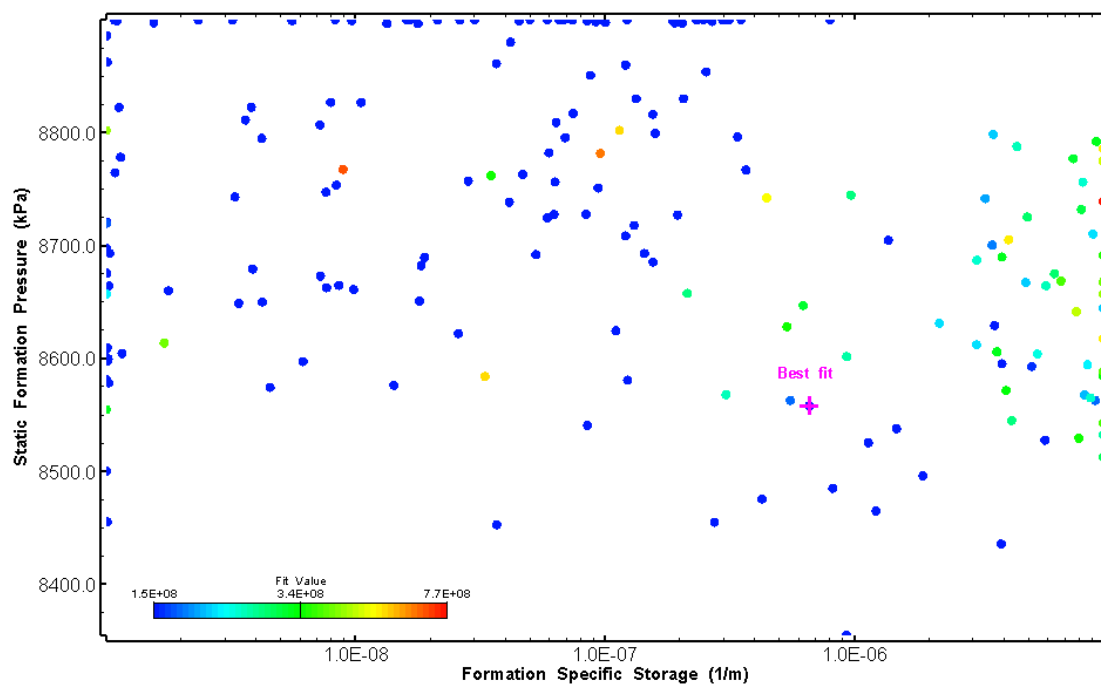


Figure 324: HT027 XY-scatter plot showing estimates of specific storage and static formation pressure from perturbation analysis

## 28.0 HT028 (924.00 – 944.02 M)

HT028 was selected to test a deep fractured interval. 15 broken fractures were observed in the core. No indication of flow was recorded during FFEC logging post-drilling.

The test was initiated with a shut-in pressure recovery phase (PSR). A pulse withdrawal test (PW) with a shut-in recovery was completed after the PSR phase.

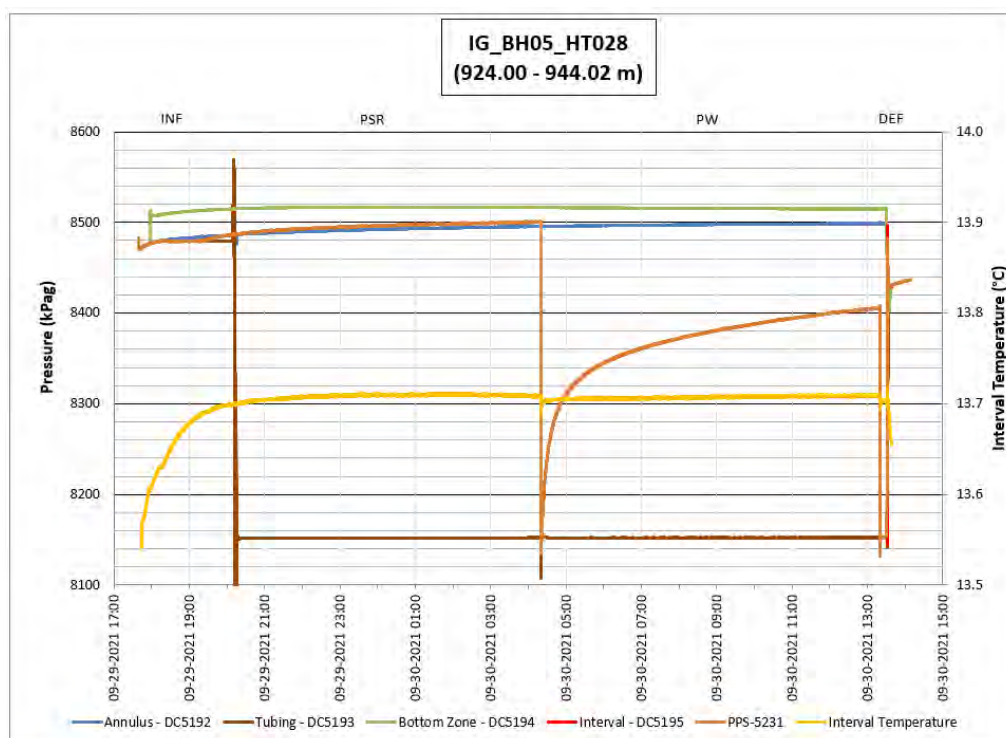
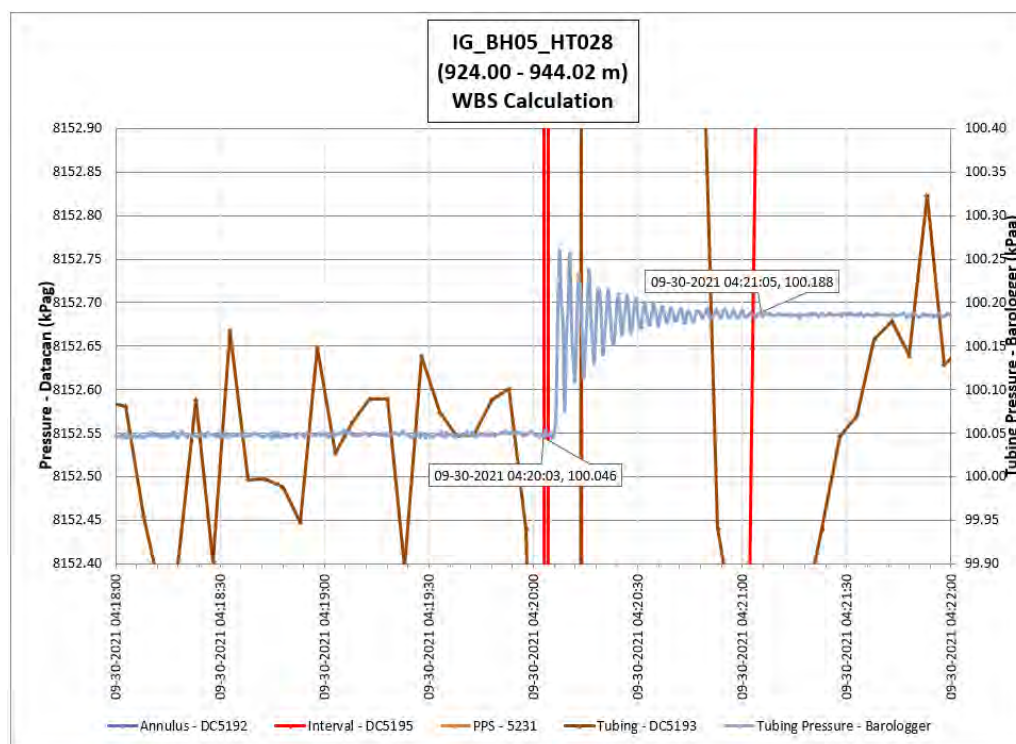


Figure 325: HT028 Annotated test plot showing monitored zone pressure and interval temperature.



**Figure 326: HT028 Tubing pressure during DHSIV activation. DHSIV Closed Wellbore Storage Estimate =  $7\text{E-}11 \text{ m}^3/\text{Pa}$**

**Table 27: Summary of Analysis Results – HT028**

	Formation conductivity	Skin zone conductivity	Static formation pressure	Formation specific storage	Radial thickness of skin	Flow dimension
	[m/s]	[m/s]	[kPa]	[1/m]	[m]	[–]
Best Fit	5E-14	3E-12	8476	2E-07	1.31E-01	2.6
Minimum	6E-15	4E-13	8400	1E-09	3E-02	1.1
Maximum	4E-12	5E-10	8550	1E-05	1E-00	2.7
Mean	2E-13	2E-11	8487	3E-07	2E-01	2.2
Median	9E-14	3E-12	8483	2E-07	2E-01	2.2
Geometric mean	1E-13	4E-12	8487	2E-07	2E-01	2.2

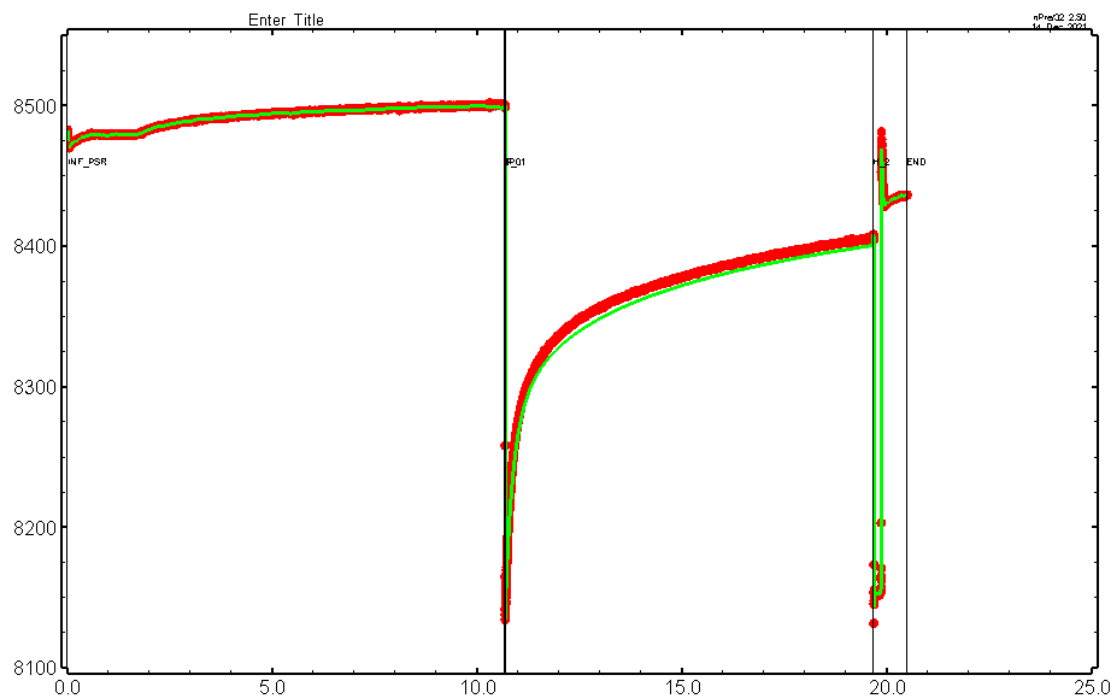


Figure 327: HT028 Pressure plot showing best-fit simulation and best fit results

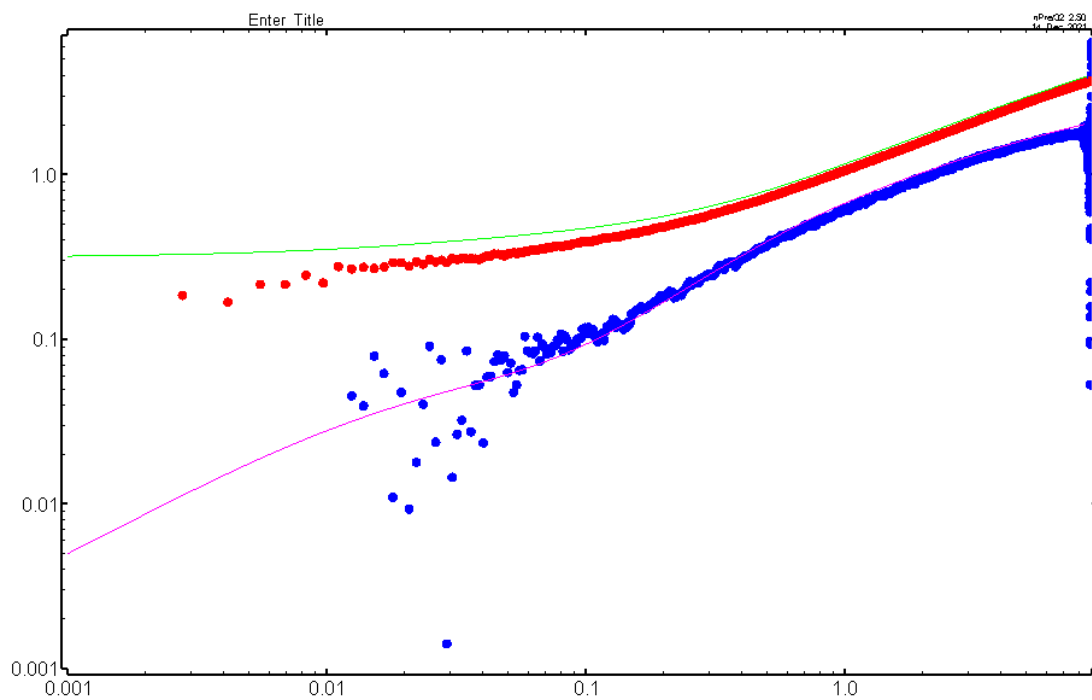


Figure 328: HT028 Deconvolved pressure change and derivative plot of the PW sequence showing best-fit simulation

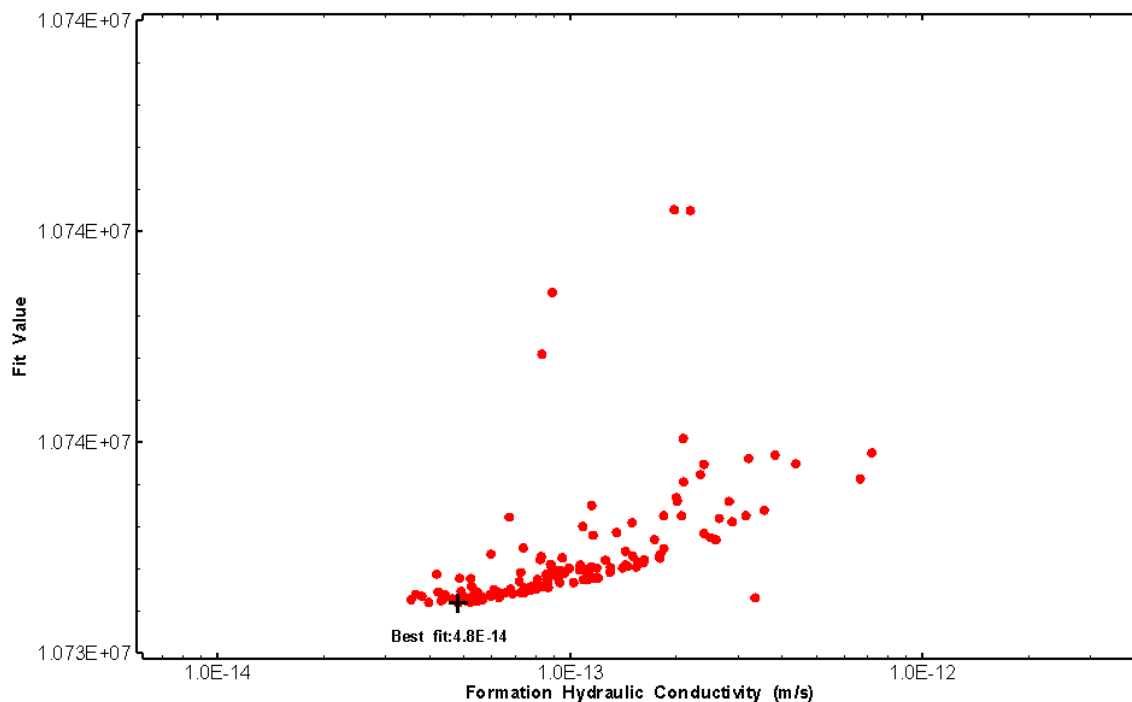


Figure 329: HT028 XY-scatter plot of formation hydraulic conductivity vs. fit value

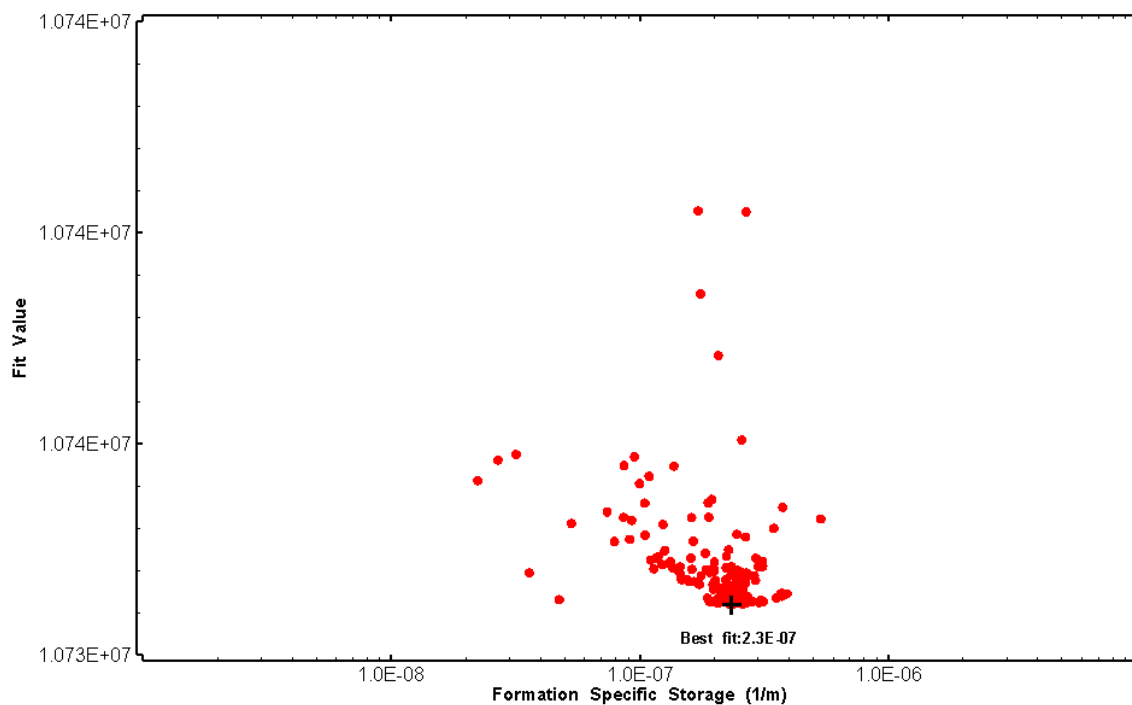


Figure 330: HT028 XY-scatter plot of formation specific storage vs. fit value

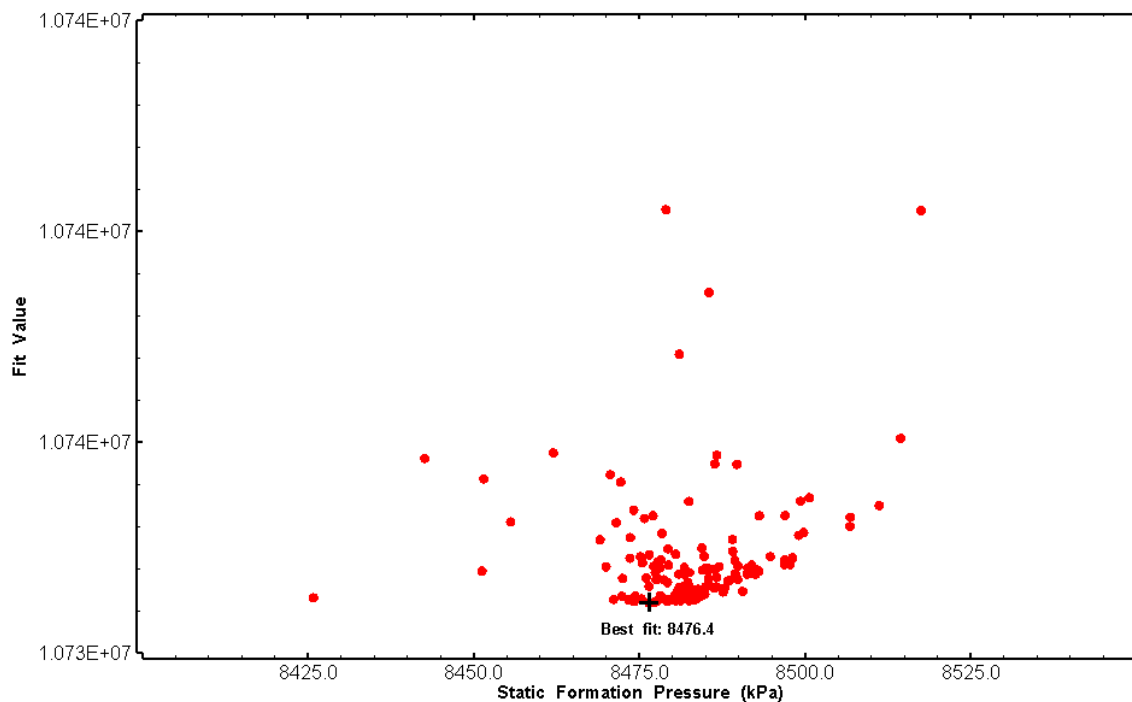


Figure 331: HT028 XY-scatter plot of static formation pressure vs. fit value

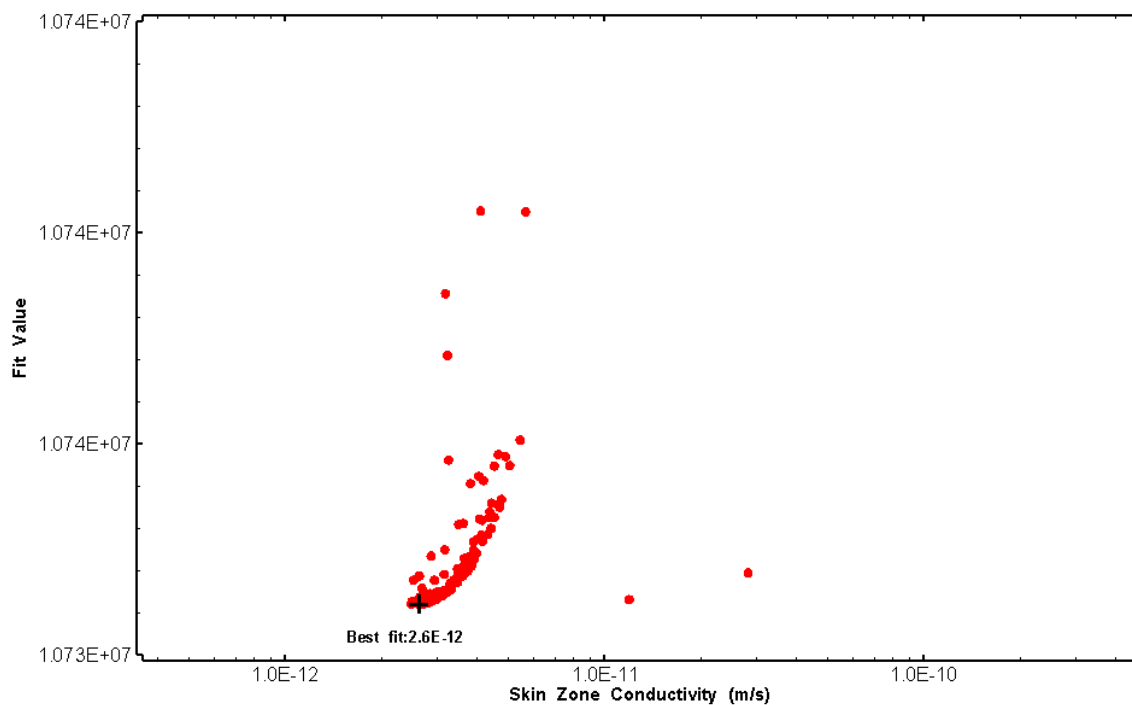


Figure 332: HT028 XY-scatter plot of skin zone conductivity vs. fit value

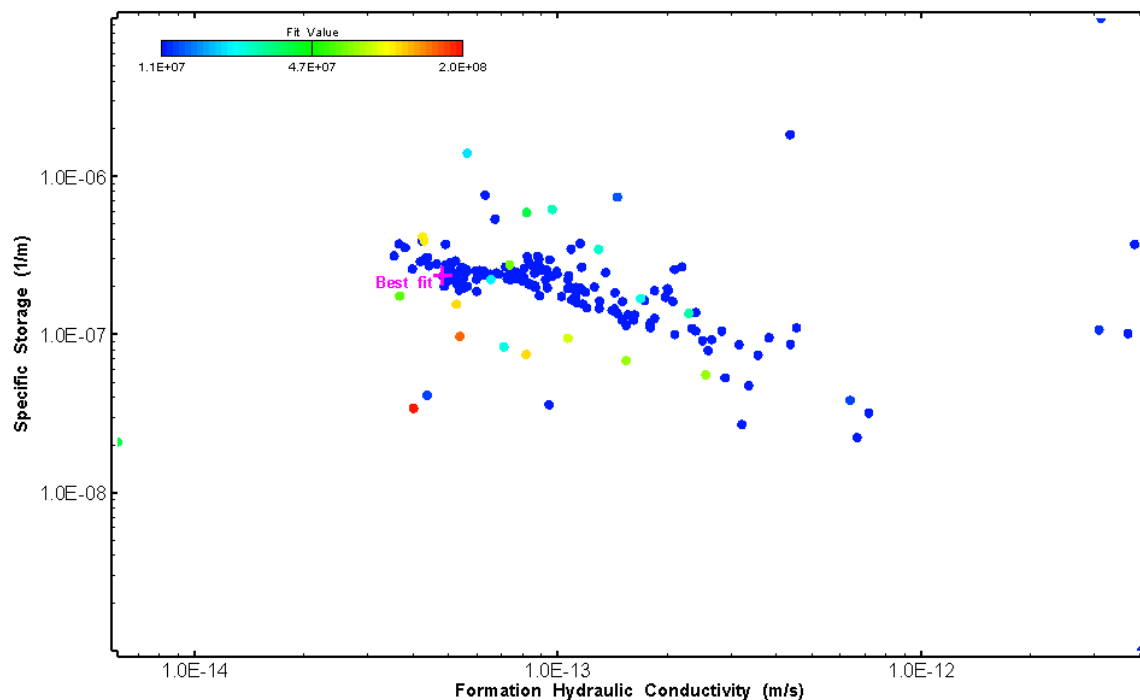


Figure 333: HT028 XY-scatter plot showing estimates of formation hydraulic conductivity and specific storage from perturbation analysis

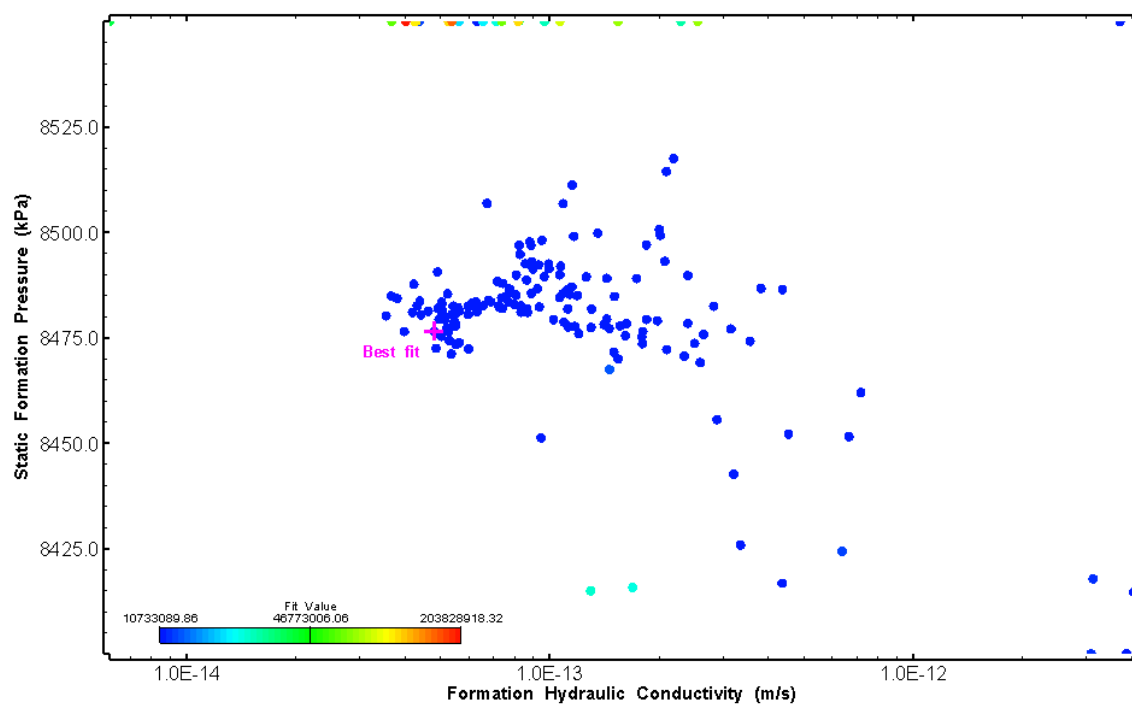


Figure 334: HT028 XY-scatter plot showing estimates of formation hydraulic conductivity and static formation pressure from perturbation analysis

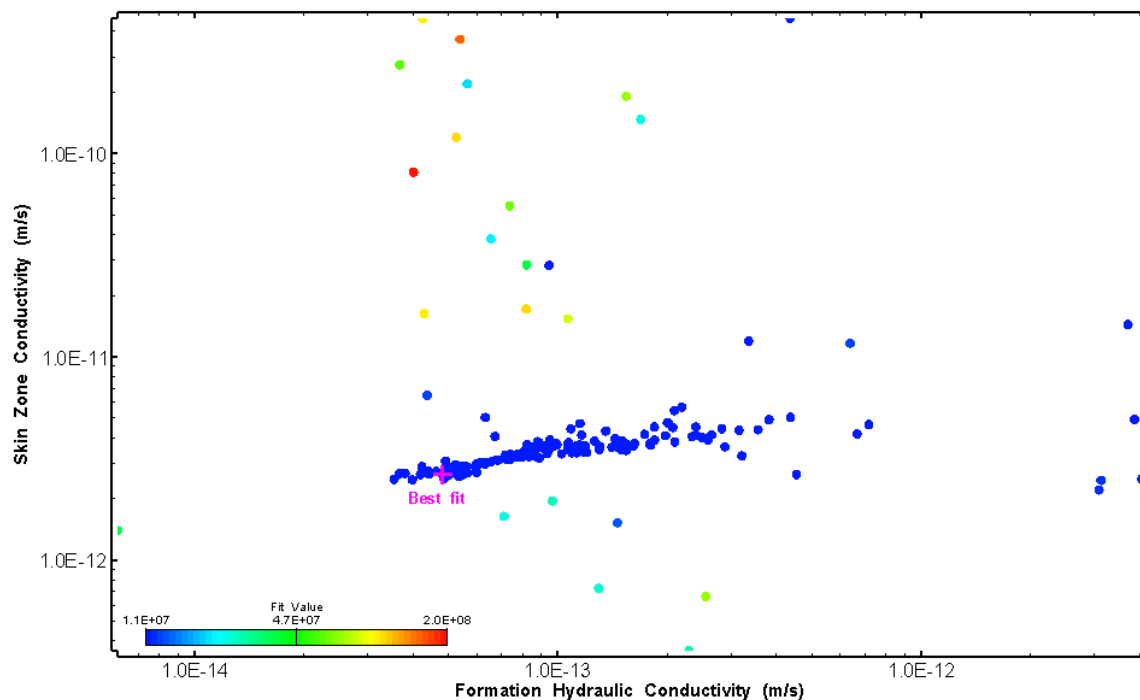


Figure 335: HT028 XY-scatter plot showing estimates of formation hydraulic conductivity and skin zone conductivity from perturbation analysis

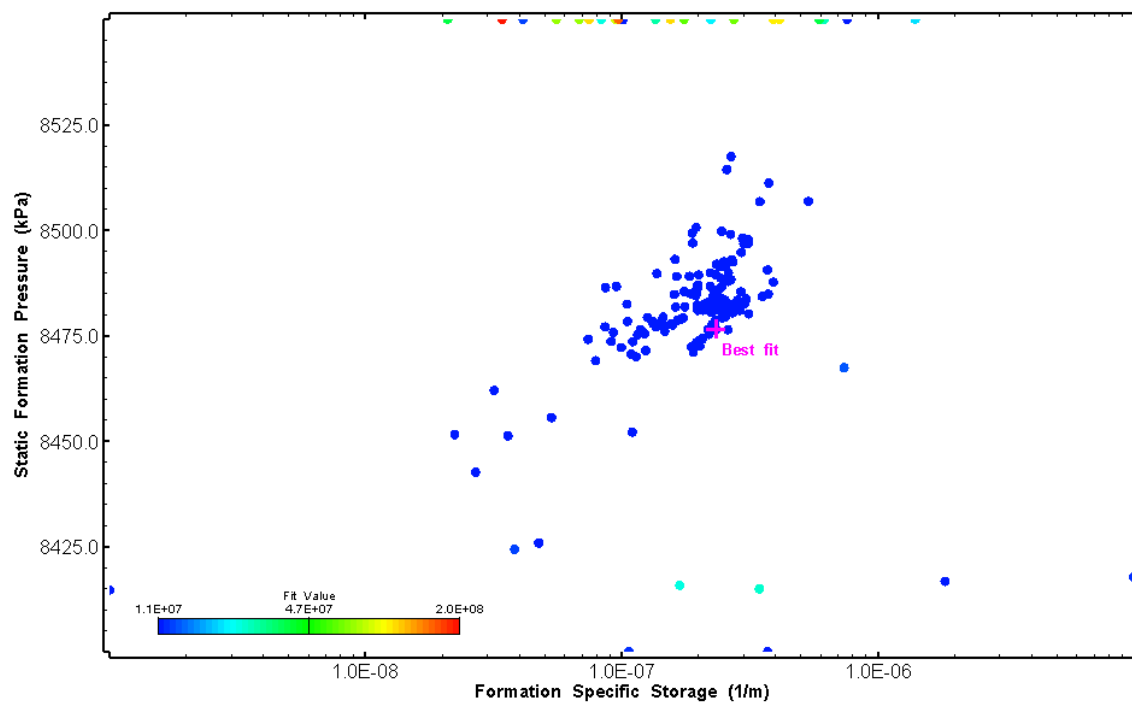


Figure 336: HT028 XY-scatter plot showing estimates of specific storage and static formation pressure from perturbation analysis



## 29.0 HT029 (945.00 – 965.02 M)

HT029 was selected to test a deep fractured interval. 18 broken fractures were observed in the core. No indication of flow was recorded during FFEC logging post-drilling.

The test was initiated with a shut-in pressure recovery phase (PSR). A pulse withdrawal test (PW) with a shut-in recovery was completed after the PSR phase.

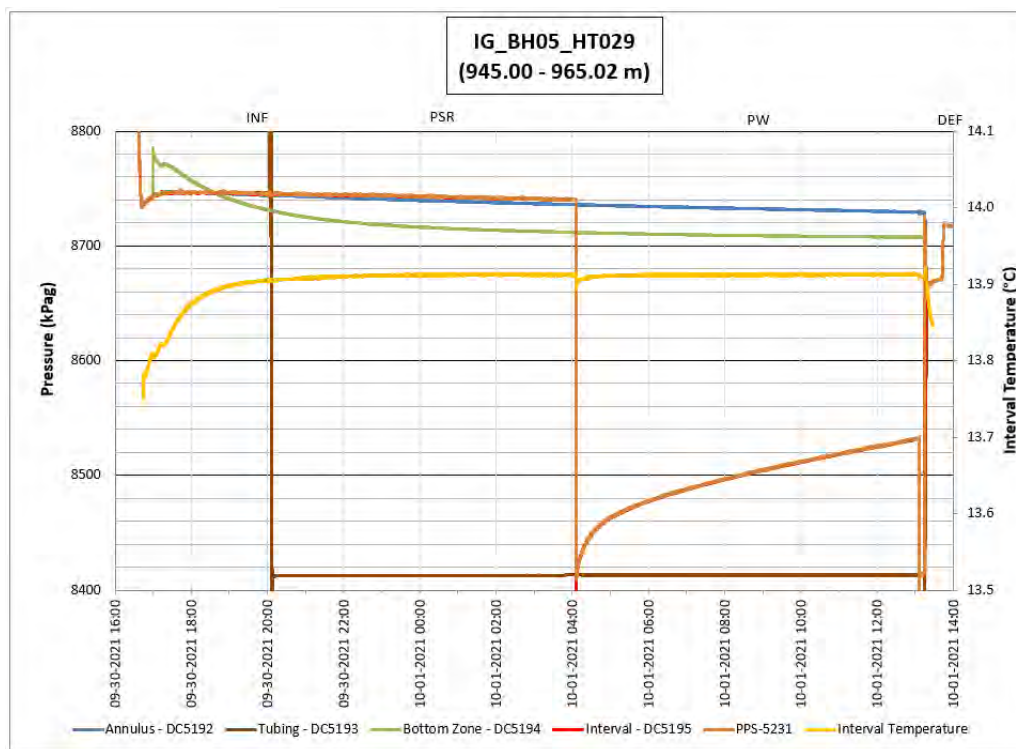


Figure 337: HT029 Annotated test plot showing monitored zone pressure and interval temperature.

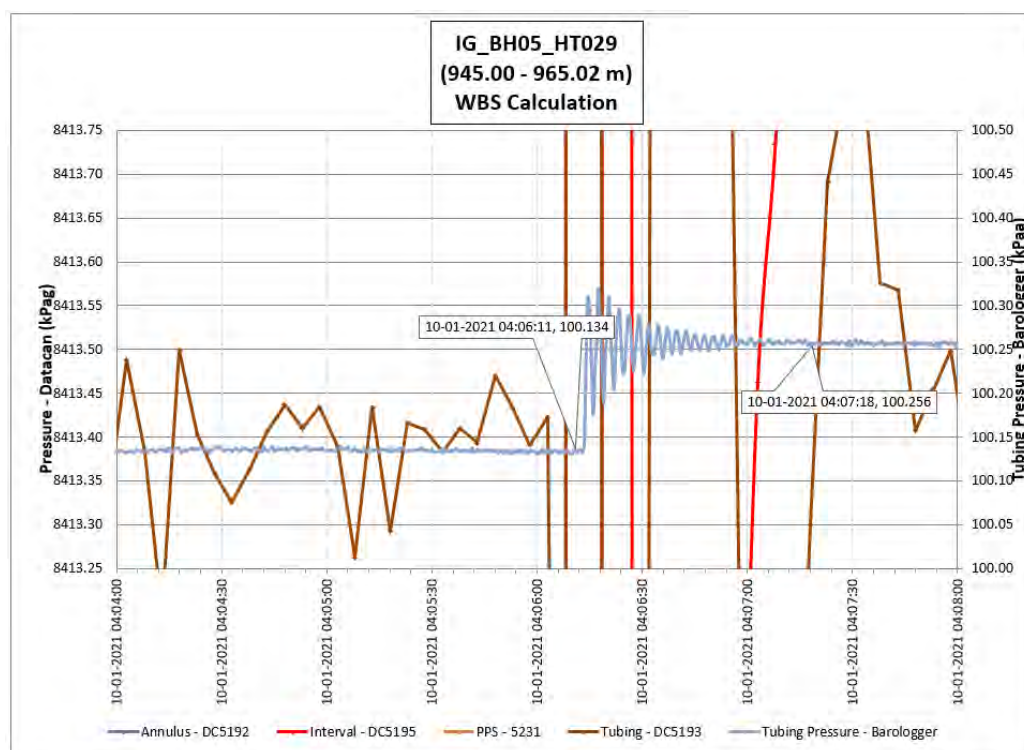


Figure 338: HT029 Tubing pressure during DHSIV activation. DHSIV Closed Wellbore Storage Estimate =  $7\text{E-}11 \text{ m}^3/\text{Pa}$

Table 27: Summary of Analysis Results – HT029

	Formation conductivity	Skin zone conductivity	Static formation pressure	Formation specific storage	Radial thickness of skin	Flow dimension
	[m/s]	[m/s]	[kPa]	[1/m]	[m]	[–]
Best Fit	4E-14	3E-13	8747	2E-08	6.08E-02	2.5
Minimum	1E-15	7E-14	8560	1E-09	1E-03	1.0
Maximum	1E-11	1E-10	8750	1E-05	1E+00	2.6
Mean	8E-13	1E-12	8713	7E-07	1E-01	1.9
Median	1E-13	4E-13	8749	5E-08	7E-02	1.9
Geometric mean	1E-13	4E-13	8713	4E-08	8E-02	1.9

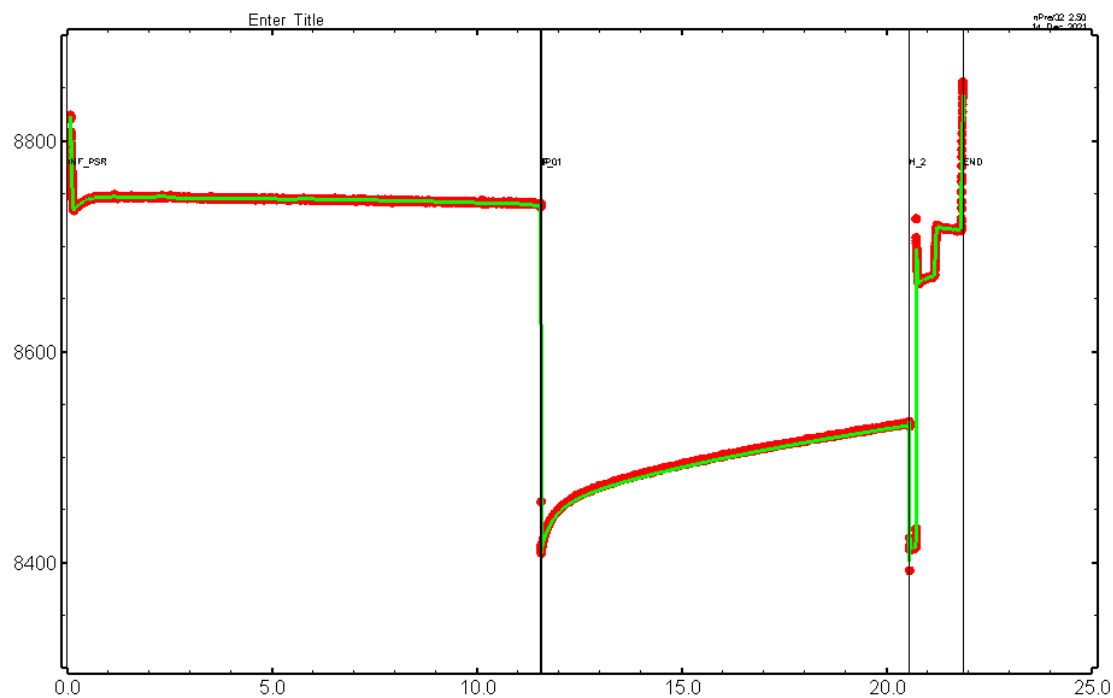


Figure 339: HT029 Pressure plot showing best-fit simulation and best fit results

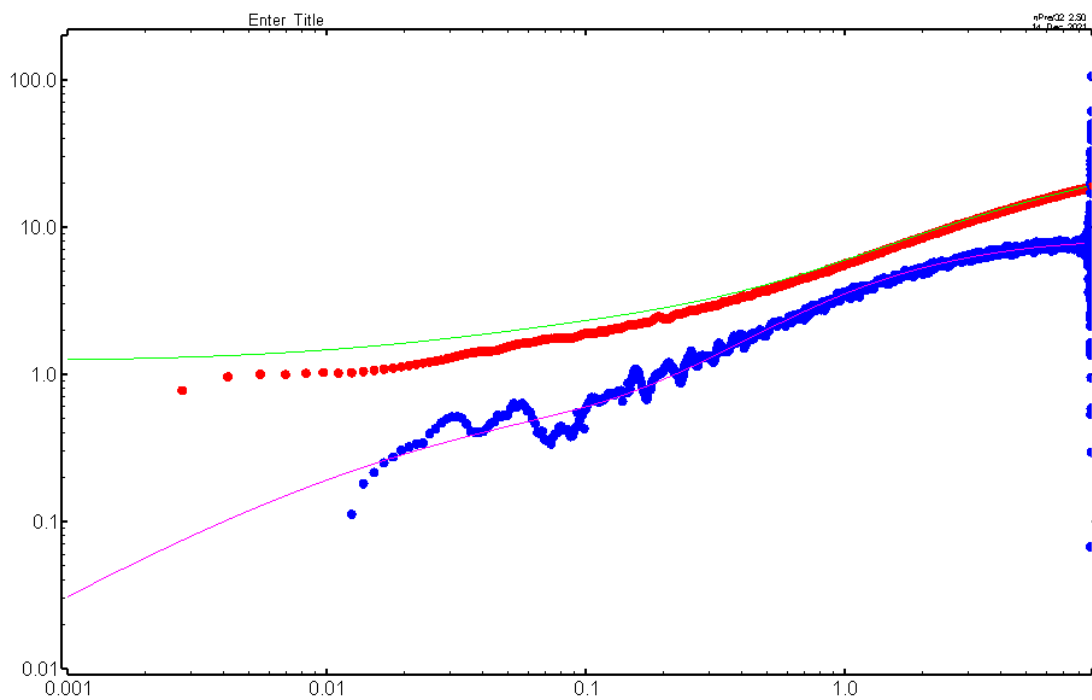


Figure 340: HT029 Deconvolved pressure change and derivative plot of the PW sequence showing best-fit simulation

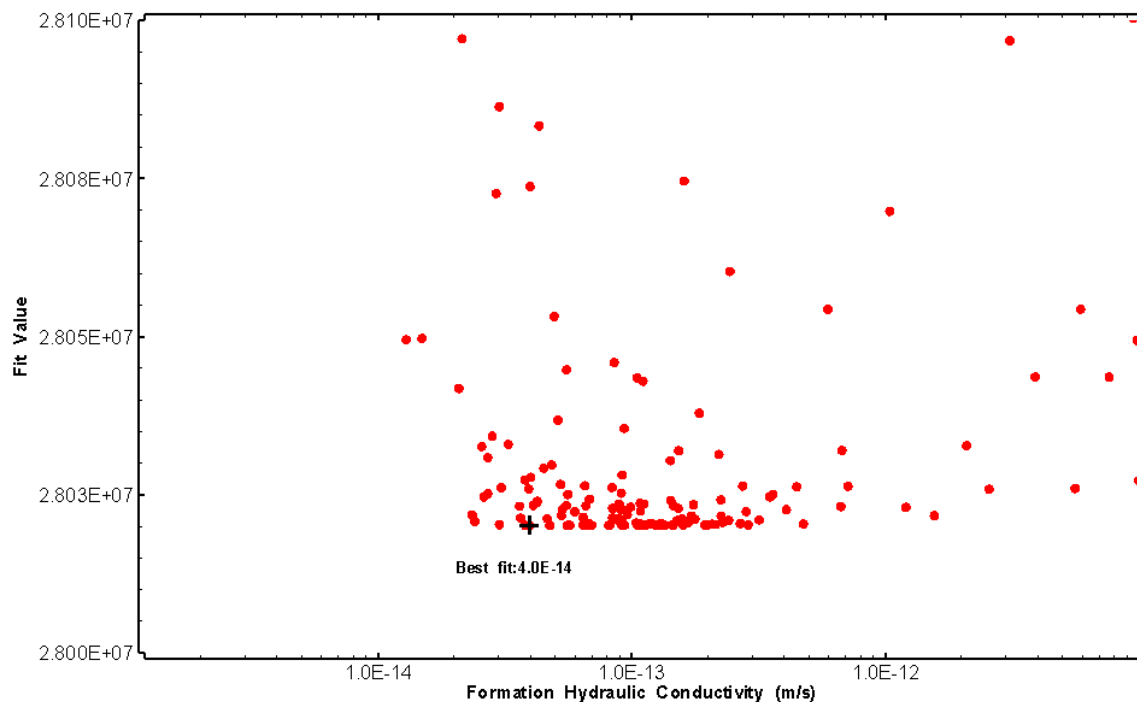


Figure 341: HT029 XY-scatter plot of formation hydraulic conductivity vs. fit value

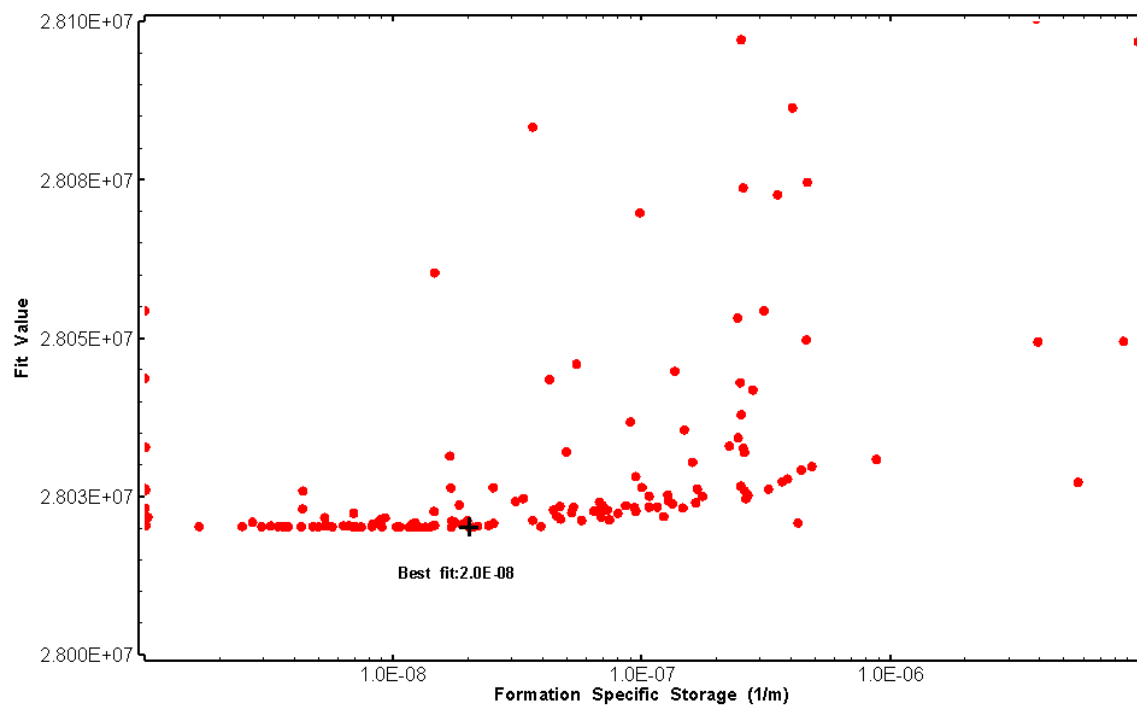


Figure 342: HT029 XY-scatter plot of formation specific storage vs. fit value

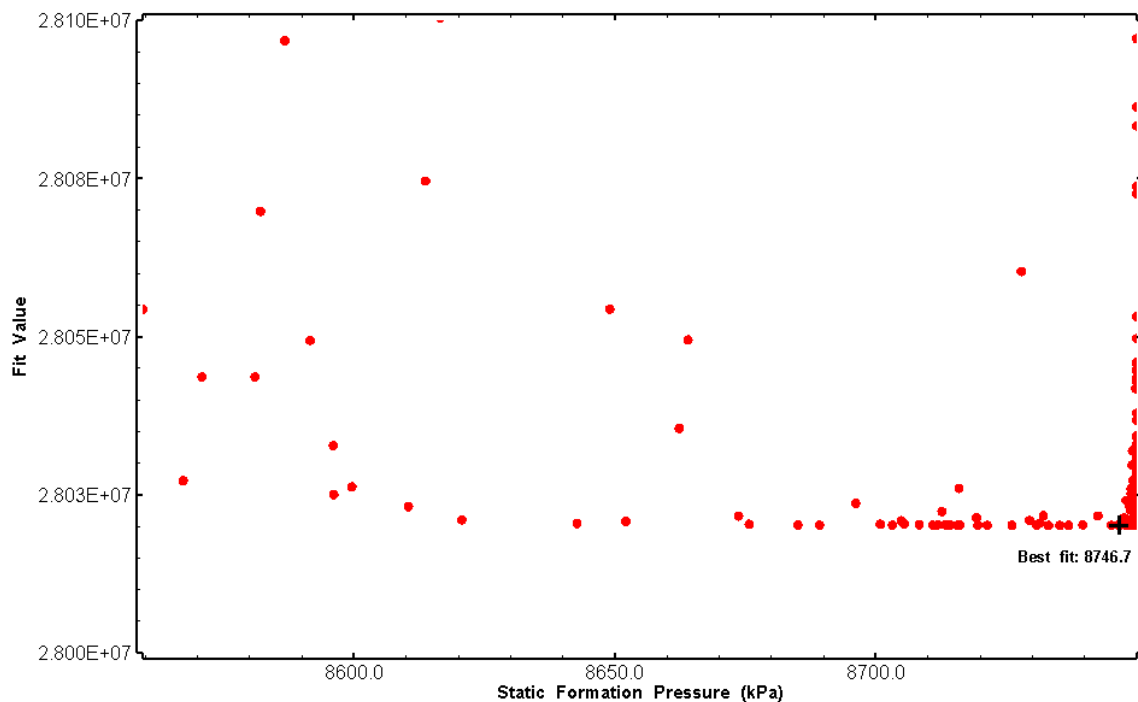


Figure 343: HT029 XY-scatter plot of static formation pressure vs. fit value

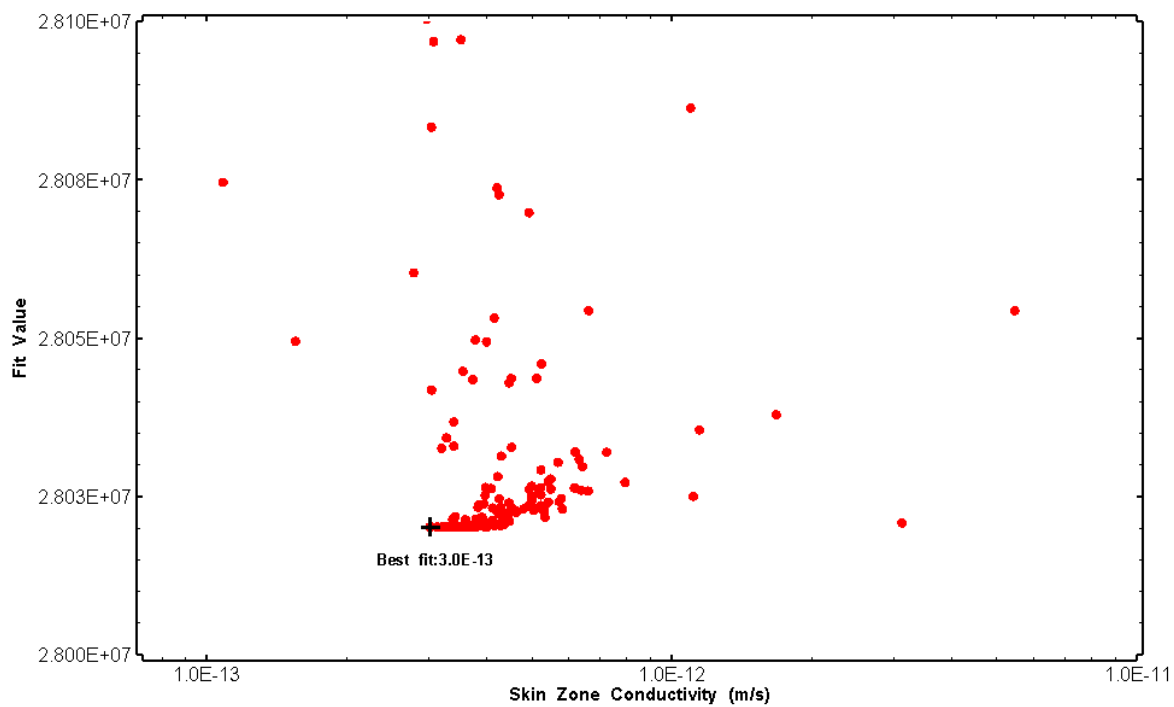


Figure 344: HT029 XY-scatter plot of skin zone conductivity vs. fit value

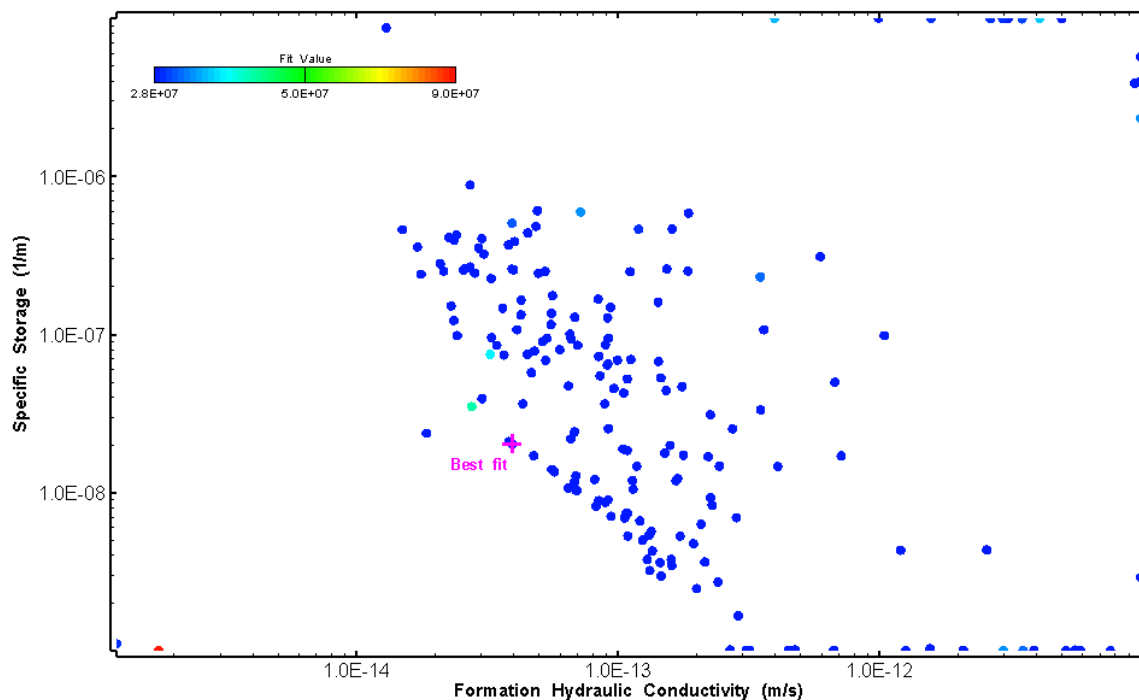


Figure 345: HT029 XY-scatter plot showing estimates of formation hydraulic conductivity and specific storage from perturbation analysis

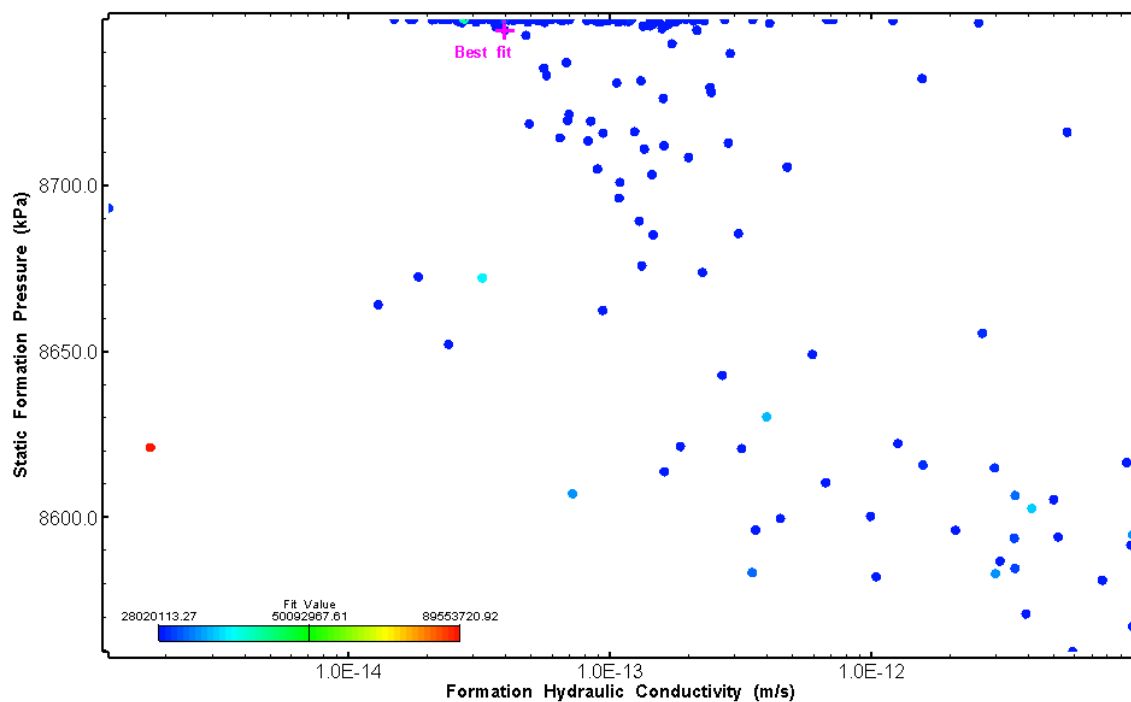


Figure 346: HT029 XY-scatter plot showing estimates of formation hydraulic conductivity and static formation pressure from perturbation analysis

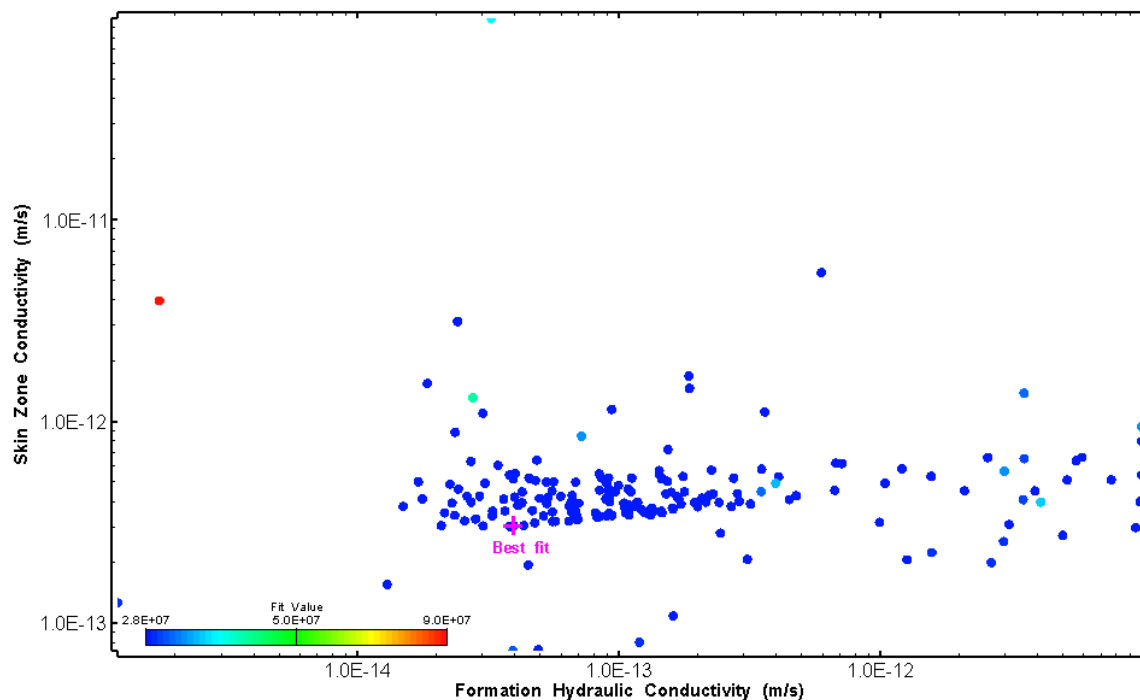


Figure 347: HT029 XY-scatter plot showing estimates of formation hydraulic conductivity and skin zone conductivity from perturbation analysis

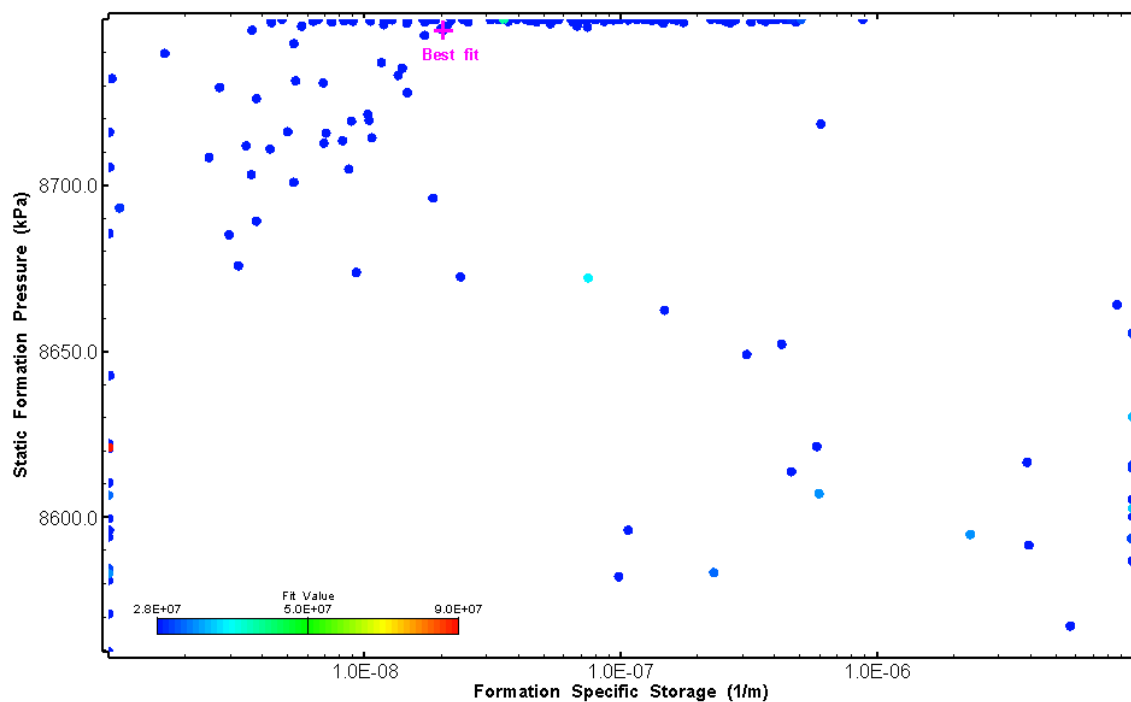


Figure 348: HT029 XY-scatter plot showing estimates of specific storage and static formation pressure from perturbation analysis

### 30.0 HT030 (967.00 – 987.02 M)

HT030 was selected to test a deep fractured interval containing dykes. 25 broken fractures were observed in the core. No indication of flow was recorded during FFEC logging post-drilling.

The test was initiated with a shut-in pressure recovery phase (PSR). A pulse withdrawal test (PW) with a shut-in recovery was completed after the PSR phase.

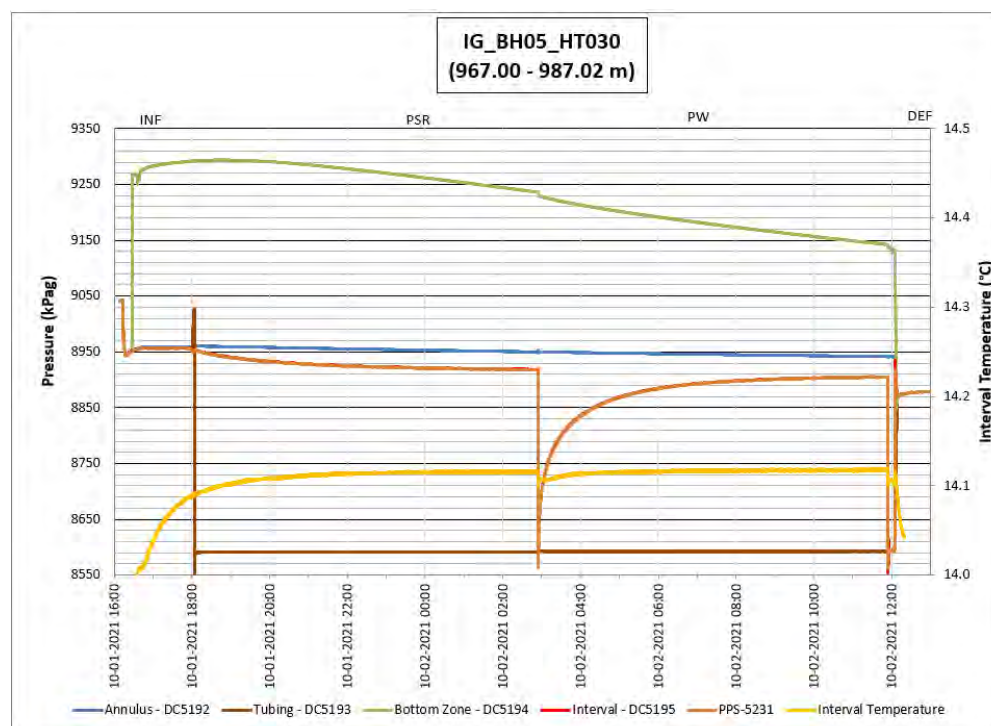
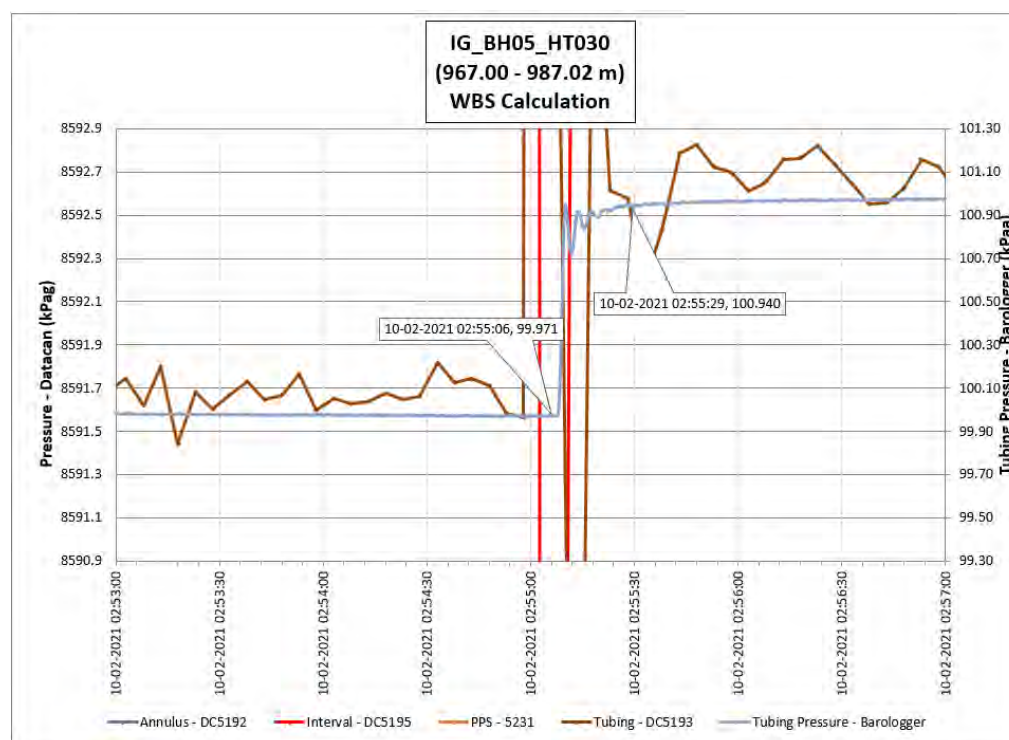


Figure 349: HT030 Annotated test plot showing monitored zone pressure and interval temperature.





**Figure 350: HT030 Tubing pressure during DHSIV activation. DHSIV Closed Wellbore Storage Estimate =  $5E-10 \text{ m}^3/\text{Pa}$**

**Table 27: Summary of Analysis Results – HT030**

	Formation conductivity	Skin zone conductivity	Static formation pressure	Formation specific storage	Radial thickness of skin	Flow dimension
	[m/s]	[m/s]	[kPa]	[1/m]	[m]	[–]
Best Fit	2E-12	1E-10	8911	2E-07	1.86E-01	3.0
Minimum	2E-12	7E-11	8888	1E-08	1E-03	1.5
Maximum	1E-10	1E-08	8950	9E-06	1E+00	3.0
Mean	3E-11	1E-09	8916	6E-07	3E-01	2.1
Median	2E-11	2E-10	8914	8E-08	3E-01	2.1
Geometric mean	2E-11	4E-10	8916	1E-07	2E-01	2.1

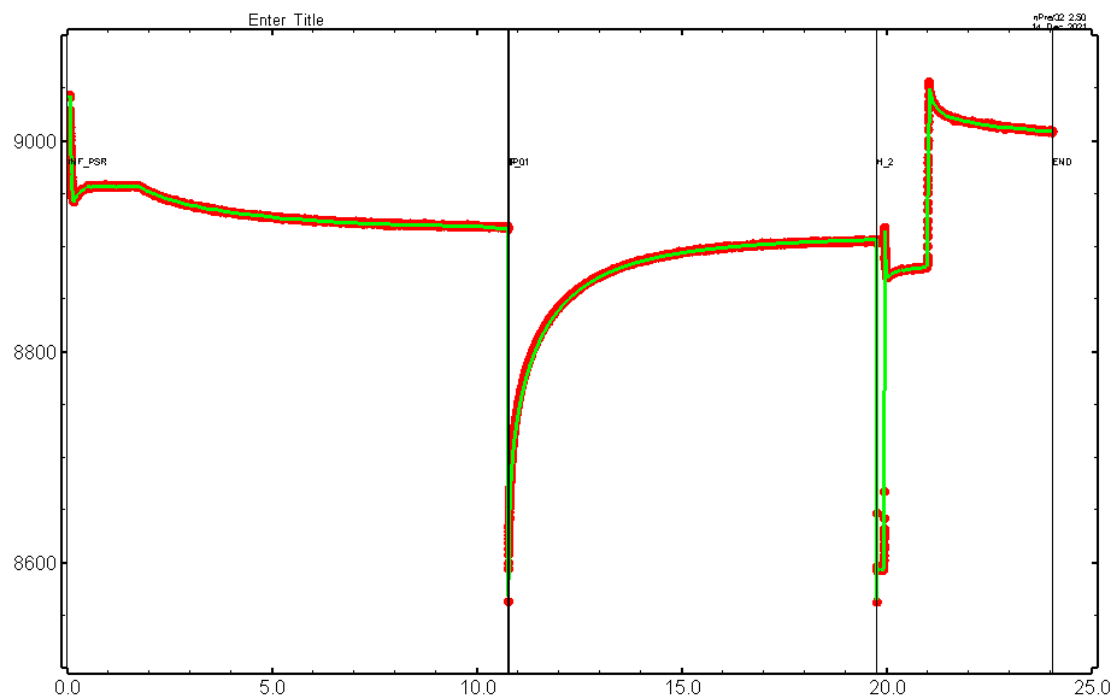


Figure 351: HT030 Pressure plot showing best-fit simulation and best fit results

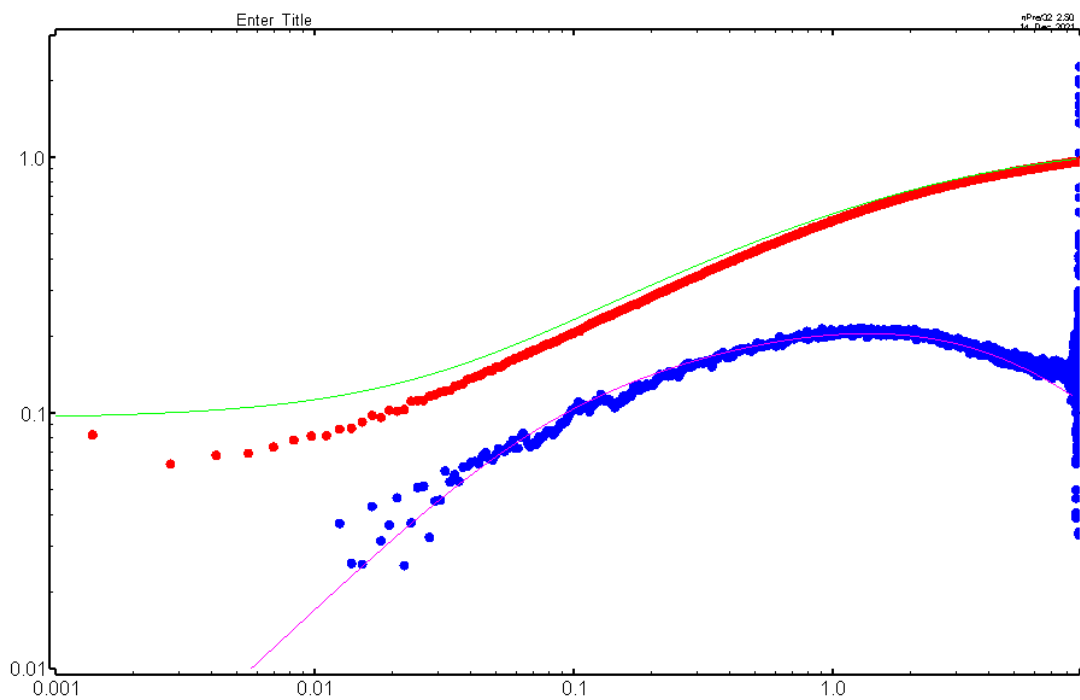


Figure 352: HT030 Deconvolved pressure change and derivative plot of the PW sequence showing best-fit simulation

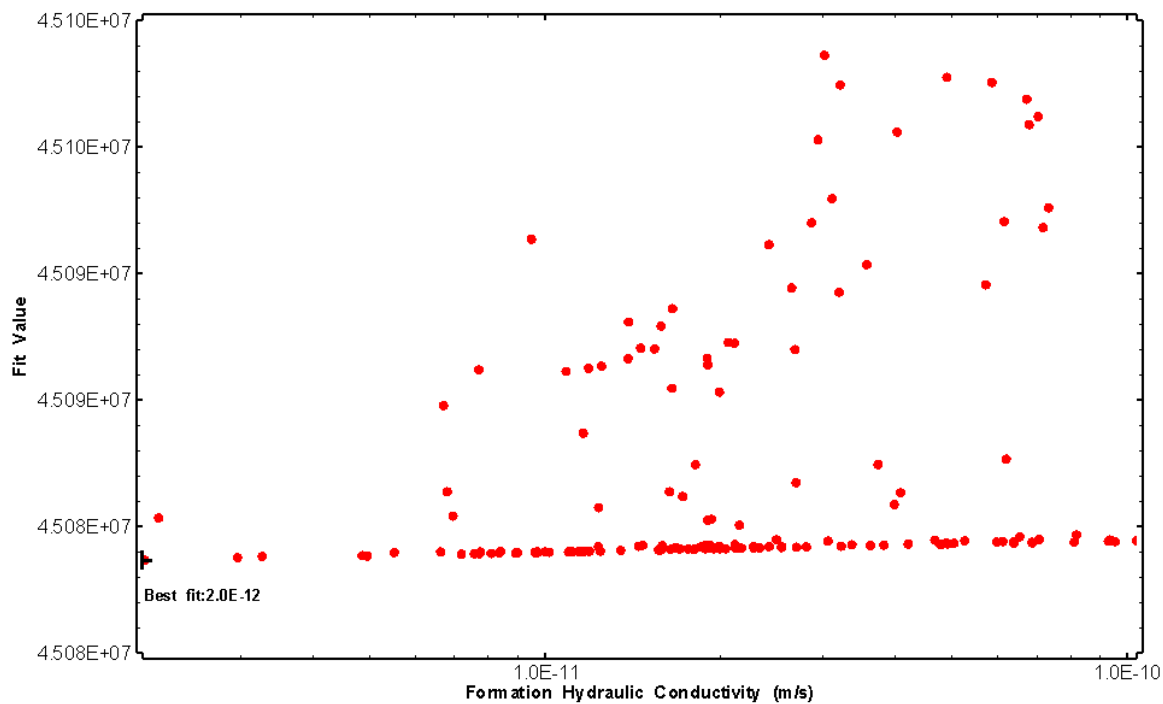


Figure 353: HT030 XY-scatter plot of formation hydraulic conductivity vs. fit value

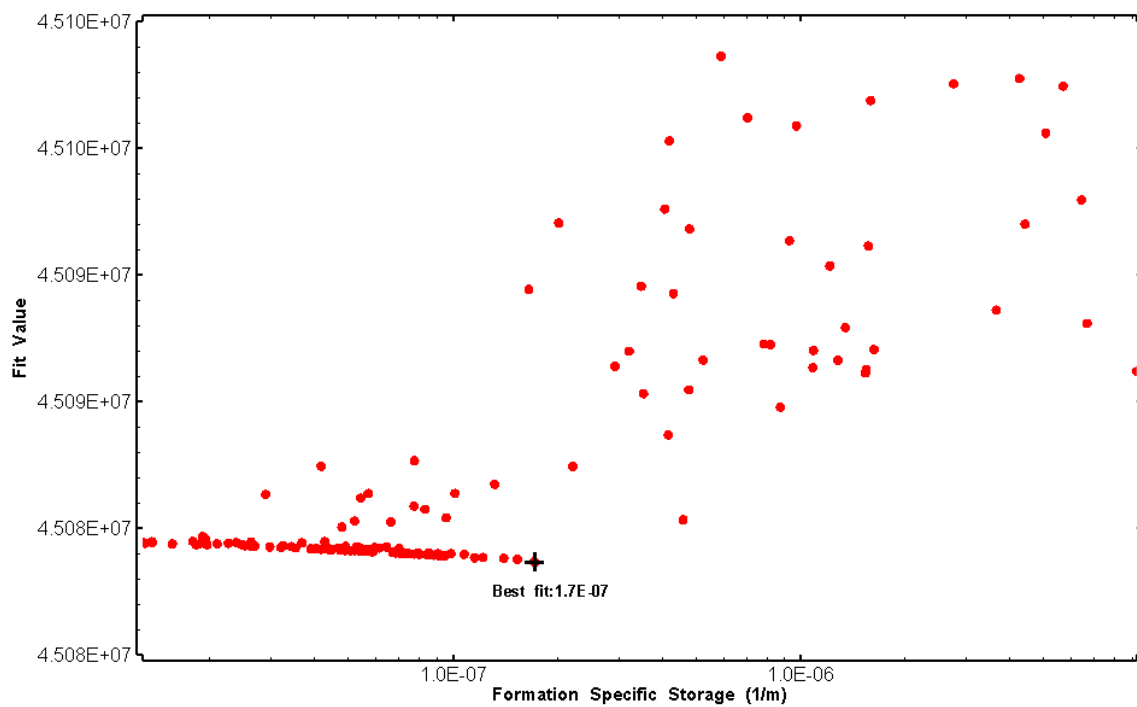


Figure 354: HT030 XY-scatter plot of formation specific storage vs. fit value

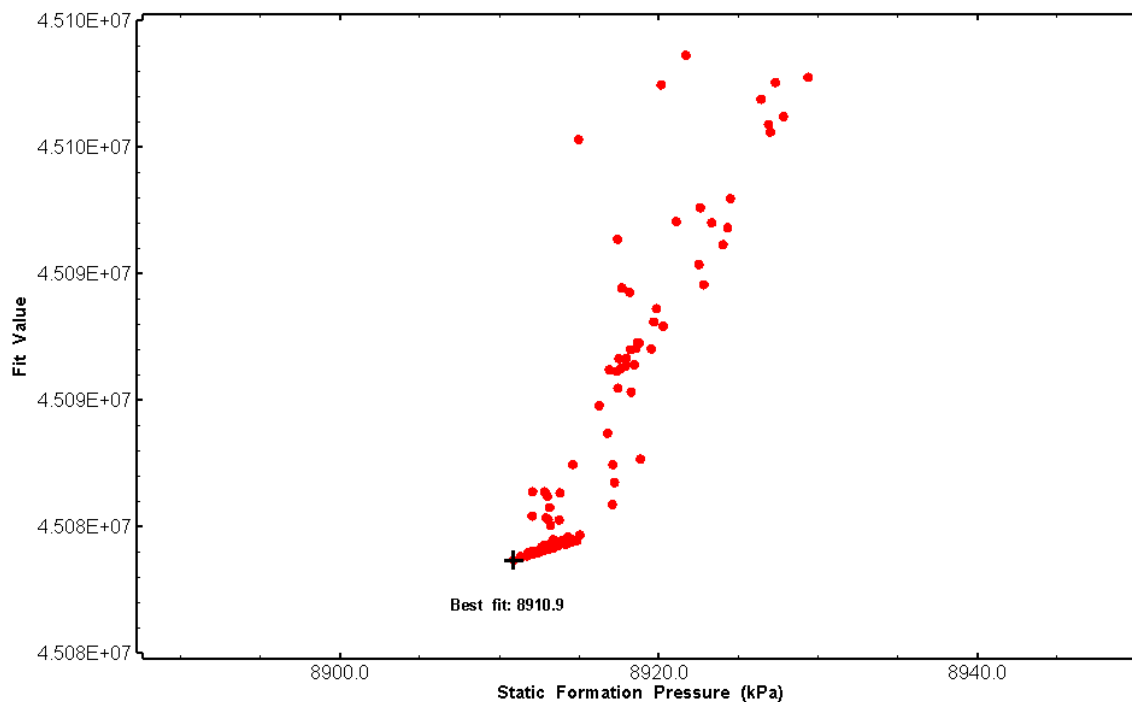


Figure 355: HT030 XY-scatter plot of static formation pressure vs. fit value

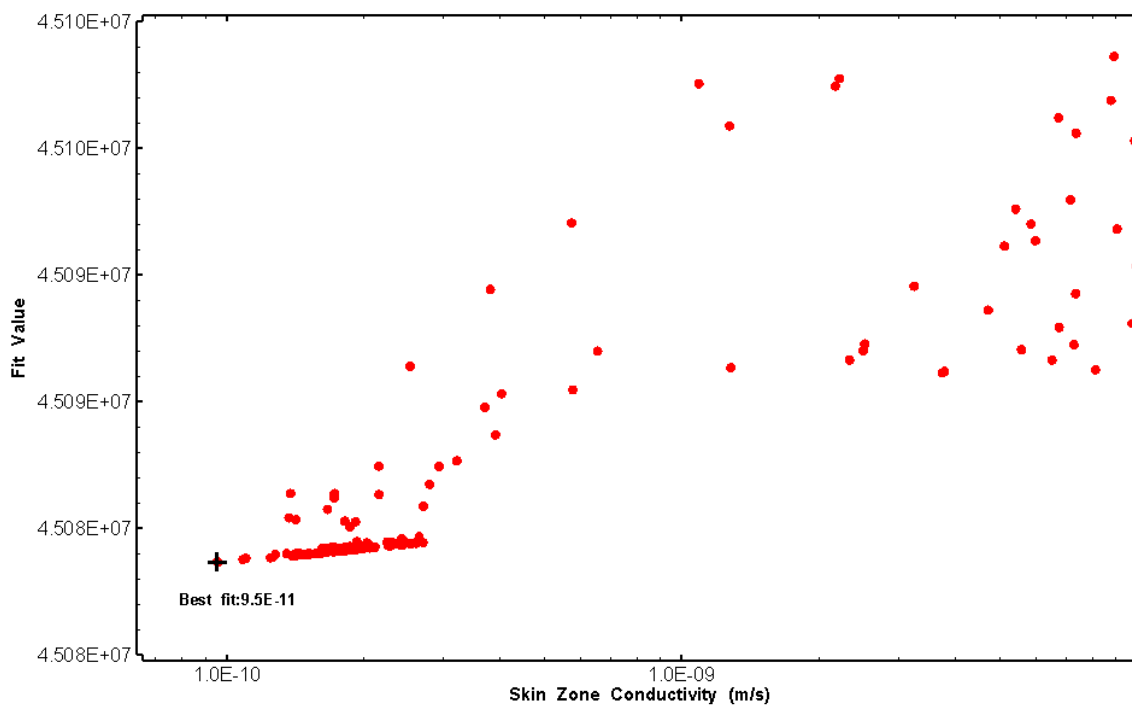


Figure 356: HT030 XY-scatter plot of skin zone conductivity vs. fit value

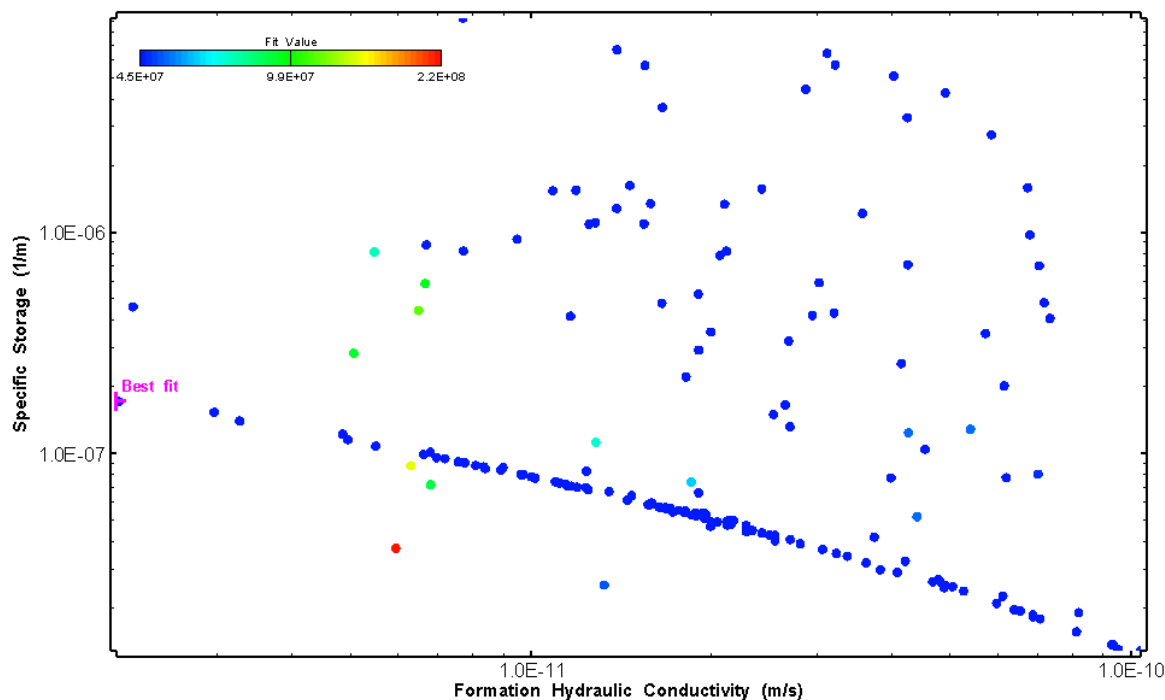


Figure 357: HT030 XY-scatter plot showing estimates of formation hydraulic conductivity and specific storage from perturbation analysis

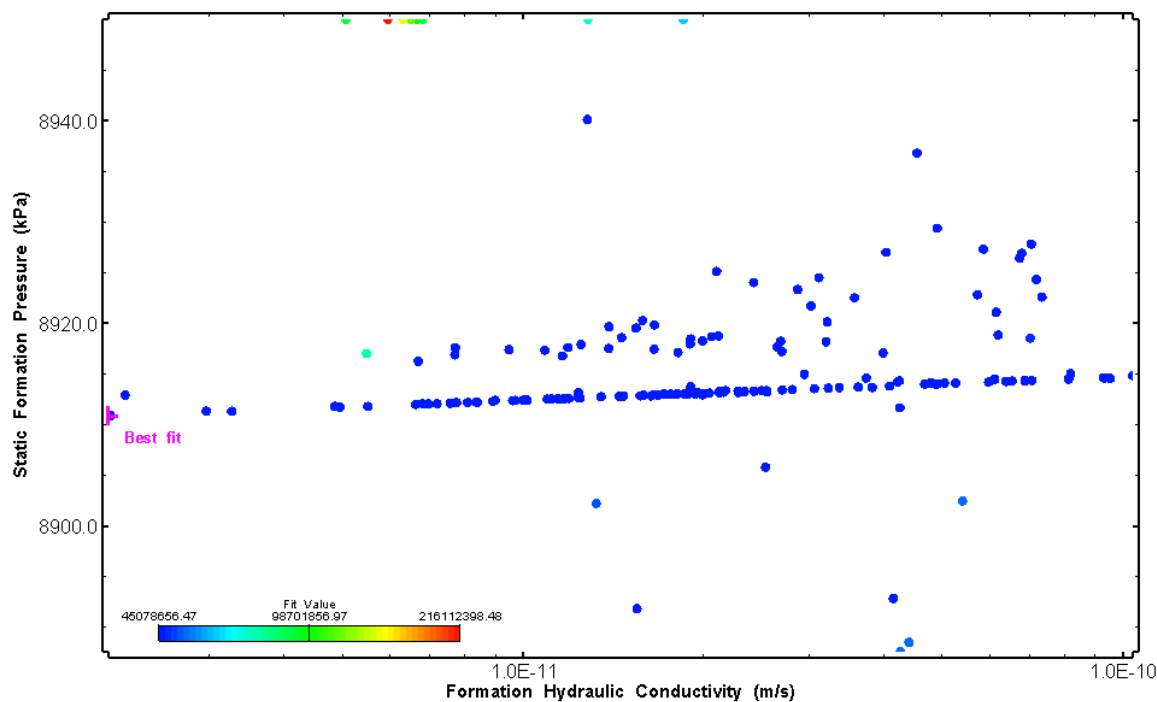


Figure 358: HT030 XY-scatter plot showing estimates of formation hydraulic conductivity and static formation pressure from perturbation analysis

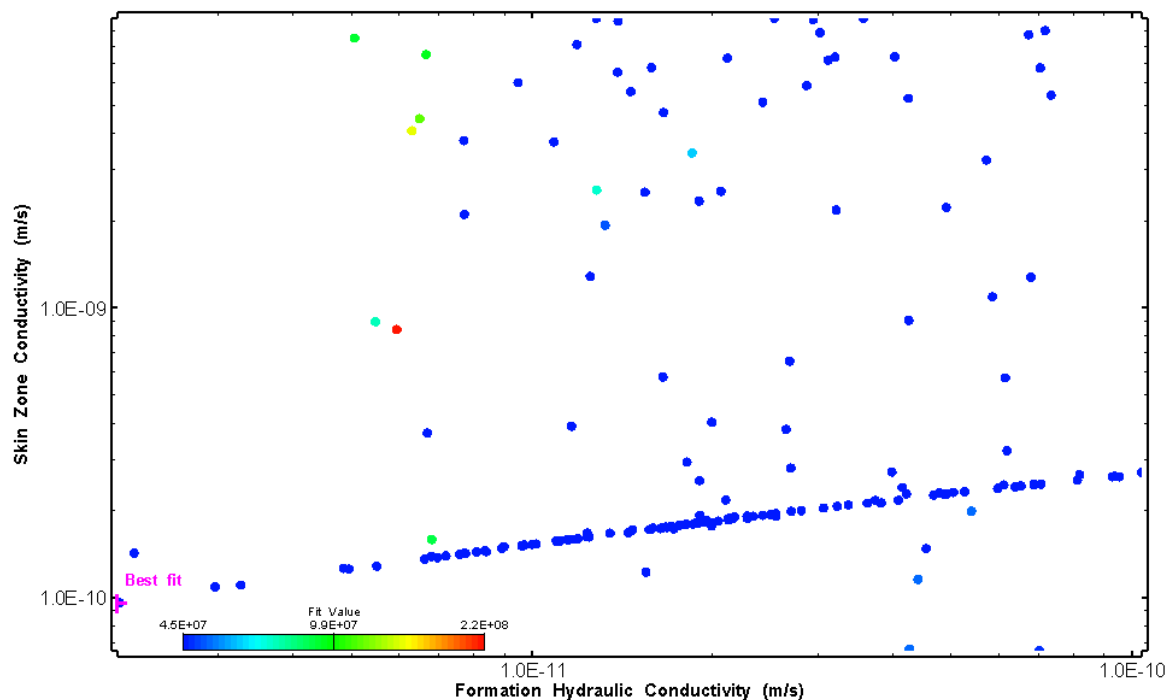


Figure 359: HT030 XY-scatter plot showing estimates of formation hydraulic conductivity and skin zone conductivity from perturbation analysis

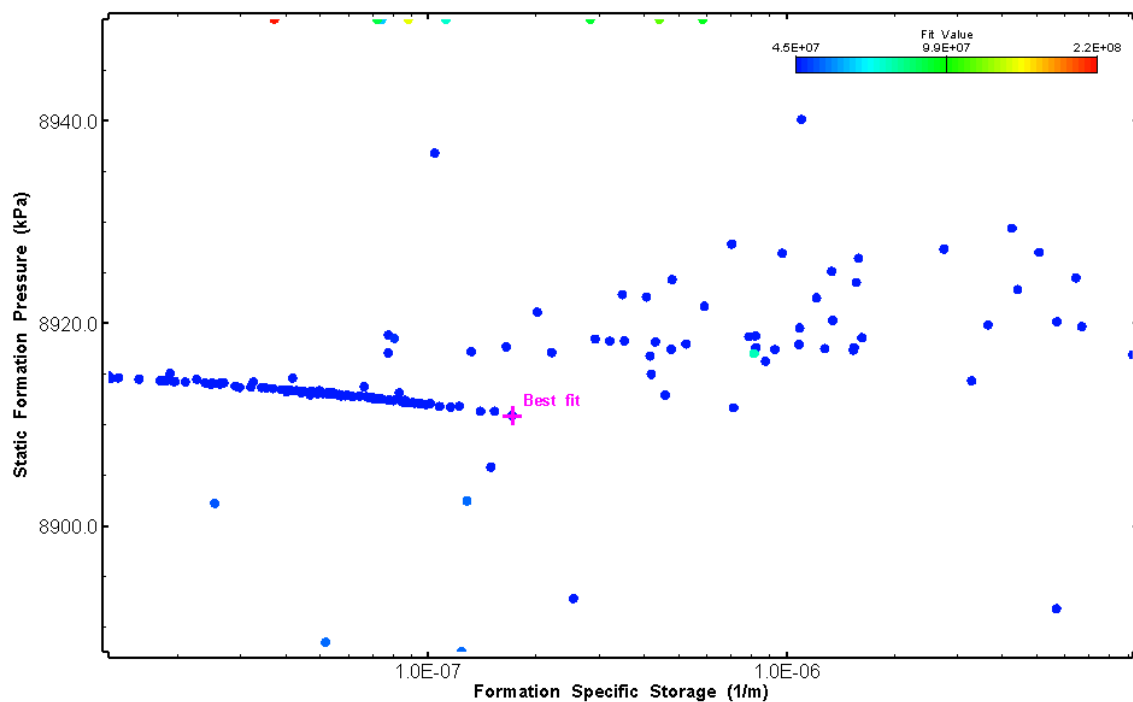


Figure 360: HT030 XY-scatter plot showing estimates of specific storage and static formation pressure from perturbation analysis

## 31.0 LT001 (40.86 – 60.88 M)

LT001 was completed to confirm that the tool performance met the project's requirement of accurately measuring test interval hydraulic conductivity down to  $10^{-13}$  m/sec. LT001 was conducted within the well surface casing.

The test was initiated with a shut-in pressure recovery phase (PSR). A slug withdrawal test (SW) followed by a slug withdrawal shut-in (SWS) phase were completed after the PSR phase.

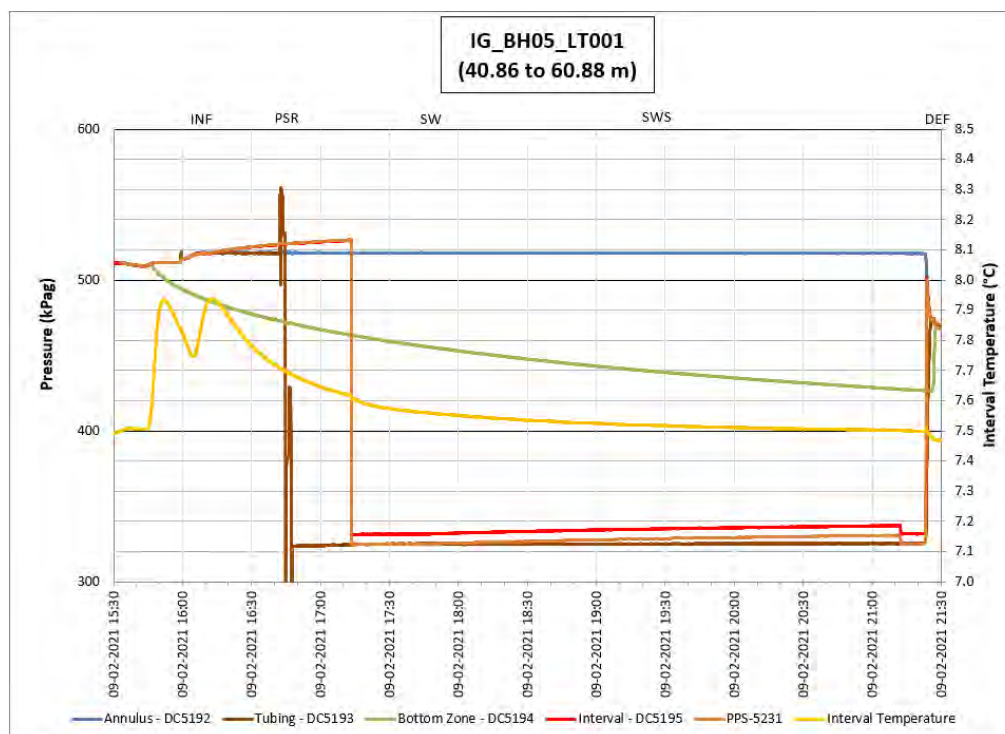
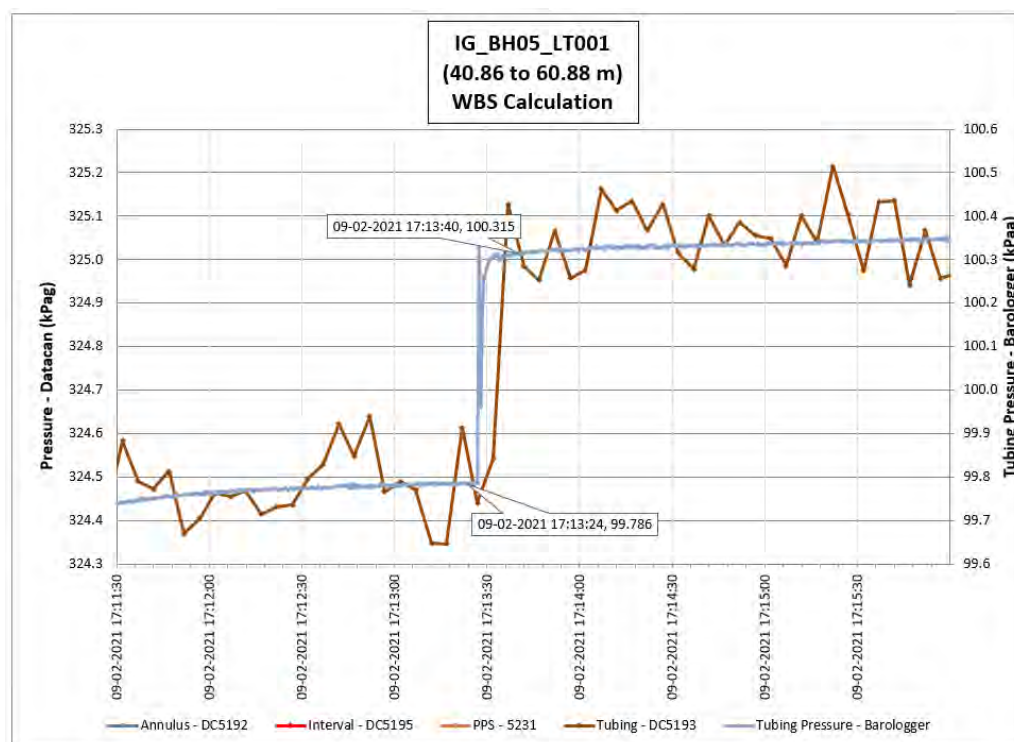


Figure 361: LT001 Annotated test plot showing monitored zone pressure and interval temperature.



**Figure 362: LT001 Tubing pressure during DHSIV activation. DHSIV Closed Wellbore Storage Estimate = 5E-10 m3/Pa**

**Table 2: Summary of Analysis Results – LT001**

	Formation conductivity	Skin zone conductivity	Static formation pressure	Formation specific storage	Radial thickness of skin	Flow dimension
	[m/s]	[m/s]	[kPa]	[1/m]	[m]	[–]
Best Fit	4E-15	1E-11	460	5E-08	3.27E-01	2.7
Minimum	1E-15	6E-14	425	1E-09	1E-03	1.0
Maximum	1E-11	1E-11	605	5E-06	1E-00	3.0
Mean	7E-13	4E-12	502	4E-07	2E-01	1.7
Median	1E-13	3E-12	498	7E-08	2E-01	1.6
Geometric mean	1E-13	3E-12	501	6E-08	9E-02	1.6



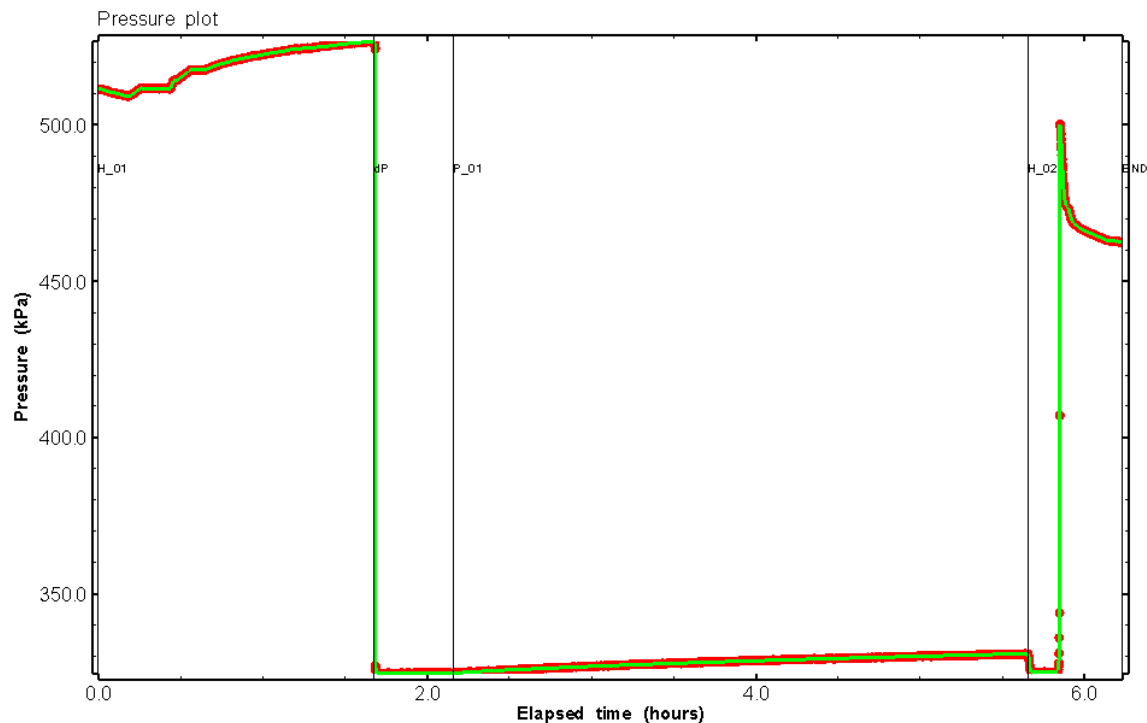


Figure 363: LT001 Pressure plot showing best-fit simulation and best fit results

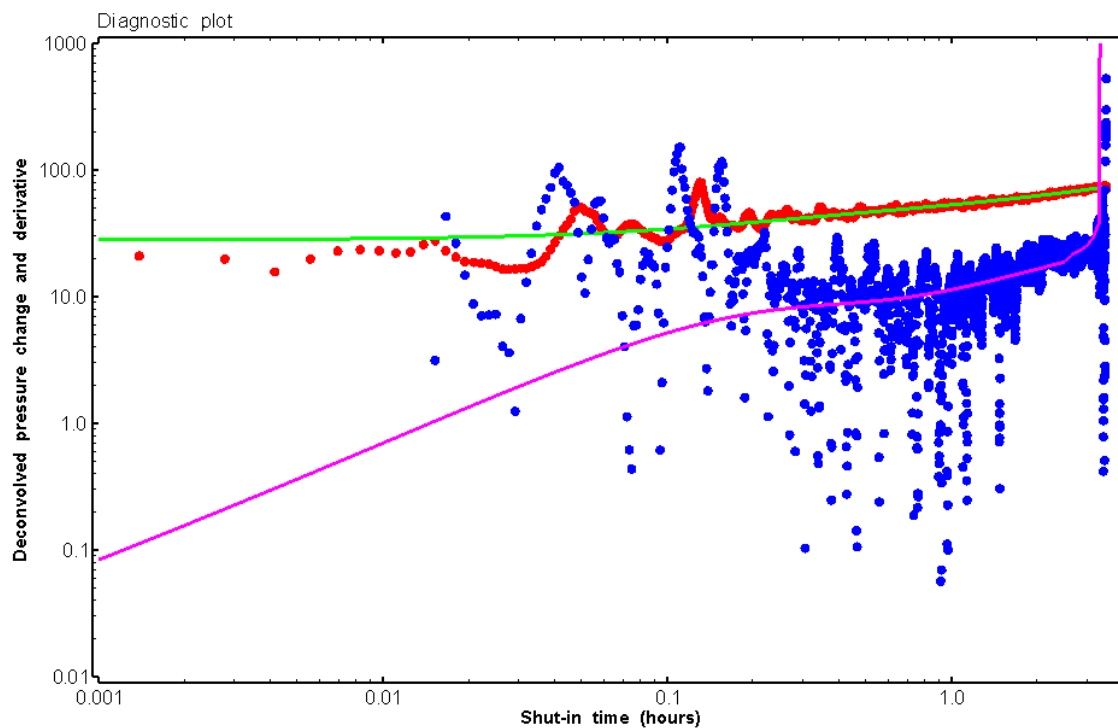


Figure 364: LT001 Deconvolved pressure change and derivative plot

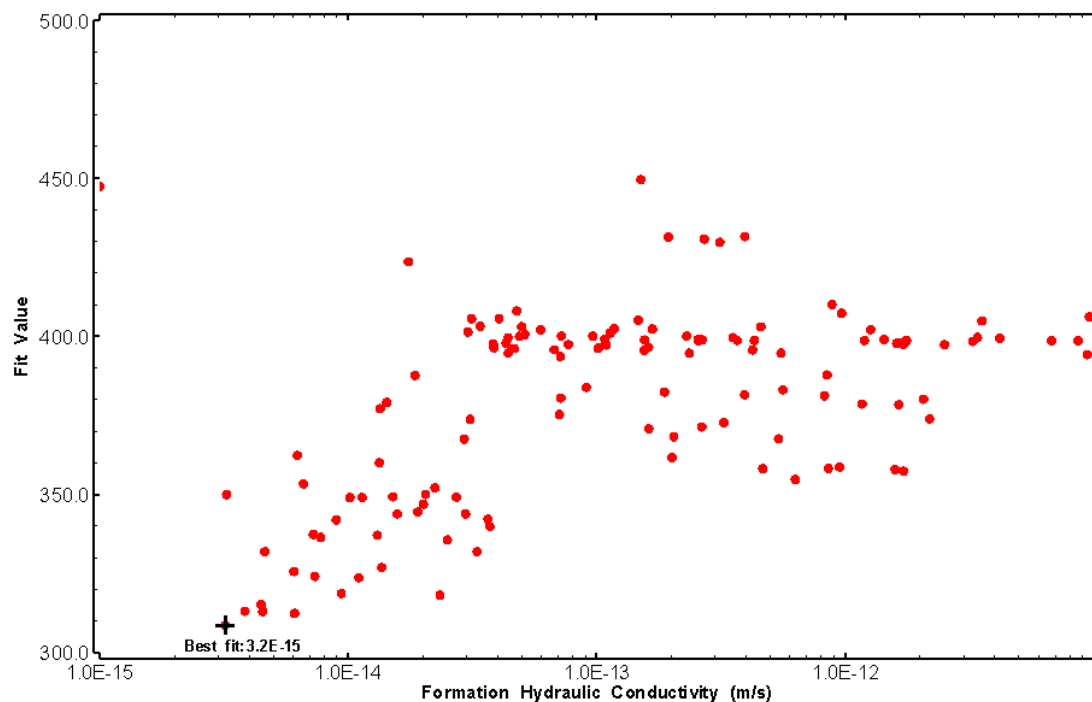


Figure 365: LT001 XY-scatter plot of formation hydraulic conductivity vs. fit value

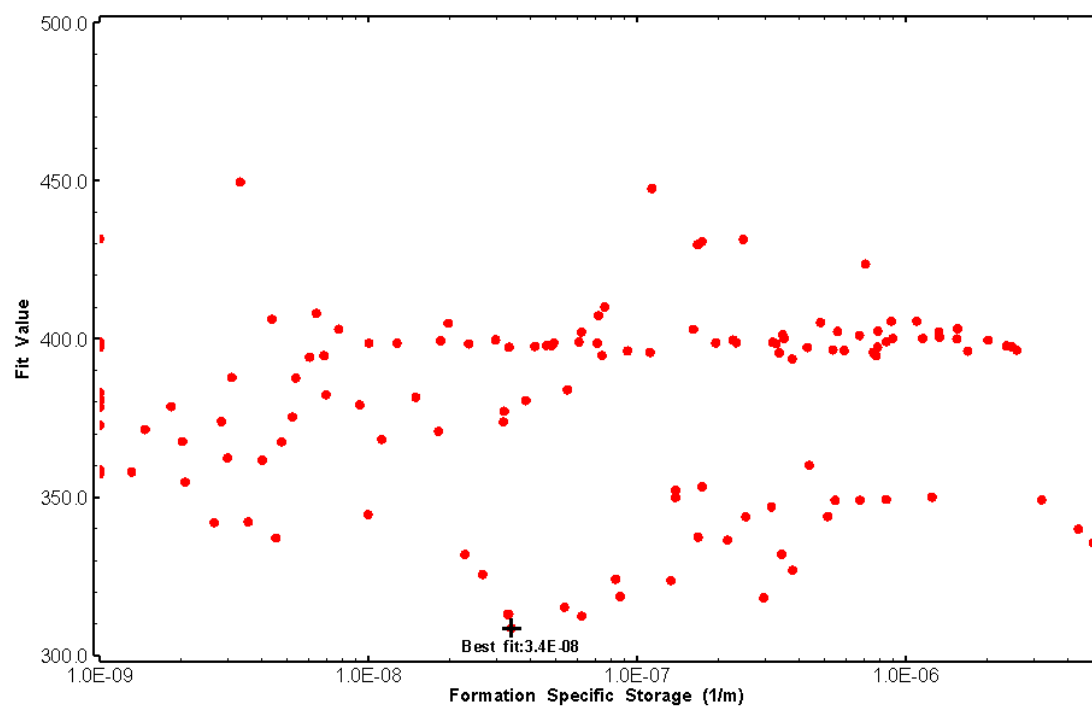


Figure 366: LT001 XY-scatter plot of formation specific storage vs. fit value

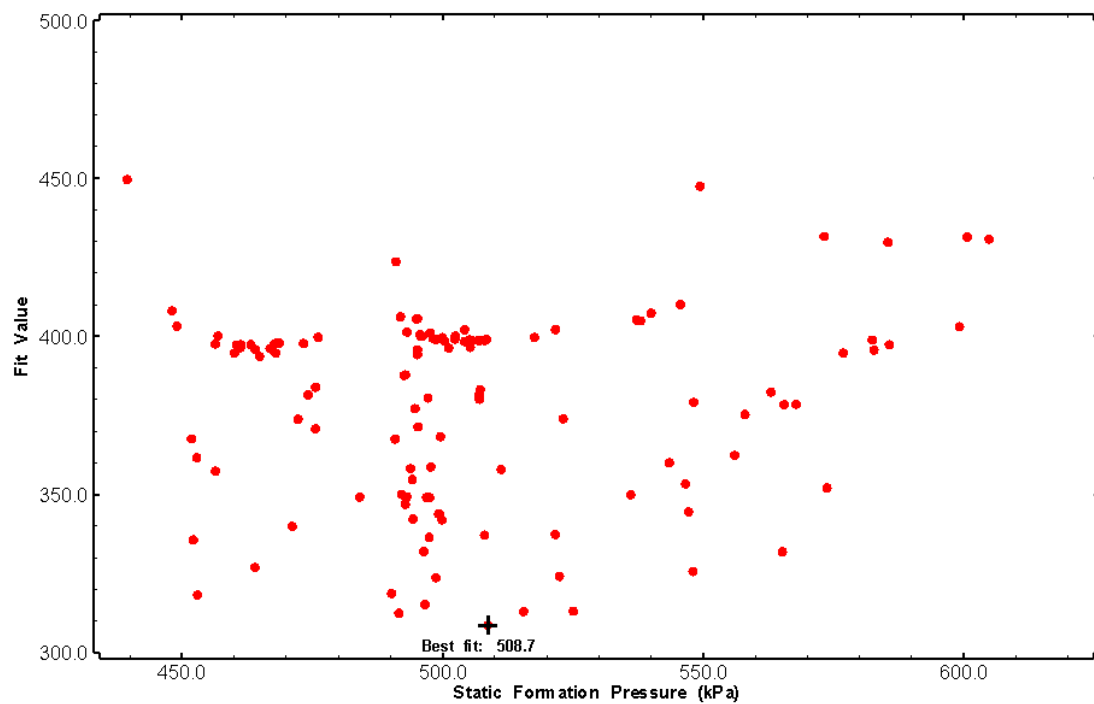


Figure 367: LT001 XY-scatter plot of static formation pressure vs. fit value

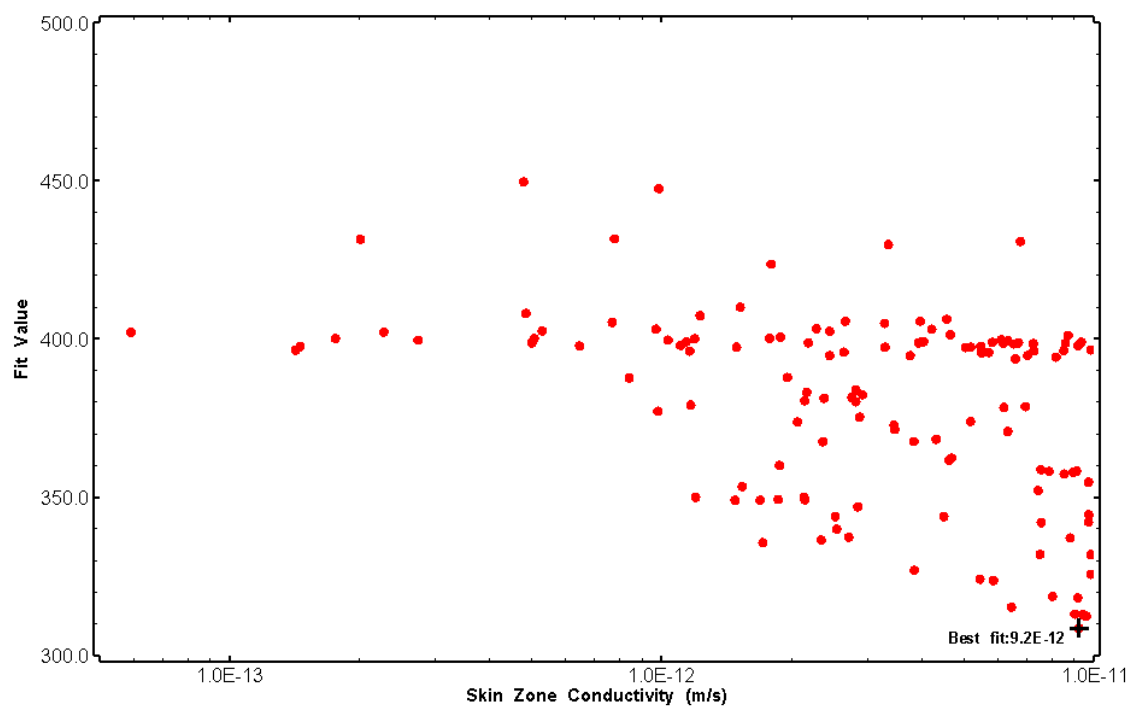


Figure 368: LT001 XY-scatter plot of skin zone conductivity vs. fit value

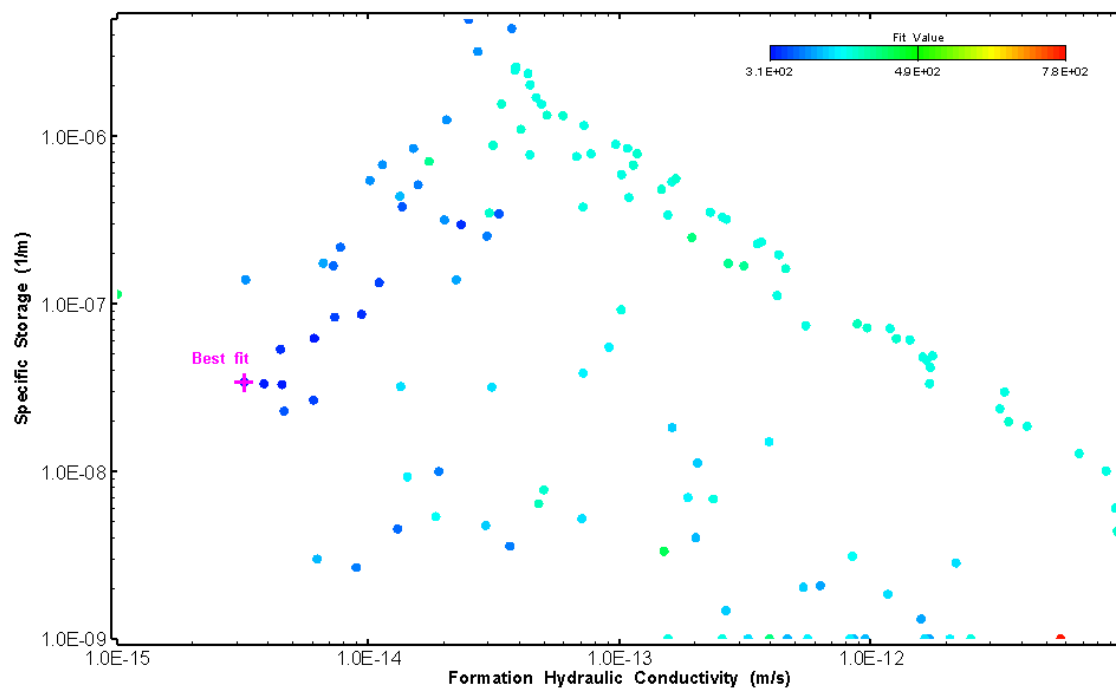


Figure 369: LT001 XY-scatter plot showing estimates of formation hydraulic conductivity and specific storage from perturbation analysis

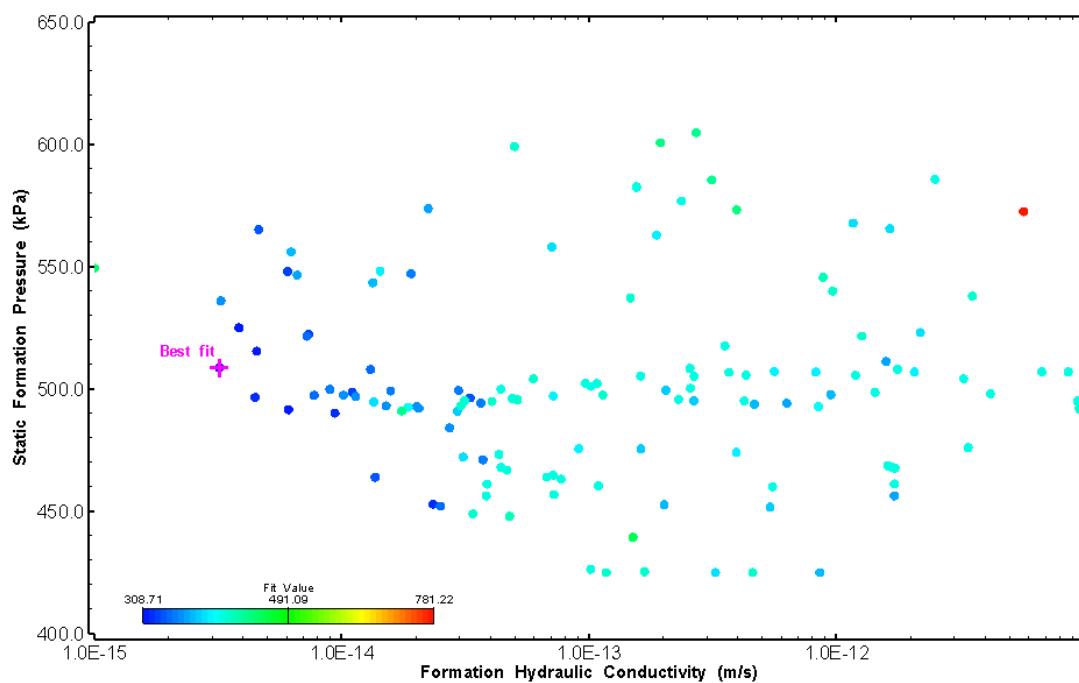
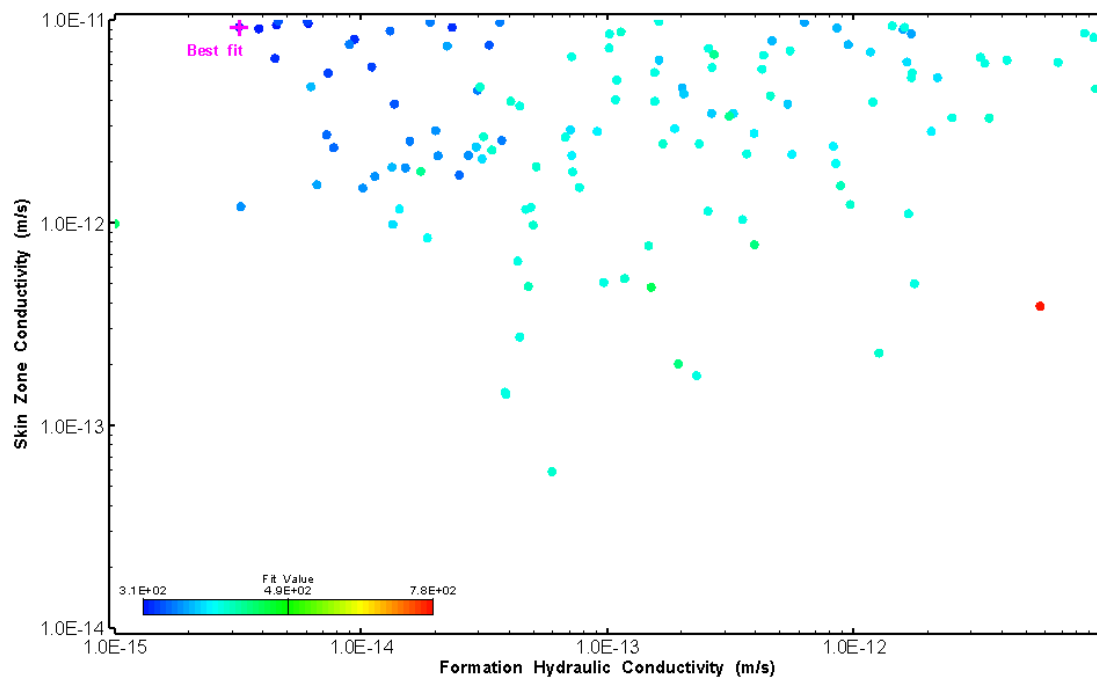
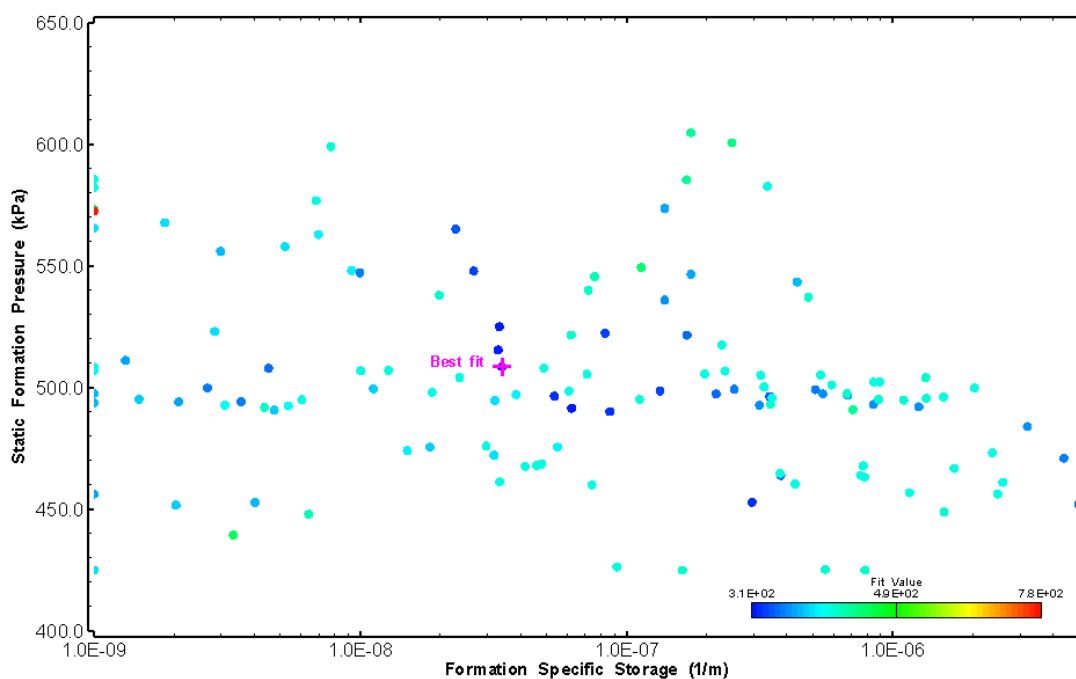


Figure 370: LT001 XY-scatter plot showing estimates of formation hydraulic conductivity and static formation pressure from perturbation analysis



**Figure 371: LT001 XY-scatter plot showing estimates of formation hydraulic conductivity and skin zone conductivity from perturbation analysis**



**Figure 372: LT001 XY-scatter plot showing estimates of specific storage and static formation pressure from perturbation analysis**

## 32.0 LT002 (40.86 – 60.88 M)

LT002 was completed to confirm that the tool performance met the project's requirement of accurately measuring test interval hydraulic conductivity down to  $10^{-13}$  m/sec. LT002 was conducted within the well surface casing.

The test was initiated with a shut-in pressure recovery phase (PSR). A slug injection test (SI) followed by a slug injection shut-in (SIS) phase were completed after the PSR phase.

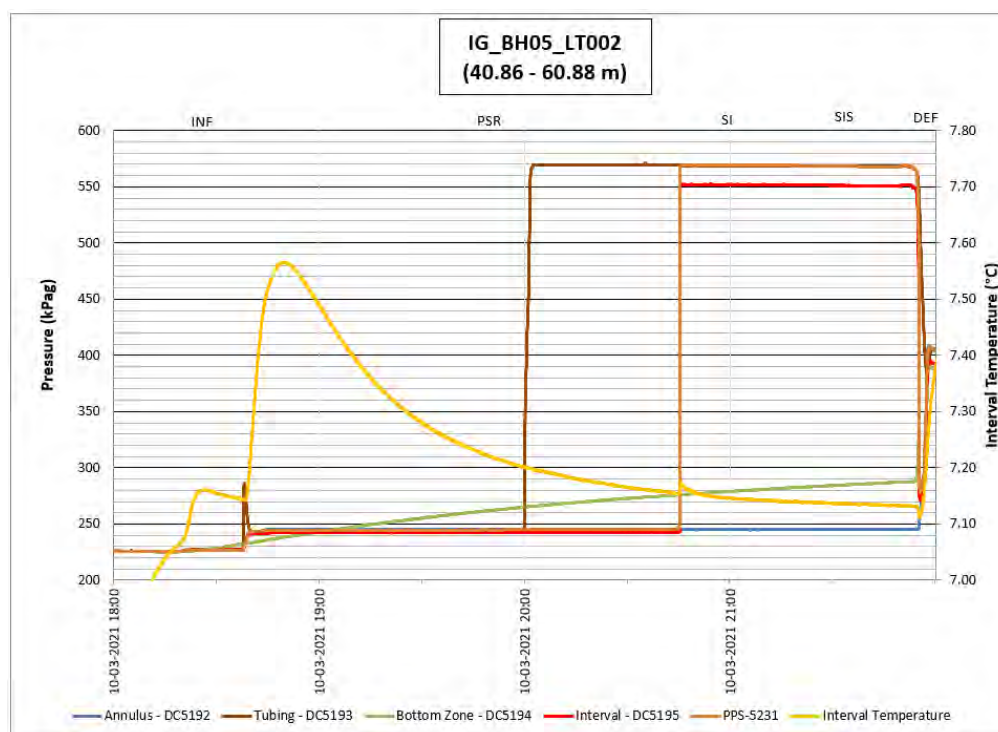


Figure 373: LT002 Annotated test plot showing monitored zone pressure and interval temperature.

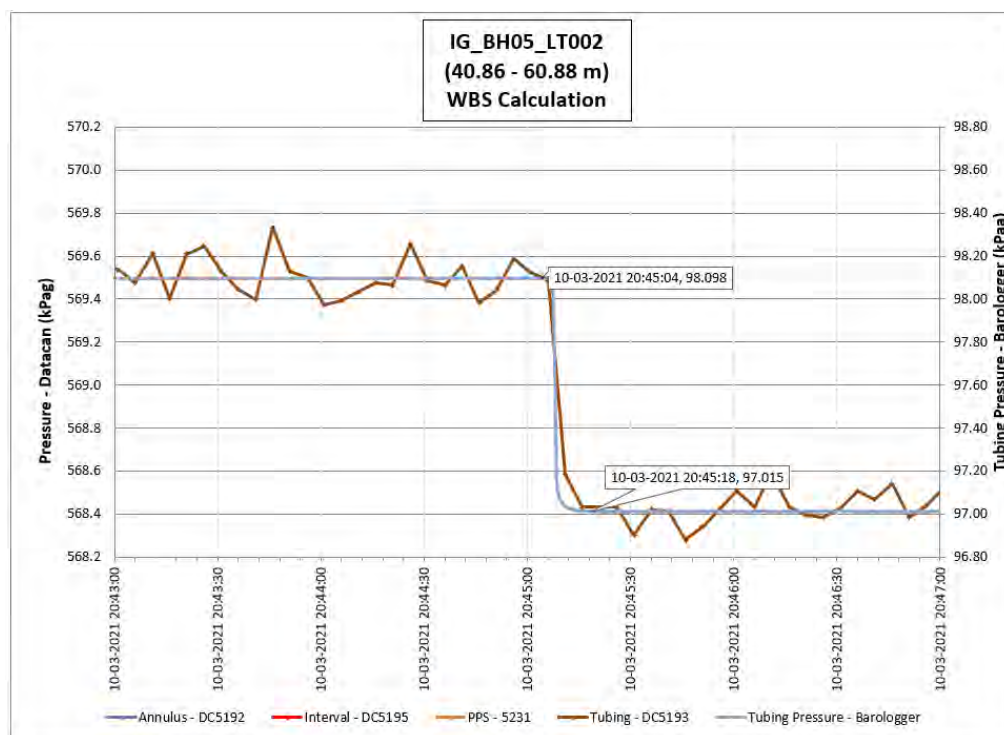


Figure 374: LT002 Tubing pressure during DHSIV activation. DHSIV Closed Wellbore Storage Estimate =  $6\text{E-}10 \text{ m}^3/\text{Pa}$

Table 3: Summary of Analysis Results – LT002

	Formation conductivity	Skin zone conductivity	Static formation pressure	Formation specific storage	Radial thickness of skin	Flow dimension
	[m/s]	[m/s]	[kPa]	[1/m]	[m]	[–]
Best Fit	1E-14	2E-13	326	8E-06	8E-03	1.7
Minimum	1E-15	4E-14	160	1E-10	1E-04	1.0
Maximum	1E-12	1E-12	360	1E-05	1E+00	3.0
Mean	2E-13	3E-13	290	1E-06	3E-01	1.4
Median	8E-14	3E-13	293	8E-08	2E-01	1.2
Geometric mean	7E-14	3E-13	284	8E-08	2E-01	1.3

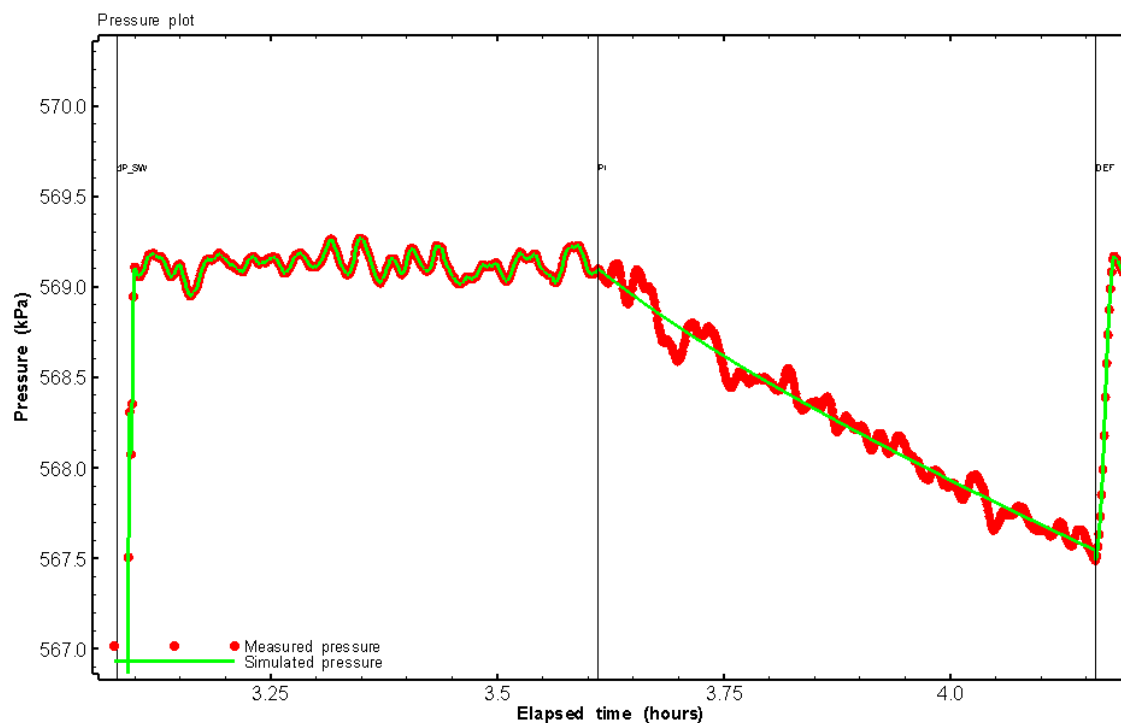


Figure 375: LT002 Pressure plot showing best-fit simulation and best fit results

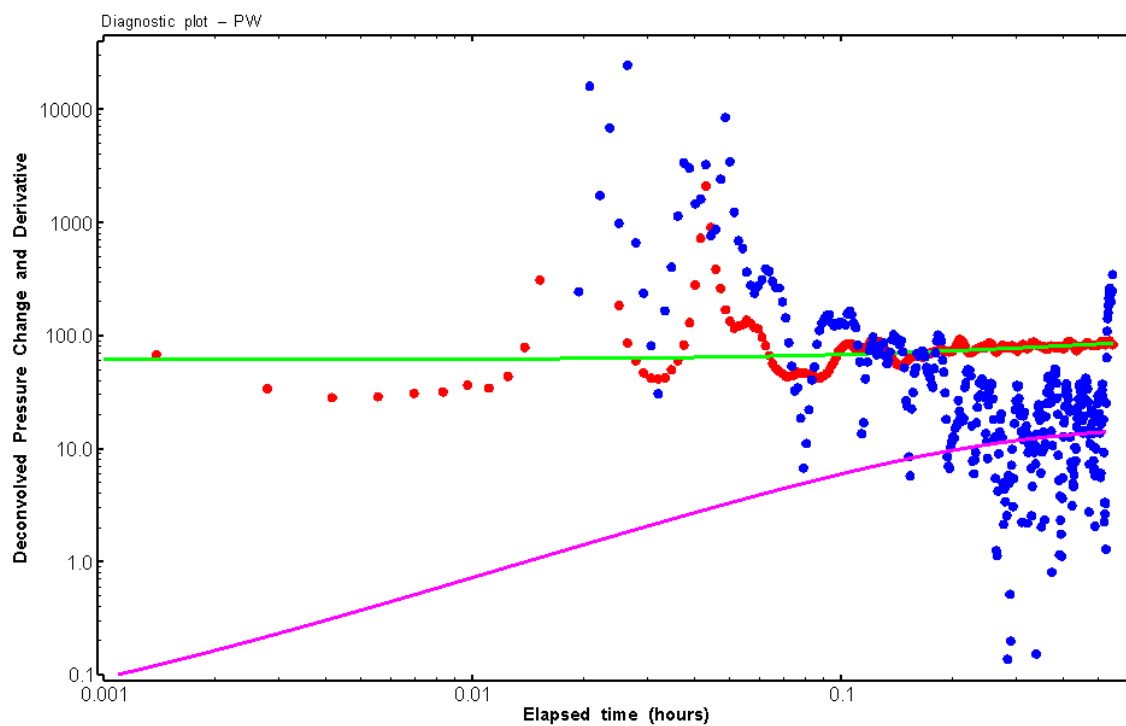


Figure 376: LT002 Deconvolved pressure change and derivative plot



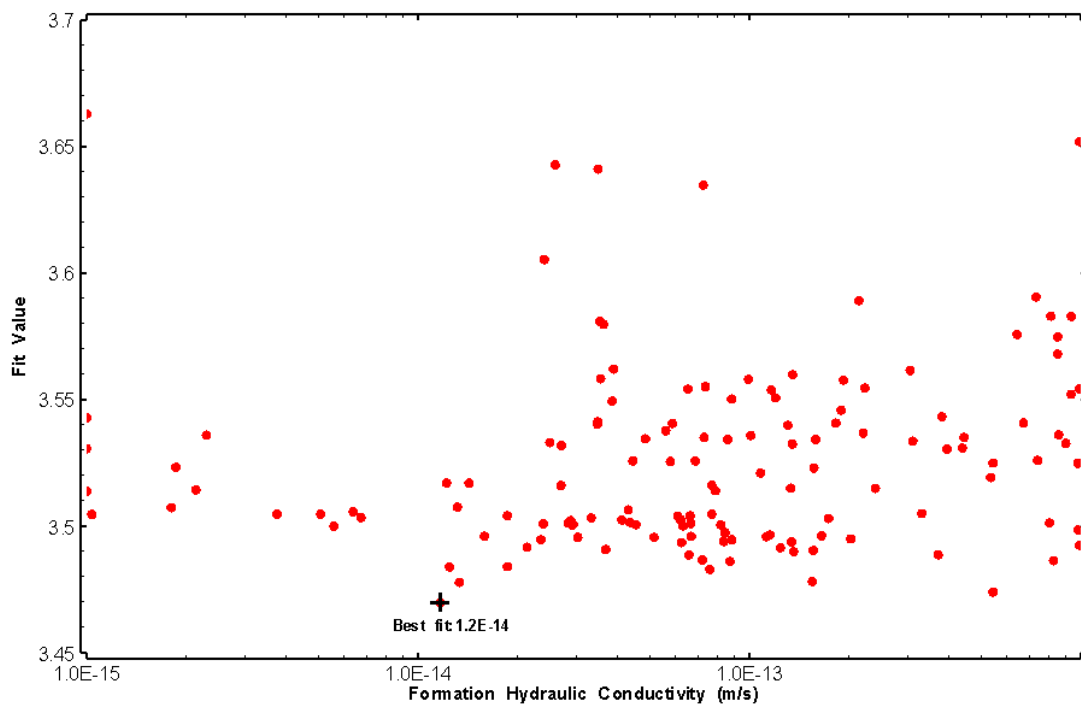


Figure 377: LT002 XY-scatter plot of formation hydraulic conductivity vs. fit value

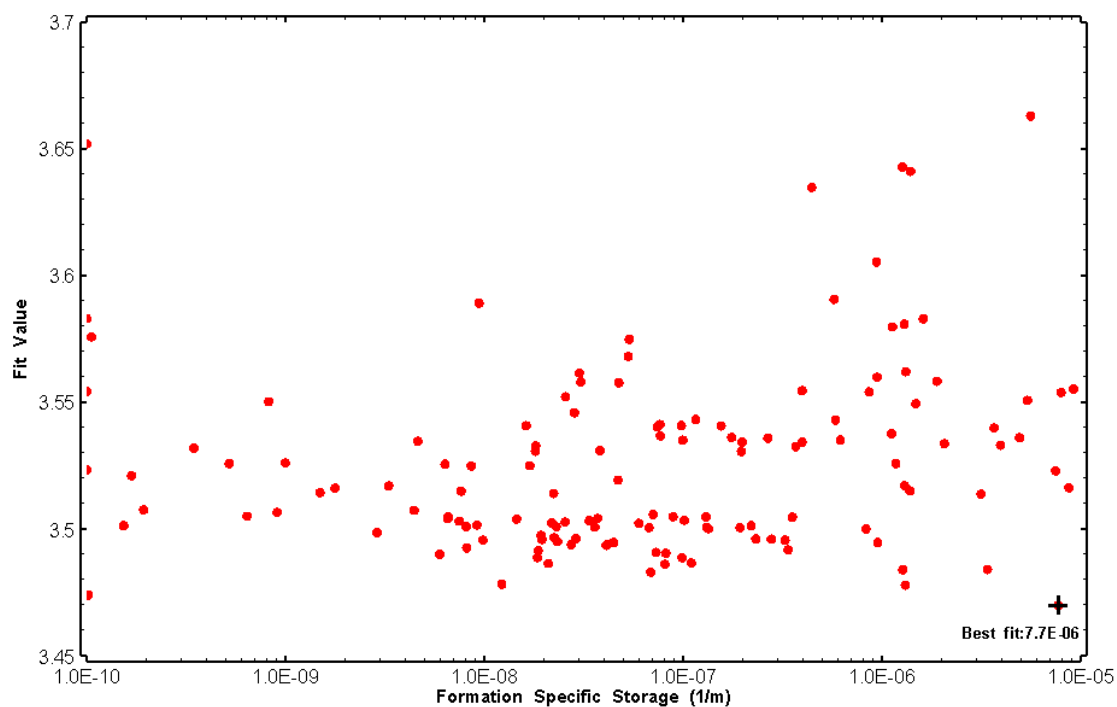


Figure 378: LT002 XY-scatter plot of formation specific storage vs. fit value

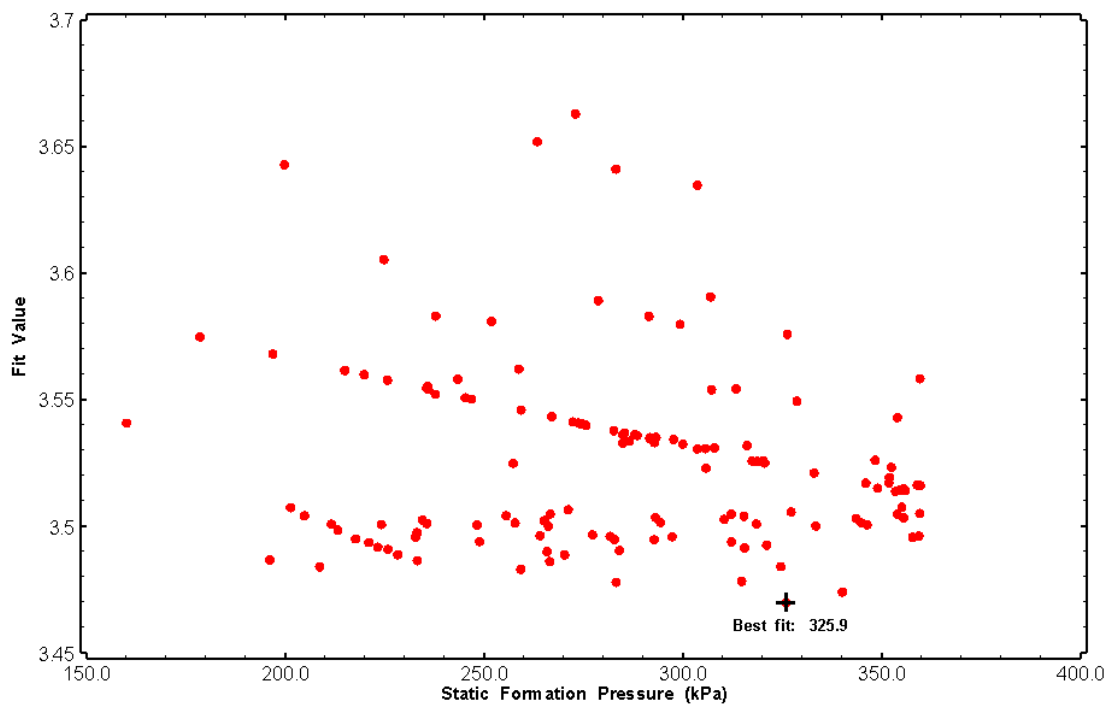


Figure 379: LT002 XY-scatter plot of static formation pressure vs. fit value

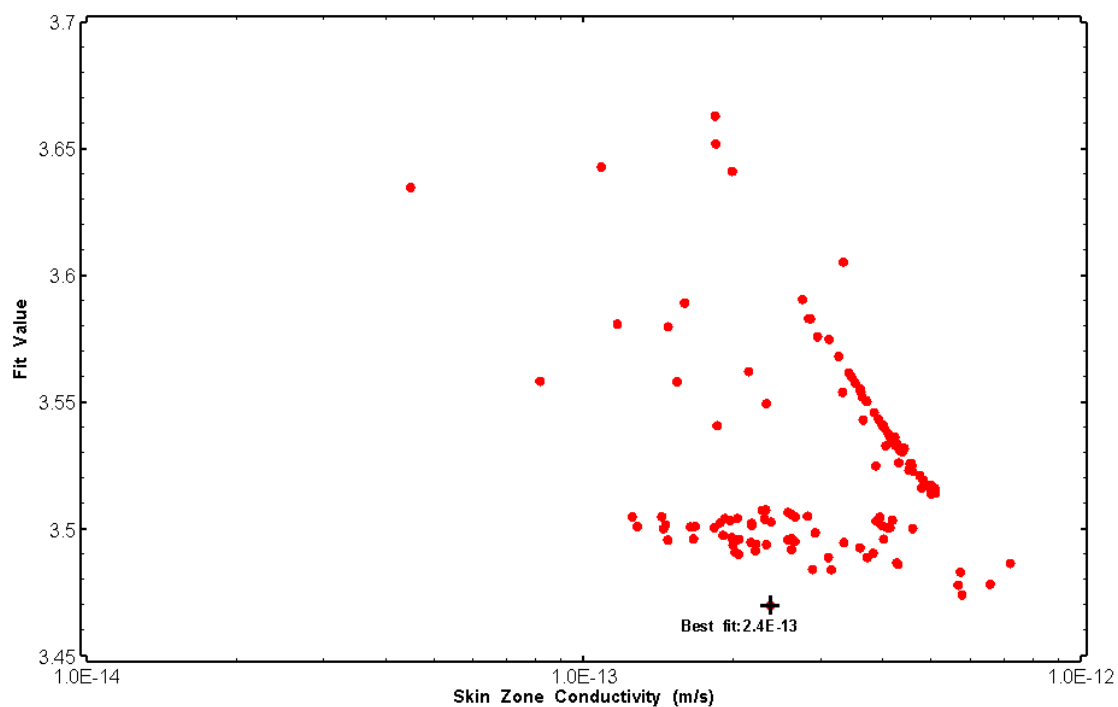
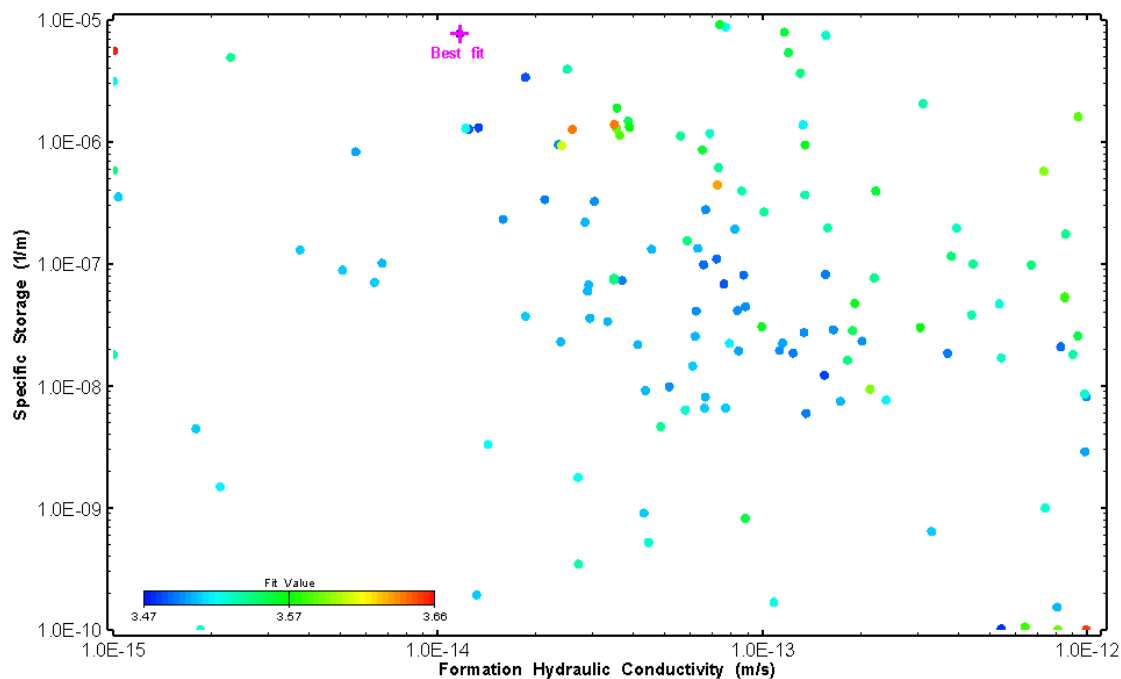
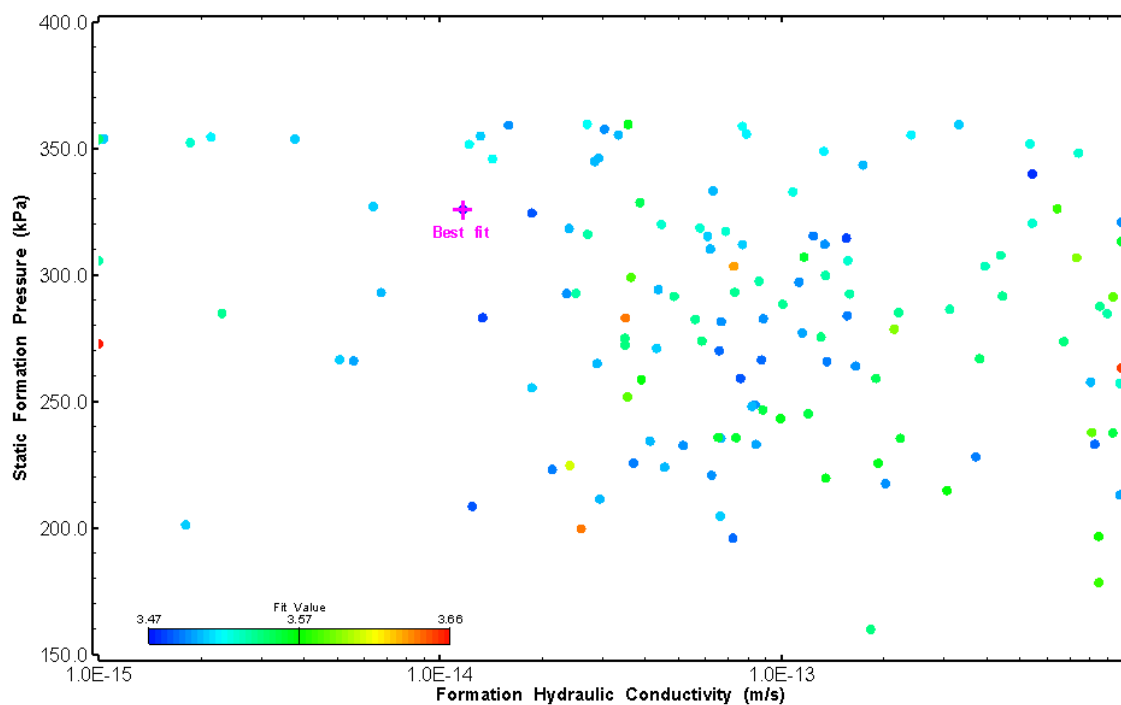


Figure 380: LT002 XY-scatter plot of skin zone conductivity vs. fit value



**Figure 381: LT002 XY-scatter plot showing estimates of formation hydraulic conductivity and specific storage from perturbation analysis**



**Figure 382: LT002 XY-scatter plot showing estimates of formation hydraulic conductivity and static formation pressure from perturbation analysis**

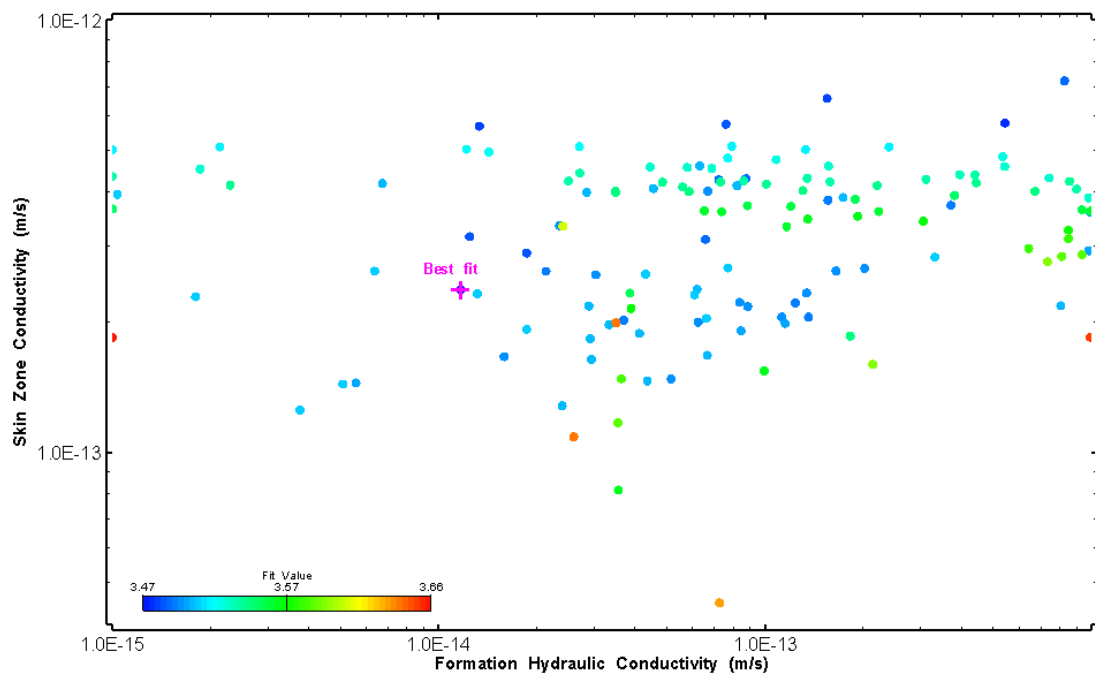


**Figure 383: LT002 XY-scatter plot showing estimates of formation hydraulic conductivity and skin zone conductivity from perturbation analysis**

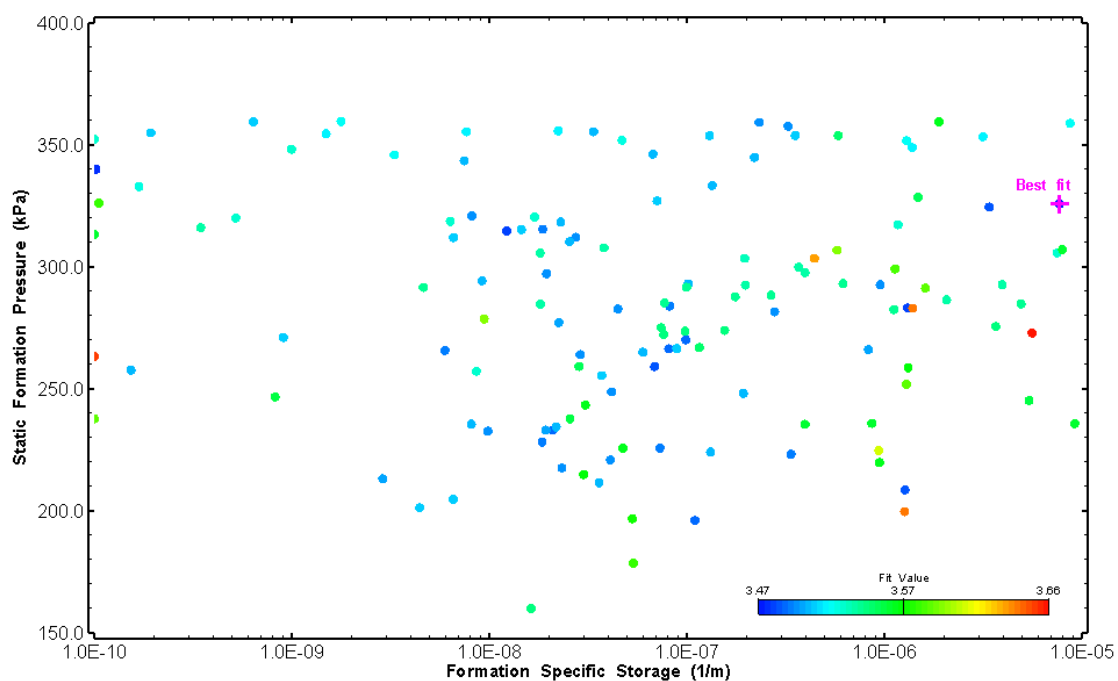


**Figure 384: LT002 XY-scatter plot showing estimates of specific storage and static formation pressure from perturbation analysis**

